

COMPUTER SIMULATION OF A MOTORCYCLE AND DUMMY RIDER
IN IMPACT

A Thesis Submitted for the Degree of Doctor of Philosophy

By

Lai-Sheung Melissa Mo, M.Sc., B.Sc.Hons.

Department of Mechanical Engineering, Brunel University.

May 1996

ABSTRACT

This thesis is concerned with the simulation model of an OPAT dummy rider on a Norton motorcycle in different configured impacts with a rigid barrier. The mathematical equations used in describing the mass-spring-damper-based impacts have been given. The software used in designing the mathematical model have also been outlined. The simulation model was then calibrated against full scale crash tests by means of film analysis and the processed digitised measurements. This led to the investigations into numerical processing of differentiation and integration. A parametric study was also conducted to examine injury to the dummy rider based on some varying parameters. The simulation model was further verified by different configurations and also an introduction of an airbag. Finally, the model was extended to a HYBRID3 dummy rider on the same motorcycle in different configured impacts with a motor car. It is hoped that after the validations and verifications have been performed to examine the robustness of the simulation model, it can assist in the analyses of motorcycle impacts with the less frequent need of conducting a full scale crash test, so that safety design of a motorcycle can be established.

ACKNOWLEDGEMENTS

The author would like to thank the following for their help in the development of this thesis:

- (a) Professor Alan Yettram and Dr. Murdo Macaulay for their knowledge and guidance.
- (b) Dr. Julian Happian-Smith of Sunderland University, for his engineering and computer programming expertise.
- (c) Dr. Bryan Chinn and staff of T.R.L. who had provided valuable data and technical information of the subjects being investigated in this work.
- (d) Professor David Taylor for his statistical advice.

CONTENTS

1.	INTRODUCTION	1
2.	REVIEW OF PREVIOUS RESEARCH	3
2.0	Introduction	3
2.1	Leg Protection	3
2.2	Airbags	7
2.3	Mathematical Modelling	10
3.	THE CONTACT MODEL	12
3.0	Introduction	12
3.1	Uni-directional Spring-Damper System	12
3.2	Two-Body Impact System	15
4.	THE SYSTEM MODEL	19
4.0	Introduction	19
4.1	SD/FAST And ACSL	19
4.2	The Development Phase	21
4.3	The Execution Phase	26
4.4	Head Contacts	29
5.	PROGRAMMING AND COMPUTATION	33
5.0	The General System	33
5.1	Coordinate System	35
5.2	Force Generation	38
5.3	Permanently Deformed Impacts	42
5.4	Torque Generation	44
5.5	The Jointed Dummy	45
5.6	The Front Fork System	50

6.	CALIBRATION AND VALIDATION	54
6.0	Introduction	54
6.1	Data Collection	54
6.2	Calibration	59
6.3	Validation	67
7.	NUMERICAL PROCESSING	70
7.0	Introduction	70
7.1	Differentiation	72
7.1.1	Piecewise Spline Interpolation	73
7.1.2	Cubic Splines	73
7.2	Integration	82
7.2.1	The Butterworth Filter	82
7.3	Overview	90
8.	PARAMETRIC STUDY	92
8.0	Introduction	92
8.1	The Independent And Dependent Variables	95
8.2	The Statistical Analysis	98
8.3	Correlation Coefficients	100
8.4	The Linear Relationship Between Forces And The Independent Variables	101
8.5	Multiple Linear Regression	103
8.6	The Variability Component R^2	105
8.7	Stepwise Multiple Linear Regression	106
8.8	Partial Correlation Coefficient	114
8.9	Analysis Of Variance (ANOVA)	120

8.10	Multivariate Analysis Of Variance (MANOVA)	127
8.11	Overview	131
9.	ANALYSIS OF SPECIFIC FEATURES	136
9.0	Introduction	136
9.1	The Datum Simulations	138
9.1.1	Run 1 (Figure 9.1)	139
9.1.2	Run 2 (Figure 9.2)	139
9.1.3	Run 3 (Figure 9.3)	140
9.2	Simulations With Minimal Outer Fairing	142
9.2.1	Run 4 (Figure 9.4)	143
9.2.2	Run 5 (Figure 9.5)	143
9.2.3	Run 6 (Figure 9.6)	144
9.3	Different Sized Dummies	146
9.3.1	Runs 1, 7 And 8 (Figures 9.1, 9.13, 9.14)	147
9.3.2	Runs 2, 9 And 10 (Figures 9.2, 9.15, 9.16)	148
9.3.3	Runs 3, 11 And 12 (Figures 9.3, 9.17, 9.18)	149
9.4	Different Seated Positions	151
9.4.1	Run 13 (Figure 9.25)	152
9.4.2	Run 14 (Figure 9.26)	153
9.5	Airbag Characteristics	154
9.5.1	Run 15 (Figure 9.29)	155
9.5.2	Run 16 (Figure 9.30)	156
9.5.3	Run 17 (Figure 9.31)	157
9.5.4	Run 18 (Figure 9.33)	158
9.5.5	Run 19 (Figure 9.34)	158
9.6	Overview	160

10. CONVERSION OF DUMMY TO HYBRID3	162
10.0 Introduction	162
10.1 The Design Of The HYBRID3	162
10.2 The Computer Runs	165
10.3 Observations	165
10.4 Comparisons	166
10.5 Discussion	168
11. EXTENSION OF SIMULATION FOR IMPACT INTO A MOTOR CAR	170
11.0 Introduction	170
11.1 The Design Of An Automobile	170
11.2 Data Collection	172
11.3 The Computer Runs	173
11.4 Observations	174
11.5 Comparisons	175
11.6 Discussion	177
12. CONCLUSIONS AND FURTHER WORK	179
12.0 General Conclusions	179
12.1 Overall Conclusions	183
12.2 Further Work	185
REFERENCES	188
BIBLIOGRAPHY	192
APPENDIX A.1 USE OF PROGRAM	194
A.1.0 Introduction	194
A.1.1 Compilation	194
A.1.2 Running Of The Program	197
A.1.3 The ACSL Command File	203

A.1.4	Modifying The Parameters	205
A.1.5	Changes To The Current Program	208
APPENDIX A.2	MATHEMATICAL DERIVATIONS	211
A.2.0	Introduction	211
A.2.1	Cubic Spline Interpolation	211
A.2.2	The Butterworth Filter	213

CHAPTER 1

INTRODUCTION

Investigations into vehicle crashworthiness, accident statistics, experimental protection devices and dummy rider development, have all had a long established history. Considered physically and intuitively, the impact dynamics of the combination of rider, motorcycle and target is undoubtedly a very sensitive system, see Figures 1.1 and 1.2. Expressed mathematically one would say that it could be quite ill-conditioned. Small changes to any part of the model, or to any input to it, might result in large changes in response. This is because the model comprises elements which are quite "loosely" connected together, such as the dummy due to the joints and in the case of the motorcycle due to the front fork rotation. This is quite apart from the three main elements themselves being separate. This is perhaps why mathematical modelling of motorcycle and rider impact remains relatively rare. One of the first such research attempts is the Dynamics of Motorcycle Impact [1] prepared for the U.S. Department of Transportation in 1973. There a series of crash tests were carried out and computer programs were written to calculate the relevant equations of motion. The computer programs were written in FORTRAN IV and the fourth-order Runge-Kutta formulae were used to integrate the mathematical differential equations.

Since then, Happian-Smith [2] had developed a two-dimensional simulation model of a motorcycle with a simple pendulum-rider in frontal impacts. However, the advance in computer technology and software had progressed and the Advanced Continuous Simulation Language [3] was used for programming. This is an extension to the FORTRAN language with built-in numerical methods, including the various Runge-Kutta formulae, as the choice of solving differential equations. The intention of the current work is to extend this two-dimensional model into three-dimensions with a more elaborate dummy rider, and to examine the effect of impact into various targets. The aim of the work is to investigate safety features - those in the hands of the designers and those in the hands of the riders. A full scale crash test involves high cost and long man hours both in the preparation of instrumentation and the analysis of results stage. A computer model will eliminate the cost in the long term where frequent computer runs with variations in the configuration of impact can be applied easily. Furthermore, it is the intention of the current work to extend the mathematical model in accordance with the very recent International Organization for Standardization (ISO) specified standards [4] for motorcycle and rider impact simulation.



Figure 1.1 Photograph of a full scale crash test where the target is a barrier. Courtesy of TRL.



Figure 1.2 Photograph of a full scale crash test where the target is a motor car. Courtesy of TRL.

CHAPTER 2

REVIEW OF PREVIOUS RESEARCH

2.0 Introduction

Such is the rarity of mathematical simulation modelling of such a system as being considered here, this chapter will also review the recent developments into various proposed safety aspects of motorcycle research, chiefly the use of leg protection and airbags in motorcycles. Bly [5] mentioned that different designs of leg protectors result in different effects to the overall rider injury, and also that airbags can contribute to injury reduction in some circumstances. Although its beneficial effects have well been observed in car accidents, in both cases, cars and motorcycles, further development is still needed.

2.1 Leg Protection

The Transport Research Laboratory (TRL) has had a long history in the development of leg protection [6]. Chinn et al [7] had conducted a series of crash tests, for unmodified motorcycles, and motorcycles with hard and soft leg protectors, in order to evaluate the effect on an Occupant Protection Accident Test (OPAT) 50 percentile dummy rider. It was found that there was a

decrease in damage on the rider from (a) the unmodified motorcycle, to (b) one with hard leg protectors and least of all, to (c) one with soft leg protectors. This was also the same trend for the dummy's forward velocity. In general, it was found that the motorcycle with a hard leg protector absorbed negligible kinetic energy, but the soft leg protector absorbed some 5 - 10% of the kinetic energy.

However, Tadokoro et al [8] had also conducted a series of crash tests with their Crushible Leg Protector (CLP). It was found that although the CLP had prevented fracture to the lower leg, it had the tendency to move injury to the upper leg and hip area. Furthermore, it may potentially increase injury to the head and chest, since a higher ejection velocity was recorded in the tests compared to when a standard motorcycle was used.

This was also the findings by Sakamoto [9] when a series of crash tests was conducted. It was found that not only fracture to the lower leg had not decreased, but overall injury to other parts of the rider's body had occurred.

However, at TRL where research was still continuing, Chinn et al [10] had conducted crash tests with standard i.e. no leg protection, with fairings-only and "U.K." leg protection fitted motorcycles over a range of impact angles. It was found that in general the leg protector had absorbed a significant level of

energy thus reducing injury to the upper and lower legs. Attention was also paid to injury to other parts of the rider, especially the head. It was found that in the 0 - 30° angle impact, the rider's head was prevented from hitting the vehicle into which the motorcycle impacted. In the head-on impacts, the acceleration recorded on the rider's head was lower in the motorcycle fitted with "U.K." leg protection than the standard and with fairings-only motorcycles. More importantly however, where a motorcycle with "U.K." leg protection had also an airbag fitted, the head acceleration was significantly lower.

This benefit of combining a leg protector and an airbag was also confirmed by Spörner et al [11]. They found that in a motorcycle to car impact, the lower leg is injured most severely. However, because of the available time of up to 100ms between first contact and the impact of the legs against the vehicle, changes in the motion can produce effects to the rider's overall injury, such as rotation of the upper part of the body, thus causing additional loading to the head. A solution to this is to combine leg protection with an airbag such that this gives the body extra height which would otherwise be pressed down as a result of the body's rotation, where the airbag can act to cushion this rotation.

This indicates the potential benefit of a fitted airbag in a motorcycle, but the argument into the potential benefit of the

leg protector is still in the balance. Rogers [12] carried out four tests in two configurations; a 0° offset to the front of the car, and a 30° impact to the side of the car, for both a standard motorcycle and one fitted with TRL leg protection. The findings were that the TRL leg protectors had resulted in increased leg and head injuries in the side impact, and although the leg protector had prevented leg injury in the offset frontal impact, there was an increase in rider ejection thus causing head to ground impact. In addition, Rogers also applied computer simulation to verify the effects of leg protection.

The use of computer simulation had also been adopted by Chinn et al [13]. A simple motorcycle with leg protectors/fairings was modelled and impacted on a flat, rigid inclined barrier. It was found that the leg protectors/fairings reduced the likelihood of the rear of the motorcycle swinging towards the barrier thus reducing the chance of leg injury. However, this is dependent on the value of friction between the leg protecting fairing and the barrier in affecting the angular velocity in a yawing direction, therefore, further design work into the optimum position of the fitted fairings is needed.

However, while the differences between various conclusions exist, the benefit of computer modelling is clear such that it is a less costly tool in being able to simulate easily many variations in the configuration of impact, and so indicate the trend of likely

events during impact.

2.2 Airbags

Airbags fitted to motor cars have been well-researched and have been standardised in several makes of cars. However, airbags fitted in motorcycles are still being investigated and so far are not available in production models.

Similar to the research into leg protection, TRL had an established history in monitoring the effect of airbags fitted in motorcycles. Chinn et al [14] had conducted a series of impacts with unmodified, pre-inflated and impact-activated airbags fitted to motorcycles. It was found that motorcycles with airbags had reduced the linear kinetic energy of the rider compared to the rider on the unmodified motorcycle. In the case of the impact-activated airbag the reduction was 30%, but significantly, though impractical, the pre-inflated version had reduced the energy by 78%. This showed the benefit of the cushion effect on the rider upon impact.

This was further investigated by Finnis [15]. Two different sized airbags were mounted on large and small sized motorcycles and tested against a standard motorcycle in car impacts. It was found that head velocity and kinetic energy had both reduced against

the standard motorcycle, with a trend of greater reduction and hence better benefit in the case of motorcycles with a large airbag. In particular, where a large bag of 90 litre (120 litre when fully inflated) was fitted on a large motorcycle, the rider's head was prevented from impacting the target.

However, the effectiveness of airbags fitted on motorcycles had also been disputed. Ramet et al [16] carried out four tests using human cadavers to examine the effect of a 155 litre bag inflation on the trajectory, and possible trauma to the rider. It was found that in all four cases the riders did not experience a forward motion upon the inflation of the airbag, but were subjected to a violent push backwards, hence causing excessive hyperextension of the neck. However, this approach to airbag testing is quite different to the conventional procedure where dummy riders are used, and therefore care must be taken if results from this work is to be compared to that where dummies are used.

Zellner et al [17], along with the collaboration of Ramet et al [16], conducted a preliminary programme carried out by the motorcycle industry and various research institutes. A series of motorcycles with differently designed airbags, and a standard motorcycle, were used in crash tests with both stationary and moving cars, at two different impact angles. Along with these, computer simulation runs were used to predict the outcome. In general, it was found that there was no chest, abdomen and legs

injury but in all cases where an airbag was fitted, there was a potentially fatal level of neck torque. This was less in the cases of standard motorcycle, suggesting that there should be further developments in the neck biofidelity of the dummy employed and the injury criteria used with regard to an airbag fitted motorcycle, as the large neck torque was not predicted by their computer simulation in some cases.

Despite the different conclusions amongst the various establishments on the effect of airbags, or indeed, that of the leg protector, computer simulation is still, nevertheless, a useful tool in providing the trends of impact behaviour. Happian-Smith et al [18] had developed a two-dimensional computer simulation program of a motorcycle and rider impacting a flat, rigid, vertical barrier. The airbag system modelled is a rider-restraint type i.e. one which has the intention of keeping the rider attached to the motorcycle. This has the benefit that the forward energy of the rider can be absorbed by the airbag without transferring any extra vertical or rotational motion to the rider. The program was put to a computer run, and the main findings were that an airbag of 100 litre can adequately restrain a motorcyclist at an impact velocity of 13.4ms^{-1} ; the airbag should be fully inflated before contact; airbag size, pressure and friction appear to be the most important variables; and more importantly, the simulation indicated that an airbag system could be developed to reduce rider injuries during head-on impacts.

2.3 Mathematical Modelling

Mathematical modelling of car occupant impact has been well established especially in the motor industry, but remains a relative newcomer in terms of motorcycle impact. Happian-Smith had contributed greatly in this respect, but this early work involved only a two-dimensional representation of motorcycle impact. One of the earliest works [19] made detailed experimental tests and modelling of the different types of front wheels, and the effect of a motorcycle impacting onto a flat rigid barrier. This showed that the construction of the front wheel had a considerable effect on the overall dynamic behaviour of the system.

Happian-Smith et al [20] then proceeded to develop a three-dimensional model of a simple motorcycle in glancing impact with a rigid barrier. A rider had been modelled as an integral part of the motorcycle and thus the development of the model was still in its infancy. However, it was observed that the points of contact between the motorcycle and the barrier is of vital importance, especially as the angle of impact becomes more oblique, and also the varying direction of friction is dependent on parameters such as angle of impact, initial velocity and time. These findings were not possible with the earlier two-dimensional model.

Nieboer et al [21] had also conducted their own development in computer simulation of motorcycle impact. Though their approach to modelling is quite different to that in which Happian-Smith et al had employed ACSL, in that Nieboer et al had made use of the MADYMO [22] simulation program. But the common points are that it is necessary to gather as much data as possible, and subsequent calibrations are needed to match the simulation to the experimental crash tests.

Yettram et al [23] had extended the computer simulation program, first written by Happian-Smith, into a three-dimensional version with a more elaborate dummy rider. During the development of the model, data regarding crash conditions, material properties of both motorcycle and the dummy rider, and geometric and inertial properties were gathered, and the model was calibrated to four crash configurations. After calibration, the model was then put to a parametric study [24] in order to examine the trends of impact events with regard to the variation of some important variables. This research formed the basis of this thesis.

CHAPTER 3

THE CONTACT MODEL

3.0 Introduction

In this chapter the basic dynamic principle describing the impact between two bodies will be given. This was modelled by Happian-Smith [2] and will be employed in the current development of a three-dimensional simulation model of a dummy rider on a motorcycle impact onto a flat rigid barrier, and subsequently into a motorcar.

There are two distinct types of impacts in this simulation model both of which are based on a mass-spring-damper system. One involves a body of given material properties hitting against a rigid body, whilst the other involves two deformable bodies each having its own material characteristics. This chapter will not deal with the determination of material values, but will give a broad outline description of each of the two modelled impacts.

3.1 Uni-directional Spring-Damper System

Consider a simple mass-spring-damper equation described below:

$$m\ddot{x} + kx + d\dot{x} = 0$$

where $m\ddot{x} = F$, F being the total force
 $kx = F_{\text{spring}}$, F_{spring} being the spring force
and $d\dot{x} = F_{\text{damper}}$, F_{damper} being the damper force.

This is representative of a body of mass m with one degree of freedom, given the material characteristics k , the spring stiffness, and d , the damping value, of the body.

The above is the basic force derivation for a compliant body impacting onto a rigid body which is considered to have infinite mass and stiffness. In the simulation model such rigid bodies will be the barrier and the road.

It must be stated that the force F acts in the line of action between the two bodies. Frictional forces in accordance with a right-handed co-ordinate system are also defined by using the coefficients of friction such that, say

$$F_y = \mu_y \cdot F,$$

and $F_z = \mu_z \cdot F.$

To give a more detailed description of the derivation of forces, consider the diagrammatic representation of a body approaching towards a plane in Figure 3.1a.

Body A is moving with velocity \dot{A} towards body B, in this case, a plane representing the stationary barrier such that $\dot{B} = 0$. Body A is of mass m and given spring stiffness k and damping value d . It is also given a radius l representing its maximum possible deformable depth. R is the compression distance between points A and B such that B is a perpendicular projection of A onto the plane. In terms of a three-dimensional co-ordinate system, R is defined as:

$$R = [(A_x - B_x)^2 + (A_y - B_y)^2 + (A_z - B_z)^2]^{1/2} \quad (3.1)$$

The rate of A approaching onto B is termed the compression velocity, \dot{R} , and is found by differentiating (3.1) such that

$$\begin{aligned} 2R\dot{R} = & 2(A_x - B_x)(\dot{A}_x - \dot{B}_x) + 2(A_y - B_y)(\dot{A}_y - \dot{B}_y) \\ & + 2(A_z - B_z)(\dot{A}_z - \dot{B}_z) \end{aligned}$$

therefore
$$\dot{R} = \frac{(A_x - B_x)(\dot{A}_x - \dot{B}_x) + (A_y - B_y)(\dot{A}_y - \dot{B}_y) + (A_z - B_z)(\dot{A}_z - \dot{B}_z)}{R} \quad (3.2)$$

Now consider when impact is being made as represented in Figure 3.1b.

When body A is in contact with plane B, the compression distance R is still the perpendicular projection of A onto B. However, the deformation distance c is beyond point B and is defined as

$$c = l - R$$

This is the deformable length of the body A such that the spring force is defined as

$$F_{\text{spring}} = k.c$$

The compression velocity between points A and B is \dot{R} such that the damping force is defined as

$$F_{\text{damper}} = d.\dot{R}$$

The two forces are summed to give the total force and subsequent frictional forces can be derived as mentioned earlier. Note that since the barrier is considered to be a rigid body of infinite mass and stiffness, the spring-damper system is uni-directional such that the derived forces are only considered as applied to body A.

3.2 Two-Body Impact System

Consider the two-mass-spring-damper system shown in Figure 3.2a.

Imagine the local displacement of x_2 is measured relative to x_1 such that x_1 is the local unknown contact distance between the two masses, therefore

force on mass m_1

$$F_1 = k_1 x_1 + d_1 \dot{x}_1 \quad (3.3)$$

and force on mass m_2

$$F_2 = k_2 (x_2 - x_1) + d_2 (\dot{x}_2 - \dot{x}_1) \quad (3.4)$$

For equilibrium, $F_1 = F_2$, which implies

$$k_1 x_1 + d_1 \dot{x}_1 - k_2 (x_2 - x_1) - d_2 (\dot{x}_2 - \dot{x}_1) = 0$$

such that

$$\dot{x}_1 = \frac{-k_2 (x_2 - x_1) - k_1 x_1 + d_2 \dot{x}_2}{d_1 + d_2} \quad (3.5)$$

In our mathematical simulation of a two-body impact system, mass m_1 can be represented by a spherical body, given a certain deformable radius, and mass m_2 can be represented by a plane with deformable characteristics. This will be our mathematical basis to simulate contact between the dummy's limb and a certain part of the motorcycle.

To illustrate the mathematical evaluation in more detail, consider the diagrammatic representation between the two bodies before impact, as shown in Figure 3.2b. Point A is the centre of gravity of mass m_1 . Point B is the perpendicular projection of point A onto the plane. C is the extension of point B with respect to point A. It is of fixed distance as from point B. x_1 is the compression distance, of mass m_1 , to be found once contact is made. In the case shown in Figure 3.2b, x_1 is measured from the point A, which is the origin of this local system, and is of distance R.

Consider when contact is made between the two masses, as shown in Figure 3.2c. Both bodies are being compressed. Their respective deformable distances are determined by the compression distance x_1 such that for mass m_1 , the deformable distance, in the opposite direction of travel, is found by

$$-(R - x_1)$$

and for mass m_2 , the deformable distance is

$$D - (AC - x_1)$$

In accordance with equation (3.5), the compression velocity is thus

$$\dot{x}_1 = \frac{-k_2(D-(AC-x_1)) + k_1(R-x_1) + d_2\dot{AC}}{d_1 + d_2} \quad (3.6)$$

where \dot{AC} is the compression velocity of the distance AC.

similarly, the force on mass m_1 is

$$F_1 = k_1(R-x_1) - d_1\dot{x}_1 \quad (3.7)$$

and the force on mass m_2 is

$$F_2 = k_2(D-(AC-x_1)) - d_2(\dot{AC}-\dot{x}_1) \quad (3.8)$$

These forces are applied to the respective bodies along the line of action. Frictional forces can also be derived as mentioned earlier. They are also applied to the bodies, along with the main force, in a localised right-handed co-ordinate system.

These are the mathematical concepts in modelling bodies in impact. The main output of interest is the force. This is in accordance with ACSL which acts as an integrator, for which the computation principles will be described later.

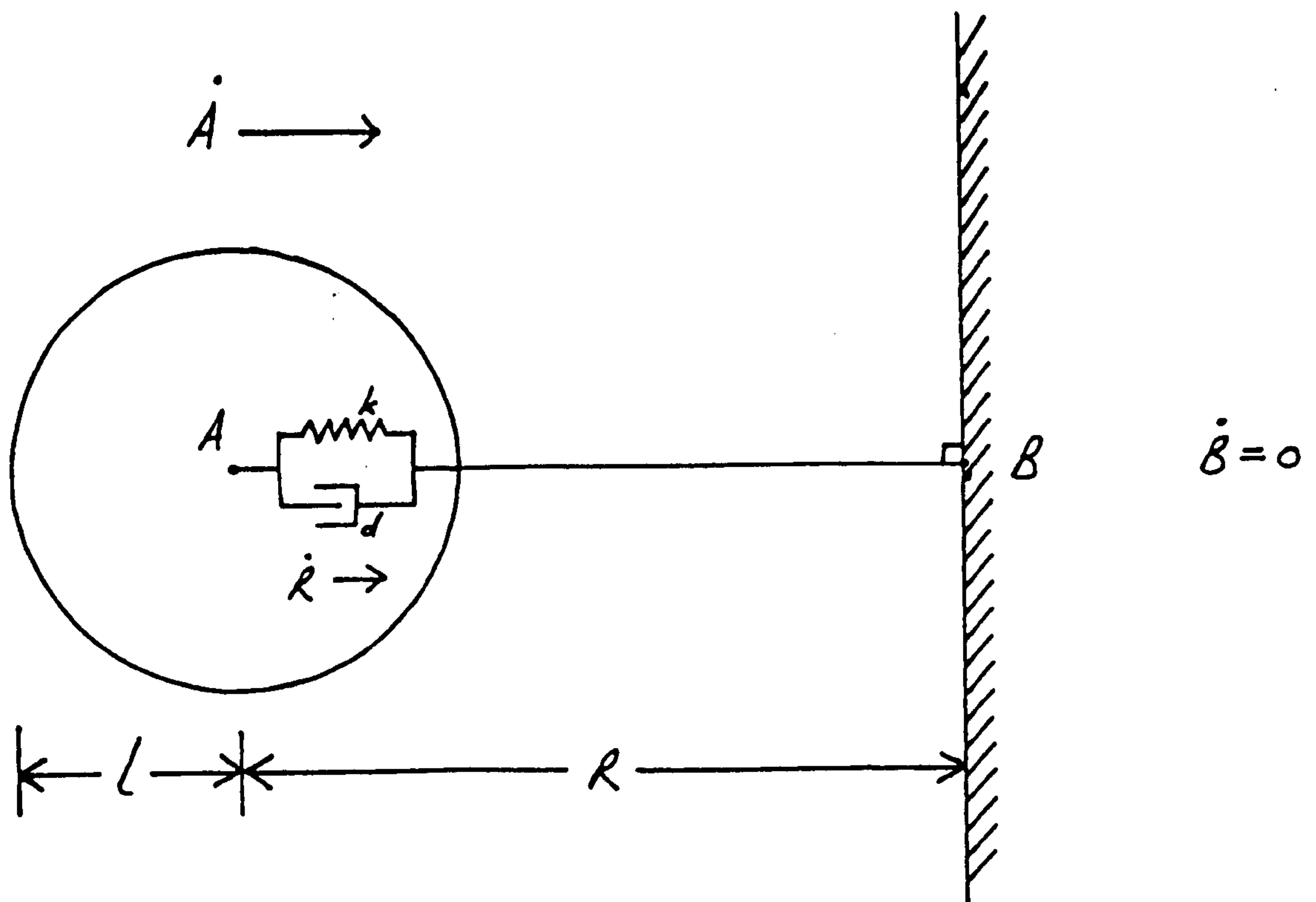


Figure 3.1a Representation of a body A approaching towards a rigid plane B.

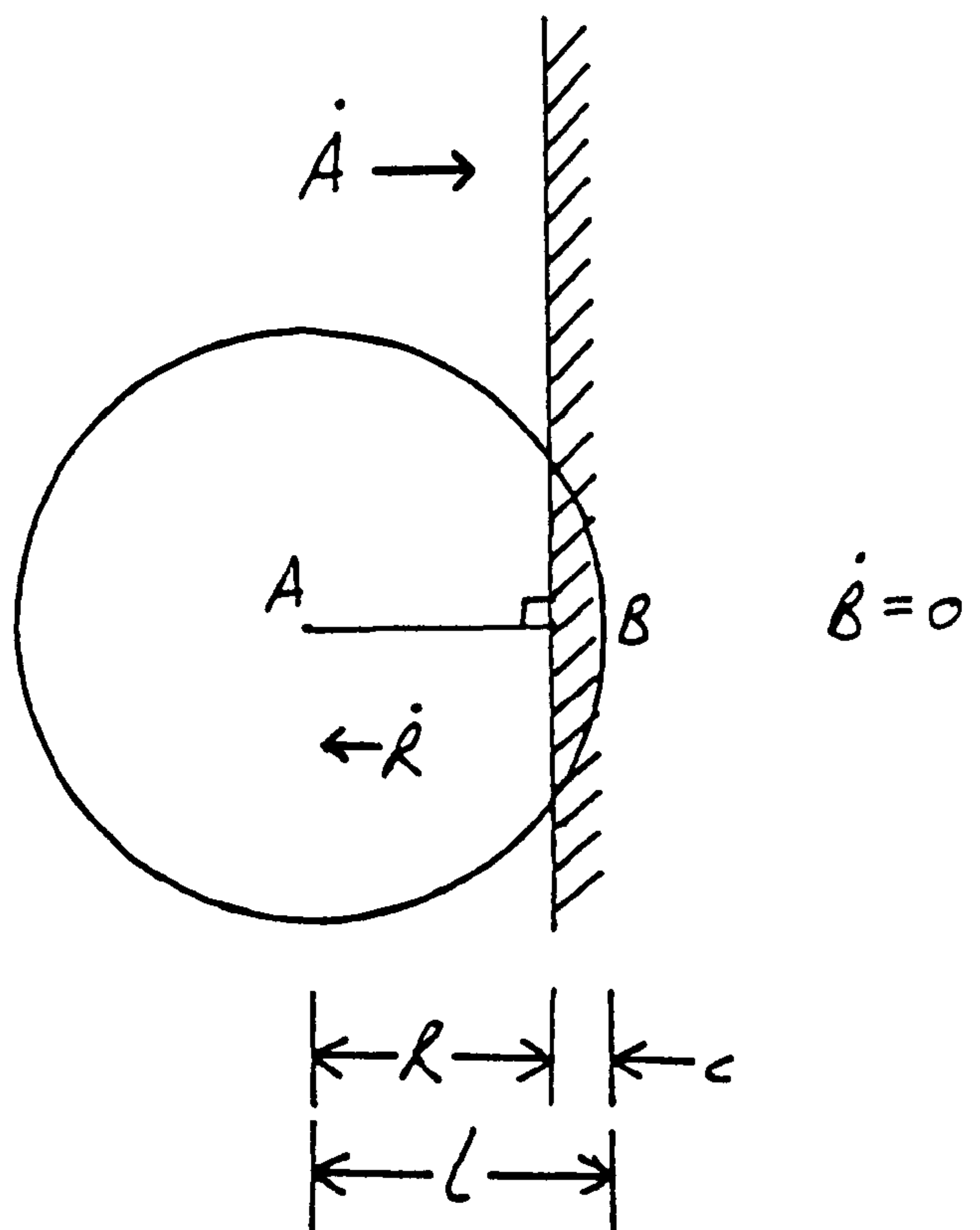


Figure 3.1b Representation of body A being compressed by plane B.

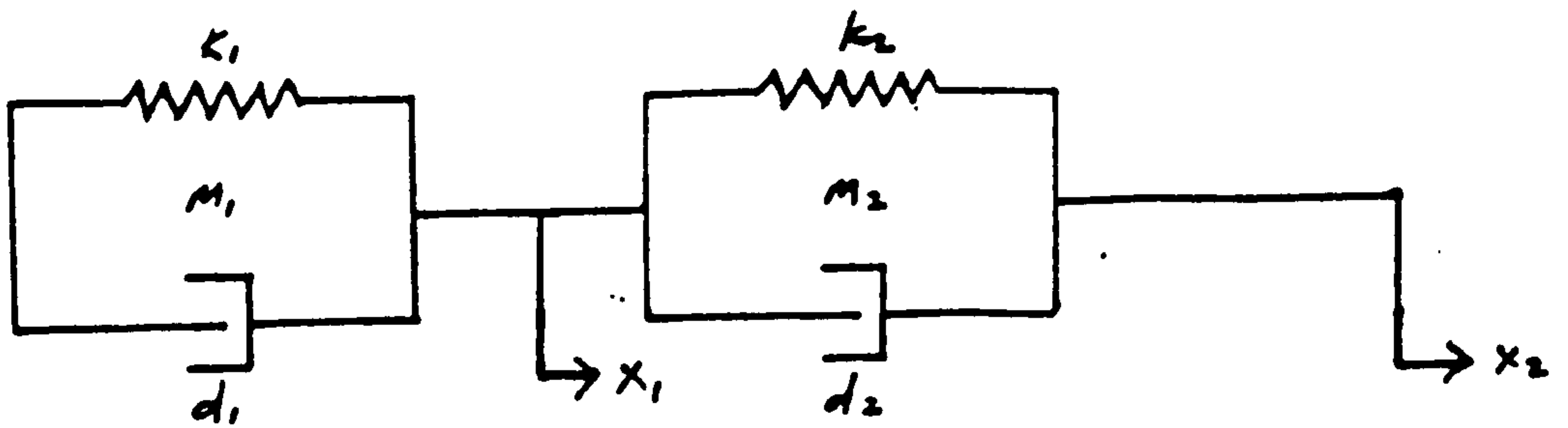


Figure 3.2a A two-mass-spring-damper system.

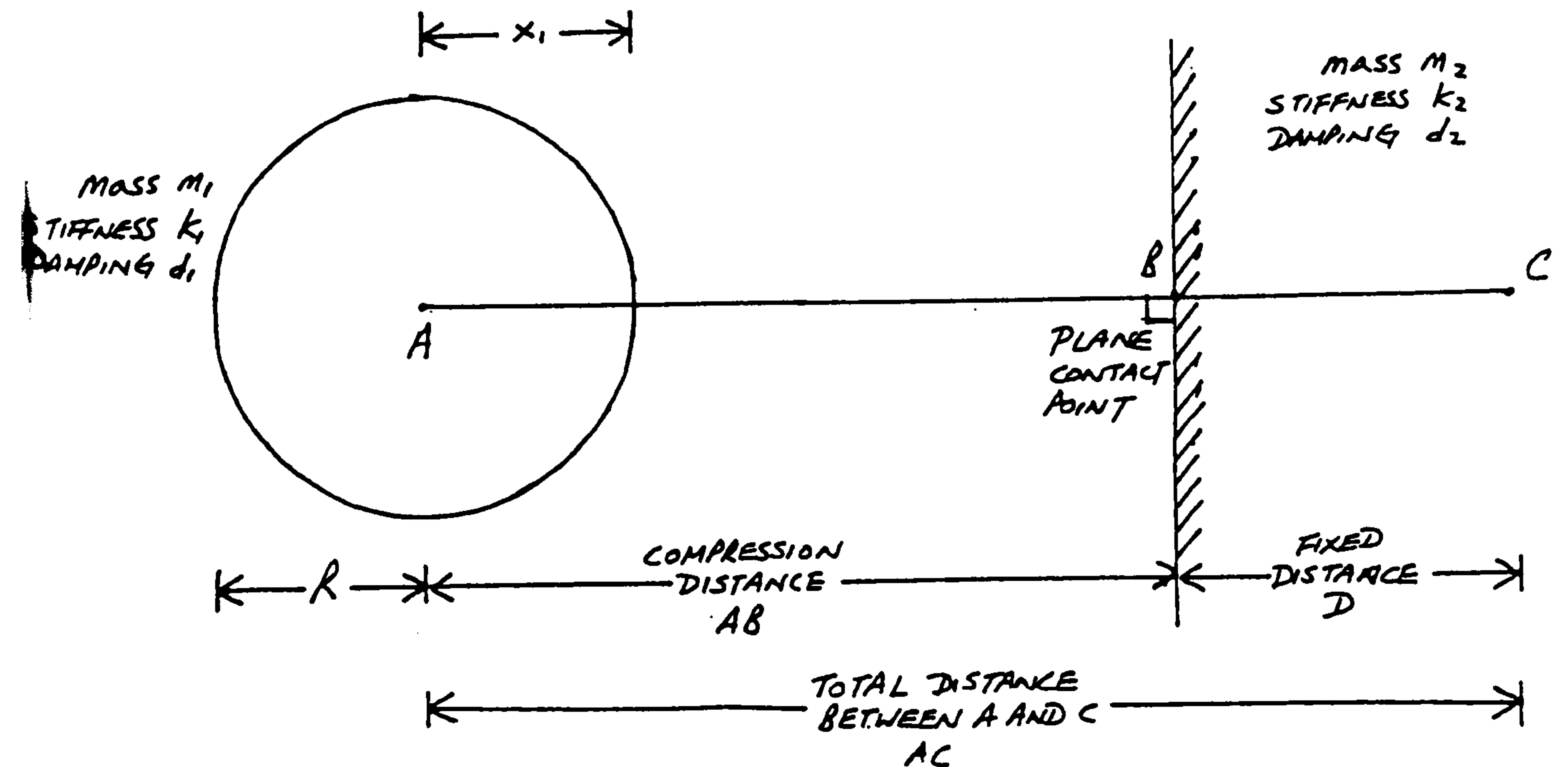


Figure 3.2b Representation of a body A approaching towards a deformable plane B.

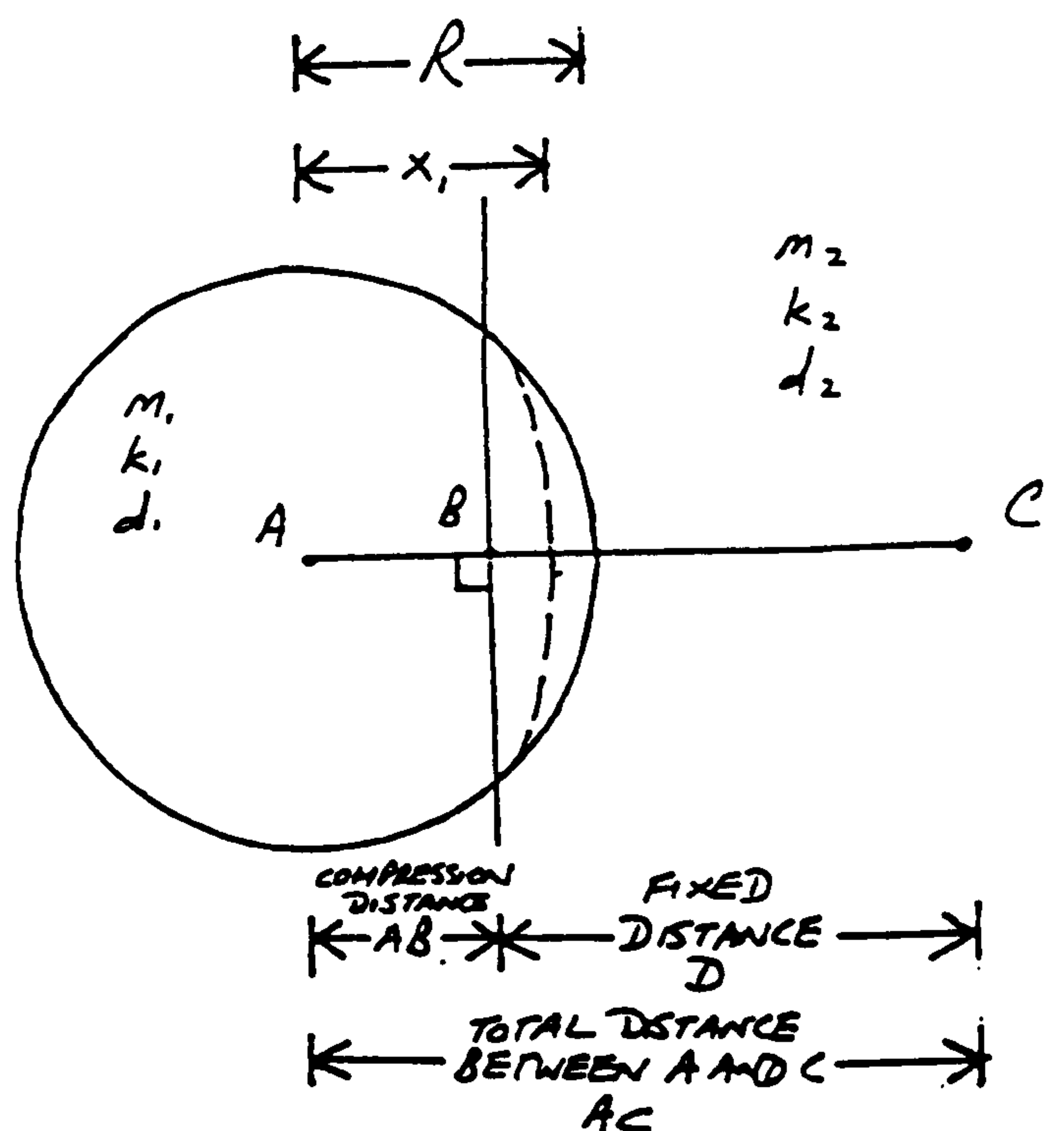


Figure 3.2c Representation of contact between body A and plane B.

CHAPTER 4

THE SYSTEM MODEL

4.0 Introduction

In the previous chapter the derivations of the contact equations have been given. They were first incorporated into an ACSL program written by Happian-Smith [2]. However, subsequent modifications have been introduced. This was because of the following three factors: to reduce programming difficulties; to minimise expensive computational time; and to model the simulation more realistically given further data and information.

This chapter will deal with the original model and the factors which led to its modification to the current state. But to begin with, a brief description of the software employed in the modelling process will be given.

4.1 SD/FAST And ACSL

The software SD/FAST (Symbolic Dynamic/Fast) is a library of routines to be used in the development of various mechanical systems comprising links and joints. The user's first task is to design the proposed system, using the available joints within the

SD/FAST package, to connect bodies representing the mechanical parts of the system, with dimensions, masses and inertias to be supplied by the user. After such a data file has been created SD/FAST then produces the relevant routines, written in FORTRAN, to interpret the dynamic information of the system. However, these parameters, such as displacements, velocities and accelerations, need to be manipulated by another programming language, such as a simple FORTRAN program or a sophisticated simulation language such as ACSL.

ACSL (Advanced Continuous Simulation Language) is a simulation language where the user can program a proposed continuous system. It offers integration functions to single variables or specified arrays and thus acts as an integrator of the system. ACSL is therefore very compatible with SD/FAST such that SD/FAST provides symbolic dynamical information, and ACSL integrates and feeds back the current system states to SD/FAST for the next phase. This can be demonstrated by the events in Figure 4.1.

It can be argued that one can solely employ either SD/FAST and FORTRAN programming, or ACSL on its own to model the proposed system. This is quite simply true, but ACSL as a controller of the program is a much more convenient language for this purpose than FORTRAN, as a sophisticated simulation can be modelled more easily. The use of SD/FAST library routines provides easy access and valuable dynamic information of the system, which would

otherwise require long and difficult programming from the user.

4.2 The Development Phase

As mentioned earlier, the first task the user needs to do in employing SD/FAST for simulation modelling is to design the proposed system, using facilities available within SD/FAST. This means that in the present case there are two SD/FAST data files to be constructed. One describes the geometric layout and mechanical connection of the dummy whilst the other describes those of the motorcycle.

To design an SD/FAST data file, one would choose a particular body as the main or datum body of the system such that remaining bodies of the system are connected directly and indirectly relative to this main body. Geometric layouts of these bodies are defined in a right-handed-coordinate system. Joints connecting the bodies can be one dimensional translational joints, or one, two or three dimensional rotational joints. Mass and inertia properties are specified by the user. To achieve a better understanding of how to approach a design, it is best to have a diagrammatic representation of the proposed system. Figure 4.2a shows the construction of a dummy rider first proposed by Happian-Smith.

In Happian-Smith's proposed dummy construction, the pelvis is chosen to be the main body. The lower torso, right hip and left hip are constructed by specifying the geometric distances relative to the pelvis. However, for the upper torso, this is specified relative to the lower torso. Likewise the two femora are specified relative to the two hips.

We can also see the different type of joints connecting the various bodies in Happian-Smith's design. Note that the dotted line denotes joints connecting to, or actually on, a body of specified zero mass and inertia. It is this aspect of massless and inertialess bodies that leads to a change in the design of the dummy. The current design is shown in Figure 4.2b.

We can observe that there is no massless or inertialess body in the design featured in Figure 4.2b. This is because in the original design, the massless and inertialess bodies have created mathematically ill-conditioned constraints. In the SD/FAST manual [25] it states that 'massless and inertialess bodies are not allowed if there exists any joint axis on which an applied load would accelerate only the massless or set of massless bodies, or would produce a rotational acceleration only on a body or set of bodies with no inertia about the axis of rotation, since this would produce infinite accelerations'. Referring back to Figure 4.2a, the legs, which are of primary importance to this research study, are constructed with a combination of massed and non-

massed bodies. In theory the massless bodies between the lower legs and the ankles would pose no basic numerical problem. However, bodies from the hips down to the knees will create mathematical singularities because between the hips and the knees there are areas where more than one massless and inertialess body have been inserted. Indeed only the femora are bodies with relevant masses and inertias. These massless and inertialess bodies will inevitably create mathematical problems since any force or torque applied to these bodies cannot be transmitted along the system. It was to deal with this point that a re-design of the dummy was necessary.

A second factor also contributed to this decision. The original dummy's legs are indeed very sophisticated. All the joints specified no doubt create more degrees of freedom to the legs, but this would then result in a more complicated model, thus unnecessarily prolonging computational time. However, would these extra massless and inertialess bodies and their joints give any valuable information or rather just give much complicated information difficult to comprehend? In addition, what properties could we assign to the flexibilities of these joints to feed into the program in order to achieve sensible results?

Based on the above factors, it was decided that a less complicated design, but with all the relevant and sensible features of a jointed dummy is more suitable, especially in this

early stage of modelling. As mentioned earlier, a diagrammatic representation of this design is in Figure 4.2b. A copy of the SD/FAST data file is in Figure 4.2c.

As one can see from Figure 4.2c that the coordinate system is a right-handed cartesian system, such that gravity is defined by assigning the z-axis with the value of -9.8066. It is important to define gravity for simulation modelled on this planet. In addition, it is equally important to choose a datum body in the proposed model such that other bodies in the model are directly, or indirectly linked to the datum body. In our case, the datum body is named 'pelvis'.

For every body its mass and inertias are assigned. The linkage between different bodies are connected by using SD/FAST defined joints, with geometrical dimensions between the bodies defined by using the 'inbtojoint' and 'bodytojoint' statements. Let us go through the following example.

The definition of 'ltorso', which is a mnemonic for 'lower torso' in our model, is assigned to the statement 'body = ltorso'. It is connected to the inboard body pelvis by a gimbal joint. The associated statements are 'inb = pelvis' and 'joint = gimbal'. The next two statements concerned with the mass and inertias definition of the lower torso. Then the statements of 'inbtojoint' and 'bodytojoint'. These, respectively, described

the three-dimensional distances from the inboard body, pelvis, to the gimbal joint, and the current body being defined, lower torso, to the gimbal joint. The following 'pin' statements defined the rotation of axes allowed by the joint used. This is indicated by assigning a number '1' to the corresponding cartesian axis. In this case, there are three 'pin' statements since a gimbal joint is a three-directional rotational joint.

The reader will notice that most of the numerical definitions are succeeded by a question mark. This is a useful feature allowed in SD/FAST such that a question mark indicates the flexibility of updating the value in future simulation, without re-defining the basic mechanical construction of the model. Another important point is that all the numerical declarations are dimensionless. This aspect is to be declared by the programmer in the simulation program, so as long as the declarations are consistent in a chosen system, there is no need to declare this aspect in the actual mechanical construction of the model.

The design of the motorcycle remains virtually the same as from how Happian-Smith first modelled it. A representation is given in Figure 4.3a.

As can be seen, the motorcycle c.g. (centre of gravity) is chosen to be the main mass. The headstock is a massless and inertialess body with a three-dimensional gimbal joint. In this situation

this body is between two others which have mass and inertia and thus no numerical complications arise. A slider joint connects the headstock and the front wheel. This gives the simulation a pair of telescopic front forks. The rear wheel is connected to the c.g. by means of a single rotational pin joint. A copy of the SD/FAST data file describing the layout and construction of the motorcycle is given in Figure 4.3b. Note that initially the front wheel hangs vertically down from the headstock. The headstock is rotated about a transverse axis to position the front wheel as shown in Figure 4.3a.

This brings the current dummy construction of 16 masses with a total for the compliant joints of 35 degrees of freedom. Similarly, the motorcycle is constructed of 4 masses with 11 degrees of freedom.

After these data files have been created, they are put to run under SD/FAST in order to create the relevant SD/FAST 'Dynamics' file, 'Information' file and 'Analysis' file. These are now ready to be accessed by the ACSL simulation program.

4.3 The Execution Phase

In Figure 4.1 we can see the events in an execution cycle. In reality, it is the ACSL program where the proposed simulation is

programmed, but it accesses SD/FAST for dynamical information about the dummy rider and the motorcycle. The cycle will repeat itself until a terminal time of simulation, specified by the user, is reached.

In the 'Accelerations' arrow we see that dynamical information is passed to the ACSL integration box. This arrow represents how details such as accelerations, velocities and displacements are passed to the main ACSL program. However, the state vectors, which represent the velocities of the defined jointed positions, are integrated by ACSL to obtain the current states. These, along with any generated forces, are fed back into the SD/FAST dynamic system for the next cycle.

In general, the mathematical modelling of contacts between different surfaces remains basically the same as described in the previous chapter. There are of course numerous opportunities for improvements. These will be described in the next two chapters. There is, however, one major modification involving the contact between two moving massed objects.

Recall the evaluation of the compression velocity \dot{x}_1 described in the previous chapter. In the original model by Happian-Smith this evaluation remained the same. However, here the compression distance x_1 , is calculated differently. Consider the following diagram in Figure 4.4.

The evaluation of the distance x_1 is dependent on the exact instant when body A touches a plane such that

$$AB - R = 0 \quad (4.1)$$

In ACSL there is a facility known as SCHEDULE which will determine a function as it crosses the value zero either from the positive or the negative direction. But to determine the exact zero crossing time a lot of computational time is needed. This will become cost-ineffective in the long run, therefore a modification has been made to determine the distance x_1 , as described in the previous chapter.

In addition, the determination of x_1 is obtained by integrating \dot{x}_1 . This requires an initial condition, say x_{ic} . In the early version, this initial condition varies at every computational step and is assigned to be the mid-distance between A and B. In the actual integration, a further parameter, say x_{add} , is added on to x_1 and this parameter is assigned to be

$$x_{add} = AB - x_1 \quad (4.2)$$

This has the effect of putting the distance x_1 on the plane before contact is made. This is best represented in Figure 4.5.

This can be difficult to comprehend, i.e. the fact the 'contact

point' is on the plane before contact is made. Therefore, modifications were made to obtain the version described in the previous chapter, where the initial condition is set to the radius R in the beginning and does not vary, and the evaluation of x_1 is such that it is on the rim of object A and will remain so during impact.

This is the major alteration to Happian-Smith's original model. However, the mathematical concept remains the same, only the determination of the contact distance has been updated. There is one major update with regard to the head's contact with the barrier and is given in the following section.

4.4 Head Contacts

In the early stage of the model, the dummy rider and the motorcycle were to impact onto a flat, vertical rigid barrier. It was later learnt from TRL that in their crash test, the barrier is of height 1.22m with a horizontal deformable barrier top covered with foam. It has been decided that all existing contacts, with respect to the barrier, remain the same, with the addition of a contact between the dummy's head and the barrier top. The top has been given appropriate characteristics representing the material with which it was covered.

The head is then allowed to contact the vertical face and/or the padded top of the barrier with regard to the position of the c.g. of the head. However, the head is not allowed to touch both surfaces at the same time. A switch is employed to determine which barrier surface is within the allowable contact for the head. This can be demonstrated in Figure 4.6.

In Figure 4.6 the head is well within contact capability with the vertical and the top face of the barrier as represented by positions A and C respectively i.e. a perpendicular from the head c.g. will hit the vertical or horizontal surface. This capability will be signalled by a switch containing a value zero. When the head is in position B or D the head is neither within the boundaries defined by the vertical or the top face of the barrier and it will be indicated so by assigning a non-zero value to the switch.

This is an adequate arrangement for possible contacts between the head and relevant surface of the barrier. However, it was eventually discovered that a mathematical singularity exists with regard to the location of the head. Let us consider the positions of the c.g. of the head as shown in Figures 4.7a, 4.7b and 4.7c.

In Figure 4.7a the head is considered to be in contact with the barrier top. As it gradually lowers and moves backwards, as shown in Figure 4.7b, it is not considered to be touching either the

barrier top or the vertical face of the barrier. As the motion continues, the head is considered to be in contact with the vertical face of the barrier as shown in Figure 4.7c.

In such a case of impact, which has every likelihood of occurring, two potential problems exist. We must remind ourselves that ACSL is a continuous simulation language, and the situation in Figure 4.7b represents a discontinuity of the force function. Because of this discontinuity the two forces generated in Figures 4.7a and 4.7c will be in a form of step function. This is one of the two potential problems, but the severity will grow depending on how steep is the step function of the force. For example, in Figure 4.7c, as the head dives down and is considered to be in contact with the vertical face, the amount of compressible surface of the head would be an unrealistic large amount if the c.g. of the head is very near to the barrier face. This very sudden large force gives rise to the second problem. In terms of mathematical modelling, a force will be generated regardless, but such would be the compression, the material characteristics of the head will produce an unlikely high force thus producing a singularity into the system.

To prevent this mathematical discontinuity, a compliant cylinder or rod is inserted along the edge of the barrier separating the vertical and top face of the barrier. This 'rod' is given material characteristics such that a force could be generated

whilst the head is within the quadrant of area outside the boundaries of the two barrier faces. This can be seen in Figure 4.8a. A three-dimensional representation of the barrier can be seen in Figure 4.8b.

In Figure 4.8 the positions A and C represent contact between the head and the vertical, and the top face of the barrier respectively. However, when the head is in position B, which in this representation is still capable of touching the barrier, it is considered to be in contact with the simulated cylinder. The difference in the force calculation depends on the 'compression distance', which unlike in the other cases, where the compression distance is the perpendicular projected distance from the head c.g. onto the targetted plane, this distance is simply the distance between the head c.g. and the prescribed contact point on the simulated cylinder.

By introducing this force generation, the risk of mathematical singularity should be greatly reduced. Though the force function, should the head pass from one plane to another, may not be perfectly smooth and continuous, it would at least prevent sharp discontinuity thus reducing the awkwardness of step functions. It will be seen later in Chapter 9 that the modification of introducing the compliant cylinder did not always prevent an excessively large force arising between the head and the vertical face of the barrier.

Development Phase

Execution Phase

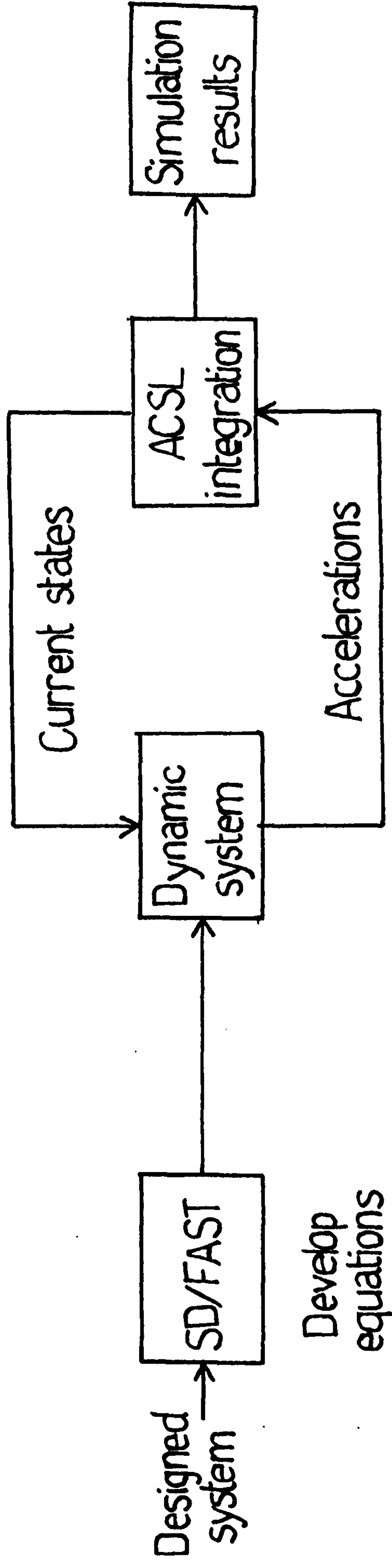


Figure 4.1 Simulation cycle.

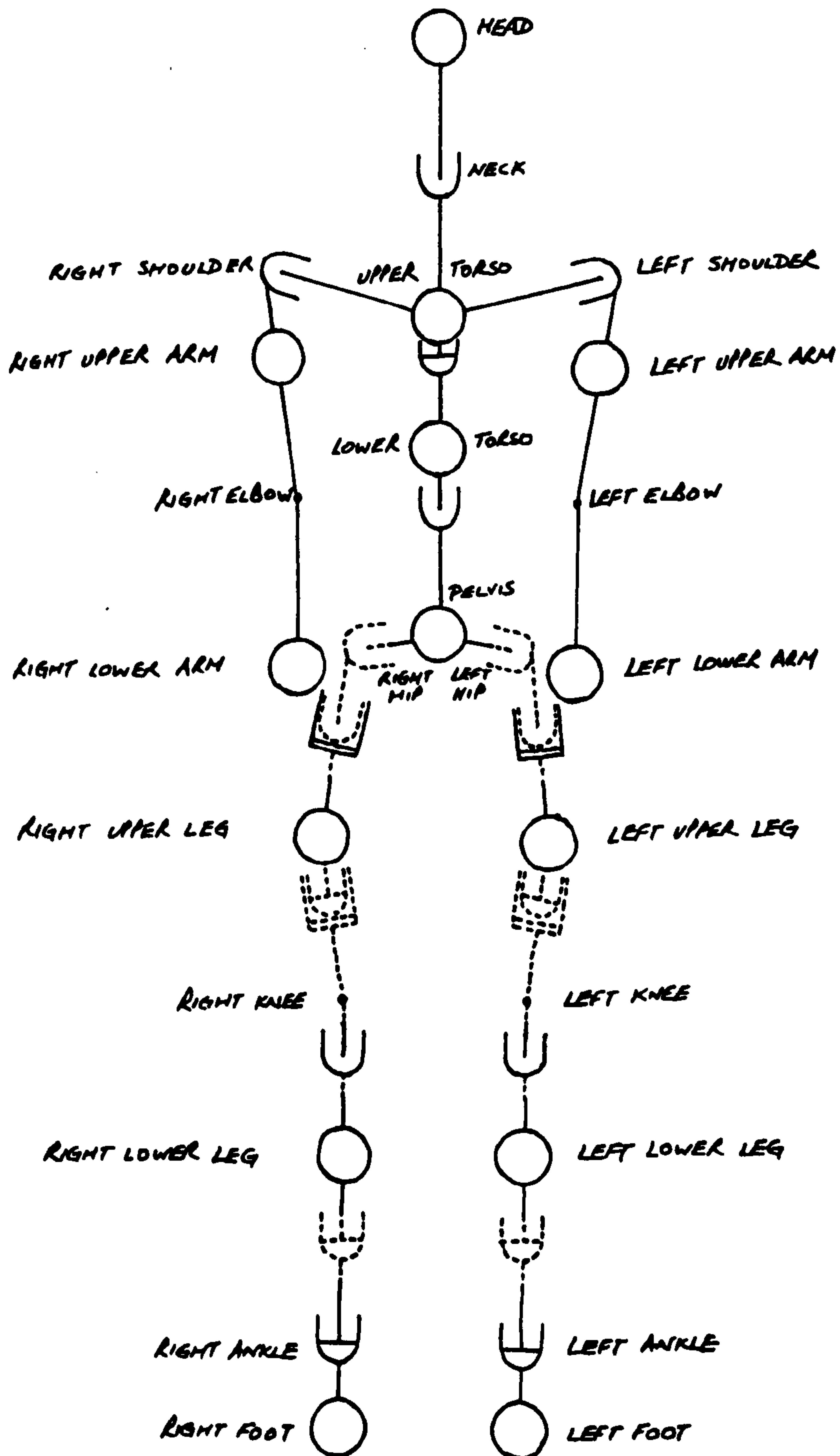
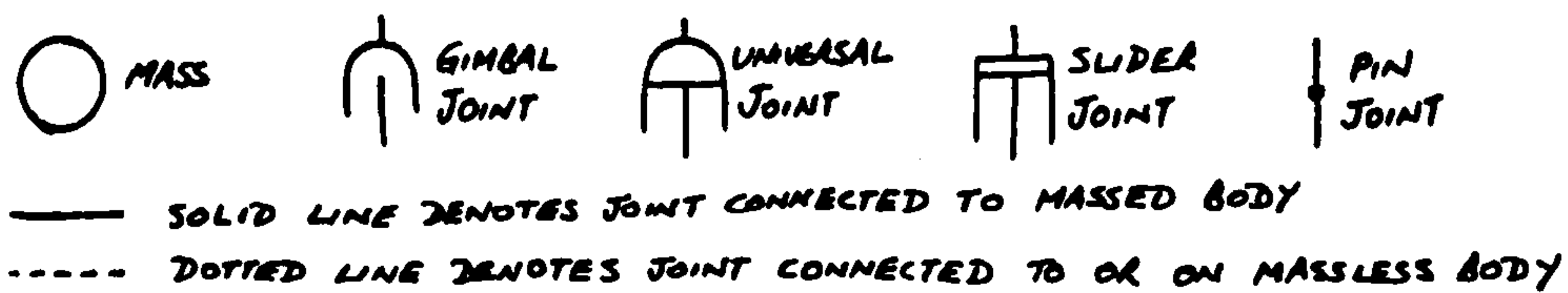


Figure 4.2a The original proposed dummy model.

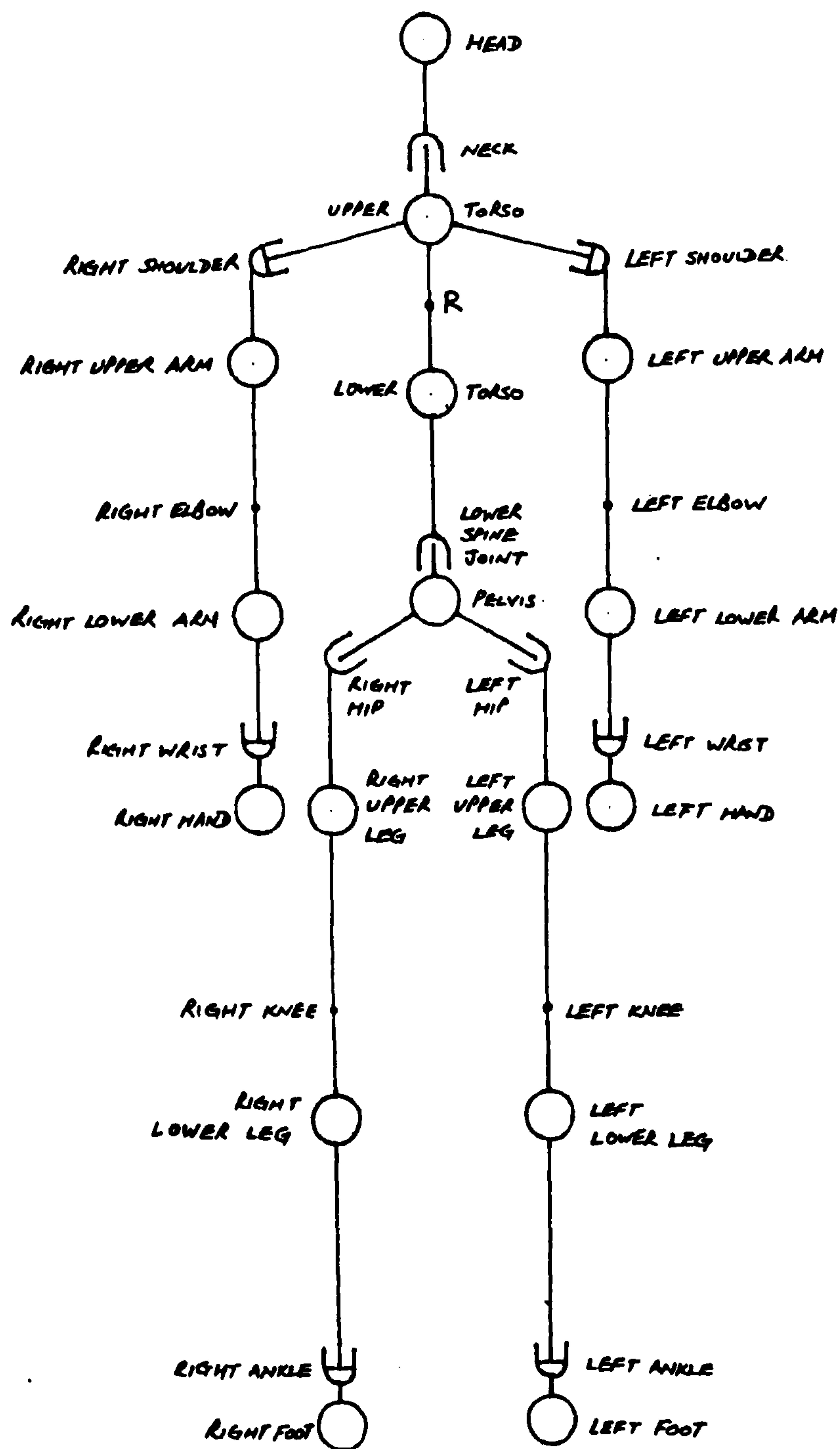


Figure 4.2b The revised model representing a 50 percentile OPAT dummy.

simple OPAT dummy model

gravity = 0.0 0.0 -9.8066?
body = pelvis
mass = 13.6?
inertia = 0.1398? 0.1045? 0.1029?

body = ltorso inb = pelvis joint = gimbal
mass = 6.09?
inertia = 0.1086? 0.0563? 0.0797?
inbtojoint = 0.0? 0.003329? 0.069?
bodytojoint = 0.0? -0.007671? -0.159?
pin = 1 0 0
pin = 0 1 0
pin = 0 0 1

body = utorso inb = ltorso joint = pin
mass = 9.33?
inertia = 0.1663? 0.0863? 0.1221?
inbtojoint = 0.0? -0.0235? 0.098?
bodytojoint = 0.0? 0.0235? -0.098?
pin = 1 0 0
prescribed = 1?

body = head inb = utorso joint = gimbal
mass = 5.686?
inertia = 0.04045? 0.0498? 0.01897?
inbtojoint = 0.0? 0.016347? 0.089?
bodytojoint = 0.0? -0.019653? -0.107?
pin = 1 0 0
pin = 0 1 0
pin = 0 0 1

body = uarmr inb = utorso joint = ujoint
mass = 2.312?
inertia = 0.0195? 0.0211? 0.001?
inbtojoint = 0.2? 0.0? -0.051?
bodytojoint = 0.0? 0.0? 0.111?
pin = 1 0 0
pin = 0 1 0

body = larmr inb = uarmr joint = pin
mass = 1.425?
inertia = 0.0067? 0.00674? 0.0005?
inbtojoint = 0.0? 0.0? -0.164?
bodytojoint = 0.0? 0.0? 0.113?
pin = 1 0 0

body = handr inb = larmr joint = ujoint
mass = 0.64?
inertia = 0.00143? 0.0018? 0.00049?
inbtojoint = 0.0? 0.0? -0.14?
bodytojoint = 0.0? 0.0? 0.064?
pin = 1 0 0
pin = 0 0 1

body = uarm1 inb = utorso joint = ujoint
mass = 2.312?
inertia = 0.0195? 0.0211? 0.001?
inbtojoint = -0.2? 0.0? -0.051?
bodytojoint = 0.0? 0.0? 0.111?
pin = 1 0 0
pin = 0 1 0

body = larm1 inb = uarm1 joint = pin
mass = 1.425?
inertia = 0.0067? 0.00674? 0.0005?
inbtojoint = 0.0? 0.0? -0.164?
bodytojoint = 0.0? 0.0? 0.113?
pin = 1 0 0

body = handl inb = larm1 joint = ujoint
mass = 0.64?
inertia = 0.00143? 0.0018? 0.00049?
inbtojoint = 0.0? 0.0? -0.14?
bodytojoint = 0.0? 0.0? 0.064?
pin = 1 0 0
pin = 0 0 1

body = uplegr inb = pelvis joint = gimbal
mass = 8.036?
inertia = 0.1048? 0.1051? 0.0105?
inbtojoint = 0.12? 0.02? -0.07?
bodytojoint = 0.0? 0.0? 0.185?
pin = 1 0 0
pin = 0 1 0
pin = 0 0 1

body = lwlegr inb = uplegr joint = pin
mass = 3.304?
inertia = 0.06574? 0.06621? 0.00357?
inbtojoint = 0.0? 0.0? -0.225?
bodytojoint = 0.0? 0.0? 0.118?
pin = 1 0 0

body = footr inb = lwlegr joint = ujoint
mass = 1.434?
inertia = 0.0065? 0.0068? 0.00231?
inbtojoint = 0.0? 0.0? -0.292?
bodytojoint = 0.0? 0.0? 0.045?
pin = 1 0 0
pin = 0 1 0

body = upleg1 inb = pelvis joint = gimbal
mass = 8.036?
inertia = 0.1048? 0.1051? 0.0105?
inbtojoint = -0.12? 0.02? -0.07?
bodytojoint = 0.0? 0.0? 0.185?
pin = 1 0 0
pin = 0 1 0
pin = 0 0 1

body = lwleg1 inb = upleg1 joint = pin
mass = 3.304?
inertia = 0.06574? 0.06621? 0.00357?
inbtojoint = 0.0? 0.0? -0.225?
bodytojoint = 0.0? 0.0? 0.118?
pin = 1 0 0

body = foot1 inb = lwleg1 joint = ujoint
mass = 1.434?
inertia = 0.0065? 0.0068? 0.00231?
inbtojoint = 0.0? 0.0? -0.292?
bodytojoint = 0.0? 0.0? 0.045?
pin = 1 0 0
pin = 0 1 0

Figure 4.2c A SD/FAST definition of the OPAT dummy.

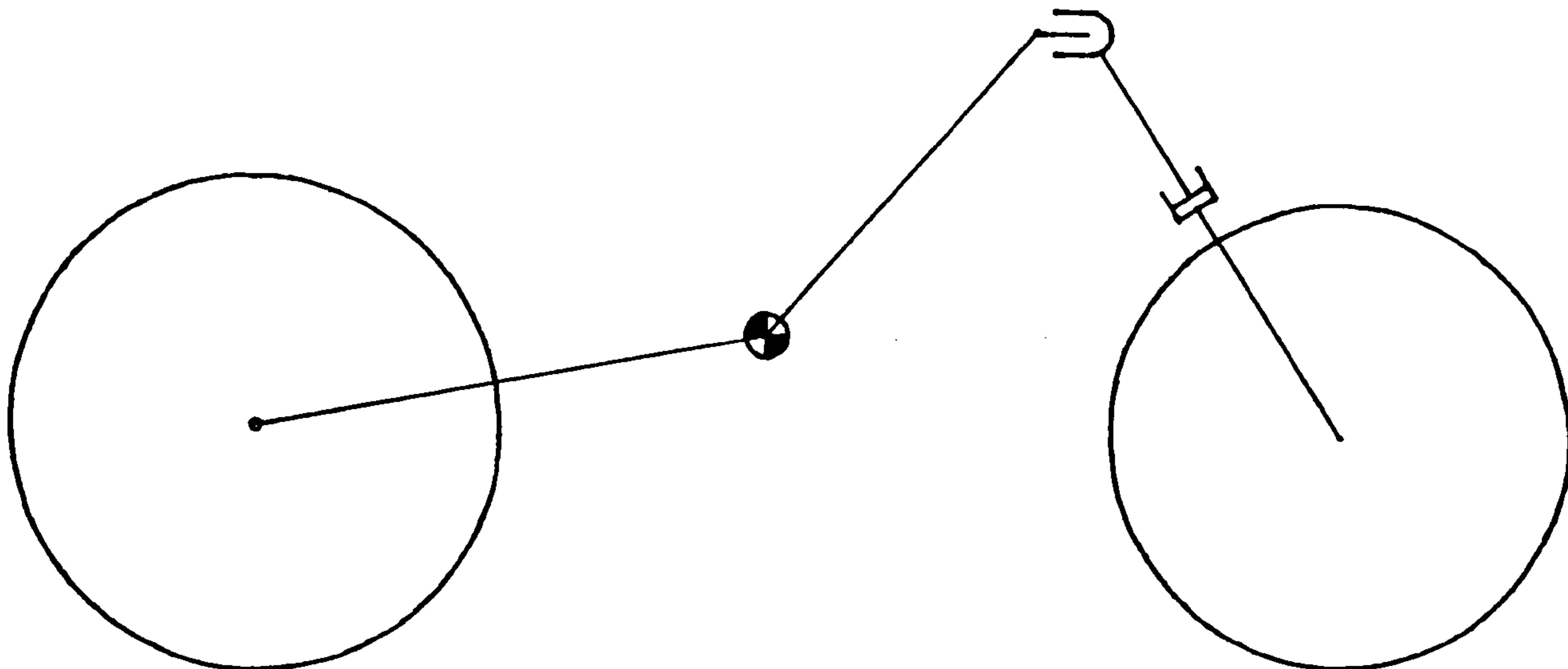


Figure 4.3a The model representing a Norton Commander motorcycle.

```
# Simple motorcycle model with a front wheel and
# bendy front forks that steer.
```

```
gravity = 0.0 0.0 -9.8066?
```

```
body      = cycle
mass      = 188.7?
inertia   = 58.675? 13.85? 34.78?
```

```
body      = stock  inb = cycle  joint = gimbal
mass      = 0.0?
inertia   = 0.0? 0.0? 0.0?
inbtojoint = 0.0? 0.37? 0.44?
bodytojoint = 0.0? 0.0? 0.0?
pin       = 1 0 0
pin       = 0 1 0
pin       = 0 0 1
```

```
body      = wheel  inb = stock  joint = slider
mass      = 19.4?
inertia   = 0.5104? 0.28887? 0.28887?
inbtojoint = 0.0? 0.0? -0.37?
bodytojoint = 0.0? 0.0? 0.365
pin       = 0 0 1
```

```
body      = rrwhl  inb = cycle  joint = pin
mass      = 12.9?
inertia   = 0.5104? 0.28887? 0.28887?
inbtojoint = 0.0? -0.71? -0.12?
bodytojoint = 0.0 0.0 0.0
pin       = 1 0 0
```

Figure 4.3b A SD/FAST definition of the Norton Commander motorcycle.

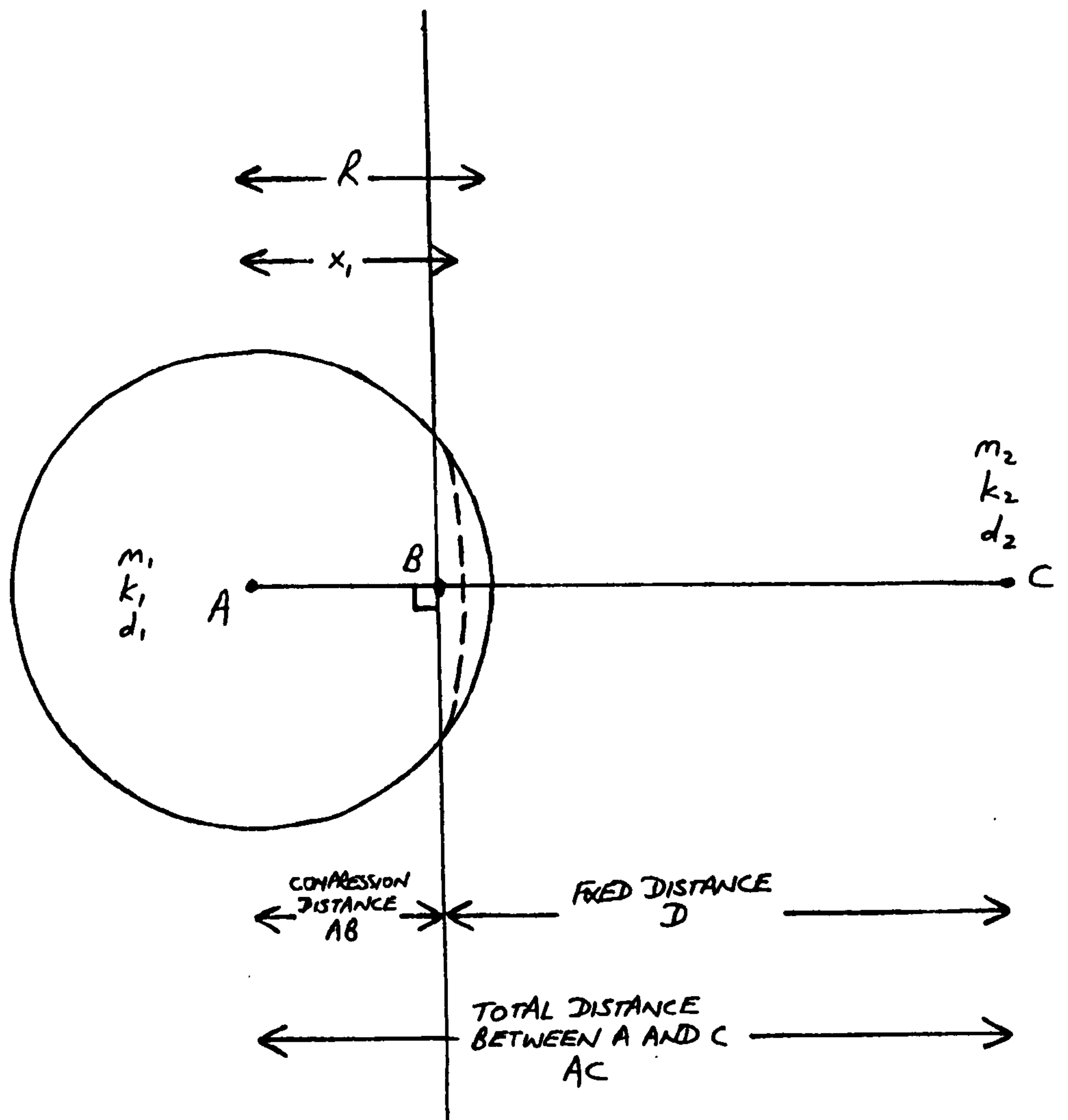


Figure 4.4 The original proposed contact evaluation involving the use of SCHEDULE in ACSL programming.

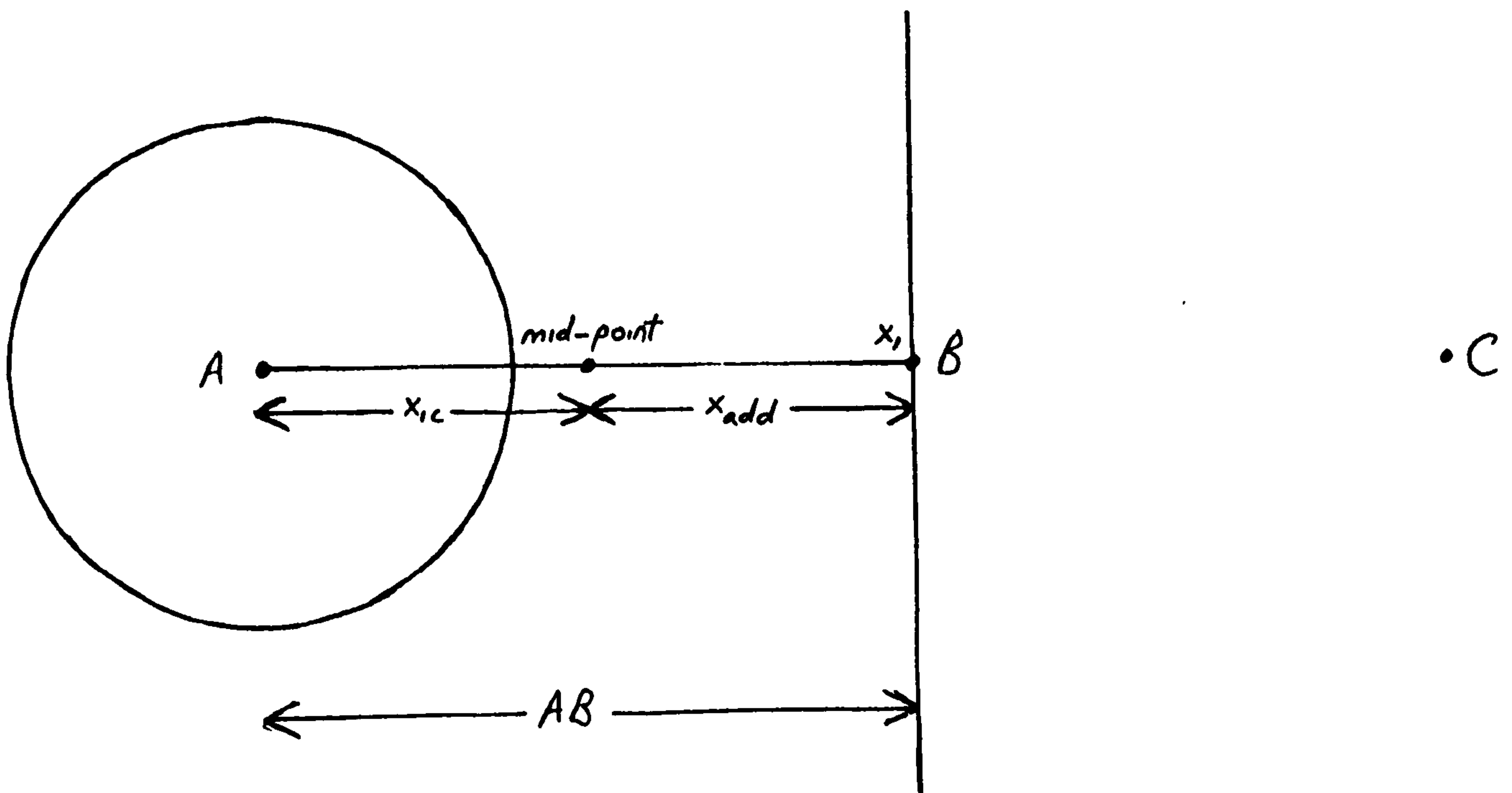


Figure 4.5 The original proposed contact evaluation where initial condition varies at every computational step.

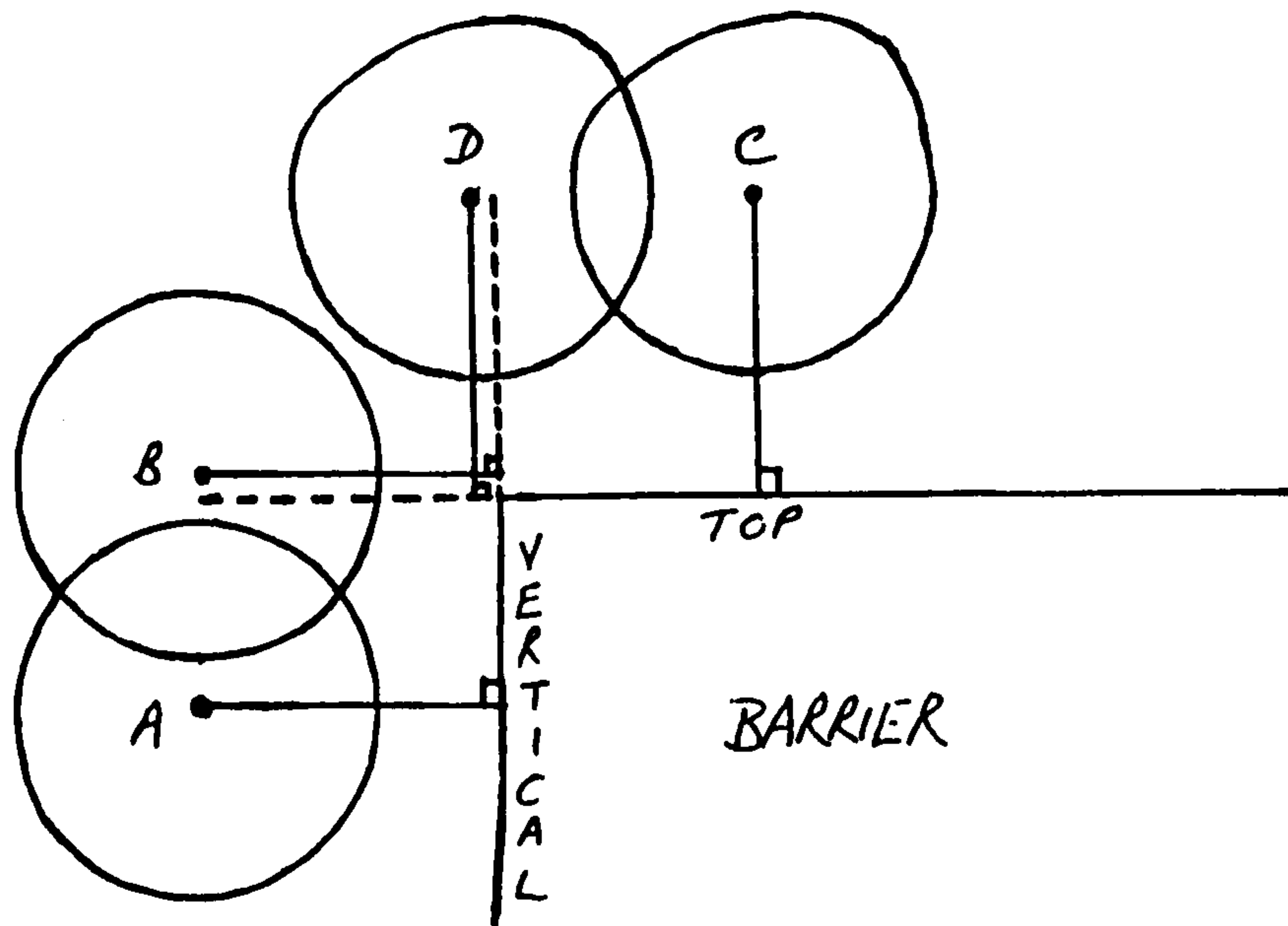


Figure 4.6 Representation of potential head to barrier contacts at points A and C, but not at B and D.

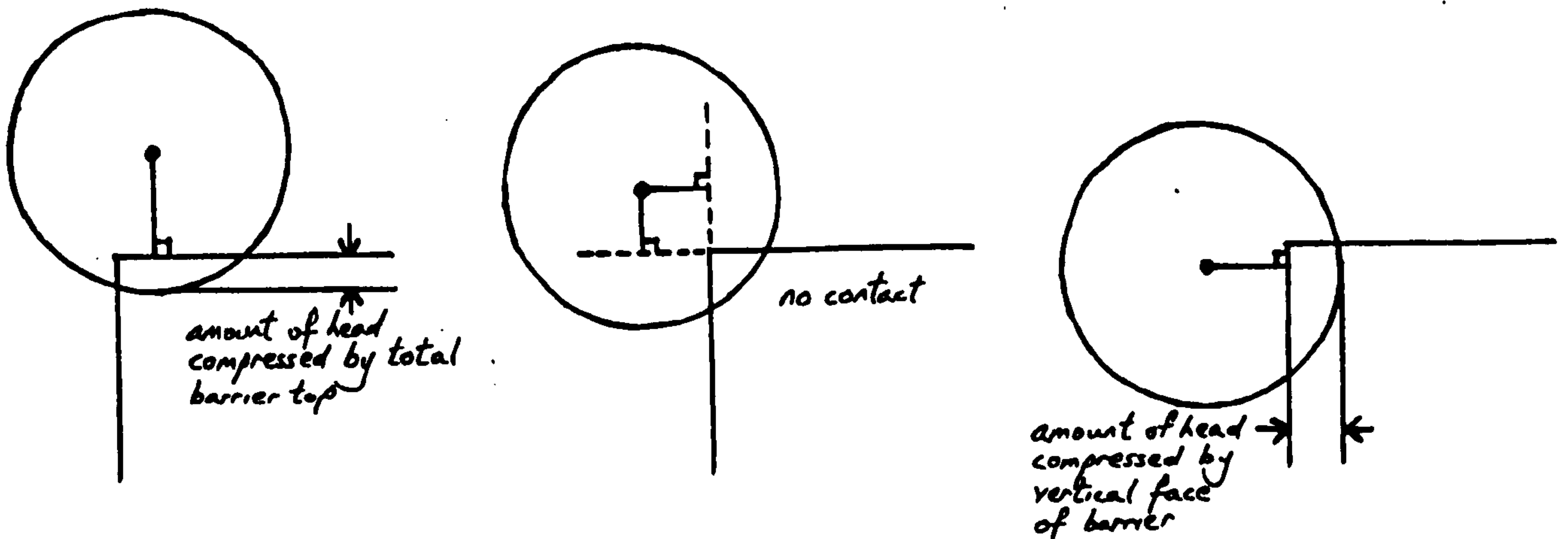


Figure 4.7a Figure 4.7b Figure 4.7c
The severity of step force generation as head passes from top of the barrier, through a quadrant of 'no contact' area, to touching the vertical face of the barrier.

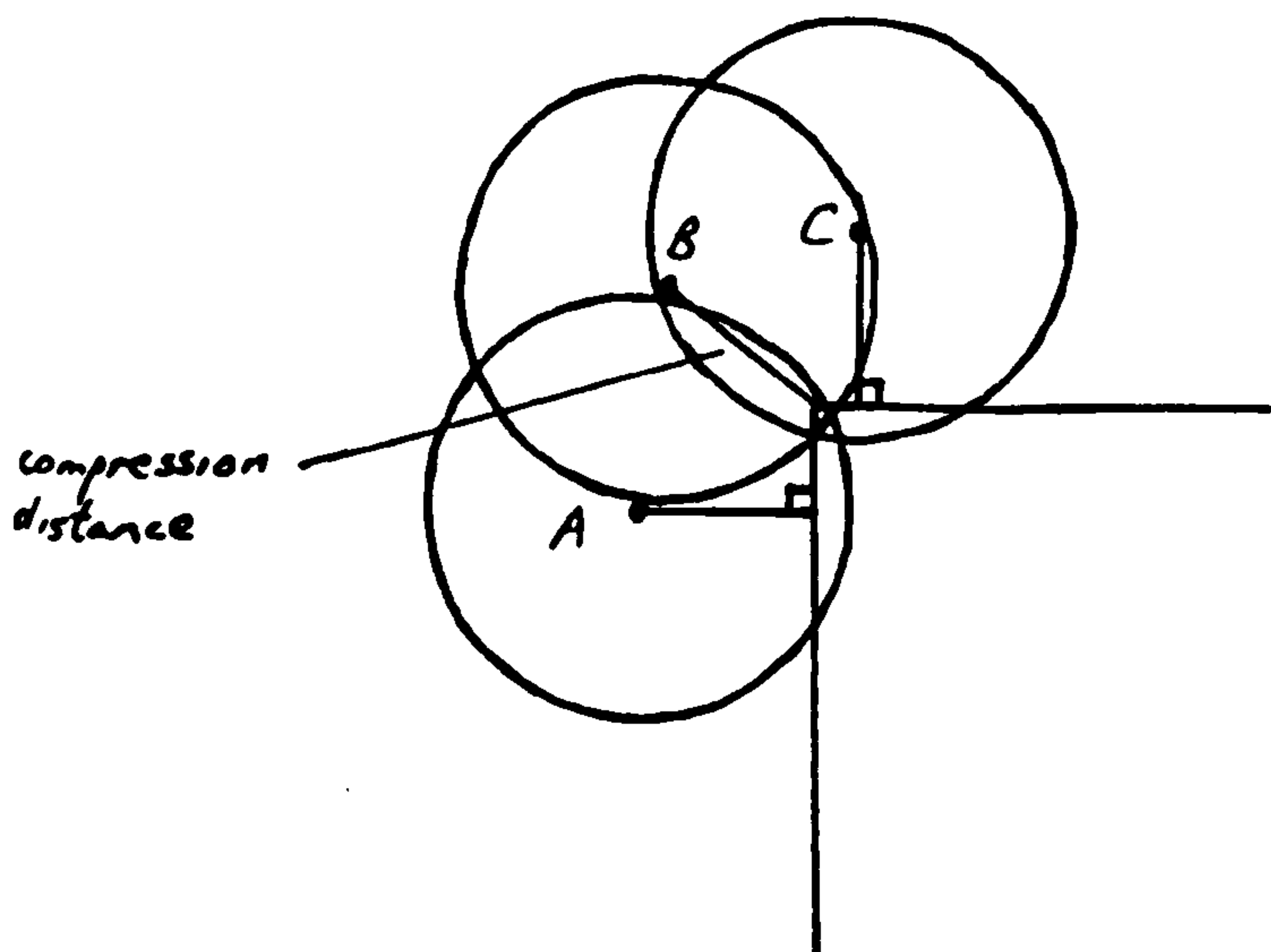


Figure 4.8a
The mathematical discontinuity is prevented by inserting a compliant rod along the edge of the barrier.

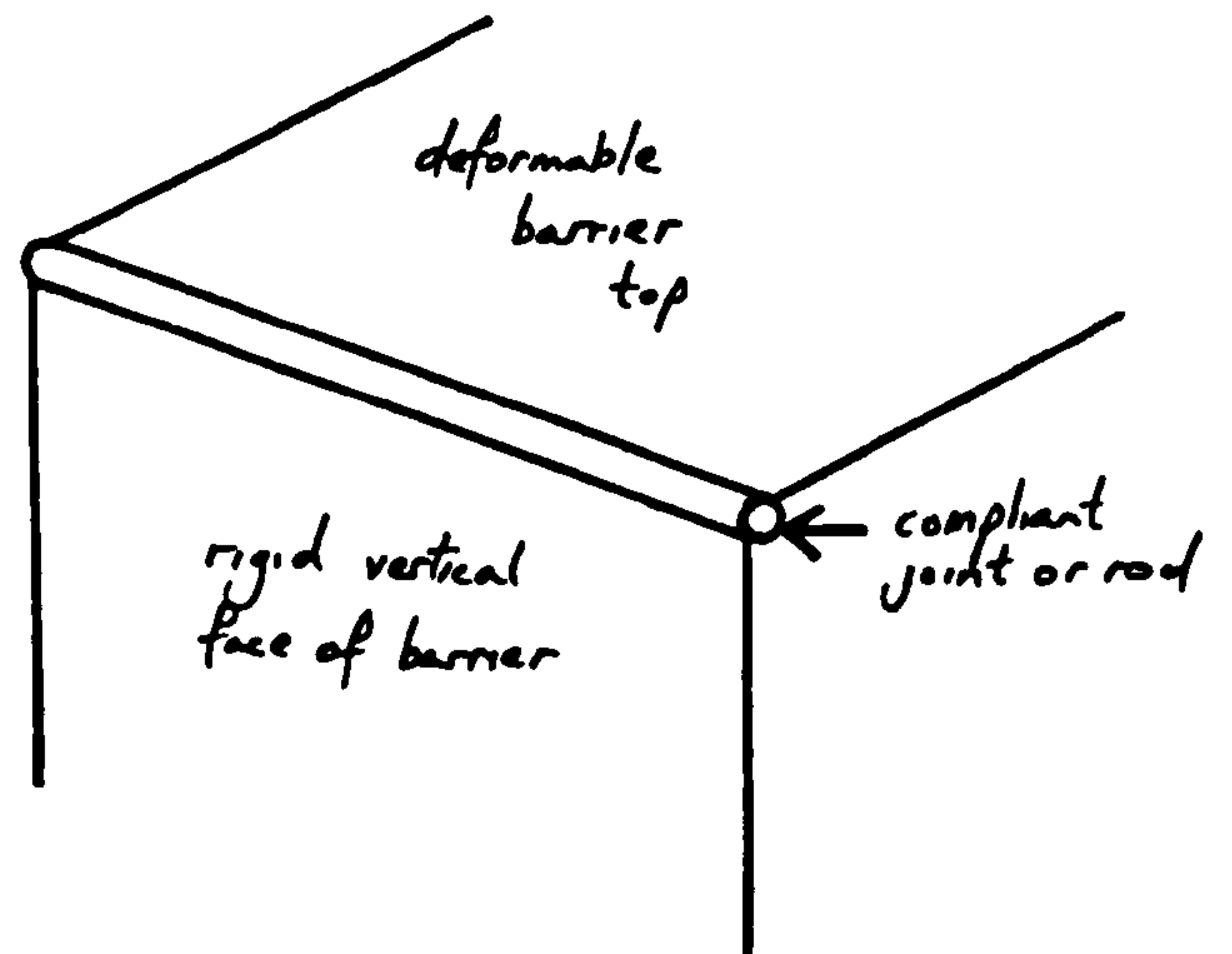


Figure 4.8b
The mathematical discontinuity is prevented by inserting a compliant rod along the edge of the barrier.

CHAPTER 5

PROGRAMMING AND COMPUTATION

5.0 The General System

As mentioned earlier in the previous chapter, the main program is written in ACSL. An SD/FAST library of routines is employed for the dynamic description of the dummy rider and the motorcycle, and is linked to the ACSL main program. The SD/FAST routines are written in FORTRAN. Output results from ACSL are in the form of numerical data, and plots of these data in a two-dimensional graphical format. In addition, computer graphics packages are used to enhance the research and development of the simulation by presenting the results in a three-dimensional visualisation form. Figure 5.1 shows the general processes during the running and completion of a typical program execution.

In the MODEL stage, the construction of the proposed dummy rider and motorcycle is designed by the user. This will be in two SD/FAST format data files. They are then run under the SD/FAST executable to create the FORTRAN-based dynamic and library files. These will be compiled by a FORTRAN compiler to produce object codes.

In the PROGRAM stage the actual ACSL simulation program is

written. It is then compiled for execution. The workings of the coded simulation will be described later.

ACSL provides a facility called a 'command' file, where certain parameters already set in the program can be updated. These can include the initial conditions to the equations set in the model. They are illustrated in the INPUT stage.

During RUNTIME, ACSL acts as the controller of the system and in addition it also acts as an integrator. In the ACSL program the simulation model is described, but it links to SD/FAST to receive kinematics information about the dummy rider and the motorcycle. It determines if contact is made between two specified surfaces, and evaluates the force value based upon the contact information. ACSL also evaluates the current states of the SD/FAST-modelled dummy rider and the motorcycle. These are the displacements and velocities of the joints within the two models. After ACSL has computed all the required calculations, the relevant data are passed back to SD/FAST, and a new cycle starts again until the simulation reaches the user-prescribed finish time.

Outputs from ACSL are in numerical data form, and graphical plots of these numerical data. It facilitates the research and development to the simulation model if a computer graphics package is employed to produce three-dimensional representations of these numerical data. Any necessary refined adjustments or

incorrectly simulated motion can be highlighted by the visualisation and thus modifications can be made. Two such packages have been used. They are VIEWWLD [26], pronounced 'view-world' and GEOMVIEW [27]. These only show stick-type models of the subjects but have the advantage of showing detailed translation displacements and joint rotations of the models.

The above describes the general actions of the system. We shall proceed with the functions and logic of the actual ACSL program in the following sections.

5.1 Coordinate System

In our normal daily lives, we measure distances relative to some convenient point of reference, usually centred around our habitat, such as the distance between one's house and one's place of work. In a computer simulation, however, these points of reference need to be expressed relative to some sort of standardised frame of reference, such as in polar coordinates, complex number fields, or in simple Cartesian coordinates.

In our mathematical simulation the Cartesian coordinate system is used. This is the standardised right-hand rule system. The actual location of our simulation lies anywhere within this frame of reference. One may argue that the precise location may not be

very important and is sometimes unrealistic. This is certainly true. The important issue here is that the model is referenced to a standardised coordinate system. This is an important concept especially when angle-related issues are concerned.

Recall in the previous chapter, the construction of a model in a SD/FAST data file format is such that a main, datum body is described, along with its mass and inertia. The next body, known as the outboard body, is described in terms of its location relative to the main body which is now known as inboard body. The next outboard body is described yet again relative to the previous inboard body which is in turn relative to the main body. This forms a tree system with successive outboard bodies described relative to their previous inboard bodies, and the ultimate root is the initial main body. This format of describing a model is obviously very localised, i.e. all parts are relative to the main, datum body.

Indeed the local coordinate system is a very important area in accessing the SD/FAST subroutines. When data are fed back into the SD/FAST subroutines they need to be expressed in their local frames with respect to the particular bodies to which they refer. When data are extracted from the SD/FAST subroutines they are, however, expressed in the global frames in accordance with the global coordinate system to which the system is related.

Therefore we can say that the ACSL program describes the set-up of the simulation in a global coordinate system. The SD/FAST models are constructed locally, but are placed, by means of specifying the positions of the main bodies, in two global three-dimensional positions, which are consistent to each other and also with relation to the simulated surroundings. This is one of two important points with reference to global and local coordinate systems in our simulation. The second point involves only ACSL and is of vital importance in force generation.

As mentioned earlier in Chapter 3 a contact point is defined as the projected perpendicular point from the centre of gravity of a body onto a plane. If a force exists, its direction is very important. The main force acts in the line of action between the two bodies, with frictional forces acting orthogonally in accordance with a Cartesian coordinate system. However, this system is generally not in line with the globally defined system already prescribed within the program. It is therefore necessary, and numerically consistent, to pre-set a local-axes system on the surface of the plane, and to devise a direction cosine matrix to transform the relevant vector, such as the force, to its appropriate coordinate system, such that

$$\begin{bmatrix} x_L \\ y_L \\ z_L \end{bmatrix} = \begin{bmatrix} \text{D.C} \\ \text{G to L} \end{bmatrix} \cdot \begin{bmatrix} x_G \\ y_G \\ z_G \end{bmatrix} \quad (5.1)$$

where

$$\begin{bmatrix} x_G \\ y_G \\ z_G \end{bmatrix} = \begin{bmatrix} \text{D.C.} \\ \text{G to L} \end{bmatrix}^T \cdot \begin{bmatrix} x_L \\ y_L \\ z_L \end{bmatrix} \quad (5.2)$$

G denotes the global coordinate system, L denotes the local coordinate system, D.C. denotes the matrix of direction cosines and T denotes the transpose of the matrix.

So when a vector of force is defined and expressed in its local coordinates, the direction cosine matrix D.C. will transform the relevant information into global coordinates in alignment with the program. The transpose of the D.C. matrix reverses the operation given the globalised vector.

5.2 Force Generation

The basic principles of defining a contact point between a body with material characteristics and a rigid body, and also between two bodies with non-rigid material properties, have been described in the previous chapter. Here we will outline how an external force is generated when two bodies are considered to have impacted, and the role of the generated force vector in the program.

Consider the list of events as follows:

- (i) define the contact point between a body and a plane
- (ii) define the contact point velocity in global coordinates
- (iii) convert this global coordinate velocity to contact velocity in contact plane local coordinates
- (iv) evaluate the compression and compression velocity between the two bodies
- (v) generate the contact force by using data from (iv) and the material properties of the two bodies
- (vi) define the frictional forces using (v) and (iii), and form a vector of forces in contact plane local coordinates
- (vii) transform this local force vector into global coordinates
- (viii) transform the global forces into SD/FAST local coordinates
- (ix) apply the local force vector back to SD/FAST
- (x) evaluate energy using (iii) and (vi)

Note that since ACSL is a continuous simulation language, the above events will be carried out regardless of whether the two bodies are in contact or not.

The generation of a force lies in (v) where a force is considered to exist when the compression distance between the body and the plane is less than the prescribed radius of the body. In the event of contact not considered to have occurred, the force value

is simply zero but the events following will still be executed.

This list of events is carried continuously between any two bodies that are coded in the program for possible contact. In the case of a body with material properties impacting onto a rigid body, the event (ix) is only applicable to the compliant body. In the case of both bodies with compliant characteristics, (ix) is applicable to both.

To achieve a better understanding of events involving global and local coordinates, consider Figure 5.2 where a body and plane are located somewhere in our global 3-D space.

In our plane of interest, a local right-handed axes system is pre-defined and a direction cosine matrix transforming the axes system (x,y,z) to (x',y',z') is formed. To determine if the body is in contact with the plane, a perpendicular projection from the centre of gravity of the body is made onto the plane. If the contact point falls within the boundary of points $(P1,P2,P3,P4)$ defining the area of the plane, an integral value of zero is assigned to a switch key to indicate the contact point is within our plane of interest. Forces can therefore be generated by determining the compression distance from the body's centre of gravity to the contact point against the radius of the body, along with the properties of the bodies.

However, in Figure 5.2 it is shown that the contact point CP'' falls below points $P3$ and $P4$. The point will still be on the same equation of plane defined by points $(P1, P2, P3, P4)$, but it is not within the area of interest. In this case the integral value of the switch will be given a value of one of 1, 2, 3 or 4, which corresponds to whether the point CP'' falls outside the boundaries defined by $(P1, P2)$, $(P2, P3)$, $(P3, P4)$ or $(P4, P1)$ respectively. To maintain the contact point within our boundary of the plane, CP'' is extended until it reaches the nearest boundary and is assigned as CP' . However, a force would not be generated since only an integral value of zero for the switch key can indicate that the true contact point actually falls within the boundary defined by the four points.

When an external force does exist, it is evaluated by how much the body has been compressed and its material characteristics. The frictional forces are defined by multiplying the main force with the coefficient of friction. Their directions are determined by the directions of the contact velocity in contact plane local coordinates as in event (iii). Finally, energies are evaluated by integrating the product of force and velocity, both local to the contact plane, along their respective axes. This is equivalent to the product of force and distance moved.

The above describes how an external force is generated if contact was made, and the role of this force. Note that the list of

events is still executed even when contact is not considered to have been made, and in this case the external force is simply assigned zero and therefore all subsequent related force vectors, local or global, are just null vectors.

However, up until now, we have only been concerned with damped elastic impacts between two compliant bodies or one compliant and one rigid body. There is a further case, involving bodies of elasto-plastic material, where deformation will stay permanently. Such an example is the front wheel impacting onto the barrier and resulting in plastic collapse of both the wheel and the forks.

5.3 Permanently Deformed Impacts

For impact involving permanent deformation, the determination of contact point is still defined in the same way. However, the generation of force involves actual measured force-deflection readings, and rebounding and unloading characteristics are used. In addition, the deformed state of the body will remain as the compressive spring of the body bottoms out.

Consider Figure 5.3 where a body is being compressed by a plane.

In Figure 5.3a the body is compressed by the amount denoted as DIS_0 . DIS_0 is then used to access the force-deflection readings

to obtain a force value, and this amount of compression is being recorded as DISMAX for future use. Meanwhile, the unloading characteristics are being accessed to obtain unloading distance NXODIS. This is used to set the new compression distance such that it equals to DISMAX-NXODIS, if rebounding force is to occur.

The above will repeat itself if at any time the current compression DIS is greater than the previously recorded DISMAX. In these cases, the current maximum compression DISMAX will be continuously updated along with the new compression distance NEWZER.

Now consider the case when the body starts to rebound, as illustrated in Figure 5.3b. In this case the current compression DIS_1 is less than the recorded maximum DISMAX. DIS_1 will be used to obtain a rebounding distance REBO such that it equals to DIS_1 -NEWZER. If REBO is positive, as in the case of Figure 5.3b, a rebounding force is obtained by accessing the rebound-force characteristics using the distance REBO.

However, if REBO is negative, as illustrated in Figure 5.3c, the current compression DIS_2 is thus less than the recorded compression distance NEWZER. In this case, with REBO being negative, there will be no force generated such that contact had not been made.

The value of NEWZER is thus the permanent deformed distance of the body unless the value of DISMAX is exceeded, which implies that the body is further being compressed. In such a case, NEWZER will be updated as the new permanent deformed distance. For further information regarding the modelling of this type of impact, see [2].

5.4 Torque Generation

The forces described in previous sections have been forces generated from impacts between two bodies. In this section we shall explain the generation of rotational torques about the joints that make up the two models, the dummy rider and the motorcycle.

Recall that an SD/FAST model is made up of bodies, with masses and inertias specified, connected by various joint arrangements. The linear forces are impact forces of these bodies but with bodies' depths and material properties specified within the ACSL program. The rotational torques are the responding joint movements triggered by the bodily impacts. They are generally defined by the following formula.

$$\tau = -k.(q-q_{ic}) - d.u \quad (5.3)$$

Where τ = torque,
 k = stiffness,
 d = damping,

and q and u are the state vectors of the SD/FAST model. They represent the rotation and angular velocity of a joint about a particular axis, q_{ic} being the initial position of this particular joint.

Therefore, given the stiffness and damping parameters of a joint, the torques about its relevant axes can be evaluated using the above formula. However, there are two special cases where the generations of torques are somewhat more involved, and they are

- (i) the torques about the dummy's joints,
- (ii) and the torques of the front fork system.

We shall explain each of these two cases in more detail.

5.5 The Jointed Dummy

The OPAT dummy is built to be representative of a 50 percentile human male. Therefore, the range of movements are made to be similar to the human's movement such that, for example, we can only bend our head forwards or backwards to a certain degree

relative to the upright position.

The ranges of articulation associated with the dummy's joints have been supplied by TRL. They have also measured torques generated by the joint's movements. However TRL have only measured these force functions through narrow ranges of the allowable articulation, therefore we need to extrapolate the unknown forces outside the limiting ranges they supplied with sensible estimated spring stiffnesses.

Consider the flow diagram in Figure 5.4 where it demonstrates how hinge torques are generated, which is a form of ACSL MACRO in the program.

At the beginning of the simulation, all hinges are set to their initial positions. They are then compared with the current hinge positions during the simulation. The amount of movement of any particular hinge is recorded into 'movement'. The rate of movement is checked against zero to determine the existence of torque. At this stage there will be two separate cases depending upon this hinge velocity. Before we proceed we need to introduce 'motion', for recording rotation made during a computational time-step; its significance will be described later.

In Case I where the hinge velocity is found to be zero, we can naturally assume there is no hinge torque. However, the current

position of a particular joint can be different to its initial position such that we cannot allow the amount of rotation made to be the true movement made by this particular joint. This apparent movement is caused by movement of the next connecting joint, usually the one that constructs the inboard body. This can be demonstrated in Figure 5.5.

Imagine a connecting rod jointed at A and B as shown in Figure 5.5a. At this stage the joints are at rest such that no rotation has been applied to either of the joints, i.e. the linkage is in a straight line.

In Figure 5.5b we have set the initial positions of the joints as would be at the start of the simulation. Joint A has been rotated through an angle of α . As it rotates it carries the next connecting joint B such that from joint A onwards they form a straight line. We then rotate joint B through an angle of β such that joint B is seen to have rotated a total angle of $(\alpha+\beta)$ measured clockwise from the vertical. The angle between joints A and B is θ .

In Figure 5.5c only joint A has been further rotated through an angle γ in the anti-clockwise direction. The new position of joint A is now at an angle α' . Since joint B has not been rotated θ therefore remains constant. However joint B has also been carried by the rotation of joint A to its new position by an

angle of γ , such that its current position is at an angle of $(\alpha' + \beta)$ measured clockwise from the vertical. But note the actual joint B has not been rotated.

Referring to Case I, we therefore need to record any movement made into 'motion' even though the hinge velocity is zero, otherwise set motion to zero.

Case II occurs when a hinge velocity exists. Because of the insufficient information of measured torques mentioned earlier, torques are generated using the conventional equation (5.3) and information supplied by TRL. Referring to Figure 5.4 we therefore have torque C being the spring stiffness multiplied by the amount of rotation moved. Torque A is the measured force supplied by TRL. Because of the sign convention associated with the axes system, there is a force table for torques generated when rotation is anti-clockwise, and another table for torques generated when rotation is clockwise. This depends on the sign of the joint velocity which indicates the quadrant of displacement.

Since TRL only supplied torques measured through narrow ranges of articulation, end-stop spring effects have been assigned towards these limiting ranges. This implies that torques increase rapidly around these regions. However, since ACSL is a continuous language such that any sudden change of state, especially the

rapid growth in force, would resemble a step function, it would be wise to eliminate these sudden high forces so as to avoid the mathematical problem of singularity. This problem is eliminated by choosing the smaller force between torques C and A such that, should the above mentioned problem have occurred, the force function is compensated by the traditional stiffness multiplied by rotation format. This torque is then assigned to torque E.

The sign of this torque is also checked such that the spring reacts opposite to the rotation. This is determined by the direction of the velocity.

After the spring torque has been determined, it is summed up with the damping torque which was derived from a damping value multiplied by the angular velocity. The negative sign indicates the opposite reaction to the displacement.

This is how the hinge torques of the dummy's joints are calculated. But there is one more important detail to record. The current displacement of the hinge's rotation, whether it is still at rest or rotated, needs to be stored for the next cycle of calculation. This is done by assigning the current value of 'motion' into another parameter called 'current motion'. When the program exits from the MACRO, the newly obtained value in 'current motion' is then put back into the parameter 'motion' in the main program.

The storing of the current joint's rotation is performed this way due to the structure of ACSL programming. The reader should be aware that the parameter 'motion' is used to hold the continually updated current rotation, after it has been used to check if movement was made, therefore it may seem a redundant step to store this current rotation into 'current motion', only to put it back into parameter 'motion' after exit from the flow diagram. However, since ACSL is a continuous simulation language, it does not allow any parameter, upon entry and exit from the same MACRO, to have its current value altered, since this will lead to unsortable programming such that ACSL would not know whether to perform checking 'motion' first, or assigning current 'motion' first. But by using a substitution parameter to hold the newly updated displacement, it can be put back to the actual 'motion' parameter outside the MACRO.

5.6 The Front Fork System

The bending of the front fork is another special case of measuring torques. It is based on the deflection of a beam to obtain the bending moment and maximum deflection. With this information known it is required to determine the amount of torque generated due to rotation moved and its direction of rotation.

Consider the front fork layout illustrated in Figure 5.6.

In the figure the notations are

M = bending moment,

l = length of front fork,

θ = angle rotated

and $\dot{\theta}$ = rate of rotation.

Note that in accordance with the right-hand rule, the directions of the rate of rotation are thus indicated. However, angle of rotation is evaluated by

initial unloaded position - current loaded position

thus the sign will be opposite to that of its angular velocity.

Now consider the flow diagram in Figure 5.7.

The current rotation made is determined by comparing the initial unloaded position and the current loaded position as written above. The sign of this value is stored in SIGNFK. Its importance will become apparent later in the flow diagram.

This current angular deflection is compared with the maximum deflection to determine which deformable region the front fork

is in, and also the amount of bending moment. If the current deflection exceeds the maximum allowable deflection the front fork has obviously exceeded the elastic limit thus the plastic bending moment. If the current deflection is within the maximum allowable deflection the front fork is in elastic region, and the amount of bending moment is assigned as the ratio of current and maximum deflection of the elastic bending moment.

Having determined the amount of bending moment due to the amount of deflection, torque generated due to the spring is then calculated. There will be four cases based on the amount of deflection, and they are demonstrated in Figure 5.8.

The sign of the current rotation is tested. If the sign is negative, as shown in Figures 5.8a and 5.8b, spring torque is assigned to the larger value between the ratio of torque and the total torque. This ratio is assigned as current rotation divided by maximum rotation.

If the sign of the current rotation is positive, as shown in Figures 5.8c and 5.8d, spring torque is assigned to the smaller value between the said ratio of torque and total torque.

This approach of determining the amount of torque has the effect of assigning variable torque, depending on the current deflection while the fork is in elastic region. When it is in the plastic

region, the torque is set automatically to its total value. However, if the front fork is in the plastic region we need to redefine the initial unloaded position by allowing the recoverable elasticity to occur. This is done as follows:

$$\begin{aligned} \text{initial unloaded position} = \\ \text{current loaded position} + \text{SIGNKF}(\text{maximum deflection}) \end{aligned}$$

The sign SIGNFK has the effect of determining the direction of the recoverable elasticity rotation as shown in Figure 5.9.

In accordance with the right-hand rule, when SIGNFK is positive, the addition of maximum rotation will be anti-clockwise. Similarly, subtraction will be in the clockwise direction. The total torque is then calculated by summing the spring torque and the product between the damping value and the velocity of rotation as shown in Figure 5.7.

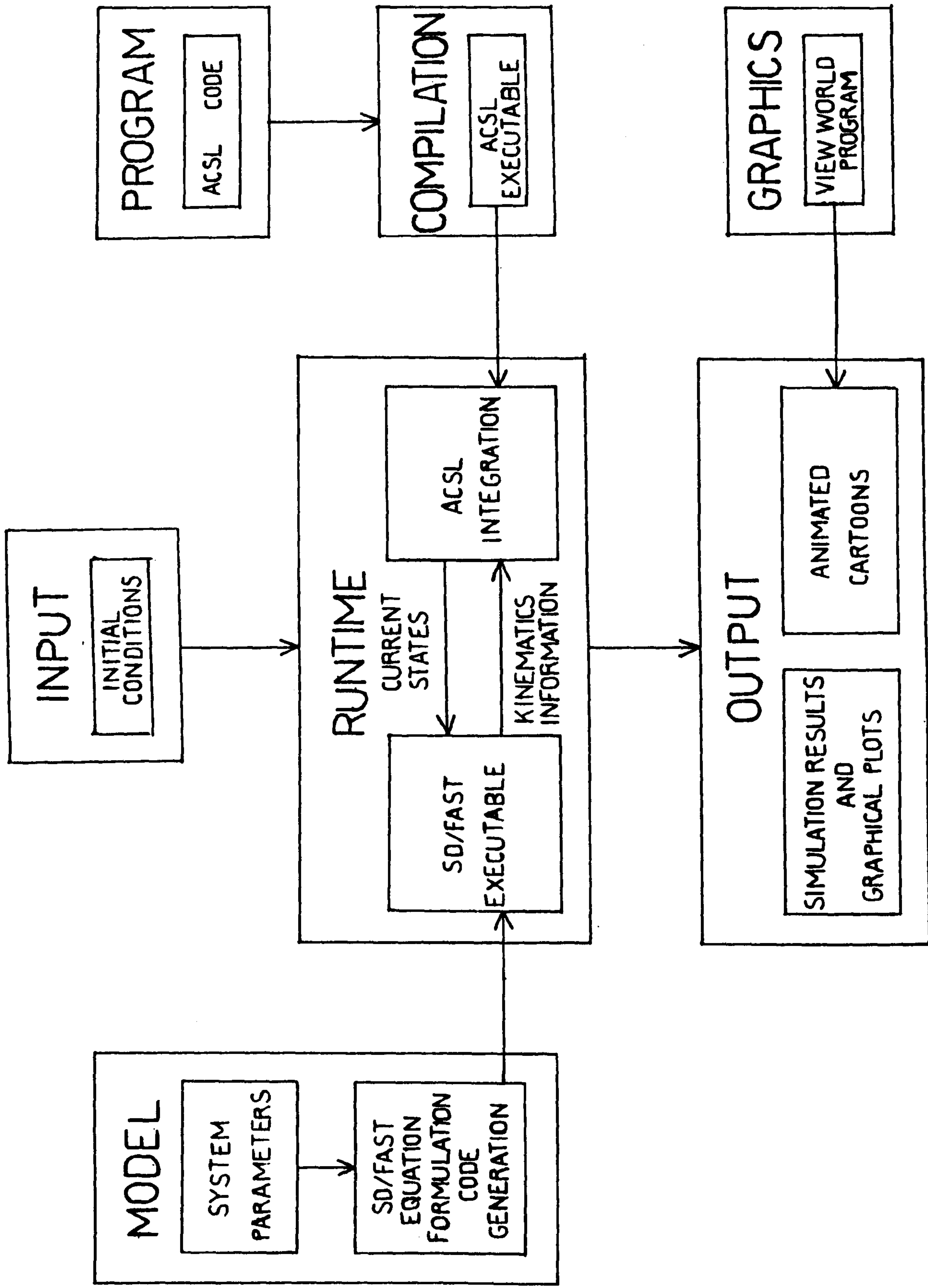


Figure 5.1 Computational scheme.

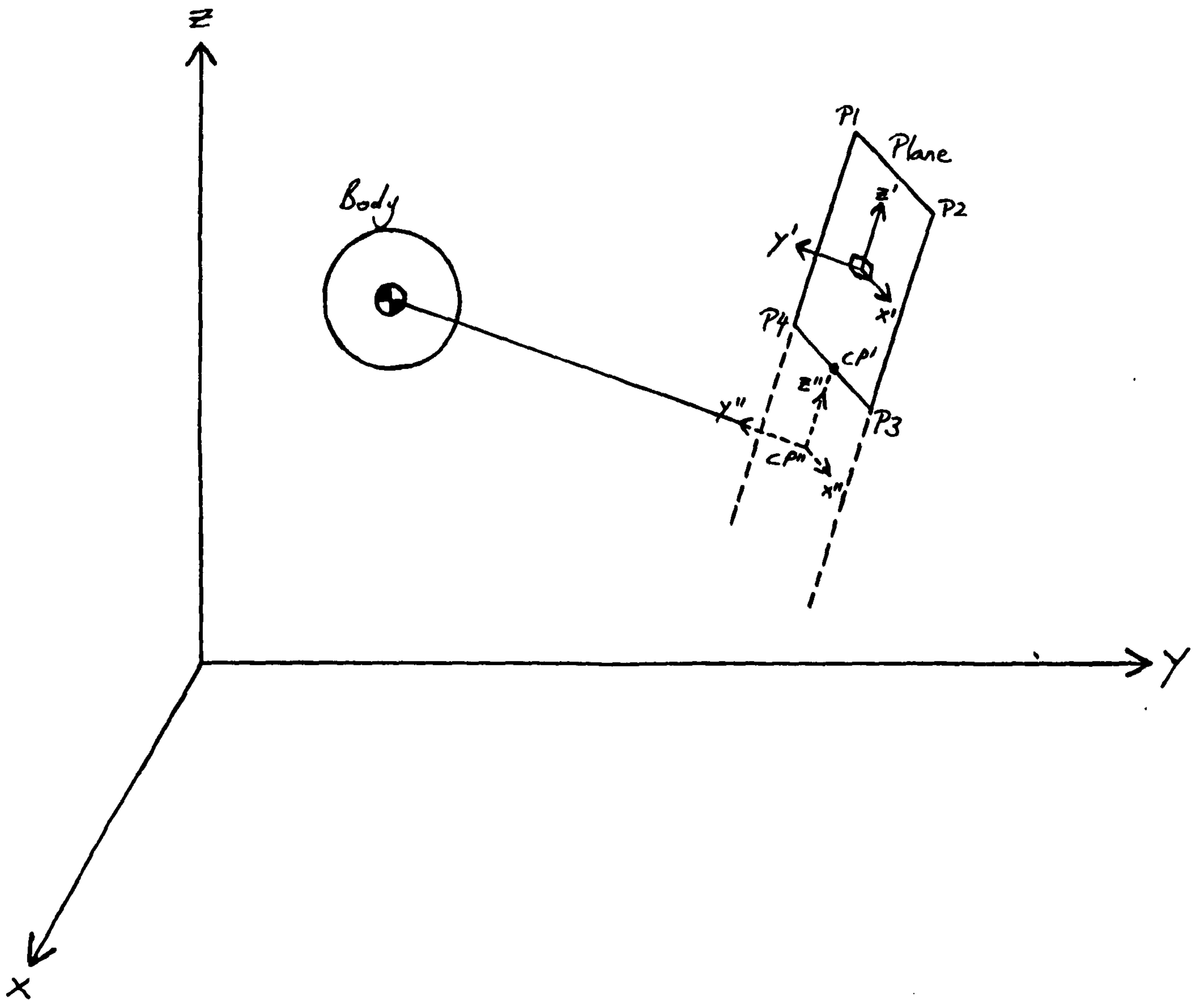


Figure 5.2 Determination of body to plane contact.

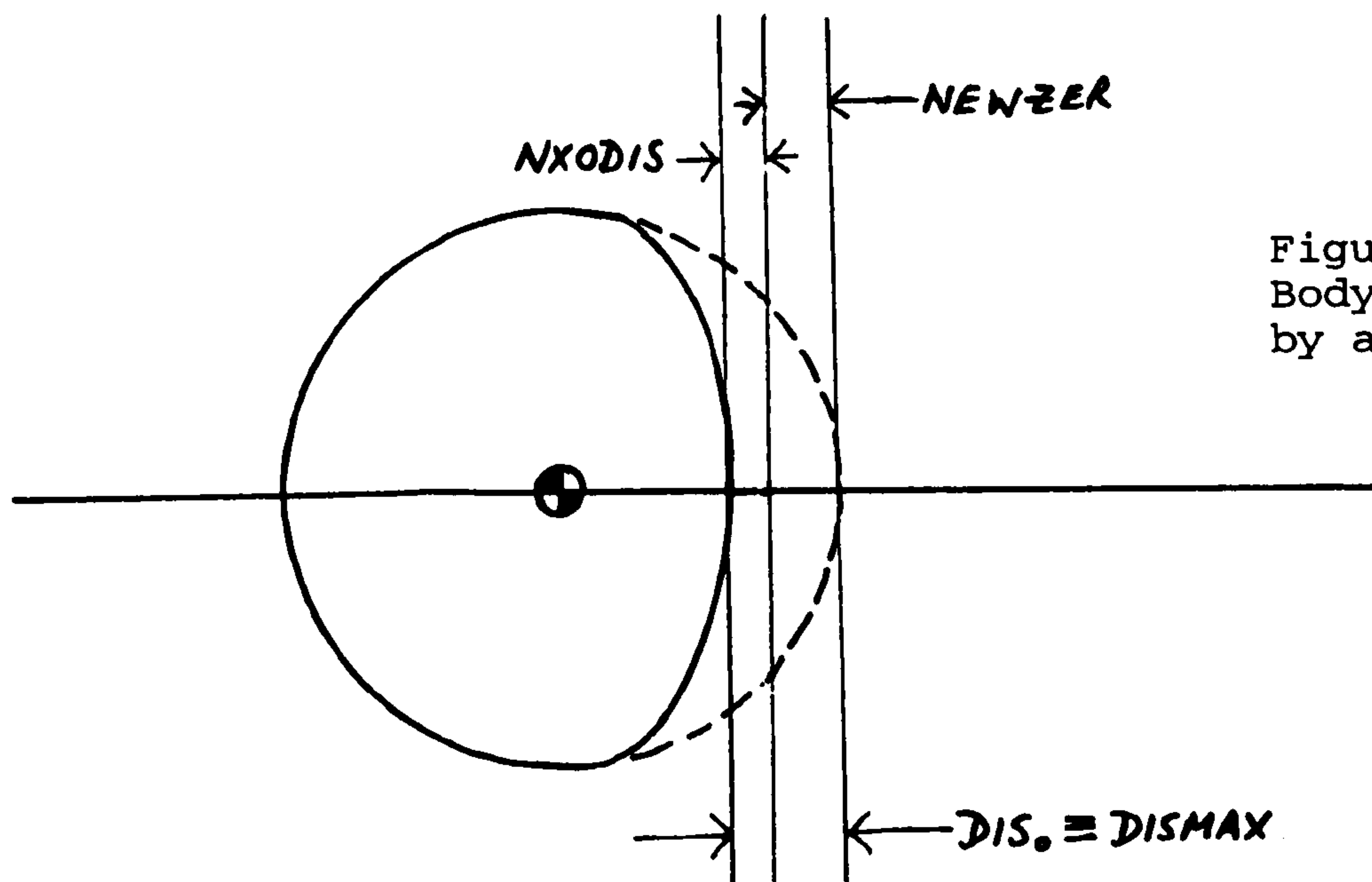


Figure 5.3a
Body is compressed
by amount DIS_0 .

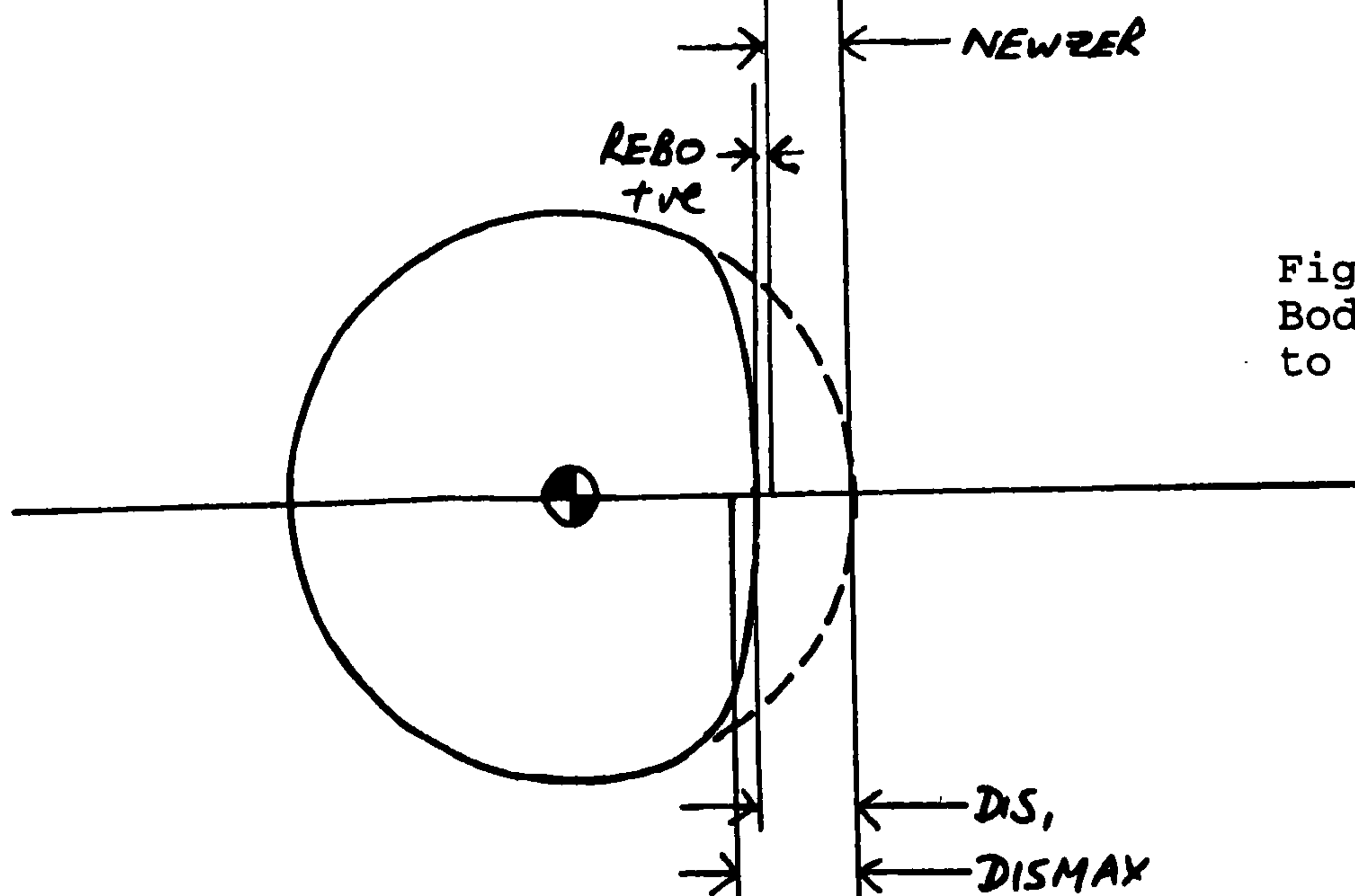


Figure 5.3b
Body starts
to rebound.

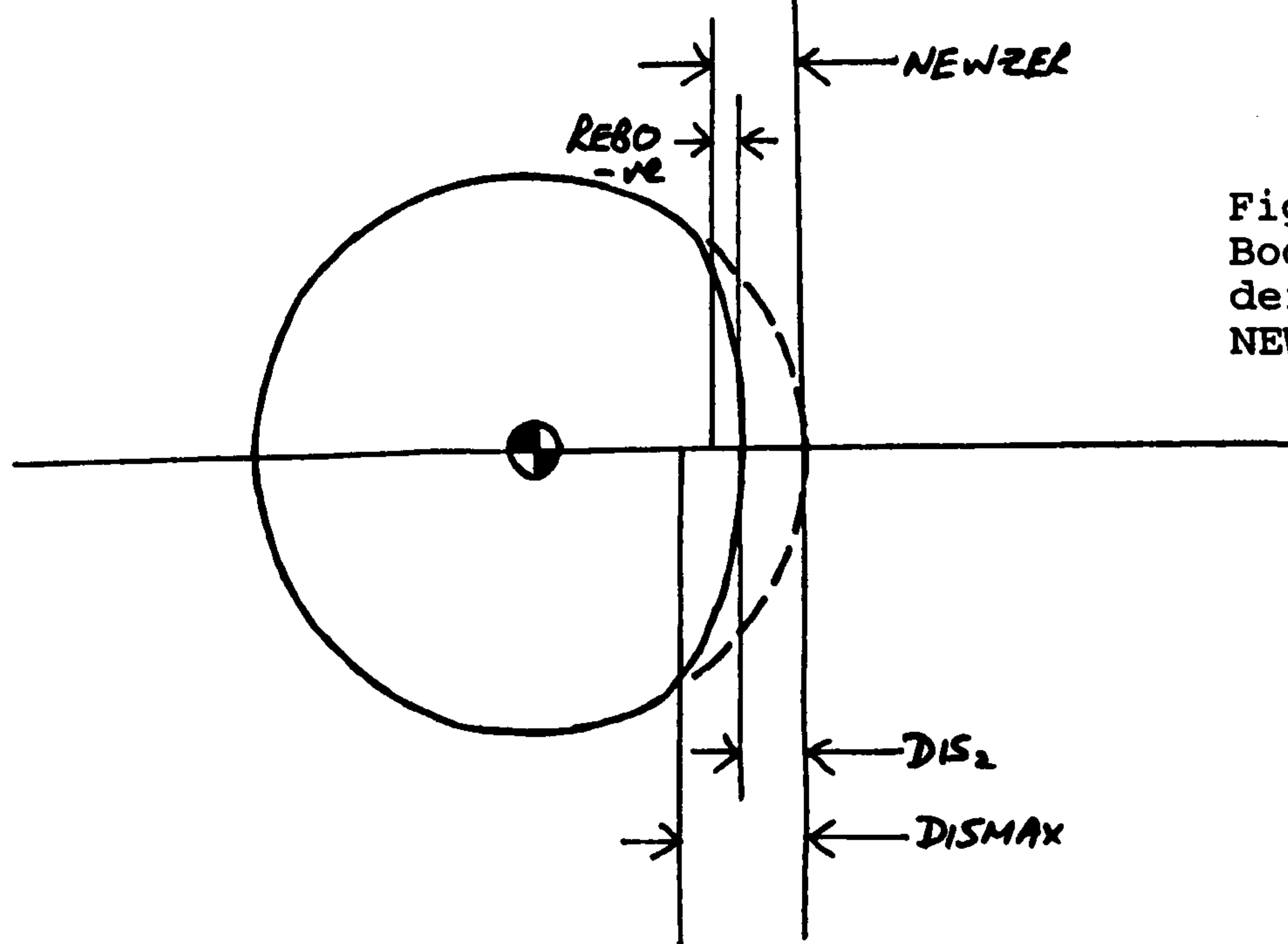


Figure 5.3c
Body is permanently
deformed by amount
 $NEWZER$.

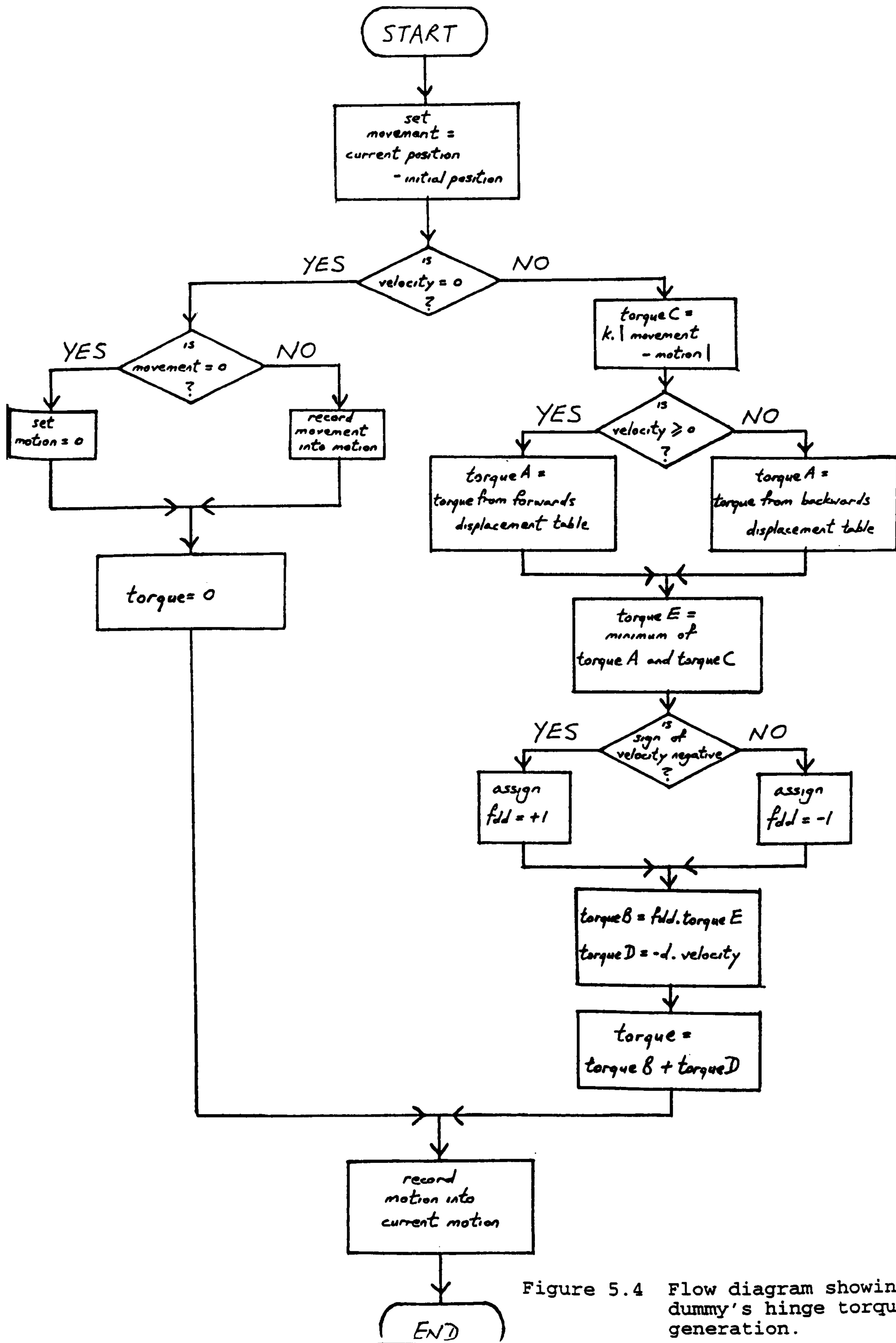


Figure 5.4 Flow diagram showing dummy's hinge torque generation.



Figure 5.5a
Joints A and B
at rest.

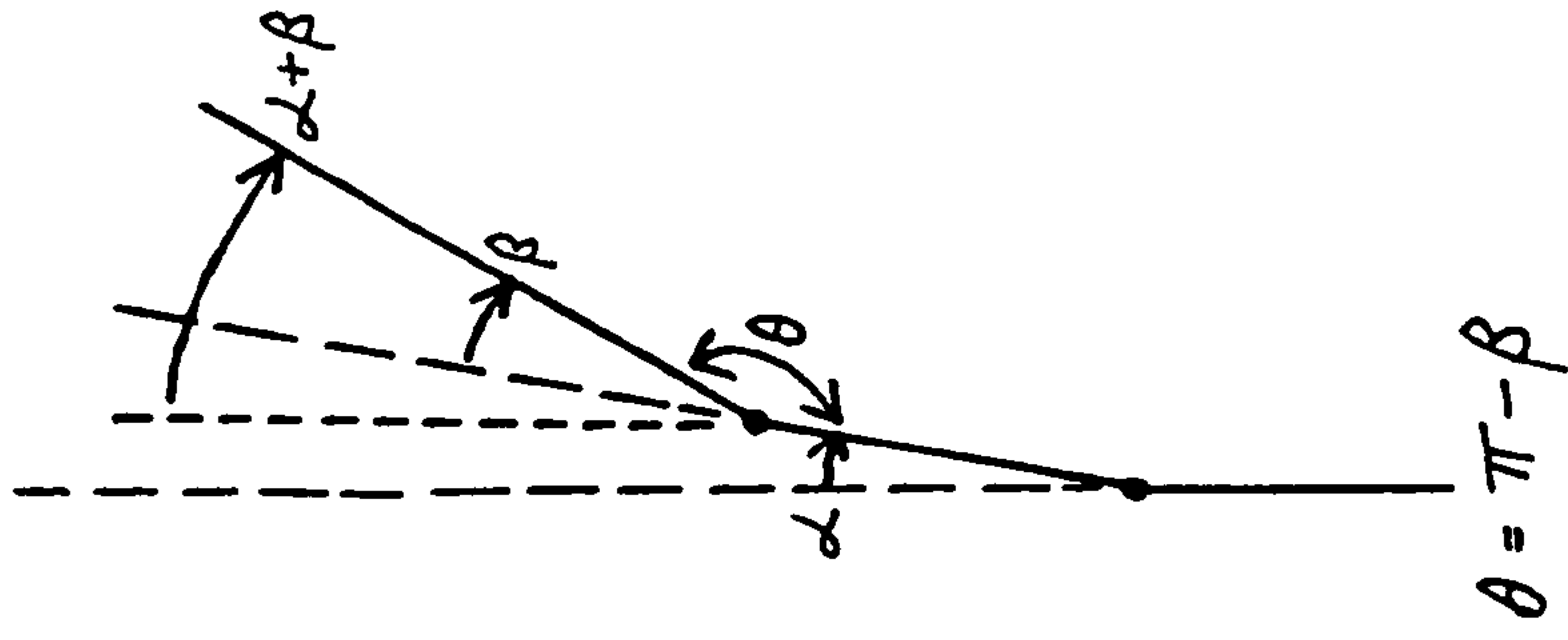


Figure 5.5b
Joint A rotated an angle α ,
joint B rotated an angle β .

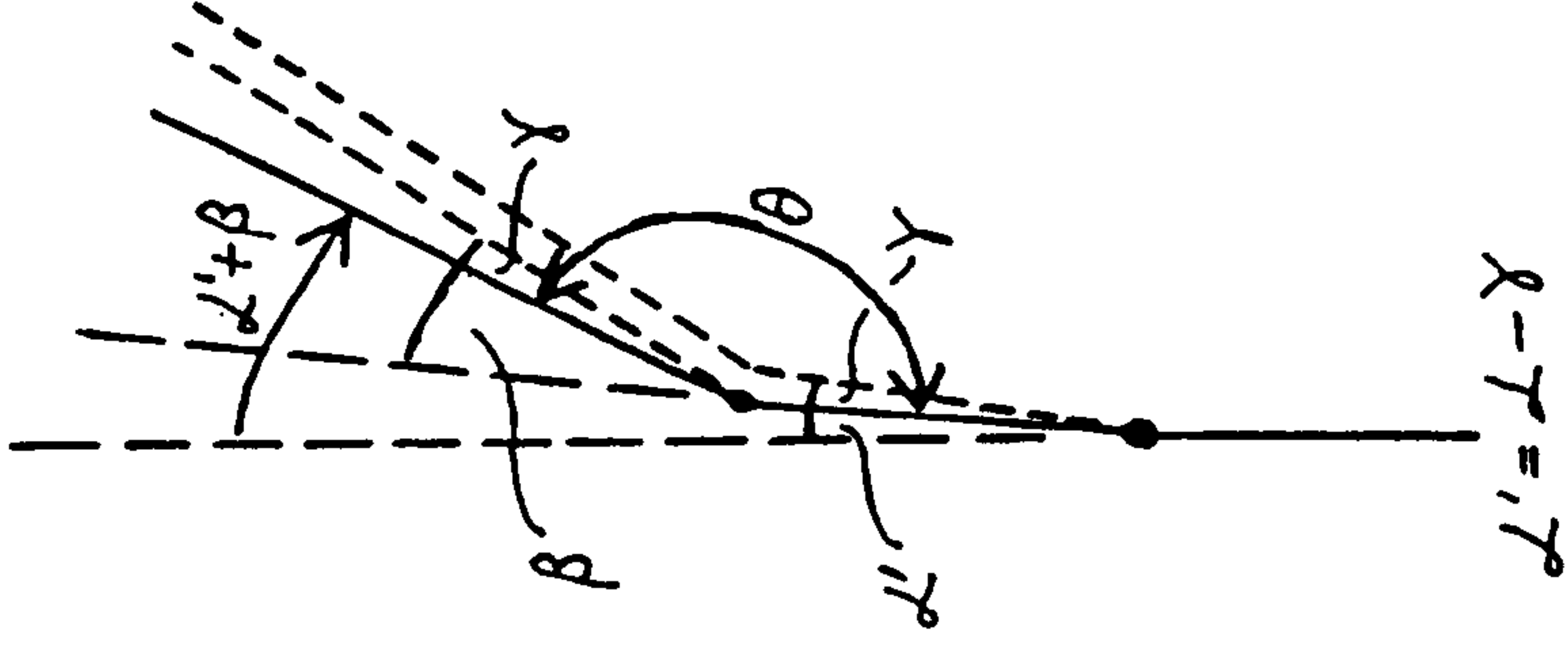


Figure 5.5c
Joint A rotated an angle γ ,
joint B had moved but not
rotated.

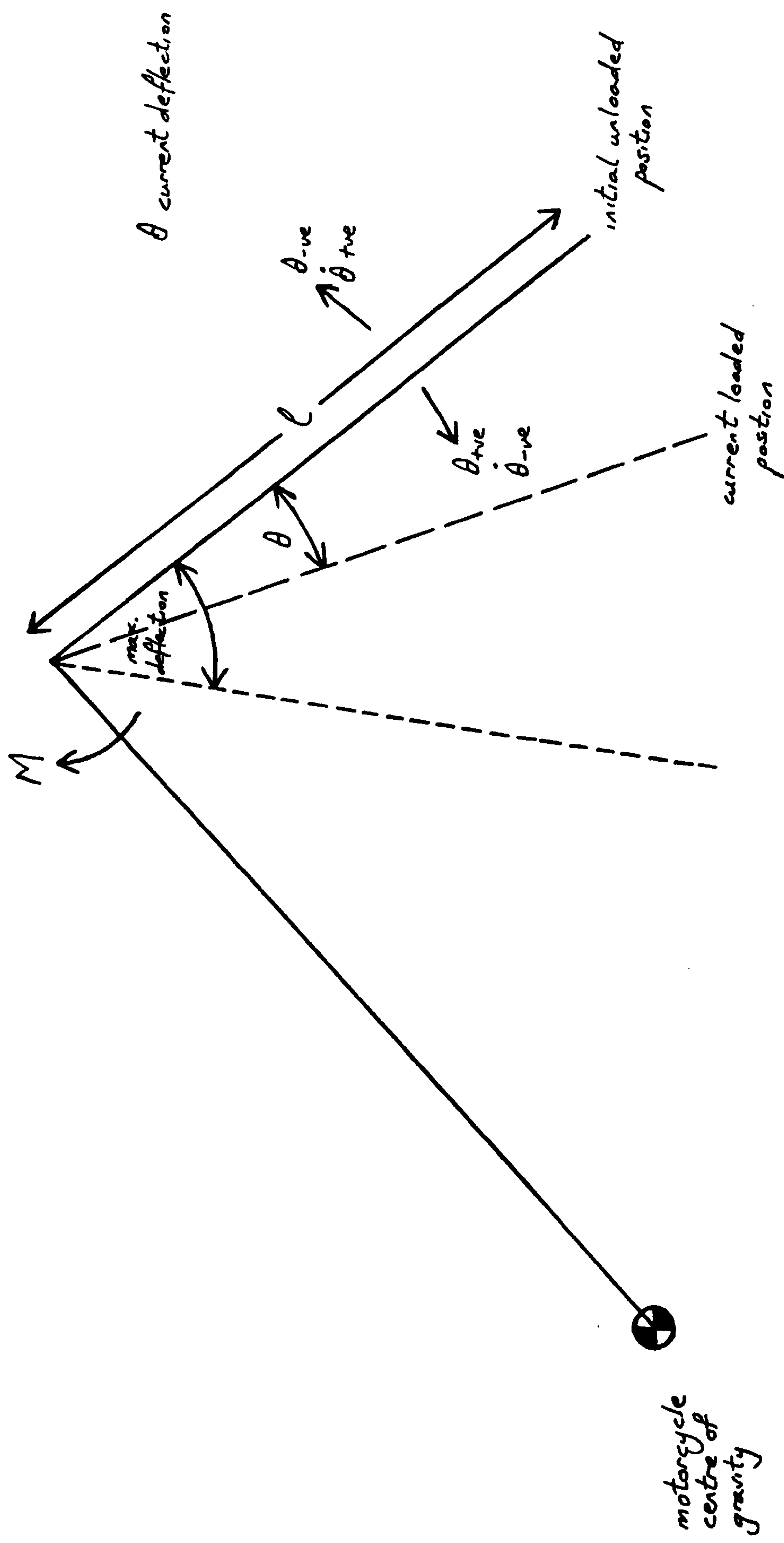


Figure 5.6 The front fork system.

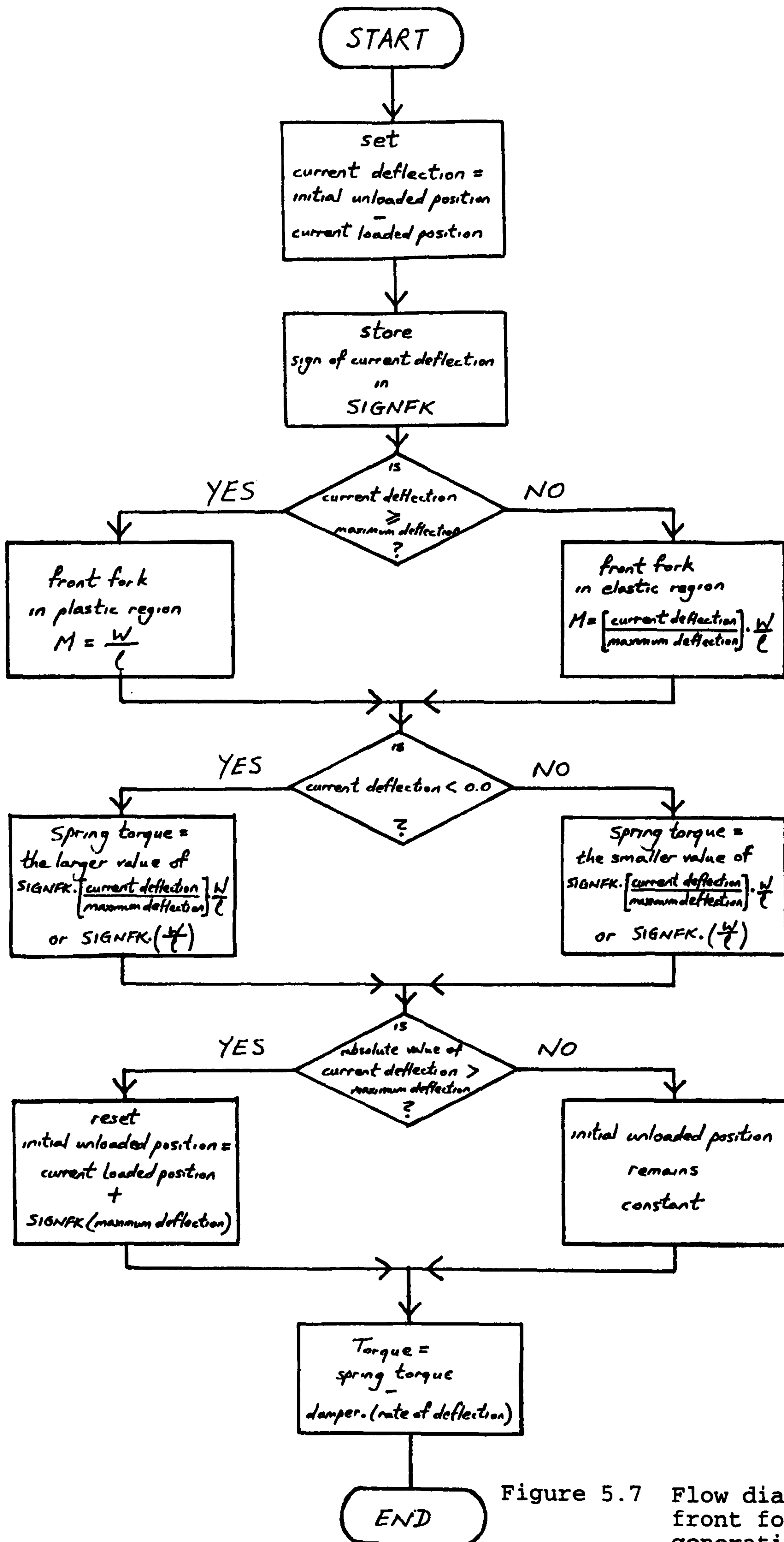


Figure 5.7 Flow diagram showing front fork torque generation.

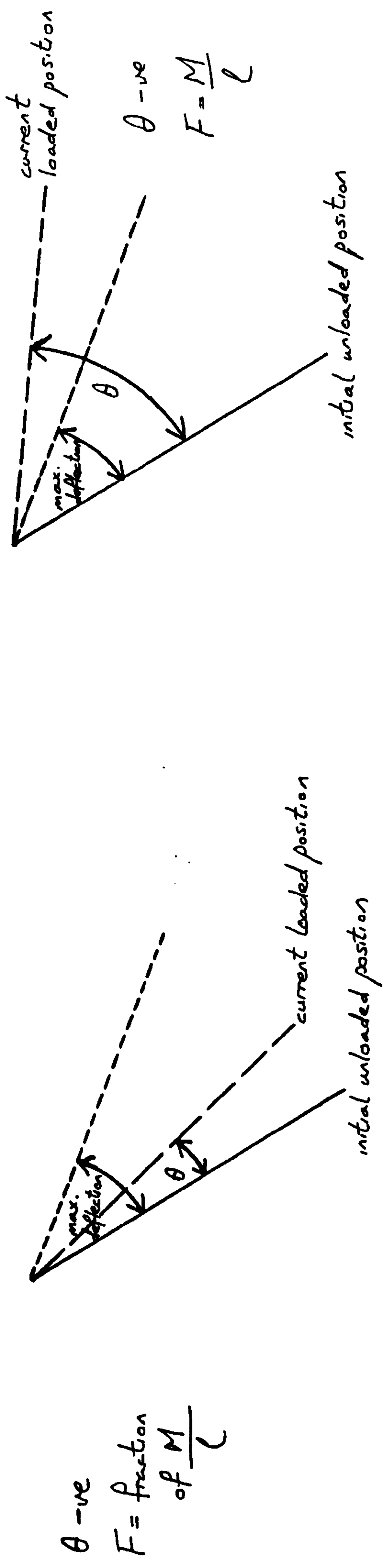


Figure 5.8a Front fork rotated anti-clockwise, but within maximum deflection.
Figure 5.8b Front fork rotated anti-clockwise, but exceeded maximum deflection.

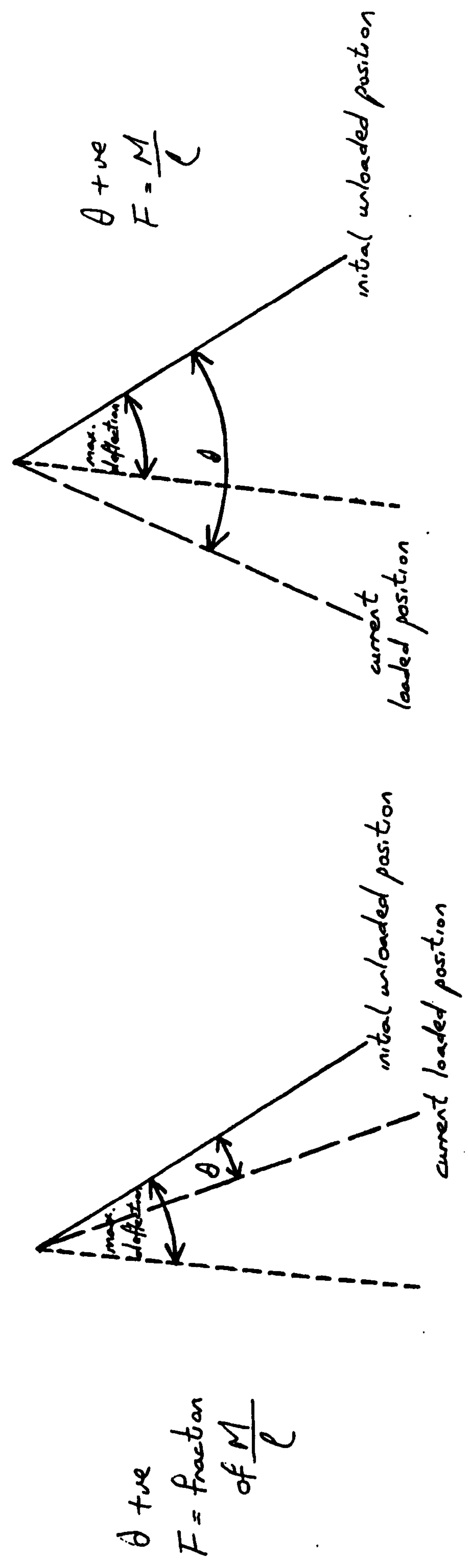


Figure 5.8c Front fork rotated clockwise, but within maximum deflection.

Figure 5.8d Front fork rotated clockwise, but exceeded maximum deflection.

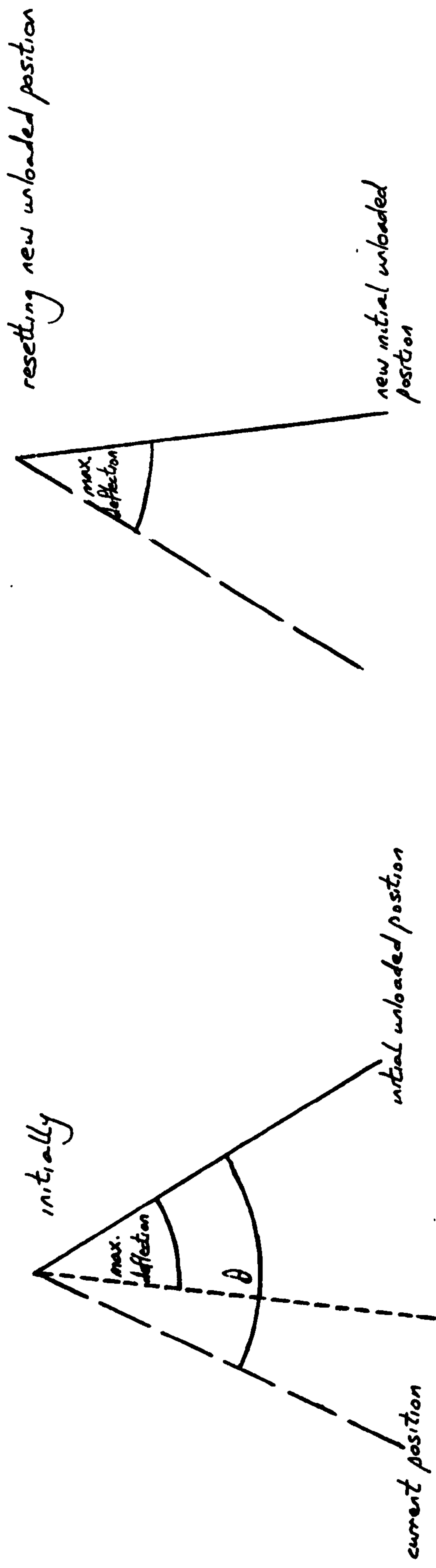


Figure 5.9a Front fork is in plastic region and had deflected clockwise.

Figure 5.9b Front fork is set to this new initial unloaded position when SIGNFK is positive.

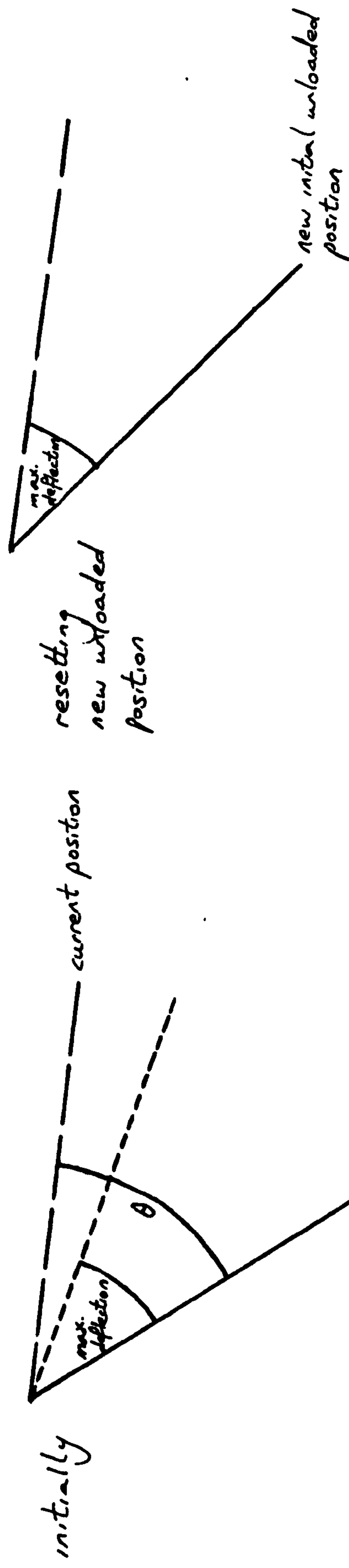


Figure 5.9c Front fork is in plastic region and had deflected anti-clockwise.

Figure 5.9d Front fork is set to this new initial unloaded position when SIGNFK is negative.

CHAPTER 6

CALIBRATION AND VALIDATION

6.0 Introduction

In order to produce meaningful results from a simulation model, the model needs to be calibrated and validated. This will need realistic data to be put into the model and the result calibrated against a real-life event. In our case this means a full scale crash test. However, in order to develop a model that is capable of simulating events under different situations, it is wise to calibrate the model against crash tests of a variety of different configurations. Four such tests have been carried out at TRL and indeed TRL is the key supplier of material data. After the calibration has been regarded as satisfactory, TRL specified another four track tests for the validation process.

This chapter will describe the data and methodology used in the development stage, the difficulties encountered and subsequent solutions employed during and leading to the completion of the calibration. A description of the validation process will also be given.

6.1 Data Collection

The basic program has been coded in ACSL. Data files describing the construction of a dummy rider and a motorcycle have also been developed using SD/FAST. The combination of software has produced a reasonably well-working simulation model. However, prior to the calibration stage, all the data used, such as the stiffness and damping properties of the front wheel, have to be obtained, by direct measurement or estimated from engineering experience. If one is to aim for more realistic computer simulation one needs realistic data to put into the system. These data were to be provided by TRL.

TRL did provide some typical material data. For the motorcycle, typical areas such as the front wheel and the petrol tank, were chosen for quasi-static impacts in order to obtain force-deflection characteristics. It is obvious that one cannot perform these tests on every inch of the motorcycle, and also the fact that material characteristics will vary depending on different factors such as the impactor, the location, and the speed, thus it would be unrealistic to expect that 'exact' material properties can be obtained for every part of the model. However, whatever data TRL had gathered are used in the model as approximating datum functions say, $f(x)$, and then factors are employed to accommodate different configurations of impacts, such as $2*f(x)$. Some typical results provided by TRL are shown in Figures 6.1, 6.2 and 6.3.

In Figure 6.1 the force-deflection curve of the front wheel of the motorcycle is shown. This is done by placing the front wheel on a test rig where a load was applied to it. One can see the actual curve as recorded by the load cell, but a continuing gradual stiffening function has been added at the end of the tested curve as shown by the 'dashed' part of the curve. This is done so that if the simulation model reaches beyond the tested crushing point of the front wheel, the front wheel is modelled as being increasingly stiff in order to prevent a body apparently passing through another body in the simulation.

Figure 6.2 shows the force-deflection characteristics when a ram loaded the side of the fairing. It shows the crushing and unloading of the first cycle as the ram reached the end of its travel, and subsequent reloadings as the ram was brought forwards for further tests. These readings have all been used to model the fairing characteristics. Note that at the end of the second test, the curve has been extended steeply to model increasing stiffness, as before.

In Figure 6.3 the stiffness-deflection characteristics of the dummy's knee being forced against the side of the petrol tank is shown. The curve is essentially a two-step function with the tank offering no stiffness at one part of the impact. This highlights the total shattering of the fibre glass material. This in itself is not a problem to model, but the step-function nature of the

curve does offer a complication. Since ACSL is a continuous language and the step-function will offer discontinuity into the system, ramping effects have been introduced around the sudden changes of the curve, as shown as the 'dashed' part of the curve in Figure 6.3, in order to minimise the rapid discontinuities of the curve.

TRL also provided data characteristics for the OPAT dummy. They have taken segments of the dummy for impact tests, and the results are in the format of stiffness against deflection, and damping against deflection. Figures 6.4, 6.5, 6.6 and 6.7 show some of these recorded curves. Note that on the the deflection axes are the recorded 'normalised' deflection defined as

$$\frac{R - d}{R}$$

where R = radius of the segment
and d = compressed displacement.

This has the effect of representing the non-contact situation when $(R-d)/R > 1.0$, on the point of contact when $(R-d)/R = 1.0$, and during contact when $(R-d)/R < 1.0$.

In Figures 6.4a and 6.4b the recorded stiffness and damping values of the dummy's pelvis against normalised deflection are shown respectively. Similarly, the stiffness and damping

characteristics of the helmetted head, the upper leg and the knee are shown in Figures 6.5a and 6.5b, 6.6a and 6.6b, and 6.7a and 6.7b respectively.

As one can observe, the femur can be compressed more deeply than the rest of the samples, whereas the pelvis offered more resistance. Damping curves were obtained from tests using a series of drop heights and fitting the best approximate curve to the recorded values. In the simulation program the start and end points have been accommodated by quoting the same starting value at a point where $(R-d)/R \geq 1.0$, say 1.5, and quoting an even higher value than the last available compressed reading. This is done so that ACSL can extrapolate values beyond the range, if necessary.

As the data provided by TRL are mostly in graphical form, they were digitised and converted into their representative numerical forms. These were typed into the program in the form of tables and accessed where appropriate.

A note about accessing these tables as data functions in the program is needed. We must bear in mind that these data functions are limited, and indeed they are only basic guides of their particular materials tested from either one, or several different conditions from which the best fitted estimates were derived. Therefore in the event of different configuration of impacts,

namely impact angle and speed, factors are used to maximise or minimise these data functions. In addition, due to the limited available data, i.e. some parts of the motorcycle have not been tested, therefore a made-up table, based on prior knowledge and engineering experience, has been constructed and used as datum. Such an example is the motorcycle seat.

After all the relevant data have been gathered and inserted into the program, the model is ready to run with both the dummy and the motorcycle now described as having tested values. The results produced will need to be compared with data from real track tests thus adjustments could be made to the various factors, so that good correlation of overall behaviour could ensue. This is then the reason for carrying out a calibration exercise.

6.2 Calibration

TRL has specified the following four different configurations of impacts of a standard motorcycle, for the calibration, they are:

<u>Run</u>	<u>Impact Angle</u> <u>(in degrees)</u>	<u>Velocity</u> <u>(in miles per hour)</u>	<u>Velocity</u> <u>(in metres second)</u>
1	90	30	13.4
2	60	30	13.4
3	60	20	8.9
4	30	30	13.4

TRL then carried out these four full scale crash tests and supplied filmed videos and photographic frames of the tests. In addition, they have also supplied displacement, velocity and acceleration information on various parts of the dummy rider and motorcycle. These are in graphical forms. TRL extracted the displacement data from high speed film. This is done by digitising a particular location on the subject, where a marker is placed, through a succession of continuous still frames. The function obtained is then differentiated to obtain velocity.

Based on the information provided, the program was then edited accordingly to the different configuration and run. Typical CPU times, depending on the different configuration, can vary from 3 to 10 hours. This vast difference in CPU time is very dependent on the type of impact and the travelling speed. For example, run 3 was found to take 3 hours to complete, whilst run 1 took 10 hours. This is because the travelling speed in run 3 is 10 miles per hour less than that of run 1, which means that events occurred more slowly and in the simulation larger time steps were possible. In addition, run 1 being a head-on impact, invariably means that all activities can only revolve around the pitching axis, unlike the oblique impacts where motion about all three axes will take place.

The output results were examined in two different forms. One form involved the comparisons of the simulated result, in graphical

curves, with the digitised curves supplied by TRL. The other used simple computer graphics packages [26] and [27] to display rider and motorcycle movements in animated form, for comparison with the film video and photographic frames supplied by TRL.

The four simulation models were of course being continuously updated, whenever discrepancies were found after comparing with TRL's data. It was a time-consuming process to refine the model so that the program could produce a simulation as closely matching as possible to the real crash test. Usually an update involved only one or two parameters to be changed, such as when the simulated front wheel is seen to have bounced off the barrier too rapidly as compared to the real test, a consideration then could be a higher value for the coefficient of friction between the wheel and the barrier. However, one must be prepared for the fact that there is a limited degree in which a computer model can re-produce the real event of necessity as the model contains simplifications and approximations.

It was also discovered that reliable inputs played a critical role in computer modelling. It may be obvious to the reader that this should be the case, but a slight variation in say, the angle of impact, will contribute to a major difference say, in the simulated motorcycle's trajectory but which may or may not be so in real life. Since the present simulation model is limited in its degree of realism, therefore it is essential that sensible

inputs are used in order to produce sensible outputs.

During the development process it was discovered that the runs specified by TRL had deviated somewhat during their crash runs. It is obvious that a crash test may not be carried out at exactly the specified angle of impact, or the specified speed, or both. This has certainly happened to the four runs and the following are the revised configurations.

<u>Run</u>	<u>Impact Angle</u> <u>(in degrees)</u>	<u>Velocity</u> <u>(in miles per hour)</u>	<u>Velocity</u> <u>(in metres second)</u>
1	90	27.4	12.4
2	57	27.96	12.5
3	50	20.58	9.2
4	30	30.87	13.8

Furthermore, the digitised and differentiated curves on the various parts of the two subjects proved to have been unreliable. In a computer model, it is a simple task to extract dynamical information say, of the motorcycle centre of gravity, but in a real-life event, it is highly unlikely that a marker is put on the exact position of the centre of gravity of a motorcycle, thus the nearest sensible position, in preparation for film digitising, is chosen. However, this misplaced position will produce different dynamical information if compared to the simulated information of the motorcycle centre of gravity.

These are some of the inconsistencies found but revised during the calibration stage. In addition, it had also been a process of further developing the model. In the simulation, the motorcycle is constructed with panels of planes onto which the rider can impact. The necessary ones have already been constructed, such as the seat and the fairing planes, but it was observed during an oblique impact, that the dummy's nearside leg penetrated through the engine area of the motorcycle. This is obviously not possible in real life and had not been anticipated, thus two extra planes have been inserted onto the sides of the engine to model such eventual contacts.

Another example was the impact between the dummy's lower legs and the knee-restraints. The lower legs have been modelled to be capable of impact onto the knee-restraints, if it should occur, but on further examination it was seen the lower legs still penetrated too deeply into these planes. This is because there was only one targetted area, namely the centre of gravity on each lower leg, modelled for impact, thus leaving areas lower than this point having no resistance for compression. Having made this observation, a further location, around the ankle area, was made to be capable for impacting onto the knee-restraints.

The above is a general summation of the effects made and lessons learnt during the calibration stage. With regards to the overall allowable impact areas for both the dummy rider and the

motorcycle at the present stage, consider Figures 6.8, 6.9 and 6.10.

In Figure 6.8 the potential contact areas of the dummy for impacting onto the barrier or motorcycle is shown. Each area uses the data supplied by TRL and is given a radius to represent the compressible depth of the flesh. Figure 6.9a shows the impact areas of the motorcycle for impacts onto the barrier and the road. These can happen in both frontal and oblique impacts. Figure 6.9b shows the impact areas of the motorcycle in the case of side impact onto the barrier.

In Figure 6.10 possible impacts between the dummy rider and the motorcycle are shown. For illustrative purpose only the springs and dampers on one side of the motorcycle are shown. As can be seen this concentrated mainly on the leg areas of the dummy, but the pelvis and the lower torso are also constructed for possible contacts on the rear end and upper surface of the petrol tank.

After various modifications the model had reached the stage where the programs could be considered to produce simulation results of a reasonable qualitative nature. One can continue endlessly to achieve even more realistic simulated representation, but one also needs to judge procedures accordingly, and of course with factors such as time and costs, an exit from the calibration stage must occur. To illustrate the final results from the four

simulations, consider Figures 6.11, 6.12, 6.13, 6.14 and 6.15.

Figure 6.11 shows the pelvis fore-and-aft displacement for runs 1 to 4. Figure 6.12 shows the corresponding velocities. Similarly, the head fore-and-aft displacement for runs 1 to 4 are shown in Figure 6.13, and Figure 6.14 contains the corresponding velocities. In each case the graph starts just prior to front wheel impact onto the barrier and ends just after head impact. It may come to the reader's attention that the simulated displacement, in general, is a better match to TRL's data than that of the simulated velocity. This is in accordance with the well-known fact that acceleration is usually not smooth, but as integration is applied within ACSL, the subsequent function is effectively filtered. This explains the good match for the displacement. As for the velocity, since the velocity data TRL supplied is obtained by digitising through a succession of film data to obtain displacement and then differentiated, it will invariably introduce mathematical noise thus the degree of correlation is not as close as that for the displacement.

Figure 6.15 shows the front wheel impact force on the barrier for the four runs. In run 1 where the angle of impact is 90° one can see the front wheel being progressively crushed against the barrier as the wheel and forks collapsed towards the end of the simulation. In both run 2 and run 3 where the angle of impact is 60° one can see that the front wheel had struck onto the barrier

with highest force at the beginning of the impact, but oscillated down in value towards the end. This is consistent with the front wheel striking the barrier but then yawing away from the barrier. Notice the peak values where they also demonstrated the contributory factor of the impact velocity. In run 4 where the angle of impact is 30° the front wheel is seen to strike hard onto the barrier but yawed away rather quickly.

The above are the results in numerical graphical forms. To demonstrate the other technique used in comparing results, consider the Geomview [27] computer graphics package frames in Figures 6.16, 6.17, 6.18, 6.19 and 6.20. Note that the red lines form the frame of the dummy rider, the green lines form the structure of the motorcycle with line segments representing the petrol tank, and the blue lines represent the confined space of impact and the height and angle of the barrier.

In Figure 6.16 run 1 is shown 50ms into the impact. This is around the period where the front wheel and the front forks collapsed. In Figure 6.17 run 2 is shown 100ms into impact. One can see the motorcycle had rolled and yawed. In Figure 6.18 run 3 is shown 100ms into impact. As can be seen, the motorcycle had started to yaw away from the barrier, but the rider was still travelling in the fore-and-aft direction. In Figure 6.19 run 4 is shown 50ms into impact. There we could see the front wheel had left the barrier and started to yaw away.

In Figure 6.20 a sequence of events in run 1 is shown. Each frame is separated by 20ms. One can observe the front wheel hit the barrier, then being crushed, along with front forks, by the barrier. This caused the dummy rider making frontal contact with the petrol tank and the knee-restraints. As the motorcycle pitched this produced a torque causing the dummy to swing forwards towards the barrier.

6.3 Validation

For the validation stage, TRL had specified the following four configurations of impacts of a motorcycle with leg protection device attached, and they are:

<u>Run</u>	<u>Impact Angle</u> <u>(in degrees)</u>	<u>Velocity</u> <u>(in miles per hour)</u>
1	90	40
2	60	10
3	45	40
4	30	30

Having learnt the lesson of discrepancy in input, actual angles of impact and velocities at the instant of impact were checked against TRL's staged crash tests, and they have been revised in the following table.

<u>Run</u>	<u>Impact Angle</u> <u>(in degrees)</u>	<u>Velocity</u> <u>(in metres second)</u>
1	88	17.3
2	60	4.5
3	45	16.3
4	30	12.0

These configurations were fed into the computer program and run. Since this is similar to a test case, with only the knowledge learnt during the calibration process, it has been just a process of relying on judgement and experience to determine whether each simulation is reasonably representative of the intended impact, the output data were then passed on to TRL. In general, three of the runs seemed to perform correctly, the exception being run 1.

In run 1 the revised angle is 88° . This was put as the barrier angle in the program. However, the subsequent simulation is that when the motorcycle first struck onto the barrier, with the contributory factor of high speed, the whole front wheel yawed rapidly away from the barrier in an almost right angle fashion. This led to the dummy rider hitting the motorcycle at a near frontal impact on its nearside body thus producing a torque swinging the motorcycle away from the barrier. In a real-life event a 2° discrepancy from a frontal impact may or may not produce such a dramatic impact. However a mathematical model is sensitive and an impact angle of 88° or 92° represents a bi-stable region when slightly out of the exact head-on angle of 90°

would lead to the events happening on one side or the other. This is a critical region but if the discrepancy was $\pm 5^\circ$ subsequent events may be more stable. This led to the decision of quoting impact angle say, θ , in the range $85^\circ < \theta < 90^\circ$ to be exactly 90° in future work. The full details of the calibrations and validations were presented to TRL in [23] and [24].

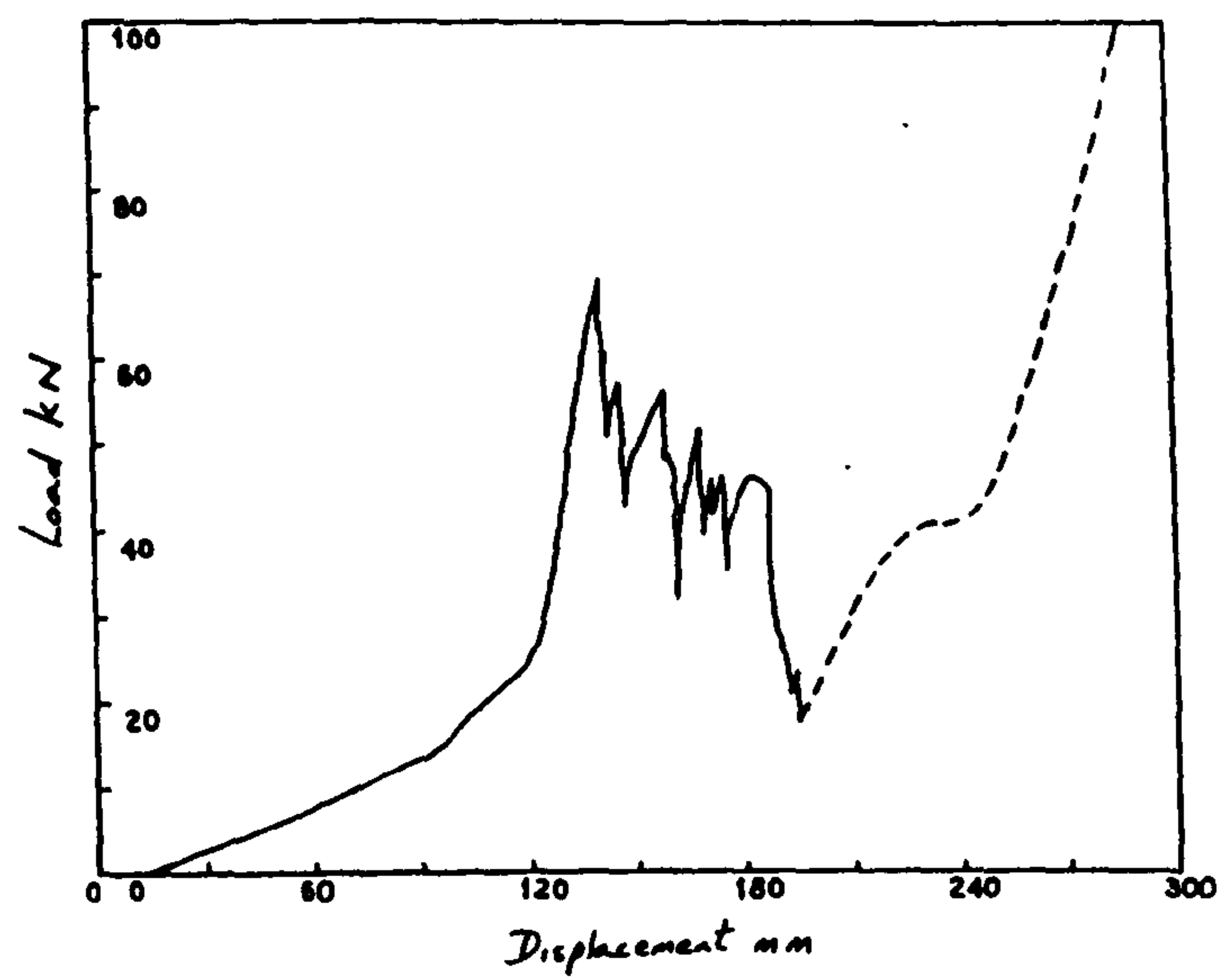


Figure 6.1 Force-deflection curve of the front wheel.

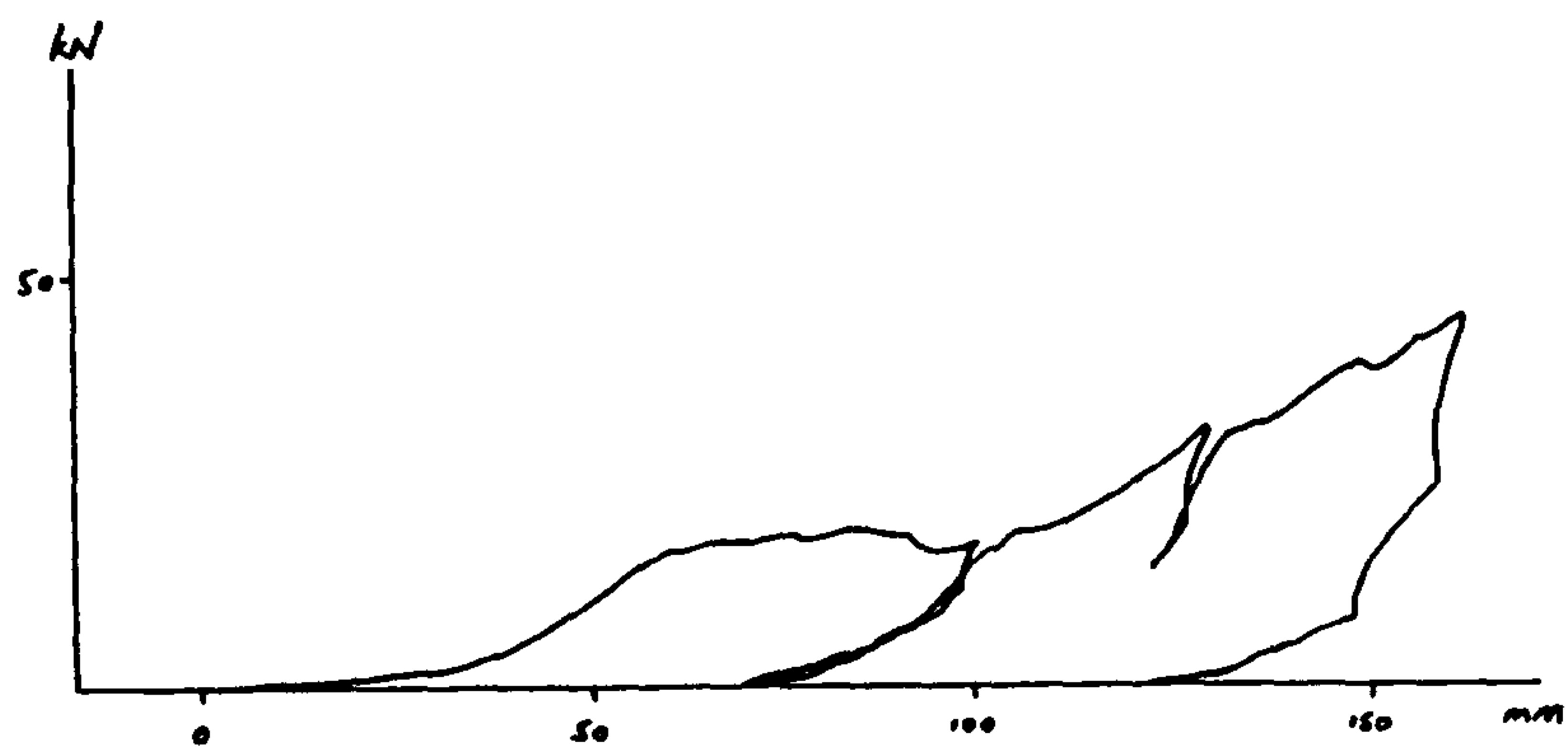


Figure 6.2 Force-deflection curve of the fairing.

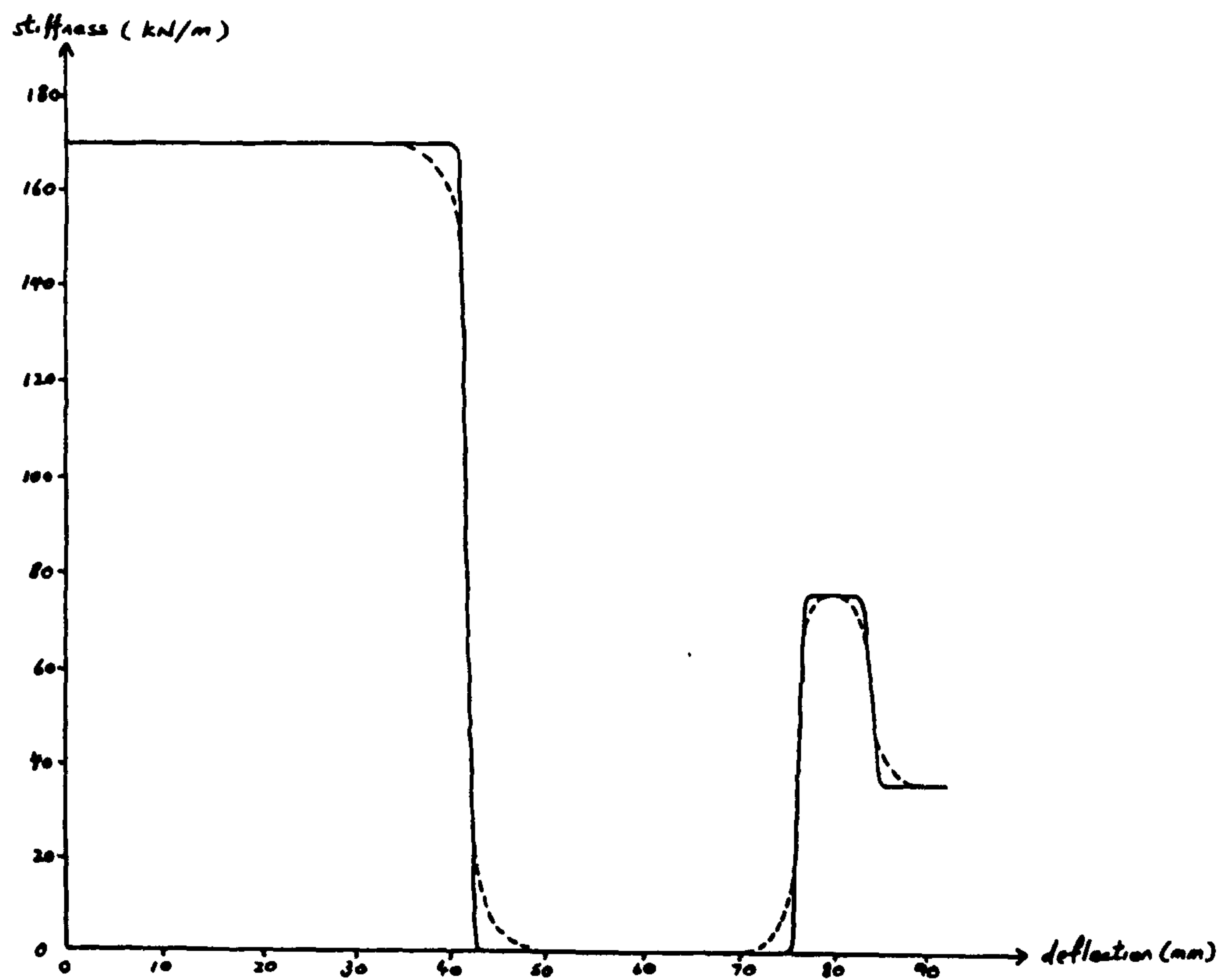


Figure 6.3 Stiffness-deflection curve of the knee against the petrol tank.

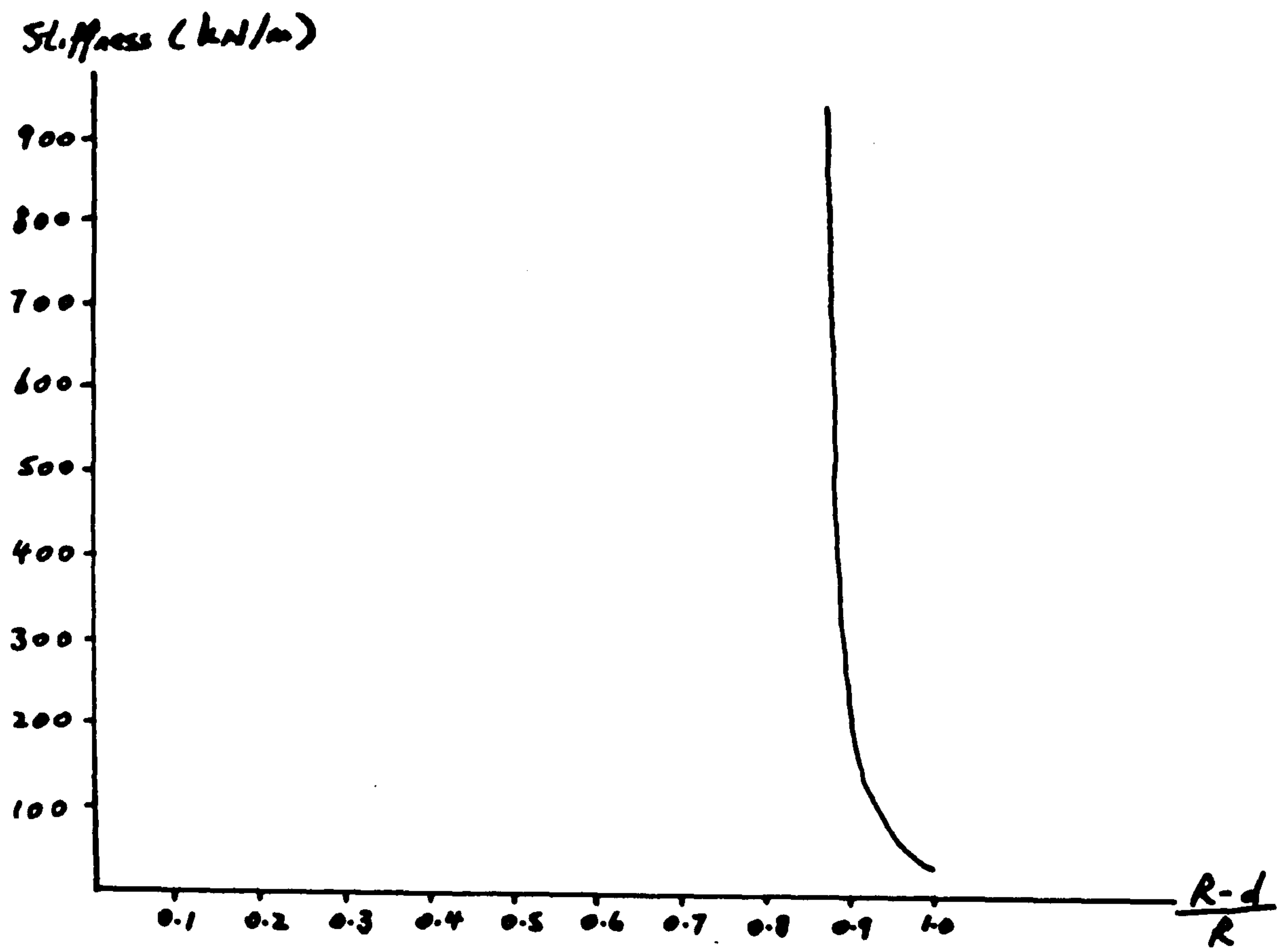


Figure 6.4a Stiffness against normalised deflection of the pelvis.

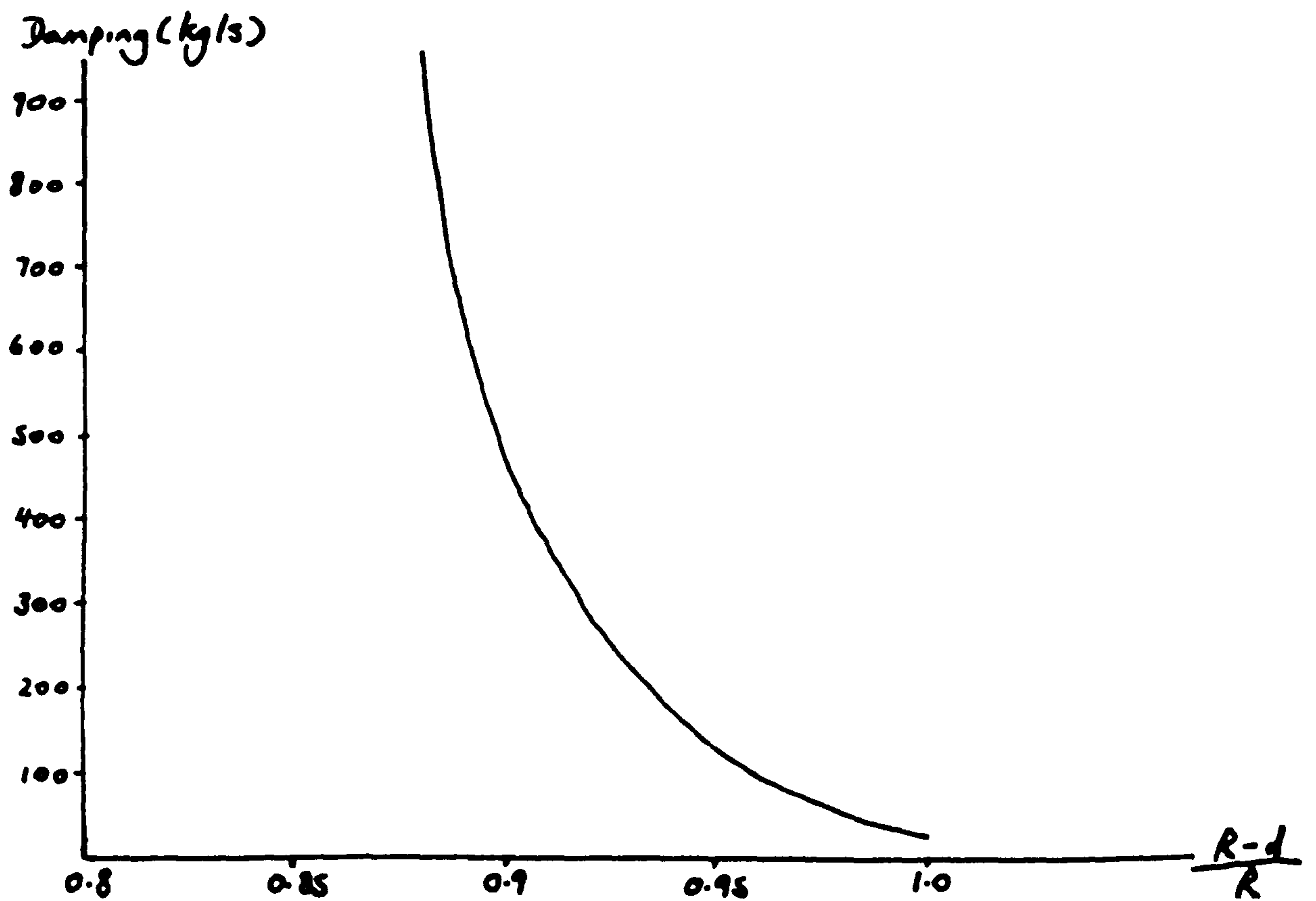


Figure 6.4b Damping against normalised deflection of the pelvis.

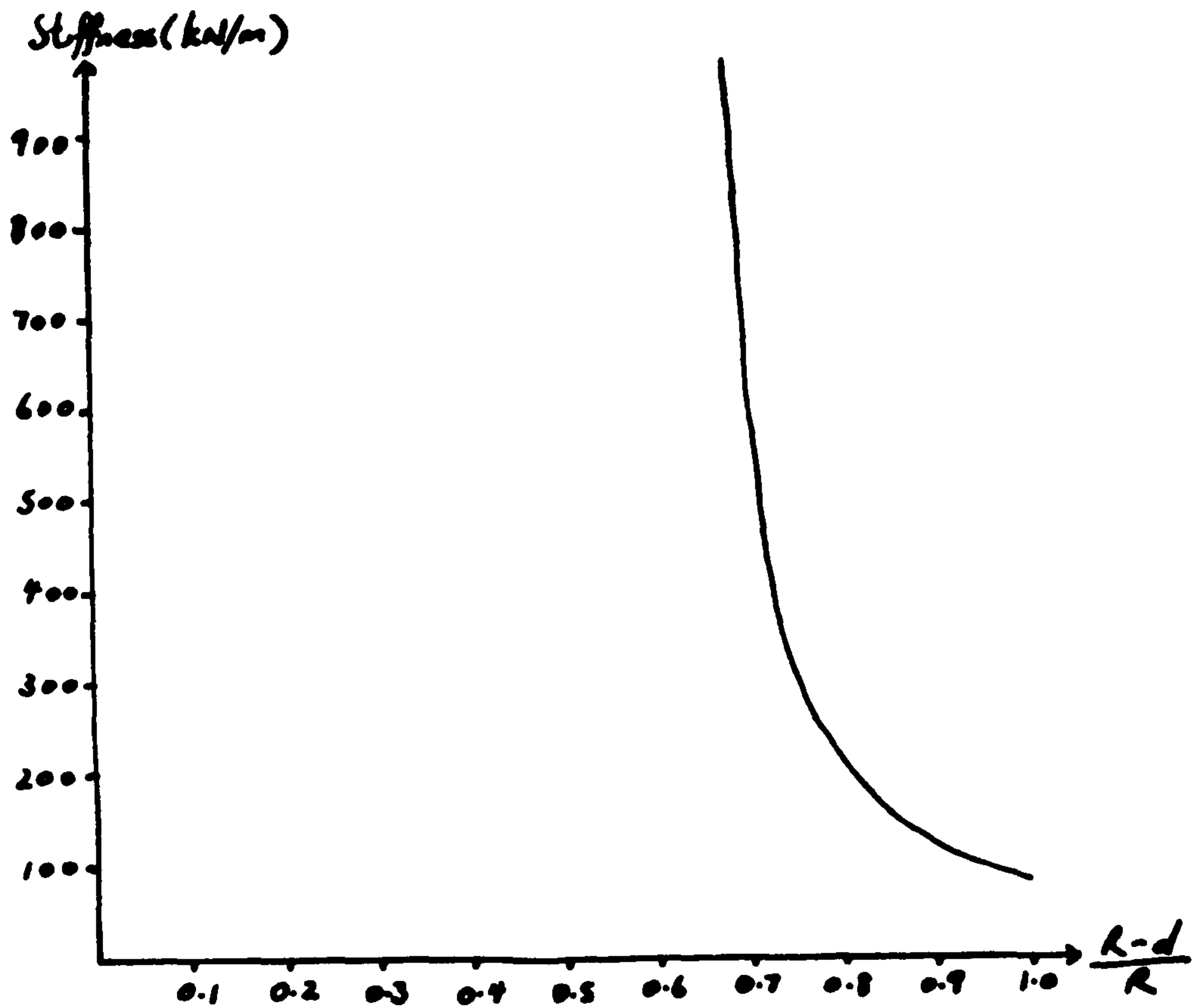


Figure 6.5a Stiffness against normalised deflection of the helmetted head.

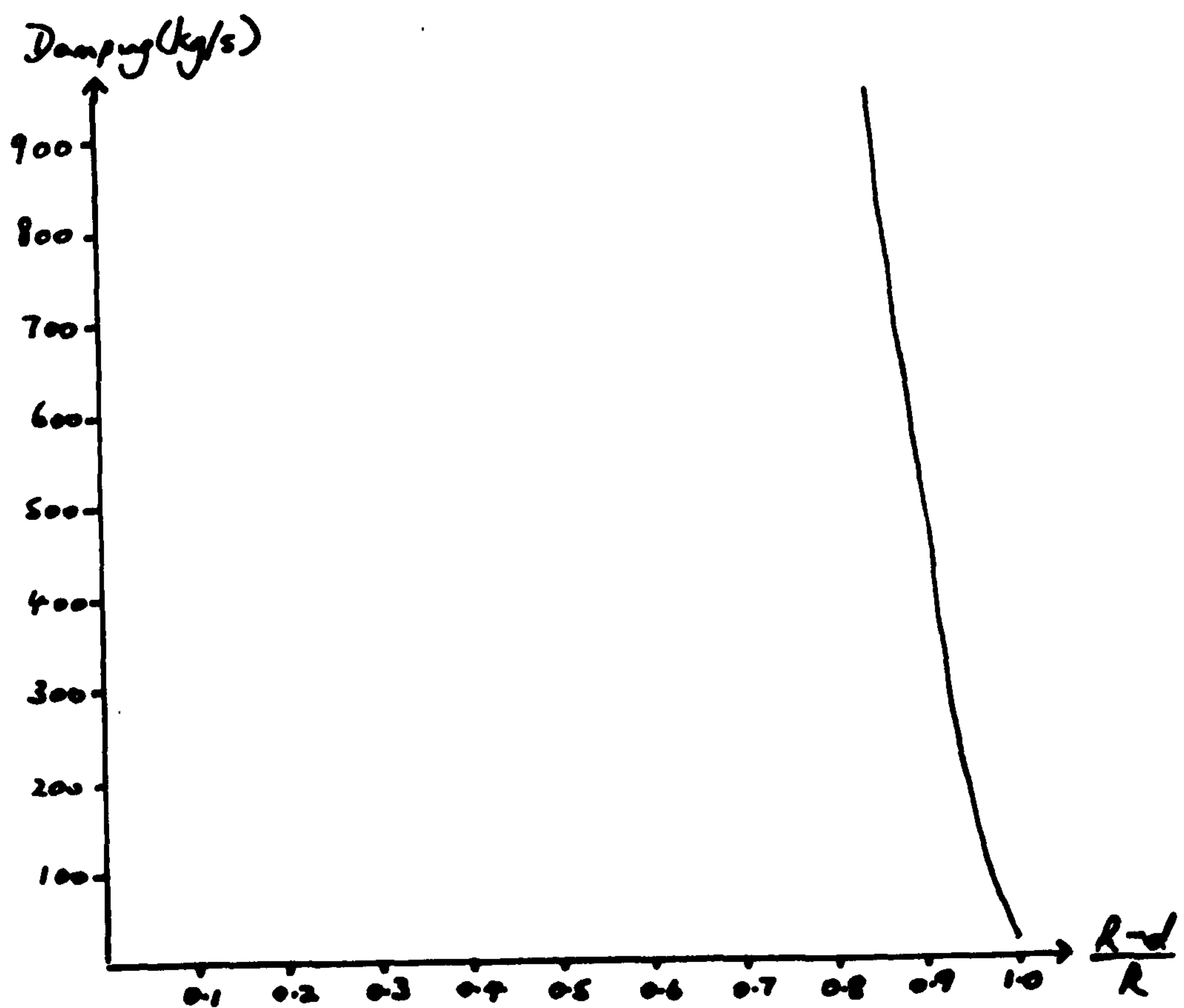


Figure 6.5b Damping against normalised deflection of the helmetted head.

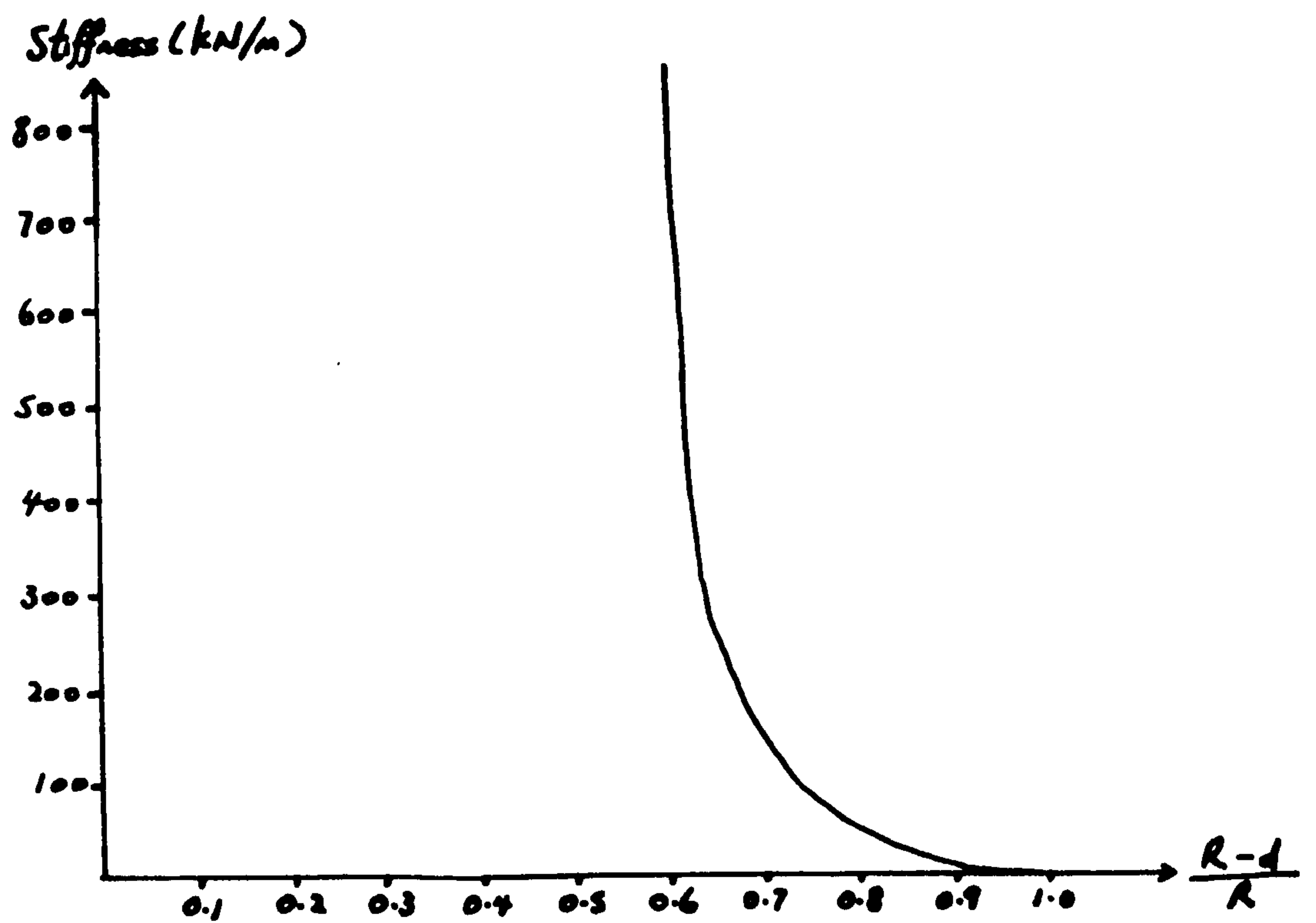


Figure 6.6a Stiffness against normalised deflection of the upper leg.

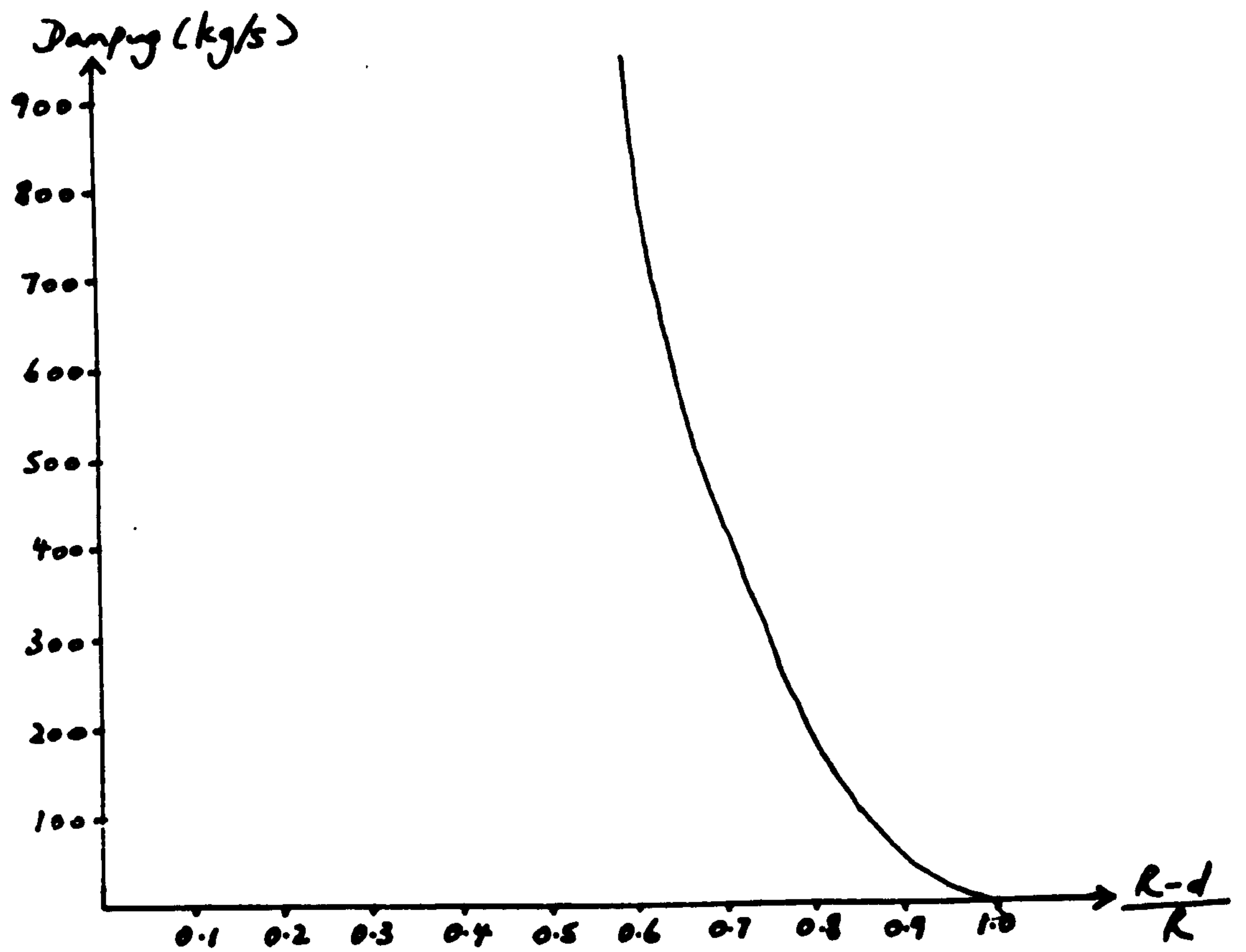


Figure 6.6b Damping against normalised deflection of the upper leg.

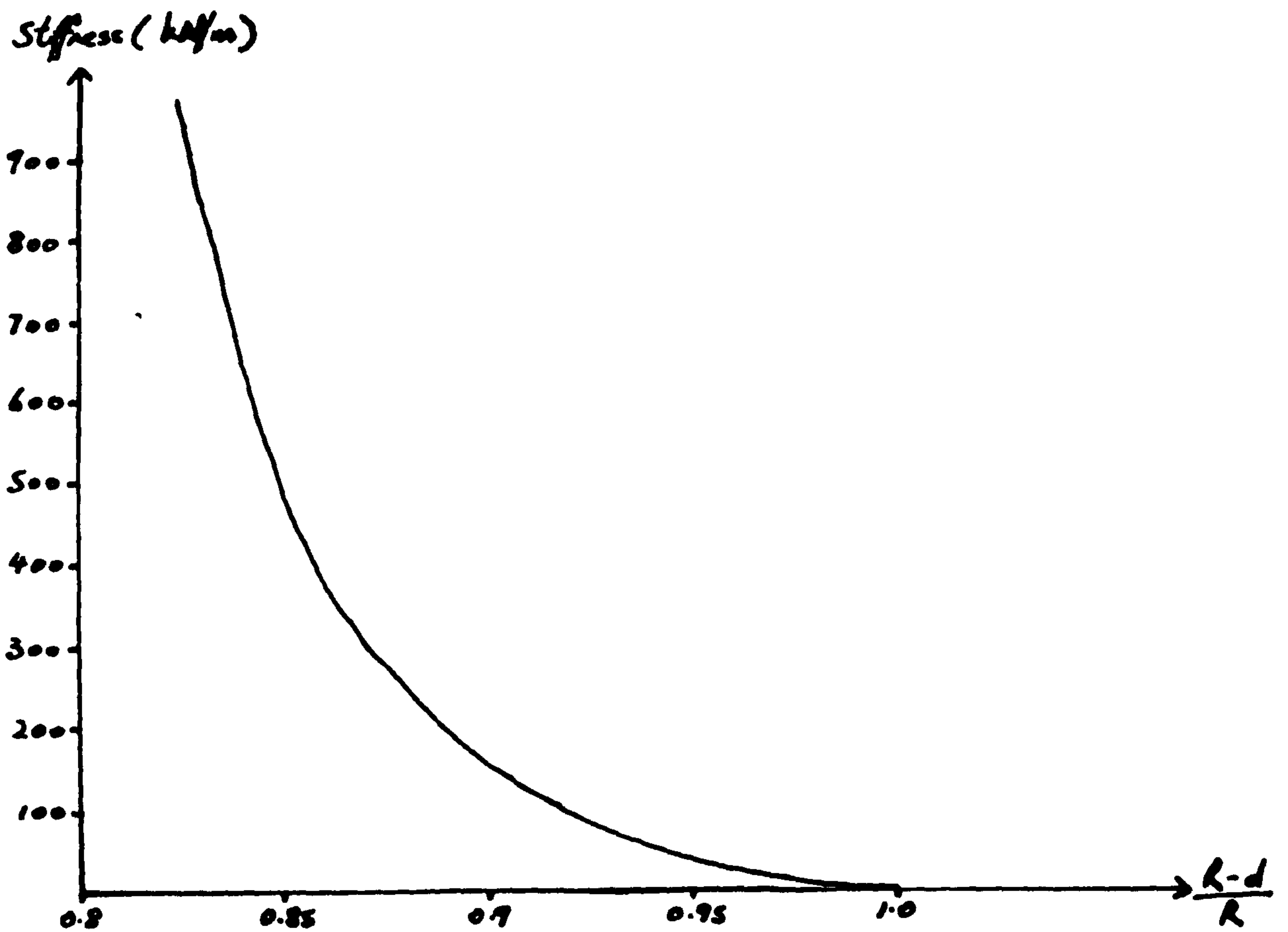


Figure 6.7a Stiffness against normalised deflection of the knee.

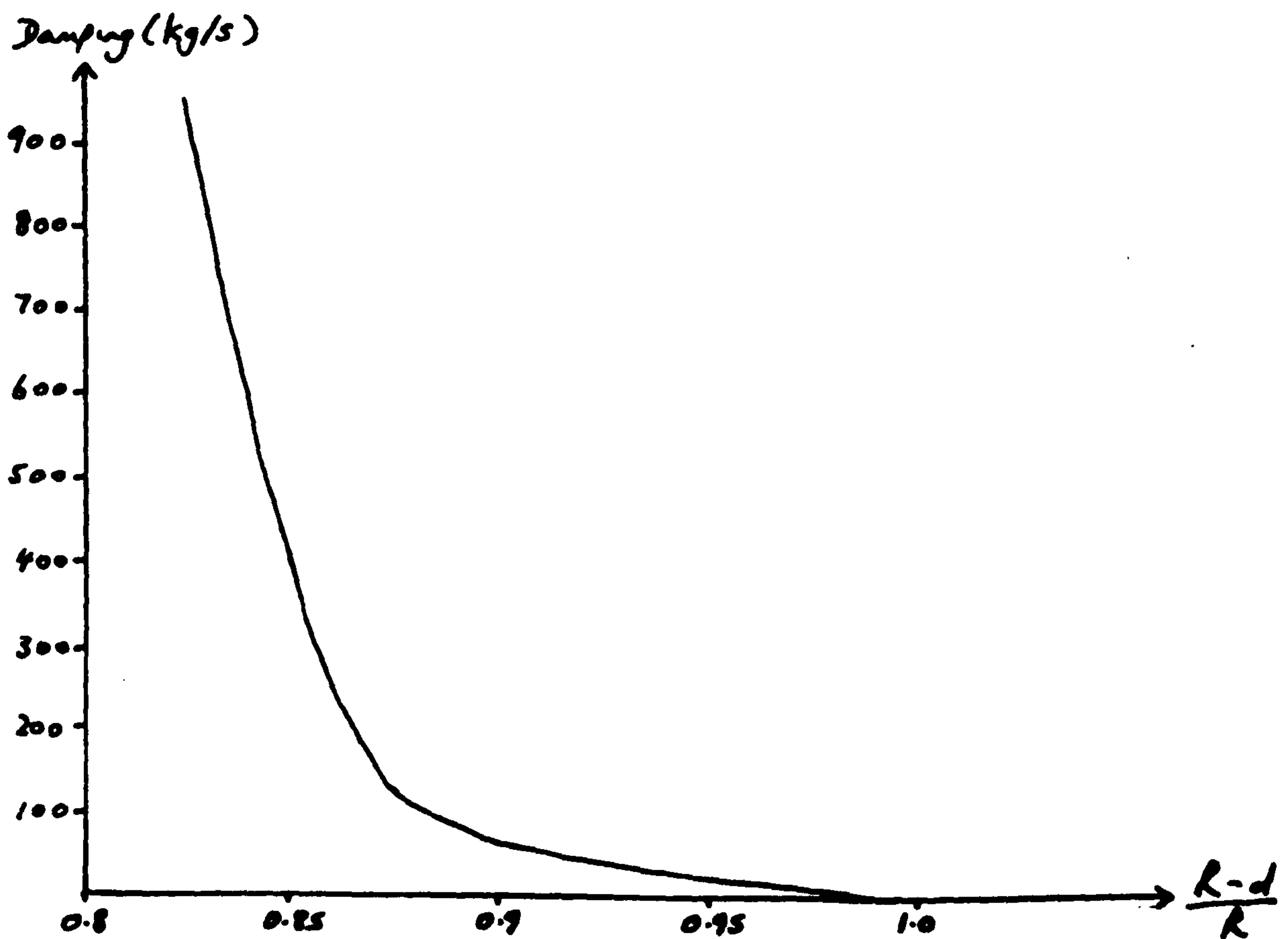


Figure 6.7b Damping against normalised deflection of the knee.

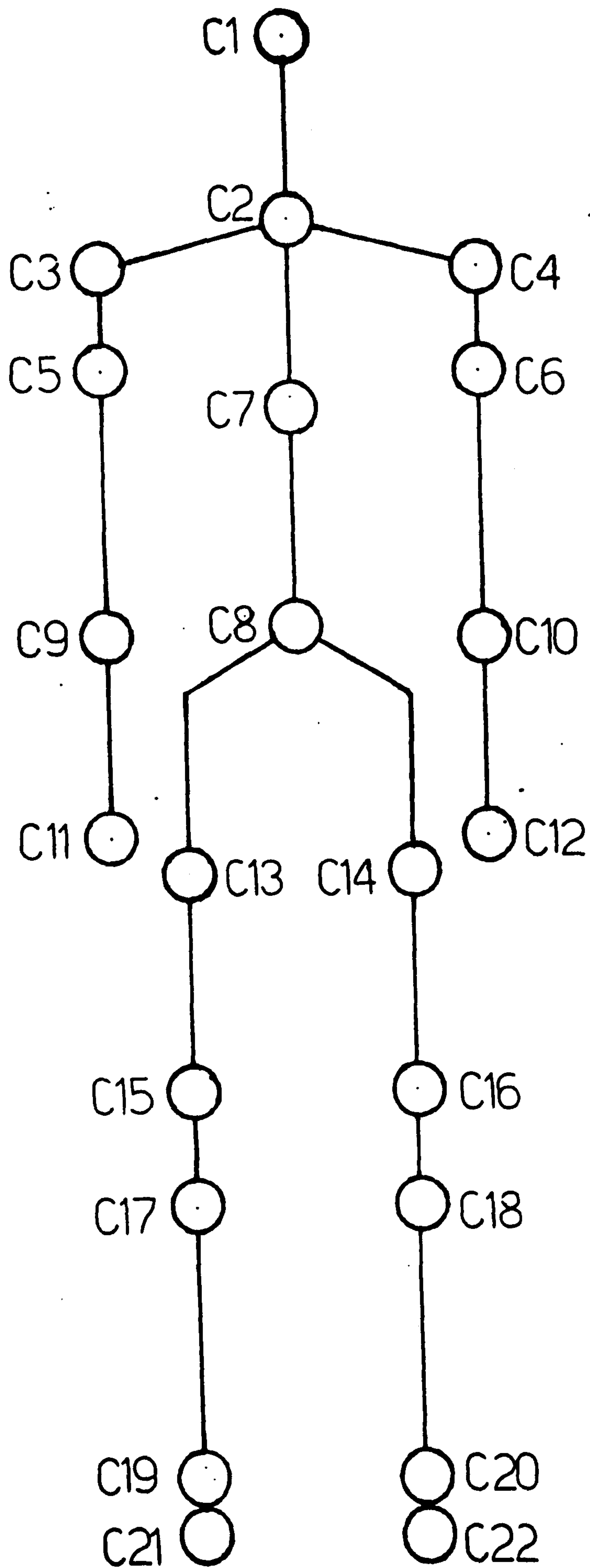


Figure 6.8 Potential contact areas on the dummy for barrier and motorcycle impacts.

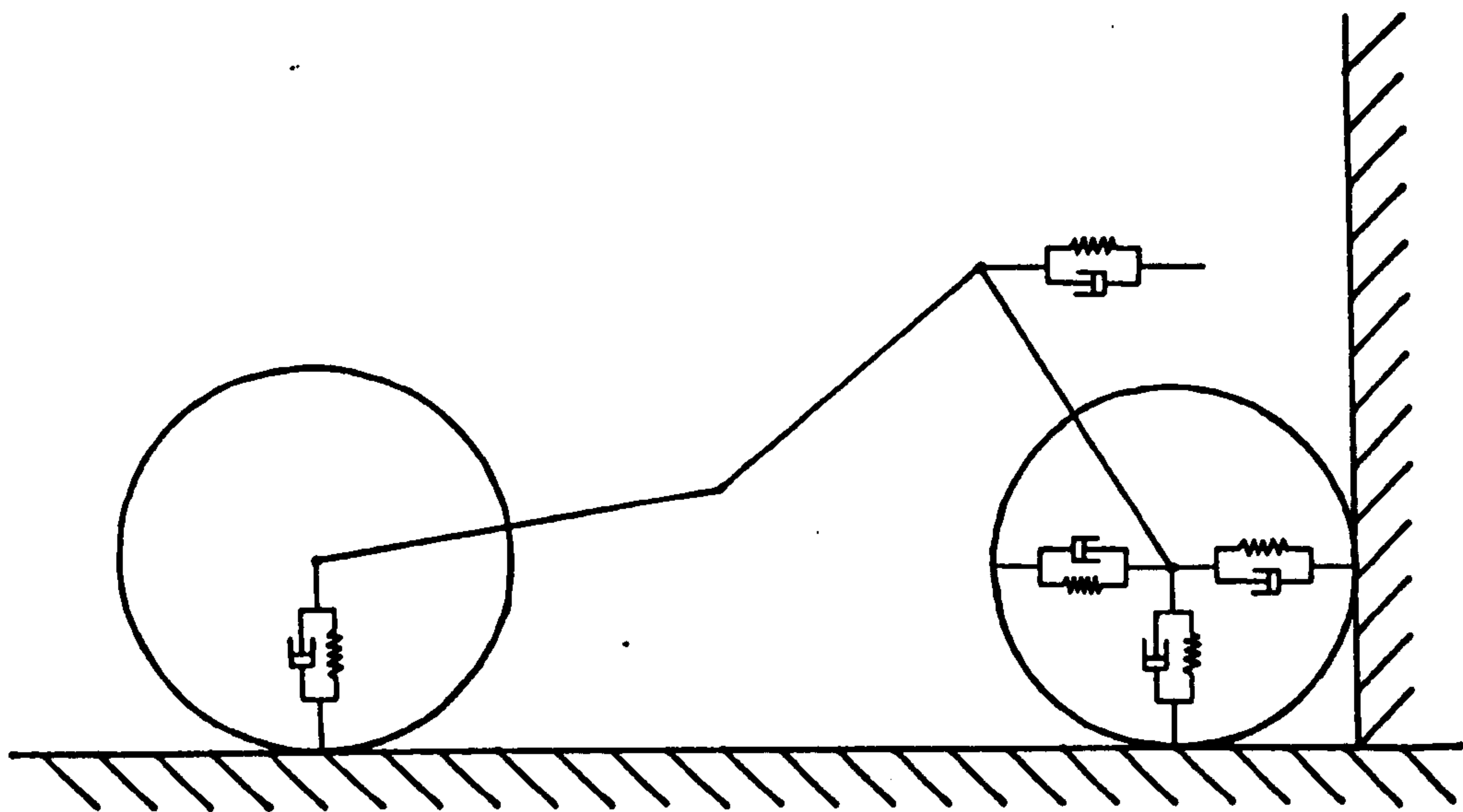


Figure 6.9a Potential contact areas on the motorcycle for frontal and oblique barrier impacts.

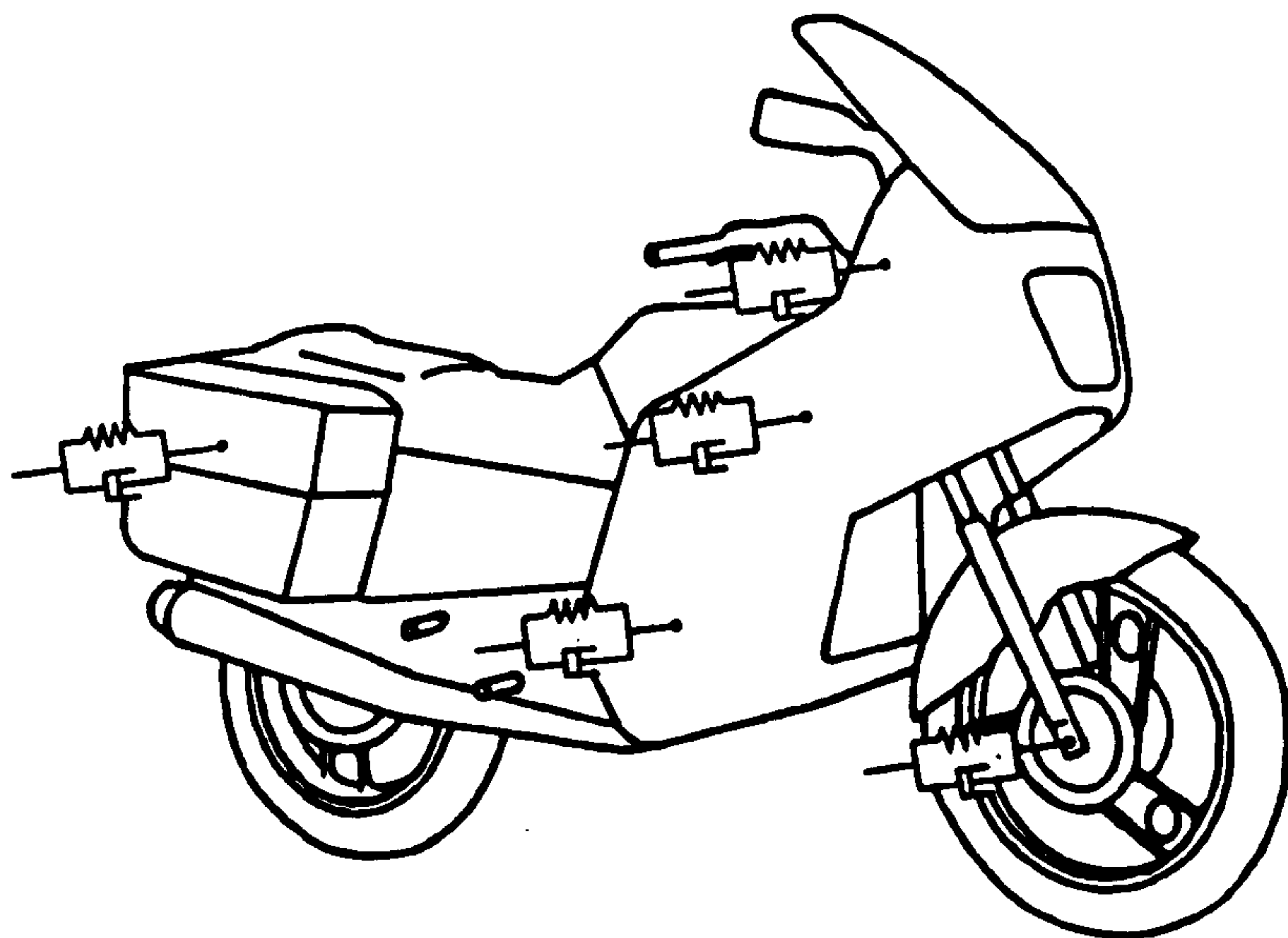


Figure 6.9b Potential contact areas on the motorcycle oblique barrier impacts.

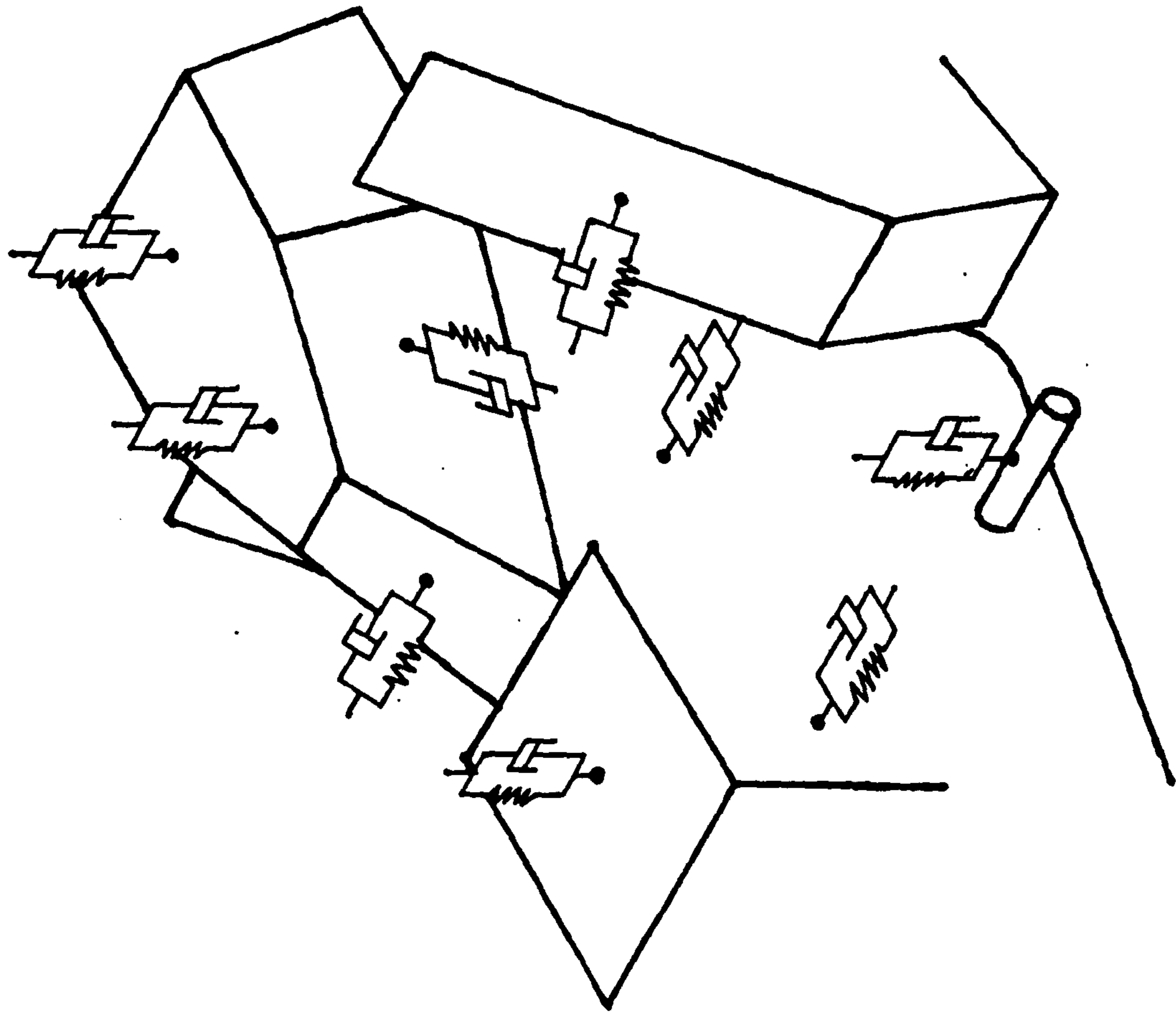


Figure 6.10 Possible impacts between dummy and motorcycle.

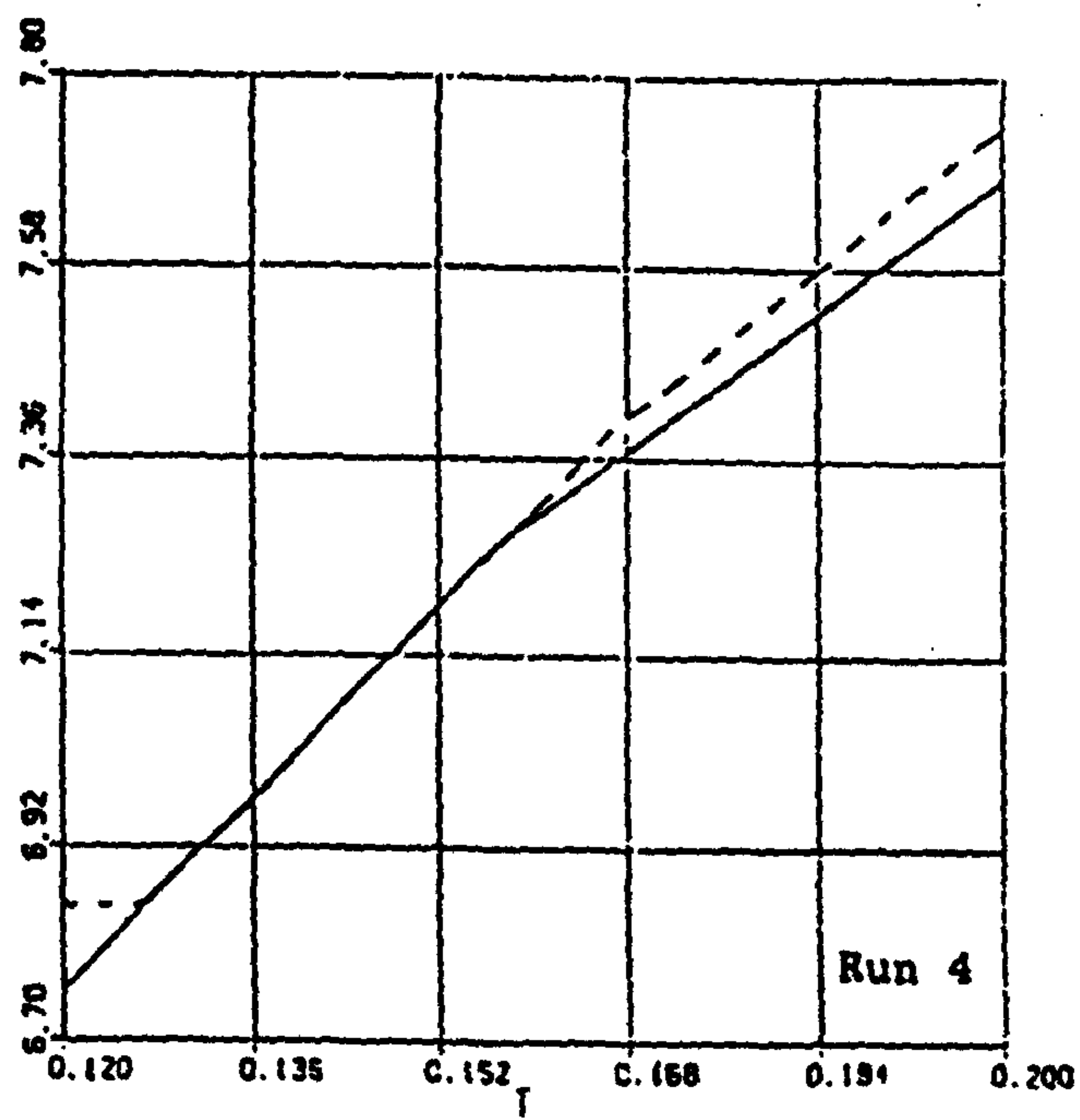
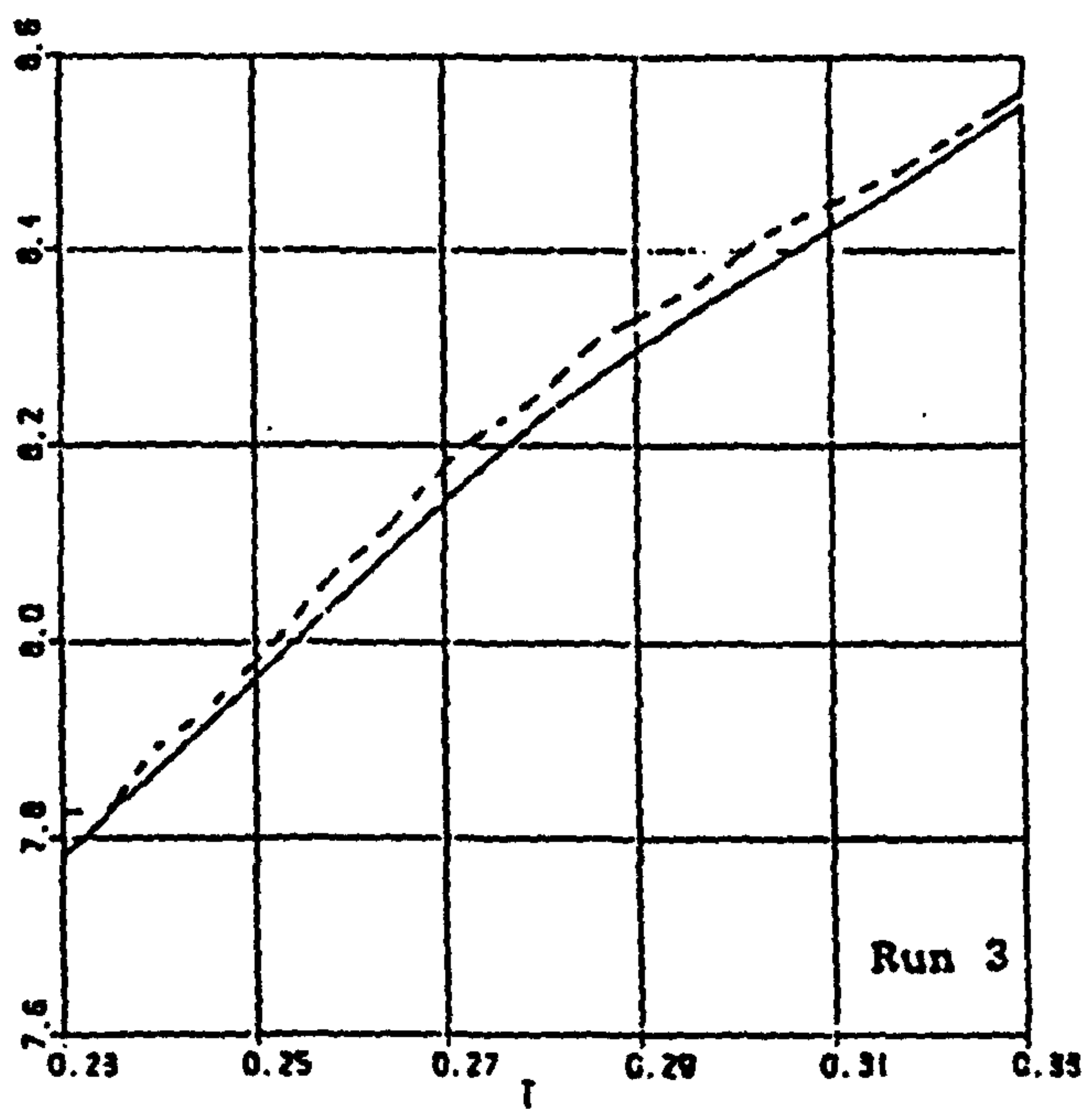
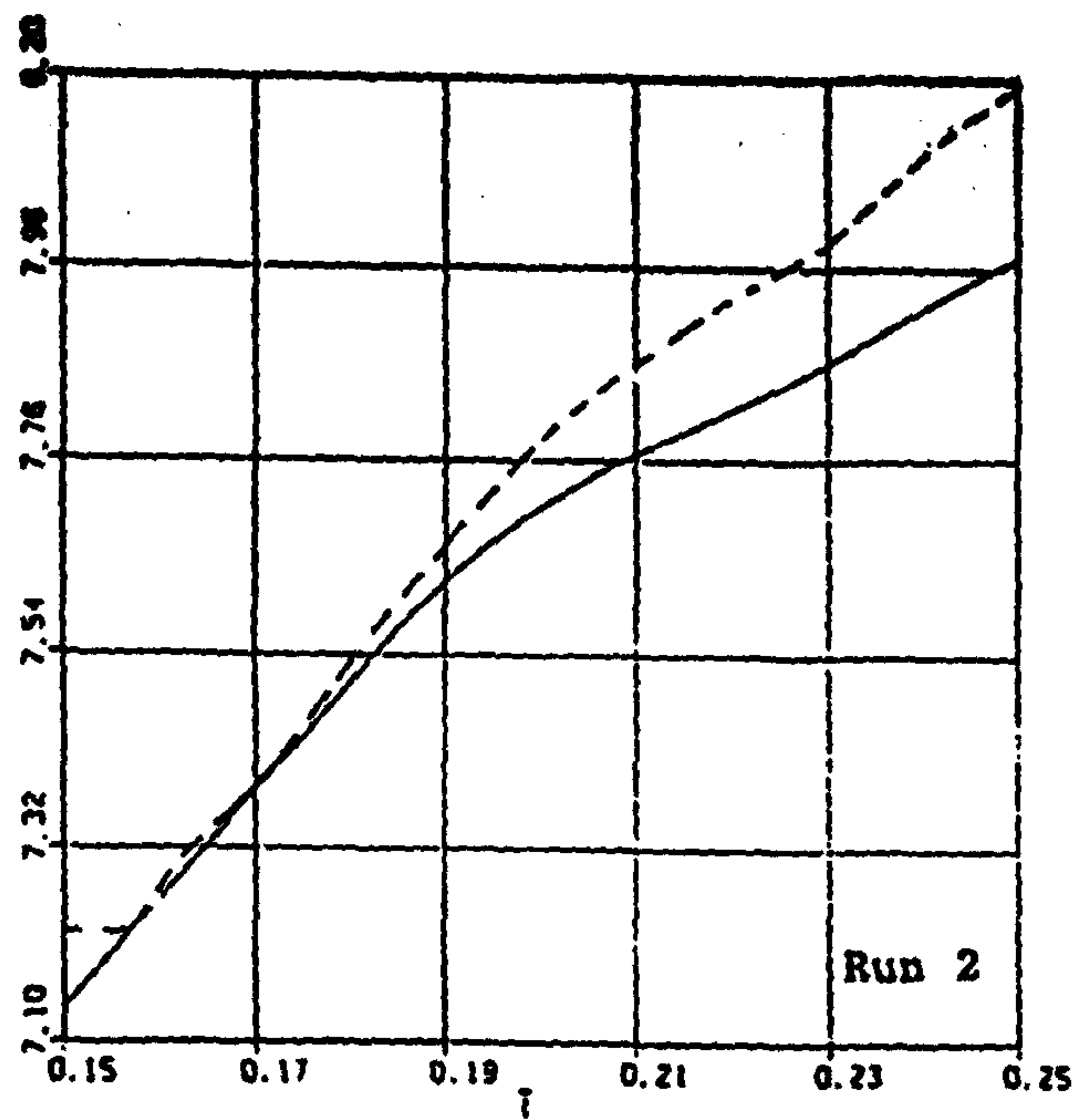
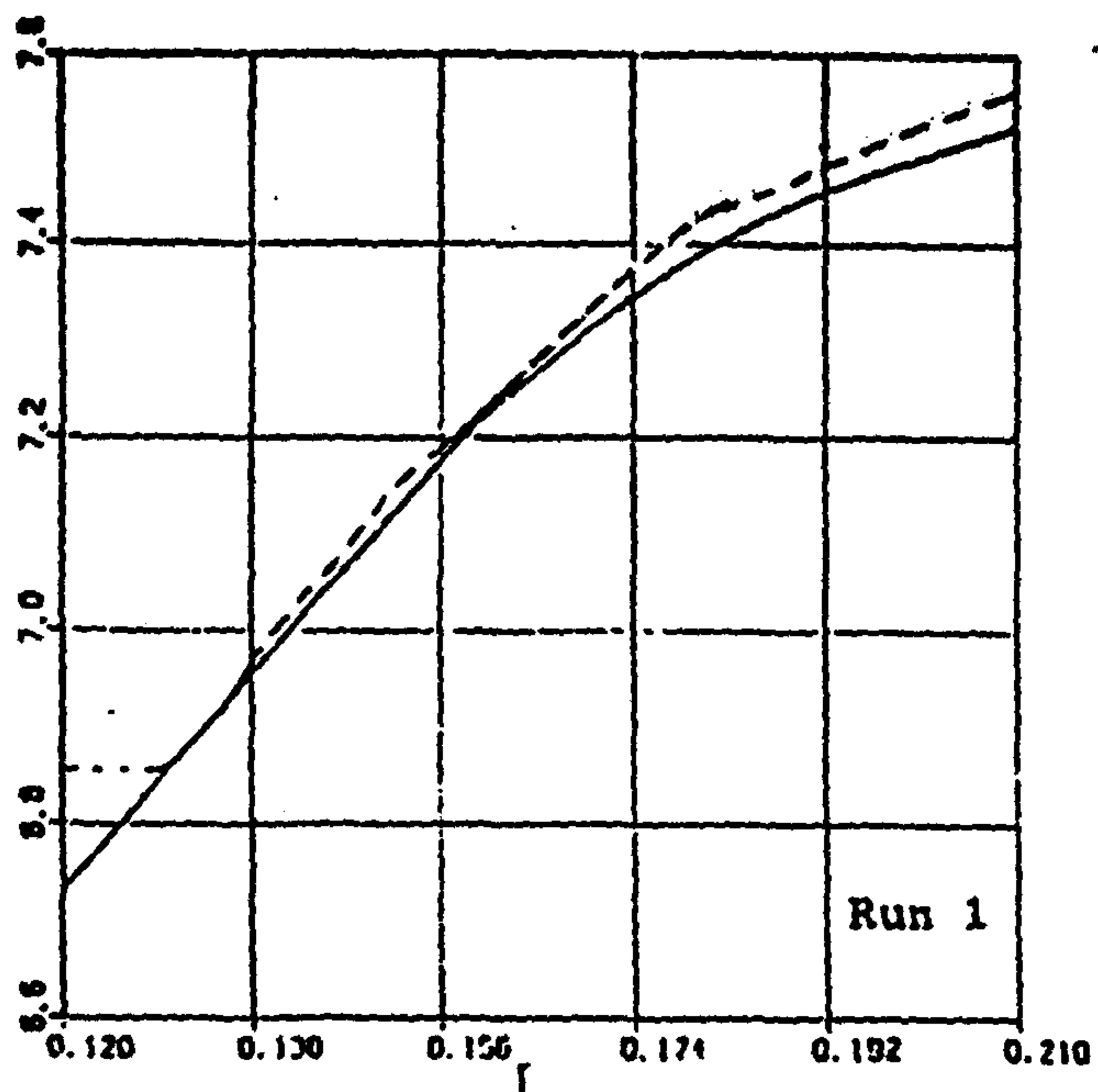


Figure 6.11 Pelvis fore-and-aft displacement (m) against time (s) for runs 1 to 4, from just before front wheel impact to just after head impact. Simulation — , from film data ---.

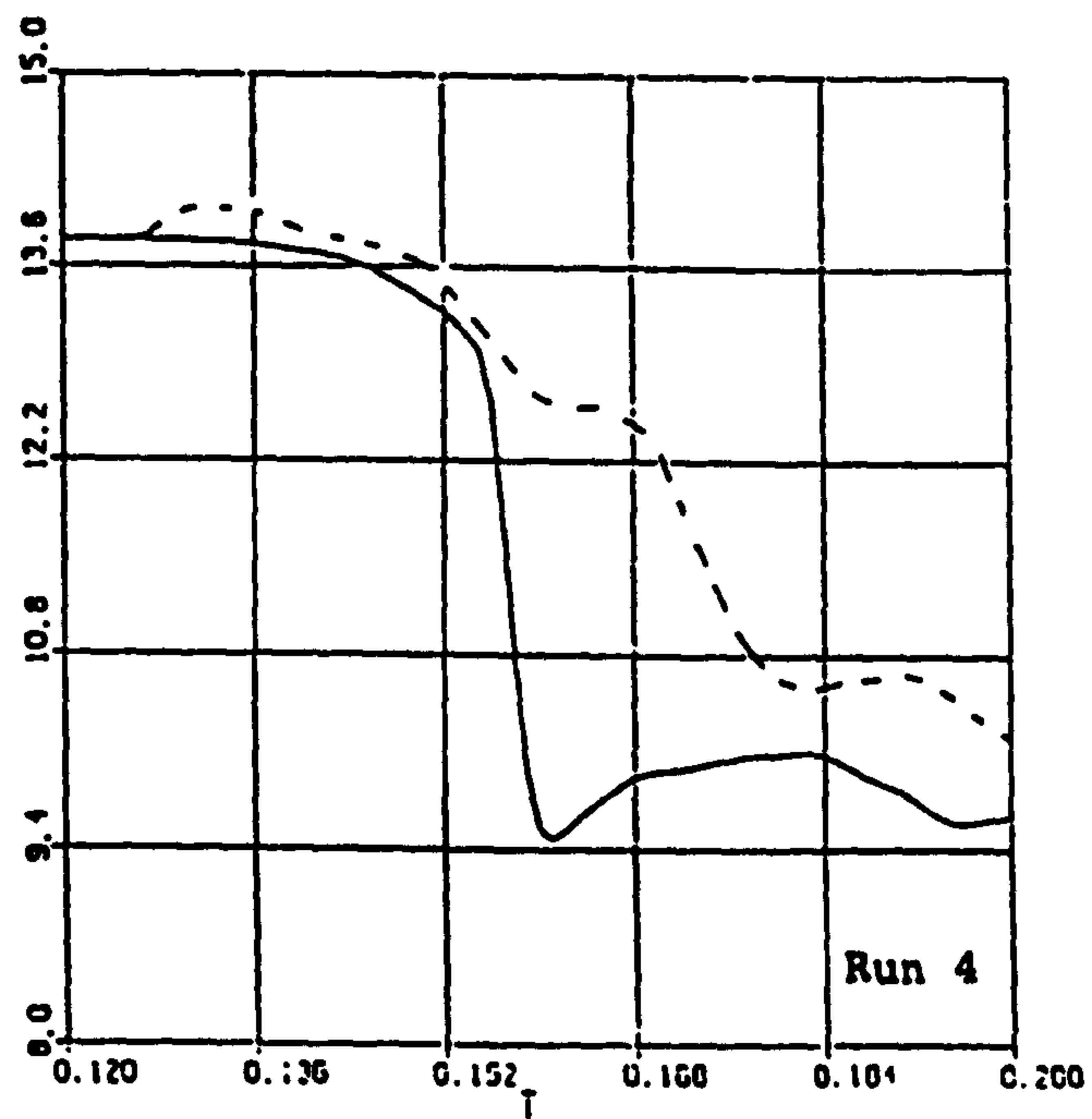
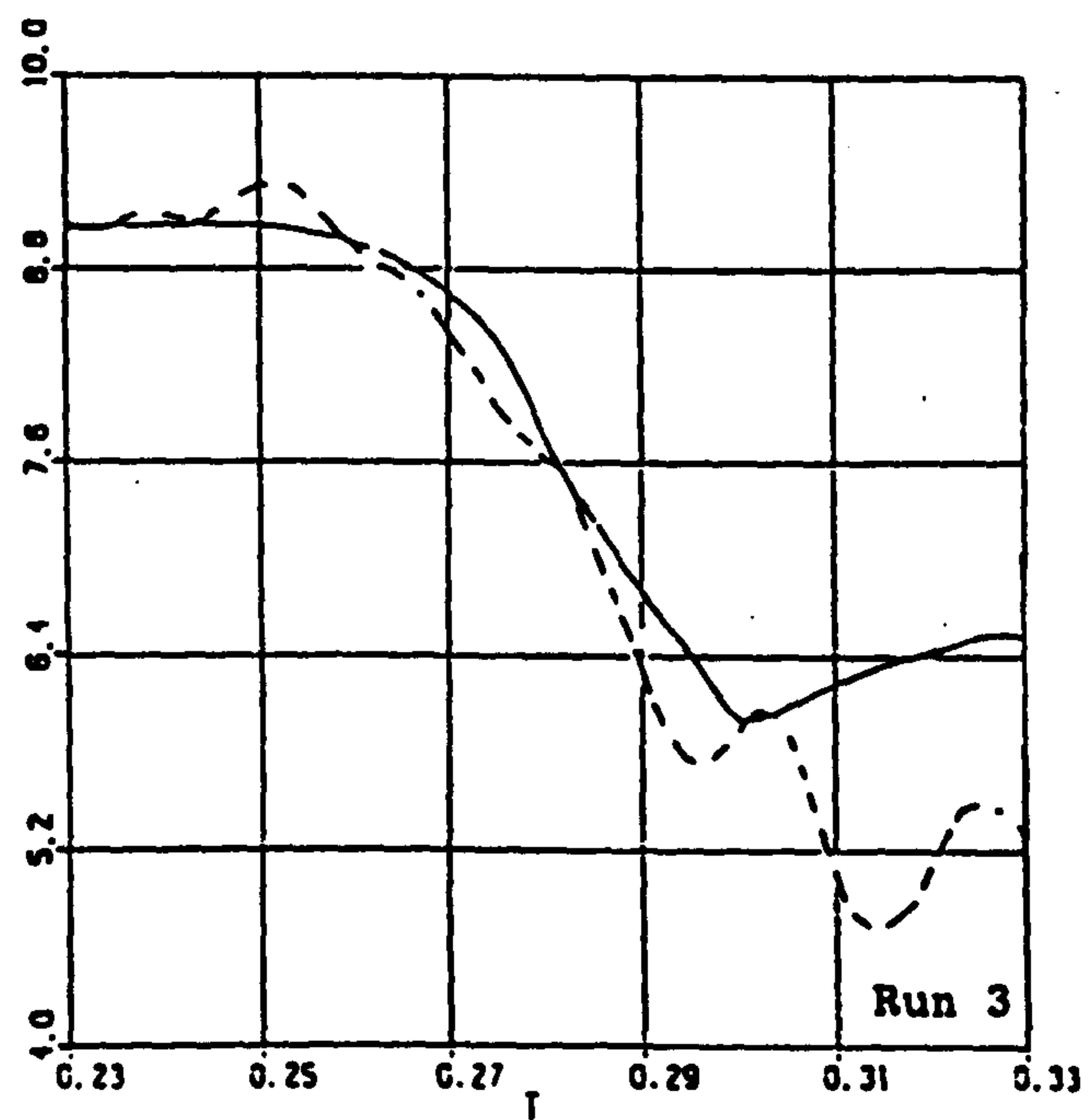
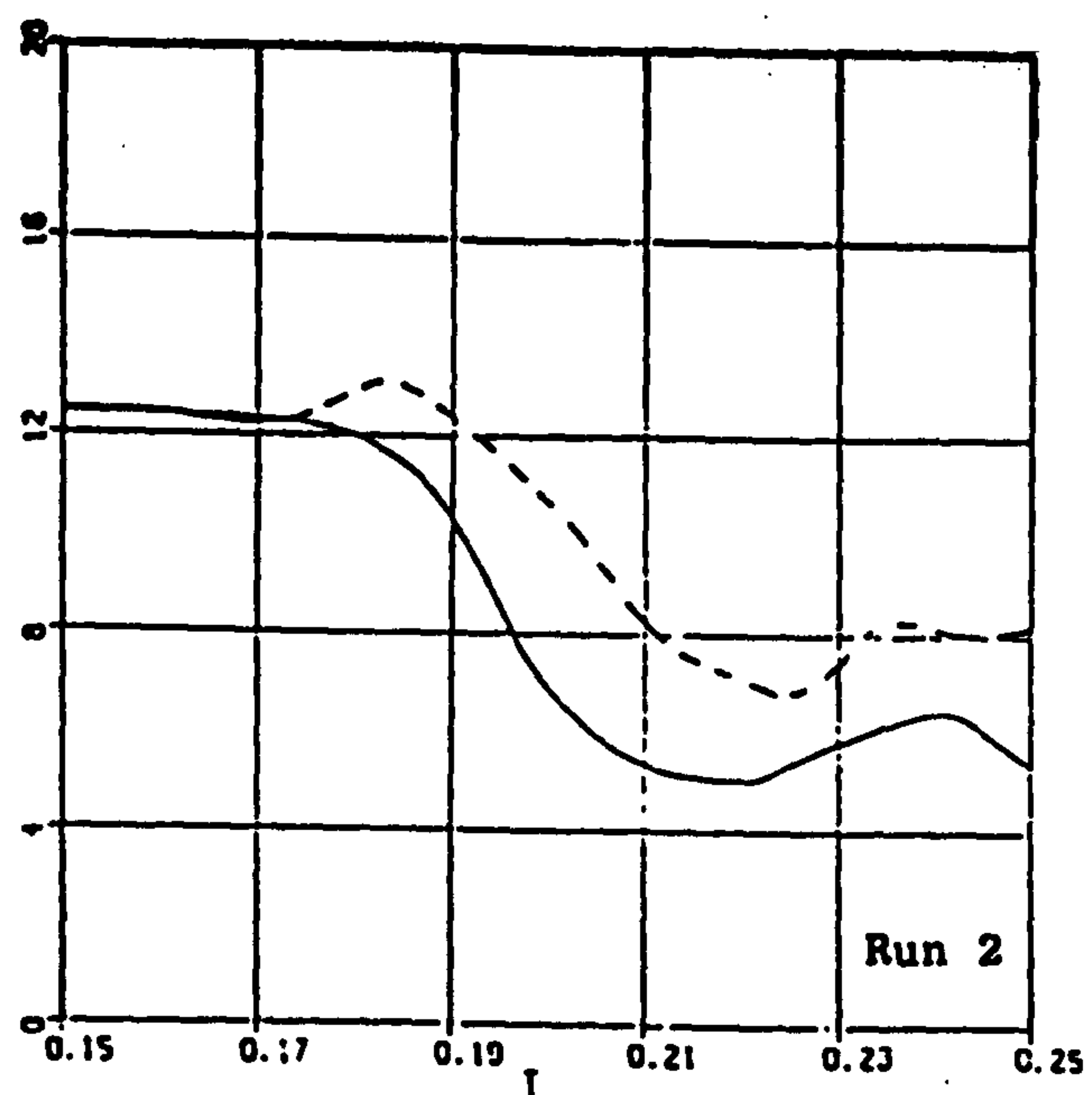
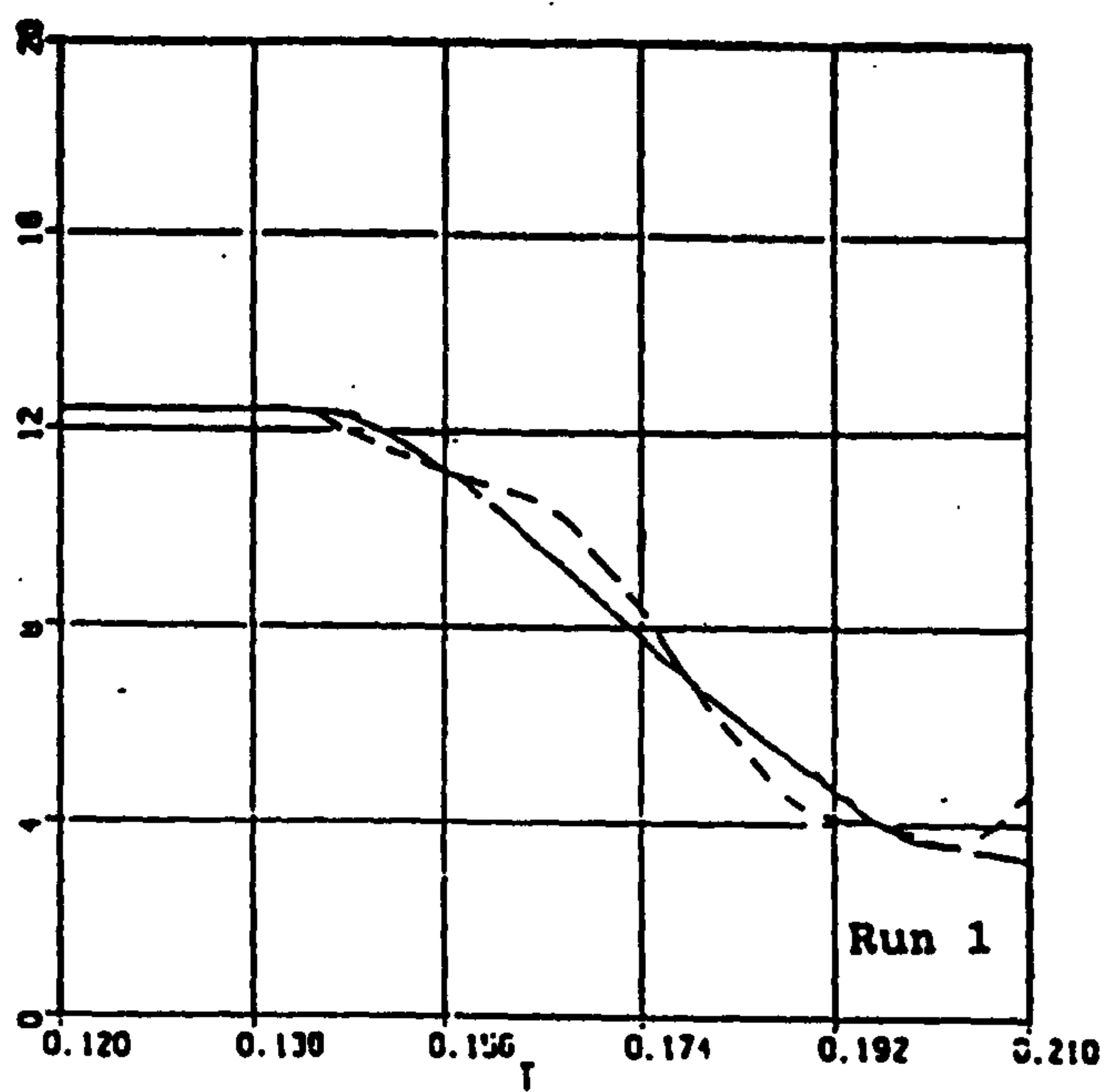


Figure 6.12 Pelvis fore-and-aft velocity (m/s) against time (s) for runs 1 to 4, from just before front wheel impact to just after head impact. Simulation —, from film data ---.

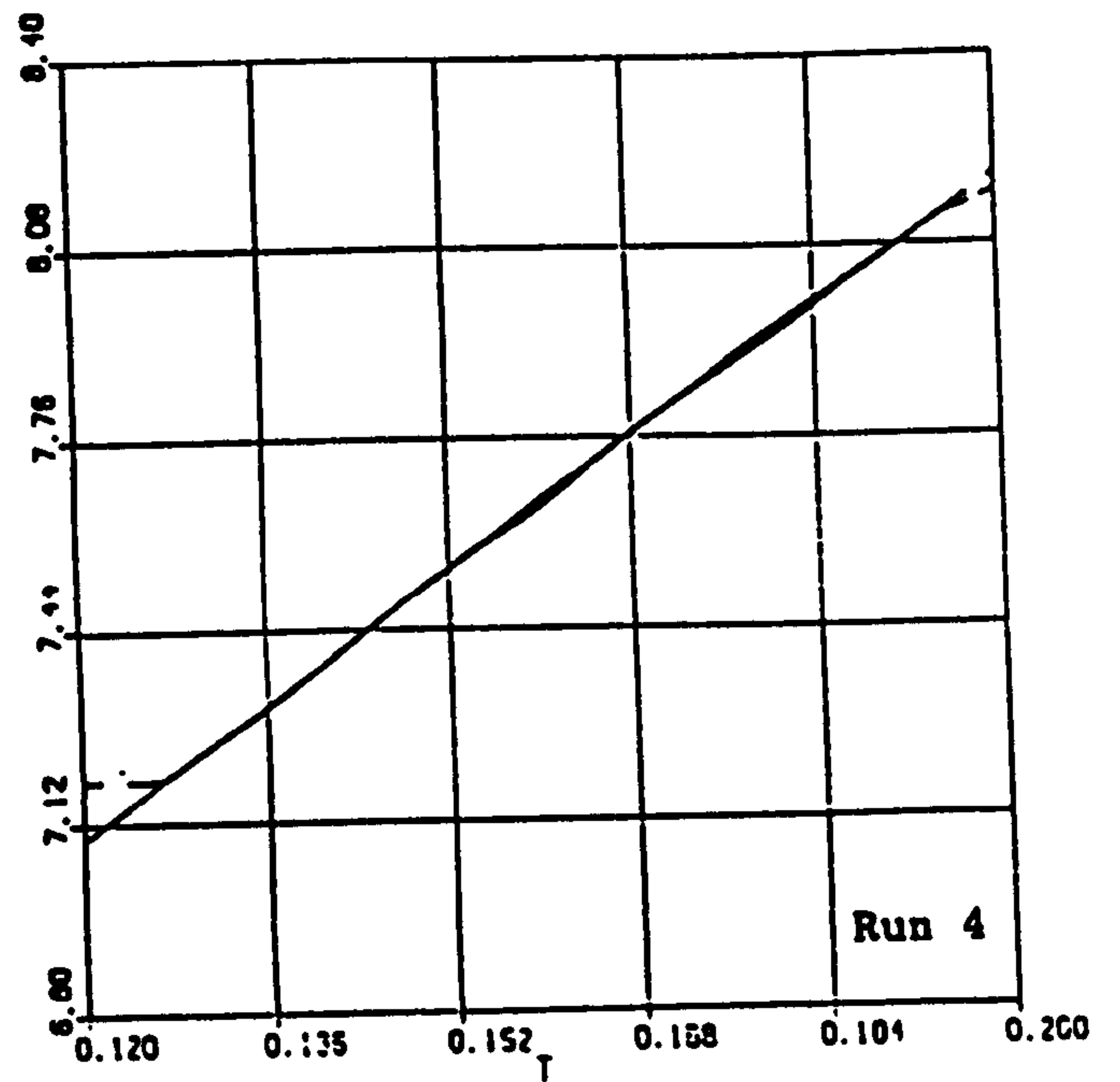
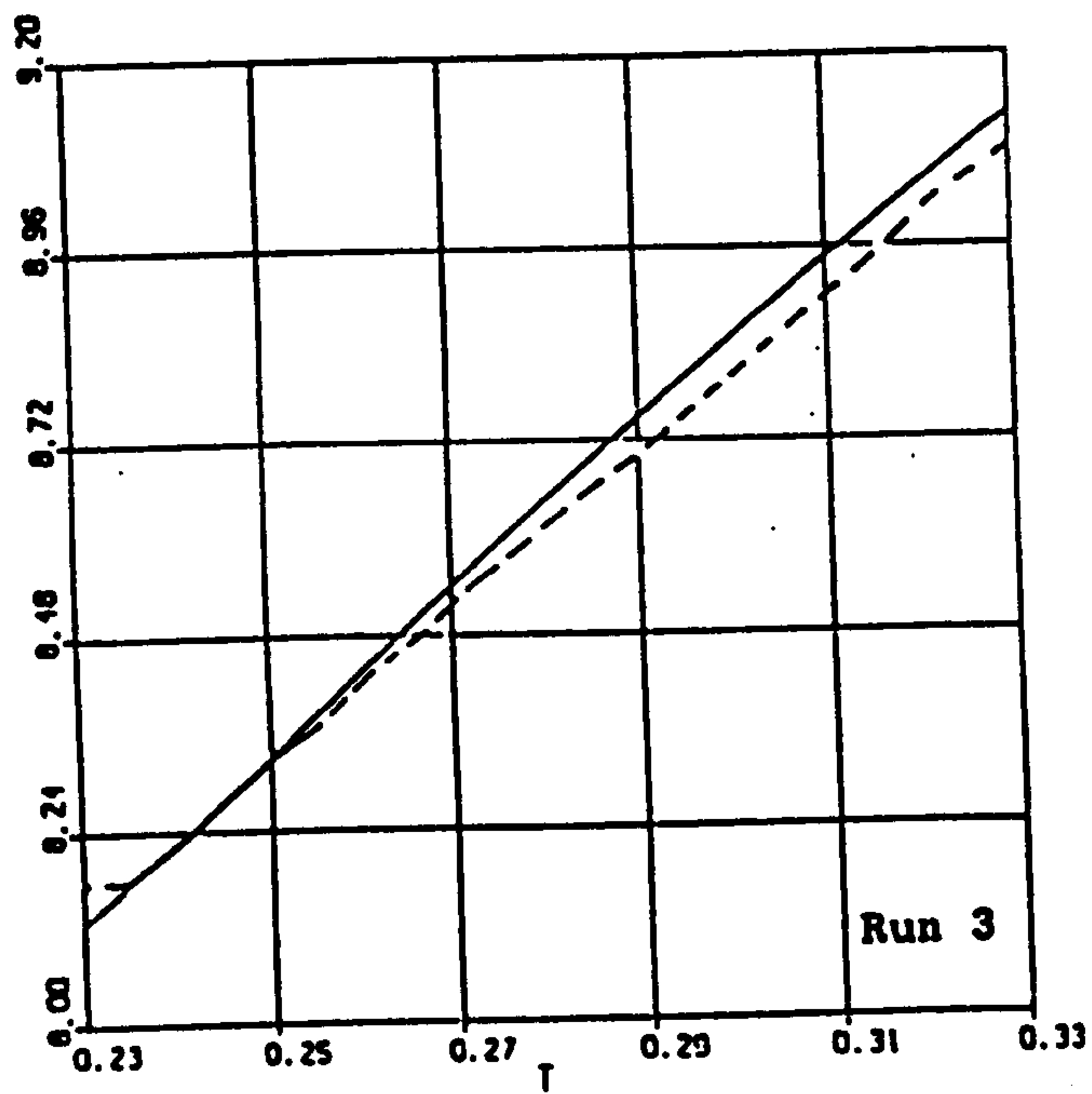
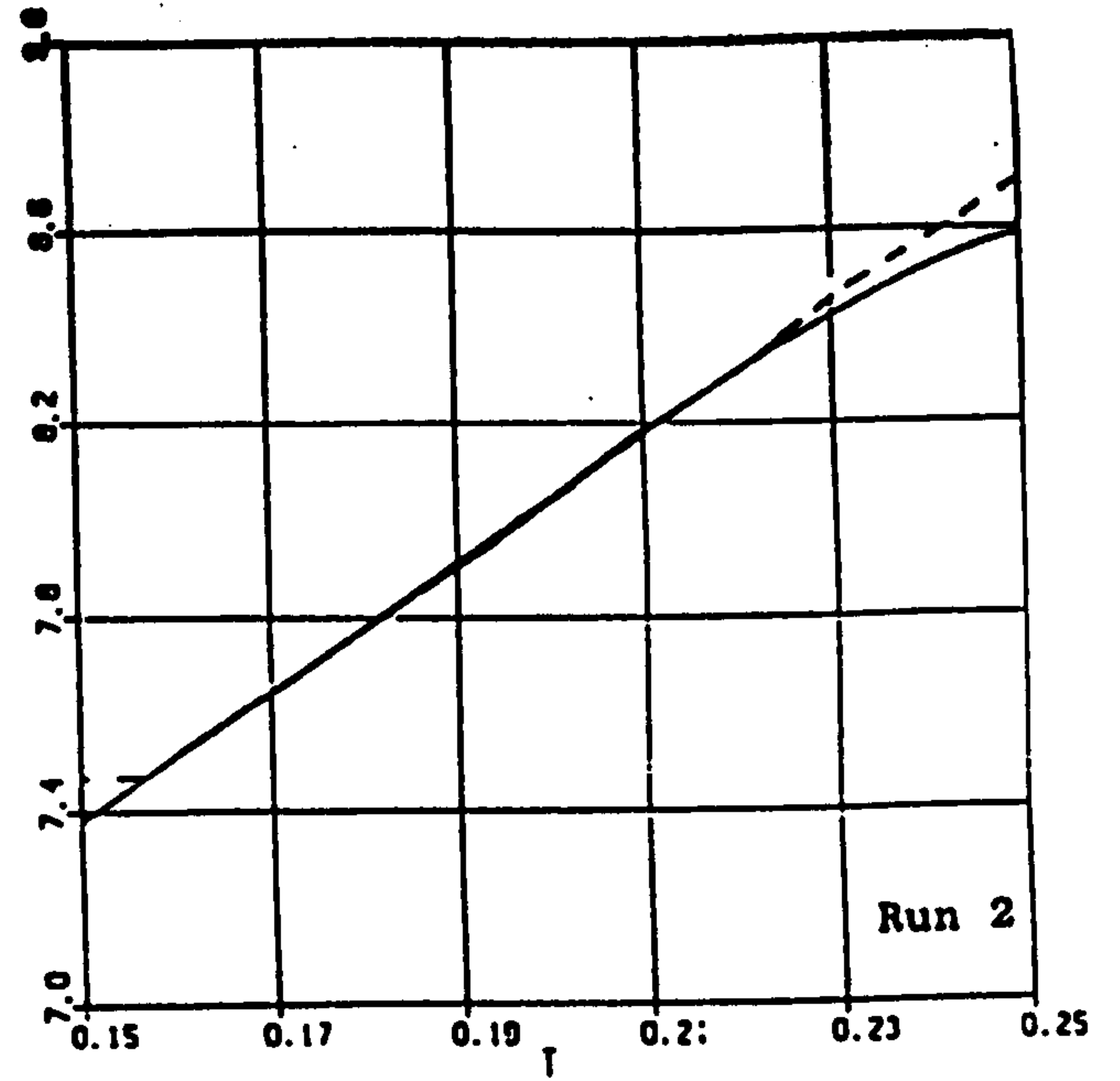
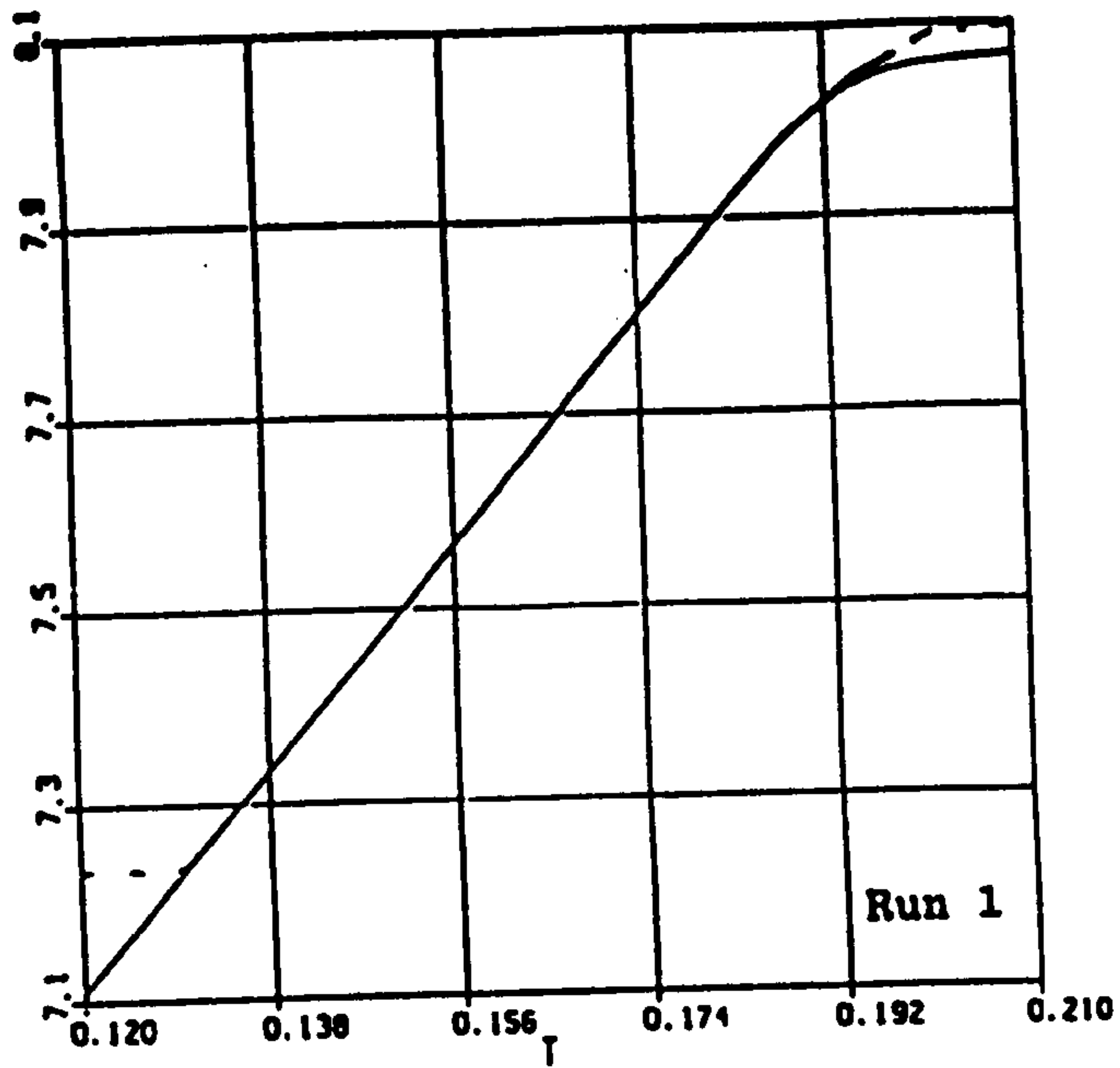


Figure 6.13 Head fore-and-aft displacement (m) against time (s) for runs 1 to 4, from just before front wheel impact to just after head impact. Simulation —, from film data - - -.

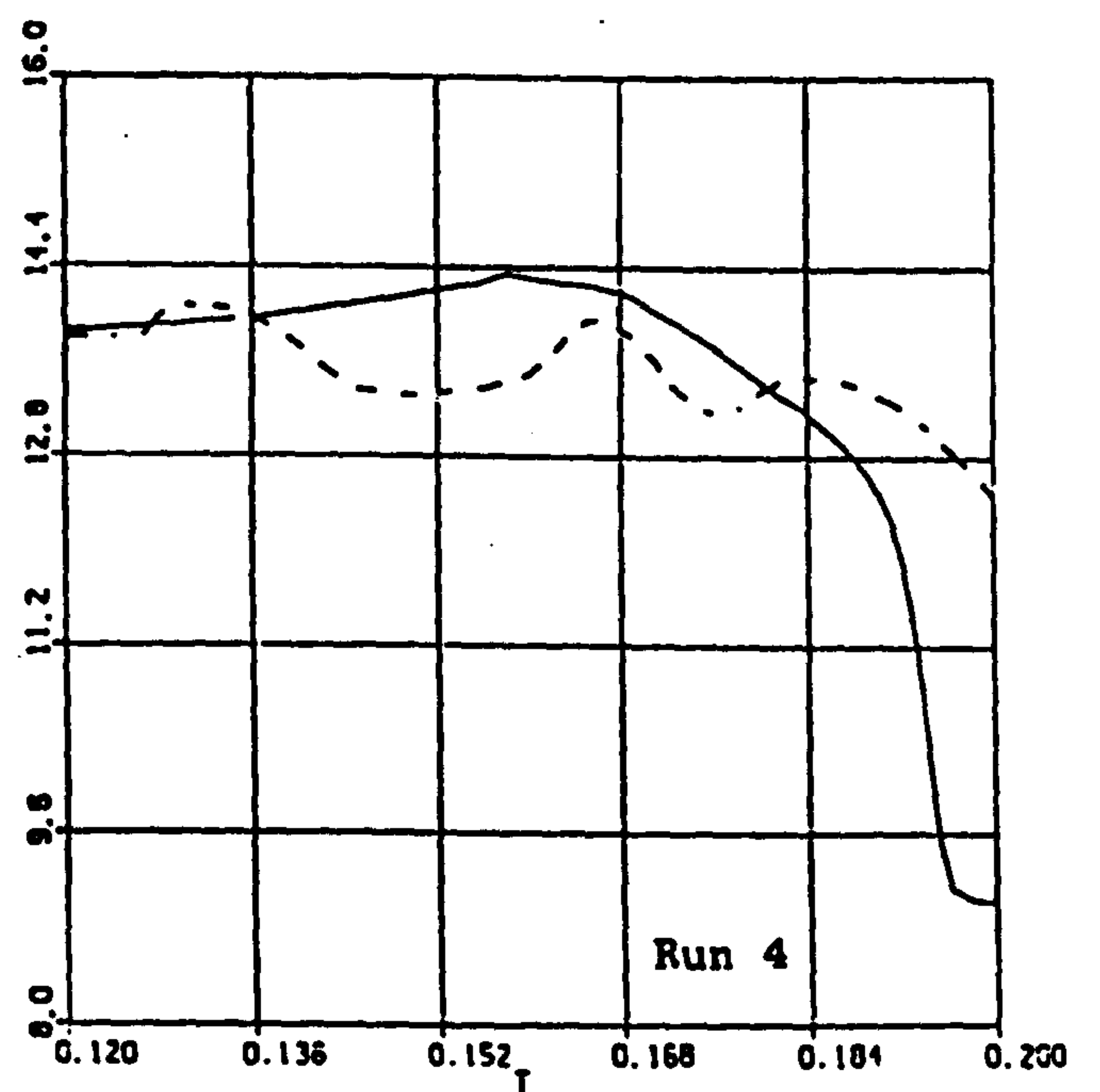
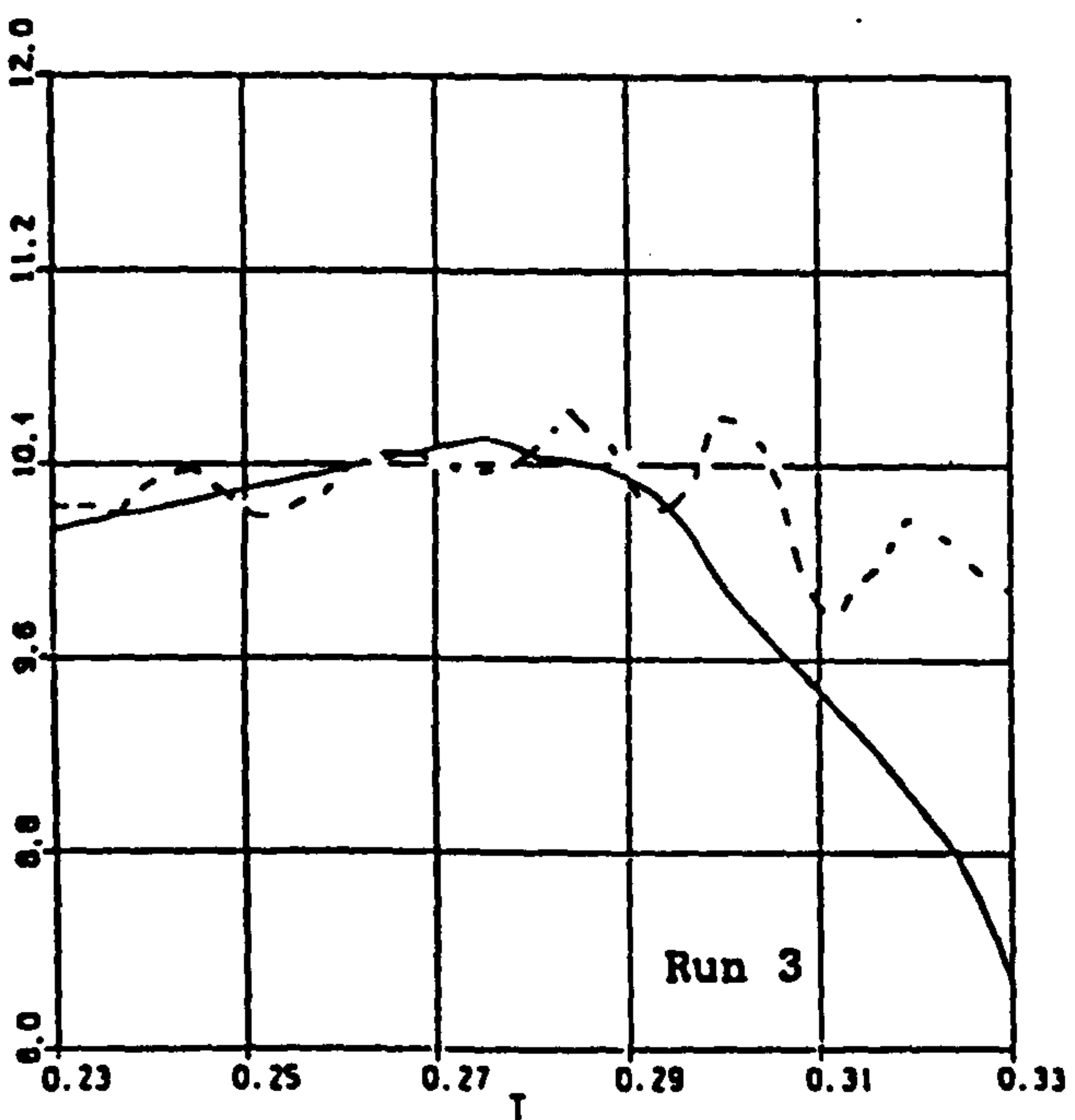
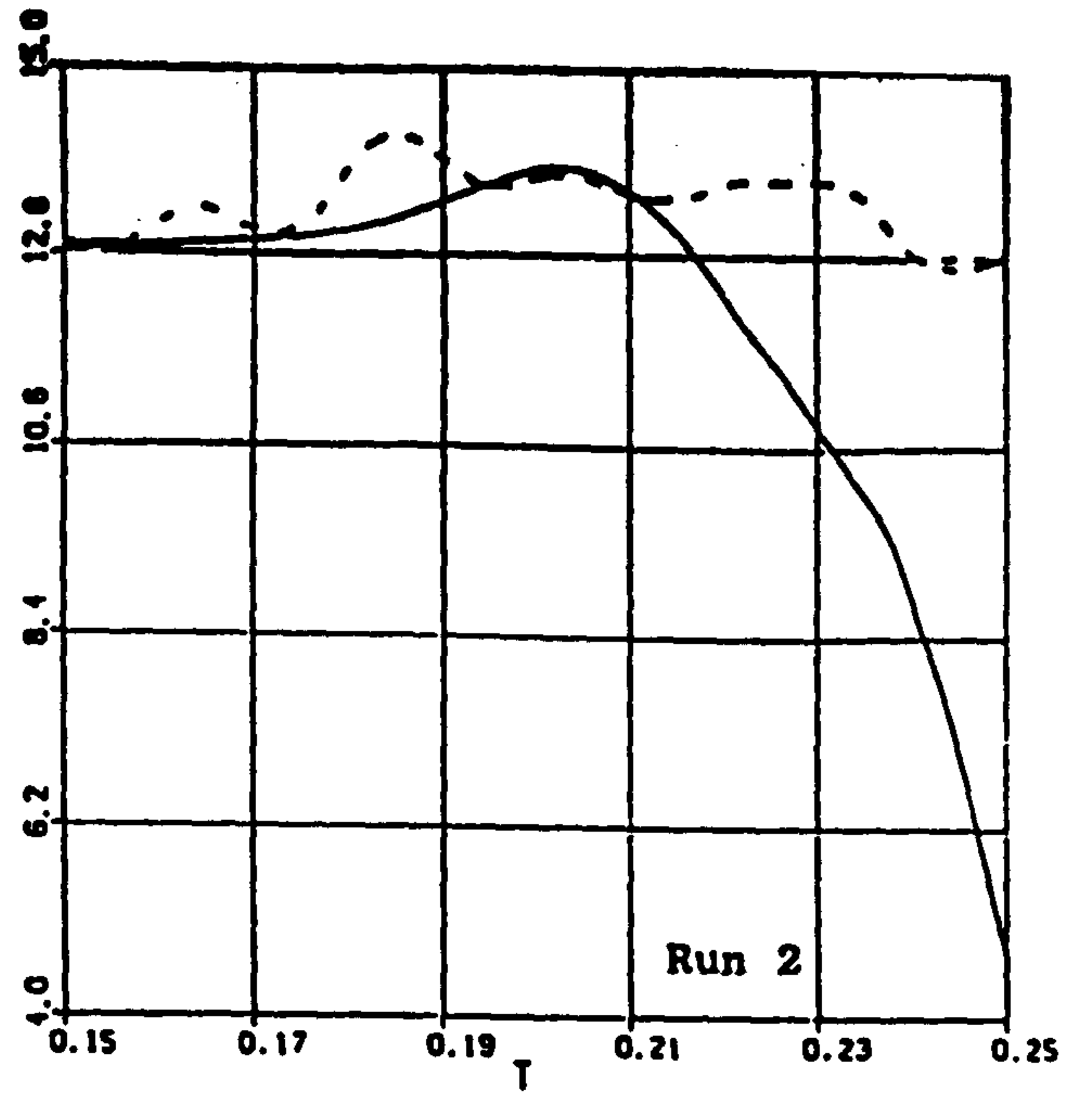
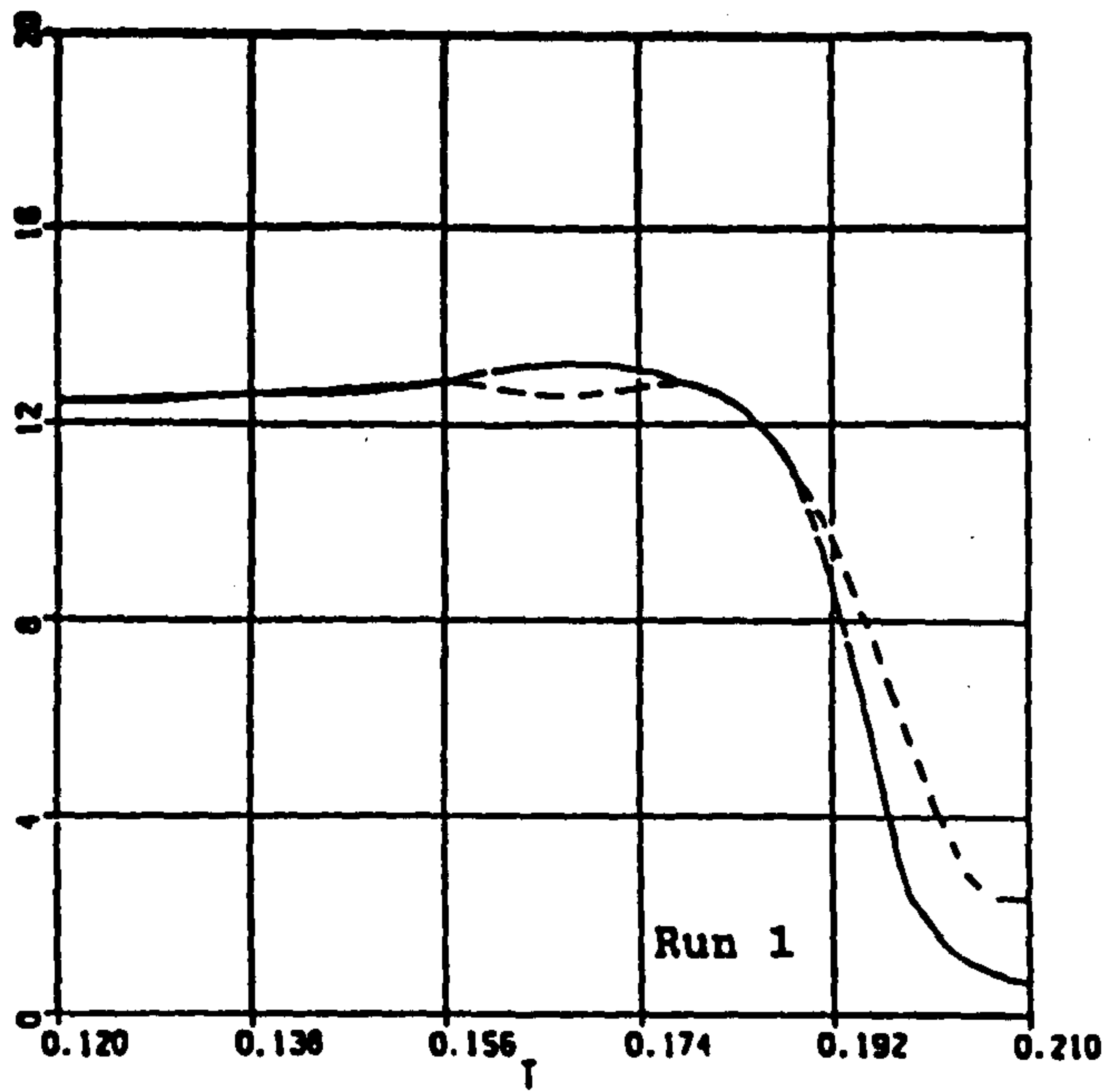


Figure 6.14 Head fore-and-aft velocity (m/s) against time (s) for runs 1 to 4, from just before front wheel impact to just after head impact. Simulation—, from film data---.

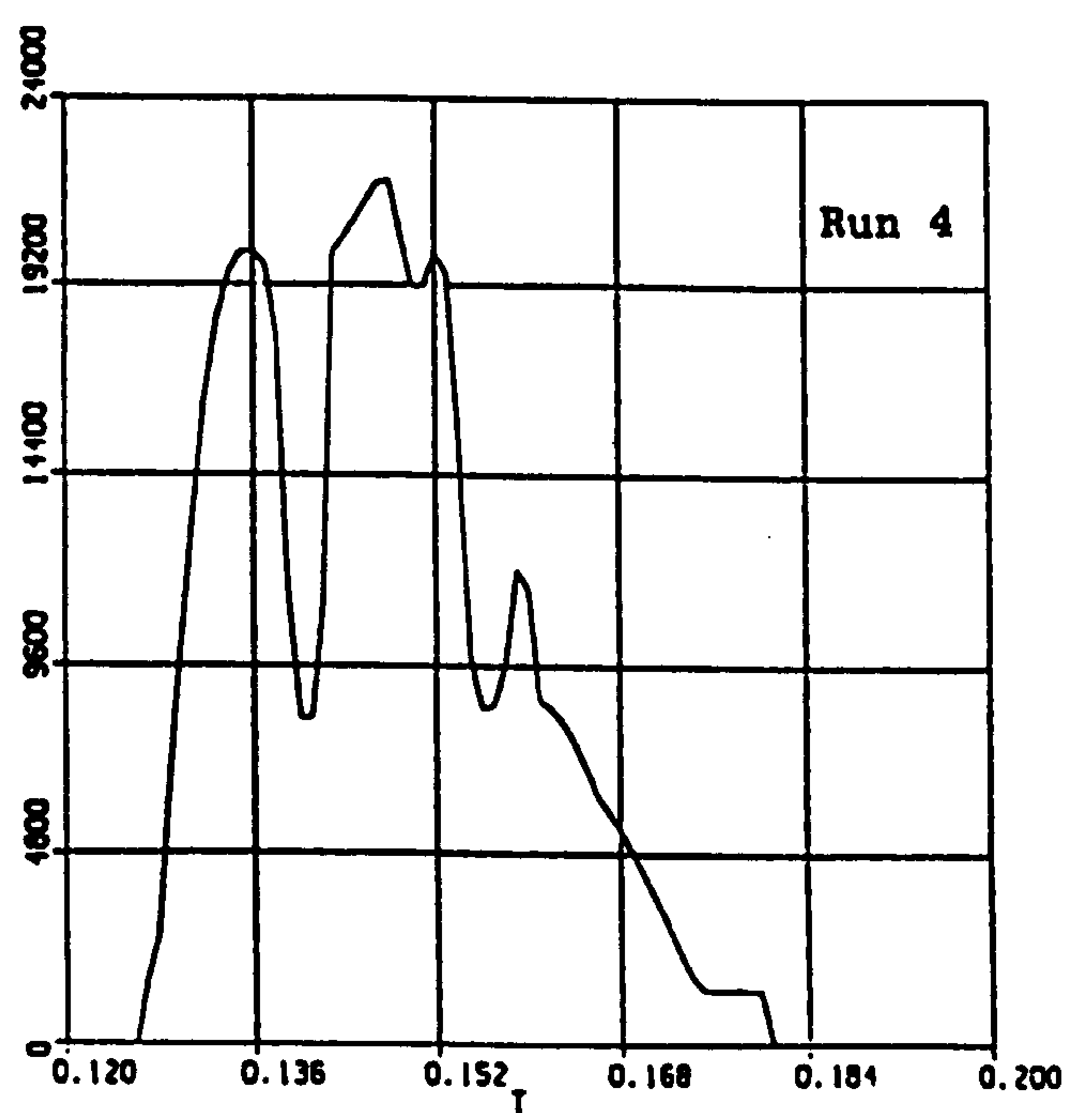
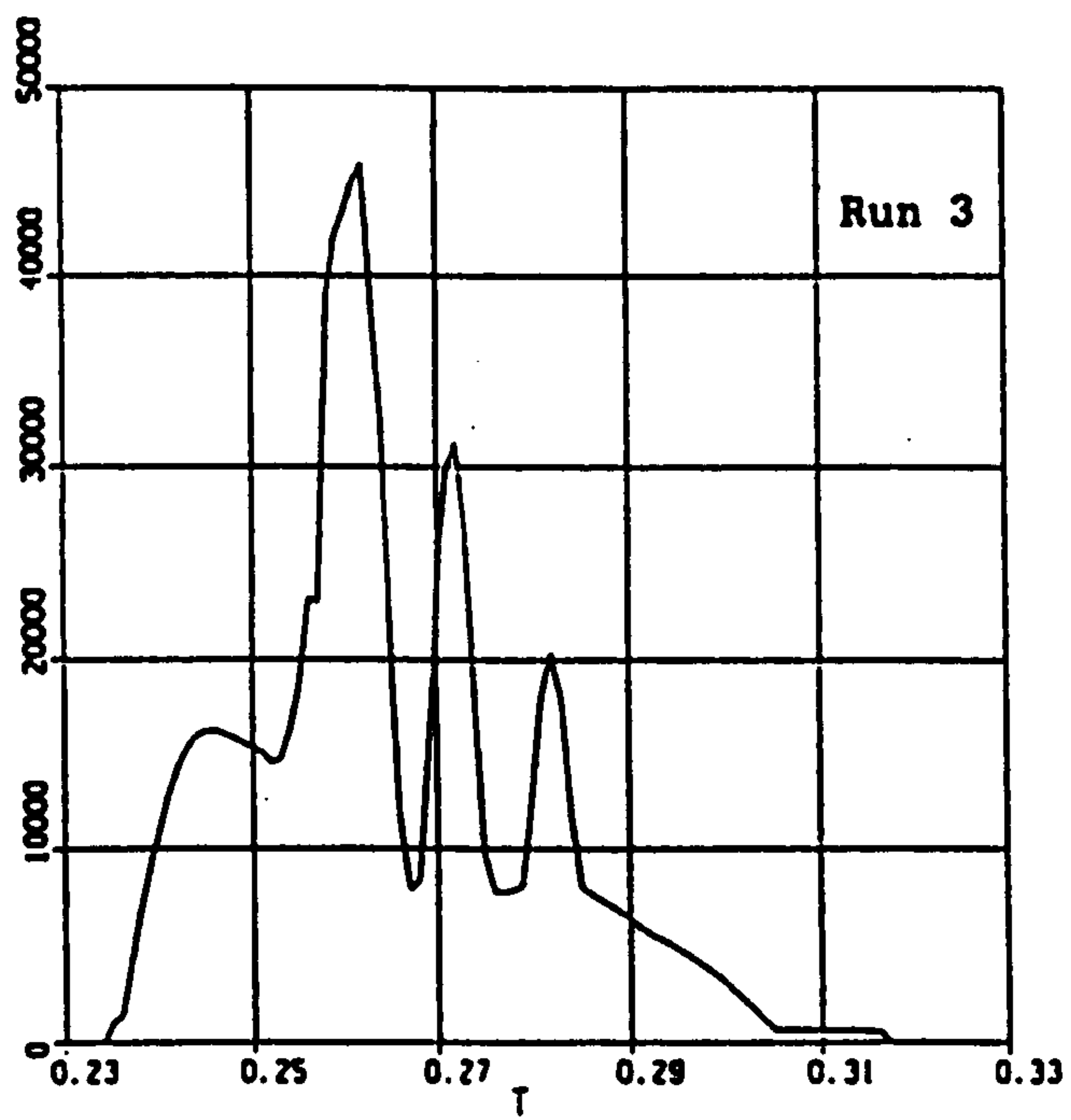
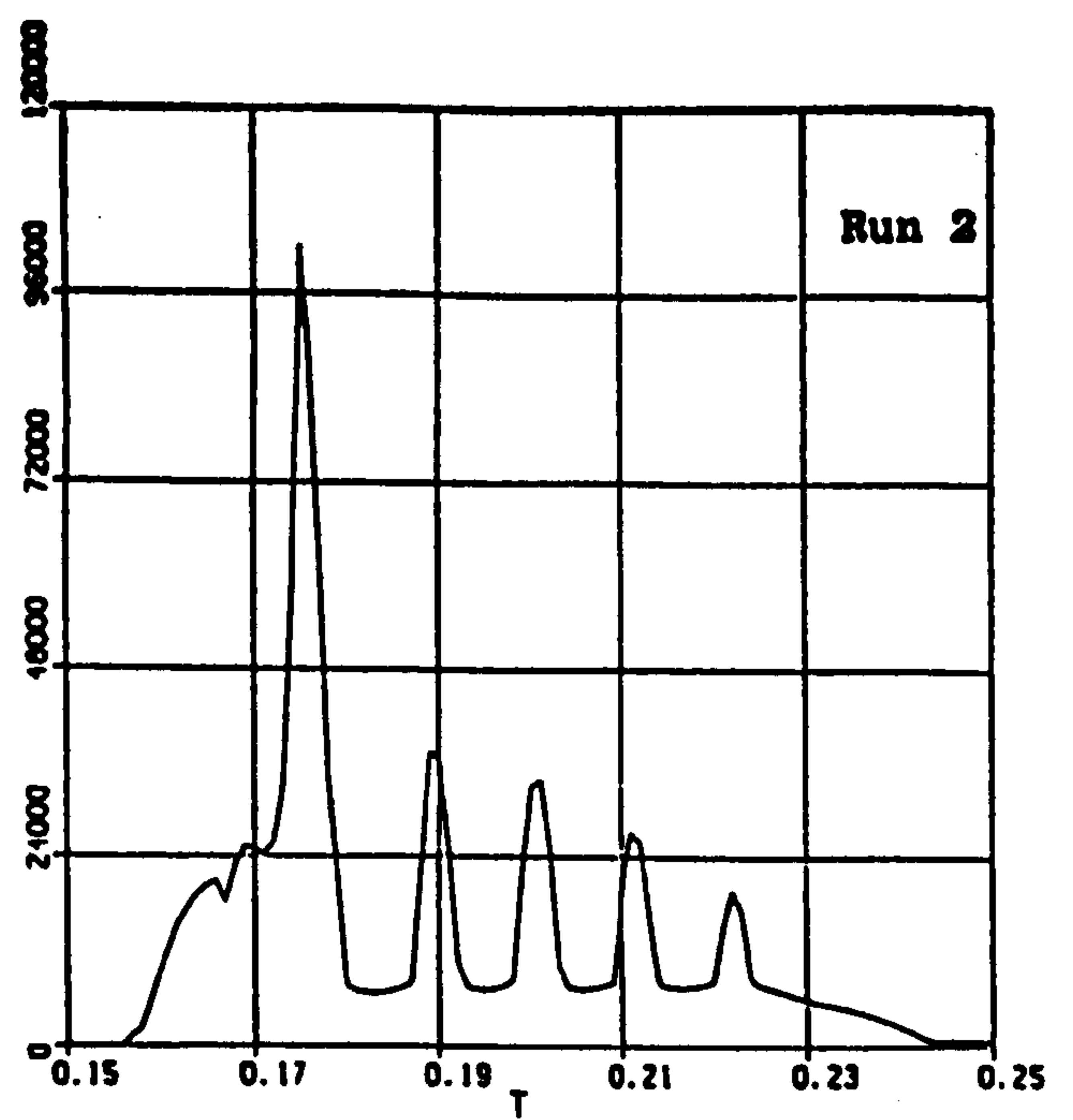
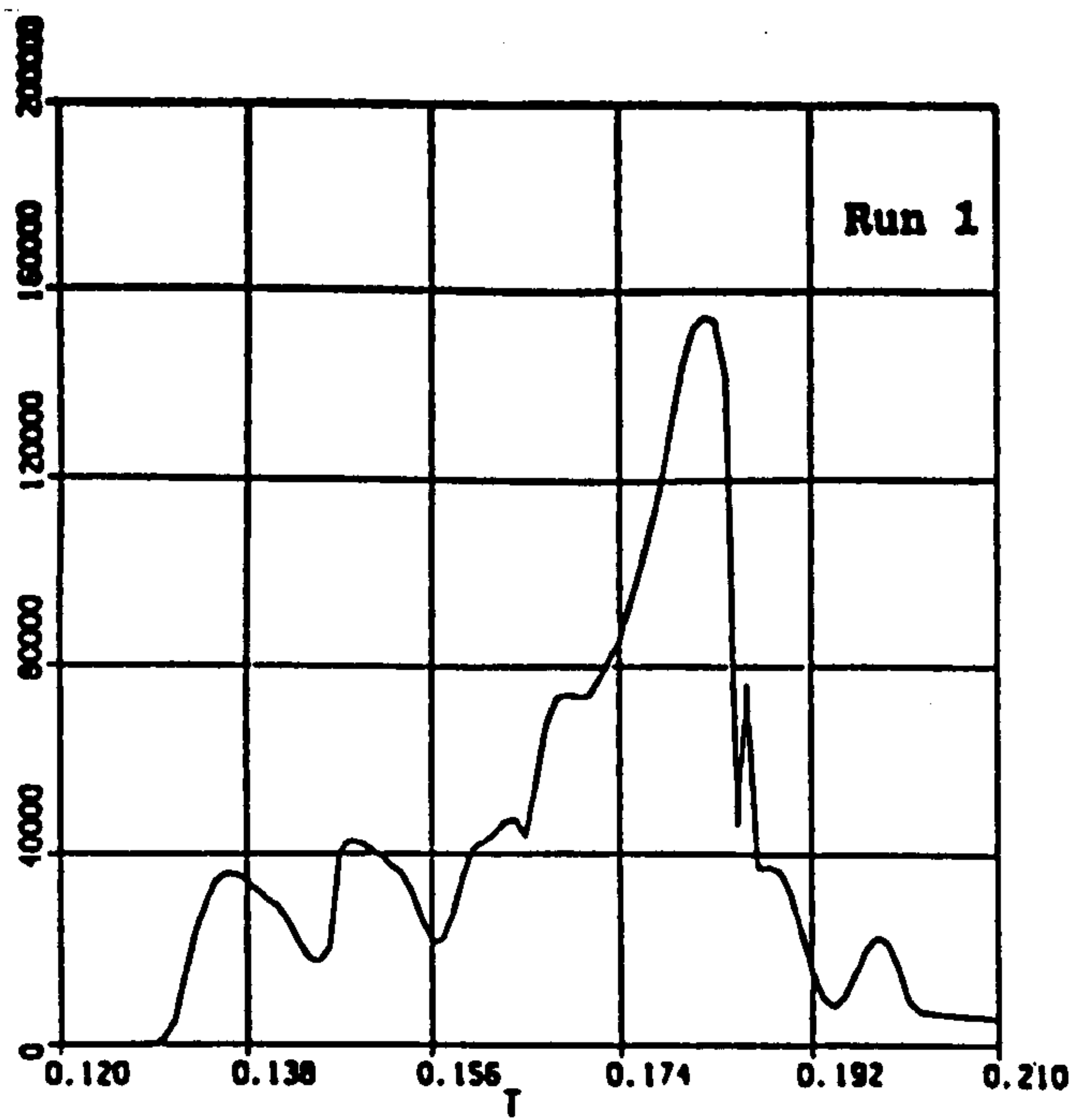


Figure 6.15 Front wheel impact force (N) against time (s) for runs 1 to 4.

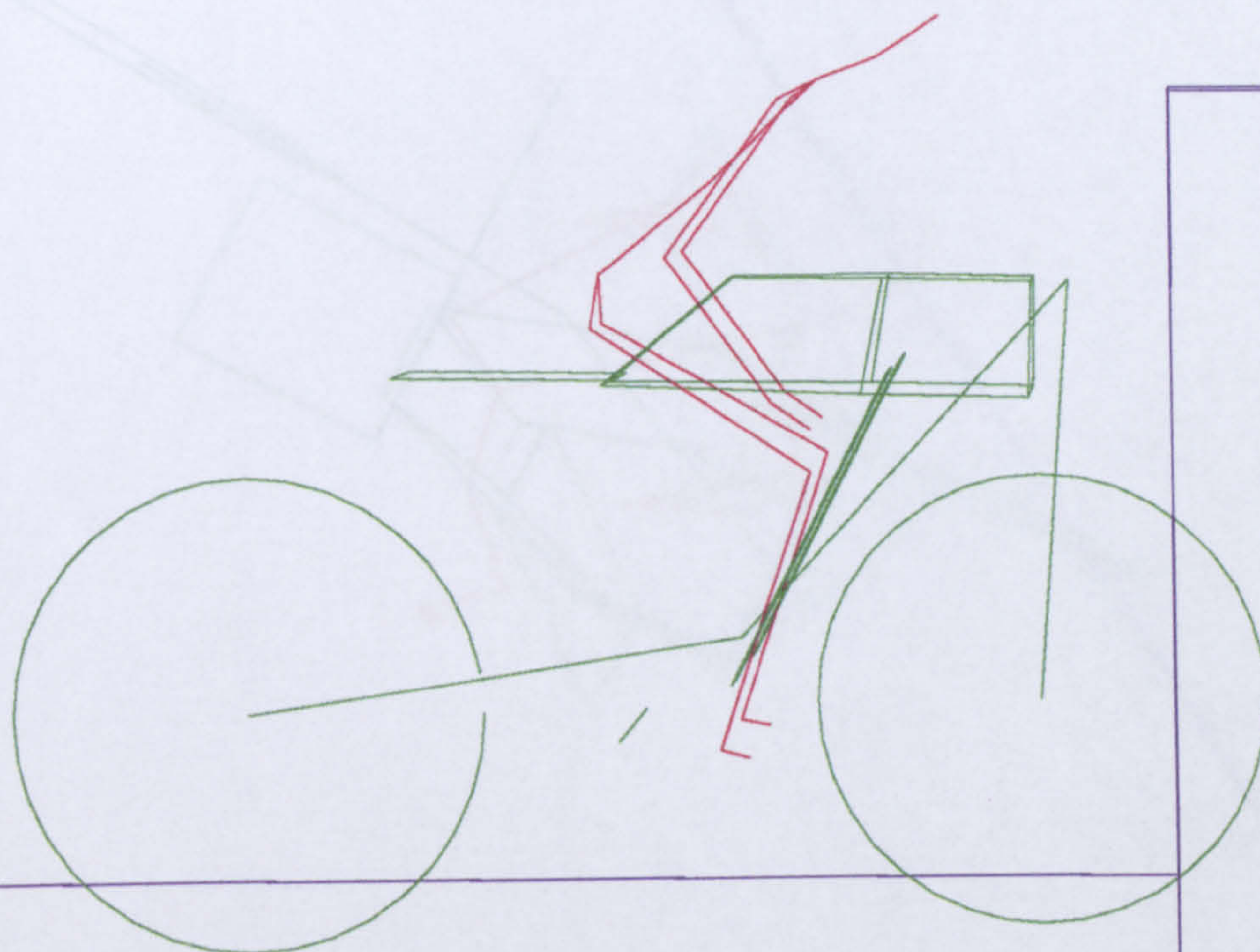


Figure 6.16 Run 1 at 50ms into impact



Figure 6.17 Run 2 at 100ms into impact

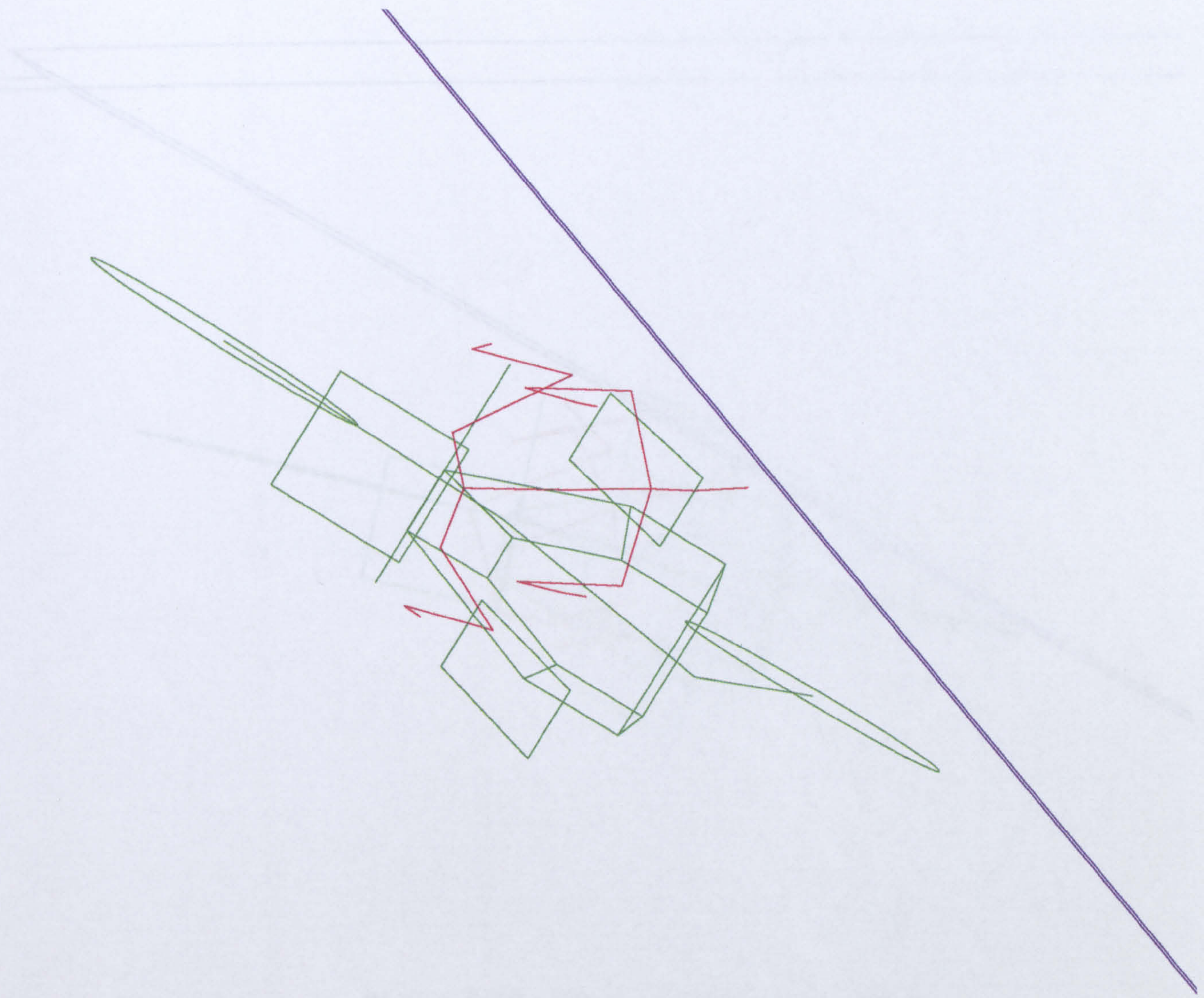


Figure 6.18 Run 3 at 100ms into impact

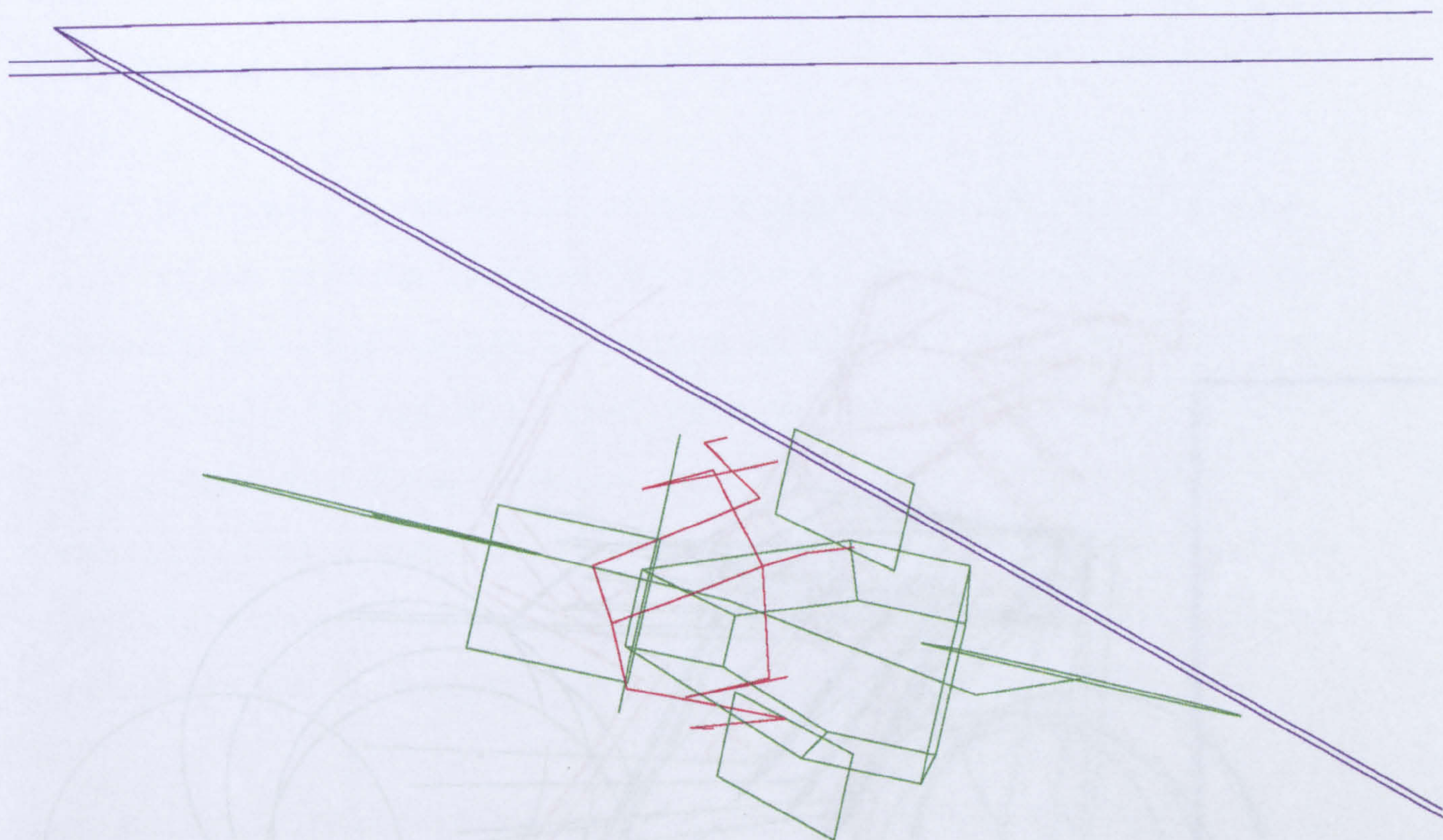


Figure 6.19 Run 4 at 50ms into impact

7.3 Introduction

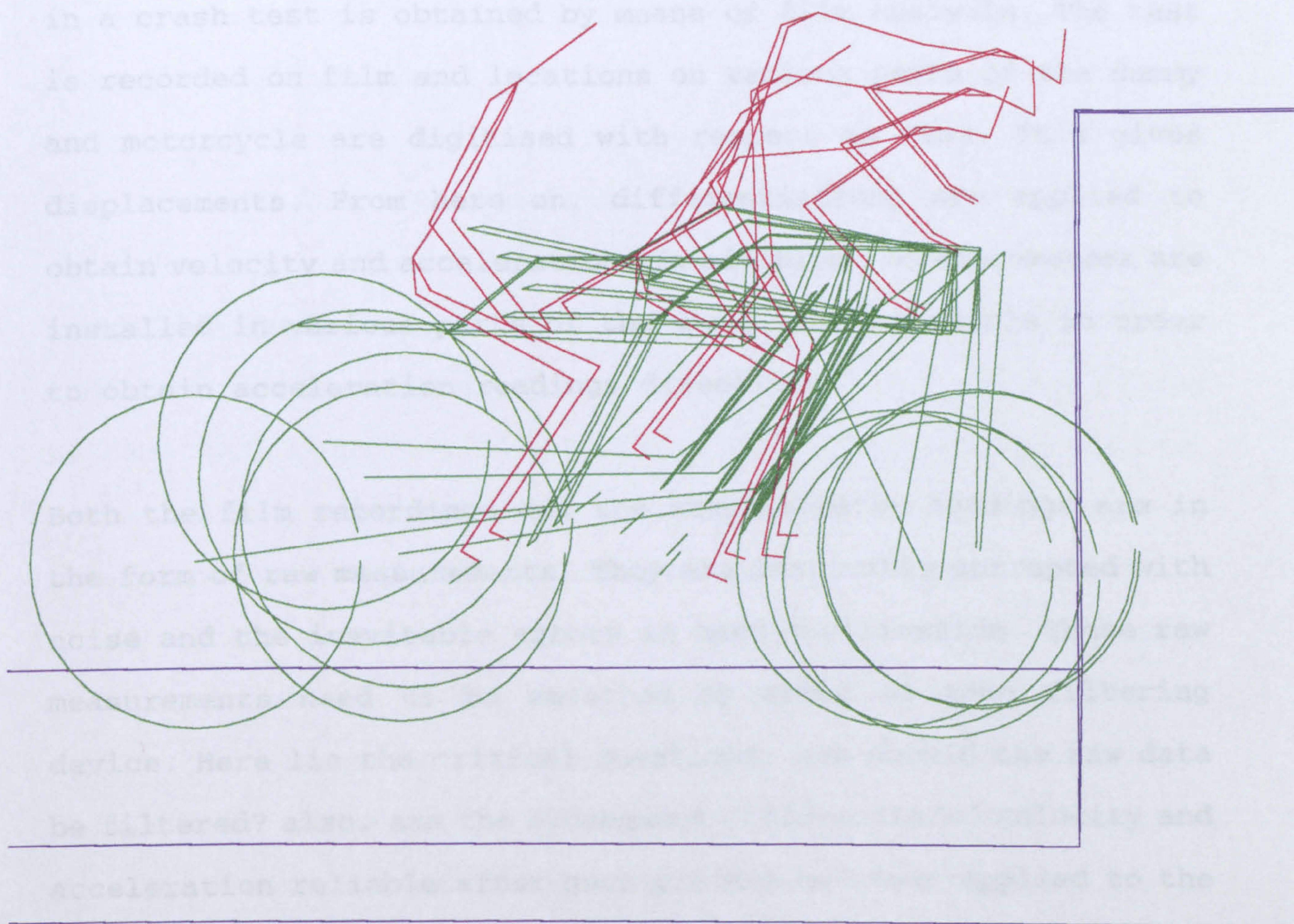


Figure 6.20 A sequence of Run 1 at 20ms intervals

CHAPTER 7

NUMERICAL PROCESSING

7.0 Introduction

At TRL dynamic information of the dummy rider and the motorcycle in a crash test is obtained by means of film analysis. The test is recorded on film and locations on various parts of the dummy and motorcycle are digitised with respect to time. This gives displacements. From here on, differentiations are applied to obtain velocity and acceleration. In addition, accelerometers are installed in various parts of the dummy and motorcycle in order to obtain acceleration readings directly.

Both the film recordings and the accelerometer readings are in the form of raw measurements. They are inevitably corrupted with noise and the inevitable errors in hand digitisation. These raw measurements need to be smoothed by means of some filtering device. Here lie the critical questions: how should the raw data be filtered? also, are the subsequent differentiated velocity and acceleration reliable after such process has been applied to the initial raw data, the displacement? Similarly, accelerometer readings are filtered and integrated but are they reliable?

In this chapter we shall investigate both differentiation and

integration using 'readings' computed by the simulation program. In other words, we shall test some typical ACSL computed outputs of displacement, velocity and acceleration, by alternative means. For example, if we consider the ACSL computed acceleration, we will investigate if there is a need, or what of the outcome, if filtering process was applied, and the influence on the subsequent integrated velocity and displacement. Similarly in the reverse mode, will differentiation carry corruption to its subsequent derivatives?

Though computed simulation results are not corrupted with noise in electronic instrumentation, as in the case of a real-life event, the mathematical model will, however, produce resonance and thus vibrational effects on the system. This is due to the mathematical modelling of the simple mass-spring-damper system, where effectively one has only the stiffness and damping parameters to achieve the required material characteristics. To simulate as 'close' a mathematical model as possible to a real-life event one can input more realistic stiffness and damping values, thus reducing the mathematical resonance. However, it is unlikely to achieve all the critical values, as would be in a real-life event, into a mathematical model where there is a high degree of impacts involving many different material properties. This highlights the fact that a simulation model can produce overall performance of an event, but not the 'exact' replica of the refined real-life situation. Thus, computed results such as

forces and accelerations are sometimes full of peakedness when observed in graphical forms. This is the point of applying different filtering procedures so as to examine the effects and thus determine whether or not there is any need to process numerically the output from the simulation.

7.1 Differentiation

In the differentiation part of this investigation, the procedure is to take the displacement coordinates, computed by ACSL, and to fit an analytically defined curve onto them. After a successful function has been obtained; i.e. one which gives a good fit, it is to be differentiated once to give velocity and twice to give acceleration. Comparisons can then be made with the corresponding velocity and acceleration computed within the ACSL simulation program.

There are numerous methods to fit a curve onto a set of points

$$(x_1, y_1), (x_2, y_2), \dots, (x_n, y_n),$$

such as linearization, polynomial approximation and spline interpolation. Here we shall consider the latter case. For mathematical derivation consult Appendix A.2.

7.1.1 Piecewise Spline Interpolation

Piecewise spline interpolation is a technique that the curve to be approximated is subdivided between the chosen nodes, such that between two successive sub-intervals, say $[x_i, x_{i+1}]$ and $[x_{i+1}, x_{i+2}]$, the interpolated function $S_i(x)$ and $S_{i+1}(x)$ respectively, will pass through the common 'interior knot'. This can be illustrated in Figure 7.1.

7.1.2 Cubic Splines

Out of the variety of piecewise spline interpolations, cubic splines are readily used. These are polynomials of degree three on each sub-interval, $S_i(x)$, such that the first two derivatives of $S_i(x)$ are continuous. However, the construction of cubic splines does not assume that the derivatives of the interpolant S agree with those of the original function f , even at the nodes.

An ACSL computed displacement of the dummy's chest is chosen to be fitted by the use of cubic spline interpolation. This is from the L4 simulation crash test: impact angle at 90 degrees with initial velocity of 30mph.

The interpolation is carried out by the use of NAG routines (Numerical Algorithms Group, [28]). The user is required to

prescribe the corresponding knots subdividing the curve into splines. The NAG routines used will determine a cubic approximation $S(x)$ to the set of data points, and evaluate the approximating splines, i.e. the fitted values to the displacement curve.

The fitted displacement curve was found to be very close to the actual displacement as computed by the simulation program, though numerically it was not exactly coincidental with the ACSL computed results. After differentiation was applied to the interpolated curve, its first and second derivatives were found to give satisfactory results, as can be seen in Figures 7.2a and 7.2b.

Before we proceed to examine the results, a note is needed on how the curve fitting process is done. We have been comparing resultant displacement, velocity and acceleration, but in fitting the original resultant displacement function, this was obtained by fitting each cartesian component, and applied the relevant differentiation used to each of these components. This is so because we know the resultant displacement, say R , is formulated by

$$R^2 = x^2 + y^2 + z^2$$

If differentiation was applied to R in order to obtain \dot{R} we have

$$\dot{R} = \frac{\dot{xx} + \dot{yy} + \dot{zz}}{R}$$

which is obviously different to the resultant velocity where, say R_v

$$R_v^2 = \dot{x}^2 + \dot{y}^2 + \dot{z}^2$$

Therefore each individual component needs to be manipulated independently.

Comparing the graphs in Figure 7.2b and the actual simulated displacement, velocity and acceleration in Figure 7.2a, the spline fitted displacement is visually similar to its counterpart. Though the differentiated velocity and acceleration are far from perfect, they do retain similar shapes to the simulated equivalents. Note that in the prescribing of knots the fore-and-aft displacement was prescribed five knots, the vertical displacement was prescribed 17 knots, sideways displacement being constant since it was a direct frontal impact. It was then considered to prescribe more knots in the interpolating curves to see the effect of finer spline interpolation.

The task was carried out with the fore-and-aft displacement curve being prescribed six knots, and the vertical displacement curve being prescribed 22 knots. The resulting spline interpolated curve was found to be numerically more accurate than the first

case. Differentiation was then applied. The results are in Figure 7.2c.

As can be seen, the equivalent resultant velocity curve is approaching the same profile as the simulated velocity curve. There are more details in the acceleration curve than previously, but the peak spike has actually increased.

Attempts were made to subdivide the displacement curves even finer. The fore-and-aft displacement was prescribed 18 knots and the vertical displacement was prescribed 37 knots. The fitted displacement is now even more accurate than before. Its first and second derivatives are also visually satisfactory. The graphs are in Figure 7.2d.

We can see now the velocity curve has very similar profile to the simulated velocity. The acceleration curve has more details in its shape than before, though the peak spike still has a sharp 'peakedness' to it, it has actually been reduced to nearer to its simulated equivalent.

This exercise shows that there is an increase in accuracy of the cubic spline interpolation as the number of interior knots increases. This also leads to better derivatives of the spline fitted function. However, we should bear in mind that the ACSL simulated acceleration of the dummy's chest is relatively

continuous, consequently, its velocity and displacement functions have been 'smoothed' by the process of integration.

Having made this observation, the following proposal is made: given a computed acceleration curve which consists of wiggles and sharp spikes, after integrations have been applied to obtain velocity and displacement they are found to contain sharp maxima and minima, and if the same spline fitting procedure is then made on the displacement curve, will the resulting derivatives be smooth and continuous? or will the spikey characteristics remain?

The centre of the front wheel in crash test simulation L4 was chosen to test this proposition. Its fore-and-aft and vertical displacements are shown in Figure 7.3a, sideways displacement being constant. The resultant displacement, velocity and acceleration are shown in Figure 7.3b. As can be seen, the resultant acceleration curve is full of wiggles and sharp spikes. The ACSL integrated velocity is still very peaked, and the displacement curve contains a few soft ripples.

Having had the experience of the apparent increase in accuracy due to the increase in the number of interior knots, when using cubic spline interpolation, the front wheel's fore-and-aft displacement is prescribed 34 knots and the vertical displacement is prescribed 84 knots. The resulting spline fitted equivalents of these displacements are shown in Figure 7.4a, and the

associated resultant displacement, velocity and acceleration are shown in Figure 7.4b.

We see that the spline fitted displacements are very close to the simulated equivalents, especially so in the case of the fore-and-aft direction. This leads to a close interpolation of the resultant displacement. The differentiated resultant velocity curve has a similar profile to the simulated equivalent, though there are more spikes in the region of 150ms, and some refined information being lost thereafter. However, the differentiated resultant acceleration is totally distorted. It bears no resemblance to the simulated equivalent.

The effectiveness of these fine splines is then questioned. Given an acceleration curve which consists of wiggles and sharp spikes, should one attempt to approximate its second integral coarsely so as to minimise the wiggly effect of differentiation? Or should one attempt to approximate almost all the known data points such that the approximated spline will coincide almost exactly with the original curve? Theoretically speaking, in the latter case, then if every known data is prescribed as an interior knot, the first and second derivatives of the then interpolated spline should be the same as the computer simulated velocity and acceleration.

Both cases were examined. In the first case where coarser splines

are introduced , the fore-and-aft displacement is prescribed 26 knots and the vertical, 64 knots. In the case of the vertical displacement, an attempt is made to eliminate the two spikes just before the 150ms mark. The fitted interpolations are shown in Figure 7.5a.

One can see the shape of the spline fitted fore-and-aft displacement curve is still very similar to the original. The two spikes in the vertical displacement have indeed been eliminated. Though the general profile remains, there is an addition of small peaks between 150ms and 200ms.

In Figure 7.5b the resultant displacement, velocity and acceleration, obtained through this coarser spline fitting interpolation, are shown. Compared to the ACSL simulated equivalents in Figure 7.3b, the resultant displacement is very similar, the resultant velocity does resemble in its shape, but once again, the resultant acceleration is totally unrecognisable.

However, if we compare with the finer spline interpolation in Figure 7.4b, we may agree that the graphs in Figure 7.4b are generally better than the graphs in Figure 7.5b, in that the resultant displacement and velocity of the finer splines resemble closer to the computed ones. In the case of the resultant acceleration, the coarser spline interpolation in Figure 7.5b

produces a curve of more peakedness in it. However, notice the sharpest peak in the computed acceleration in Figure 7.3b, it has somehow been captured by the coarser cubic spline interpolation.

In the second case where almost all the simulated data points are designated as interior knots, the fitted displacement, and the differentiated velocity and acceleration are shown in Figure 7.6a.

Compared to the originals in Figure 7.3b, we can see that the fitted displacement is certainly very close to the computed one, even the velocity representation is much more similar to the computed equivalent than previously. The acceleration is still unlike the computed acceleration, but the two sharp peaks in the original have been captured, and the fact if one compares to the equivalents in Figures 7.4b and 7.5b, there is certainly a feel of less 'peakedness' about the curve in Figure 7.6a, even though it still contains some sharp spikes.

One may be surprised with the outcome of the latter case, when theoretically speaking, one should gain back the original curve when the actual original curve is spline fitted with every known data point. But one major fact should be considered. The accuracy of the data points read is limited due to rounding. Also ACSL is a continuous simulation language, but data are read into the differentiation program discretely. In addition, the acceleration

of the centre of the front wheel has discontinuities and peaky spikes, therefore numerical differentiation will be sensitive and unstable. However, it appears that if the acceleration is less spikey and more continuous, such that the approximated spline will be more differentiable, its derivatives can achieve the general profiles of the computed velocity and acceleration curves. This seems to improve as the interpolating curve is prescribed with finer knots, as demonstrated in the case of the dummy's chest. But this does not mean that if every data point is prescribed as an interior knot, the derivatives gained will be the same as the computed velocity and acceleration. This is demonstrated in Figure 7.6b where the dummy's chest displacement curves are spline fitted with every known data point.

Comparing to the ACSL simulated graphs in Figure 7.2a, we see that the fitted displacement is visually identical to the simulated equivalent, even the first derivative representing the velocity does not produce any obvious discrepancy from the computed velocity. However the second derivative produces a curve holding the general profile but with numerous spikes. This is due to the splines being prescribed too finely such that the slopes will be very sensitive, and this accumulates with the second derivatives onwards. Another contributory factor is the accuracy of the computer. Rounding errors and the inaccurate definition of zero are inevitable problems with computers, and differentiation to these minute fluctuations is extremely sensitive.

7.2 Integration

Raw measurements obtained from an accelerometer are generally filtered in order to minimise the existence of randomly generated noise. In the integration part of this investigation, we shall apply this comparable procedure to an ACSL computed acceleration curve, then integrate the filtered acceleration once to give velocity and twice to give displacement. These are then to be compared with the computed equivalents to see the effect of filtering or 'smoothing'.

There are several standard filters in the field of signal processing, but since we are making a parallel operation with TRL, where the low-pass Butterworth filter is employed, we shall consider this well-known filter in this investigation. For a mathematical derivation consult Appendix A.2.

7.2.1 The Butterworth Filter

The simulated acceleration, from crash test simulation L4, of the centre of the front wheel is chosen to be filtered using the second-order Butterworth filter. This is done by using the Pro-matlab routines (The MathWorks inc., [29]). The user is required to adjust the frequency W_n such that $0 < W_n \leq 1.0$, where 1.0

corresponds to half the sampling rate. Note that this has the effect of non-filtering if W_n is set to 1.0.

In the computer simulation, the response is every one millisecond, therefore the half-sampling rate is 500 Hertz. If, for example, W_n is set to 0.2, the frequency is equivalent to 100 Hertz.

A range of different values of W_n is applied. The higher the value of W_n within the range $0 < W_n \leq 1.0$ the more noise passes through the filter, and subsequently the filtered curve still retains some of the spikey characteristics.

Figure 7.7a contains six of the filtered acceleration curves of the centre of the front wheel. The cut-off frequency of each case is also shown. Notice at 50 Hertz, equivalent to $W_n = 0.1$, the curve is 'smooth'. At 100 Hertz, the curve is still relatively smooth but has started to retain some of its original profile without too peaked a spike. At 250 Hertz onwards, the true characteristics of the original curve starts to emerge. As the cut-off frequency approaches half the sampling rate, less filtering has been made. At 500 Hertz the curve is seen to be 'un-filtered' if compare to the ACSL simulation graph shown in Figure 7.3b.

In Figure 7.7b the integrated velocity curves of the

corresponding filtered accelerations are shown. Note that the integration is done by ACSL, with the numerical values of the filtered acceleration fed into the program and the initial condition specified. The curves seem to resemble each other, indeed, there are only two regions of each of the curves which show a minute difference from the other graphs, they are: the initial decrease in velocity at around 150ms, which corresponds to the sharp peak in the acceleration curve, a discontinuity: and the minima of the velocity curve at around 185ms, which corresponds to the rapid fall in the acceleration curve.

Two observations can be made from the integration exercise. The first is the fact that the velocities are all very similar. This would imply that within the ACSL integrator there is some sort of 'smoothing' process in the numerical algorithms. Secondly, the integrated velocity of the acceleration which was filtered with the cut-off frequency at 500 Hertz, does not resemble to the ACSL computed velocity. In theory, if the acceleration was unfiltered, when it was integrated using the same software, the resulting velocity should be the same as the original computed velocity.

There is an explanation to the outcome of the second observation, and it is about the numerical accuracy of the data. We know that ACSL is a continuous simulation language with results output at a regular interval specified by the user. However, the filtered acceleration fed back to the ACSL program was read discretely,

with continuous information between successive intervals being lost, hence losing some of the important characteristics of the original acceleration. In addition, within the actual ACSL simulation numbers are computed in double-precision format, but these numbers, when outputted to a medium, are only specified to twelve significant places, and thus the accuracy of input into MATLAB had been truncated. The difference in terms of accuracy between computed and read-in data thus becomes apparent.

Just to further illustrate the smoothing process of integration, Figure 7.7c contains the second integrals of the filtered accelerations in Figure 7.7a. As can be seen, there is no visual difference between the curves. This demonstrates that on the first integration, sharp spikes were smoothed/filtered so to minimise the discontinuities as in Figure 7.7b, and thus on second integration, the effect of smoothing is such that there is no apparent difference between these different integrals.

Note the subsequent integrals of the acceleration filtered at the cut-off frequency of 500 Hertz do not agree with the original computed velocity and displacement as shown in Figure 7.3b. This is due to the loss of accuracy as explained earlier.

However, the acceleration curve of the centre of the front wheel is peaked with sharp spikes. We will employ a smoother acceleration curve, say that of the dummy's chest, to verify the

effectiveness of a filter and its subsequent integrations. This is similar to the exercise operated in the differentiation part of this investigation.

Figure 7.8a contains the filtered acceleration curves of the dummy's chest. These curves have been passed through the Butterworth filter at the same cut-off frequencies as was in the case of the centre of the front wheel. The first graph at cut-off frequency of 50 Hertz produces a smooth curve with no peaked spike, although the maximum has been reduced noticeably. The second curve at cut-off frequency of 100 Hertz is still smooth with no spike, but the peak acceleration has been retained by the filter to nearer to its true peak. From there onwards, the filter has emitted more noise as the cut-off frequency was adjusted higher. The shape of the curve gradually becomes more peaked although still retaining its general profile, until at 500 Hertz the curve is seen to be 'unfiltered'.

Figure 7.8b contains the corresponding first integral of the accelerations. Although they are all very similar, as explained before, with only minute differences between 250ms to 300ms observable, the noticeable fact is that they do resemble the simulated velocity curve in Figure 7.2a. The most obvious difference is the decrease in velocity from 200ms to 300ms. This demonstrates further the difference between continuously generated information and discretely read-in data.

Figure 7.8c contains the second integrals of the filtered accelerations. Similarly to those of the centre of the front wheel, there is no apparent difference between them, although they resemble much more the simulated displacement than in the case of the front wheel. There is a loss in displacement from 200ms to 300ms if compared to the graph in Figure 7.2a. This is due to the decrease in velocity as mentioned above.

The above demonstrates the effectiveness of filtering. It will smooth out more sharp spikes and ripples as the noise passing through the filter is being reduced. But on integration, in which itself is similar to a 'smoothing' process, integrals from functions filtered at different cut-off frequencies do not present obvious differences. It is even more so on the second integration. However, it is observed that subsequent integrals do not revert back to their simulated equivalents, when the original curve is filtered at exactly half the sampling rate, but a smoother curve with not many sharp peaked spikes will produce integrals that are more similar to their computed equivalents.

Now a question may arise about filtering computed data: is this necessary? since computer generated data are, unlike real events, exempt from randomly generated noise from instrumentation. Even if they need to be filtered, what is the range of the cut-off frequency?

The question was put back to TRL, since this is a simulation model running in parallel with the real crash test procedure at TRL. The response was that they do filter their raw measurements, using the SAE (Society of Automotive Engineers) standard of 600 Hertz.

Raw data are recorded at a much higher frequency in TRL than in this simulation model. To run the simulation procedure in accordance with TRL, one tries to operate as closely as possible with their experimental procedure. This means the nearest cut-off frequency we can apply, using the simulation model as it stands, is 500 Hertz, which is equivalent to non-filtering of data.

Before a decision is made whether to filter computed data or not, one must verify the different procedures made and justify whatever decision is finally agreed upon.

Since our simulation program has been running at a frequency of 1,000 Hertz throughout, it is not justifiable to make a comparison with what have been the procedures at TRL. It is wise to run the same computer program but at a higher frequency, say 5,000 Hertz, and then apply the filtering procedure as before, and compare the filtered data between the high frequency run and the usual low frequency run of 1,000 Hertz. After this, a judgement can be made as to whether or not to filter the simulation results, which are all of 1,000 Hertz, or to choose

a filter of a different cut-off frequency.

Figure 7.9 contains two sets of the filtered acceleration of the centre of the front wheel. Both have been passed through a Butterworth filter of half of their sampling rates, 2,500 Hertz for the high frequency run and 500 Hertz for the low frequency run, and also both at 50 Hertz. This is to demonstrate their unfiltered natures, and at a very low frequency so to examine if there would be a considerable difference between the two frequency simulations when the accelerations were filtered at the same cut-off frequency. In addition, the high frequency simulation's curve is also filtered at 500 Hertz. This is a direct comparison with the low frequency simulation.

As can be seen the general profile of the curve has been retained in the two different frequency simulations. The most noticeable differences are the peaks of the two spikes at around 160ms in the high frequency graphs, and at around 150ms in the low frequency graph. In the high frequency simulation the signals of these two spikes are higher than those in the low frequency simulation. As the cut-off frequency decreases, less noise has been passed through the filter. When the cut-off frequency is very low, the two acceleration curves are virtually identical.

Attention needs to be paid to the 500 Hertz Butterworth filter. The two different frequency acceleration curves, when filtered

at the same 500 Hertz cut-off frequency, are very similar to each other. This is with the exception of the two sharp spikes. But they are the discontinuities within the system, and in a real-life event they will surely be filtered out. Therefore it is justified that using our simulation model running at a frequency of 1,000 Hertz, we can apply a 500 Hertz Butterworth filter (in effect, non-filtering) to the data so to achieve as close as possible the SAE standard TRL employs.

7.3 Overview

It was found, within this investigation of differentiation and integration, that neither can revert their derivatives and integrals back to the original states, such that they are the same as their computed equivalents. However, below is a list of the more detailed observations of the spline fitting and Butterworth filtering processes.

- (1) The accuracy of the derivatives increases as finer splines are introduced in the original curve fitting process.
- (2) However, if all known data points are used as splines it does not lead to the exact derivatives as computed by the simulation program.
- (3) Butterworth filtering produces similar integrals but of more smooth profiles. This is even more so as cut-off frequency

is lowered, i.e. less noise being emitted from the original curve.

- (4) But when a curve is filtered at half the sampling rate, such that effectively it is unfiltered, its integrals are not the exact integrals as computed by the simulation program.

However, it has been concluded, in general that the integration process produces better results, such that they resemble more to their computed equivalents, than the differentiation process.

The final part of the investigation was concerned with the amount of noise to be filtered. It was found that TRL operates on the SAE standard of 600 Hertz. This presents us with the problem of incompatibility, since our simulation has been running on a lower frequency basis, therefore the nearest acceptable cut-off frequency is 500 Hertz, equivalent to non-filtering.

The same crash test simulation was run but at a higher frequency. It was observed that when these high frequency data are put through the Butterworth filter, the filtered data are similar to the low frequency data as the cut-off frequency is being decreased. Certainly at the same 500 Hertz cut-off frequency, it is very similar to the low frequency data except with some sharp discontinuities, which in reality would be ignored. It is concluded that within this research project, the simulated data need not to be filtered.

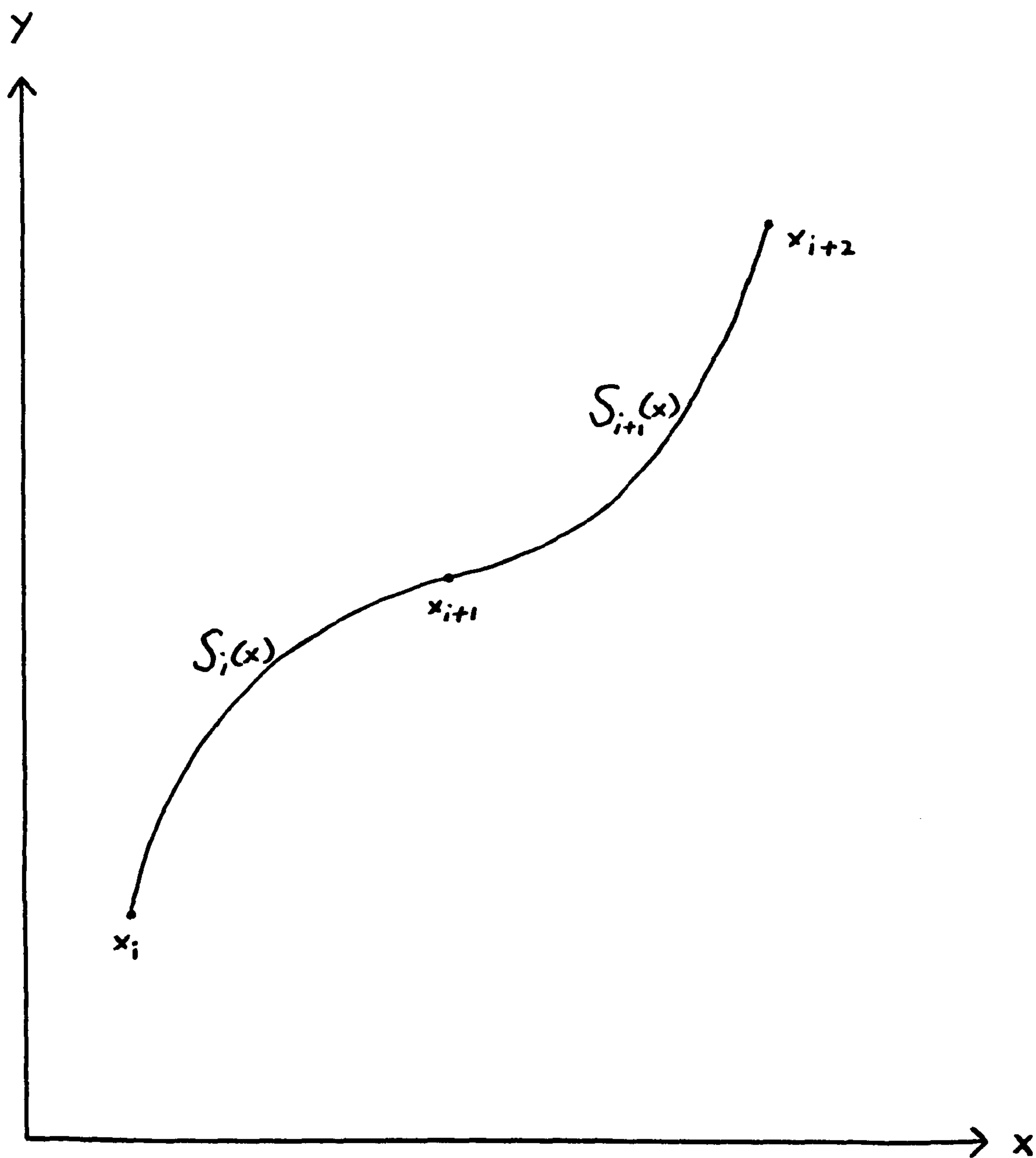


Figure 7.1 Interpolation by spline functions.

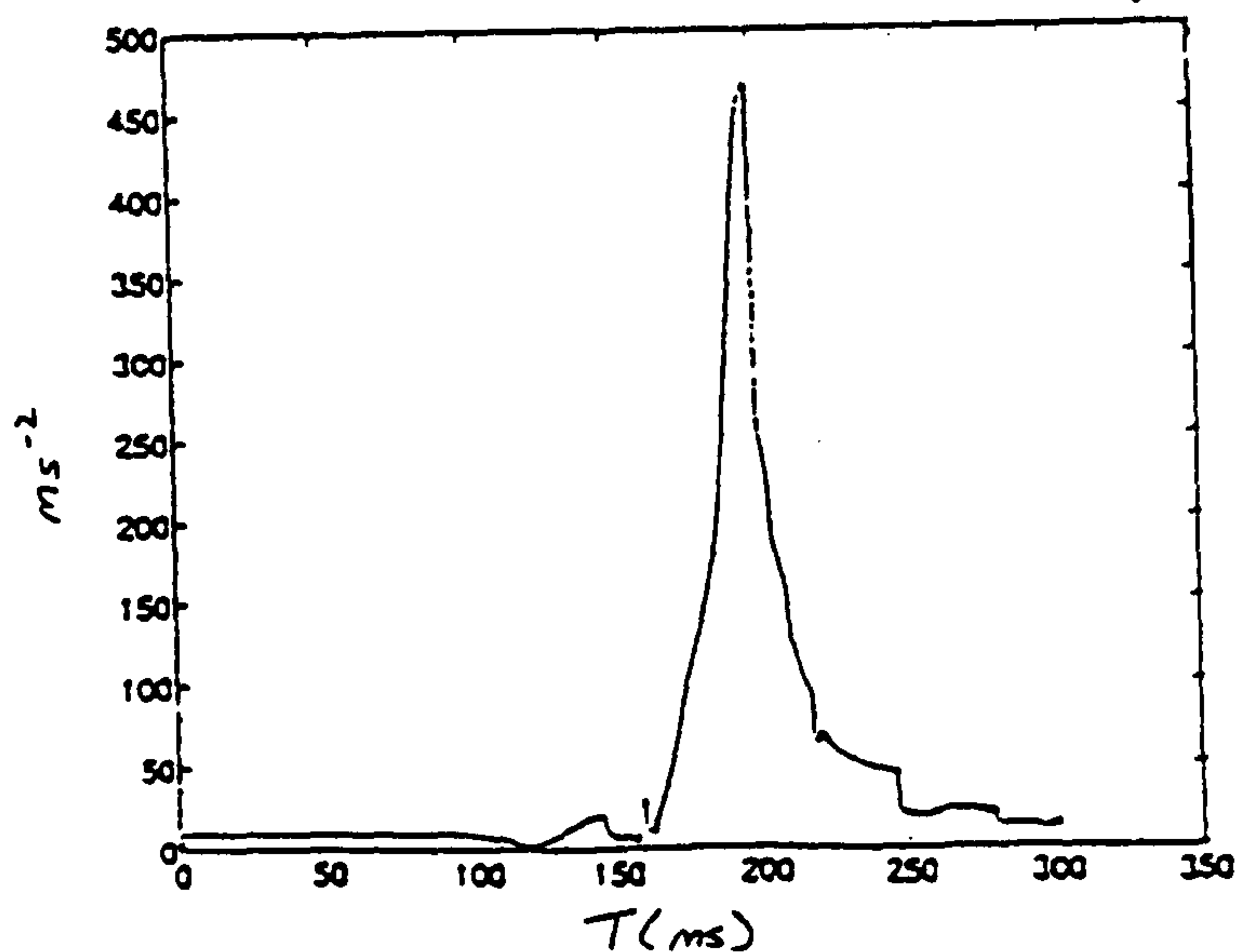
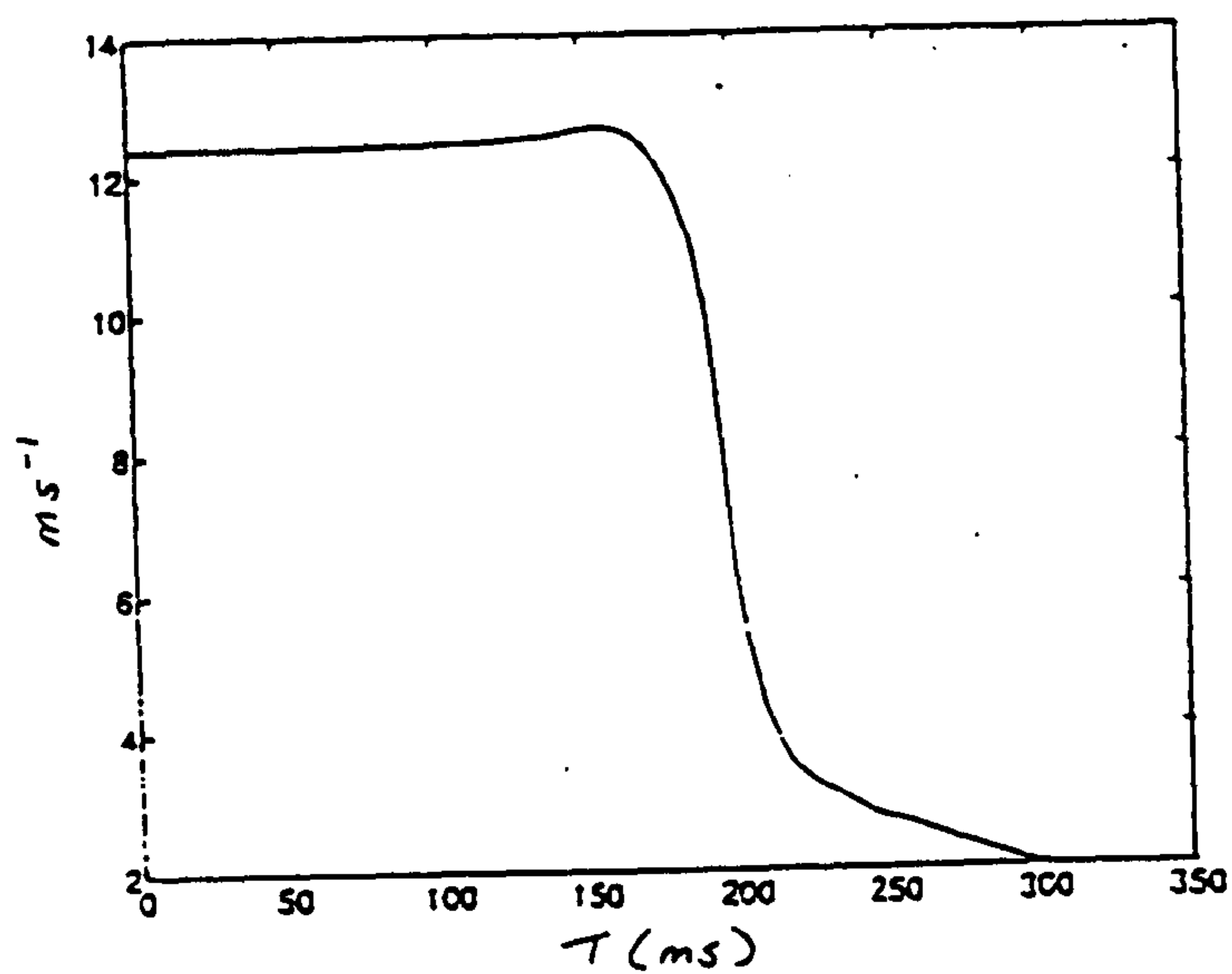
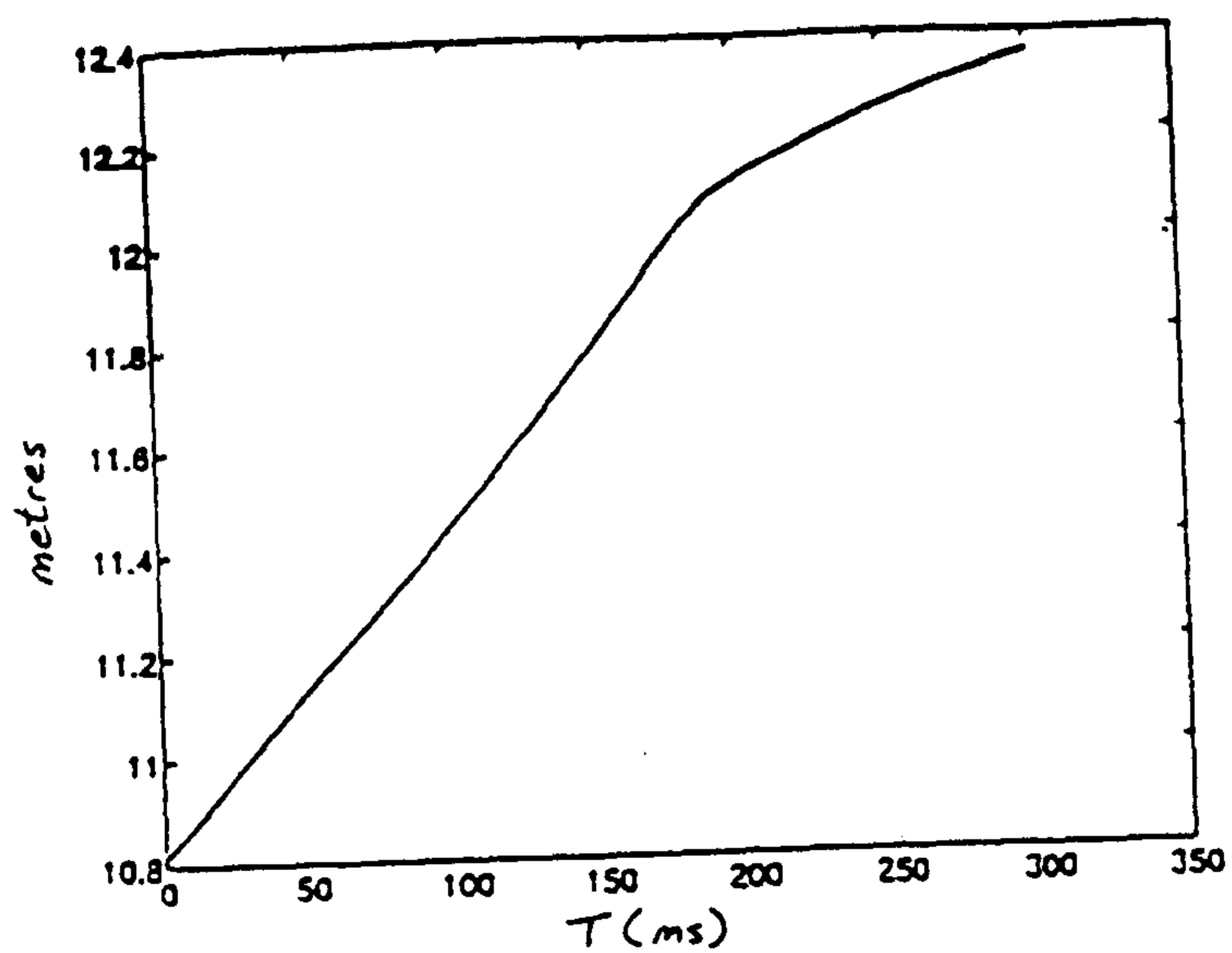


Figure 7.2a ACSL computed resultant displacement, velocity and acceleration, respectively, of the dummy's chest from the L4 test.

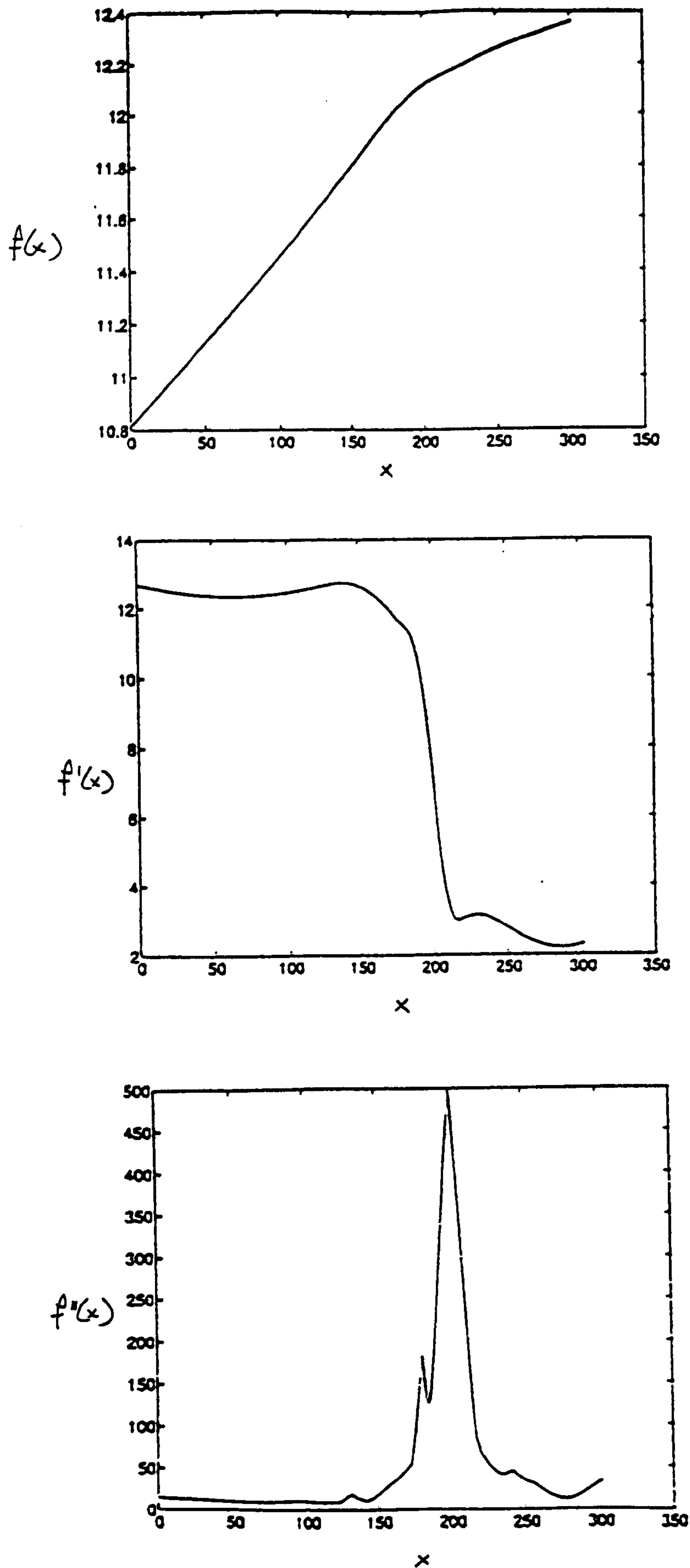


Figure 7.2b Cubic splines fitted resultant displacement of the dummy's chest, $f(x)$, and its first and second derivatives, respectively.

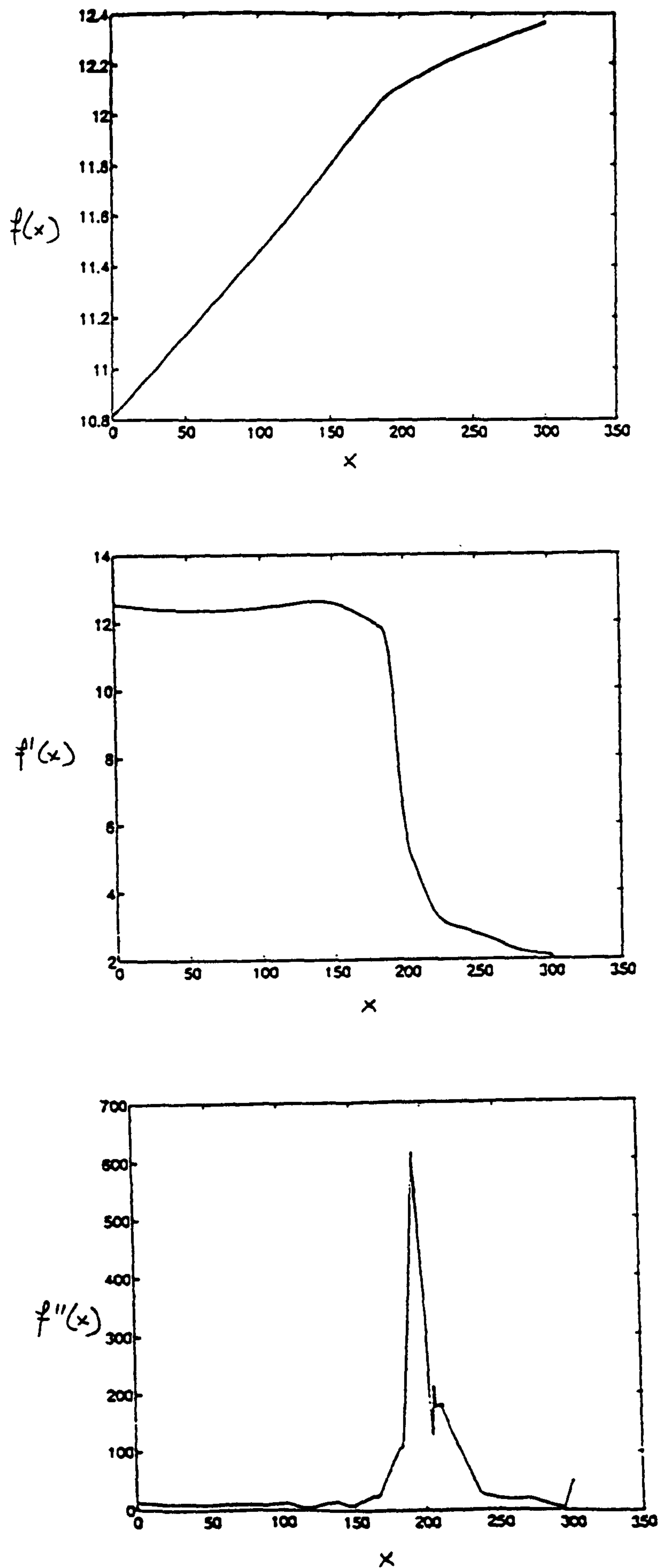


Figure 7.2c Cubic splines fitted resultant displacement of the dummy's chest, $f(x)$, where the number of interior knots had been increased, and its first and second derivatives, respectively.

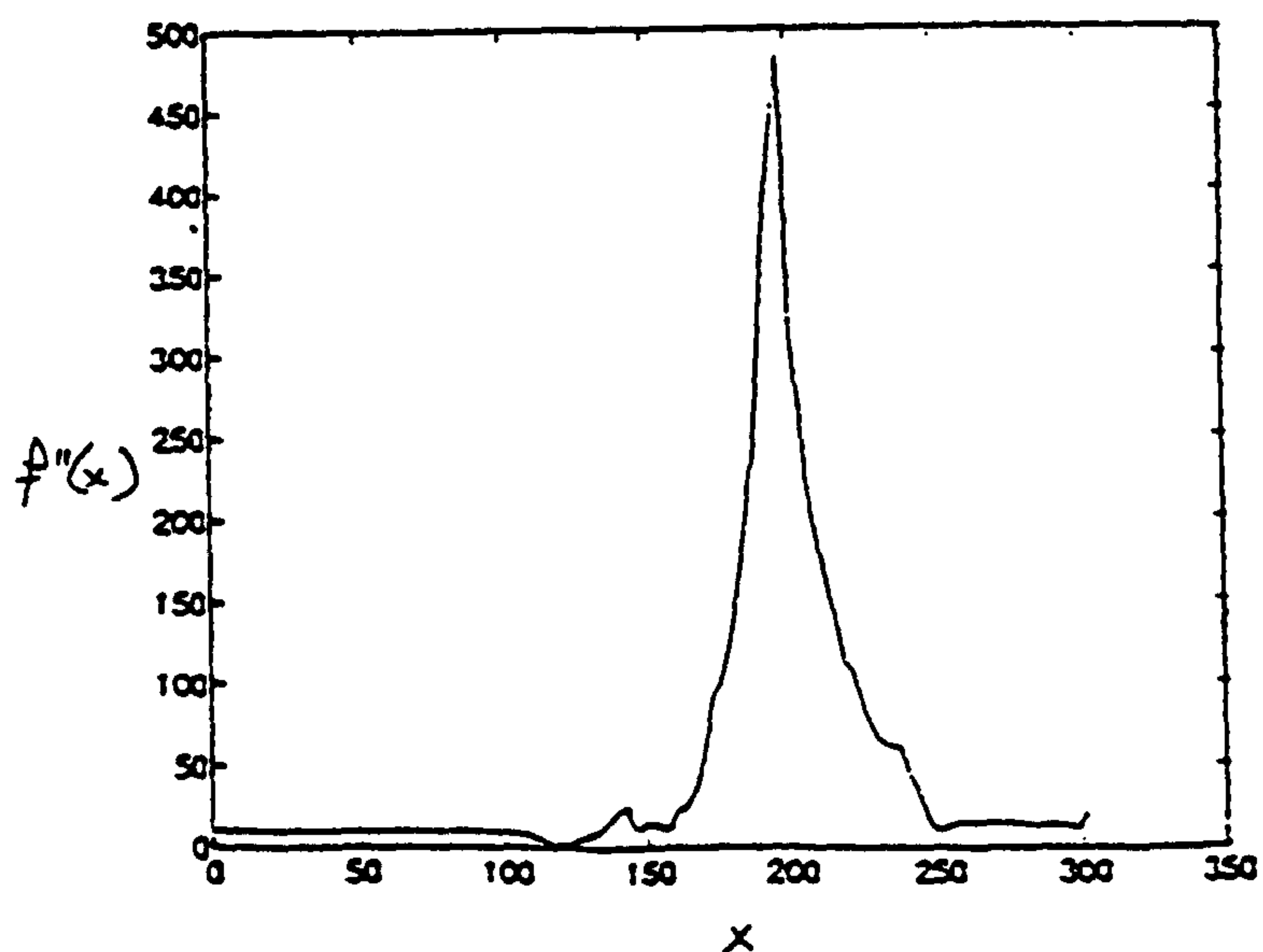
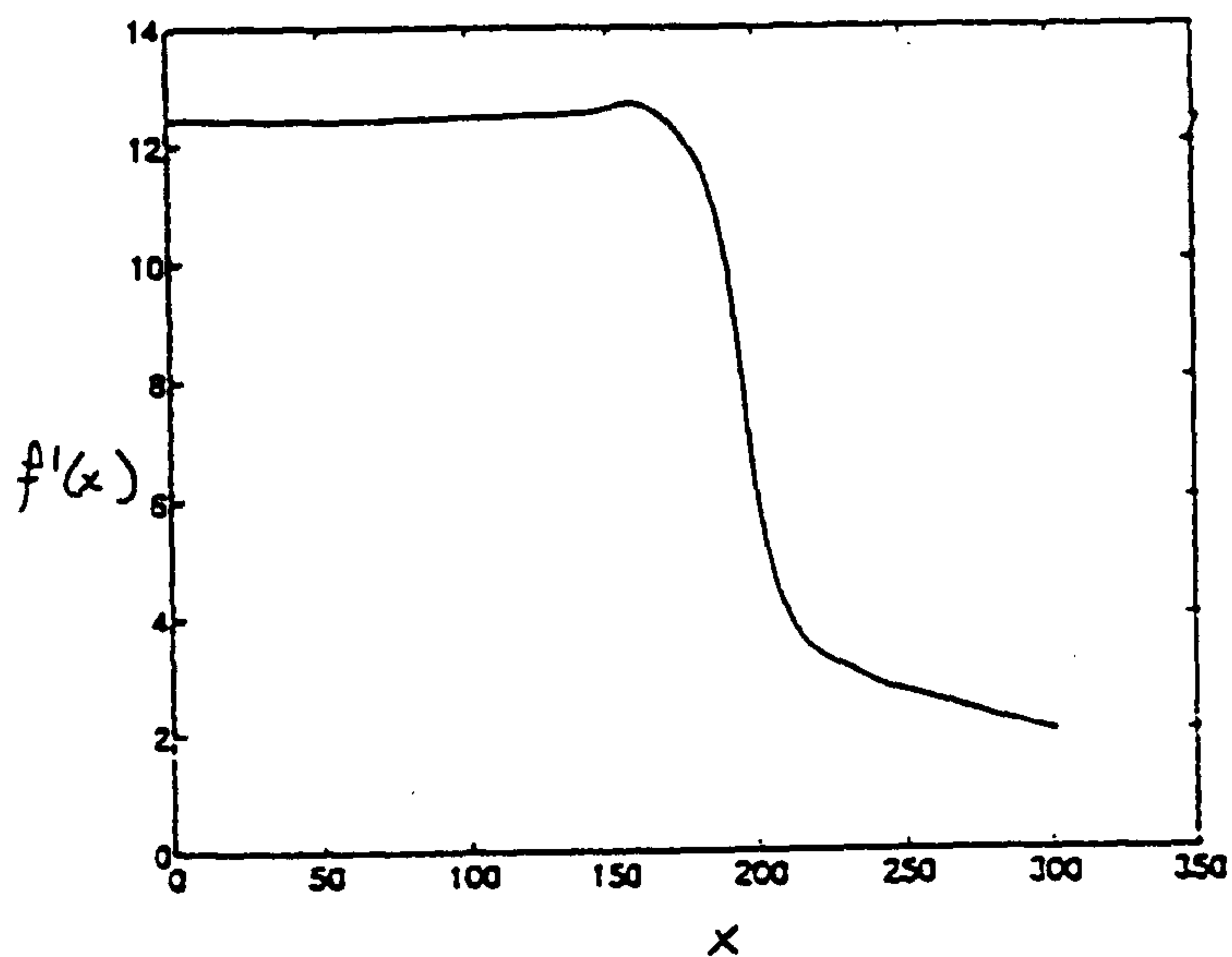
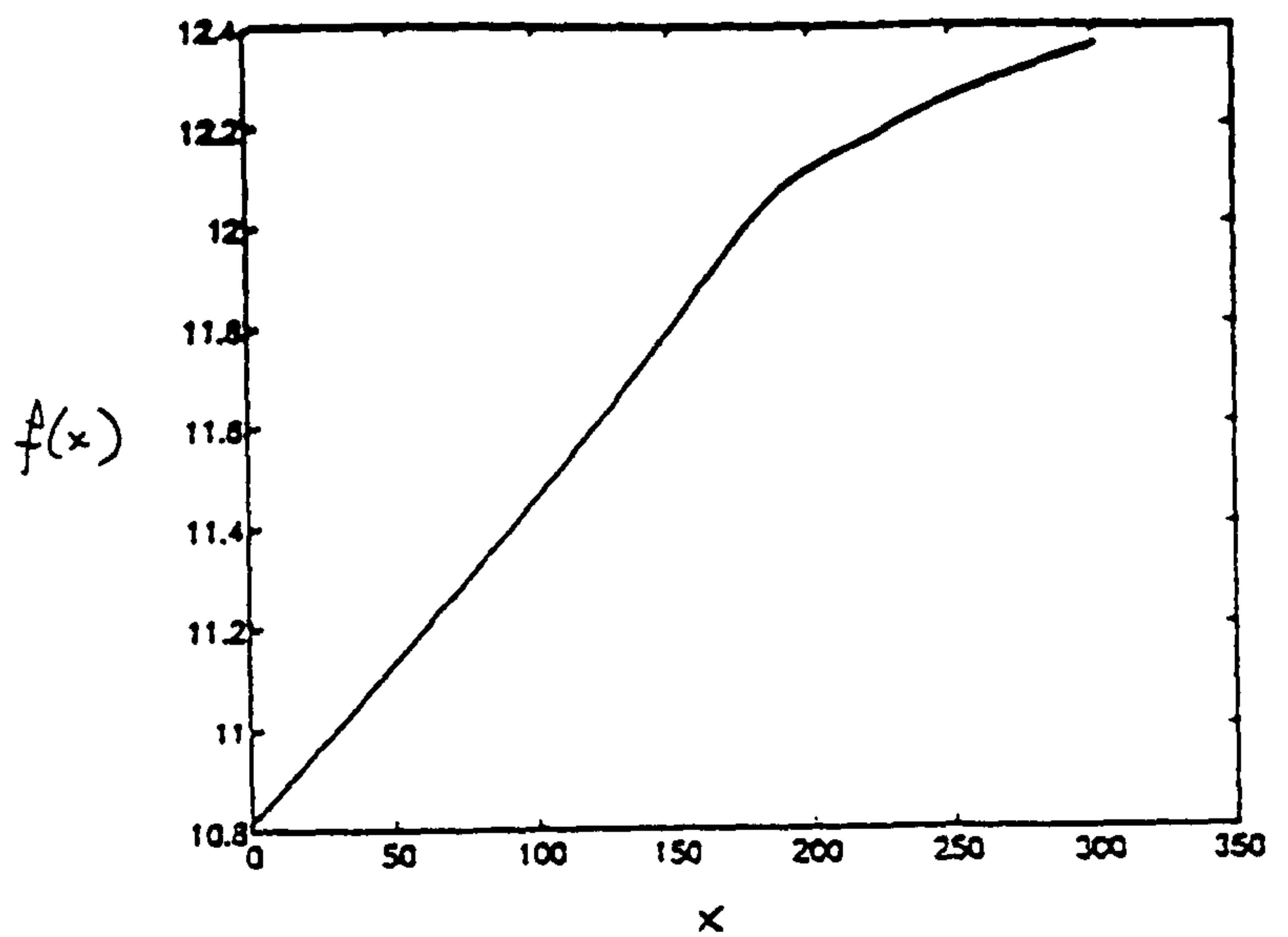


Figure 7.2d Cubic splines fitted resultant displacement of the dummy's chest, $f(x)$, where the number of interior knots had been further increased, and its first and second derivatives, respectively.

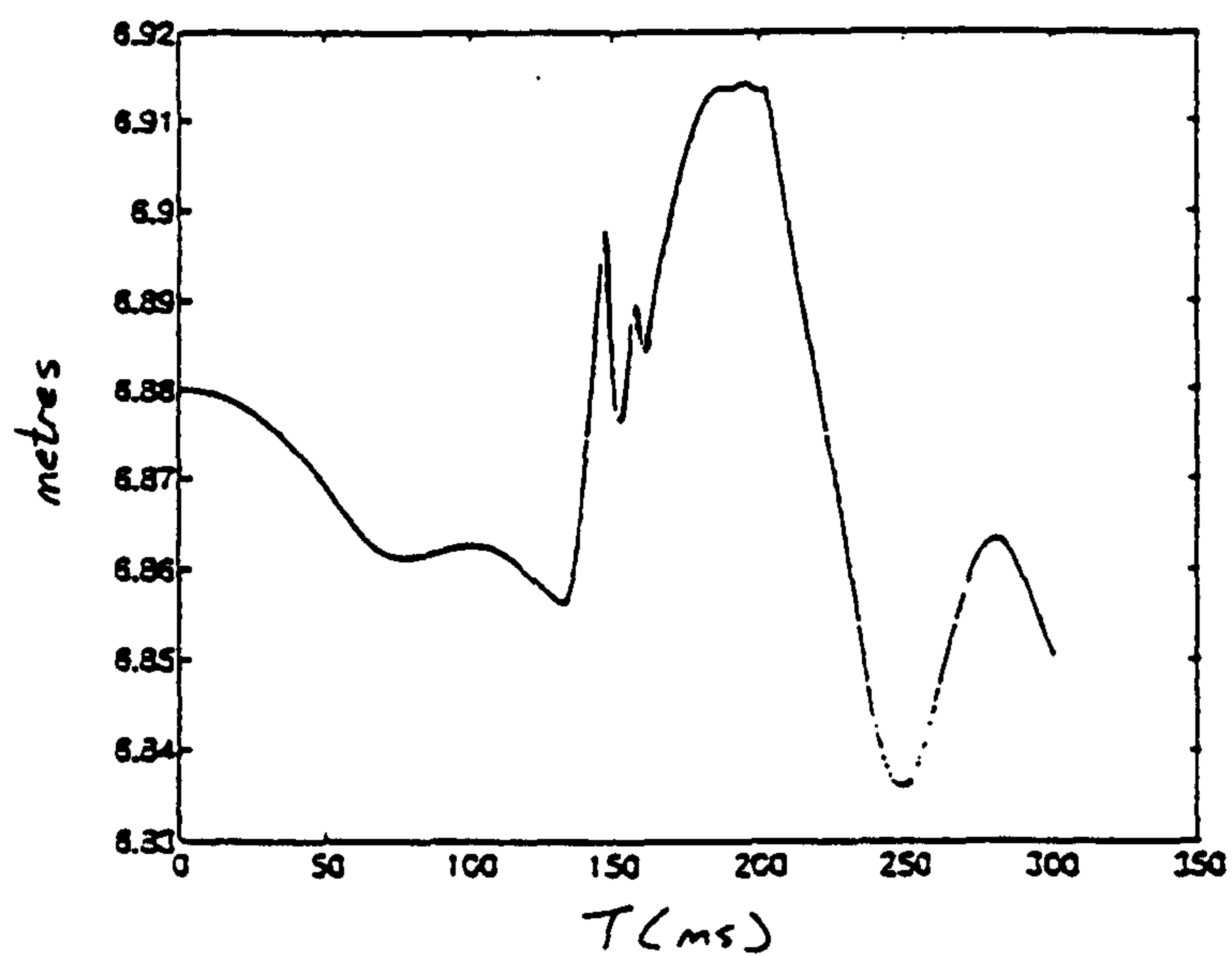
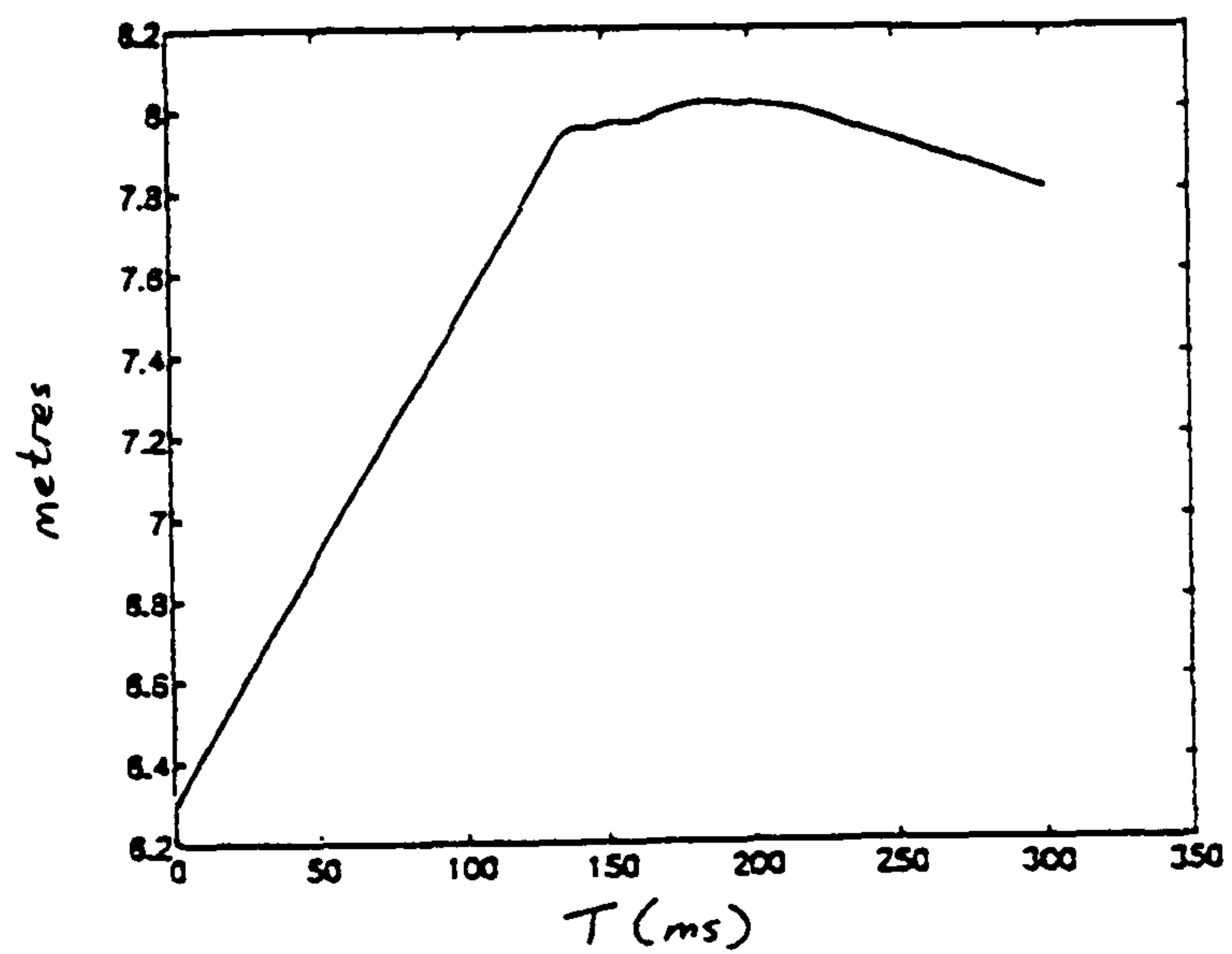


Figure 7.3a ACSL computed fore-and-aft and vertical displacement, respectively, of the centre of the front wheel from the L4 test.

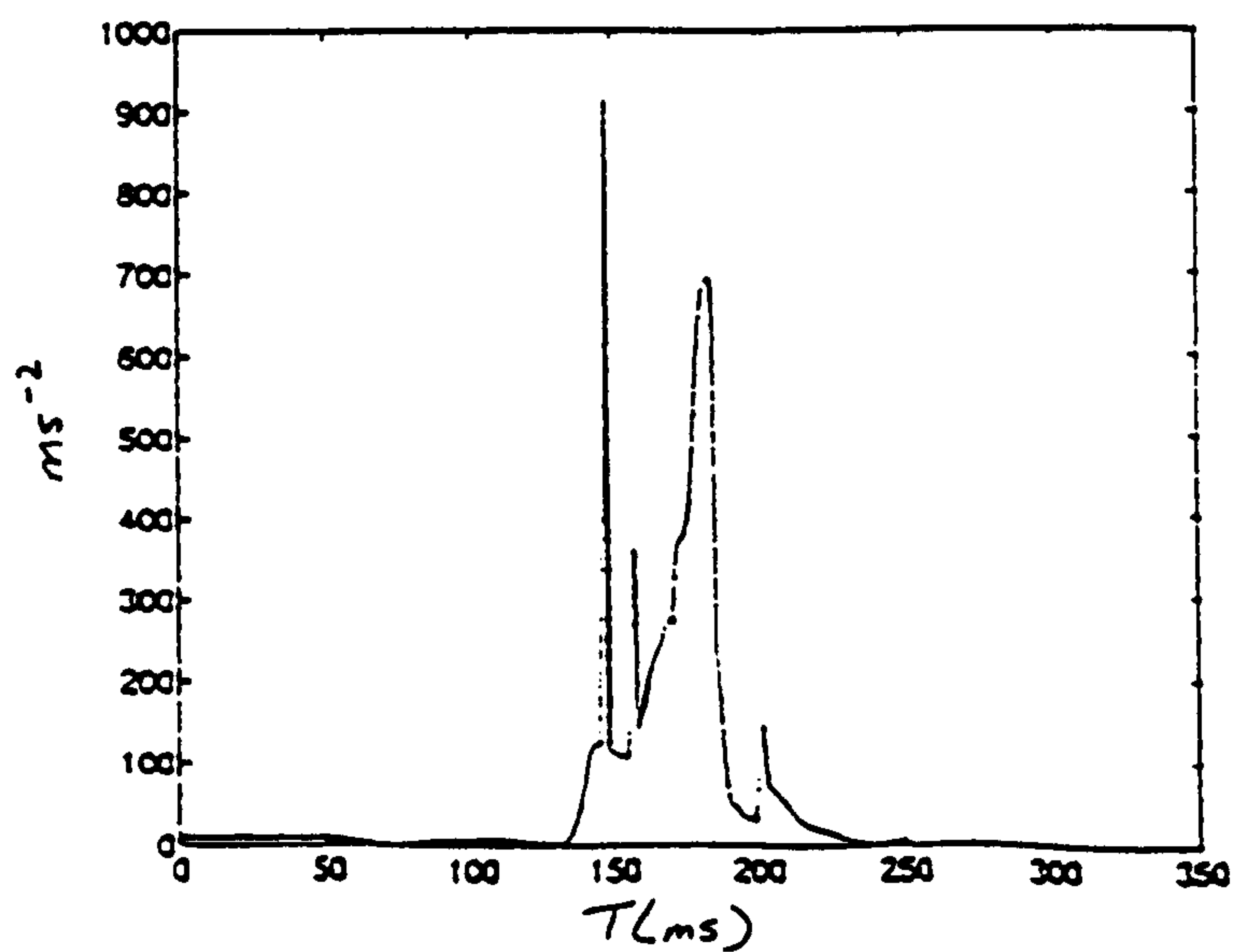
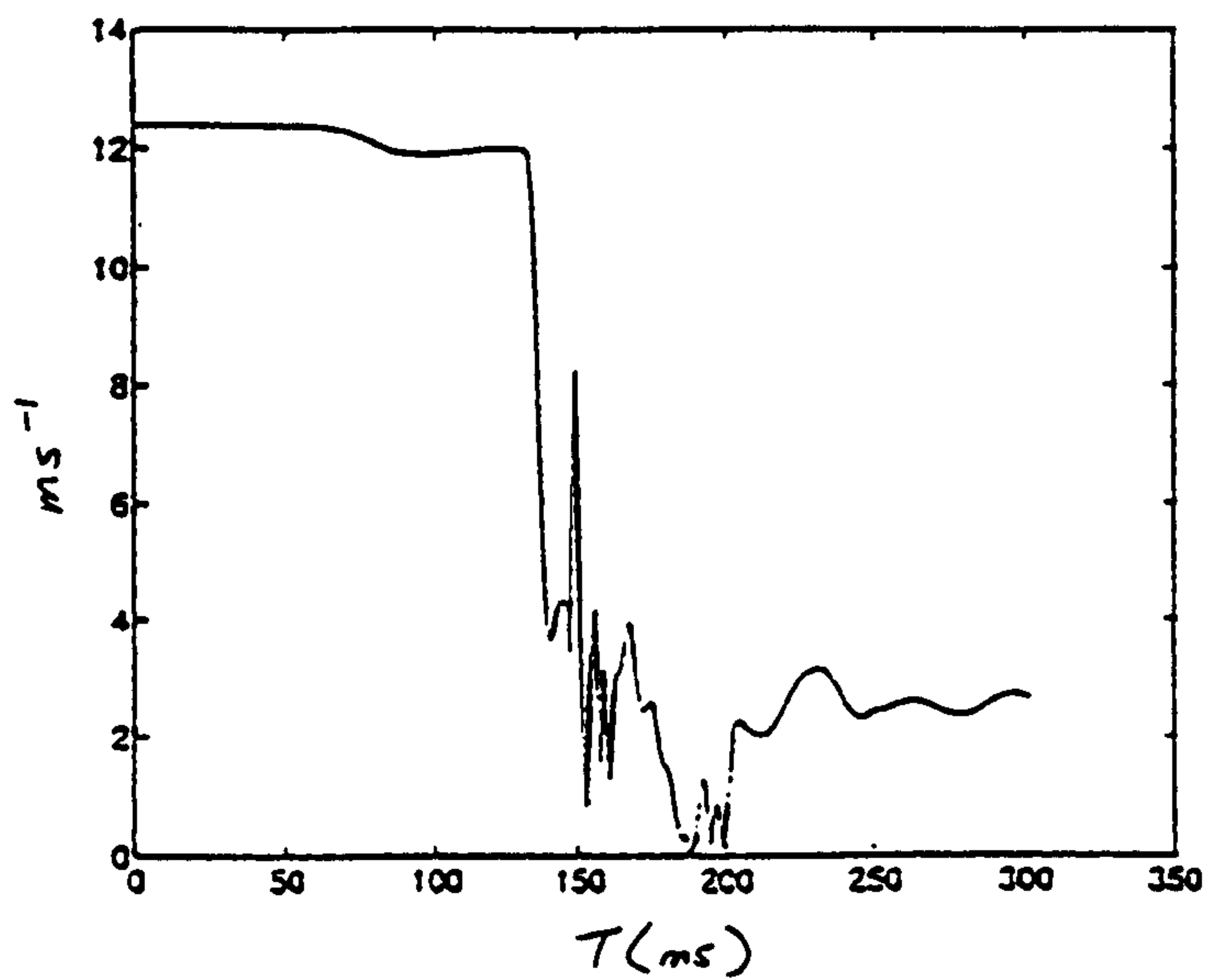
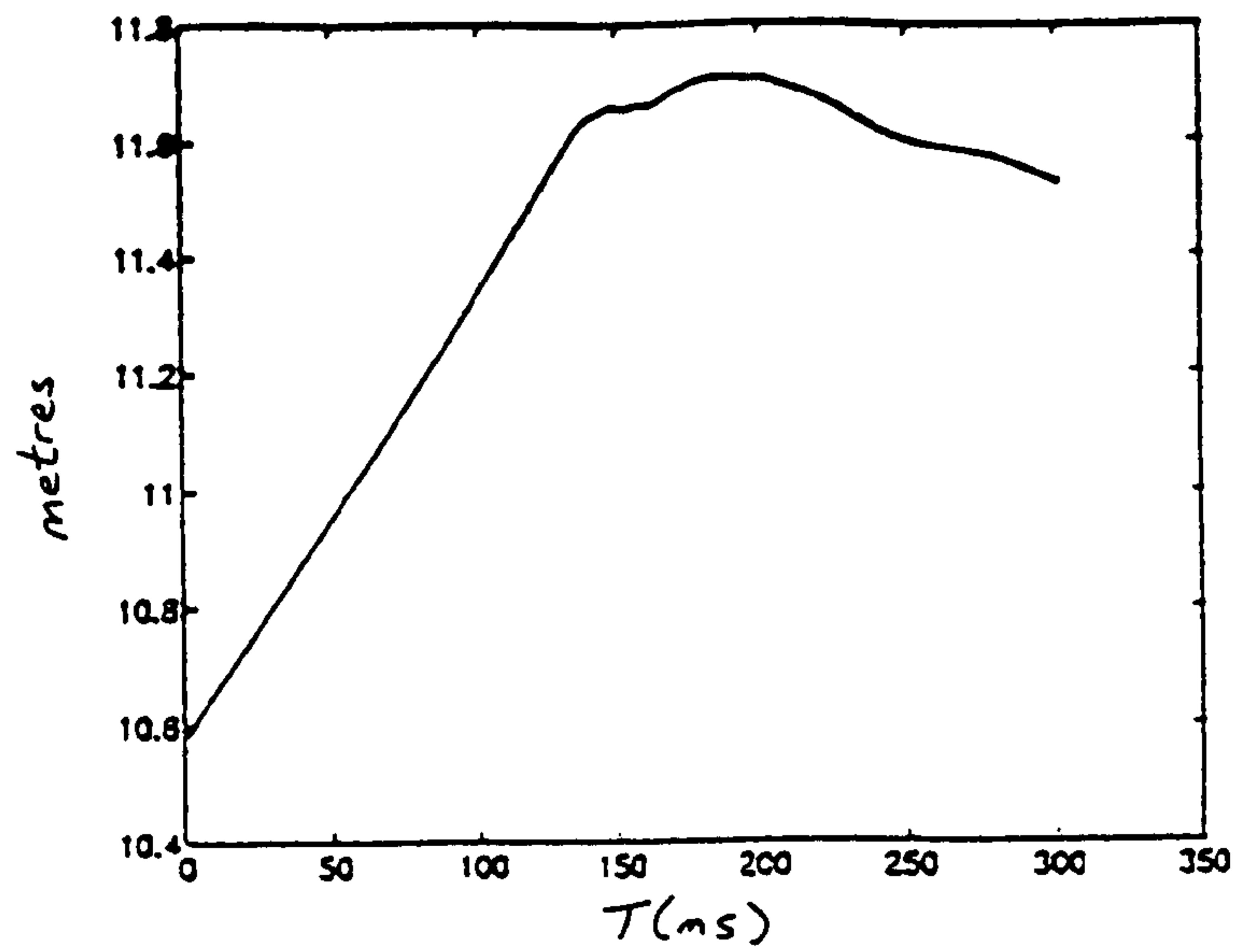


Figure 7.3b ACSL computed resultant displacement, velocity and acceleration, respectively, of the centre of the front wheel.

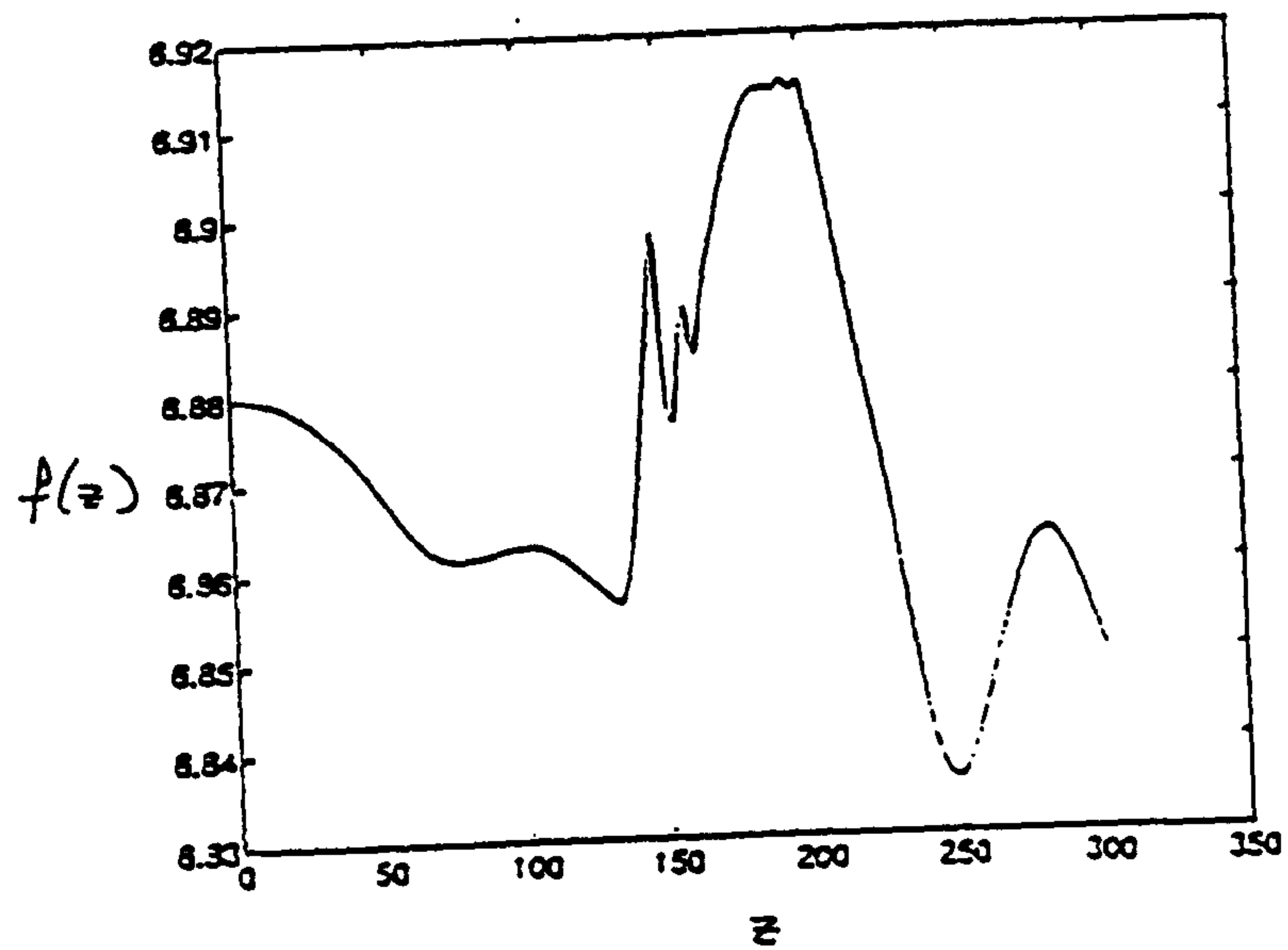
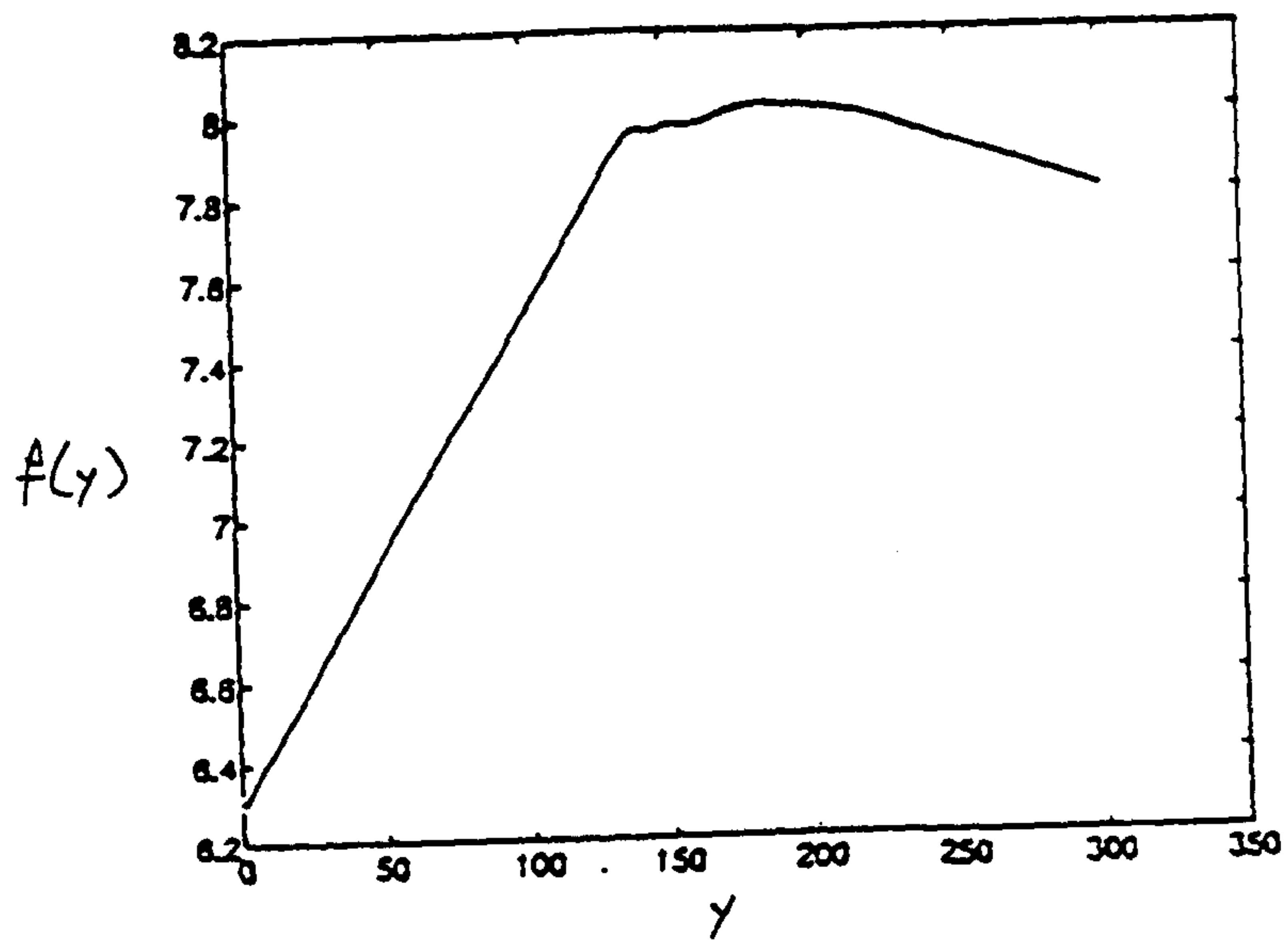


Figure 7.4a Cubic splines fitted of fore-and-aft, $f(y)$, and vertical, $f(z)$, displacements respectively, of the centre of the front wheel.

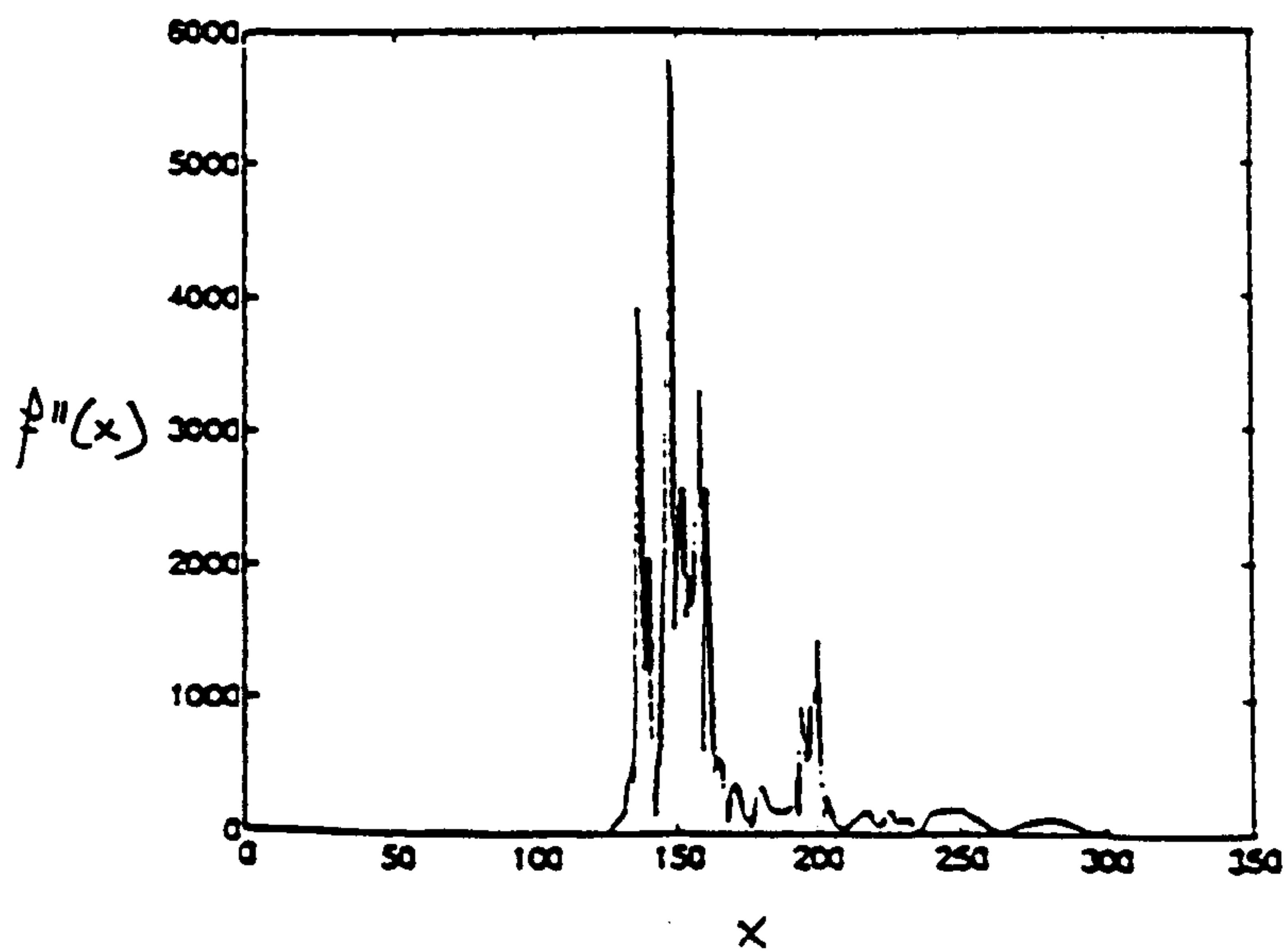
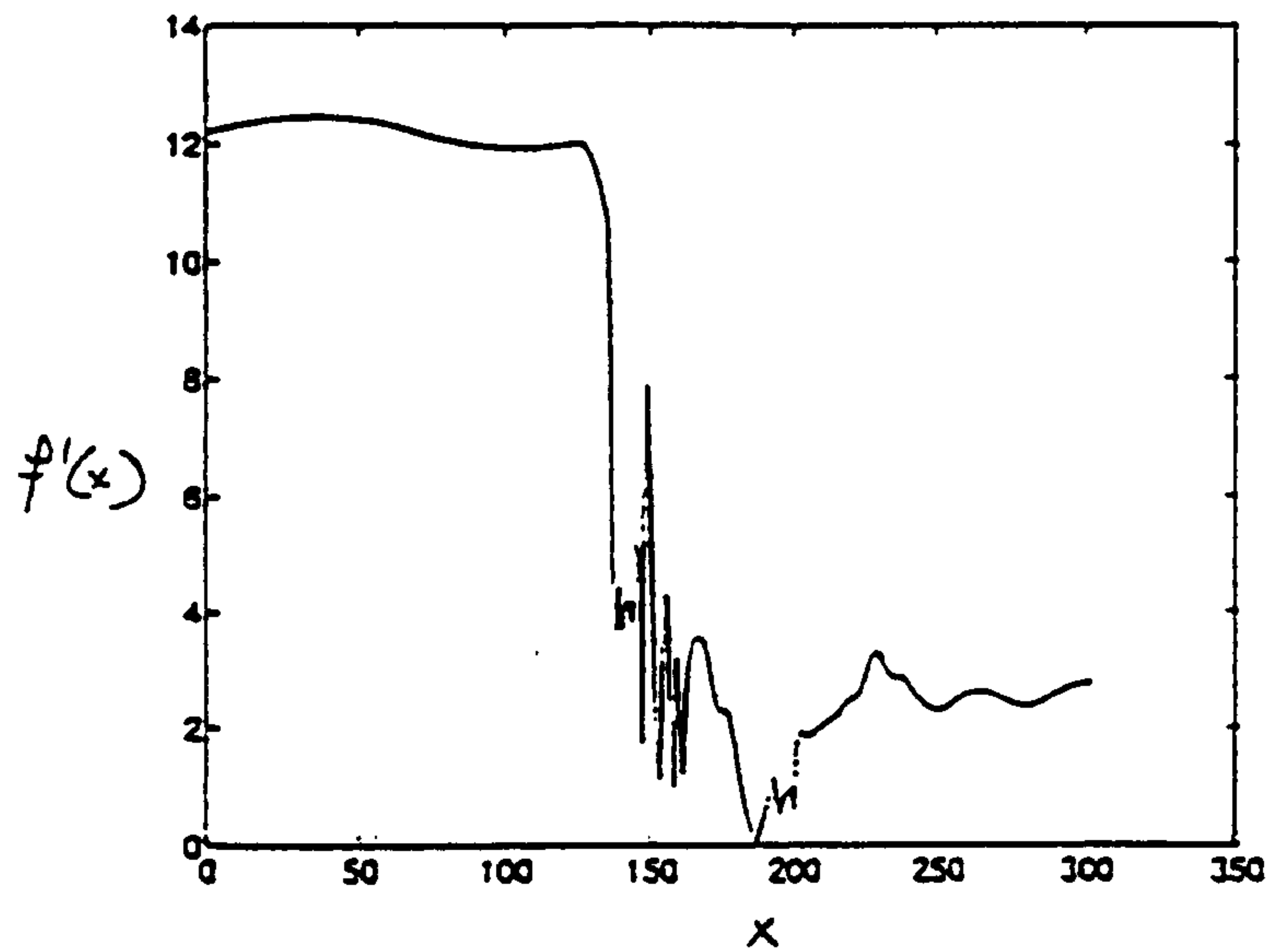
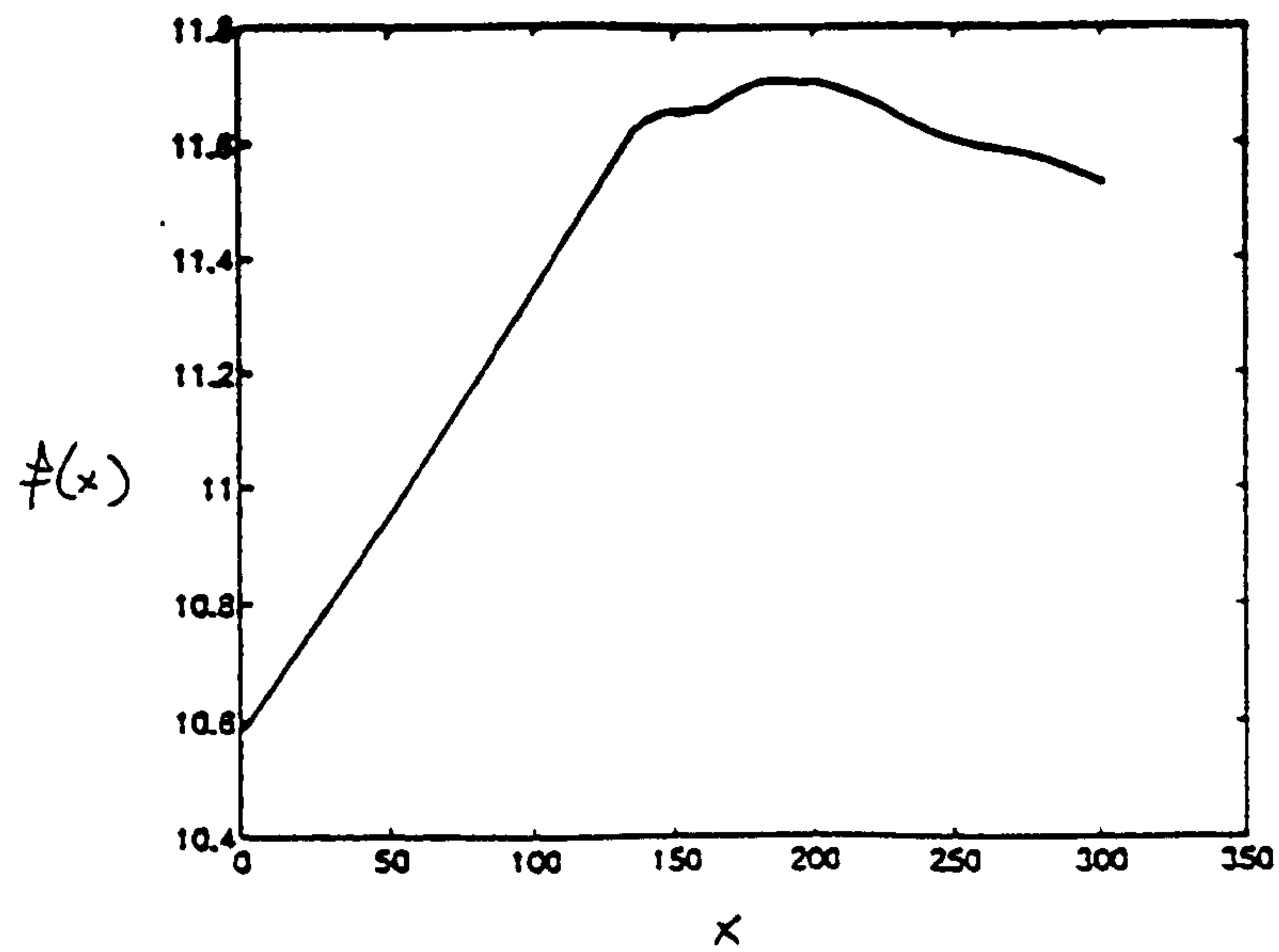


Figure 7.4b Cubic splines fitted resultant displacement of the centre of the front wheel, $f(x)$, and its first and second derivatives, respectively.

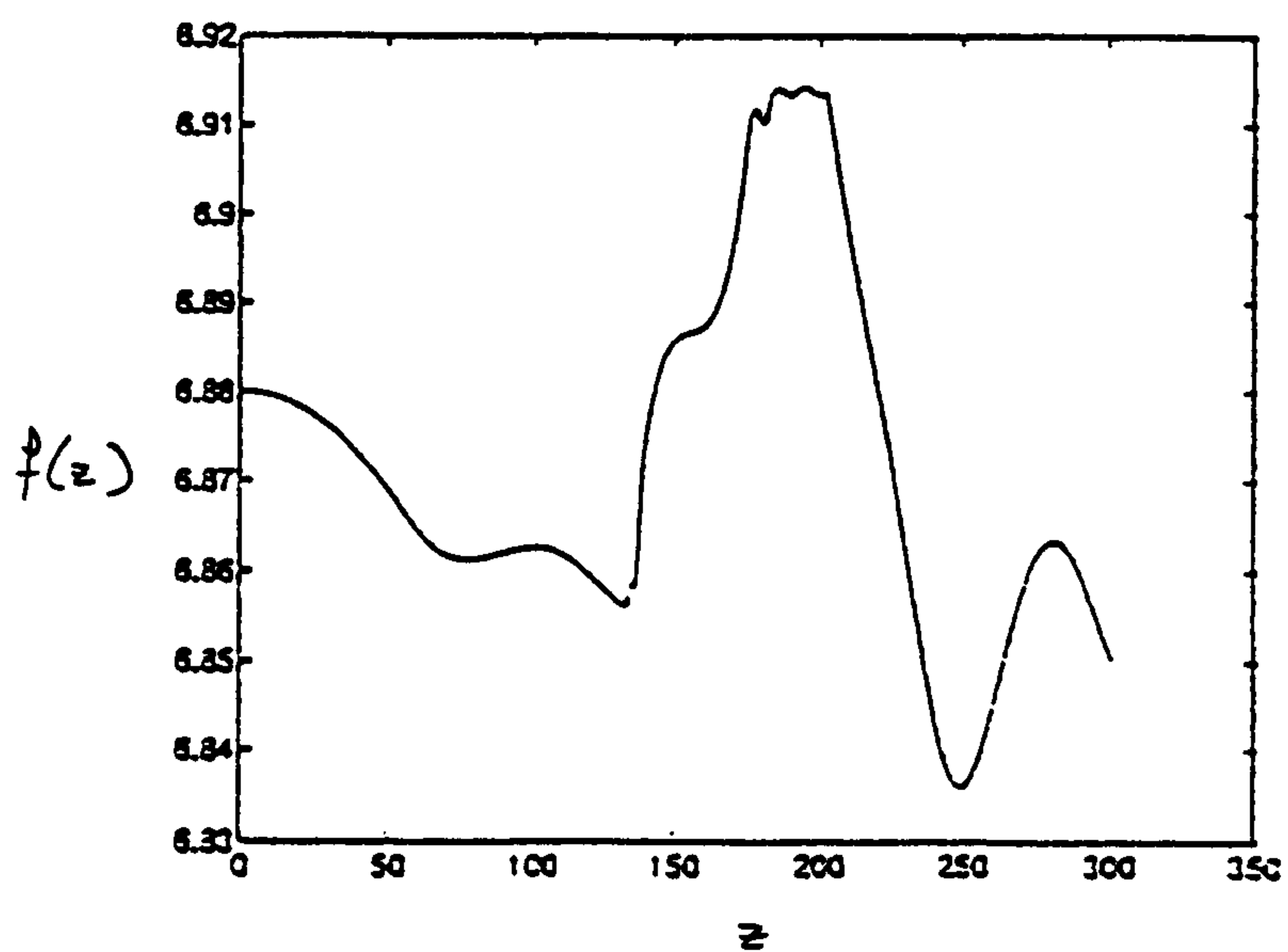
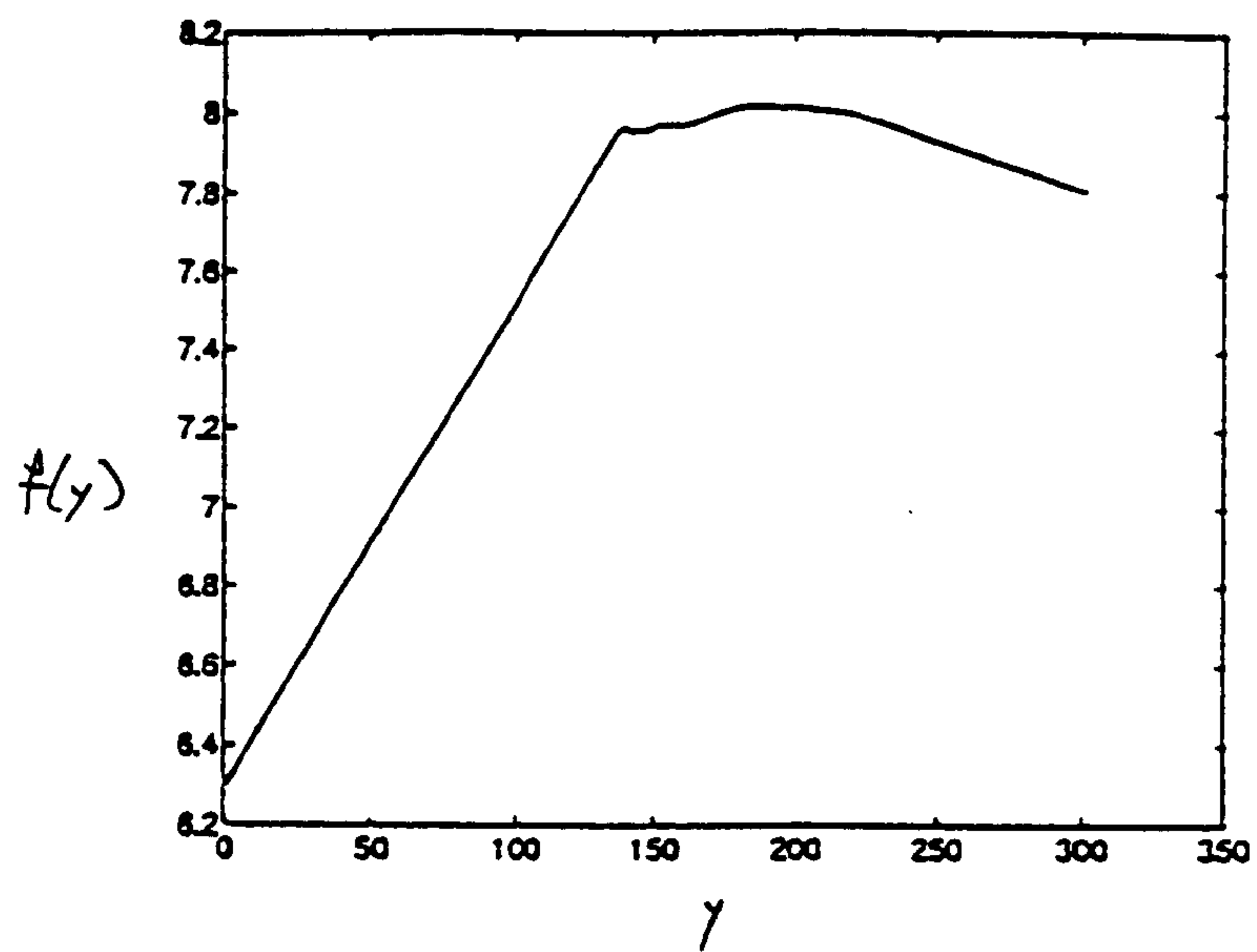


Figure 7.5a Cubic splines fitted of fore-and-aft, $f(y)$, and vertical, $f(z)$, displacements respectively, of the centre of the front wheel, where the number of the interior knots had been decreased.

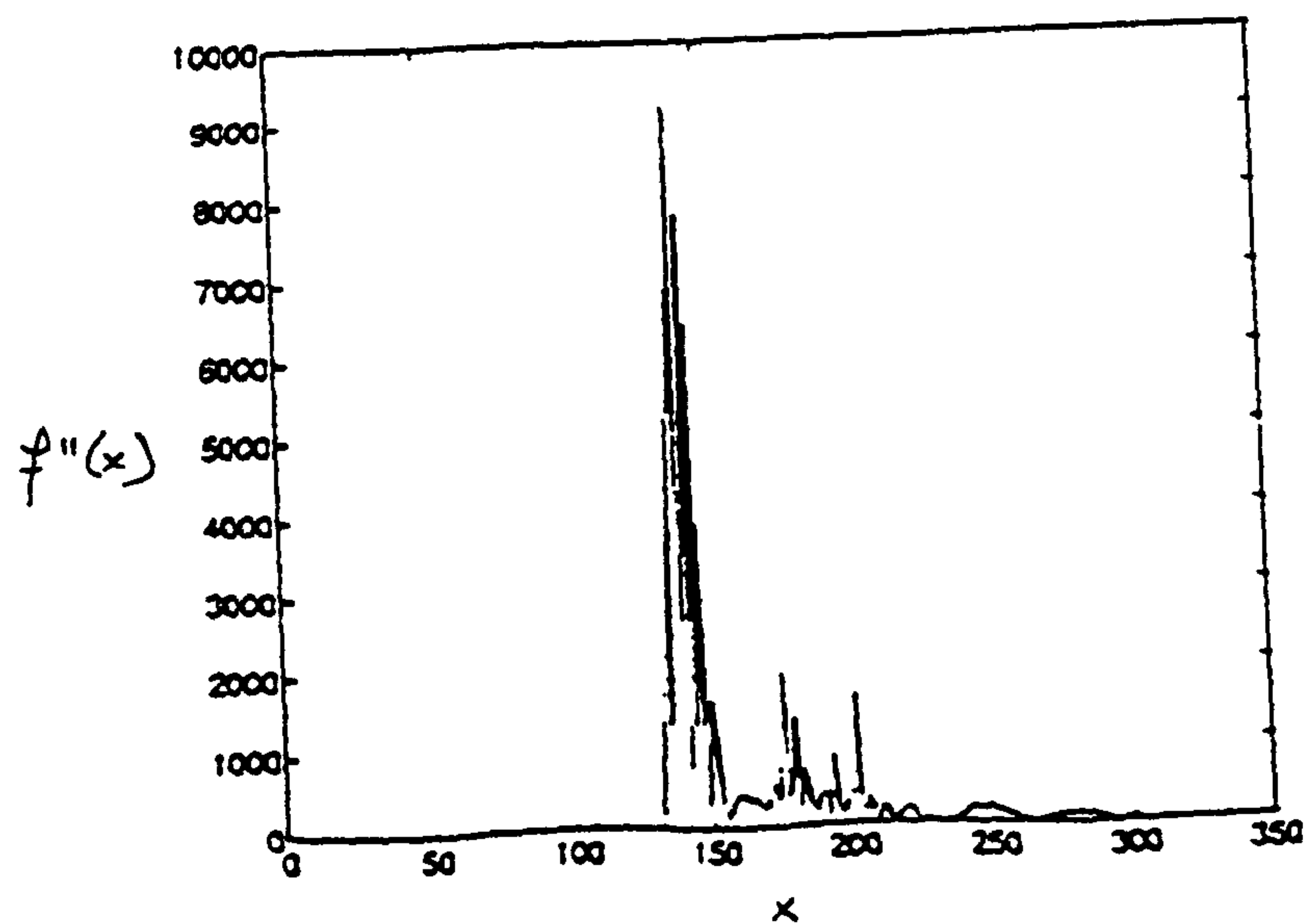
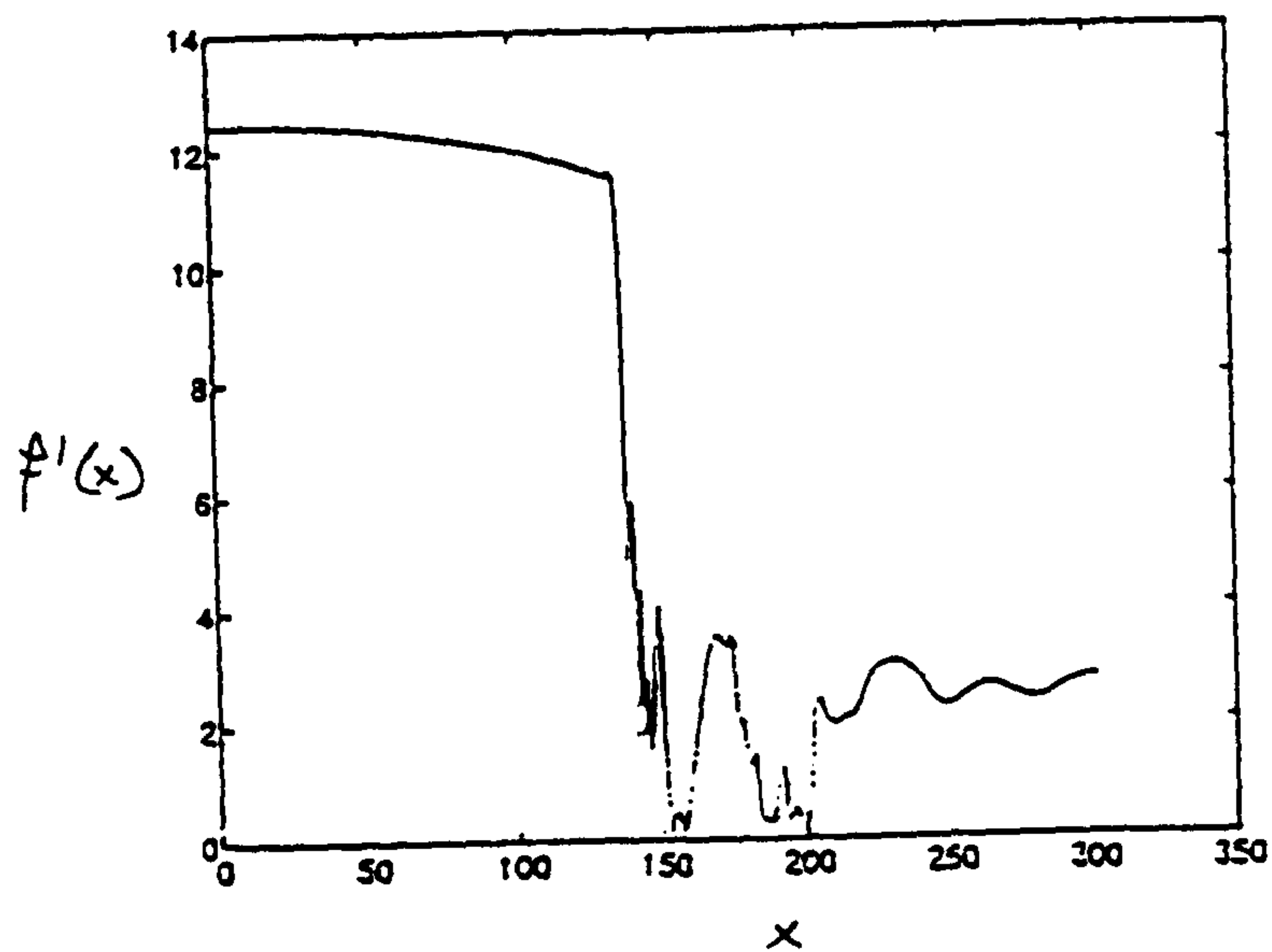
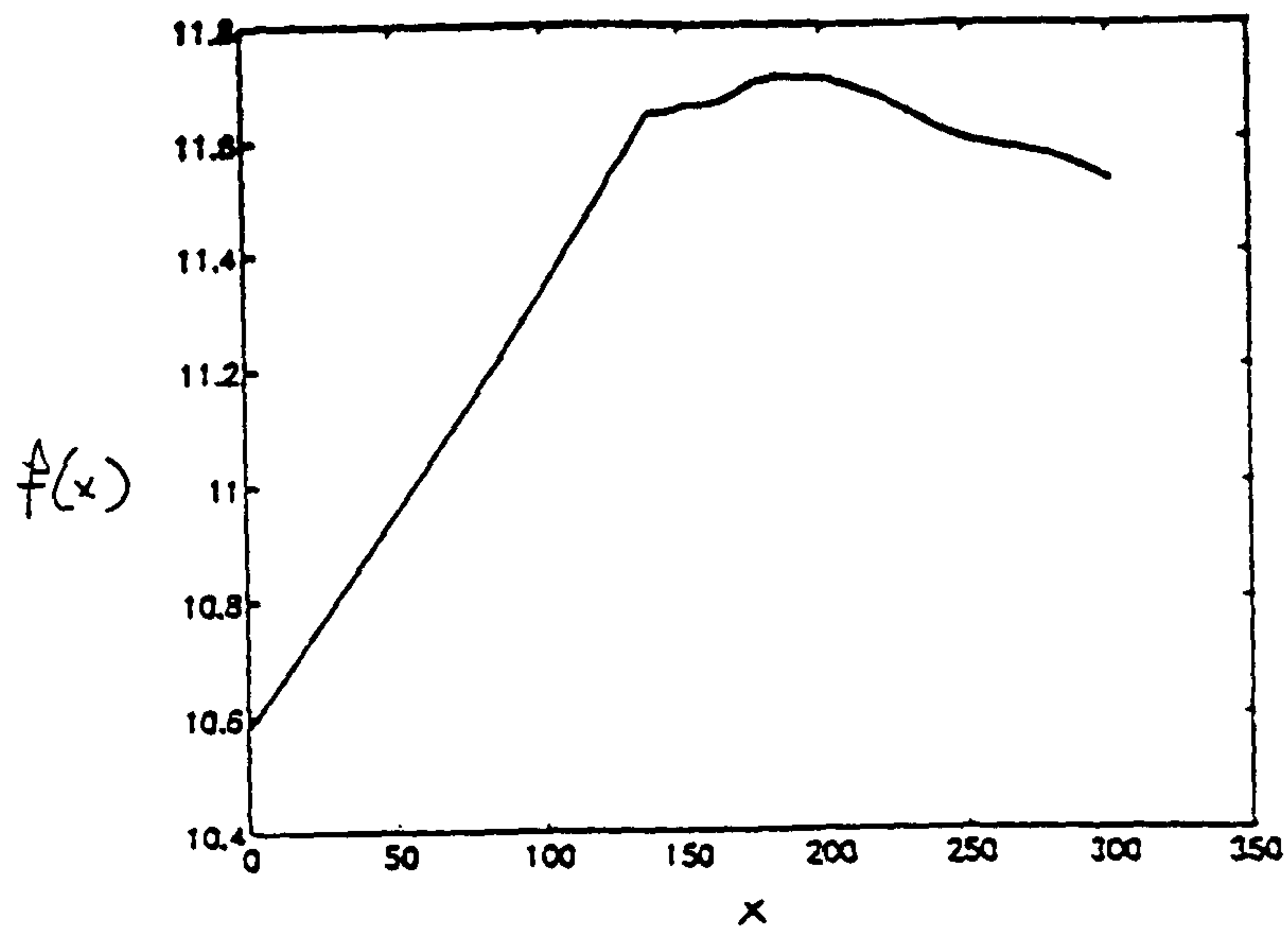


Figure 7.5b Cubic splines fitted resultant displacement of the centre of the front wheel, $f(x)$, and its first and second derivatives, respectively, where the number of interior knots had been decreased.

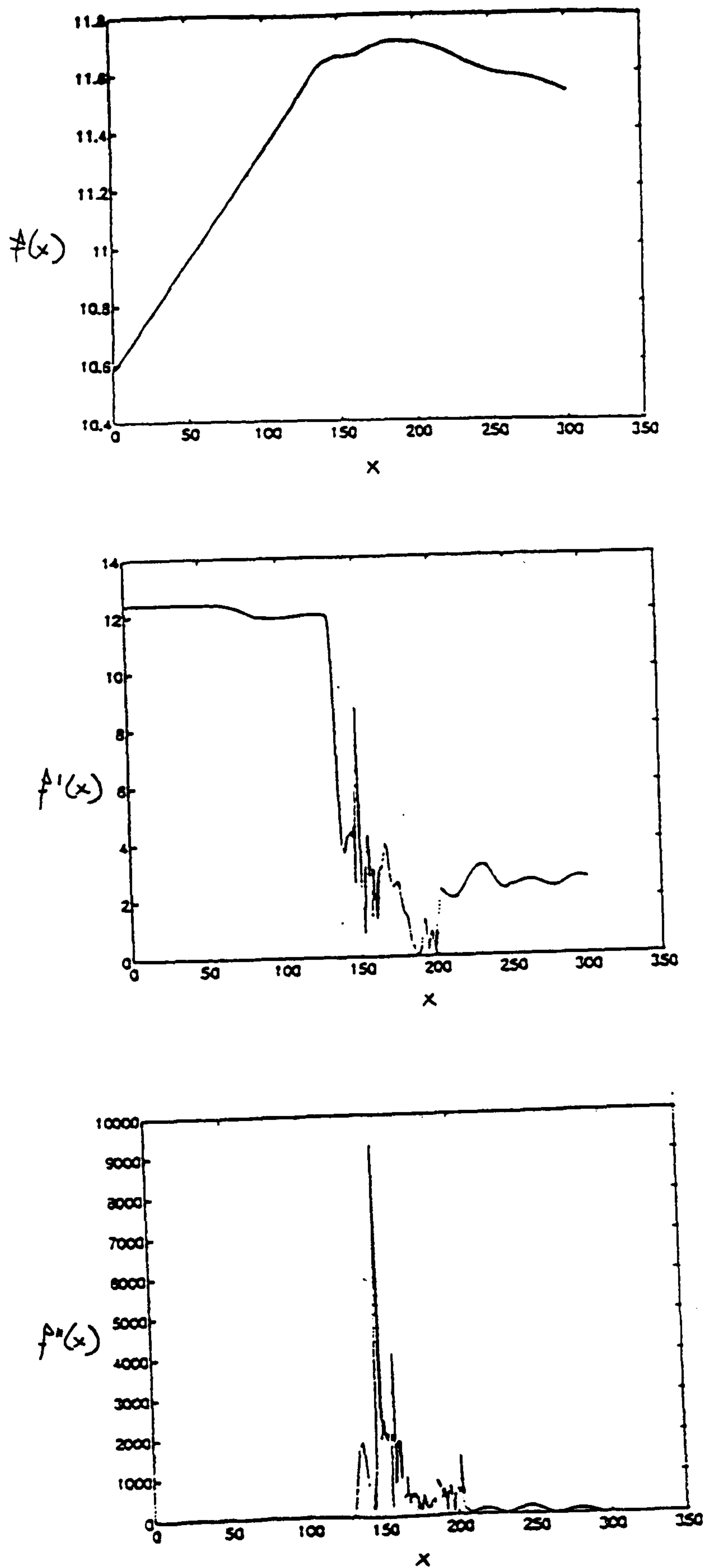


Figure 7.6a Cubic splines fitted resultant displacement of the centre of the front wheel, $f(x)$, and its first and second derivatives, respectively, where all data points were prescribed as interior knots.

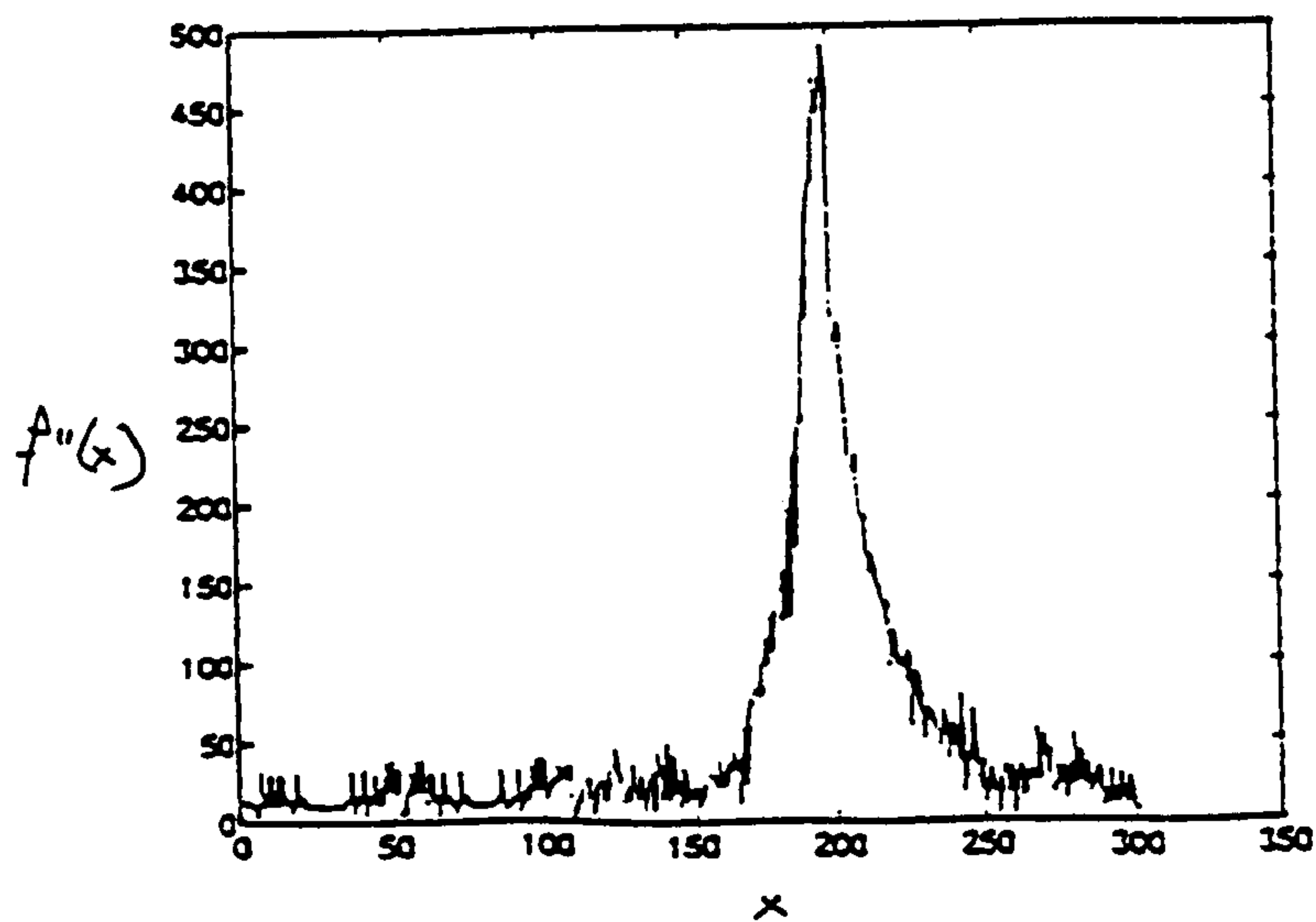
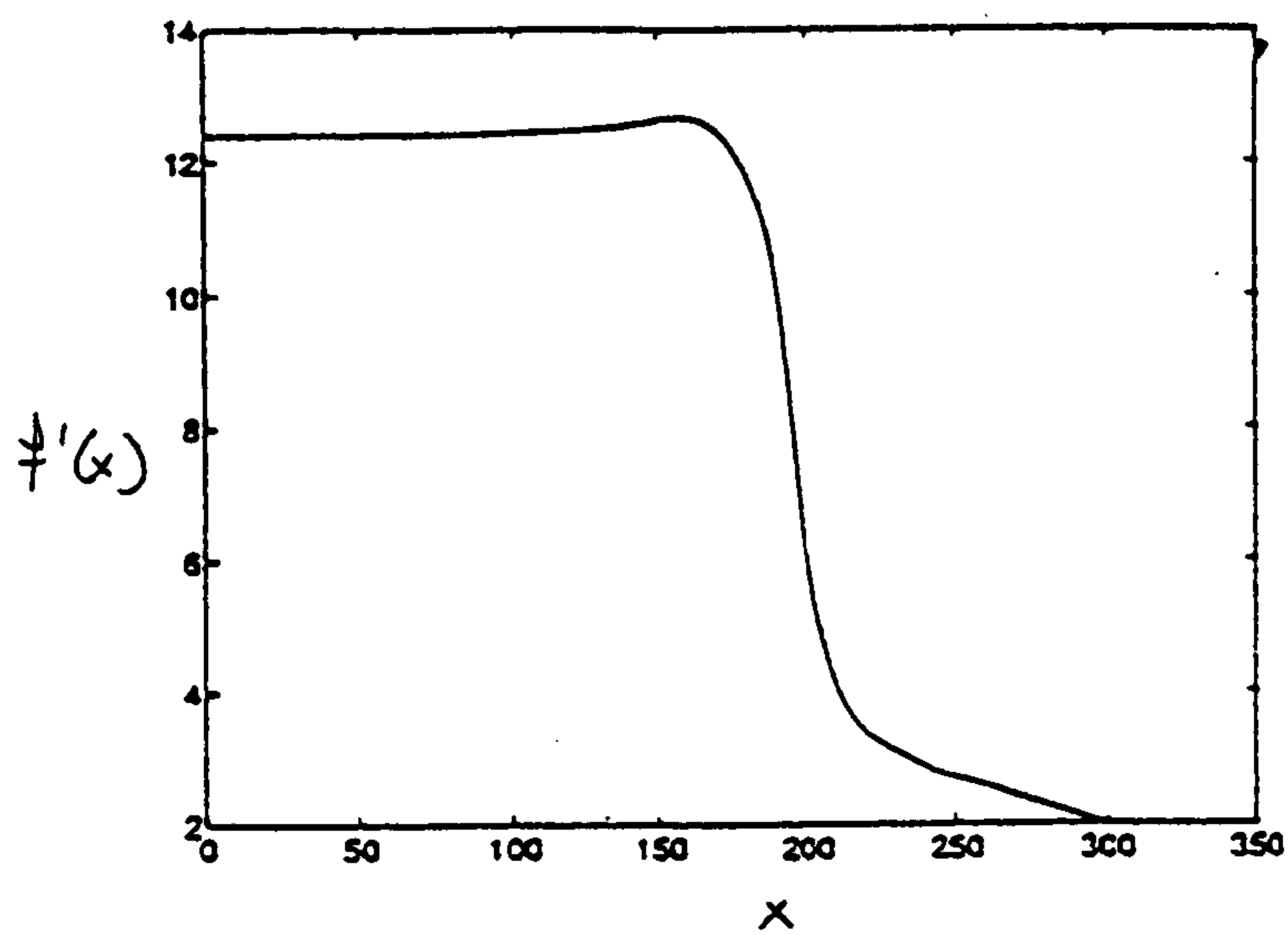
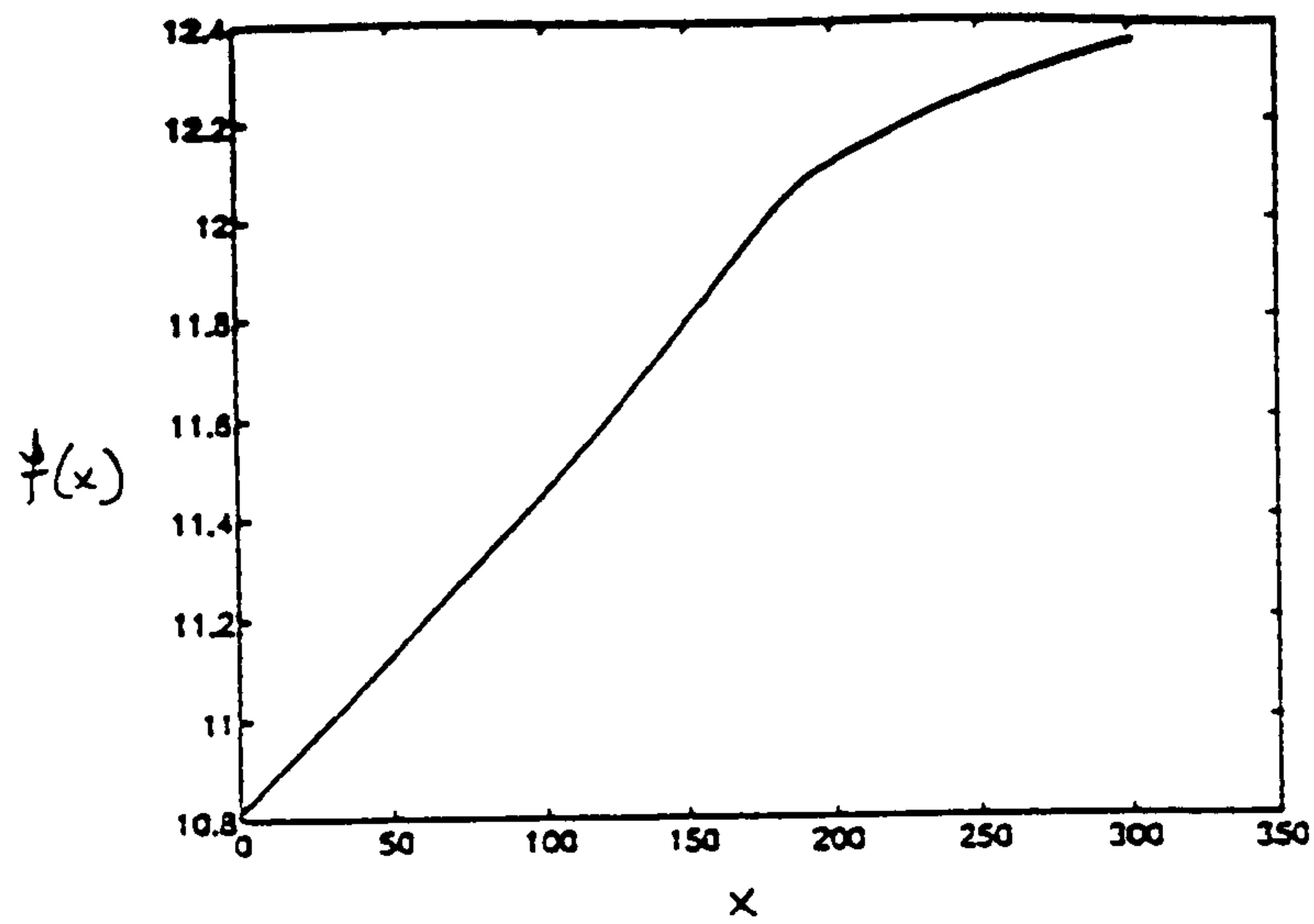


Figure 7.6b Cubic splines fitted resultant displacement of the dummy's chest, $f(x)$, and its first and second derivatives, respectively, where all data points were prescribed as interior knots.

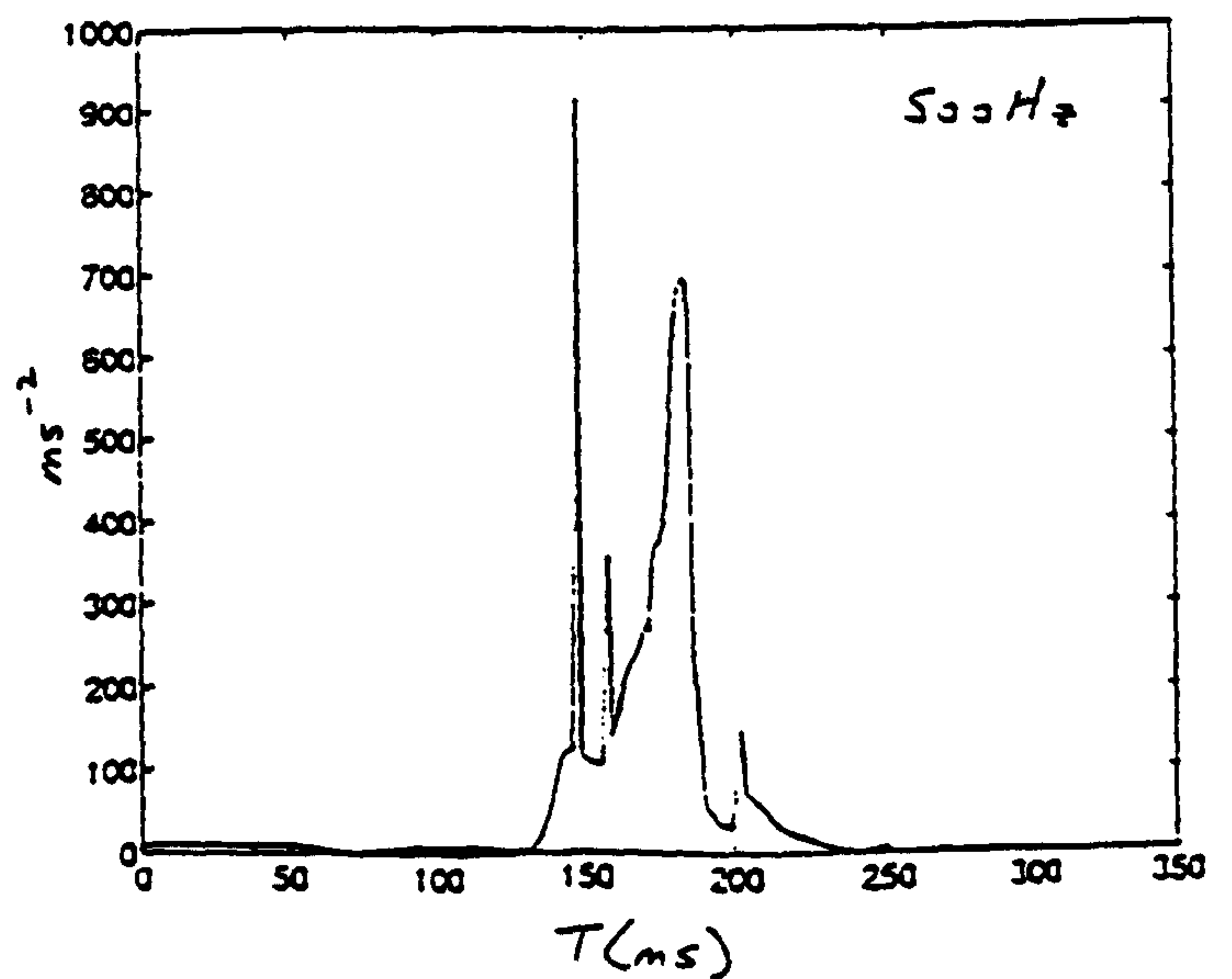
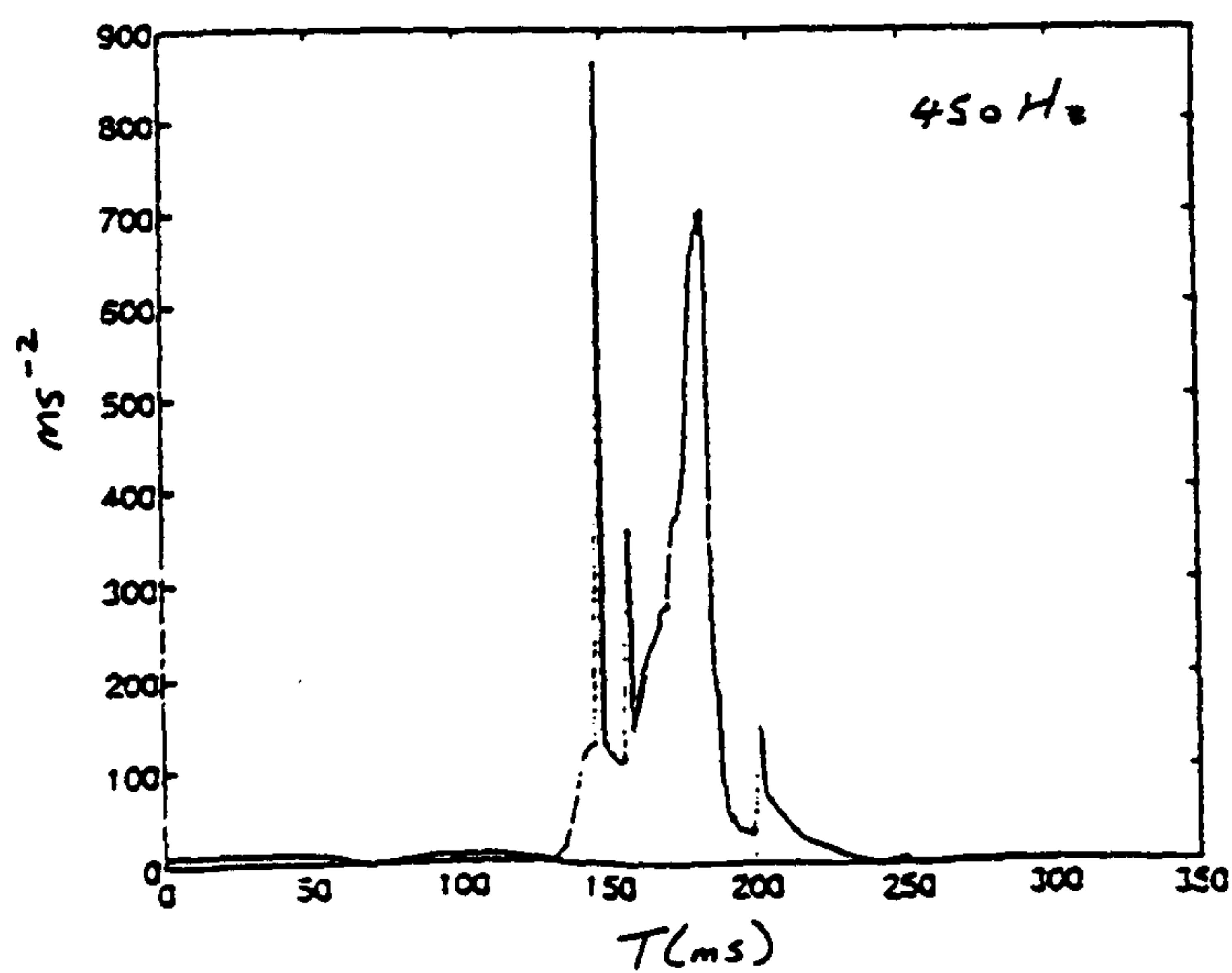
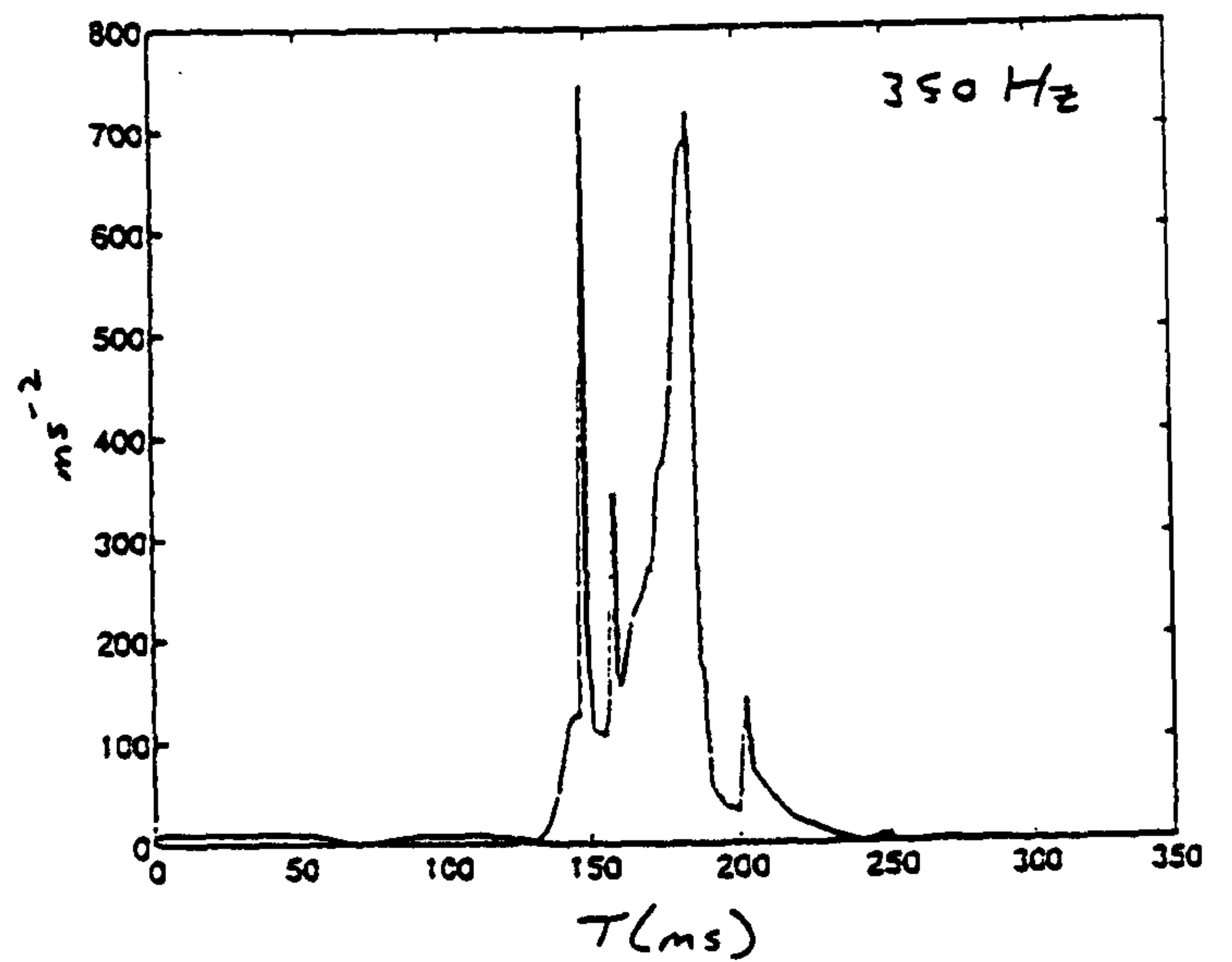
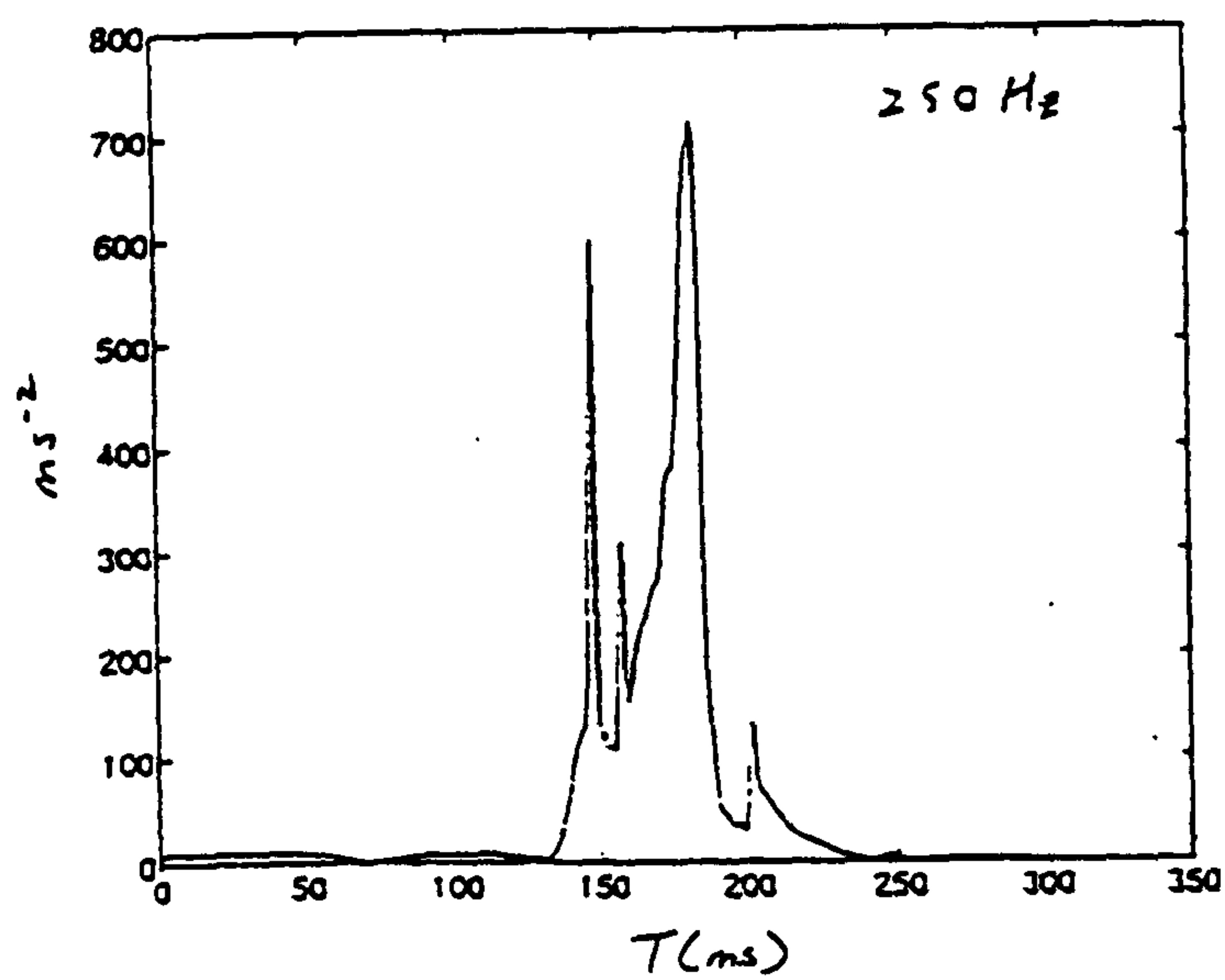
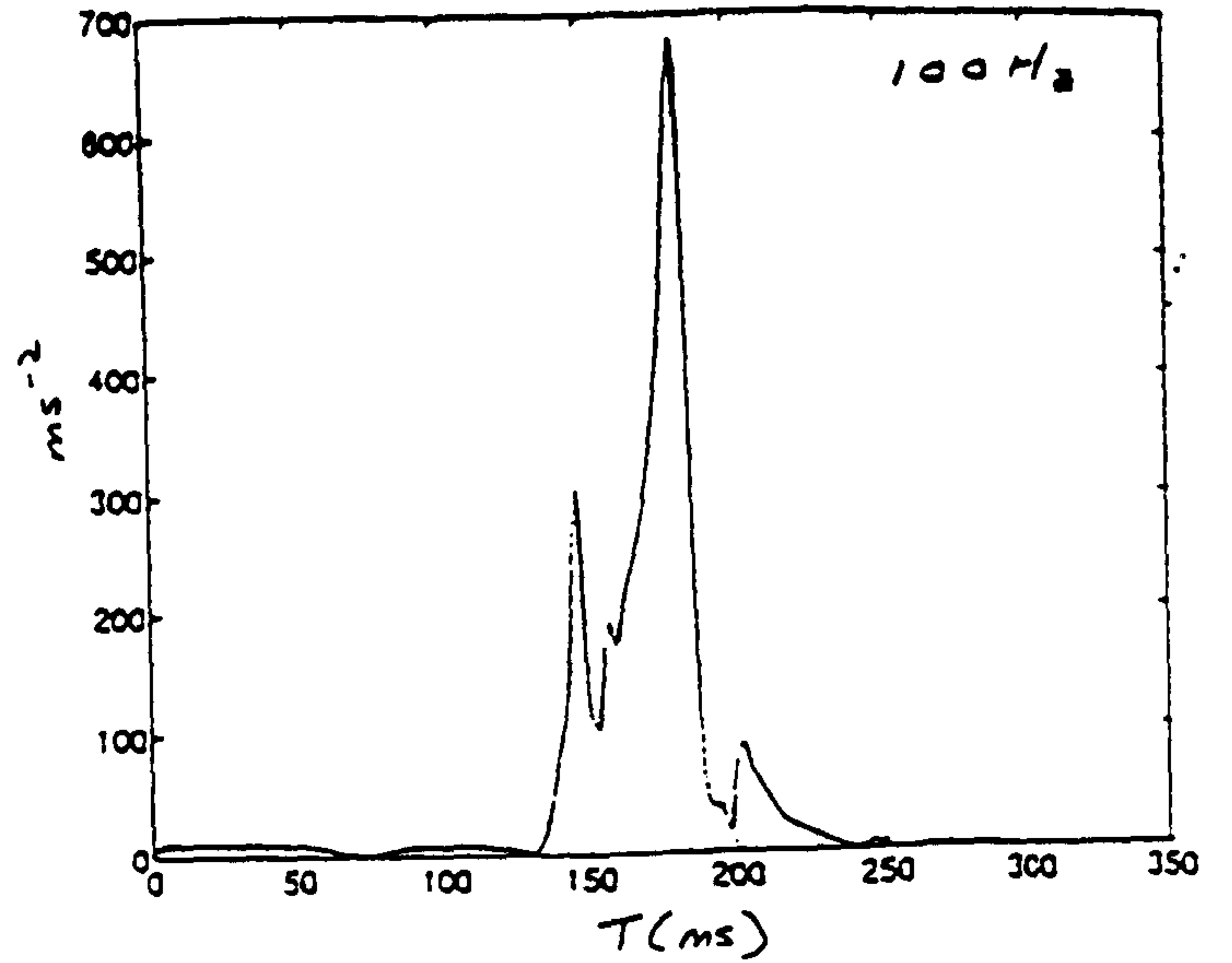
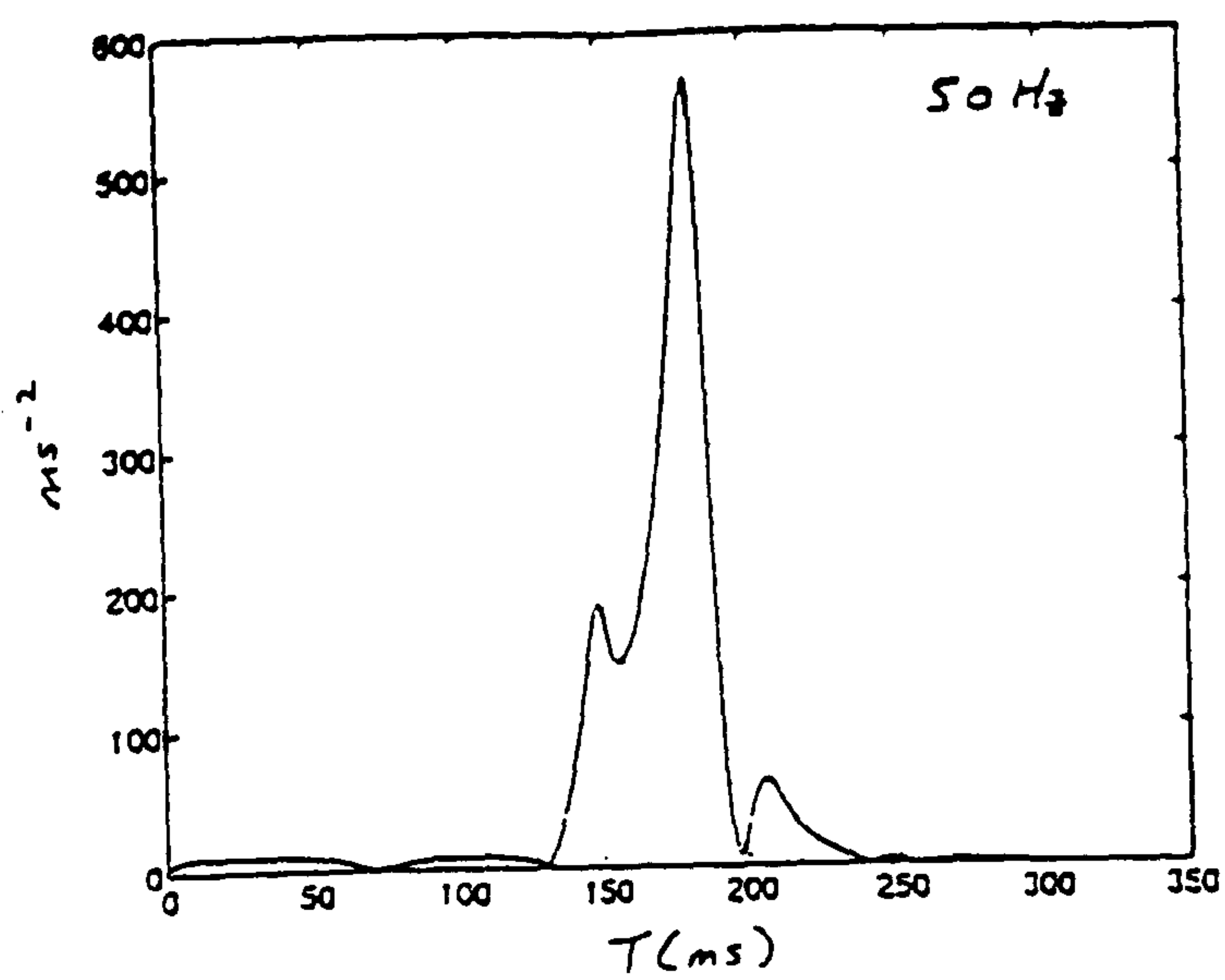


Figure 7.7a Butterworth filtered accelerations of the centre of the front wheel with varying number of cut-off frequencies.

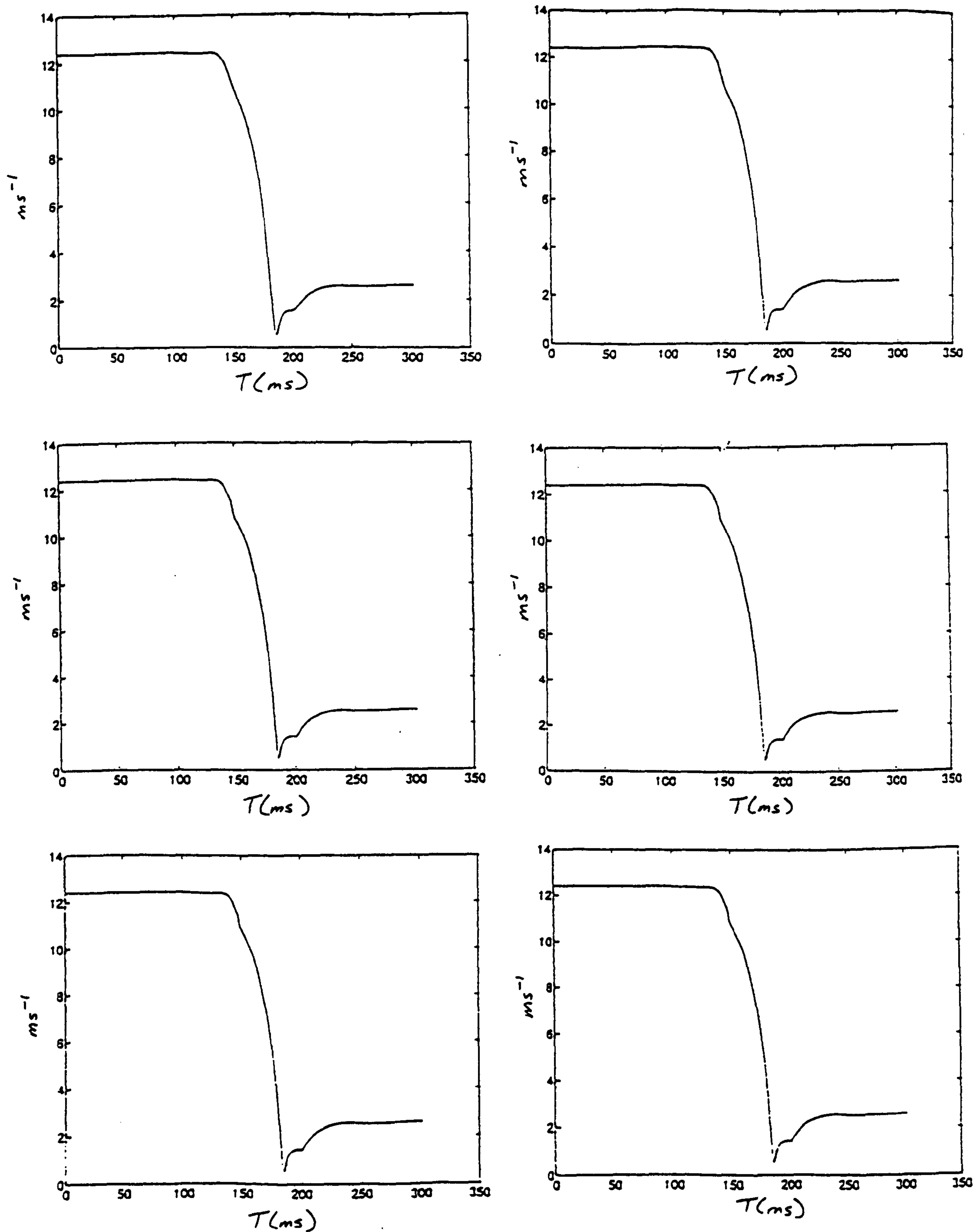


Figure 7.7b The first integral curves of the filtered accelerations.

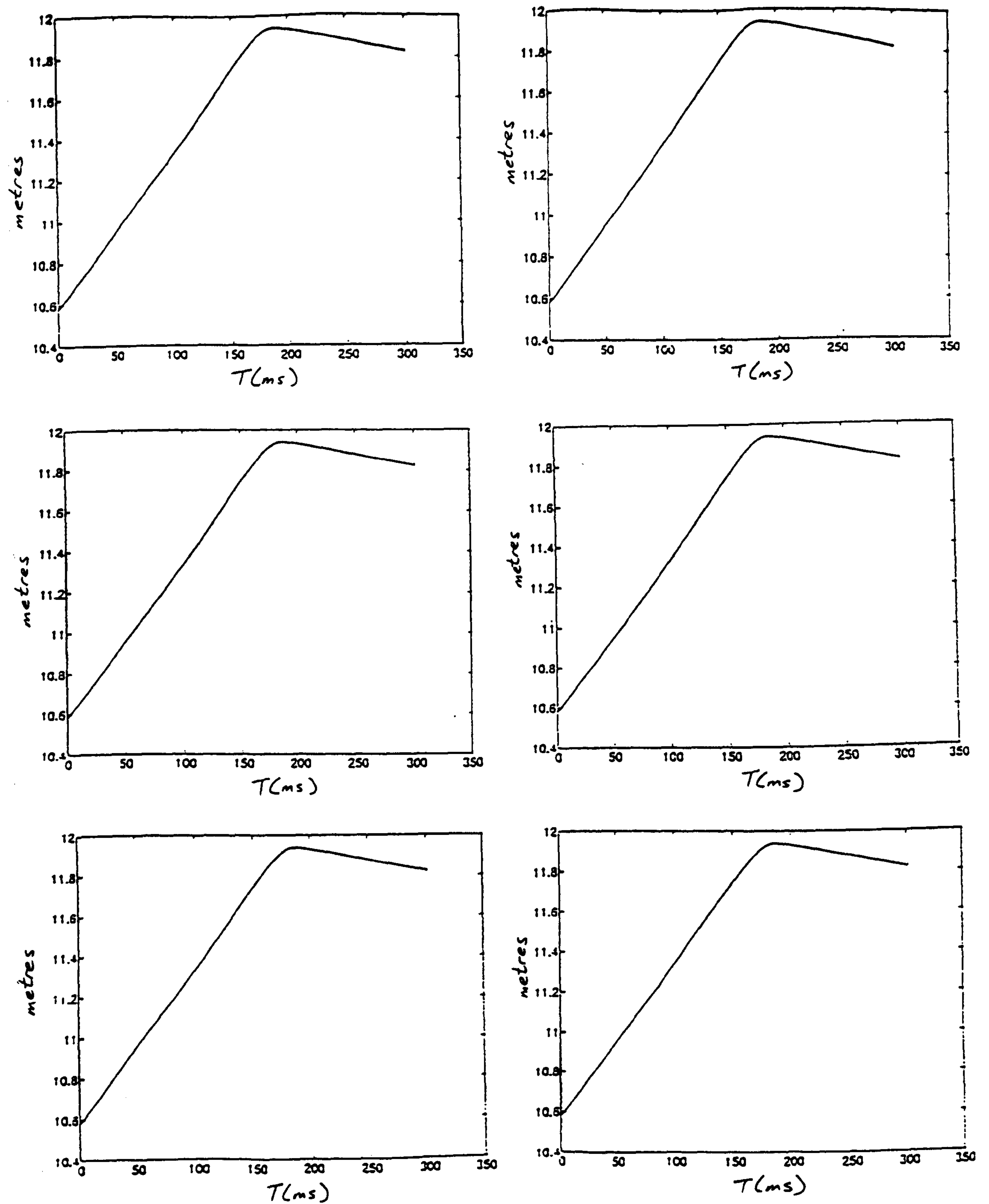


Figure 7.7c The second integral curves of the filtered accelerations.

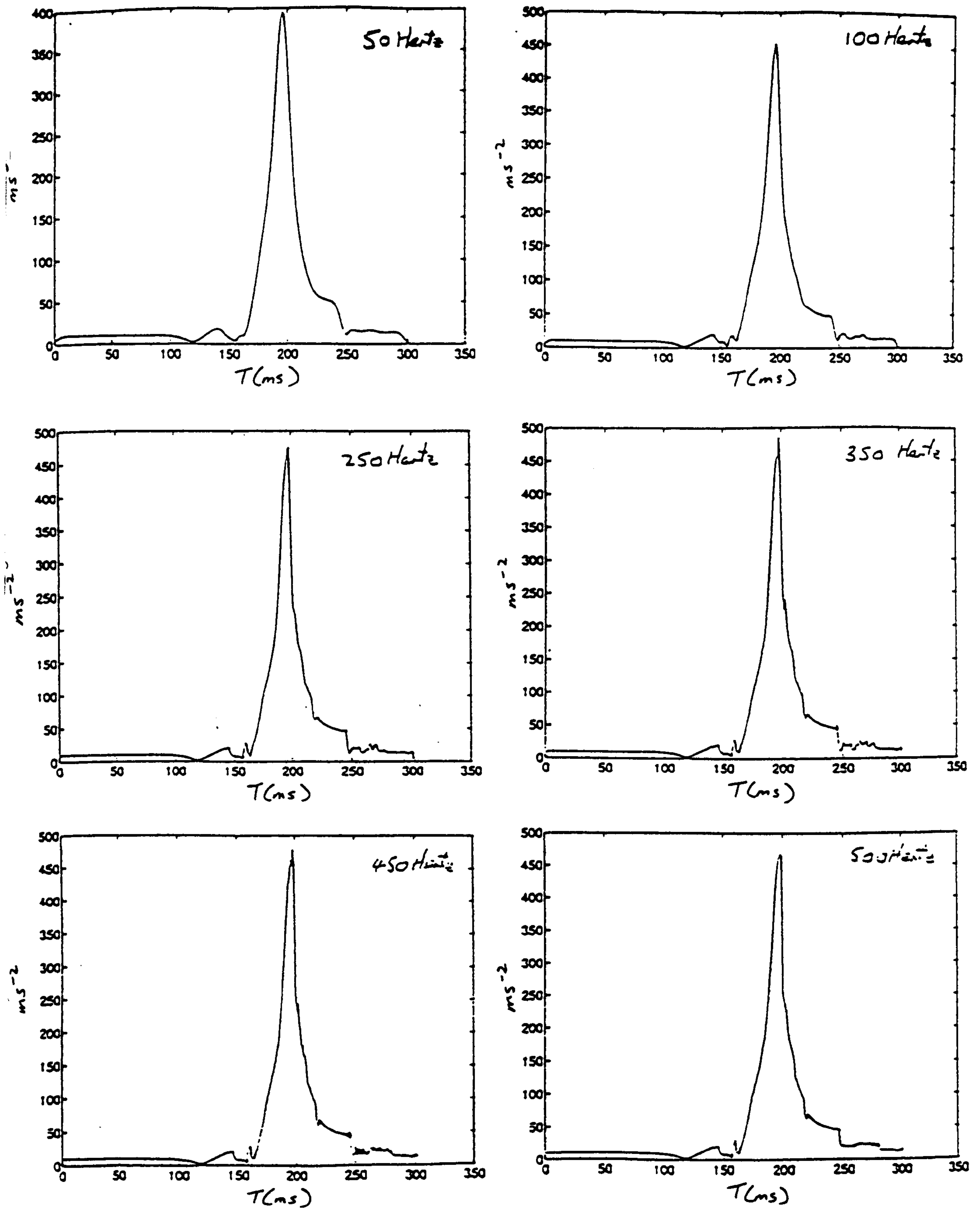


Figure 7.8a Butterworth filtered accelerations of the dummy's chest with varying number of cut-off frequencies.

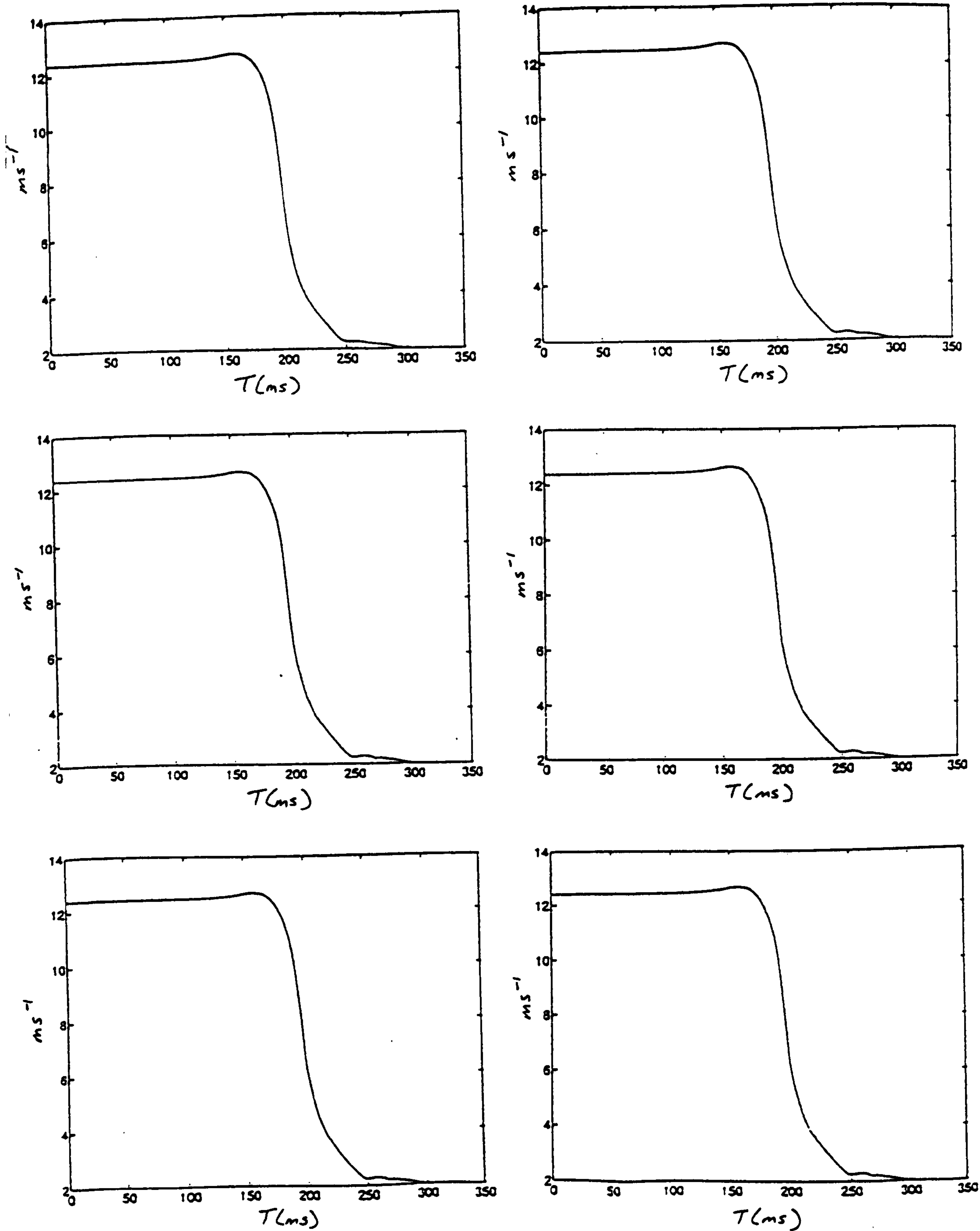


Figure 7.8b The first integral curves of the filtered accelerations.

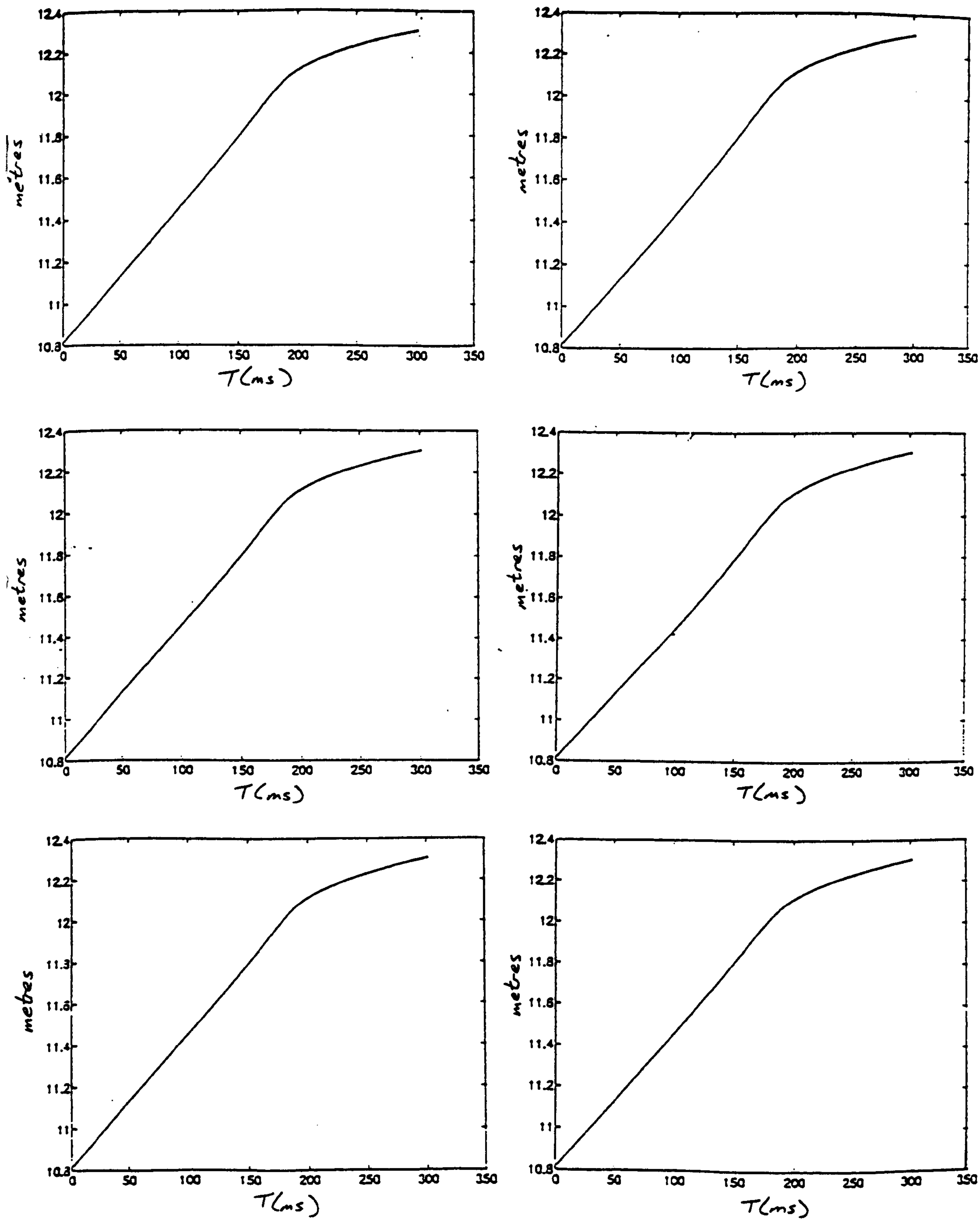
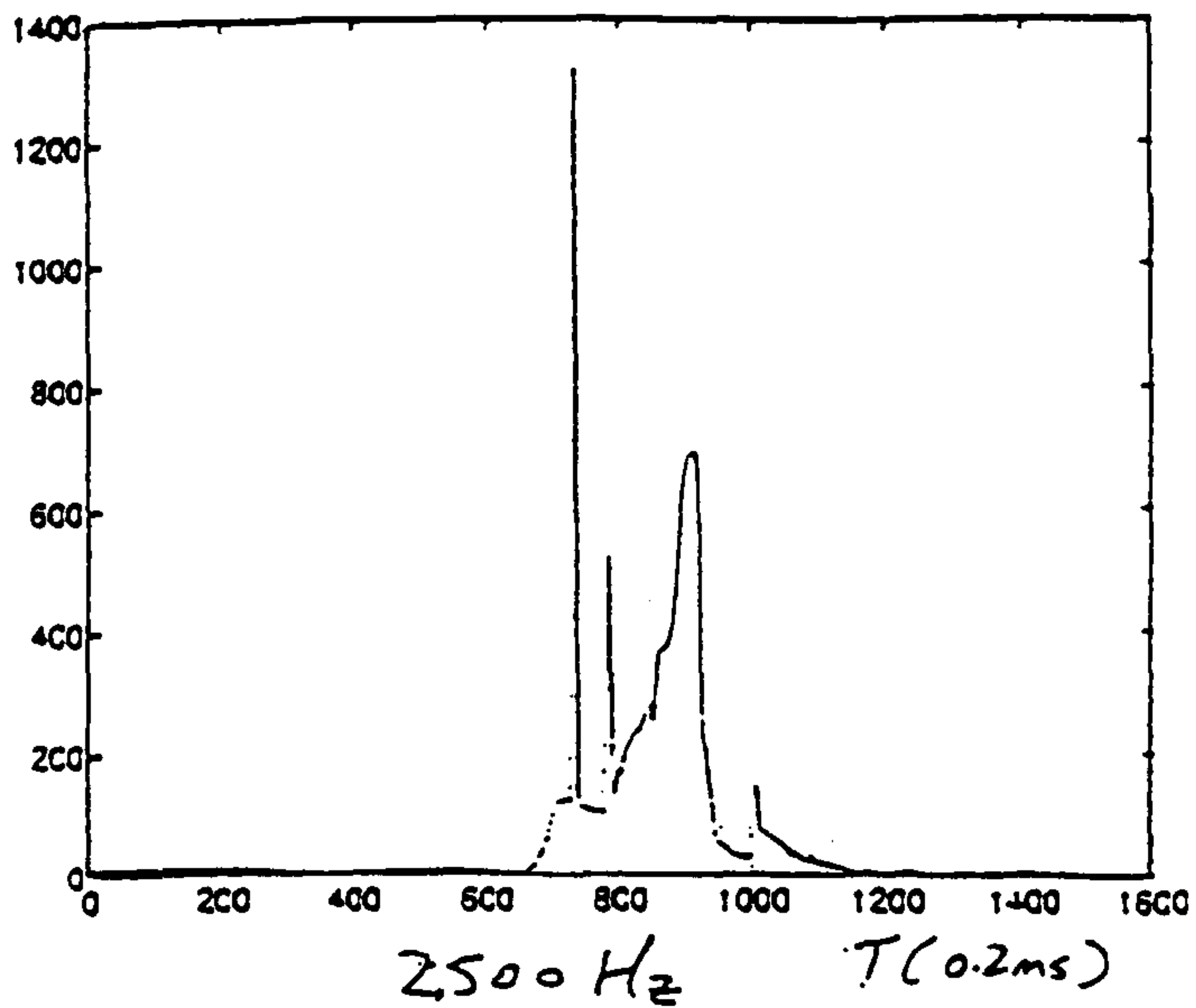


Figure 7.8c The second integral curves of the filtered accelerations.

L4 FRONT WHEEL AGAINST BARRIER (ACCELERATION)

HIGH FREQUENCY RUN
(5,000 Hz)

LOW FREQUENCY RUN
(1,000 Hz)



← These two are equivalent
to the original unfiltered
plots.

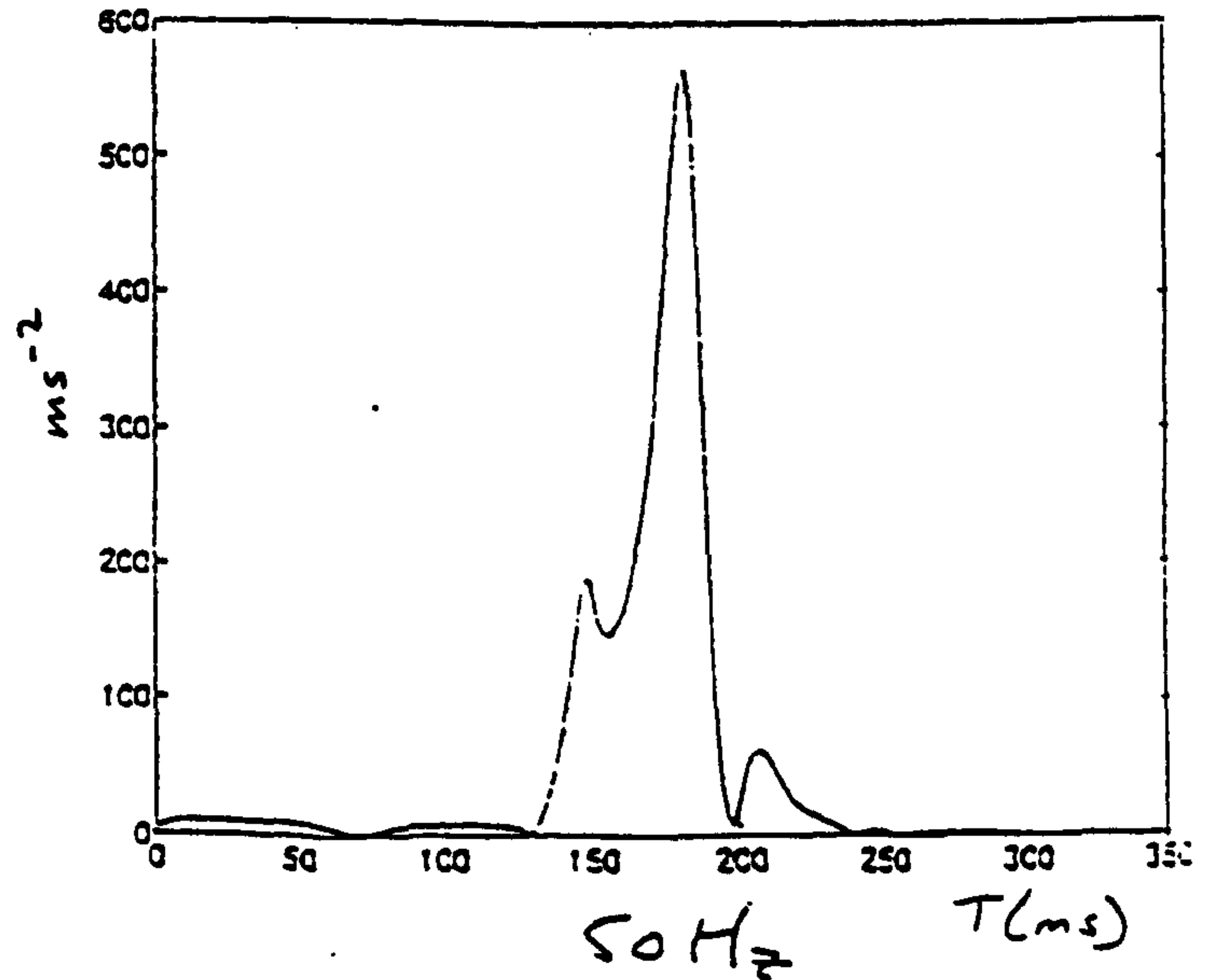
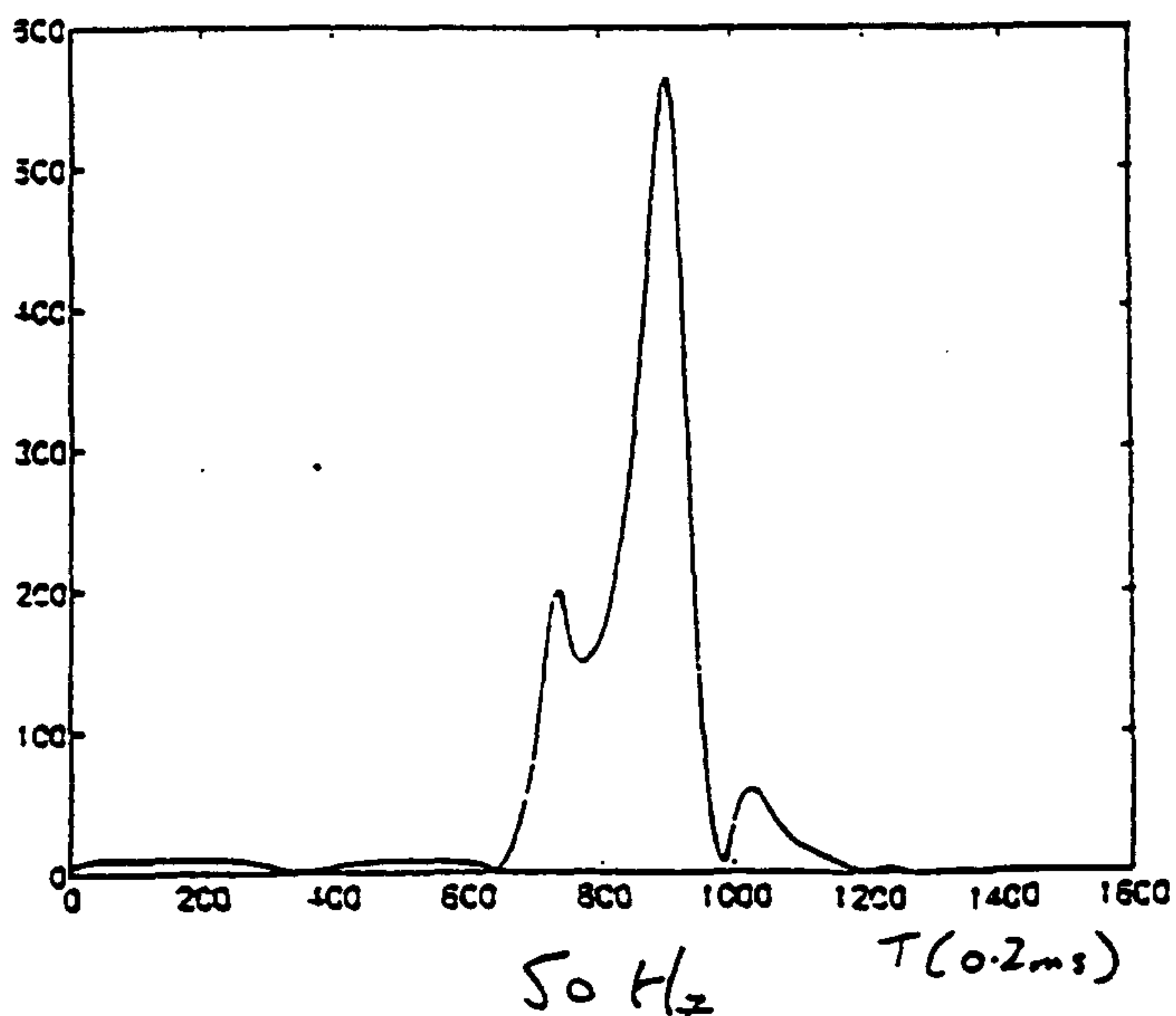
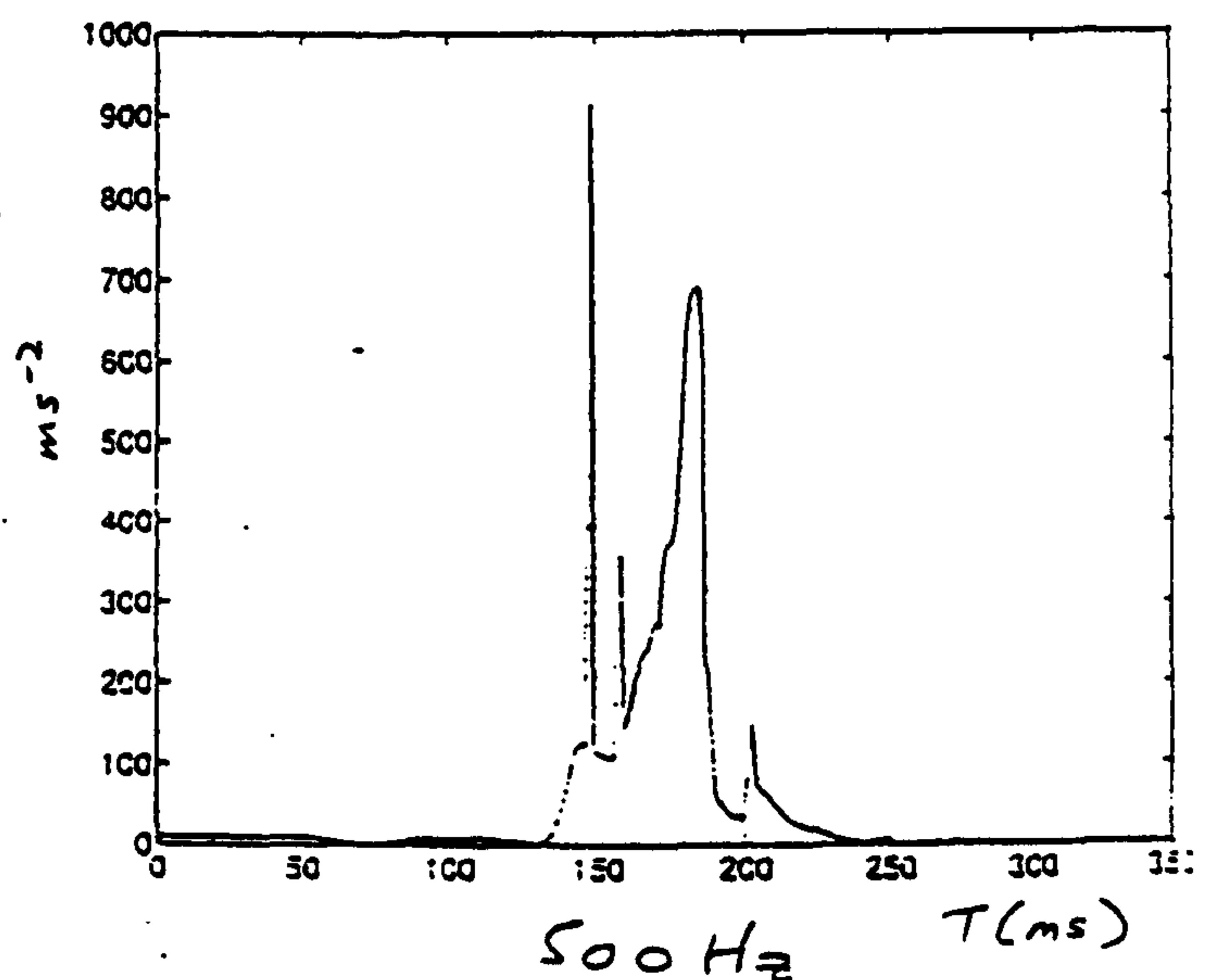
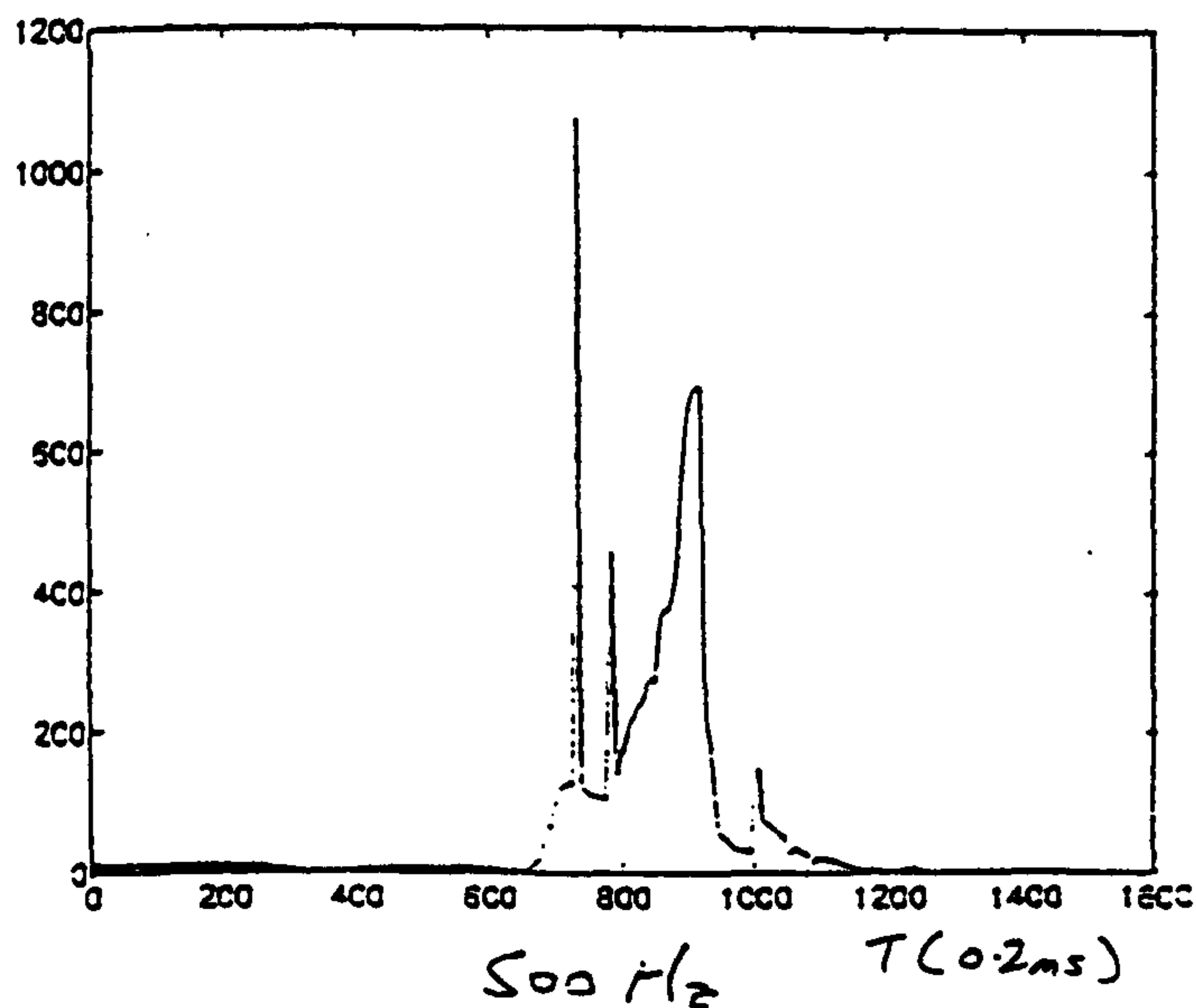


Figure 7.9 Comparison of filtered accelerations of the centre of the front wheel, where it was ACSL computed at different frequencies.

CHAPTER 8

PARAMETRIC STUDY

8.0 Introduction

In this chapter a sample of 51 runs of the simulation program is analysed statistically. By using statistical techniques, the effects of some significant aspects of the design of the motorcycle, and of the impact, can be demonstrated. The potential injuries to the dummy rider can therefore be assessed in relation to these factors.

The primary concern of this study is the potential injury to the dummy's legs under different circumstances of impact. Indeed the computer program is one which includes a simulated leg protector attached to the motorcycle. The characteristics and the design of the leg protector are therefore some of the major criteria to be investigated. This study will examine the effects of five leading variables within the simulation, they are

- (i) the initial velocity of the motorcycle and dummy rider, VEL, with range $10\text{mph} \leq \text{VEL} \leq 40\text{mph}$,
- (ii) the inclination of the barrier angle, ANG, with range $20^\circ \leq \text{ANG} \leq 90^\circ$,
- (iii) the initial distance between the seated dummy's knees to

- the knee-restraints, KR, with range $0.0\text{m} \leq \text{KR} \leq 0.1\text{m}$,
- (iv) the stiffness of the leg protector, denoted by a factor LP, with range $2.0 \leq \text{LP} \leq 20.0$ and
- (v) the profile of the leg protector, outlined by a radius RLP, with range $0.135\text{m} \leq \text{RLP} \leq 0.18\text{m}$.

These five variables will be chosen randomly, within the specified ranges, by a random number generator. This is done by incorporating a NAG subroutine into the program.

However, based on previous experience it has been found that the variables react differently under different circumstances. For example, the coefficient of friction between two surfaces is not only based on the materials of the surfaces, but also the rate of motion between the two sliding surfaces. It is impossible to obtain the true coefficient of friction, and un-economical to be precise in determining these coefficients between the vast number of different impact surfaces. Therefore, the coefficients of friction between the impacting surfaces that are of critical importance to the motion of the motorcycle and dummy rider are chosen to be appropriate to the circumstance of impact, whilst the relatively less important coefficients, such as those between motorcycle and the ground, are kept constant throughout.

In addition to the coefficients of friction between the more important impact surfaces, there are other variables, such as

stiffness factors, that are also dependent upon different situations. Therefore, these variables are chosen to be changeable in each computer run, and the determination of their values is based on previous simulation experience. They have been found to be related to the initial velocity of the motorcycle and dummy rider, the angle of the barrier, or both. The total number of changeable variables, including the five listed randomly generated variables, is chosen to be 25 and they are listed in Figure 8.1.

The number of computer simulation runs is also an important consideration in this parametric study. One can use tens, hundreds or even thousands of computer runs. But of course time and economy are two prime concerns. From previous experience, a typical computer run will take an average of 8 hours of real time to complete the simulation, and it is estimated that computer time will increase proportionally to the increase in the velocity variable. It is essential then, to select an adequate and applicable number of simulation runs.

The number of changeable variables is 25. It is advised that in a parametric study, where N is the number of variable parameters, $(2N+1)$ typical samples will be sufficient and adequate to commence the study [30]. Therefore in this parametric study, there will be a sample of 51 computer simulation runs.

8.1 The Independent And Dependent Variables

The ranges of the five independent variables have already been stated. Here we will give a more detailed account as to the chosen ranges.

The range of the velocity term, VEL, is fairly straight-forward. We want to investigate impact behaviour in a wide range of forward velocity, but it may well be beyond preventability of injury if the speed is above 40mph, hence this is the chosen upper limit.

That the barrier angle is significant is also understandable, but an explanation is needed for the upper range of 90° . It is found, by previous experience, that simulation is extremely sensitive especially in a highly unstable situation such as motorcycle impact. In reality, impact behaviour between a motorcycle and a barrier at 90° may not be so different to an impact where the barrier is at 88° . But in a mathematical model this minute difference is critical to the local dynamics, which in turn, will spread rapidly to the overall behaviour. This particular case has been proven during the development of the current model. Hence the upper limit of ANG is adjusted so that if the random number generator chooses ANG, between 85° and 90° , ANG will automatically be set to 90° .

The above ranges have been chosen in relation to road tests carried out by TRL. The following are specified by TRL who have tested and measured the relevant components.

The range of the knee to knee-restraint distance is $0.0\text{m} \leq \text{KR} \leq 0.1\text{m}$. The lower limit of 0.0m has the effect of the two knees touching the knee-restraints. The upper limit of 0.1m is one where TRL found that the dummy can sit adequately with the knees furthest away from the knee-restraints.

TRL provided the stiffness range for the leg protector, from 100KN/m to 1,000KN/m. Based upon the force-deflection table already constructed into the computer program, it is found that a stiffness factor with range 2.0 to 20.0 will cover the force range completely. Note that the factor is dimensionless.

For the different profiles of the leg protector, TRL provided a diagrammatic representation as shown in Figure 8.2.

TRL stated that a range of different shapes of leg protector can be represented within the range between the shown maximum and minimum curvatures. It is found that this can be modelled by using a radius, RLP, in the range $0.135\text{m} \leq \text{RLP} \leq 0.18\text{m}$, as shown in Figure 8.3. This has the effect of having the lower limit, 0.135m, representing the most pronounced extension of the leg protector, with the upper limit, 0.18m, representing the minimum

leg protector profile.

The above are the descriptions of the independent variables. The dependent variables in this parametric study are the various forces, if impact occurred, between the dummy's legs and the different locations of the motorcycle. A complete list is given in Figure 8.4.

Before we proceed with the analyses, we must define the direction of travel of the dummy and motorcycle with respect to the barrier. The left-hand-side of the dummy and motorcycle is the side nearer to the barrier in an oblique impact, which will be termed as the 'nearside'. Likewise, the right-hand-side will be termed as the 'offside'. This can be shown in Figure 8.5.

Out of the fourteen sets of forces, there are three noticeable distinctions. Impact did not occur in the case of KLFTT (nearside knee against upper part of petrol tank) and is withdrawn from the analysis. Only two impacts occurred in LBLFTT (nearside tibia against engine) but KTRFTT (offside knee against lower part of petrol tank) scored in all of the 51 simulation runs.

In the statistical analysis which follows note that in the case where impact occurred, it is the peak value of the generated force which is entered into the analysis. Non-impact situations are represented by the value zero.

8.2 The Statistical Analysis

A statistical analysis software package is employed in the following analyses. The software is known as SPSS (Statistical Program for Social Scientists, [31] and [32]) and comprises a wide range of statistical procedures. It is menu-driven; the users need only to prepare their data in a specific format.

In this parametric study, the following statistical analyses are used:

- (a) Correlation Coefficient
- (b) Multiple Linear Regression
- (c) Partial Correlation Coefficient
- (d) Analysis of Variance
- (e) Multivariate Analysis of Variance

The study can broadly be divided into two parts. In the first part, where procedures (a), (b) and (c) are used, the data are in their parametric states i.e. they are in their numerical forms as computed by the simulation program. In the second part, where procedures (d) and (e) are used, the data are semi-parametric such that some data are categorised by the user.

In a non-parametric analysis data are categorised in order of

merit, rank or class instead of actual raw scores. In our semi-parametric analyses the independent variables are categorised as given in Figure 8.6, into their respective groupings, but the dependent variables, forces, are to remain in their raw states, since the two analyses (d) and (e) both use the means of samples in their calculations.

One may criticize categorisation of data, according to whatever standard being is used, such that bias may be introduced. This is a valid point. But techniques such as these have the advantage of comparing data from one group with another. It will serve to indicate if the performance of the dependent variable differs between different groups, and if so, by what significant amount.

Another point worthy of mention is the order of categorisation. It is conceivable that within a particular group a dependent variable did not score well or not at all. However, non-parametric techniques are ones which do not assume the shape of the scoring distribution. Nevertheless, care needs to be taken when categorising data. In a manner of speaking, categorising data is similar to constructing a finite-element mesh, but unlike the success of finite-element techniques, too coarse a mesh in categorisation may result in the non-apparent relationship between variables, while too fine a mesh may make the extraction of a sensible relationship difficult.

The categories listed in Figure 8.6 were constructed after much consideration. Care has been taken so that variables are categorised appropriately, such as the cases of ANG and VEL, and also the numbers of categories have been adjusted according to the ranges and relevance.

8.3 Correlation Coefficient

A correlation coefficient is a measure of how linear is the relationship between two variables. The one commonly used measure is the Pearson correlation coefficient, denoted by r , and is defined as

$$r = \frac{\sum (x_i - \bar{x})(y_i - \bar{y})}{(N-1) S_x S_y}$$

where

\bar{x} = mean of the x variable

\bar{y} = mean of the y variable

S_x = standard deviation for the x variable

S_y = standard deviation for the y variable

and

N = total number of pairs of scores

Since this is a measure of strength of the linear relationship between two variables, one can conclude the highest absolute value of $r = 1$, indicates there is either a total positive or negative linear relationship, and that when $r = 0$, indicates

there is no linear relationship between the two variables.

As such, a correlation coefficient may lead to a crude indication of the relationship between two variables. However, it is a good basic starting procedure to begin an analysis, and one that will lead to an understanding of other statistical analyses.

8.4 The Linear Relationship Between Forces And The Independent Variables

Since there are fourteen possible contact points between the dummy's legs and the motorcycle, we shall examine each case individually. The correlation coefficients of interest are between the peak value of the generated force, F , if contact was made, and each of the five randomly generated values. A table of the correlated coefficients, computed by SPSS, is given in Figure 8.7.

As one can see, the correlated values are generally small, indicating not very strong linearity. On the whole, there is more linearity between F and ANG , and between F and VEL . The latter highlights the instinctive feeling that the faster the moving vehicle, the higher the tendency for injury if collision was made.

If the values are examined more closely, one can see there exists a difference in relationship between ANG and VEL. For anatomy representing the left-hand-side of the dummy there is a stronger linear relationship between F and ANG, than for the anatomy representing the right-hand-side of the dummy, where the linear strength between F and VEL is stronger. These differences may be small but it is a significant observation.

There are some coefficients marked with one or two asterisks. These are the levels of significance computed by SPSS. One asterisk indicates the correlation coefficient is significant at 5% level, while two asterisks indicate a 1% level significance. This means that if a variable is significant at 5%, it has a one in twenty chance of being subjected to randomised variation.

Most of the coefficients in the ANG and VEL columns are marked with asterisks. This shows that though the magnitudes of these coefficients are fairly low, there are high levels of significance for these two variables within the system.

The correlation coefficients between F and KR, LP and RLP are generally low, showing not much linear relationship. However, between these three randomly generated variables, KR seems to show the strongest linearity, though there are two asterisks associated with one particular correlation coefficient between F and RLP.

In short, based upon the correlation coefficients computed by SPSS among these variables, it is ANG and VEL that dominate the behaviour of the variable F.

8.5 Multiple Linear Regression

Regression is a technique which is concerned with prediction. Unlike correlation, which is concerned with measuring the strength of relationship among a set of variables, regression involves estimating some dependent or predicted variable, using information about the independent or predictor variable. Multiple regression is used when there are two or more independent variables.

The simplest form of regression technique is the multiple linear regression. It can be expressed as:

$$\hat{y}_i = \beta_0 + \beta_1 x_1 + \dots + \beta_N x_N + \varepsilon_i \quad (8.1)$$

where \hat{y}_i are the estimated values computed by the regression equation, N is the number of independent variables and ε_i are the estimated residual terms.

One can see the resemblance of an equation of a straight line in equation (8.1). Indeed it is a model of fitting a straight line

based upon the predictor variables and the observed predicted values. The β_i 's are the unknown parameters or slopes in determining a straight line. They are known as regression coefficients and are obtained by

$$\beta_i = \frac{\sum (x_i - \bar{x})(y_i - \bar{y})}{\sum (x_i - \bar{x})^2} \quad (8.2)$$

where (\bar{x}, \bar{y}) is the centroid point on the regression line.

Equation (8.2) is known as the method of least squares such that after computing the β 's from the sample, they achieved the best possible fit within the constraints of the least square model, and that they minimised the error sum of square such that

$$\sum \epsilon_i^2 = \sum (y_i - \hat{y}_i)^2 \quad (8.3)$$

is a minimum (see Figure 8.8).

In Figure 8.8, the vertical distance labelled 'regression' is the best possible fit of a straight line to the observed data (x_i, y_i) . It represents the variability of the dependent variable explained by the regression equation. The vertical distance labelled 'residual' between the predicted value \hat{y}_i and the observed value y_i is the minimised error sum of square. It represents the variability of the dependent variable unexplained by the regression.

8.6 The Variability Component R^2

In SPSS, there is a term, R^2 , called the coefficient of determination. The following are the different interpretations of the meaning of R^2 .

Simply, R^2 is the squared value of the correlation coefficient between an independent and a dependent variable. Within regression, it can be thought of as a goodness of fit of the model. But more importantly, when there are two or more independent variables in the sample, it can be thought of as the proportion of variability in the dependent variable explained by the model, and is given by

$$R^2 = \frac{1 - \text{RESIDUAL SUM OF SQUARES}}{\text{TOTAL SUM OF SQUARES}} \quad (8.4)$$

Another statistical analysis involving the use of R^2 is the hypothesis of $R^2_{pop} = 0$, the linear relationship in the model is zero. This is given by the F statistics as

$$F = \frac{\text{MEAN SQUARE REGRESSION}}{\text{MEAN SQUARE RESIDUAL}} \quad (8.5)$$

Note that if $R^2 = 0$ it does not mean there is no relationship in the model, but it means there is no linear relationship in the model.

8.7 Stepwise Multiple Linear Regression

There are different techniques in determining a multiple regression equation, of which the stepwise multiple linear regression is the most commonly used. The basic principle is that the independent variables are entered into the equation in the order of the amount of variability removed by each variable. This means the independent variable with the largest absolute correlation coefficient against the dependent variable is the first candidate.

Since there is this priority in the order of the independent variables entering into the equation, there is an added advantage of observing the changes in the successive R^2 terms. If the change in two successive R^2 is large, we can conclude that the second variable entered contributes a significant portion towards the model. Similarly, if the change is small, we can conclude that the second variable entered does not play a significant role in the regression.

There is also another statistical analysis which concerns the regression coefficient β_i . This uses the t statistics value, which is the square rooted value of the F statistics. It serves to test whether $\beta_i = 0$, in other words, whether the slope of the i th independent variable is zero.

To demonstrate the stepwise multiple linear regression using SPSS, three contact locations are chosen. They are the impact between the offside upper leg and the side of the petrol tank (ULRFTT), between the offside knee and the knee-restraint (KFRFTT) and between the offside lower leg and the knee-restraint (LFRFTT). The outputs are contained in Figures 8.9, 8.10 and 8.11 respectively.

The first variable to enter in the regression analysis of ULRFTT is VEL. The R^2 value (in row marked 'R Square') is 0.29561. This represents that 29.56% of variability in the dependent variable can be explained by VEL alone. The F statistics value is 20.56361 and its level of significance is less than 0.000005 (marked 'Signif F'), therefore we reject the null hypothesis that $R^2_{\text{pop}} = 0$.

The t statistics value is 4.535 and its level of significance is also less than 0.000005 (marked 'Sig T'). This represents that the regression coefficient associated with VEL is not zero. Indeed its value is 354.006663 in the column marked B. This represents the initial regression equation with only VEL as the first variable entered, thus

$$F = -1853.025 + (354.007) \cdot \text{VEL} \quad (8.6)$$

The second variable to enter into the equation is ANG. R^2 has now

increased to 53.88%. Note that the R^2 change is approximately 24%, therefore signifying the importance of variable ANG in the model. The F statistics shows a significance level of less than 0.000005, therefore the null hypothesis $R^2_{pop} = 0$ is rejected. Similarly, the t statistics also indicates the rejection of zero regression coefficient for ANG, and the computed value is found to be -61.660509. Note the negative slope of variable ANG. Thus, the equation now stands as

$$F = 1489.965 + (361.279) \cdot VEL + (-61.661) \cdot ANG \quad (8.7)$$

The next variables to enter into the equation are RLP, KR and LP. For these variables SPSS only printed out the final completed analysis. This is not surprising, since R^2 is now increased to 54.63%; less than one percent since the second step in the regression. This shows that the remaining three variables do not contribute any significant influence to the model. However, the F statistics level is still less than 0.000005 thus indicating that R^2_{pop} does not equal zero.

The t statistics significance levels associated with these remaining variables show that the null hypothesis of each of the regression coefficients being zero cannot be rejected. However, the final regression equation is presented as below.

$$F = 908.699 + (344.939) \cdot \text{VEL} + (-59.667) \cdot \text{ANG} \\ + (999.983) \cdot \text{RLP} + (5944.538) \cdot \text{KR} + (20.005) \cdot \text{LP} \quad (8.8)$$

The regression coefficients associated with the last three independent variables do not appear to be zero, indeed two of them are of high values. But then these independent variables are in different units, such as ANG in radians, VEL in metres per second. The equation above only represents the regression of a straight line within this sample of data; the actual magnitudes of these coefficients do not represent the relevant importance of the associated variables.

The entries under the column 'SE B' are the estimated standard of errors of the corresponding B's. The larger ones correspond with the large magnitudes of the regression coefficients, thus indicating the levels of error assumed in regressing these coefficients. This is compatible with the *t* statistics findings.

The next column marked 'Beta' contains what are known as standardised regression coefficients, and they are defined as

$$\text{BETA}_i = \frac{B_i S_i}{S_y} \quad (8.9)$$

where S_i = standard deviation of the *i*th independent variable
and S_y = standard deviation of the dependent variable

This leads to BETA's in dimensionless coefficients and they act as a more reliable guide to the relative importance of each of the independent variable. Thus

$$\begin{aligned} F(\text{ULRFTT}) = & (0.5298) \cdot \text{VEL} + (-0.4773) \cdot \text{ANG} + (0.0048) \cdot \text{RLP} \\ & + (0.0675) \cdot \text{KR} + (0.0426) \cdot \text{LP} \end{aligned} \quad (8.10)$$

Indeed these standardised regression coefficients agree with the findings of the t statistics hypotheses.

The regressed equation shows VEL being the most dominating variable, with ANG being the second major contributor. The sign of ANG is negative, suggesting its effectiveness at oblique angles. Of the three remaining variables, RLP is virtually ineffective, and the other two contributed insignificantly.

The same procedure can be applied to regressions of KFRFTT (Figure 8.10) and LFRFTT (Figure 8.11). Notice in regression of KFRFTT there is an extra step where the variable KR is entered singly by SPSS, rather than being printed out with RLP and LP in the final stage of the regression, as with the cases of ULRFTT and LFRFTT. This may highlight the relative importance of KR in the regression of the KFRFTT case. Indeed the R^2 change is 57% from 50.5% when ANG is entered.

Based upon the standardised BETA regression coefficients we have

the following two equations:

$$\begin{aligned} F(KFRFTT) = & (0.5678) \cdot VEL + (0.4463) \cdot ANG + (-0.2329) \cdot KR \\ & + (0.0159) \cdot RLP + (-0.1123) \cdot LP \end{aligned} \quad (8.11)$$

$$\begin{aligned} F(LFRFTT) = & (0.5367) \cdot VEL + (0.4143) \cdot ANG + (0.0090) \cdot RLP \\ & + (-0.1251) \cdot KR + (-0.1159) \cdot LP \end{aligned} \quad (8.12)$$

The two regression equations appear different to that of ULRFTT, but share similarities between themselves. The signs of the ANG variables are both positive, suggesting these two forces are more linearly related to steep to head-on angles. The coefficients associated with the RLP terms are still basically small, suggesting they are relatively unimportant in the regressions, but for KR and LP, not only the magnitudes of their coefficients have been increased if compared with the ULRFTT regression, but the signs have changed to negative.

The negative sign of the regression coefficient associated with KR variable suggests that F is more linearly related to shorter gap distance between the knee and the knee-restraint. This is so especially in the case of KFRFTT where the magnitude is relatively high. The magnitudes of the LP regression coefficients are smaller, but the negative signs suggest F is more linearly related to a softer leg protector, in both cases.

It may not be a surprise that KFRFTT and LFRFTT share these similarities and that ULRFTT behaves quite differently from these two forces. This is because KFRFTT and LFRFTT are impact forces between the offside knee, the offside lower leg and the knee-restraint, they are then different locations on the same limb impacting onto the same object. The force ULRFTT, is between the right upper leg, which is seated horizontally, and the side of the petrol tank, a different object.

Figure 8.12 is a table containing all the BETA regression coefficients as computed by SPSS, between the independent variables and the various forces. In general, the entries under the columns ANG and VEL are of higher magnitudes than to those entered under columns KR, LP and RLP, thus demonstrating ANG and VEL are the two most dominating variables in the whole system.

The entries under column VEL, with the exception of one LBLFTT, are all positive. This indicates the linearized relationship between F and the positive slope of VEL, such that F will have a tendency to increase given the increase in the value of VEL. Similarly, most of the entries under ANG are also positive, showing the tendency for F to increase when the angle of impact is getting steeper. This is so with the exception of three cases, and they are the forces between the offside upper leg and the right-hand-side of the petrol tank.

The right-hand-side in this simulation is the side of the dummy and the motorcycle away from the barrier. When the barrier is inclined at an oblique angle, the motorcycle will first impact onto the barrier on its left-hand-side, causing the motorcycle to rotate towards its right-hand-side, away from the barrier. However, in the meantime, the dummy rider is still travelling in the original fore-and-aft direction such that as the motorcycle yaws, the offside upper leg will impact onto the side of the petrol tank. At less oblique angles, the likelihood of the motorcycle impacting the barrier onto its side is reduced, thus reducing the motorcycle's yaw motion. This explains the negative slopes of the variable ANG when regression is performed on the offside upper leg. Figure 8.13 is a three-dimensional diagram of the relationship between F, ANG and VEL. F being the force on the offside upper leg, ULRFTT.

For the entries under columns KR, LP and RLP in Figure 8.12, it seems the values are generally low, but in a randomised pattern. On closer inspection, the variable KR possesses higher magnitude of the BETA regression coefficient on more occasions, with RLP being very close to zero at times, to having a relatively reasonable regression coefficient. The LP regression coefficient is more stable, generally around the 0.1 mark.

Notice the signs of these three variables tend to be negative when the impact occurs on both of the lower legs. Bearing in mind

a negative sign for KR means a closer distance between the knee and the knee-restraint; for LP it means the leg protector is constructed with softer material; and for RLP it means a fuller profile of the shape of the leg protector, therefore, based on this regression analysis, it seems that the two lower legs will tend to suffer more injury when these three factors are as stated.

8.8 Partial Correlation Coefficient

Earlier we have measured the strength of linear relationships among the different sets of variables. It was found that the velocity variable VEL dominates the overall system, closely followed by the angle of impact variable, ANG. The linear strength between the remaining three variables and the forces were small.

However, this does not necessarily mean that these three variables, KR, RLP and LP, are totally insignificant. This is important as these three factors are in the hands of the motorcycle designer whereas VEL and ANG are not. If the dominant effects of ANG and VEL are somehow minimised or even suppressed, there may emerge a more accurate relationship between F and the three other variables. SPSS provides such a facility known as the Partial Correlation Coefficient.

The partial correlation coefficient is a technique closely related to multiple linear regression. It measures the linear strength between two variables while the linear effects of other variables in the sample are adjusted. This provides us with a technique to detect any hidden relationship, dominant feature and/or the relative significance of variables in a sample.

Figure 8.14 contains the partial correlation coefficients between KR, LP, RLP and the different impact forces, when ANG and VEL are controlled separately. We shall investigate these coefficients following our examples ULRFTT, KFRFTT and LFRFTT.

Consider first when the variable ANG is controlled. The partial correlation coefficient between ULRFTT and KR is 0.2218. Refer back to Figure 8.7 where the corresponding correlation coefficient, when neither ANG nor VEL is controlled, is 0.2598. The value is reduced somewhat but not significantly. Similarly for LP and RLP, the values are more or less equivalent to the corresponding correlation coefficients.

However, when the variable VEL is controlled, we see a substantial difference. The partial correlation coefficient between ULRFTT and KR is now reduced to 0.1777 from 0.2598 as previously. This indicates the relationship between F and KR is weakened by the absence of VEL, but because of the positive slope, F has the tendency to increase as KR increases. This is

also the case for the variable LP, but not for RLP where its partial correlation coefficient is now 0.0075, close to zero.

From the above, it seems that ANG has no effect on the relationships between F and the three variables, but VEL has. Indeed RLP seems to be almost dominated by VEL, and for both KR and LP, the relationship is weakened. Yet the trends seem to be that if the knee is further away from the knee-restraint, F will increase; and if the leg protector is made stiffer, F will also increase.

In the case of the KFRFTT, observations are quite different from the above. When ANG is controlled, both partial correlation coefficients for KR and LP have reduced. Because of their negative nature, it suggests that if the knee is placed closer to the knee-restraint, and if the leg protector is made softer, F will increase. The partial correlation coefficient for RLP stays quite constant thus ANG has no effect.

When VEL is controlled, the reverse happens. Both coefficients for KR and LP have increased, but because of their negative slopes, the trends are still the same as before. For RLP, the coefficient is now reduced to 0.0005. This is very close to zero, showing that RLP is totally dominated by VEL.

Therefore the more accurate relationships between KFRFTT and KR,

LP, RLP emerge. When either ANG or VEL is controlled, KFRFTT is likely to increase if the knee is placed closer to the knee-restraint, and if the leg protector is made less stiff. This relationship is made weaker if the variable ANG is controlled, but stronger if the variable VEL is controlled. ANG seems to have not much effect for the relationship between F and RLP, but VEL seems to dominate RLP completely.

The findings for the case of LFRFTT are very similar to those for KFRFTT. Once again it seems LFRFTT is likely to increase if the knee is placed closer to the knee-restraint, and if the leg protector is quite soft. RLP has not much effect.

This is not surprising. As with multiple linear regression, it was found that KFRFTT and LFRFTT shared similarities. Also the findings here using Partial Correlation Coefficients broadly agree with those by regression.

The above are observations made with either ANG or VEL controlled. Figure 8.15 contains the partial correlation coefficients when both ANG and VEL are controlled.

Using the same examples as before, we see that all three coefficients for KR, LP and RLP, in the case of ULRFTT, have been reduced substantially. All are positive with RLP reduced to 0.0160, close to zero. This demonstrates that relationships have

been greatly weakened by the absence of ANG and VEL. However, the coefficient for LP is 0.0879, a weak linear strength, but for KR it stands at 0.1136. Though more than halved from its original correlation coefficient, but perhaps it is still an indication of an increase in F if the knee is placed further away from the knee-restraint.

For both KFRFTT and LFRFTT, the coefficients for KR and LP have been increased significantly. Because the increases are in the negative direction, they show the tendency of increase in F if the knee is placed closer to the knee-restraint, and if the leg protector is made softer. Note that the increases in these coefficients are sometimes doubled. This demonstrates the stronger relationships between these variables once the dominant effects of ANG and VEL are being controlled.

The RLP coefficients, however, have been greatly reduced in both the KFRFTT case and the LFRFTT case. This shows that this variable is greatly dominated by either ANG or VEL or both. As we have found out earlier, this term is dominated by VEL.

If we glance at Figure 8.15, one can broadly divide the findings into two main groups. A group containing forces on the upper legs and a group of forces on the lower legs.

In general, for the group representing relationships on the lower

legs, the coefficients for both KR and LP have increased. The increases are in the negative direction, suggesting increase in F if knee to knee-restraint distance is reduced, and if the leg protector is made progressively less stiff. For coefficients associated with the RLP term, though most of them are small, they are all of negative signs, some even changed from their positive slopes when computed as correlation coefficients. This suggests the trend of increase in F if the profile of the leg protector is made more pronounced.

In the group containing relationships on the upper legs, most of the coefficients have been reduced, suggesting weaker relationships once ANG and VEL have been controlled. The coefficients are broadly positive with the exceptions of the KTLFTT (nearside knee against lower part of petrol tank) and KTRFTT cases.

In the KTLFTT case, relationship between the force and KR is close to zero. For LP, the coefficient increases negatively, suggesting the effect of a softer leg protector. The RLP coefficient shows little change.

In the KTRFTT case, though the coefficient between the force and KR is small, it has been changed from a positive slope to a negative one. This suggests the trend of increase in F as the knee is placed closer to the knee-restraint. The change from

positive to negative slope also applies to the RLP term, suggesting an increase in F as the profile of the leg protector is made more pronounced. These two findings broadly agree with those of the group containing impact forces on the lower legs, with the exception that the slope of the LP coefficient is positive, although the magnitude is reduced. This indicates an increase in F as the leg protector is made stiffer.

This may highlight the position of the knee being sensitive in an impact. Indeed the knee is the connecting joint between the upper and the lower legs. Because of the lack of simulated flesh surrounding the dummy knee, and therefore the knee being extremely stiff, forces generated against it may be inordinately high.

8.9 Analysis Of Variance (ANOVA)

Analysis of variance is a technique which divides the total variance in a population of observed data, into different portions. This has the effect of categorising the data into different pre-determined classes, though some classifications may be deterministic, such as the gender of interviewees in a research survey. However, proportions of score ratings into classes such as low, medium and high are sometimes due to human judgement or experience. Note also it is the independent variable

that is to be categorised into different groups, with the dependent variable, or the scores, being partitioned into appropriate groups.

The partitioning of the total variation concerns with the sum of squares of the difference between the groups, denoted by $SS(\text{between})$, and the sum of squares of the difference within the groups, denoted by $SS(\text{within})$. When there is only one independent variable and one dependent variable, the total sum of squares can be expressed as:

$$SS(\text{total}) = SS(\text{between}) + SS(\text{within}) \quad (8.13)$$

And the null hypothesis, H_0 , to be tested is

H_0 : There is no relationship between
the independent variable and the
dependent variable

If H_0 is true, it implies that the population means of the categorised groups are identical such that

$$\mu_1 = \mu_2 = \dots = \mu_N = \mu, \text{ a constant.} \quad (8.14)$$

This implies that variation among group means should be no greater than variation within individual groups, as expressed in

the following null hypothesis:

$$H_0 : \sigma^2_{\text{between}} = \sigma^2_{\text{within}} \quad (8.15)$$

This is known as 'One-Way Analysis of Variance'.

When there are two independent variables the partition of the total variation is divided into four components. They are the sum of squares for each variable, their interaction, and the residual. This can be expressed as:

$$\begin{aligned} SS(\text{total}) = SS(\text{variable 1}) + SS(\text{variable 2}) + \\ SS(\text{interaction}) + SS(\text{residual}) \end{aligned} \quad (8.16)$$

The null hypothesis, H_0 , to be tested is:

$$H_0 : \text{There is no interaction between} \\ \text{the two independent variables}$$

This is known as 'Two-Way Analysis of Variance'. In SPSS, it is denoted simply as ANOVA.

Let us proceed with SPSS using our examples, namely ULRFTT, KFRFTT and LFRFTT.

Figures 8.16a and 8.16b contain the ANOVA output computed by SPSS

for the force ULRFTT. The two independent variables in the first analysis of variance are ANG and VEL, as shown in Figure 8.16a. The dependent variable being F. We see the significance levels under the column marked 'Main Effects' are both less than 0.00005. This means that the mean force values from the categorised group of ANG and VEL are not all the same. The significance level for the '2-Way Interactions' between ANG and VEL is also less than 0.00005. This indicates that there is an interaction between ANG and VEL in the generation of F.

If we look at the three-dimensional plot in Figure 8.17a, we will see the relationship between ANG and VEL in generating F. We see the higher forces are mostly clustered in an area where ANG ranges from 35° to 55° , and where VEL ranges from 14ms^{-1} to 18ms^{-1} . This demonstrates the impact between the offside upper leg and the side of the petrol tank is more severe at these angles, where the motorcycle spins to the side after the front wheel impacted onto the barrier. The high velocities demonstrate the rapid rotation of the motorcycle.

In Figure 8.17b the independent variables are ANG and RLP, the dependent variable still being that of the force ULRFTT. We see the F values are no longer significant, so that we cannot reject the null hypothesis that there is no interaction between ANG and RLP. Indeed if we look at the appropriate plot in Figure 8.17b, we see that the higher values are still mostly contained in the

range 35° to 55° , but these values lie across the whole spectrum of RLP.

For the force KFRFTT, the analyses are in Figures 8.18a and 8.18b. In Figure 18a the independent variables are ANG and VEL. We see all the F values are significant thus we reject the null hypothesis that there is no interaction between ANG and VEL. Let us look at the appropriate plot in Figure 8.19a.

We see that for $ANG < 50$ the forces are mostly low or no contact. From there on, forces increase as both ANG and VEL increase, indeed the two highest forces are around the $ANG = 80$ and $VEL = 18$ locations. This highlights the severity of the impact force at more head-on angles and high velocity.

Figure 8.18b contains the analysis of variance when the independent variables are ANG and RLP. The 2-way Interaction significance level indicates there is an interaction between ANG and RLP. If we look at the corresponding plot in Figure 8.19b, we see for $ANG < 50$ there are mostly low forces or no contact, as before. However, for $ANG > 50$, the distribution is more diverse.

We see when $ANG = 90$, there is a range of values across the range of RLP. This is understandable since for head-on impacts, the forces between the knee and the knee-restraint will be

independent of the shape of the leg protector. The two high indicators, the two highest forces, are around $ANG = 80^\circ$. High values also occur at one range of RLP which represents the less pronounced profile of a leg protector. This is a curious result from the combination of ANG and RLP, but perhaps this is due to the high velocity as discovered in the first analysis.

Perhaps the best indicators of interaction between ANG and RLP are the forces in the centre of the contour plot. They indicate a barrier angle ranging from 50° to 60° , with a medium profile of a leg protector. We also note that these indicators are of velocities 10ms^{-1} and upwards, as can be seen in Figure 8.19a. Though these are not the highest forces, they agree with the motion of the dummy when a motorcycle impacts on a skew angle. This is because as the motorcycle rotates, the dummy is still travelling forwards, so it would be more likely that the dummy's knees will impact more severely onto the knee-restraints if aimed at a more direct angle.

Figures 8.20a and 8.20b contain the analyses for the force LFRFTT. As before the first analysis contains independent variables ANG and VEL, whilst the second contains independent variables ANG and RLP. In both analyses the interaction terms show significant interactions between the variables. Let us look at the corresponding plots in Figures 8.21a and 8.21b.

There are similar patterns in both figures to those of the force KFRFTT, but even more concentrated. In the plot for ANG and VEL, the high forces are indeed in the left upper corner. In the plot for ANG and RLP, the forces are mostly low or no contact occurred, with exception of a few high lying across $ANG = 90$. As mentioned before, these are independent of the shape of the leg protector. The other higher forces, as before, lie in the left upper corner of the plot. Unlike the corresponding plot for KFRFTT, there does not seem to be an effect around the mid-ranges of ANG and RLP. However, it is conceivable that the knees are more likely to impact onto the knee-restraints before the lower legs, by which time, the motorcycle will spin round even more to the offside of the dummy.

The combination of these results may seem curious. One might expect there would be more interaction between ANG and RLP for the impact force ULRFTT than would be forces KFRFTT and LFRFTT, since the latter two hit the knee-restraint rather than the side of the tank. This is because the interaction between ANG and RLP will be most effective on an inclined barrier whilst totally independent when the barrier is directly in front of the motorcycle. However, if we look onto the contour plot in Figure 8.17b, we see most of the high indicators are located at $ANG = 50$ or below. This demonstrates the effectiveness of a skew angled barrier. But their scatter across the lower half of the plot, which is unlike the equivalent plots for KFRFTT and LFRFTT, where

the high indicators are more concentrated in a specific area, namely the right upper corner, may be the reason why the interaction term did not show its significance.

In general, there is interaction between variables ANG and VEL for most of the forces. This agrees with the findings from the regression technique. There is also interaction between variables ANG and RLP, but curiously, only for forces between the knees and the knee-restraints, and for forces on the lower legs. For forces on the upper legs, interaction terms are insignificant.

8.10 Multivariate Analysis Of Variance (MANOVA)

Multivariate analysis of variance (MANOVA) is a statistical technique similar to ANOVA, with the exception that there are two or more dependent variables in the analysis. The hypothesis is to test if there is interaction between the independent variables based upon the dependent variables.

The dependent variable in our analysis has always been the force, if impact had occurred, between a location on the dummy and an area of the motorcycle. To assemble more than one dependent variable in the analysis we can broadly divide all the impact forces into two groups: one group involving impacts between the upper legs and the sides of the petrol tank, and one group

involving the impacts between the lower legs and the knee-restraints. Within each group, there exist two sub-groups of impacts occurring on the left-hand-side and on the right-hand-side. To continue our examples, we will consider impacts on the right-hand-side of the dummy.

For the impacts between the dummy's offside upper leg and the right-hand-side of the petrol tank, there are three sets of forces; they are ULRFTT, KRFTT and KTRFTT. From the MANOVA outputs computed by SPSS, it is found that the multivariate tests are only significant for the interaction between ANG and VEL, and between KR and LP. The outputs are listed in Figures 8.22a and 8.22b respectively.

In Figure 8.22a we can see that the Hotellings multivariate test of significance indicates we can reject the null hypothesis that the ANG-by-VEL interaction is 0, and the univariate F-test suggests that F1, equivalent to ULRFTT, is highly significant to the different categories of ANG and VEL. These are in the top third of Figure 8.22a. The following sections give the equivalent multivariate and univariate tests of significance for each of the independent variables. Thus we can see that the means of the forces do differ for the different categories of VEL, with forces ULRFTT and KTRFTT highly significantly so; and the means of the forces also differ for the different categories of ANG, with force ULRFTT highly significant. In both cases, the force KRFTT

does not show any significance at all. This may be due to the fact that KRFTT only scored few contacts.

In Figure 8.22b we see the KR-by-LP interaction is significant, so are the independent variables when taken individually. However, this time only the force KRFTT shows that its mean differs for the different categories of the independent variables.

For the impacts between the dummy's offside lower leg and the knee-restraint, there are three sets of forces; they are KFRFTT, LFRFTT, LLFRFTT. From the MANOVA analyses, they are found to be significant for the interaction between ANG and VEL, ANG and KR, ANG and RLP, and VEL and RLP. The outputs are listed in Figures 8.23a, 8.23b, 8.23c and 8.23d respectively.

In Figure 8.23a we can see that all the forces are confidently significant for the ANG-by-VEL interaction, as well as the two independent variables when taken individually. This indicates that the means of the forces do differ for the different categories of ANG and VEL.

In Figure 8.23b we see that the Hotelling test of significance shows that we can reject the hypothesis that the ANG-by-KR interaction is 0. However, the univariate test does not show any particular force of significance. This is the case when KR is

taken individually. But forces LFRFTT and LLFRFTT do show that they differ to the different categories of ANG variable.

In Figure 8.23c we see that all the tests show there is clear evidence to reject the null hypothesis. This indicates that there is strong interaction between ANG and RLP for the scores of these forces.

Figure 8.23d shows that there is still sufficient significance to reject the null hypothesis that the interaction between VEL and RLP is 0. However, no particular force shows any significance to the combined categories. This is the same when RLP is taken singly. The univariate test of VEL shows us not to reject that the means of forces do not differ to the different categories of VEL.

These are the findings from SPSS using MANOVA analysis. However, this does not lead to any strong conclusion, except for the interaction between ANG and VEL, about the effect of these variables when combined together. Indeed, the only convincing results are those of ANG and VEL, and the interaction of ANG and RLP in the case of the lower legs impacting onto the knee-restraints. This particular finding is consistent with the finding by ANOVA.

8.11 Overview

We have examined the results analysed by different statistical techniques, as computed by SPSS. Here, we will summarize these analyses and draw out some general conclusions.

From the correlation coefficients between forces and the five independent variables, it was observed that ANG and VEL correlate stronger with F. The coefficients between F and VEL are mostly positive, indicating the increase in VEL leads to increase in F. The coefficients between F and ANG are also mostly positive, except for the offside upper legs of the dummy where they are negative. This indicates the offside upper legs impacting onto the side of the petrol tank, after the motorcycle had hit an inclined barrier on the left-hand-side thus producing clockwise yaw motion.

Of the three remaining independent variables, KR, RLP and LP, the linear strength of the correlation is weak. However, out of the three, KR possesses the strongest correlation with F though this may not be of any significant value.

In stepwise multiple linear regression the equations in regressing the forces are once again dominated by ANG and VEL. The coefficients associated with ANG are negative in the equations describing forces on the dummy's right upper leg. This

is consistent with the findings by correlation coefficient. The signs of the slopes of VEL are mainly positive.

Of the three remaining variables in the equations, the signs of the slopes of KR are generally positive on the upper legs, but negative on the lower legs. This is also the case for the slopes of LP. This suggests that the forces on the lower legs have the tendency to increase, if impact occurred, as the knees are placed nearer to the knee-restraints, and if the leg protector is made less stiff. However, the signs of the slopes of RLP are more diverse and less conclusive.

In correlation coefficient analysis the coefficients given are the direct measures of linear strength between the independent variable and the dependent variable. Multiple regression gives the best regressed equation with the inclusion of all the independent variables. Partial correlation, however, will give the linear strength of an independent variable when the effect of some other independent variable is disregarded. This has the advantage of highlighting the potential importance, or otherwise, of the variable in question.

We have observed the two most dominant variables are ANG and VEL. It would be appropriate to extract these two factors out of the analysis so that the effects of KR, LP and RLP can be demonstrated. We see that when this happens, the relationships

between these variables and the upper legs are greatly weakened, but for the lower legs, certain tendencies have emerged.

When ANG and VEL are held constant, the forces on the lower legs have the tendency to increase if the knees are placed nearer to the knee-restraints, and if the leg protector is made less stiff, also if the shape of the leg protector is more pronounced. There is one exception for the right knee impacting onto the side of the petrol tank, where the partial correlation coefficient for the stiffness of the leg protector indicates that this force has the tendency to increase, if the leg protector is made stiffer.

The above analyses are based on parametric results from the computer simulation. Here we will summarize the findings by ANOVA and MANOVA. These two techniques are non-parametric in that the user needs to categorise the variables into classes.

In ANOVA there is only one dependent variable. Independent variables are taken to test if there is interaction between them based on the scoring of the dependent variables. We find that interaction exists between ANG and VEL, and between ANG and RLP interaction exists only for the lower legs.

In MANOVA the same principle applies but there are two or more dependent variables. It is therefore logical to separate forces on the upper and lower legs as dependent variables. The findings

are consistent to those by ANOVA, where interaction exists between ANG and VEL, and between ANG and RLP on the lower legs.

For forces on the right upper leg, the highest ones concentrated in a cluster at around 35° to 50° barrier range, and the velocity range of 14ms^{-1} to 18ms^{-1} . This illustrates the yaw motion of the motorcycle, and the effectiveness of a high travelling velocity.

For forces on the lower legs, they have the tendency to increase as barrier angles approach 90° , and as velocity increases. This illustrates the fact that the lower legs impact onto the knee-restraints when the motorcycle hit the barrier at an approachingly head-on angle.

For forces on the lower legs in terms of the interaction between ANG and RLP, there are two small clusters of high forces. One cluster indicates the head-on angle of 90° , with the shape of the leg protector at its widest limit. The other cluster of high forces indicates the barrier angle at around 80° , but the shape of the leg protector is at its least wide limit.

One may ask that when the angle of impact approaches head-on, is the shape of the leg protector relevant to the injury on the rider's legs? However, experience has shown us that mathematical modelling is extremely sensitive. An angle of 88° will result in completely different patterns or trajectories of the motion of

the dummy and the motorcycle to those of 90° , whereas in real-life events may be similar. Because of this all angles greater than 85° were given the value of 90° exactly. This casts doubt on whether the different effect found for leg protector shape is genuine.

Though SPSS did not show interaction involving the variables KR and LP, it is worth investigating these particular forces at the 80° mark. Findings show these cases are of high velocities, with knees, in general, placed nearer to the knee-restraints, but of different ranges of stiffness of the leg protector. This may not be conclusive, but we can see the consistency of the findings in variables VEL and KR.

- (1) FORVEL - initial velocity for motorcycle (BIKEVL) and dummy rider (DMYVL)
- (2) PLANG - barrier angle
- (3) YGLBAR - y-coordinate for extension of barrier
- (4) WHLFRM - stiffness factor assigned to front wheel to barrier impact (WHLSTT) and to front wheel to motorcycle frame impact (CNGSTT)
- (5) MCYSTT - stiffness factor assigned to linear headstock to barrier impact
- (6) SDFAIR - stiffness factor assigned to radial headstock to barrier impact (STKSTT) and fairing to barrier impact (FARSTT)
- (7) PANSTT - stiffness factor assigned to pannier to barrier impact
- (8) FFMEWY - local y-axis friction coefficient assigned to front wheel to barrier impact (MEWWHLY) and to front wheel to motorcycle frame impact (MEWCNGY)
- (9) FFMEWZ - local z-axis friction coefficient assigned to front wheel to barrier impact (MEWWHLZ) and to front wheel to motorcycle frame impact (MEWCNGZ)
- (10) MEWMCYY, MEWMCYZ - local y-axis and z-axis friction coefficients respectively, assigned to linear headstock to barrier impact
- (11) TAKMEW - friction coefficient, assigned to local y-axis (MEWYB) and z-axis (MEWZB) of fairing to barrier impact, and local x-axis (MEWXTK) and z-axis (MEWZTK) of petrol tank to barrier impact
- (12) FLMEW - friction coefficient, assigned to local y-axis (MEWPANY) and z-axis (MEWPANZ) of pannier to barrier impact, and local x-axis (MEWXLP) and z-axis (MEWZLP) of knee-restraint to barrier impact
- (13) RHEAD - radius of head
- (14) FARDIS - knee to knee-restraint distance
- (15) LGPSTT - stiffness factor assigned to leg protector to barrier impact
- (16) RLEGP - radius of leg protector
- (17) LPXIC - x-coordinate of centre of radius of leg protector
- (18) LPYIC - y-coordinate of centre of radius of leg protector
- (19) TSTOP - time of simulation
- (20) BIKPOS - initial y-coordinate position of centre of gravity of motorcycle
- (21) DUMPOS - initial y-coordinate position of centre of gravity of dummy rider
- (22) FCSPIN - stiffness factor for dummy spine joint
- (23) FCNECK - stiffness factor for dummy neck joint
- (24) FCHIP - stiffness factor for dummy hip joint
- (25) FCKNEE - stiffness factor for dummy knee joint

Figure 8.1 A list of the 25 changeable variables.

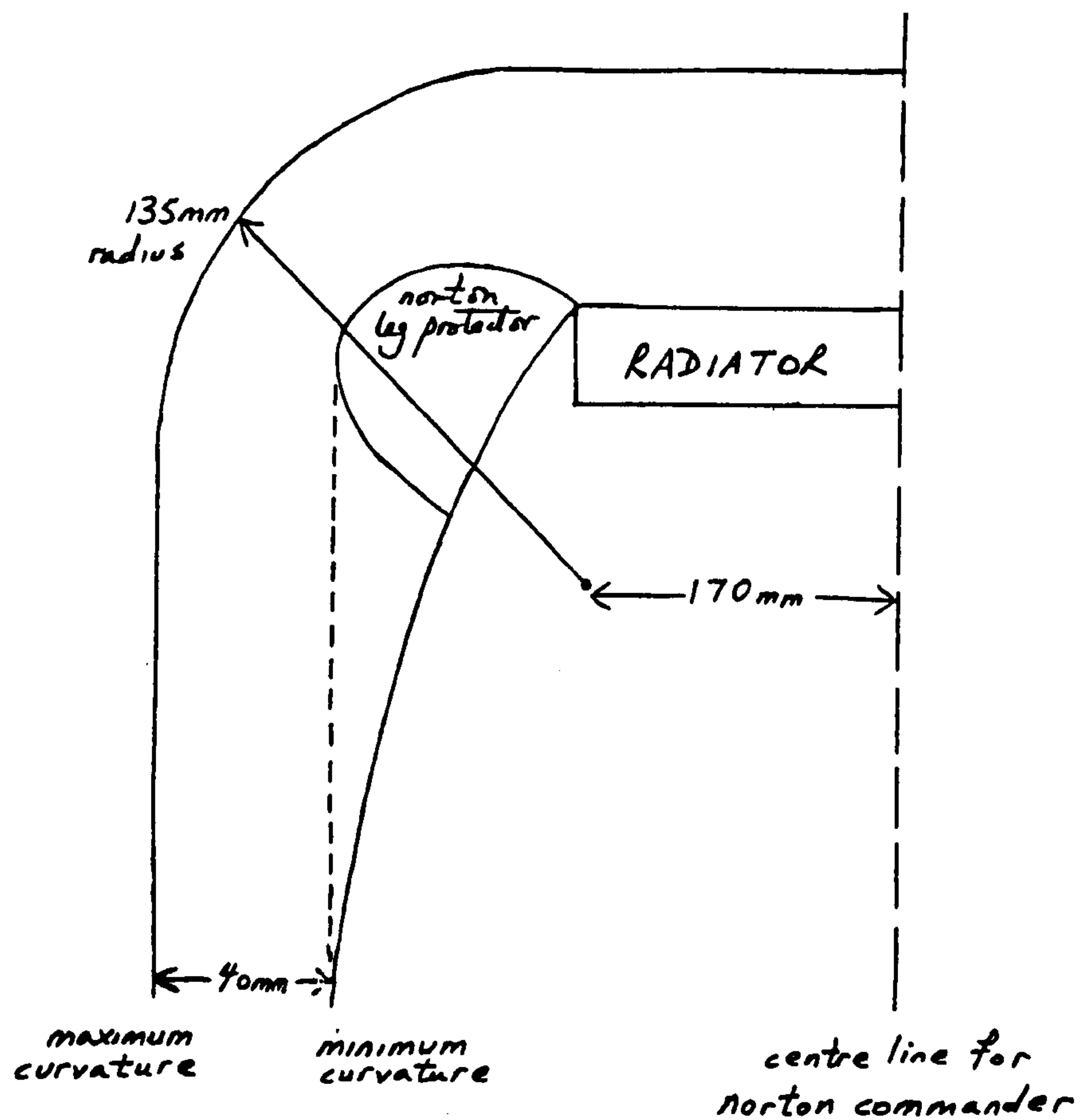


Figure 8.2 The upper and lower limits of the leg protector profile.

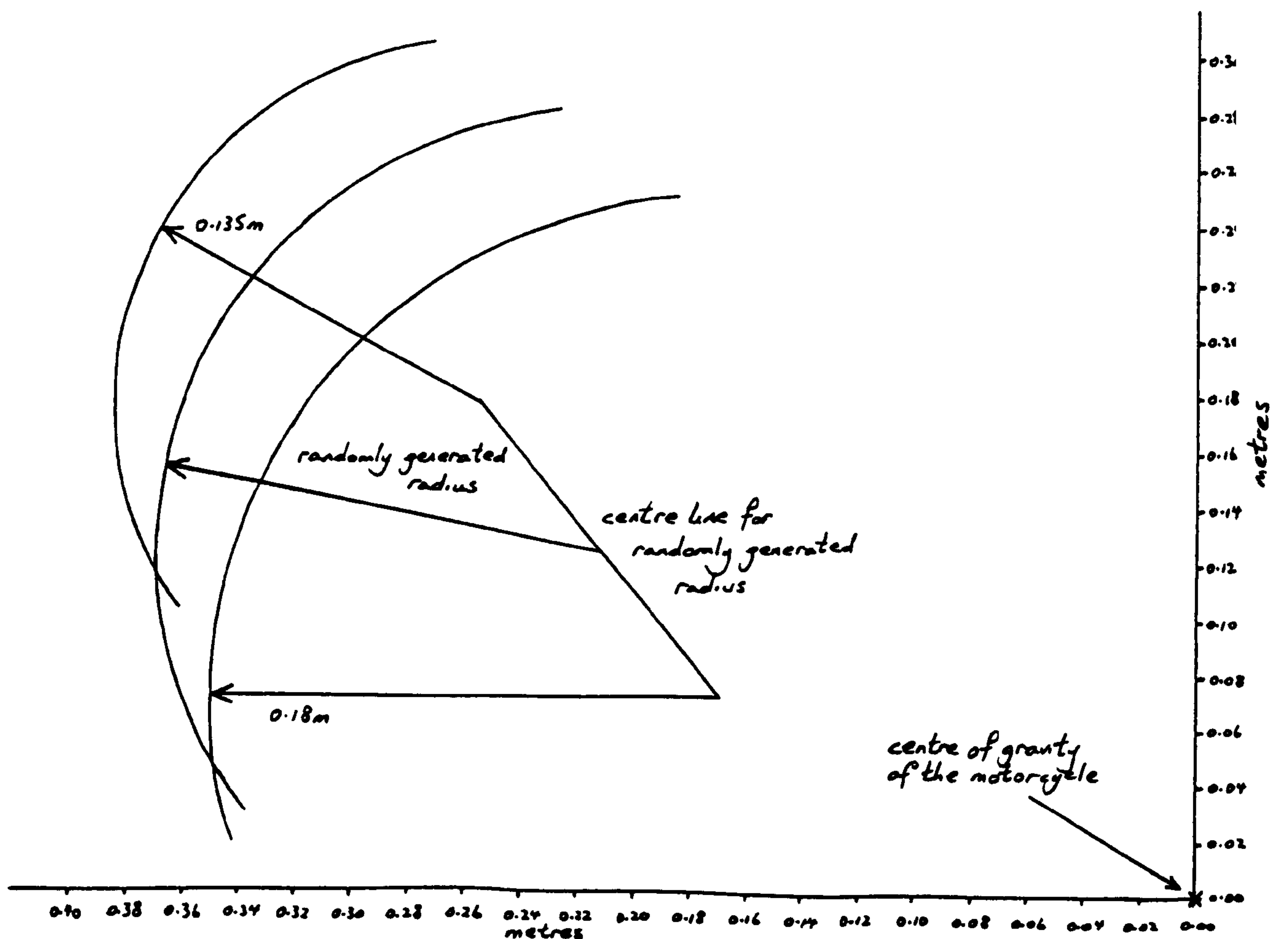


Figure 8.3 The modelling of the leg protector profile by the use of RLP.

FORCE	LOCATION ON DUMMY RIDER	LOCATION ON MOTORCYCLE
ULLFTT	dummy's left femur	port side of petrol tank
ULRFTT	dummy's right femur	starboard side of petrol tank
KLFTT	dummy's left knee	upper part of port side of petrol tank
KRFTT	dummy's right knee	upper part of starboard side of petrol tank
KTLFTT	dummy's left knee	lower part of port side of petrol tank
KTRFTT	dummy's right knee	lower part of starboard side of petrol tank
KFLFTT	dummy's left knee	left knee-restraint
KFRFTT	dummy's right knee	right knee-restraint
LBLFTT	dummy's left tibia	port side of engine
LBRFTT	dummy's right tibia	starboard side of engine
LFLFTT	dummy's left tibia	left knee-restraint
LFRFTT	dummy's right tibia	right knee-restraint
LLFLFTT	dummy's left ankle	left knee-restraint
LLFRFTT	dummy's right ankle	right knee-restraint

Figure 8.4 A list of target areas for contact between the dummy rider and the motorcycle.

$$20^{\circ} \leq \text{ANG} \leq 90^{\circ}$$

$20^{\circ} \leq \text{ANG} < 30^{\circ}$	$30^{\circ} \leq \text{ANG} < 40^{\circ}$	$40^{\circ} \leq \text{ANG} < 50^{\circ}$	$50^{\circ} \leq \text{ANG} < 60^{\circ}$	$60^{\circ} \leq \text{ANG} < 70^{\circ}$
2	3	4	5	6
$70^{\circ} \leq \text{ANG} < 80^{\circ}$	$80^{\circ} \leq \text{ANG} < 85^{\circ}$	$\text{ANG} = 90^{\circ}$		
7	8	9		

$$4.4 \text{ ms}^{-1} \leq \text{VEL} \leq 17.0 \text{ ms}^{-1}$$

$4.4 \text{ ms}^{-1} \leq \text{VEL} < 8.9 \text{ ms}^{-1}$	$8.9 \text{ ms}^{-1} \leq \text{VEL} < 11.4 \text{ ms}^{-1}$	$11.4 \text{ ms}^{-1} \leq \text{VEL} < 17.0 \text{ ms}^{-1}$
1	2	3

$$\text{VEL} = 17.0 \text{ ms}^{-1}$$

4

$$0.0 \text{ m} \leq \text{KR} \leq 0.1 \text{ m}$$

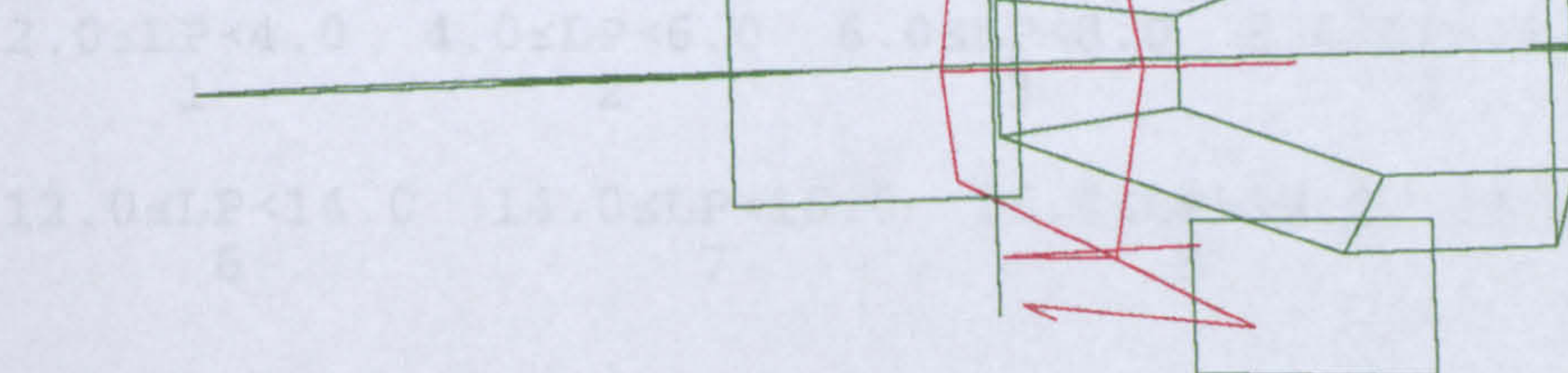
$0.0 \text{ m} \leq \text{KR} < 0.01 \text{ m}$	$0.01 \text{ m} \leq \text{KR} < 0.02 \text{ m}$	$0.02 \text{ m} \leq \text{KR} < 0.03 \text{ m}$	$0.03 \text{ m} \leq \text{KR} < 0.04 \text{ m}$	$0.04 \text{ m} \leq \text{KR} < 0.05 \text{ m}$
0	1	2	3	4

$0.04 \text{ m} \leq \text{KR} < 0.05 \text{ m}$	$0.05 \text{ m} \leq \text{KR} < 0.06 \text{ m}$	$0.06 \text{ m} \leq \text{KR} < 0.07 \text{ m}$	$0.07 \text{ m} \leq \text{KR} < 0.08 \text{ m}$	$0.08 \text{ m} \leq \text{KR} < 0.09 \text{ m}$
4	5	6	7	8

$0.08 \text{ m} \leq \text{KR} < 0.09 \text{ m}$	$0.09 \text{ m} \leq \text{KR} < 0.1 \text{ m}$
8	9



nearside



offside

Figure 8.5 Direction of travel

Figure 8.6 Categorization of impact points

$$20^{\circ} \leq \text{ANG} \leq 90^{\circ}$$

$20^{\circ} \leq \text{ANG} < 30^{\circ}$ 2	$30^{\circ} \leq \text{ANG} < 40^{\circ}$ 3	$40^{\circ} \leq \text{ANG} < 50^{\circ}$ 4	$50^{\circ} \leq \text{ANG} < 60^{\circ}$ 5	$60^{\circ} \leq \text{ANG} < 70^{\circ}$ 6
$70^{\circ} \leq \text{ANG} < 80^{\circ}$ 7	$80^{\circ} \leq \text{ANG} < 85^{\circ}$ 8	$\text{ANG} = 90^{\circ}$ 9		

$$4.4\text{ms}^{-1} \leq \text{VEL} \leq 17.8\text{ms}^{-1}$$

$4.4\text{ms}^{-1} \leq \text{VEL} < 8.9\text{ms}^{-1}$ 1	$8.9\text{ms}^{-1} \leq \text{VEL} < 13.4\text{ms}^{-1}$ 2	$13.4\text{ms} \leq \text{VEL} < 17.8\text{ms}^{-1}$ 3
$\text{VEL} = 17.8\text{ms}^{-1}$ 4		

$$0.0\text{m} \leq \text{KR} \leq 0.1\text{m}$$

$0.0\text{m} \leq \text{KR} < 0.01\text{m}$ 0	$0.01\text{m} \leq \text{KR} < 0.02\text{m}$ 1	$0.02\text{m} \leq \text{KR} < 0.03\text{m}$ 2	$0.03\text{m} \leq \text{KR} < 0.04\text{m}$ 3
$0.04\text{m} \leq \text{KR} < 0.05\text{m}$ 4	$0.05\text{m} \leq \text{KR} < 0.06\text{m}$ 5	$0.06\text{m} \leq \text{KR} < 0.07\text{m}$ 6	$0.07\text{m} \leq \text{KR} < 0.08\text{m}$ 7
$0.08\text{m} \leq \text{KR} < 0.09\text{m}$ 8	$0.09\text{m} \leq \text{KR} < 0.1\text{m}$ 9	$\text{KR} = 0.1\text{m}$ 10	

$$2.0 \leq \text{LP} \leq 20.0$$

$2.0 \leq \text{LP} < 4.0$ 1	$4.0 \leq \text{LP} < 6.0$ 2	$6.0 \leq \text{LP} < 8.0$ 3	$8.0 \leq \text{LP} < 10.0$ 4	$10.0 \leq \text{LP} < 12.0$ 5
$12.0 \leq \text{LP} < 14.0$ 6	$14.0 \leq \text{LP} < 16.0$ 7	$16.0 \leq \text{LP} < 18.0$ 8	$18.0 \leq \text{LP} < 20.0$ 9	$\text{LP} = 20.0$ 10

$$0.135\text{m} \leq \text{RLP} \leq 0.18\text{m}$$

$\text{RLP} = 0.135\text{m}$ 6	$0.135 < \text{RLP} \leq 0.14\text{m}$ 5	$0.14\text{m} < \text{RLP} \leq 0.15\text{m}$ 4	$0.15\text{m} < \text{RLP} \leq 0.16\text{m}$ 3
$0.16\text{m} < \text{RLP} \leq 0.17\text{m}$ 2	$0.17\text{m} < \text{RLP} < 0.18\text{m}$ 1	$\text{RLP} = 0.18\text{m}$ 0	

Figure 8.6 Categorization of independent variables.

CORRELATION	ANG	VEL	KR	LP	RLP
ULLFTT	0.2738	0.0468	0.1470	0.0458	-0.0403
ULRFTT	-0.4807**	0.5437**	0.2598	0.2498	0.1402
KRFTT	-0.2458	0.2449	0.2152	0.1533	0.3750**
KTLFTT	0.6679**	0.3264*	-0.0299	-0.1535	0.2410
KTRFTT	-0.3139*	0.5881**	0.1249	0.2946*	0.0653
KFLFTT	0.5018**	0.4670**	-0.1849	-0.1727	0.1082
KFRFTT	0.5078**	0.5083**	-0.2116	-0.1255	0.1258
LBLFTT	0.0390	-0.1570	-0.1935	-0.1031	-0.1398
LBRFTT	0.0305	0.3152*	0.2306	-0.0610	-0.0049
LFLFTT	0.4816**	0.4590**	-0.0624	-0.1007	-0.0214
LFRFTT	0.4605**	0.4965**	-0.1078	-0.0965	0.1223
LLFLFTT	0.4659**	0.4149**	0.0006	-0.0782	-0.1160
LLFRFTT	0.4822**	0.4885**	-0.0792	-0.0823	0.0759

Figure 8.7 Correlation coefficients between various forces and the independent variables.

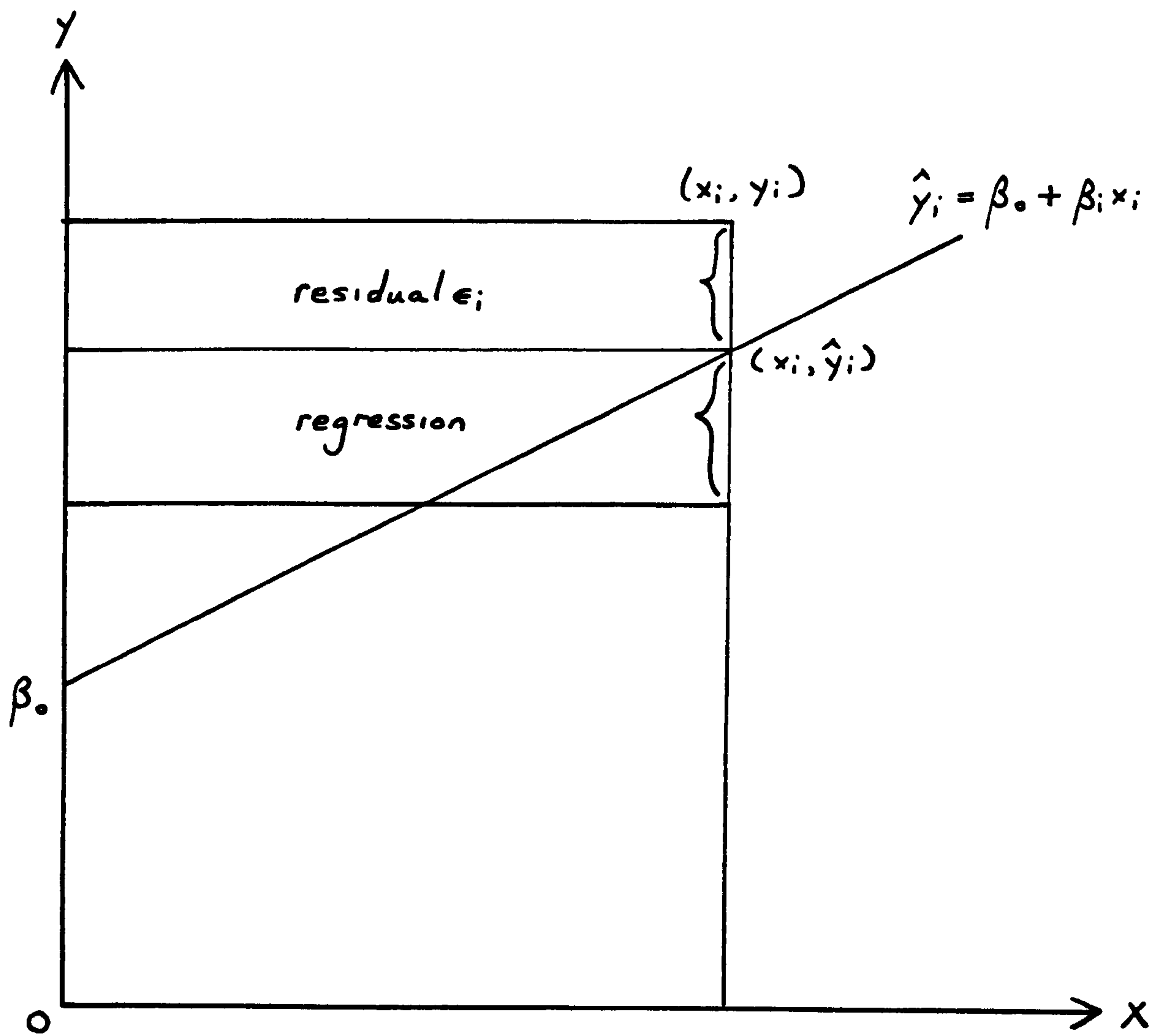


Figure 8.8 Regression by the least square model.

***** MULTIPLE REGRESSION *****

Listwise Deletion of Missing Data

Equation Number 1 Dependent Variable... F

Block Number 1. Method: Stepwise Criteria PIN .0500 POUT .1000
 ANG VEL KR LP RLP

Variable(s) Entered on Step Number
 1... VEL

Multiple R .54370
 R Square .29561
 Adjusted R Square .28123
 Standard Error 2293.16783

Analysis of Variance

	DF	Sum of Squares	Mean Square
Regression	1	108136179.35491	108136179.35491
Residual	49	257672316.92945	5258618.71285

F = 20.56361 Signif F = .0000

----- Variables in the Equation -----

Variable	B	SE B	Beta	T	Sig T
VEL	354.006663	78.065971	.543699	4.535	.0000
(Constant)	-1853.025483	913.113816		-2.029	.0479

Variable(s) Entered on Step Number
 2... ANG

Multiple R .73400
 R Square .53876
 Adjusted R Square .51954
 Standard Error 1874.86914

Analysis of Variance

	DF	Sum of Squares	Mean Square
Regression	2	197082050.98751	98541025.49375
Residual	48	168726445.29685	3515134.27702

F = 28.03336 Signif F = .0000

----- Variables in the Equation -----

Variable	B	SE B	Beta	T	Sig T
VEL	361.278818	63.842261	.554868	5.659	.0000
ANG	-61.660509	12.257874	-.493228	-5.030	.0000
(Constant)	1489.965018	999.498936		1.491	.1426

Variable(s) Entered on Step Number
 3... RLP
 4... KR
 5... LP

Multiple R .73912
 R Square .54629
 Adjusted R Square .49588
 Standard Error 1920.47619

Analysis of Variance

	DF	Sum of Squares	Mean Square
Regression	5	199838200.35952	39967640.07190
Residual	45	165970295.92484	3688228.79833

F = 10.83654 Signif F = .0000

----- Variables in the Equation -----

Variable	B	SE B	Beta	T	Sig T
VEL	344.938993	69.679453	.529773	4.950	.0000
ANG	-59.667498	12.779484	-.477285	-4.669	.0000
RLP	999.983467	21443.66390	.004844	.047	.9630
KR	5944.537898	9546.617823	.067488	.623	.5366
LP	20.004684	51.046954	.042556	.392	.6970
(Constant)	908.698772	3332.304939		.273	.7863

End Block Number 2 All requested variables entered.

Figure 8.9 Multiple regression output with
 dependent variable being ULRFTT.

Text cut off in original

```

      MULTIPLE REGRESSION * * *
Listwise Deletion of Missing Data

Equation Number 1      Dependent Variable..  F

Block Number 1.  Method: Stepwise      Criteria  PIN  .0500  POUT  .1000
      ANG      VEL      KR      LP      RLP

Variable(s) Entered on Step Number
1..      VEL

Multiple R      .50825
R Square      .25832
Adjusted R Square      .24318
Standard Error      2566.33043

Analysis of Variance
      DF      Sum of Squares      Mean Square
Regression      1      112398280.85122      112398280.85122
Residual      49      322716542.60811      6586051.88996

F =      17.06611      Signif F = .0001

----- Variables in the Equation -----
Variable      B      SE B      Beta      T      Sig T
VEL      360.915688      87.365205      .508251      4.131      .0001
(Constant) -2364.463516      1021.884111      -2.314      .0249

Variable(s) Entered on Step Number
2..      ANG

Multiple R      .71047
R Square      .50477
Adjusted R Square      .48413
Standard Error      2118.78270

Analysis of Variance
      DF      Sum of Squares      Mean Square
Regression      2      219631297.21337      109815648.60669
Residual      48      215483526.24596      4489240.13012

F =      24.46197      Signif F = .0000

----- Variables in the Equation -----
Variable      B      SE B      Beta      T      Sig T
VEL      352.930881      72.147904      .497006      4.892      .0000
ANG      67.703087      13.852579      .496562      4.887      .0000
(Constant) -6035.058832      1129.530063      -5.343      .0000

Variable(s) Entered on Step Number
3..      KR

Multiple R      .75477
R Square      .56967
Adjusted R Square      .54221
Standard Error      1995.96110

Analysis of Variance
      DF      Sum of Squares      Mean Square
Regression      3      247873370.69783      82624456.89928
Residual      47      187241452.76150      3983860.69705

F =      20.73980      Signif F = .0000

----- Variables in the Equation -----
Variable      B      SE B      Beta      T      Sig T
VEL      392.742654      69.590992      .553070      5.644      .0000
ANG      62.513996      13.194304      .458503      4.738      .0000
KR      -25307.60236      9505.058297      -.263443      -2.663      .0106
(Constant) -5044.736365      1127.188505      -4.476      .0000

Variable(s) Entered on Step Number
4..      RLP
5..      LP

Multiple R      .76197
R Square      .58060
Adjusted R Square      .53401
Standard Error      2013.75848

Analysis of Variance
      DF      Sum of Squares      Mean Square
Regression      5      252629778.76989      50525955.75398
Residual      45      182485044.68944      4055223.21532

F =      12.45948      Signif F = .0000

----- Variables in the Equation -----
Variable      B      SE B      Beta      T      Sig T
VEL      403.207376      73.063957      .567807      5.519      .0000
ANG      60.852799      13.400215      .446319      4.541      .0000
KR      -22372.84547      10010.32072      -.232893      -2.235      .0304
RLP      3589.856113      22485.23582      .015946      .160      .8739
LP      -57.566370      53.526431      -.112285      -1.075      .2879
(Constant) -5109.289016      3494.163250      -1.462      .1506

End Block Number 2      All requested variables entered.

```

Figure 8.10 Multiple regression output with dependent variable being KFRFTT.

```

* * * * * M U L T I P L E   R E G R E S S I O N   * * * * *

Listwise Deletion of Missing Data

Equation Number 1      Dependent Variable..   F

Block Number  1.  Method:  Stepwise      Criteria  PIN  .0500  POUT  .1000
      ANG      VEL      KR      LP      RLP

Variable(s) Entered on Step Number
1..      VEL

Multiple R          .49648
R Square           .24650
Adjusted R Square   .23112
Standard Error      1545.09396

Analysis of Variance
      DF      Sum of Squares      Mean Square
Regression      1      38267663.72679      38267663.72679
Residual        49      116978452.40874      2387315.35528

F =      16.02958      Signif F = .0002

----- Variables in the Equation -----
Variable          B          SE B          Beta          T      Sig T
VEL          210.592015      52.599404      .496484      4.004      .0002
(Constant) -1676.830980      615.239157      -2.725      .0089

Variable(s) Entered on Step Number
2..      ANG

Multiple R          .66964
R Square           .44842
Adjusted R Square   .42544
Standard Error      1335.65162

Analysis of Variance
      DF      Sum of Squares      Mean Square
Regression      2      69615784.66636      34807892.33318
Residual        48      85630331.46917      1783965.23894

F =      19.51153      Signif F = .0000

----- Variables in the Equation -----
Variable          B          SE B          Beta          T      Sig T
VEL          206.274778      45.481051      .486306      4.535      .0000
ANG          36.605805      8.732476      .449476      4.192      .0001
(Constant) -3661.453896      712.040293      -5.142      .0000

Variable(s) Entered on Step Number
3..      RLP
4..      KR
5..      LP

Multiple R          .69501
R Square           .48304
Adjusted R Square   .42560
Standard Error      1335.46792

Analysis of Variance
      DF      Sum of Squares      Mean Square
Regression      5      74989760.60777      14997952.12155
Residual        45      80256355.52776      1783474.56728

F =      8.40940      Signif F = .0000

----- Variables in the Equation -----
Variable          B          SE B          Beta          T      Sig T
VEL          227.646290      48.453959      .536691      4.698      .0000
ANG          33.743581      8.886645      .414332      3.797      .0004
RLP          1215.204517      14911.57526      .009037      .081      .9354
KR          -7180.038717      6638.562830      -.125128      -1.082      .2852
LP          -35.498848      35.497222      -.115920      -1.000      .3226
(Constant) -3202.344105      2317.230679      -1.382      .1738

End Block Number  2  All requested variables entered.

```

Figure 8.11 Multiple regression output with dependent variable being LFRFTT.

REGRESSION	ANG	VEL	KR	LP	RLP
ULLFTT	0.3049	0.0117	0.1844	0.0323	-0.0713
ULRFTT	-0.4773	0.5298	0.0675	0.0926	0.0048
KRFTT	-0.2356	0.1416	0.1092	0.0207	0.3294
KTLFTT	0.6409	0.2979	0.0295	-0.1549	0.1699
KTRFTT	-0.3166	0.6000	-0.0866	0.1541	-0.0834
KFLFTT	0.4408	0.5301	-0.1794	-0.1688	0.0073
KFRFTT	0.4463	0.5678	-0.2329	-0.1123	0.0159
LBLFTT	0.0185	-0.0970	-0.1536	-0.0190	-0.0973
LBRFTT	0.0298	0.3314	0.2423	-0.2008	-0.0945
LFLFTT	0.4472	0.5211	-0.0536	-0.1214	-0.1387
LFRFTT	0.4143	0.5367	-0.1251	-0.1159	0.0090
LLFLFTT	0.4466	0.4810	0.0233	-0.1063	-0.2335
LLFRFTT	0.4437	0.5303	-0.0897	-0.1030	-0.0414

Figure 8.12 BETA regression coefficients between various forces and the independent variables.

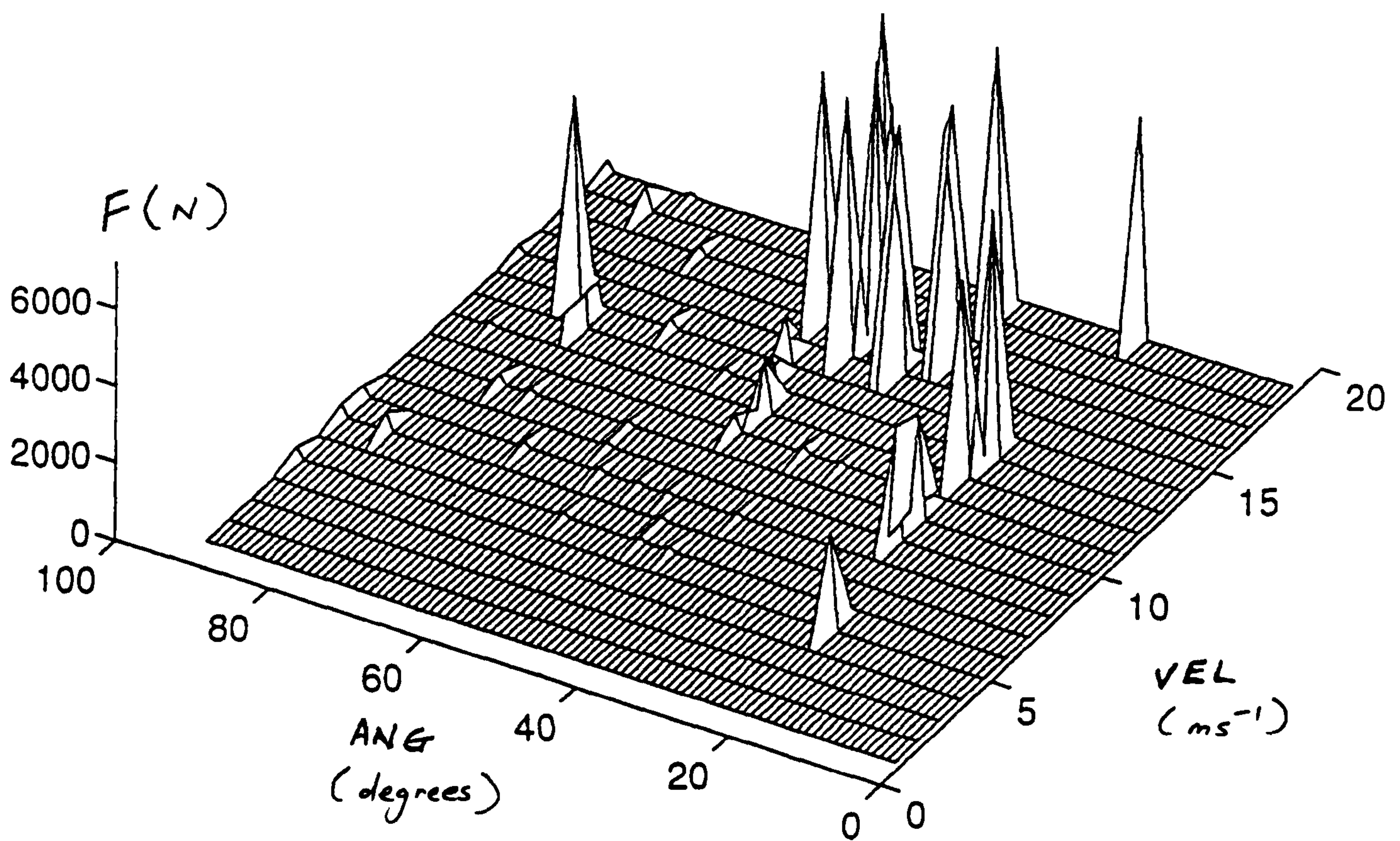


Figure 8.13 A three-dimensional diagram between force F and independent variables ANG and VEL .

PARTIAL CORRELATION	ANG controlled			VEL contrlled		
	KR	LP	RLP	KR	LP	RLP
ULLFTT	0.1945	0.0887	-0.0461	0.1405	0.0364	-0.0536
ULRFTT	0.2218	0.2095	0.1679	0.1777	0.1585	0.0075
KRFTT	0.1884	0.1235	0.3906	0.1728	0.1049	0.3348
KTLFTT	0.0860	-0.0801	0.3108	-0.1064	-0.2447	0.1752
KTRFTT	0.0863	0.2662	0.0736	0.0022	0.2089	-0.1018
KFLFTT	-0.1341	-0.1188	0.1166	-0.3270	-0.3198	-0.0082
KFRFTT	-0.1649	-0.0629	0.1374	-0.3777	-0.2830	0.0005
LBLFTT	-0.1901	-0.0987	-0.1405	-0.1663	-0.0711	-0.1056
LBRFTT	0.2373	-0.0572	-0.0054	0.1774	-0.1411	-0.0899
LFLFTT	0.0056	-0.0376	-0.0324	-0.1825	-0.2332	-0.1563
LFRFTT	-0.0495	-0.0357	0.1303	-0.2496	-0.2435	-0.0002
LLFLFTT	0.0750	-0.0140	-0.1388	-0.0970	-0.1913	-0.2477
LLFRFTT	-0.0137	-0.0163	0.0787	-0.2129	-0.2235	-0.0527

Figure 8.14 Partial correlation coefficients between various forces and three independent variables when either ANG or VEL was controlled.

PARTIAL CORRELATION	with ANG and VEL contrlled		
	KR	LP	RLP
ULLFTT	0.1900	0.0814	-0.0583
ULRFTT	0.1136	0.0879	0.0160
KRFTT	0.1408	0.0691	0.3492
KTLFTT	-0.0044	-0.1976	0.2360
KTRFTT	-0.0637	0.1638	-0.1072
KFLFTT	-0.2979	-0.2875	-0.0160
KFRFTT	-0.3620	-0.2431	-0.0060
LBLFTT	-0.1619	-0.0654	-0.1061
LBRFTT	0.1831	-0.1390	-0.0902
LFLFTT	-0.1242	-0.1832	-0.1902
LFRFTT	-0.2046	-0.1959	-0.0058
LLFLFTT	-0.0267	-0.1356	-0.2917
LLFRFTT	-0.1599	-0.1712	-0.0686

Figure 8.15 Partial correlation coefficients between various forces and three independent variables when both ANG and VEL were controlled.

*** ANALYSIS OF VARIANCE ***

by F
ANG
VEL

Source of Variation	Sum of Squares	DF	Mean Square	F	Sig of F
Main Effects	246050240	10	24605024.009	23.372	.000
ANG	96364392	7	13766341.719	13.077	.000
VEL	132932881	3	44310960.351	42.091	.000
2-Way Interactions	89228756	11	8111705.078	7.705	.000
ANG VEL	89228756	11	8111705.078	7.705	.000
Explained	335278996	21	15965666.474	15.166	.000
Residual	30529500	29	1052741.391		
Total	365808496	50	7316169.926		

51 cases were processed.
0 cases (.0 pct) were missing.

Figure 8.16a ANOVA output for force ULRFTT where independent variables are ANG and VEL.

*** ANALYSIS OF VARIANCE ***

by F
ANG
RLP

Source of Variation	Sum of Squares	DF	Mean Square	F	Sig of F
Main Effects	131202565	13	10092505.009	1.354	.271
ANG	100084313	7	14297758.948	1.919	.126
RLP	18085206	6	3014201.013	.404	.866
2-Way Interactions	100469660	19	5287876.841	.710	.768
ANG RLP	100469660	19	5287876.841	.710	.768
Explained	231672225	32	7239757.034	.972	.543
Residual	134136271	18	7452015.066		
Total	365808496	50	7316169.926		

51 cases were processed.
0 cases (.0 pct) were missing.

Figure 8.16b ANOVA output for force ULRFTT where independent variables are ANG and RLP.

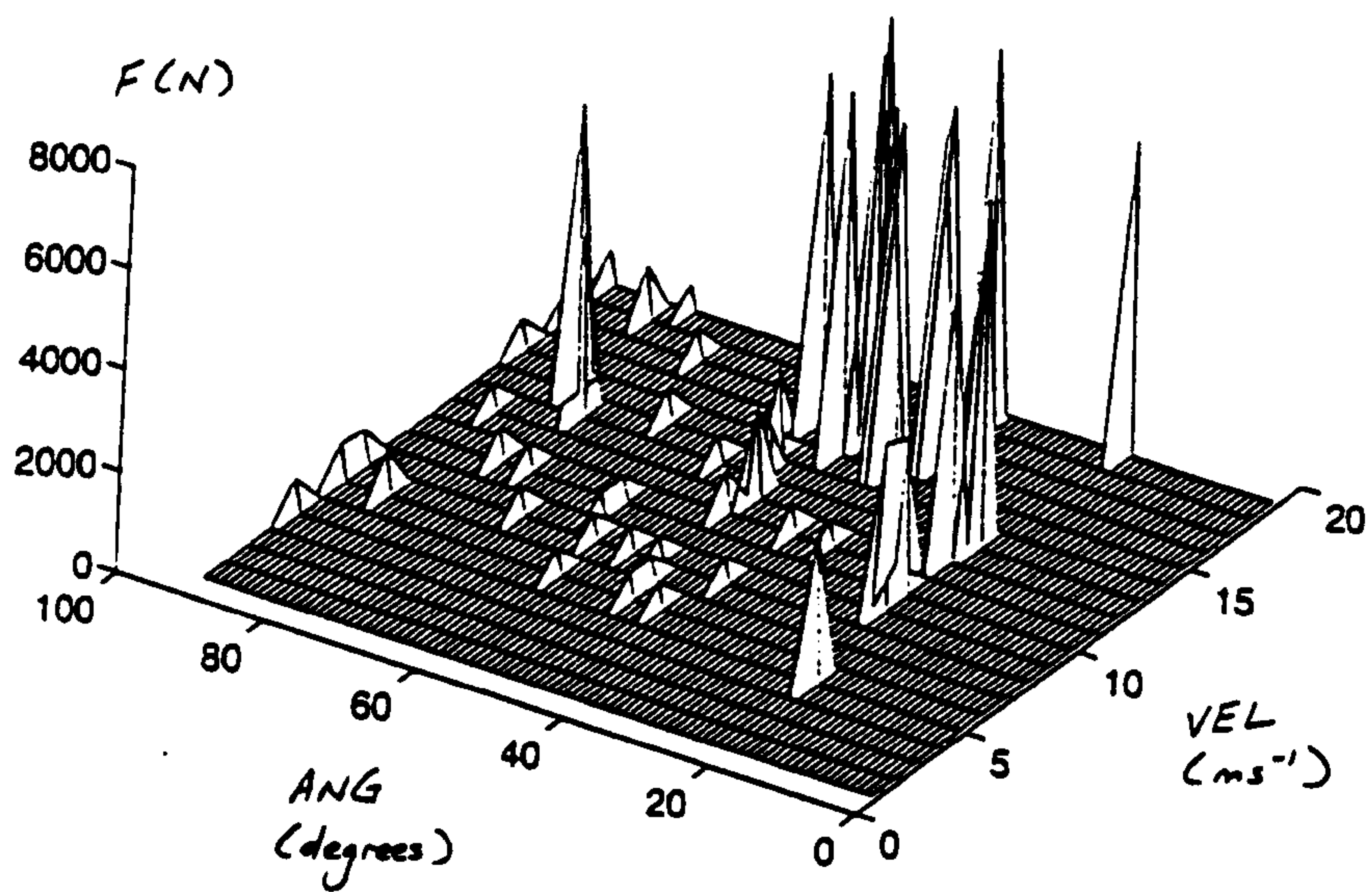


Figure 8.17a A three-dimensional diagram between ULRFTT, ANG and VEL.

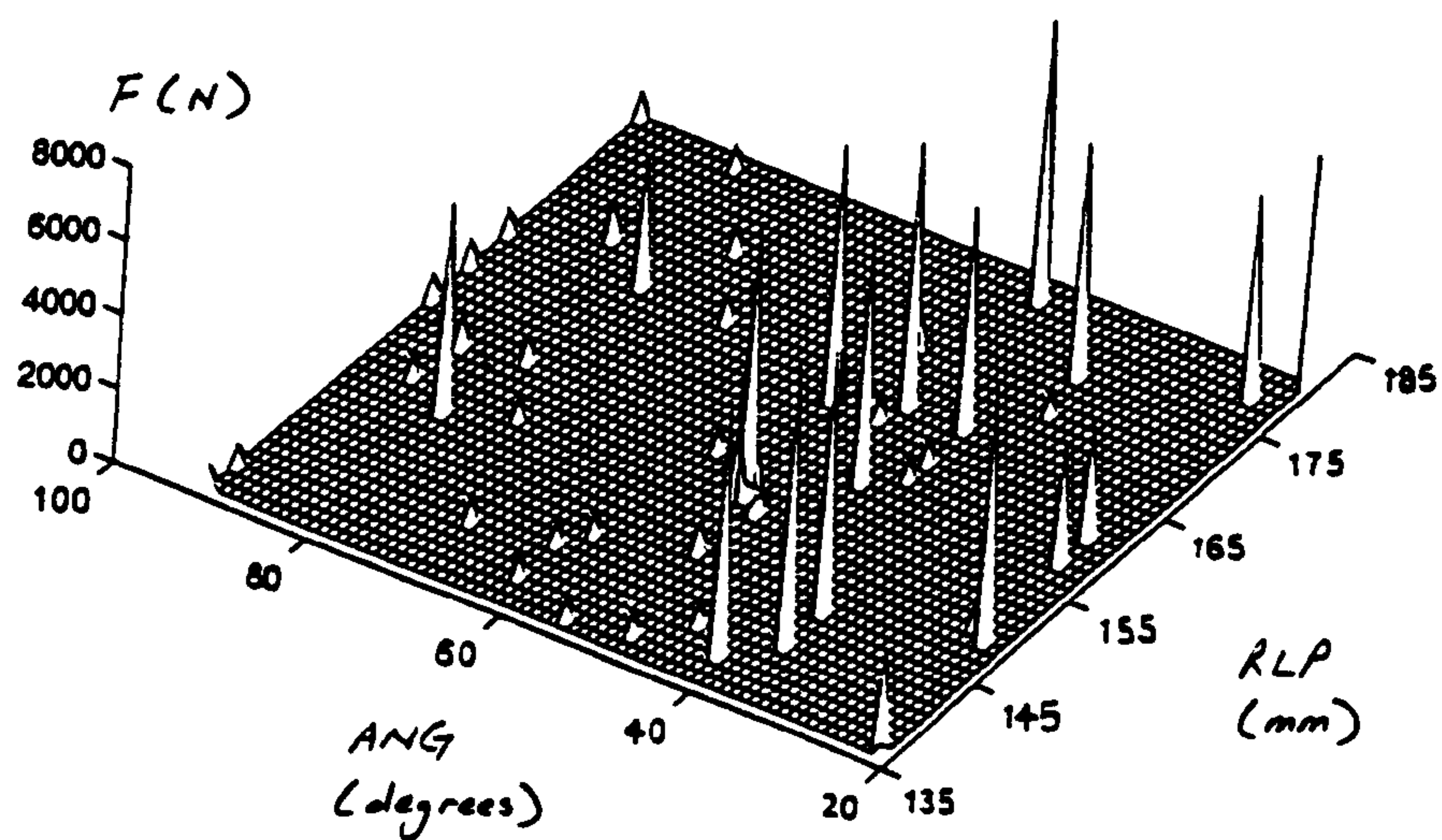


Figure 8.17b A three-dimensional diagram between ULRFTT, ANG and RLP.

*** ANALYSIS OF VARIANCE ***

by F
ANG
VEL

Source of Variation	Sum of Squares	DF	Mean Square	F	Sig of F
Main Effects	224232349	10	22423234.852	6.910	.000
ANG	135705980	7	19386568.538	5.974	.000
VEL	94152801	3	31384267.060	9.671	.000
2-Way Interactions	116770535	11	10615503.180	3.271	.005
ANG VEL	116770535	11	10615503.180	3.271	.005
Explained	341002883	21	16238232.548	5.004	.000
Residual	94111940	29	3245239.309		
Total	435114823	50	8702296.469		

51 cases were processed.
0 cases (.0 pct) were missing.

Figure 8.18a ANOVA output for force KFRFTT where independent variables are ANG and VEL.

*** ANALYSIS OF VARIANCE ***

by F
ANG
RLP

Source of Variation	Sum of Squares	DF	Mean Square	F	Sig of F
Main Effects	184635508	13	14202731.366	3.769	.005
ANG	140251543	7	20035934.741	5.317	.002
RLP	54555960	6	9092660.070	2.413	.069
2-Way Interactions	182652368	19	9613282.540	2.551	.026
ANG RLP	182652368	19	9613282.540	2.551	.026
Explained	367287876	32	11477746.126	3.046	.008
Residual	67826947	18	3768163.746		
Total	435114823	50	8702296.469		

51 cases were processed.
0 cases (.0 pct) were missing.

Figure 8.18b ANOVA output for force KFRFTT where independent variables are ANG and RLP.

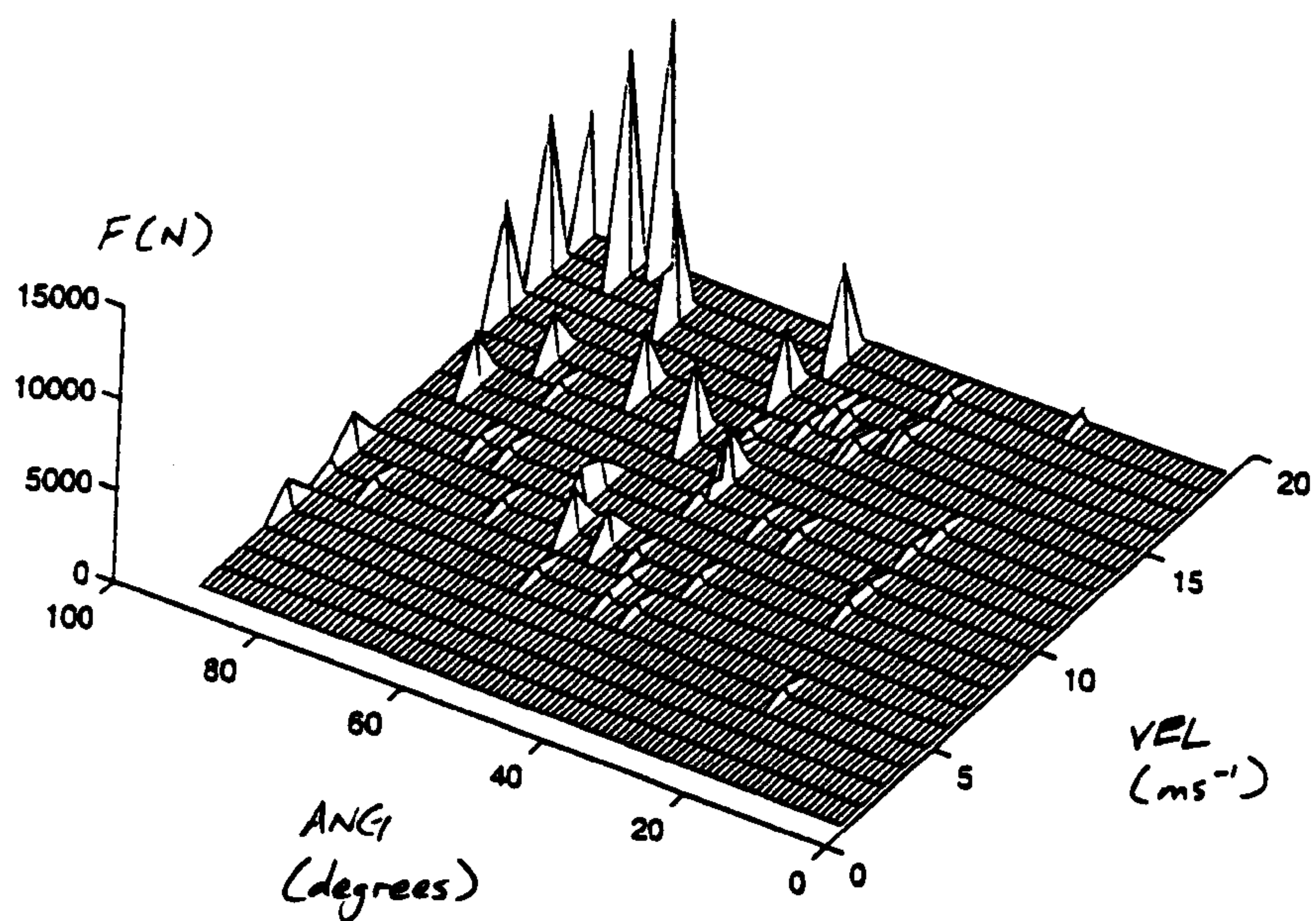


Figure 8.19a A three-dimensional diagram between KFRFTT, ANG and VEL.

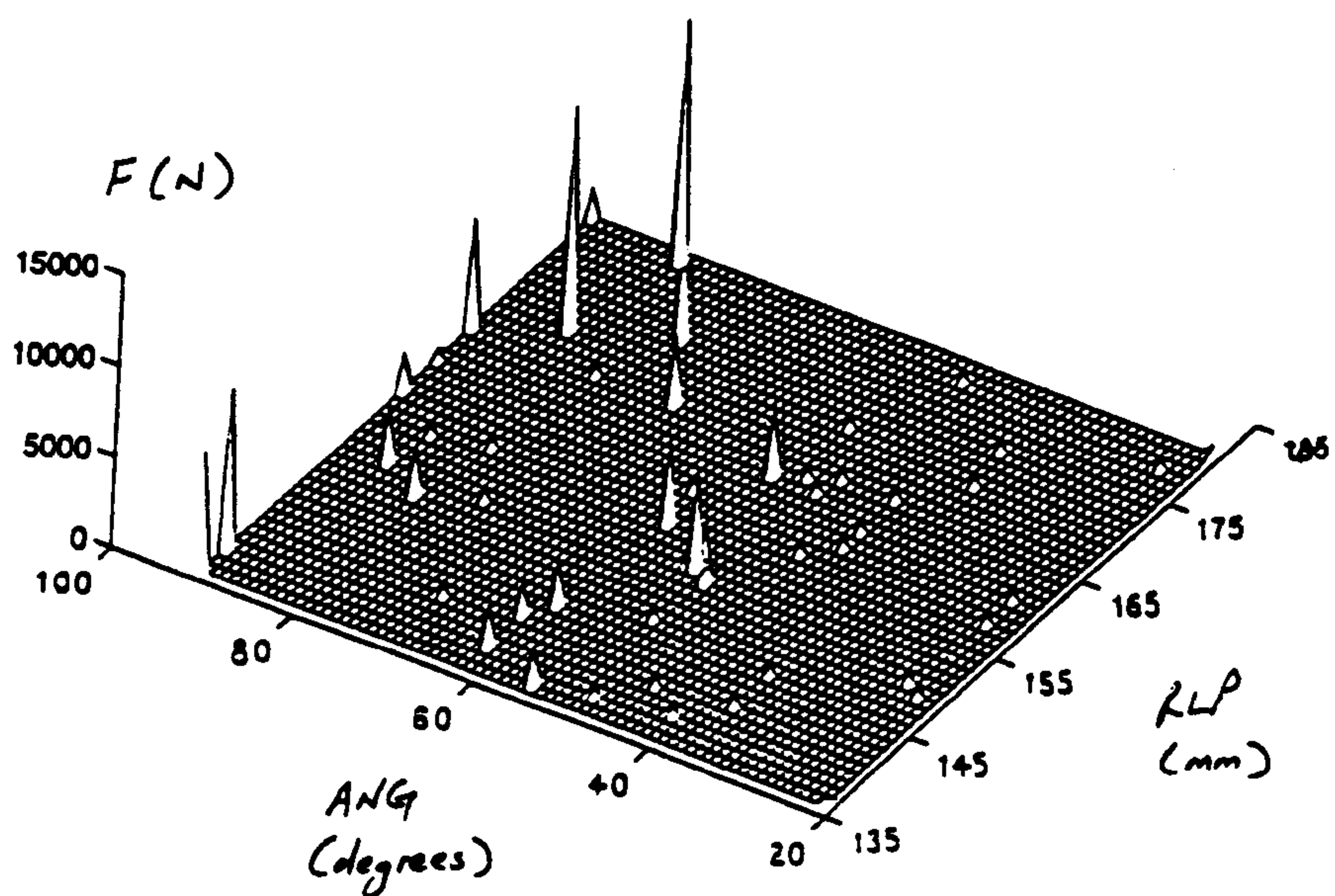


Figure 8.19b A three-dimensional diagram between KFRFTT, ANG and RLP.

*** ANALYSIS OF VARIANCE ***

by F
ANG
VEL

Source of Variation	Sum of Squares	DF	Mean Square	F	Sig of F
Main Effects	75806959	10	7580695.872	6.274	.000
ANG	39762396	7	5680342.277	4.701	.001
VEL	30253010	3	10084336.810	8.346	.000
2-Way Interactions	44398230	11	4036202.728	3.340	.005
ANG VEL	44398230	11	4036202.728	3.340	.005
Explained	120205189	21	5724056.606	4.737	.000
Residual	35040927	29	1208307.842		
Total	155246116	50	3104922.323		

51 cases were processed.
0 cases (.0 pct) were missing.

Figure 8.20a ANOVA output for force LFRFTT where independent variables are ANG and VEL.

*** ANALYSIS OF VARIANCE ***

by F
ANG
RLP

Source of Variation	Sum of Squares	DF	Mean Square	F	Sig of F
Main Effects	70523211	13	5424862.410	7.594	.000
ANG	44957129	7	6422446.980	8.991	.000
RLP	24969263	6	4161543.840	5.826	.002
2-Way Interactions	71864491	19	3782341.610	5.295	.000
ANG RLP	71864491	19	3782341.610	5.295	.000
Explained	142387702	32	4449615.685	6.229	.000
Residual	12858414	18	714356.345		
Total	155246116	50	3104922.323		

51 cases were processed.
0 cases (.0 pct) were missing.

Figure 8.20b ANOVA output for force LFRFTT where independent variables are ANG and RLP.

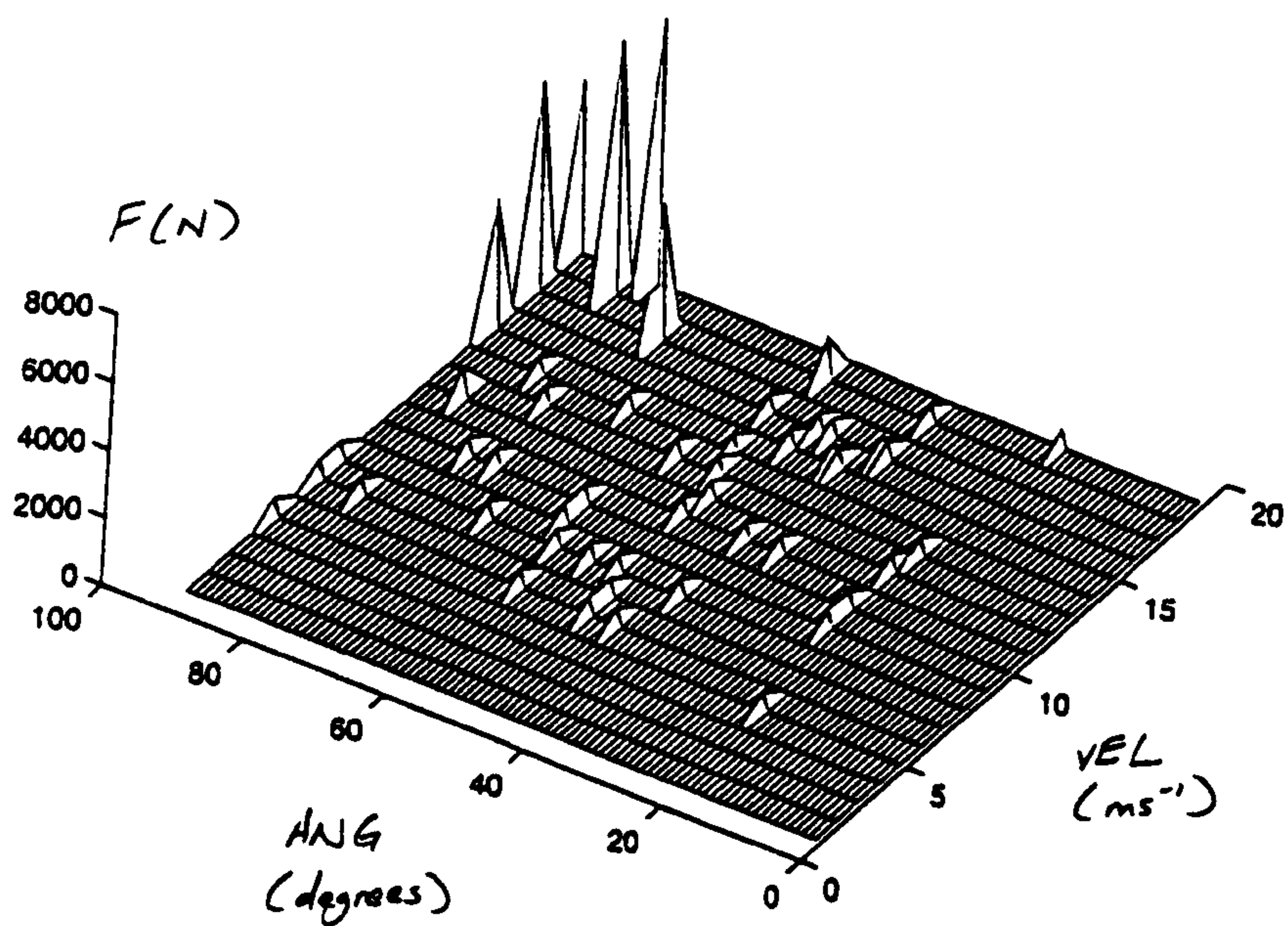


Figure 8.21a A three-dimensional diagram between LFRFTT, ANG and VEL.

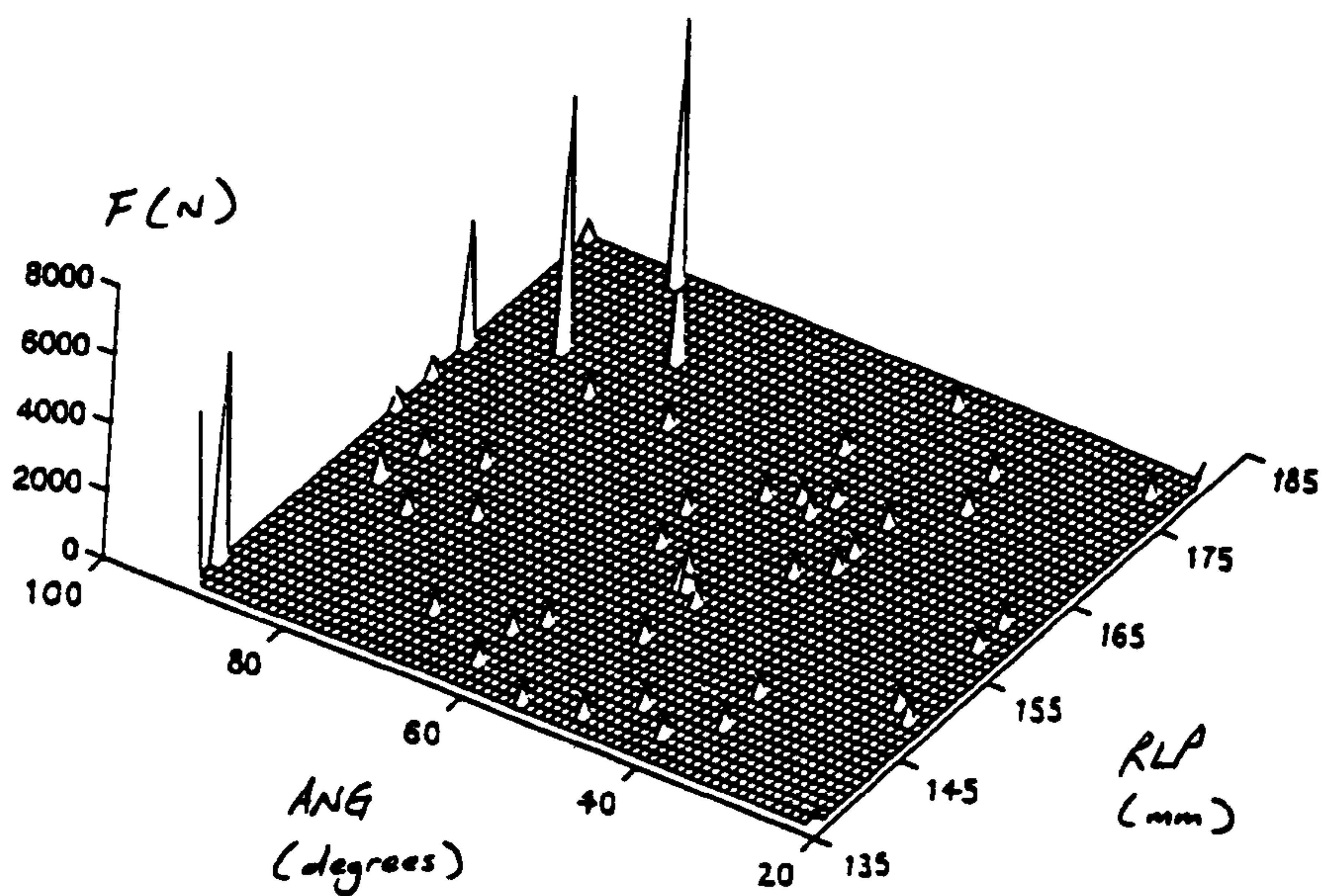


Figure 8.21b A three-dimensional diagram between LFRFTT, ANG and RLP.

***** ANALYSIS OF VARIANCE -- DESIGN 1*****

Multivariate Tests of Significance (S = 3, M = 3 1/2, N = 12 1/2)

Test Name	Value	Approx. F	Hypoth. DF	Error DF	Sig. of F
Pillais	1.42249	2.37730	33.00	87.00	.001
Hotellings	4.42008	3.43784	33.00	77.00	.000
Wilks	.10064	2.86990	33.00	80.25	.000
Roys	.76905				

EFFECT .. ANG BY VEL (Cont.)
Univariate F-tests with (11,29) D. F.

Variable	Hypoth. SS	Error SS	Hypoth. MS	Error MS	F	Sig. of F
F1	89228755.9	30529500.3	8111705.08	1052741.39	7.70532	.000
F2	10066963.8	33624566.0	915178.529	1159467.79	.78931	.649
F3	27396266.2	34993243.8	2490569.66	1206663.58	2.06401	.058

Multivariate Tests of Significance (S = 3, M = -1/2, N = 12 1/2)

Test Name	Value	Approx. F	Hypoth. DF	Error DF	Sig. of F
Pillais	1.15369	6.04038	9.00	87.00	.000
Hotellings	3.57549	10.19678	9.00	77.00	.000
Wilks	.15207	8.54840	9.00	65.86	.000
Roys	.74277				

EFFECT .. VEL (Cont.)
Univariate F-tests with (3,29) D. F.

Variable	Hypoth. SS	Error SS	Hypoth. MS	Error MS	F	Sig. of F
F1	85976043.5	30529500.3	28658681.2	1052741.39	27.22291	.000
F2	2243333.17	33624566.0	747777.723	1159467.79	.64493	.592
F3	39136794.9	34993243.8	13045598.3	1206663.58	10.81130	.000

Multivariate Tests of Significance (S = 3, M = 1 1/2, N = 12 1/2)

Test Name	Value	Approx. F	Hypoth. DF	Error DF	Sig. of F
Pillais	1.16295	2.62263	21.00	87.00	.001
Hotellings	4.18045	5.10944	21.00	77.00	.000
Wilks	.13961	3.66276	21.00	78.08	.000
Roys	.78765				

EFFECT .. ANG (Cont.)
Univariate F-tests with (7,29) D. F.

Variable	Hypoth. SS	Error SS	Hypoth. MS	Error MS	F	Sig. of F
F1	110217820	30529500.3	15745402.8	1052741.39	14.95657	.000
F2	6307181.79	33624566.0	901025.971	1159467.79	.77710	.611
F3	21330750.3	34993243.8	3047250.04	1206663.58	2.52535	.037

Figure 8.22a MANOVA output for forces ULRFTT, KRFTT and KTRFTT where independent variables are ANG and VEL.

***** ANALYSIS OF VARIANCE -- DESIGN 1*****

Multivariate Tests of Significance (S = 3, M = 6 1/2, N = 5 1/2)

Test Name	Value	Approx. F	Hypoth. DF	Error DF	Sig. of F
Pillais	1.95122	1.64158	51.00	45.00	.046
Hotellings	8.20149	1.87616	51.00	35.00	.026
Wilks	.02870	1.77855	51.00	39.51	.031
Roys	.83980				

EFFECT .. KR BY LP (Cont.)
Univariate F-tests with (17,15) D. F.

Variable	Hypoth. SS	Error SS	Hypoth. MS	Error MS	F	Sig. of F
F1	167370923	72486100.6	9845348.39	4832406.70	2.03736	.086
F2	28459938.7	9231099.99	1674114.04	615406.666	2.72034	.029
F3	74309051.5	98128919.3	4371120.68	6541927.96	.66817	.789

Multivariate Tests of Significance (S = 3, M = 2 , N = 5 1/2)

Test Name	Value	Approx. F	Hypoth. DF	Error DF	Sig. of F
Pillais	1.53992	1.97752	24.00	45.00	.024
Hotellings	4.39251	2.13525	24.00	35.00	.020
Wilks	.08614	2.12084	24.00	38.31	.018
Roys	.71284				

EFFECT .. LP (Cont.)
Univariate F-tests with (8,15) D. F.

Variable	Hypoth. SS	Error SS	Hypoth. MS	Error MS	F	Sig. of F
F1	114031836	72486100.6	14253979.5	4832406.70	2.94966	.034
F2	17568251.8	9231099.99	2196031.47	615406.666	3.56842	.016
F3	34471945.0	98128919.3	4308993.13	6541927.96	.65867	.719

Multivariate Tests of Significance (S = 3, M = 3 , N = 5 1/2)

Test Name	Value	Approx. F	Hypoth. DF	Error DF	Sig. of F
Pillais	1.55563	1.61554	30.00	45.00	.071
Hotellings	4.69077	1.82419	30.00	35.00	.044
Wilks	.08009	1.76496	30.00	38.83	.048
Roys	.73985				

EFFECT .. KR (Cont.)
Univariate F-tests with (10,15) D. F.

Variable	Hypoth. SS	Error SS	Hypoth. MS	Error MS	F	Sig. of F
F1	87872931.9	72486100.6	8787293.19	4832406.70	1.81841	.143
F2	20722901.5	9231099.99	2072290.15	615406.666	3.36735	.017
F3	24909178.1	98128919.3	2490917.81	6541927.96	.38076	.936

Figure 8.22b MANOVA output for forces ULRFTT, KRFTT and KTRFTT where independent variables are KR and LP.

***** ANALYSIS OF VARIANCE -- DESIGN 1*****

Multivariate Tests of Significance (S = 3, M = 3 1/2, N = 12 1/2)

Test Name	Value	Approx. F	Hypoth. DF	Error DF	Sig. of F
Pillais	1.67452	3.33060	33.00	87.00	.000
Hotellings	8.25585	6.42121	33.00	77.00	.000
Wilks	.04350	4.61610	33.00	80.25	.000
Roys	.86974				

EFFECT .. ANG BY VEL (Cont.)
Univariate F-tests with (11,29) D. F.

Variable	Hypoth. SS	Error SS	Hypoth. MS	Error MS	F	Sig. of F
F1	116770535	94111940.0	10615503.2	3245239.31	3.27110	.005
F2	44398230.0	35040927.4	4036202.73	1208307.84	3.34038	.005
F3	40769107.3	28187660.2	3706282.48	971988.282	3.81309	.002

Multivariate Tests of Significance (S = 3, M = -1/2, N = 12 1/2)

Test Name	Value	Approx. F	Hypoth. DF	Error DF	Sig. of F
Pillais	.71463	3.02275	9.00	87.00	.003
Hotellings	1.42895	4.07516	9.00	77.00	.000
Wilks	.37514	3.63044	9.00	65.86	.001
Roys	.55399				

EFFECT .. VEL (Cont.)
Univariate F-tests with (3,29) D. F.

Variable	Hypoth. SS	Error SS	Hypoth. MS	Error MS	F	Sig. of F
F1	109432109	94111940.0	36477369.7	3245239.31	11.24027	.000
F2	27789184.6	35040927.4	9263061.53	1208307.84	7.66614	.001
F3	21182671.8	28187660.2	7060890.61	971988.282	7.26438	.001

Multivariate Tests of Significance (S = 3, M = 1 1/2, N = 12 1/2)

Test Name	Value	Approx. F	Hypoth. DF	Error DF	Sig. of F
Pillais	1.92948	7.46697	21.00	87.00	.000
Hotellings	7.24983	8.86090	21.00	77.00	.000
Wilks	.03345	8.42212	21.00	78.08	.000
Roys	.80772				

EFFECT .. ANG (Cont.)
Univariate F-tests with (7,29) D. F.

Variable	Hypoth. SS	Error SS	Hypoth. MS	Error MS	F	Sig. of F
F1	222525167	94111940.0	31789309.5	3245239.31	9.79567	.000
F2	62823912.7	35040927.4	8974844.67	1208307.84	7.42761	.000
F3	49392296.5	28187660.2	7056042.36	971988.282	7.25939	.000

Figure 8.23a MANOVA output for forces KFRFTT, LFRFTT and LLFRFTTT where independent variables are ANG and VEL.

***** ANALYSIS OF VARIANCE -- DESIGN 1*****

Multivariate Tests of Significance (S = 3, M = 7 1/2, N = 5)

Test Name	Value	Approx. F	Hypoth. DF	Error DF	Sig. of F
Pillais	1.98554	1.44217	57.00	42.00	.108
Hotellings	193.93498	36.29193	57.00	32.00	.000
Wilks	.00128	5.34845	57.00	36.61	.000
Roys	.99481				

EFFECT .. ANG BY KR (Cont.)

Univariate F-tests with (19,14) D. F.

Variable	Hypoth. SS	Error SS	Hypoth. MS	Error MS	F	Sig. of F
F1	151628927	97389263.0	7980469.86	6956375.93	1.14722	.403
F2	57908362.7	29575657.4	3047808.56	2112546.96	1.44272	.245
F3	52424014.7	21501583.1	2759158.67	1535827.36	1.79653	.134

Multivariate Tests of Significance (S = 3, M = 3 , N = 5)

Test Name	Value	Approx. F	Hypoth. DF	Error DF	Sig. of F
Pillais	2.02977	2.92887	30.00	42.00	.001
Hotellings	25.10607	8.92660	30.00	32.00	.000
Wilks	.00880	4.80501	30.00	35.90	.000
Roys	.95771				

EFFECT .. KR (Cont.)

Univariate F-tests with (10,14) D. F.

Variable	Hypoth. SS	Error SS	Hypoth. MS	Error MS	F	Sig. of F
F1	140001099	97389263.0	14000109.9	6956375.93	2.01256	.112
F2	50601657.1	29575657.4	5060165.71	2112546.96	2.39529	.066
F3	38302385.2	21501583.1	3830238.52	1535827.36	2.49393	.058

Multivariate Tests of Significance (S = 3, M = 1 1/2, N = 5)

Test Name	Value	Approx. F	Hypoth. DF	Error DF	Sig. of F
Pillais	1.68311	2.55618	21.00	42.00	.005
Hotellings	36.83433	18.70950	21.00	32.00	.000
Wilks	.00968	6.71451	21.00	35.01	.000
Roys	.97234				

EFFECT .. ANG (Cont.)

Univariate F-tests with (7,14) D. F.

Variable	Hypoth. SS	Error SS	Hypoth. MS	Error MS	F	Sig. of F
F1	121227195	97389263.0	17318170.7	6956375.93	2.48954	.069
F2	45616398.1	29575657.4	6516628.31	2112546.96	3.08473	.035
F3	33426371.0	21501583.1	4775195.86	1535827.36	3.10920	.034

Figure 8.23b MANOVA output for forces KFRFTT, LFRFTT and LLFRFTT where independent variables are ANG and KR.

***** ANALYSIS OF VARIANCE -- DESIGN 1*****

Multivariate Tests of Significance (S = 3, M = 7 1/2, N = 7)

Test Name	Value	Approx. F	Hypoth. DF	Error DF	Sig. of F
Pillais	1.74007	1.30840	57.00	54.00	.161
Hotellings	10.99971	2.83033	57.00	44.00	.000
Wilks	.02946	1.92541	57.00	48.53	.010
Roys	.90096				

EFFECT .. ANG BY RLP (Cont.)
Univariate F-tests with (19,18) D. F.

Variable	Hypoth. SS	Error SS	Hypoth. MS	Error MS	F	Sig. of F
F1	182652368	67826947.4	9613282.54	3768163.75	2.55118	.026
F2	71864490.6	12858414.2	3782341.61	714356.345	5.29475	.000
F3	59021394.0	13266761.1	3106389.16	737042.282	4.21467	.002

Multivariate Tests of Significance (S = 3, M = 1 , N = 7)

Test Name	Value	Approx. F	Hypoth. DF	Error DF	Sig. of F
Pillais	1.22637	2.07434	18.00	54.00	.020
Hotellings	9.73061	7.92865	18.00	44.00	.000
Wilks	.06737	4.05411	18.00	45.74	.000
Roys	.90309				

EFFECT .. RLP (Cont.)
Univariate F-tests with (6,18) D. F.

Variable	Hypoth. SS	Error SS	Hypoth. MS	Error MS	F	Sig. of F
F1	175084100	67826947.4	29180683.3	3768163.75	7.74401	.000
F2	64855542.4	12858414.2	10809257.1	714356.345	15.13146	.000
F3	48357843.6	13266761.1	8059640.60	737042.282	10.93511	.000

Multivariate Tests of Significance (S = 3, M = 1 1/2, N = 7)

Test Name	Value	Approx. F	Hypoth. DF	Error DF	Sig. of F
Pillais	1.16782	1.63902	21.00	54.00	.074
Hotellings	8.81640	6.15749	21.00	44.00	.000
Wilks	.07785	3.17251	21.00	46.49	.001
Roys	.89447				

EFFECT .. ANG (Cont.)
Univariate F-tests with (7,18) D. F.

Variable	Hypoth. SS	Error SS	Hypoth. MS	Error MS	F	Sig. of F
F1	226809037	67826947.4	32401291.0	3768163.75	8.59870	.000
F2	78359291.9	12858414.2	11194184.6	714356.345	15.67031	.000
F3	64408399.3	13266761.1	9201199.90	737042.282	12.48395	.000

Figure 8.23c MANOVA output for forces KFRFTT, LFRFTT and LLFRFTT where independent variables are ANG and RLP.

***** ANALYSIS OF VARIANCE -- DESIGN 1*****

Multivariate Tests of Significance (S = 3, M = 1 1/2, N = 15)

Test Name	Value	Approx. F	Hypoth. DF	Error DF	Sig. of F
Pillais	.72936	1.56017	21.00	102.00	.074
Hotellings	1.22417	1.78768	21.00	92.00	.031
Wilks	.39593	1.67621	21.00	92.44	.049
Roys	.48307				

EFFECT .. VEL BY RLP (Cont.)
Univariate F-tests with (7,34) D. F.

Variable	Hypoth. SS	Error SS	Hypoth. MS	Error MS	F	Sig. of F
F1	42550420.9	283024777	6078631.56	8324258.14	.73023	.648
F2	16130735.6	89974679.4	2304390.80	2646314.10	.87079	.539
F3	18374465.7	73924326.1	2624923.68	2174244.88	1.20728	.326

Multivariate Tests of Significance (S = 3, M = 1 , N = 15)

Test Name	Value	Approx. F	Hypoth. DF	Error DF	Sig. of F
Pillais	.70296	1.73416	18.00	102.00	.045
Hotellings	1.11243	1.89525	18.00	92.00	.026
Wilks	.41831	1.82435	18.00	90.99	.034
Roys	.44339				

EFFECT .. RLP (Cont.)
Univariate F-tests with (6,34) D. F.

Variable	Hypoth. SS	Error SS	Hypoth. MS	Error MS	F	Sig. of F
F1	36909161.9	283024777	6151526.99	8324258.14	.73899	.622
F2	20929616.7	89974679.4	3488269.46	2646314.10	1.31816	.276
F3	19836303.0	73924326.1	3306050.49	2174244.88	1.52055	.201

Multivariate Tests of Significance (S = 3, M = -1/2, N = 15)

Test Name	Value	Approx. F	Hypoth. DF	Error DF	Sig. of F
Pillais	.32935	1.39766	9.00	102.00	.199
Hotellings	.43368	1.47773	9.00	92.00	.168
Wilks	.68648	1.44923	9.00	78.03	.182
Roys	.27123				

EFFECT .. VEL (Cont.)
Univariate F-tests with (3,34) D. F.

Variable	Hypoth. SS	Error SS	Hypoth. MS	Error MS	F	Sig. of F
F1	56389486.8	283024777	18796495.6	8324258.14	2.25804	.099
F2	23438730.0	89974679.4	7812910.00	2646314.10	2.95237	.046
F3	21872019.5	73924326.1	7290673.18	2174244.88	3.35320	.030

Figure 8.23d MANOVA output for forces KFRFTT, LFRFTT and LLFRFTT where independent variables are VEL and RLP.

CHAPTER 9

ANALYSIS OF SPECIFIC FEATURES

9.0 Introduction

It was decided, after the parametric study has been completed, that some specific features relevant to safety, should be examined in depth. These factors are applicable to both the dummy rider and the motorcycle, and their influence to the overall performance was examined against simulations selected from the 51 runs used in the parametric study.

After careful consideration, three simulations were selected as those to be taken as datum on which then certain variations would be made, and they are :

- (i) barrier angle = 46.8° ,
initial velocity = 13.7ms^{-1} ,
knee to knee-restraint distance = 0.07m,
stiffness factor of leg protector = 15.7,
radius of leg protector = 0.165m.
- (ii) barrier angle = 20.0° ,
initial velocity = 4.4ms^{-1} ,
knee to knee-restraint distance = 0.0m,

stiffness factor of leg protector = 2.0,
radius of leg protector = 0.135m.

(iii) barrier angle = 90.0° ,
initial velocity = 15.9ms^{-1} ,
knee to knee-restraint distance = 0.02m,
stiffness factor of leg protector = 4.7,
radius of leg protector = 0.138m.

These three simulation runs were chosen mainly due to their representative nature over the range of the barrier angle. However, the other factors are also generally randomised within their limited ranges such that no bias is introduced into this study.

Recall that all the 51 runs are simulations with leg protection characteristics attached to the motorcycle, and the dummy rider is a 50th percentile OPAT male seated 70° relative to the horizontal axis. The factors we are interested in examining are the variations of the above with the addition of extra safety features. Below is a list of these factors.

- I. (a) Simulations (i), (ii) and (iii) with no leg protection attached,
- (b) Simulations (i), (ii) and (iii) of a small sized female,
- and

(c) Simulations (i), (ii) and (iii) of a large sized male.

II.(a) Simulation (iii) where the dummy is seated in two attitude positions,

(b) Simulation (iii) with the addition of an airbag of three different stiffnesses, and

(c) Simulation (iii) with addition of an airbag situated on three different positions.

The list is divided into two parts since part I are the named simulations to be compared against the datum runs (i), (ii) and (iii). Part II are the named simulations to be compared against the datum run (iii). In addition, there will be one datum run in sets II(b) and II(c) where the airbag is given a particular stiffness and situated on a specified position, thus between these two sets there will be five simulation runs. Table 9.1 categorises these runs. At the beginning of the description of each run, a figure shows plan and elevation, the movement of the system.

9.1 The Datum Simulations

Before we proceed with the comparisons we shall give a brief description on the performance on each of the datum runs.

9.1.1 Run 1 (Figure 9.1)

At 50ms into impact, the dummy's head is seen to have dipped very slightly. At 60ms, the motorcycle had started to roll but the dummy is still, apparently, going forwards towards the barrier. At 70ms, the top half body of the dummy had started to yaw anti-clockwise while the motorcycle yawed in a clockwise direction, causing the offside leg to spread outwards. At 100ms, the dummy's head had hit fully against the barrier, and in the meantime, the motorcycle is nearly parallel to the barrier. From then on, the motorcycle continued yawing in a clockwise direction, and also rolling towards the ground, while the dummy is rebounding from the barrier. The simulation finished 130ms after impact.

For the forces, the dummy's head had hit the barrier edge, 2,429N, then the barrier top, 6,359N, the offside thigh against the side of the petrol tank, 6,628N, the offside knee against the tank, 8,036N, and the offside lower leg against the engine, 31N.

9.1.2 Run 2 (Figure 9.2)

In this run, the front wheel did not hit the barrier. However, the leg protector had hit the barrier and hence steered the motorcycle away from the barrier. This is the result of the combination of the oblique barrier angle and the size of the leg

protector. Since the initial velocity is slow, the motorcycle is seen not to have yawed as much as it rolled, and throughout the simulation the dummy continued diving down towards the barrier. However, the dummy had yawed anti-clockwise while the offside leg extended outwards as the motorcycle rolled towards the ground.

This is a quite a mild impact and the dummy's head did not hit the barrier. For forces, the offside thigh had hit the side of petrol tank, 2,415N, the offside knee against the tank, 1,706N, and the nearside knee against the knee-restraint, 245N.

9.1.3 Run 3 (Figure 9.3)

Up until 50ms into the impact, the front wheel was being crushed between the barrier and the motorcycle frame, causing the front forks to bend backwards. During this time the dummy was still travelling forwards such that its legs were fully impacted onto the knee-restraints. From then on, the dummy started to pitch towards the barrier. The front wheel also pitched but also started to rebound. This continued up to 100ms into the impact when the dummy's head contacted the vertical face of the barrier and such was the force generated by this contact, the dummy was thrown backwards with high acceleration.

This highlighted two potential problems. Firstly, the simulated

compliant cylinder along the top edge of the barrier, which is used for the prevention of discontinuity in the modelling, is not sufficient to eject the head away from the barrier. Thus, providing the head is simulated to have compressed by a significant amount by the vertical face of the barrier, an enormous force is generated. This led to the second problem. Because of the severity of the force, the dummy is thrown, theoretically, 'through' the motorcycle, since no contact was provided in the model for such an eventuality.

However, there are solutions to these problems. Firstly, different material characteristics can be tried in the simulation model for the compliant cylinder in order to achieve satisfactory results. Secondly, more contacts can be added between the dummy and various parts of the motorcycle, even though it may be unlikely for these contacts to occur in real-life. This of course will result in long program coding and consume large amount of CPU time. These solutions, however, are beyond the scope of this research but can be incorporated in the model in future work.

Even though the potential problems have emerged, it must be emphasized that events prior to the discontinuity are still valid. Indeed it was agreed, for data analysis purpose, that events leading up to when the head is at a 0.35m distance parallel to the barrier will be sufficient.

Thus for the forces on the other parts of the dummy rider, the dummy's lower legs including the knees, have all hit the knee-restraints. In addition, the knees have also hit the sides of the petrol tank. These forces range from 3kN to 8kN.

9.2 Simulations With Minimal Outer Fairing

These are the repeats of the three runs (i), (ii) and (iii) but with the stiffness factor of the outer fairing reset to 1.0, i.e. the outer fairing having such a minute stiffness to represent the case of effectively no outer fairing. Also, the profile of the outer fairing is set to its minimum such that its radius is 0.18m, this represents the minimal shape such that there is no absorber inside the fairing. The knee restraint was retained in its original position and at its original stiffness. Simulating the bare motorcycle with no leg protection would have involved extensive remodelling and results could not be guaranteed to be compatible to those with leg protecting fairings. Removing the knee restraints would have produced loading conditions which have not been calibrated against tests. It was decided that it was not feasible to simulate a bare motorcycle within the time available and a minimal outer fairing was the nearest that could be achieved. The following are their comparisons.

9.2.1 Run 4 (Figure 9.4)

The motions of both the dummy rider and the motorcycle are very similar to those of the datum run. On closer inspection, the motorcycle in the datum run is seen to have greater yaw and roll motions. In the same case, the offside thigh of the dummy is seen to have penetrated further into the side of the tank. This is due to the rolling effect of the motorcycle. In addition, the dummy's yaw motion is also greater in the datum run than that of the minimal outer fairing. The yaw direction is anti-clockwise.

For the forces the two runs also share the same impacts. The peak forces are all very similar with the exception that the offside thigh force, in the simulation with the leg protector, is about twice that in the simulation with minimal outer fairing. This can be explained by the rolling effect of the motorcycle as mentioned above.

9.2.2 Run 5 (Figure 9.5)

In this simulation the front wheel also did not hit the barrier but the knee-restraint is seen to have penetrated into the barrier. The motorcycle yaw and roll motions are less than those in the datum run. For the dummy, the offside thigh did not spread as far outwards as the dummy in the datum run, and the whole body

did not travel as far forwards along the petrol tank as in the datum run. This is due to the motorcycle yaw and roll motions being greater in the simulation in the datum run thus bringing the dummy with it.

For forces the offside thigh in this run is 1,168N, comparing to 2,414N in the datum run. The force between the offside knee and the petrol tank, is similar to the datum run, but unlike the datum run, the head had hit the barrier edge, though mildly at 844N.

9.2.3 Run 6 (Figure 9.6)

Up to 50ms into the impact, events have been very similar to those in the datum run. By this time, the legs have fully impacted onto the knee-restraints. At 60ms into impact, the legs have started to rebound. However, it can be seen that the rebound rate in the simulation with the minimal outer fairing is not as high as that in the datum run. This caused the pivot point, the pelvis, not to pitch as high and not travel as far backwards relative to the barrier as was the case in the datum run. Subsequently, as the pitching motion continued, the head is projected on target towards the barrier edge and barrier top. As the head hit it then rebounded, causing the dummy to be thrown upwards.

It is an interesting observation that the head had started to rebound at around 100ms into impact. This is the time that the discontinuity happened in the datum run. This demonstrates the extreme sensitivity of mathematical modelling such that only a slight difference between two very similar simulations can produce immense difference in the overall performance.

However, the initial trigger which contributed to this result can be explained. Similar to the simulation with leg protection, the dummy's legs have hit fully onto the knee-restraints. Somehow these forces are somewhat less than those suffered in the datum run. For example, the knee to knee-restraint force is 4,914N, comparing to 8,189N in its counterpart. This led to the less severe rebound on the legs and less pitching action on the pelvis. The head then subsequently hit the barrier edge with peak a force 18,013N, and the barrier top, 18,923N.

To demonstrate the relative differences in performance between the datum runs and a motorcycle with minimal outer fairing, the contact forces and head's velocities are bar charted in Figures 9.7 to 9.12. Note that the head's velocities are taken when the head is at a 0.35m distance parallel to the barrier.

For comparison between Run 1 and Run 4, which are shown in Figures 9.7 and 9.8, the only visual difference is the force on the offside thigh, where Run 1 produced a considerable higher

force than in Run 4.

In Figures 9.9 and 9.10 we can see that Run 2 had generally produced higher contact forces and higher velocities than Run 5. But between Run 3 and Run 6 as shown in Figures 9.11 and 9.12, only the contact forces are generally higher in Run 3, the head's velocities are similar.

We can therefore see that the trend is that a motorcycle with leg protection generally produced higher forces between the dummy's legs and the motorcycle, if contact occurred. However, head's velocities did not offer a definitive trend.

9.3 Different Sized Dummies

It was the intention of this study to use a 5th percentile and a 95th percentile dummy to represent the range of dummy size. However it was subsequently discovered that these sizes of dummies have not been constructed and it was not possible to obtain measurements.

TRL then found a document named 'Anthropmetric Specifications' [33], on variously sized dummies, compiled by the Transportation Research Institute at the University of Michigan. However, there are still no specific 5th and 95th percentile dummy measurements,

but there are specifications on a small female and a large male, thus these will be used in place of the intended 5th and 95th percentile dummies respectively. Table 9.2 contains the general statistics of these different sized dummies.

9.3.1 Runs 1, 7 And 8 (Figures 9.1, 9.13, 9.14)

In all three cases, the motorcycle yaw motion offered no clear visual difference, however, motorcycle roll motion increased with the increase in the size of the dummy. The dummies' offside legs spread outwards but the spine pitched higher as the size of the dummy decreased, but the head dived lower onto the barrier as the dummy increased in size.

All the dummies hit the same locations with the large sized male having extra contact between the offside knee and the knee-restraint. This is due to the longer thigh. Out of all the contact forces, three sets are of more interest in comparison.

In all three cases the heads hit the barrier edge and the barrier top. For the barrier edge, forces between datum and large sized male are similar, but are about 3,500N less than that of the small female. For the barrier top, forces between the small sized female and datum are similar, but are also about 3,500N less than that of the large sized male. This maybe due to the fact that the

large sized male, being taller, had landed more on target towards the barrier top.

The last set of forces are generated between the offside thigh and the petrol tank. There is no clear trend in this case where the small female suffered the least, 2,069N, the large male being the medium, 4,946N, and the datum being the greatest, 6,628N.

9.3.2 Runs 2, 9 And 10 (Figures 9.2, 9.15, 9.16)

In this section the motorcycle yaw motion is the least with the large sized male dummy rider. The other two motorcycles share similar yaw motion. However, there is no apparent difference in all three motorcycle roll motions.

For the dummy part, the overall performances of the small female and the datum are similar such that as the motorcycle steered slightly away from the barrier, the dummy continued to travel forwards but gradually yawed in the anti-clockwise direction. However, the large sized male reacted very differently.

As the motorcycle carrying the large sized male steered away from the barrier, the dummy actually turned towards the barrier. This is due to the fact that, unlike the other two dummies, where their heads did not contact the barrier, the large sized male

actually hit the vertical face and the edge of the barrier.

For the impact between the offside thigh and the petrol tank, this occurred in all three cases. Again the datum and the small female share similarity in terms of durations and peak values, whereas the large male's impact was mild and occurred late into impact. This is once again due to the physique of the large sized male where the impact occurred as the motorcycle rolled, by which time the large sized male had already straightened up and was yawing in an anti-clockwise direction. This led to the offside thigh touching the side of the petrol tank.

9.3.3 Runs 3, 11 And 12 (Figures 9.3, 9.17, 9.18)

This is the case where in the datum run the discontinuity occurred. In the simulation run of the small female, because of the shorter physique, her head also hit the vertical face of the barrier with force 26,585N. However, since the force is less severe than that of the datum, even though the dummy was thrown backwards and 'through' the motorcycle, the acceleration is less.

However, for the large sized male, the head did hit the barrier edge and the barrier top. This is due to his longer torso. This led to a different response to that from the other simulations such that the head rebounded and caused the whole body to bounce

upwards.

For the forces, all three pairs of legs hit the knee-restraints and the trend is that the force increases as the size of the dummy increases. There is a different pattern in the impact force between the knees and the petrol tank where the small female hit hardest but the large sized male did not hit at all.

To highlight the performance of these different sized dummies in the different configuration of impacts, the bar charts in Figures 9.19 to 9.24 contain the contact forces and the head velocities.

From the bar charted contact forces in Figures 9.19, 9.21 and 9.23, there is an indicator that the small female dummy is more likely to hit the motorcycle on her offside upper leg, indeed in the oblique impacts, but even in the head-on impact, the impact between the lower legs and the motorcycle are less severe than impacts on her upper legs. On the other hand, the large male is more likely to hit the motorcycle on his lower legs, This can be explained by the stature of each dummy, where the small female dummy has shorter legs such that when she is seated on the motorcycle her thighs are nearer to the contact targets around the sides of the petrol tank, than her lower legs which cannot extend fully towards the knee-restraints. In the case of the large male dummy, the opposite is true. When he is seated on the motorcycle, because of his longer legs, the thighs are more

spread outwards around the petrol tank, but the lower legs are nearer towards the knee-restraints. The datum 50 percentile dummy falls between these two limits.

For the velocity bar charts, where the velocities are taken when the head is at a 0.35m distance from the barrier, there exists a trend in the head's normal velocity, such that the normal velocity increases as the size of the dummy increases. There is also an indicator that the vertical velocity increases as the size of the dummy decreases, since the mass of the female dummy is lighter than the other two dummies such that for the same input of energy the female dummy will react with a higher velocity than the other two dummies. This is so except in Runs 2, 9 and 10, where the impact configuration is a barrier angle of 20° , and the velocity is 4.4ms^{-1} . However, this is the case where the nearside fairing hit the barrier before the front wheel, thus the subsequent dummy's impact is less severe.

9.4 Different Seated Positions

In all the simulation runs so far, the dummy is seated at an angle inclined to 70° relative to the horizontal. It is the intention here to position the dummy torso at different angles in order to study the trajectories of dummy and motorcycle. In order to achieve consistent comparisons, run (iii) is chosen as

the datum position.

In the track tests TRL have tried putting the OPAT dummy into various positions. Of these it was found that the dummy can sit at its most upright at 80° relative to the horizontal, and the most inclined at 37° to the horizontal. These two sitting positions were then used in the simulations.

9.4.1 Run 13 (Figure 9.25)

The dummy's legs hit the knee-restraints 50ms into impact. They then rebounded causing the dummy to pitch and the head to hit the barrier edge and the vertical face of the barrier. This is similar to the datum run such that the dummy somersaulted and went 'through' the motorcycle. However, since the force generated in the impact between the head and the vertical face of the barrier is about half of that from the datum run, the subsequent motion is not as violent as the datum. The size of the force between the head and the barrier edge is also nearly halved.

For other forces they are all very similar to the datum run. All the targetted forces between the dummy's legs and the knee-restraints, and also the petrol tank, have scored, in addition the thighs have hit the sides of the petrol tank, though only mildly at 779N. The thighs did not hit in the datum run.

9.4.2 Run 14 (Figure 9.26)

In this case the dummy's legs also hit the knee-restraints 50ms into impact, however, since the dummy torso angle is low, the head hit the vertical face of the barrier at about 60ms, which is about 30-40ms earlier than the other two runs. Also because of this low attitude, the head hit the vertical face only but not the edge. This caused the dummy to somersault but because the force generated is 162,455N, which is lower than the other two runs, the subsequent motion is quite smooth, though the unfortunate 'penetration' into the motorcycle still occurred.

For forces on the legs, they all were generated from the impacts on the knee-restraints and the sides of the petrol tank. Similar to the 80° seating position run, the thighs have also hit at 980N, which is about 200N higher than Run 13. The magnitudes of the other forces are also similar to those from the other two runs, with the exception for the forces between the knees and the petrol tank, which is about 700N less than the other two sets of forces.

The comparison between these two runs, 13 and 14, and the datum run of Run 3 are bar charted in Figures 9.27 and 9.28.

In Figure 9.27 where the contact forces are shown it can be seen

that Run 13, in general, produced the highest contacting forces. In Figure 9.28 where the head's velocities are charted, it is also Run 13 which produced the highest velocities. But on the whole, the three runs behaved very similar to each other.

9.5 Airbag Characteristics

This is the part of the exercise where it may lead to future work. This involves a mounting of an airbag on the motorcycle. Happian-Smith had already developed a two-dimensional airbag restraint simulation model [18] with a single-massed dummy rider. However, to convert the same principle into the current three-dimensional multi-massed dummy rider and motorcycle would be beyond the scope of this study, therefore at present, the airbag is represented by a collapsible plane, with measured force-deflection characteristics, mounted permanently on top of the petrol tank. This is a crude representation such that the inflation of the airbag, which in practice would be activated by the initial impact of the front wheel, is neglected. However this will give us preliminary insights of the dummy's reaction when impacted onto objects of airbag properties.

For possible contacts between the dummy and the airbag it was decided that the head and the upper torso are the most likely contact areas. The properties of the airbag are based on the

tests by Nieboer et al [34], where a sphere and circular plates of various sizes are used as impactors hitting a mounted airbag. Based on these force-deflection curves and the dimensions of the dummy's head and upper torso, estimated spring force data were obtained for use in our simulation.

For the actual comparison, airbags of three stiffnesses and situated in three different positions were chosen. Of these the above estimated stiffnesses, for the head and the upper torso, will be the datum stiffnesses. The suggestion by TRL that the airbag should incline at an angle parallel to the dummy's attitude, and situated one-third of the distance measured from the rear end of the petrol tank, will be considered as the datum. The two other stiffnesses will be taken as one-half and twice the datum stiffness. The two alternative positions will be an airbag mounted on the nearer edge of the petrol tank, and an airbag mounted on the farther edge of the petrol tank.

9.5.1 Run 15 (Figure 9.29)

At 50ms into impact, the dummy's legs have fully impacted onto the knee-restraints. These forces range from 3,134N for impacts between the knees and the sides of the petrol tank, to 8,167N for impacts between the knees and the knee-restraints. At the same time the head is seen to come into contact with the airbag. By

60ms the dummy's legs have started to rebound but the dummy's body is still in full contact with the airbag. From then on, the head started to bend backwards and rebounded. The legs have straightened up and the whole dummy is seen to have been thrown upwards and backwards. The peak forces for the impacts between the airbag and the head and also the upper torso are 29,316N and 1,184N respectively.

9.5.2 Run 16 (Figure 9.30)

In this impact the dummy's legs reacted in a very similar way to that in the datum run (indeed the forces on the legs are all very similar), however, the duration of the head impact onto the airbag lasted longer. By 60ms when the legs started to rebound the head is still in full contact with the airbag, also the penetration is further into the airbag. When the dummy started to rebound the head is seen to have bent more backwards if compared with the datum. The legs have straightened up but the spine stayed bent at an angle, which is unlike the datum where the dummy is seen to have stood up. This continued while the dummy was thrown backwards and upwards.

For the peak forces on the head and the upper torso, they are 21,996N for the head and 3,458N for the torso. This suggests that the torso had suffered more if compared to the datum but the head

had suffered less.

9.5.3 Run 17 (Figure 9.31)

The performance of this impact is very similar to the datum. The only exception is that of the head. It did not deform the airbag as deeply as it did in the datum run, and the impact duration is shorter. The neck is seen to have bent slightly less than that of the datum, but the subsequent trajectory is very similar.

For the forces, they are similar for the impact forces on the legs, but the head had suffered more at 37,979N. The upper torso's peak force is similar at 1,340N.

We can now examine these force values in Figures 9.32a, 9.32b and 9.32c. For forces between the dummy's legs and parts of the motorcycle all three runs produced similar results, but it was the force between the head and the airbag that produced a clear trend. This force increases as the stiffness of the airbag increases. However, the force between the torso and the airbag did not offer a clear trend. On the contrary, it was the least stiff airbag in Run 16 where this force is the highest. This can be explained by the fact that in Run 16, the dummy's head was in contact with the airbag fractionally longer than the other two runs, thus bringing the torso in contact with the airbag.

9.5.4 Run 18 (Figure 9.33)

The dummy's legs, along with the head and upper torso, have fully impacted onto the knee-restraints, and the airbag at 50ms into impact. The legs reacted similarly to the datum but the head and upper torso contact durations lasted longer. By 70ms, the head started to rebound. The neck had also bent backwards. From then on the dummy was being thrown upwards and backwards. However, the spine had somewhat been straightened more upright than the datum, but the pelvis did not pitch as much as in the datum case. This resulted in some slight differences in the dummy's trajectory such that it was thrown slightly higher, but not as far back as the datum.

For the forces on the legs they are still similar to those of the datum except for the forces between the knees and the knee-restraints, where they are some 500N less than those of the datum. The force between the head and the airbag is similar at 29,063N, but between the upper torso and the airbag it is 6,694N, some 5,500N higher.

9.5.5 Run 19 (Figure 9.34)

In this impact the legs have also fully impacted onto the knee-

restraints at 50ms. The force values are also similar to those of the datum. However because of the further location of the airbag, the head did not hit as early as the other simulations. At 60ms the legs have started to rebound. This caused the dummy to pitch forwards and the head hit the airbag at 70ms. The head soon started to rebound but the pitching around the pelvis continued, causing the dummy's head to hit the top of the petrol tank. Because of the non-existence of simulated contact between the head and the petrol tank, the dummy dived through the motorcycle by the pitching motion around the pelvis.

However, the peak force between the head and the airbag is still valid in the events leading up to the diving trajectory. At 34,256N this is the highest force based on an airbag of standardised stiffness. The upper torso did not hit the airbag.

For these differently positioned airbags, we can now see the difference in forces in Figures 9.35a, 9.35b and 9.35c. As with the previous comparison, the forces on the dummy's legs are all very similar in the three runs, but it was the forces between the dummy's head, torso and the airbag that offered a clear difference, especially that of the force between the torso and airbag. This force was the highest when the airbag is situated nearest to the rider, but did not occur at all when the airbag is furthest away from the rider. For the force between the head and the airbag it was highest in Run 19; the other two runs

shared similar value for this force.

9.6 Overview

Having analysed the various simulations, below are the summarised observations made within each specific comparison.

Between the motorcycle in the datum runs and one with minimal outer fairing it was observed that the dummy riding the motorcycle with minimal outer fairing had marginally suffered more on the head in oblique impacts. However, in head-on impact the dummy's legs had suffered less compared with the datum runs, but both sets of forces are well within injury criterion limit.

It must be emphasized that the above observations were made between a motorcycle with full leg protection, and one with minimal outer fairing such that this motorcycle, unlike a bare standard, is fitted with a small and soft outer fairing but the knee-restraints were retained. Direct comparison cannot be made between motorcycles with and without leg protection since this will involve extensive re-design of the current motorcycle model.

For the different sized dummies it was observed that the large sized dummy can hit the barrier, especially the barrier top, more readily than the other two dummies. Also it was observed that the

loads on the large sized dummy were the highest, indeed there was a trend of increase in load on the legs as the dummy's size increased.

When the dummy was sitting in three different attitude positions it was found that events were very similar. In all three cases the head had hit the vertical face of the barrier causing the backwards somersault motion, but was less violent in the case of the 37° torso angle since the force was comparatively low.

For the different stiffnesses of airbags, it was observed that there were two trends. The first is that there was an increase in the load on the head, for head to airbag contact, as the stiffness of the airbag increased. Secondly, the head to airbag contact duration lasted longer as the stiffness of the airbag decreased. All three subsequent motions were similar in that the head hit the airbag, then the legs started to straighten up and finally the whole dummy was thrown backwards and upwards.

When the airbag was situated in different positions, it was observed that when the airbag was at the nearest and the datum positions to the dummy they shared similarities, but when the airbag was at the farthest position the head to airbag contact came late. Indeed it occurred after the legs had hit, therefore causing the pitching motion on the dummy in a clockwise direction such that the dummy dived 'into' the petrol tank.

Run	Angle of impact ANG (degrees)	Initial velocity VEL (ms ⁻¹)	Knee to knee-restraint distance KR (m)	Stiffness of leg protector LP (unit factor)	Radius of leg protector RLP (m)	Dummy type	Seated altitude (degrees)	Airbag stiffness x	Airbag position (relative to near edge of petrol tank)
1	46.8	13.7	0.07	15.7	0.165	medium sized male	70	—	—
2	20.0	4.4	0.0	2.0	0.135	medium sized male	70	—	—
3	90.0	15.9	0.02	4.7	0.138	medium sized male	70	—	—
4	46.8	13.7	0.07	1.0	0.18	medium sized male	70	—	—
5	20.0	4.4	0.0	1.0	0.18	medium sized male	70	—	—
6	90.0	15.9	0.02	1.0	0.18	medium sized male	70	—	—
7	46.8	13.7	0.07	15.7	0.165	small female	70	—	—
8	46.8	13.7	0.07	15.7	0.165	large male	70	—	—
9	20.0	4.4	0.0	2.0	0.135	small female	70	—	—
10	20.0	4.4	0.0	2.0	0.135	large male	70	—	—
11	90.0	15.9	0.02	4.7	0.138	small female	70	—	—
12	90.0	15.9	0.02	4.7	0.138	large male	70	—	—
13	90.0	15.9	0.02	4.7	0.138	medium sized male	80	—	—
14	90.0	15.9	0.02	4.7	0.138	medium sized male	37	—	—
15	90.0	15.9	0.02	4.7	0.138	medium sized male	70	x	$\frac{1}{3}$ from near edge
16	90.0	15.9	0.02	4.7	0.138	medium sized male	70	$\frac{1}{2}$ x	$\frac{1}{3}$ from near edge
17	90.0	15.9	0.02	4.7	0.138	medium sized male	70	2x	$\frac{1}{3}$ from near edge
18	90.0	15.9	0.02	4.7	0.138	medium sized male	70	x	on near edge
19	90.0	15.9	0.02	4.7	0.138	medium sized male	70	x	on far edge

Table 9.1 Categorisation of specific computer runs

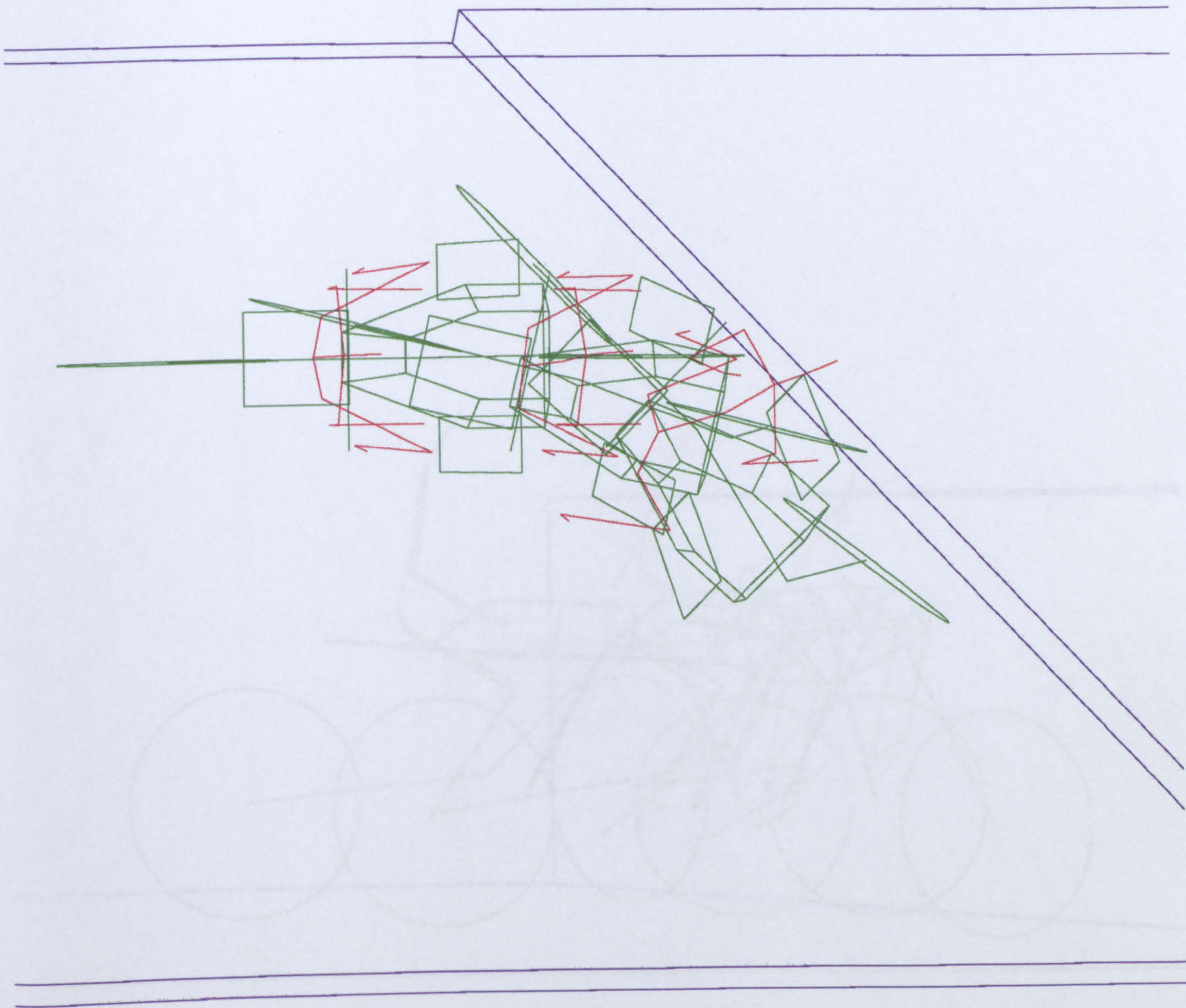


Figure 9.1a Plan view of Run 1

Figure 9.1b Elevation view of Run 1

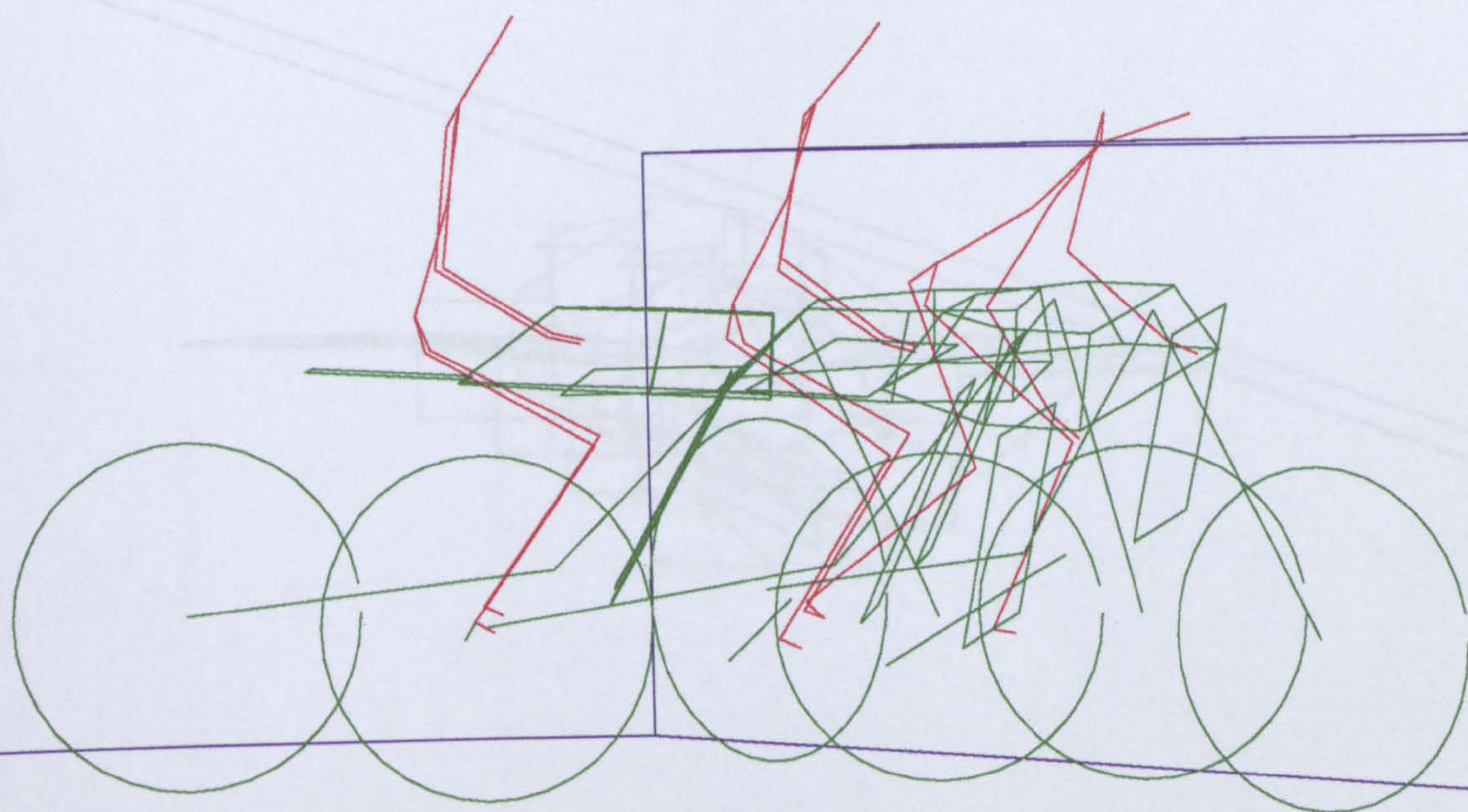


Figure 9.1b Elevation view of Run 1

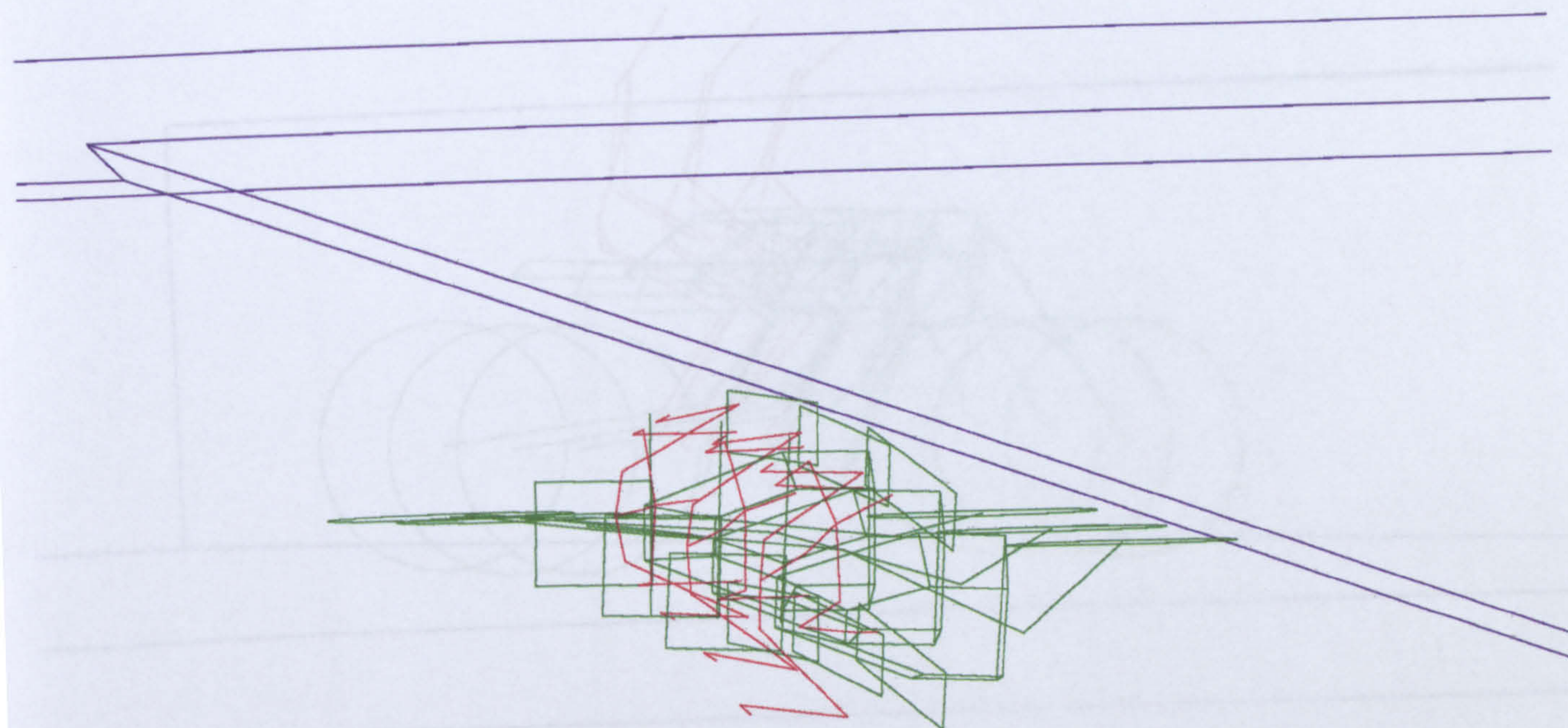


Figure 9.2a Plan view of Run 2

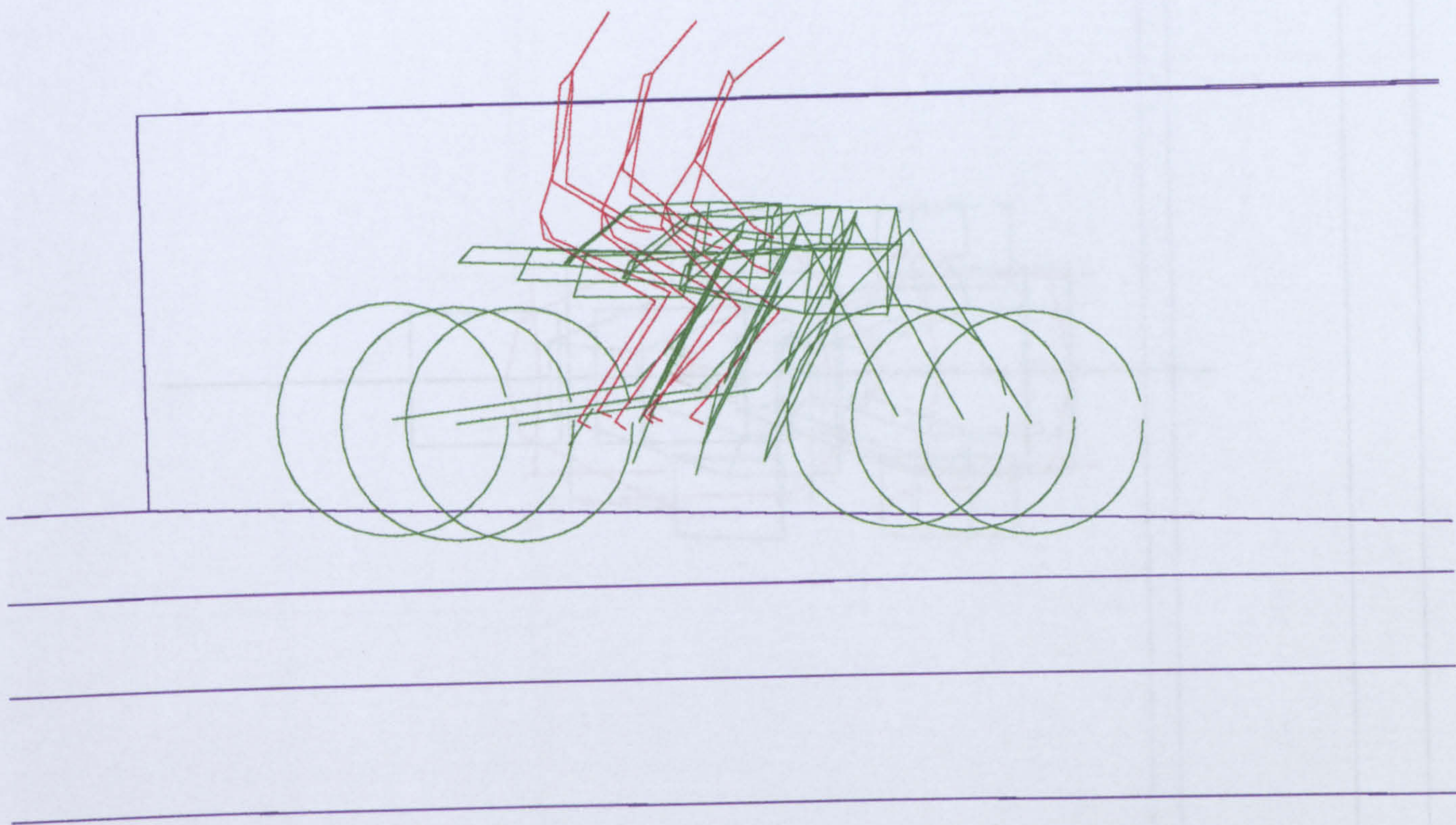


Figure 9.2b Elevation view of Run 2

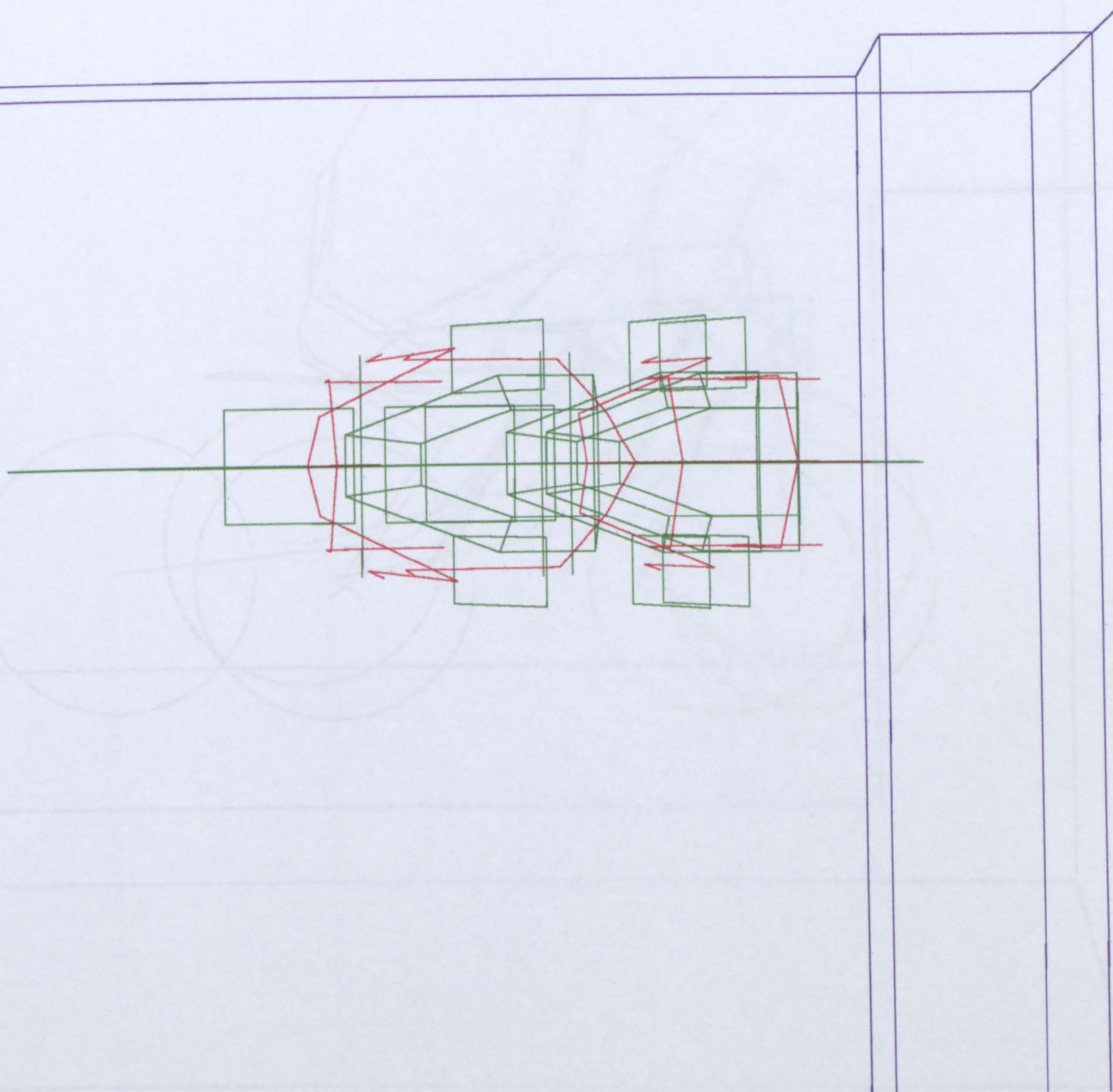


Figure 9.3a Plan view of Run 3



Figure 9.3b Elevation view of Run 3

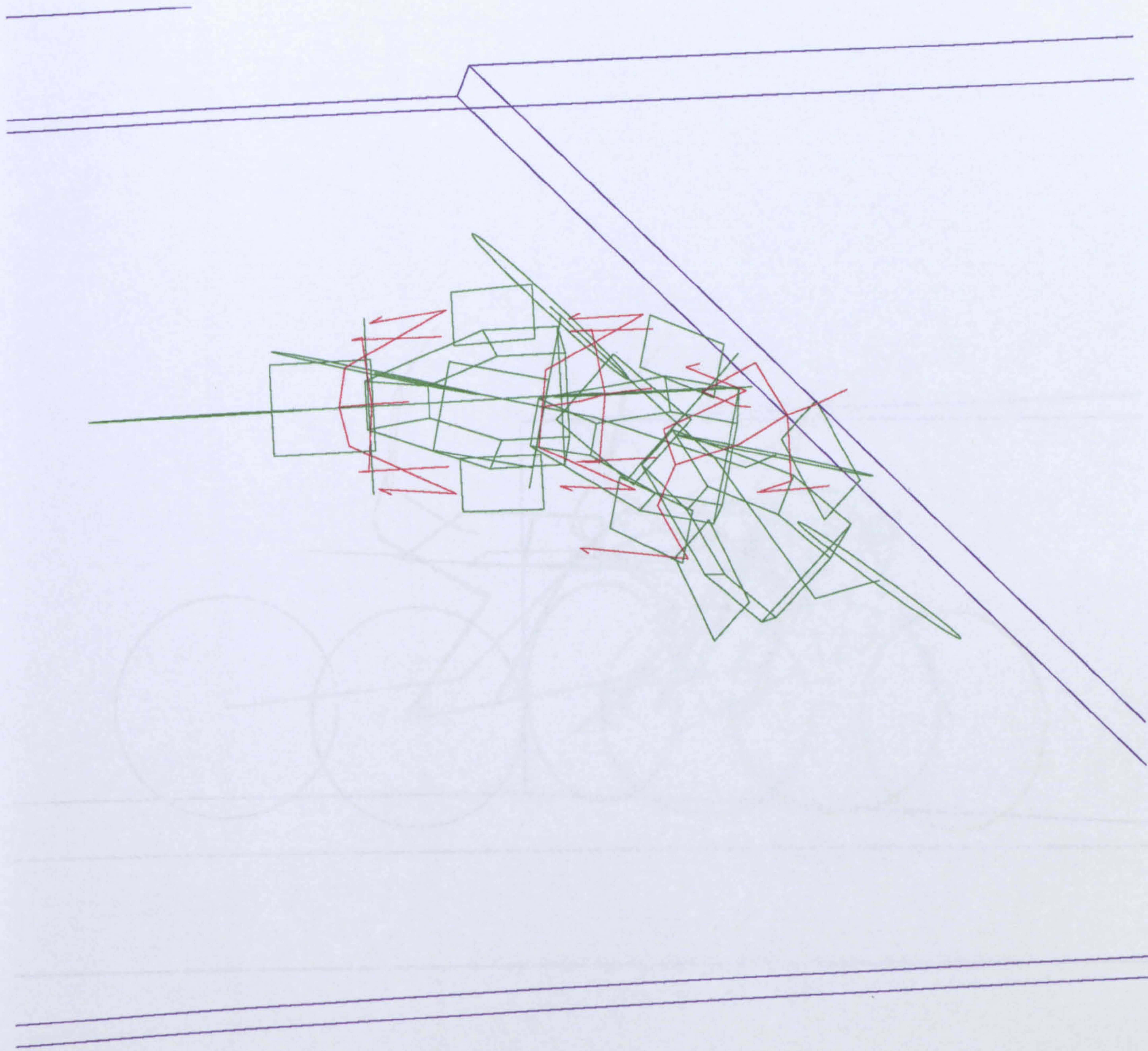


Figure 9.4a Plan view of Run 4

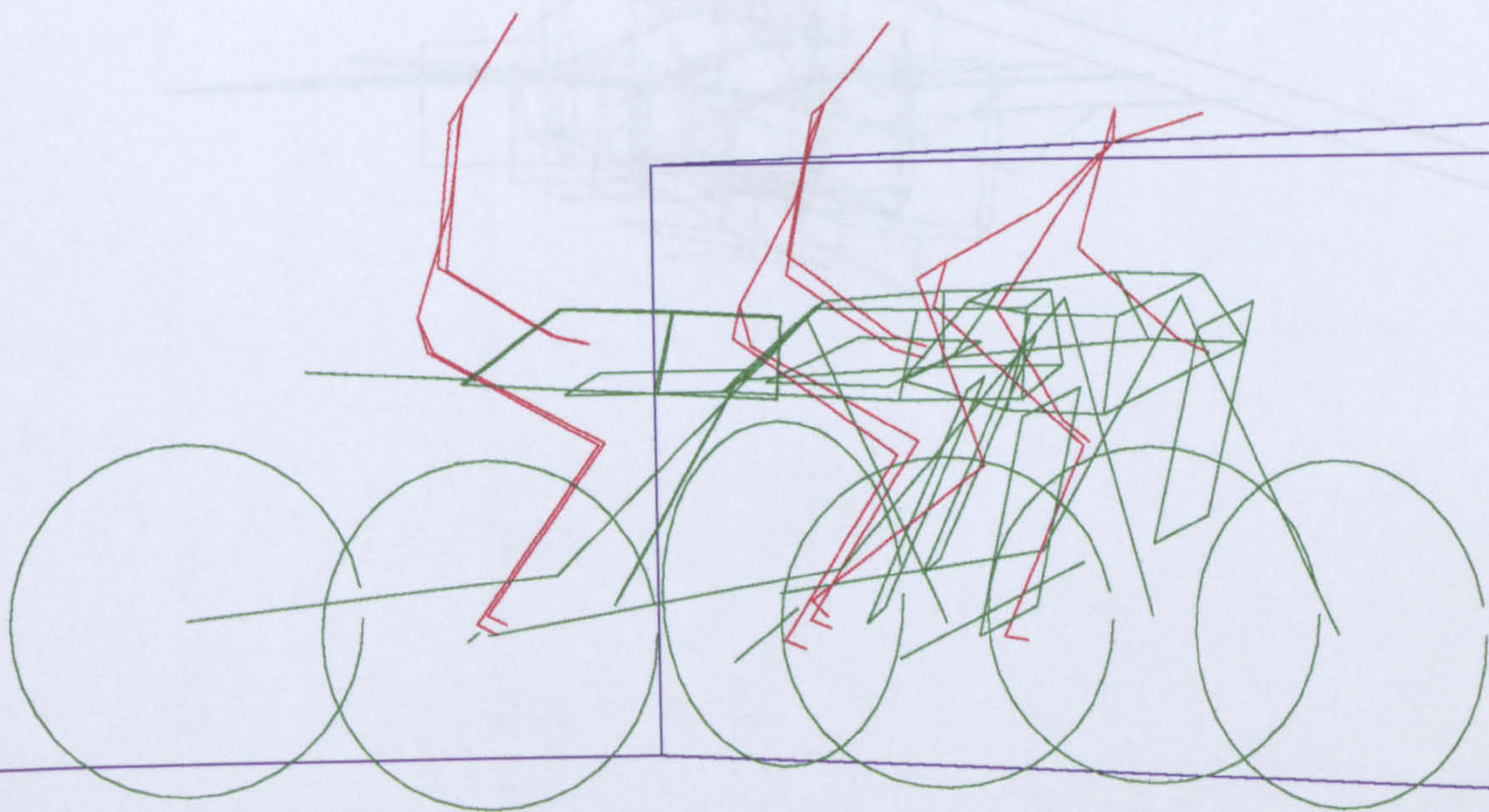


Figure 9.4a Plan view of Run 3

Figure 9.4b Elevation view of Run 4

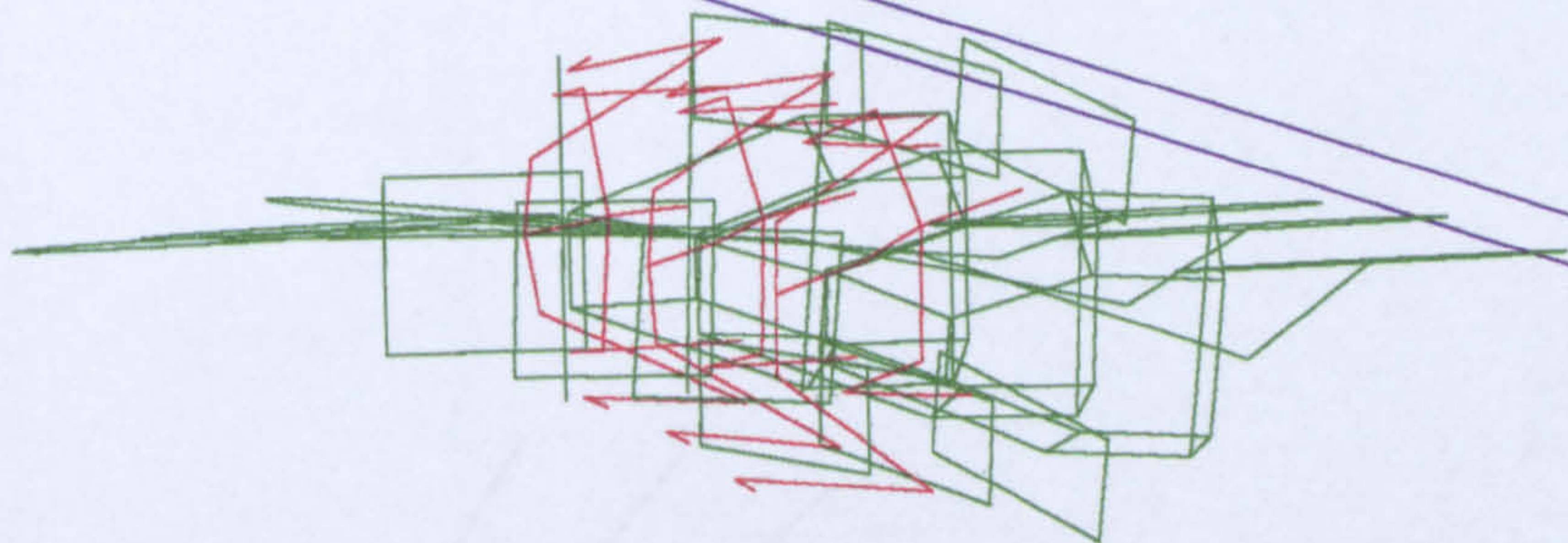


Figure 9.5a Plan view of Run 5

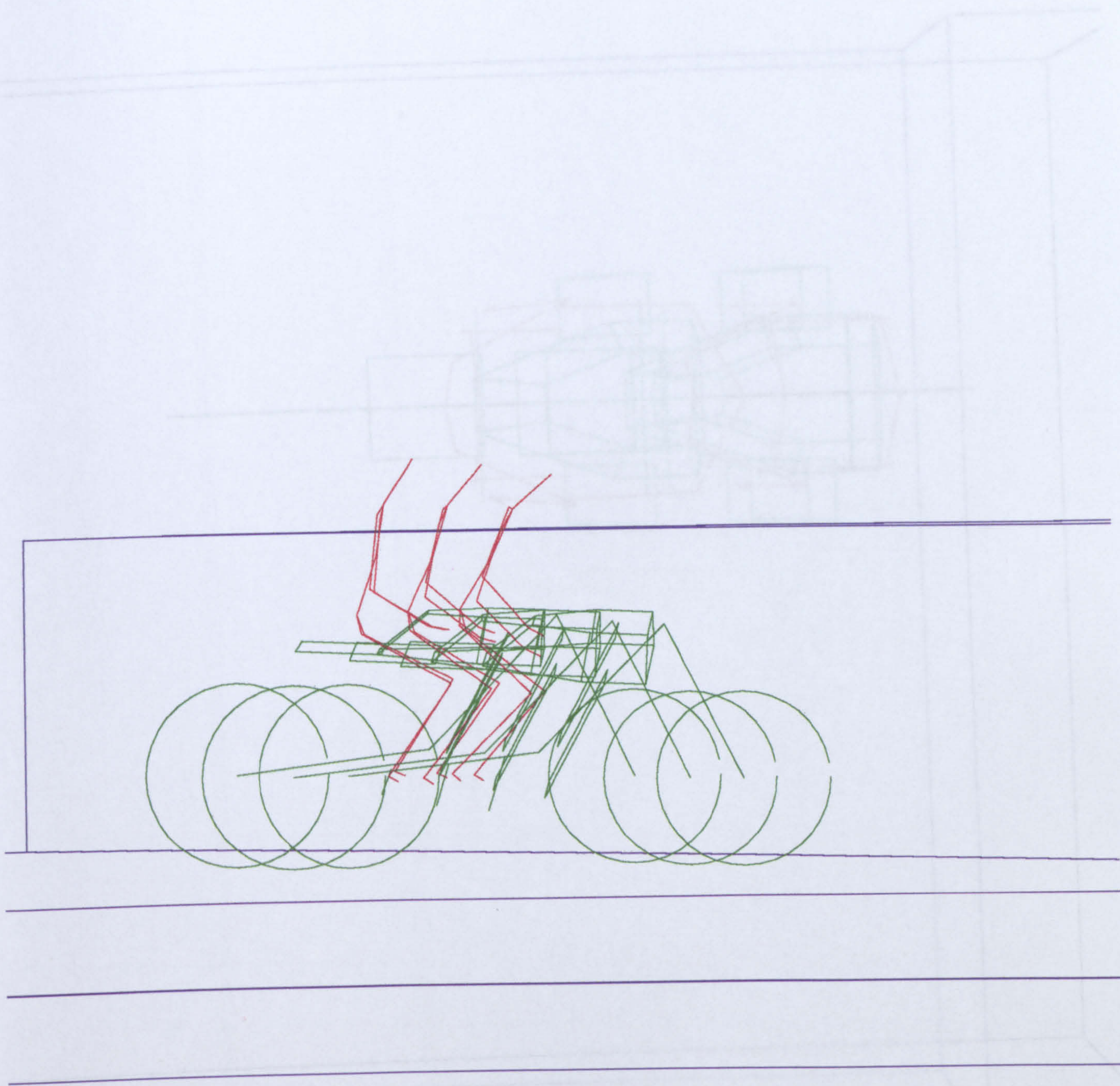


Figure 9.5b Elevation view of Run 5

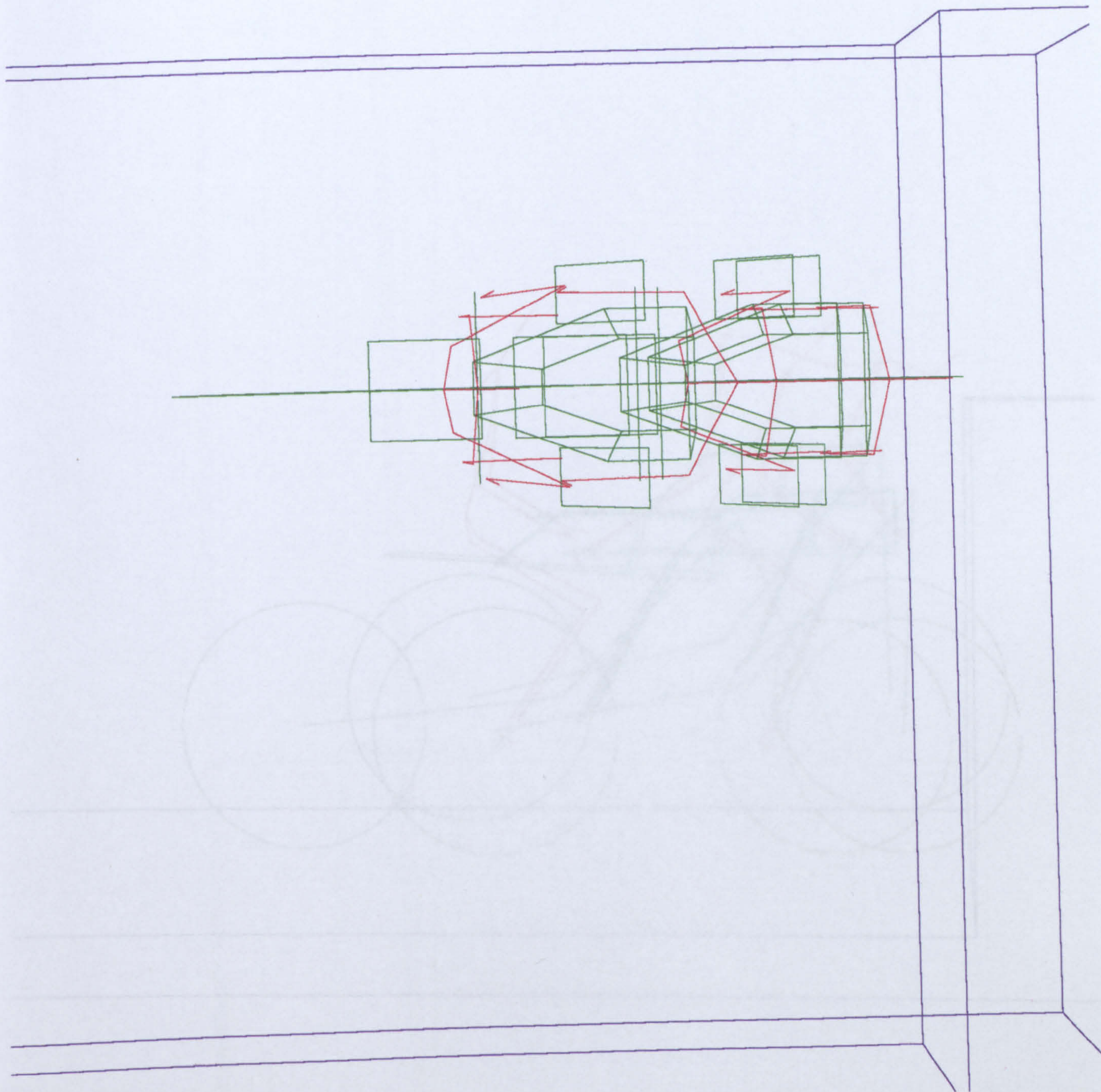


Figure 9.6a Plan view of Run 6

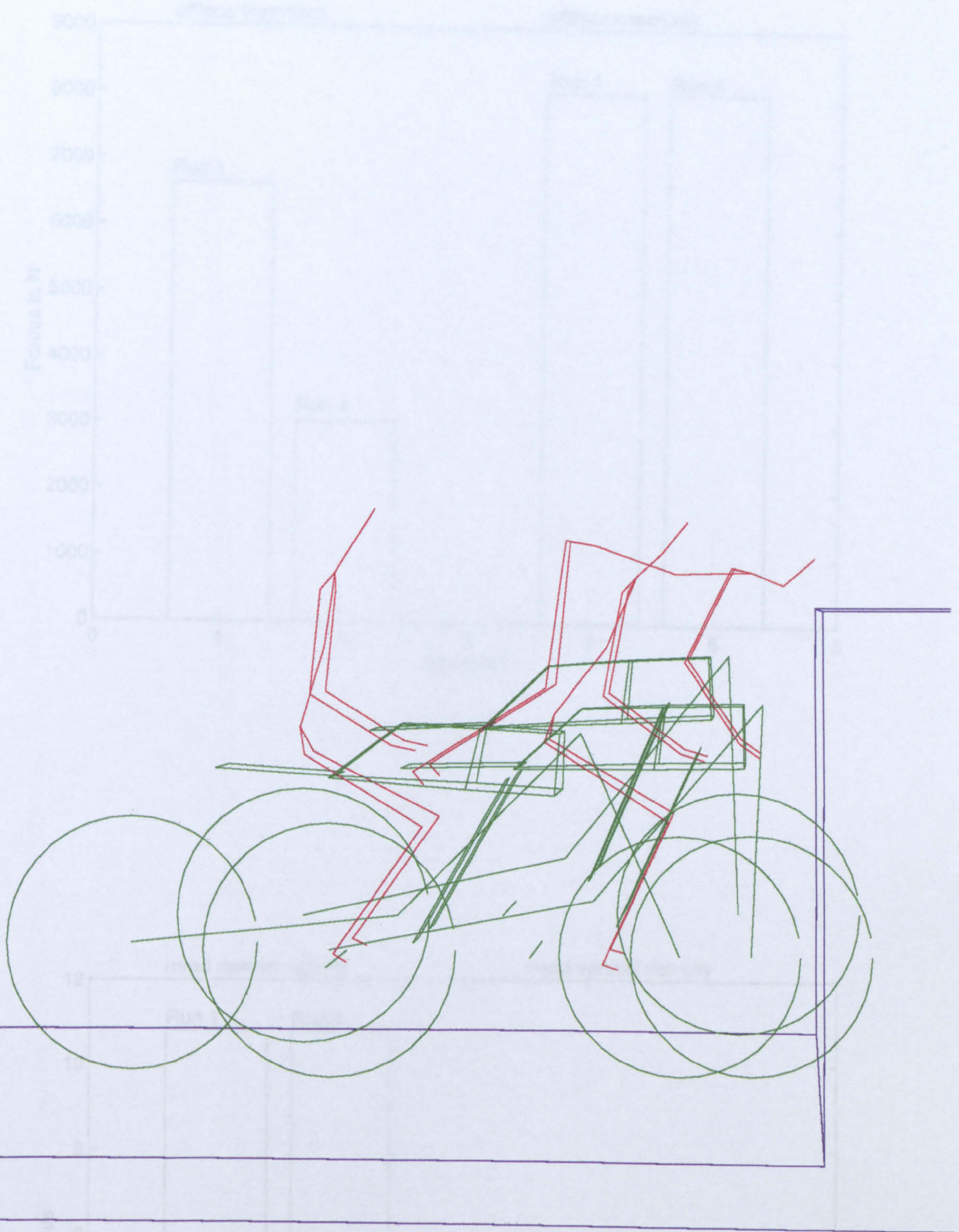
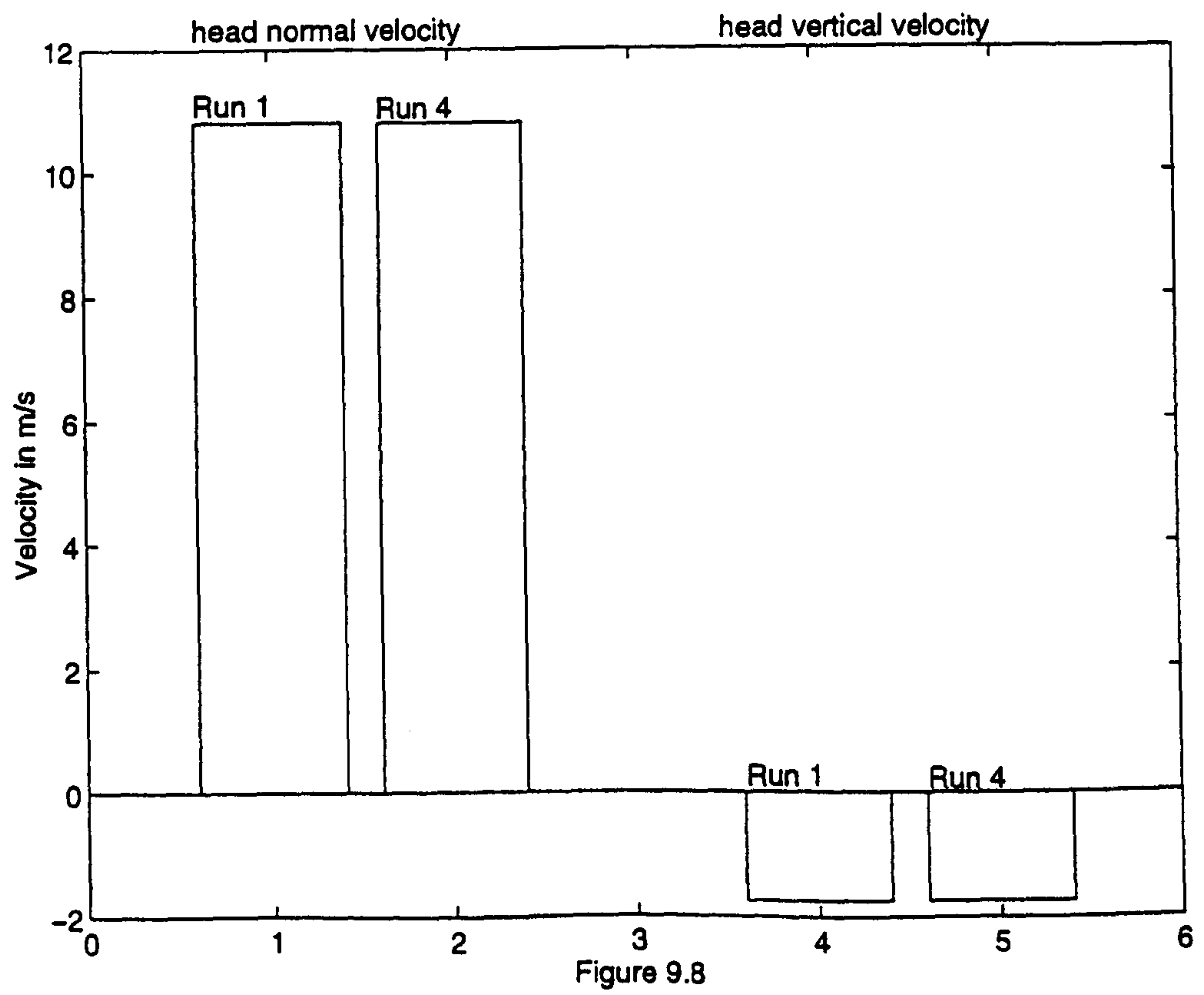
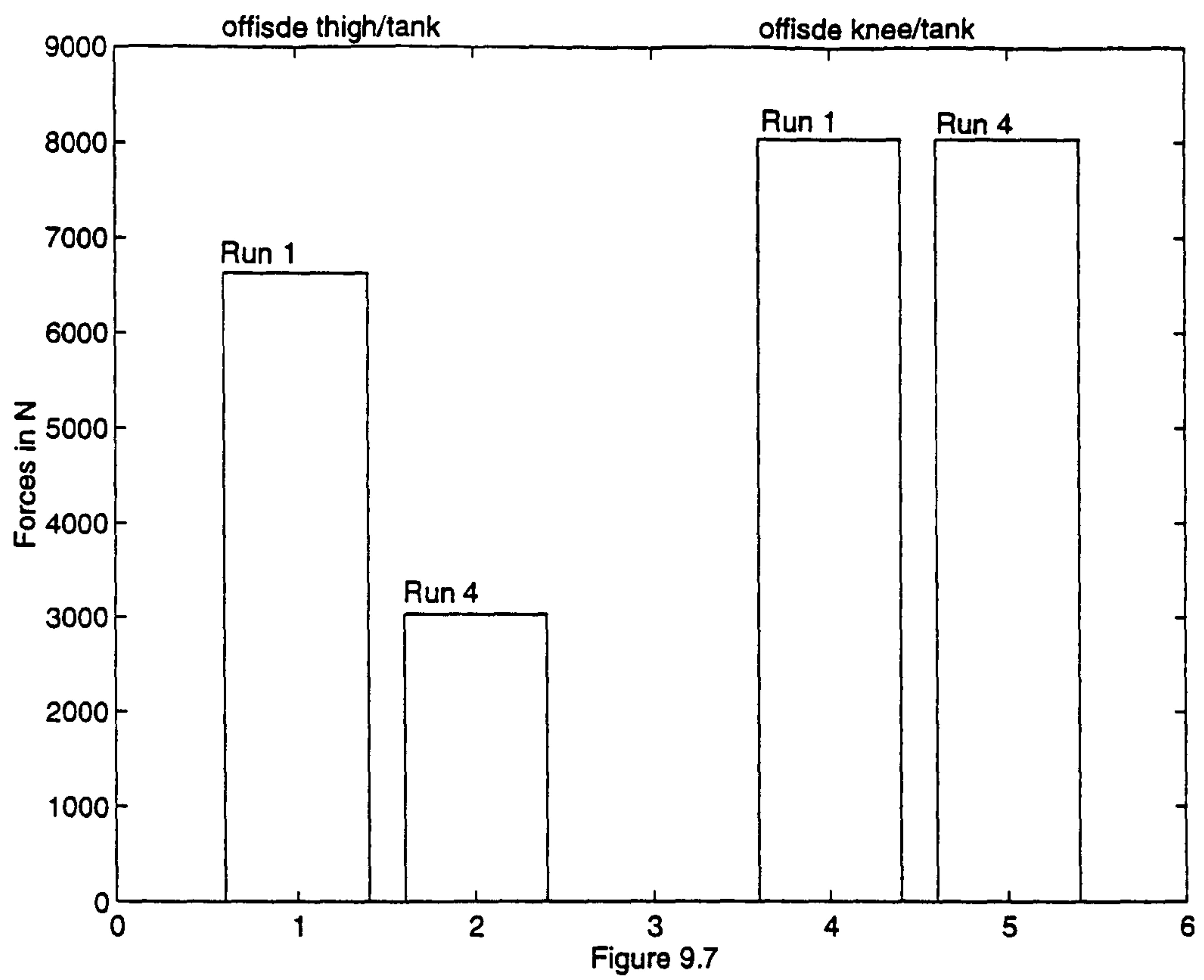
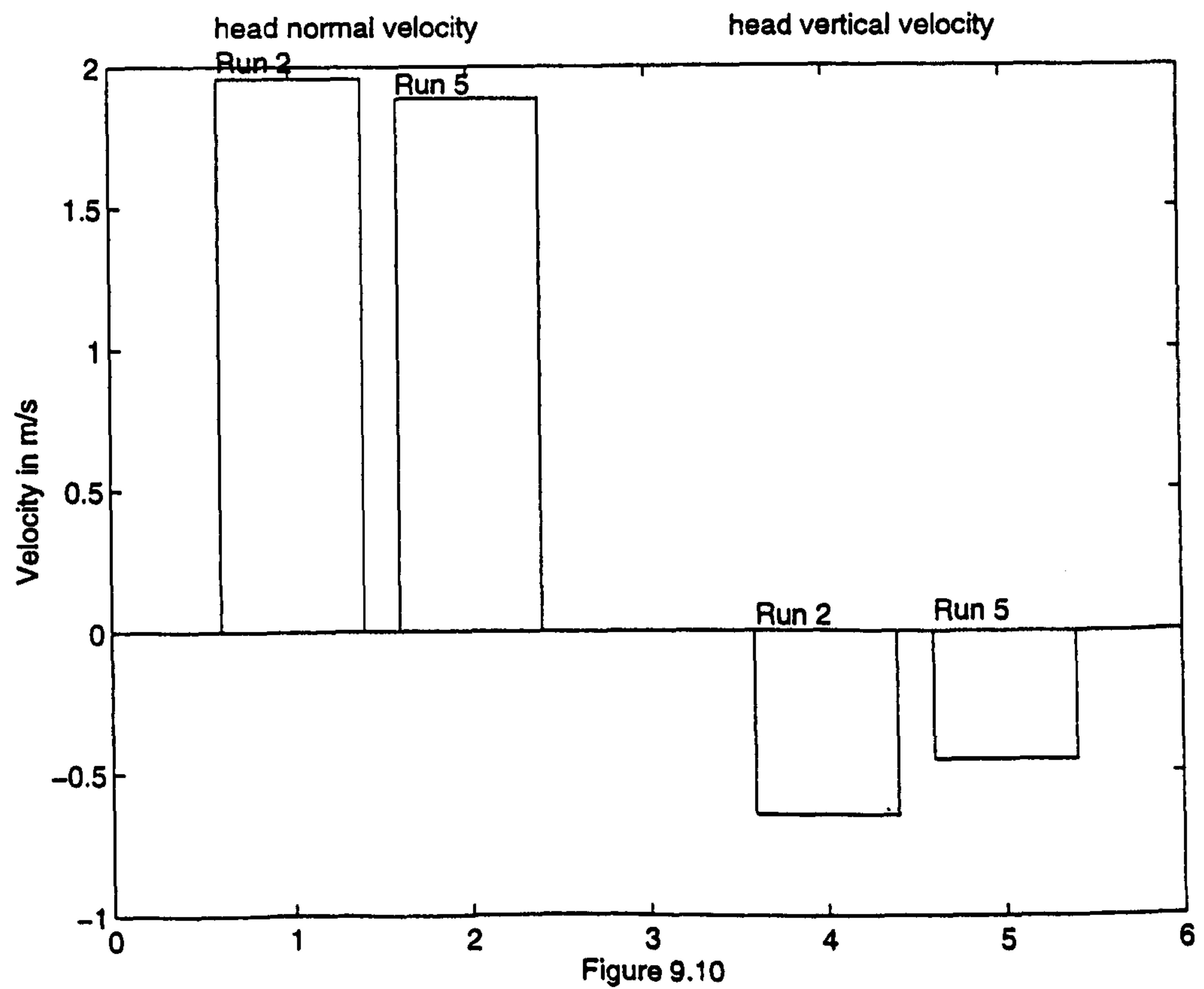
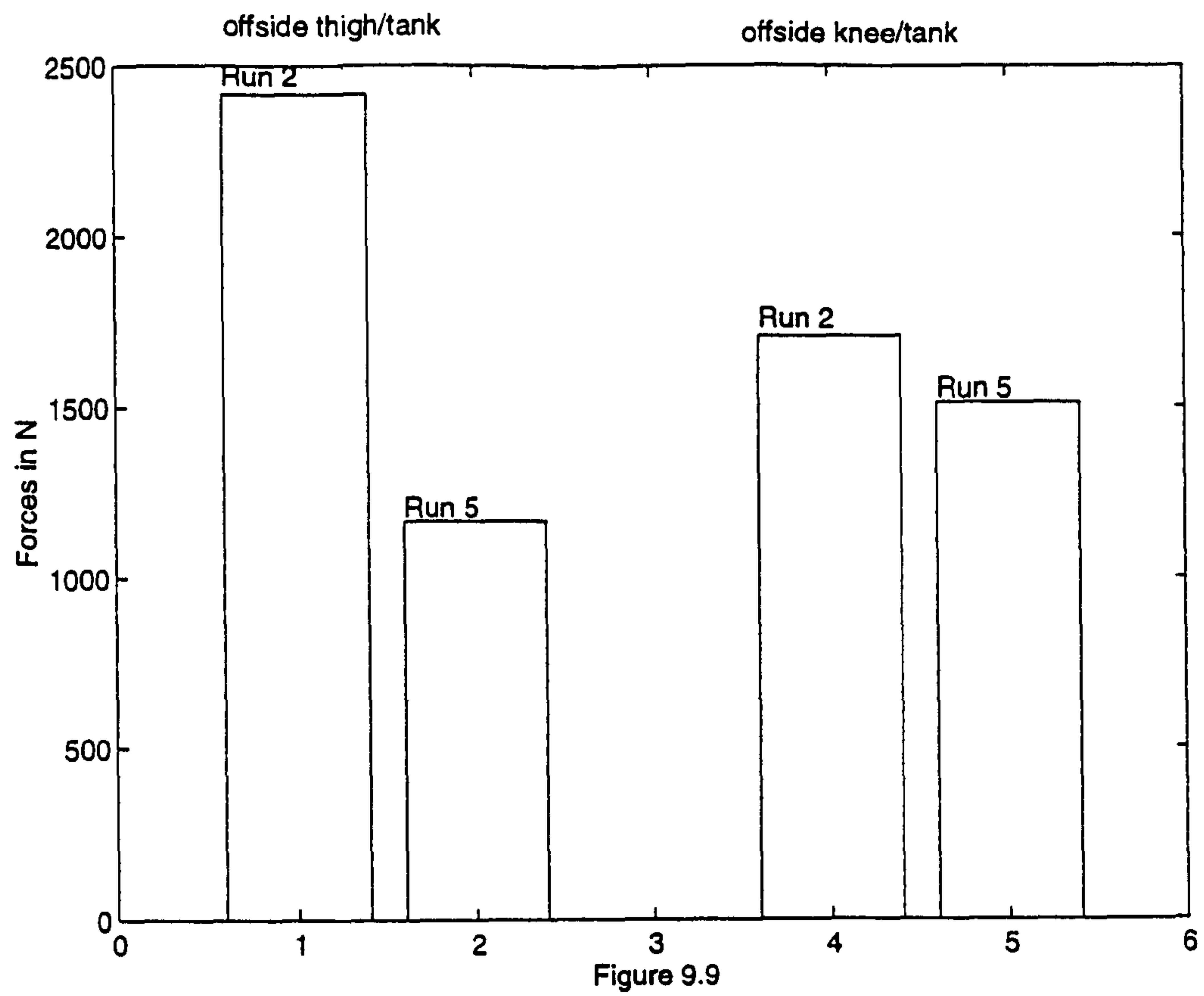
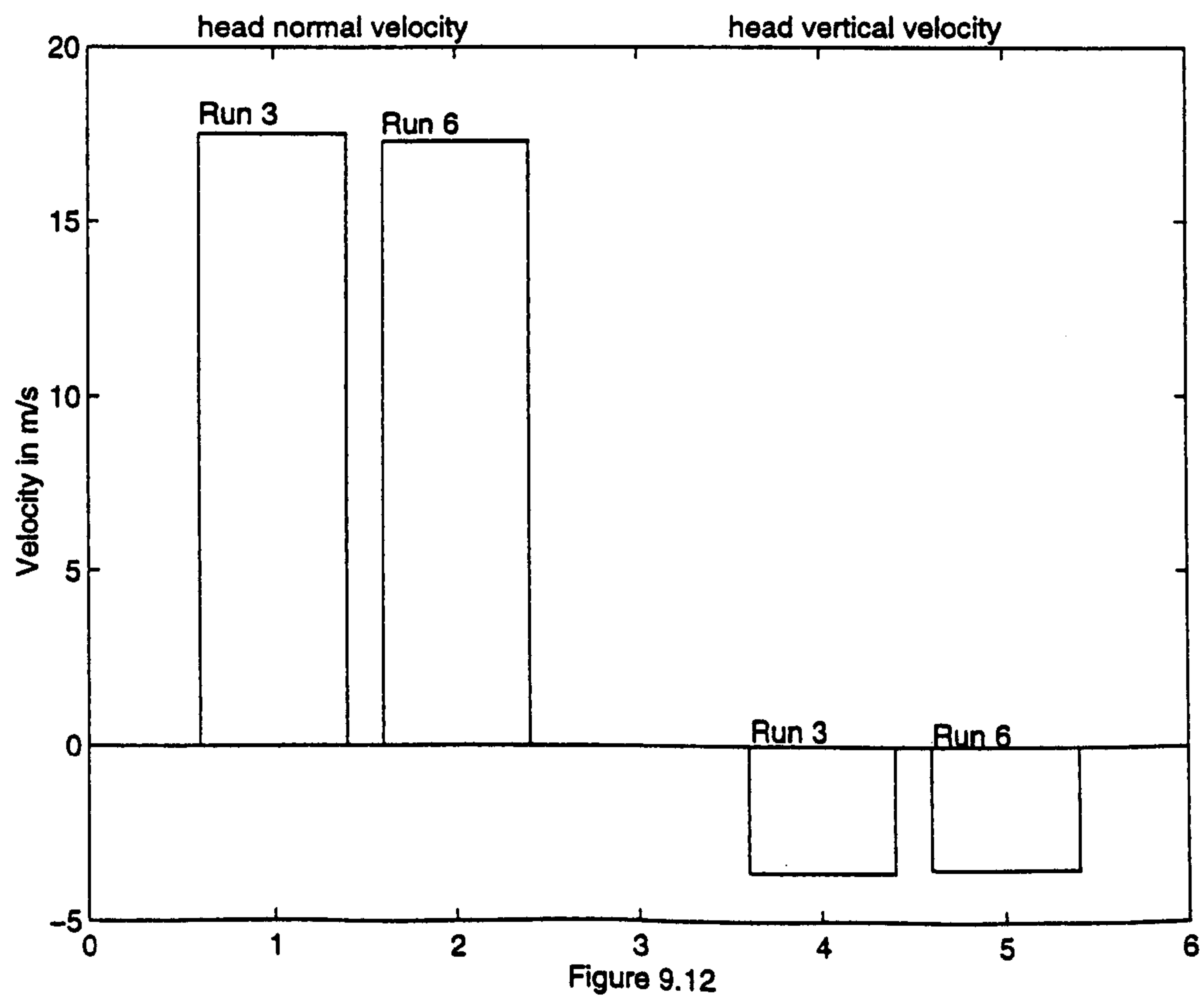
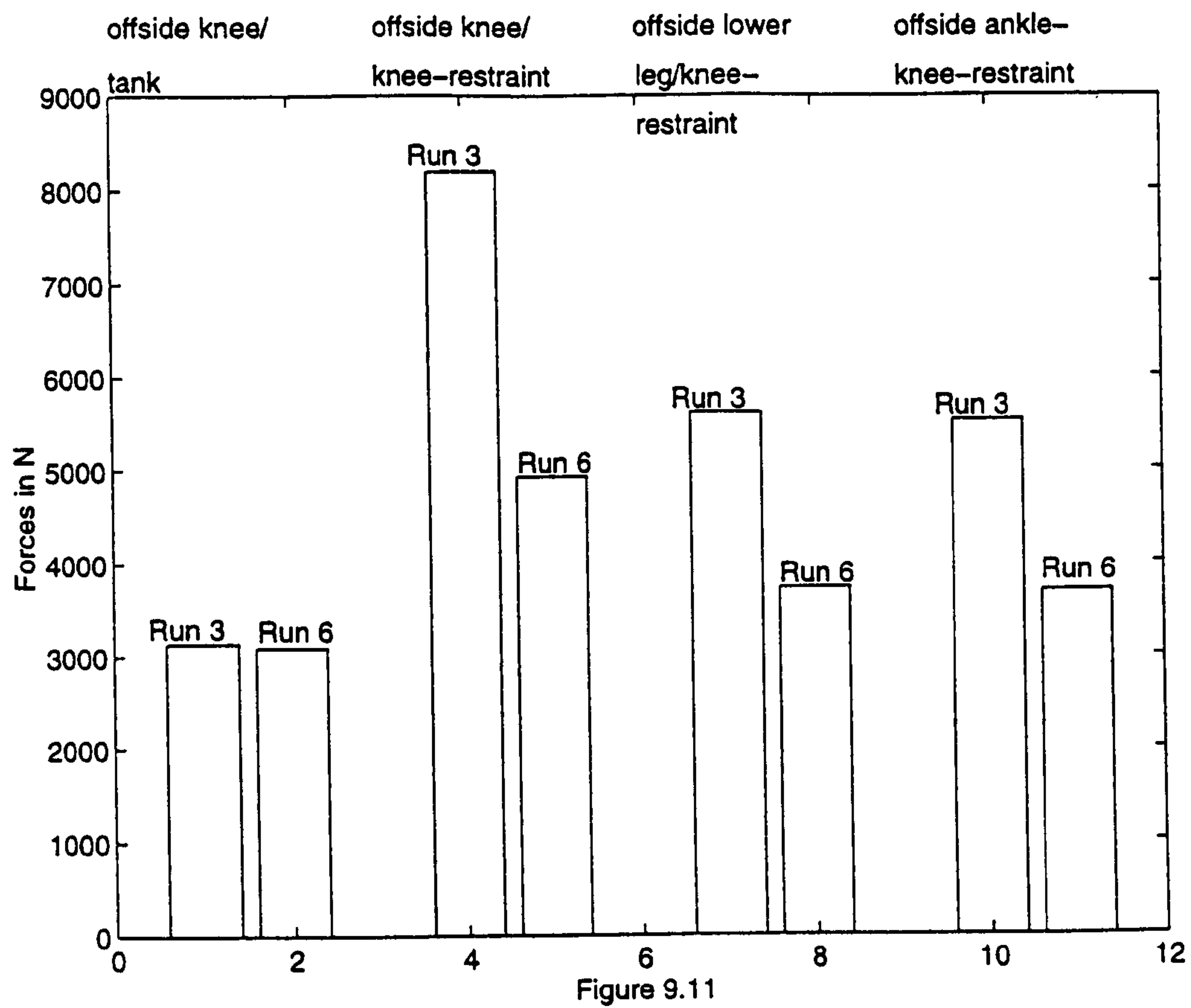


Figure 9.6b Elevation view of Run 6







Segment	Mass (kg)	Principal Moments of Inertia ($\text{kgm}^2 \times 10^{-3}$)		
		I_y	I_y	I_z
Head	4.14	20.02	22.15	14.46
Neck	0.97	1.48	1.84	2.29
Thorax	23.76	456.64	322.25	301.59
Abdomen	2.37	16.76	10.66	25.48
Pelvis	11.41	101.57	94.24	118.47
Upper Arm	1.77	11.25	12.25	2.31
Lower Arm & Hand	2.02	31.08	30.93	2.01
Upper Leg	8.61	123.09	130.15	36.71
Lower Leg	3.59	52.04	52.83	6.07
Foot	0.98	0.87	4.30	4.41

Estimated Mass and Principal Moments of Inertia for Medium Sized Male.

Segment	Mass (kg)	Principal Moments of Inertia ($\text{kgm}^2 \times 10^{-3}$)		
		I_y	I_y	I_z
Head	3.70	14.61	17.29	13.17
Neck	0.60	0.61	0.95	1.03
Thorax	12.98	154.28	116.12	120.86
Abdomen	1.61	14.34	10.15	20.57
Pelvis	6.98	32.62	28.29	57.42
Upper Arm	1.12	5.00	5.11	0.82
Lower Arm & Hand	1.14	14.15	12.94	0.83
Upper Leg	5.91	73.14	70.10	15.39
Lower Leg	2.36	26.14	26.19	2.31
Foot	0.64	0.34	1.84	1.66

Estimated Mass and Principal Moments of Inertia for a Small Female.

Segment	Mass (kg)	Principal Moments of Inertia ($\text{kgm}^2 \times 10^{-3}$)		
		I_y	I_y	I_z
Head	4.51	22.59	26.31	16.87
Neck	1.17	2.18	2.44	3.19
Thorax	32.42	735.1	547.4	490.4
Abdomen	2.95	26.2	16.5	48.1
Pelvis	16.04	172.0	155.3	195.6
Upper Arm	2.31	17.9	18.7	5.15
Lower Arm & Hand	2.43	41.4	40.0	2.8
Upper Leg	11.34	192.6	200.0	59.3
Lower Leg	5.06	83.1	83.4	9.38
Foot	1.55	1.04	7.51	7.76

Estimated Mass and Principal Moments of Inertia of a Large Male

Table 9.2 Mass and principal moments of inertias for the different sized dummies.

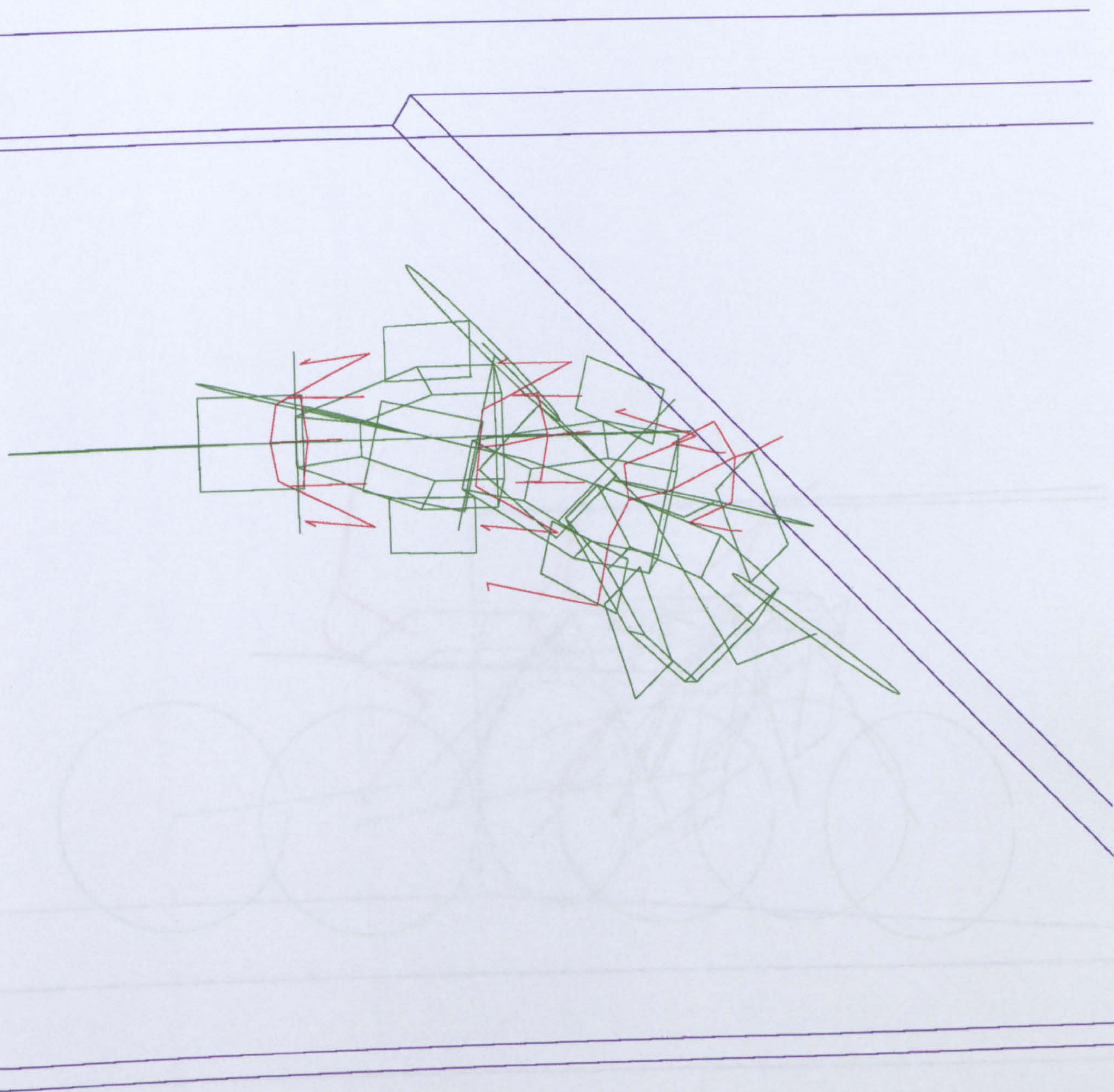


Figure 9.13a Plan view of Run 7

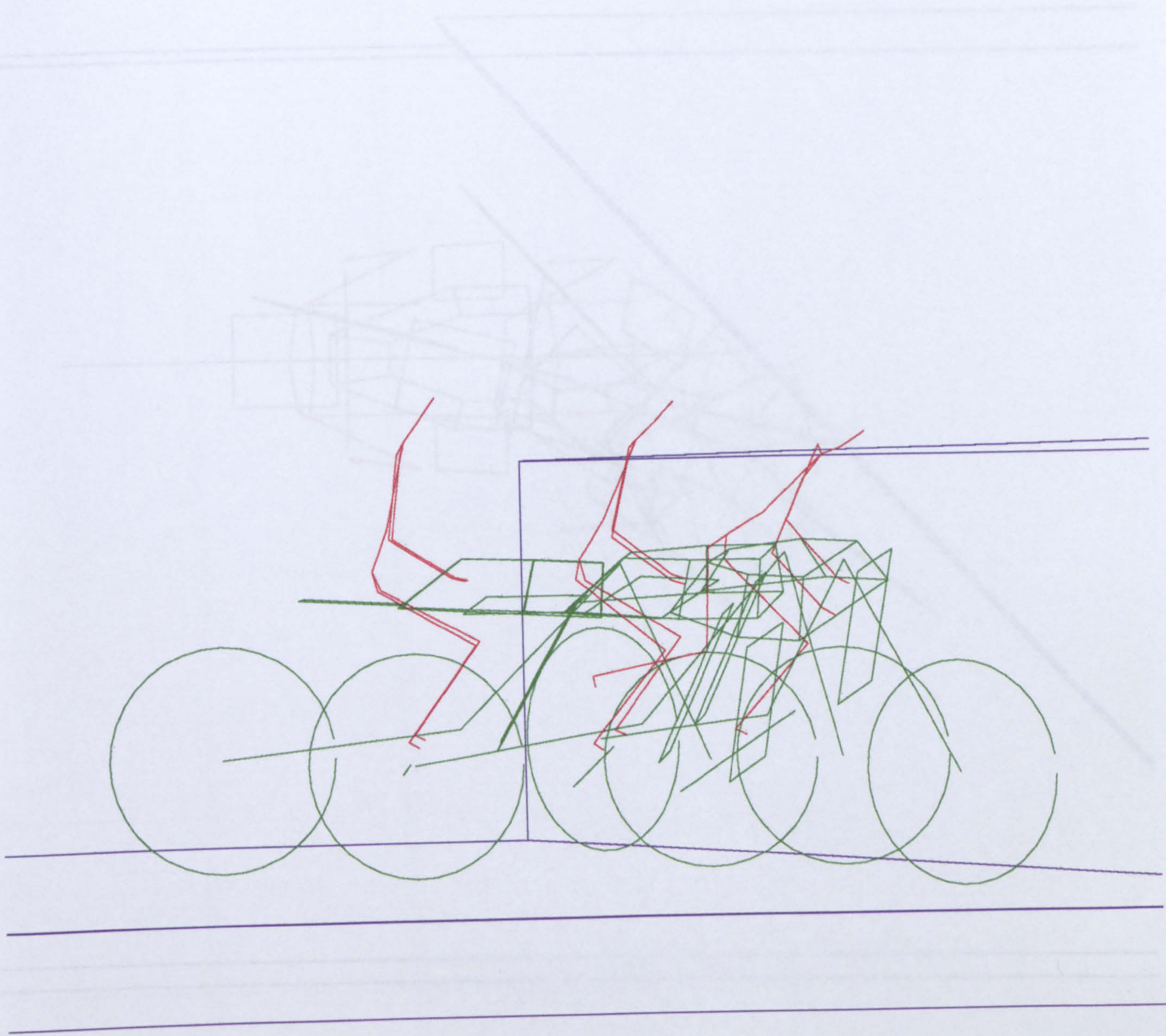


Figure 9.13b Elevation view of Run 7

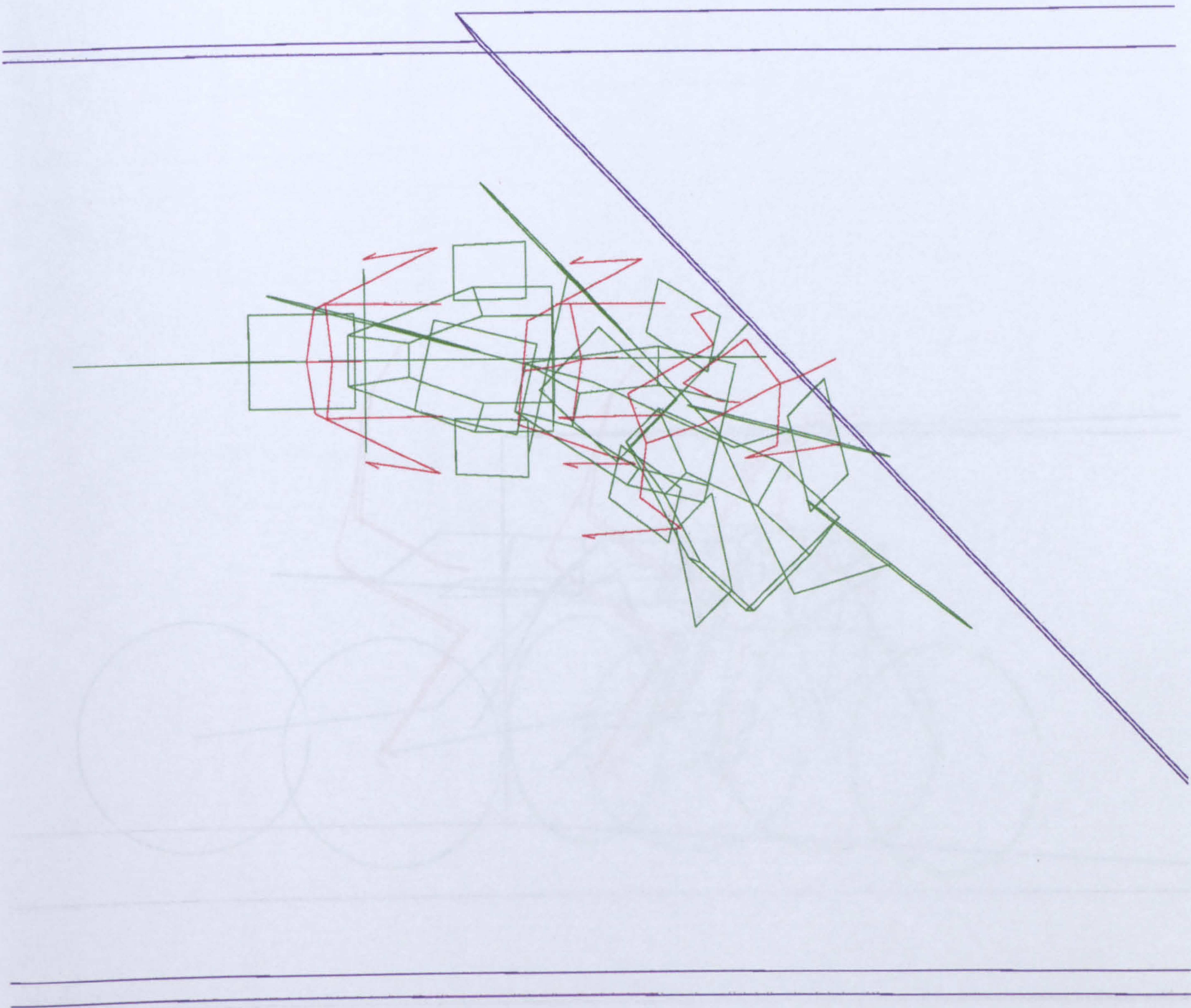


Figure 9.14a Plan view of Run 8

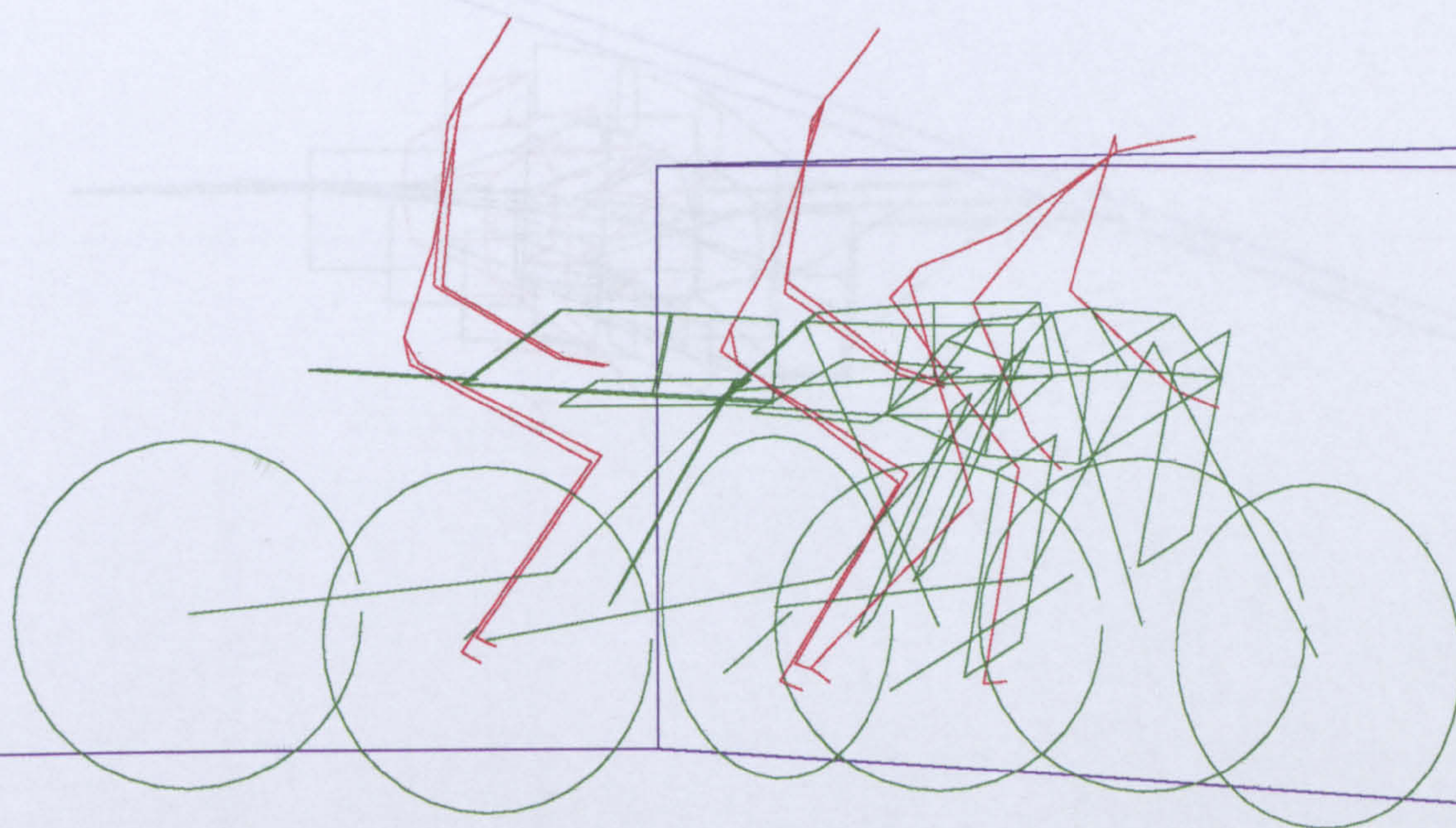


Figure 9.14b Elevation view of Run 8

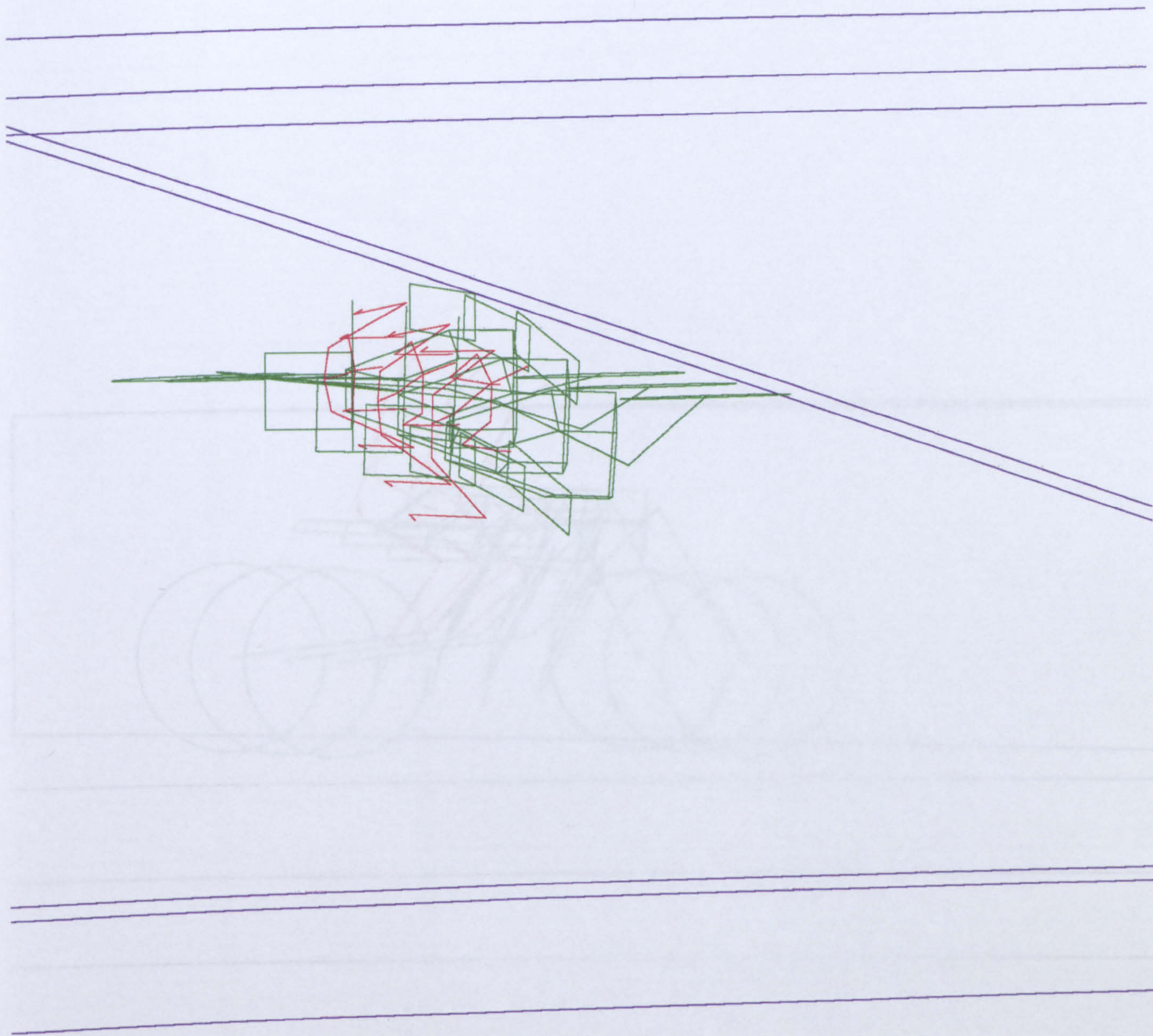


Figure 9.15a Plan view of Run 9

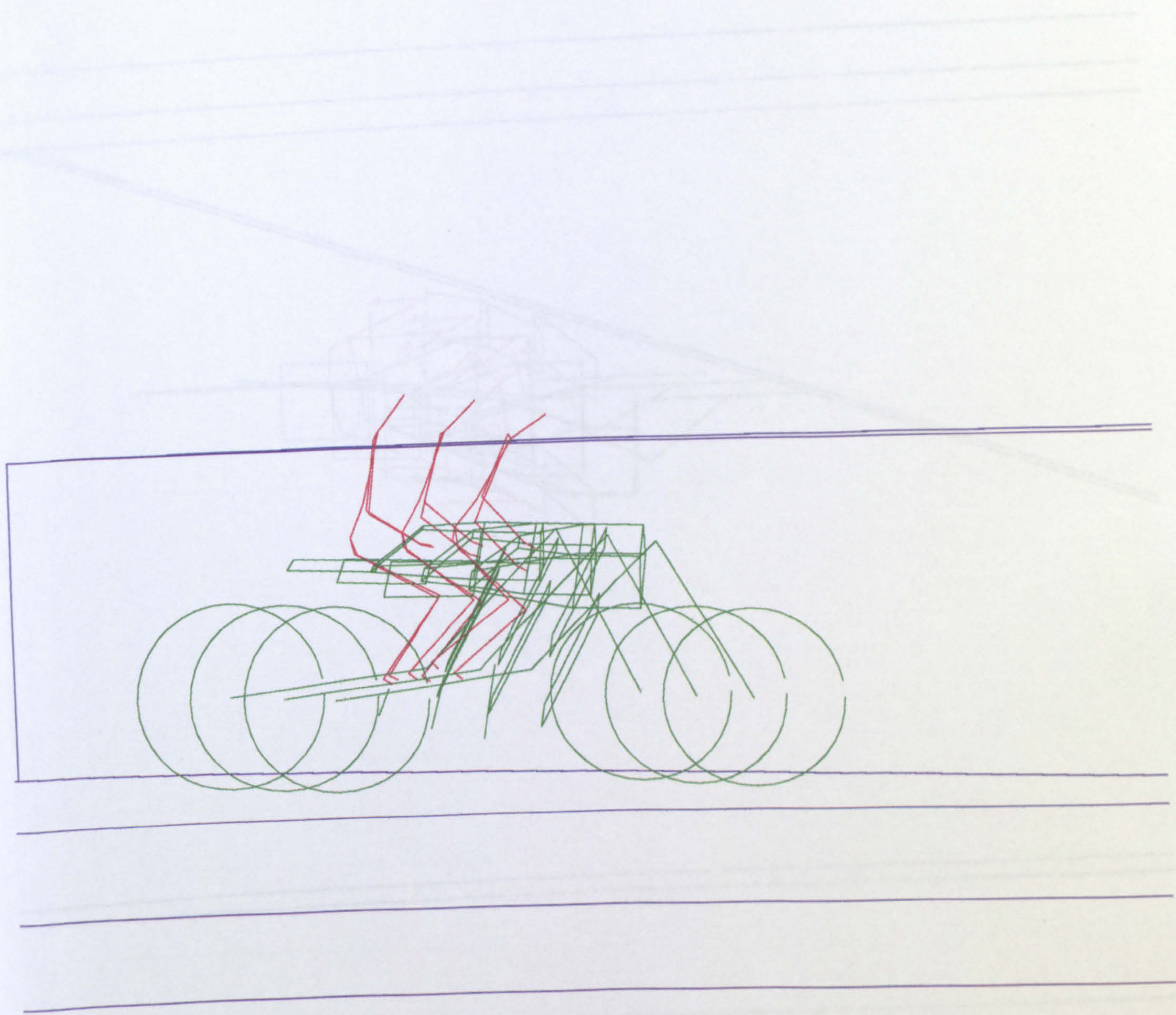


Figure 9.15b Elevation view of Run 9

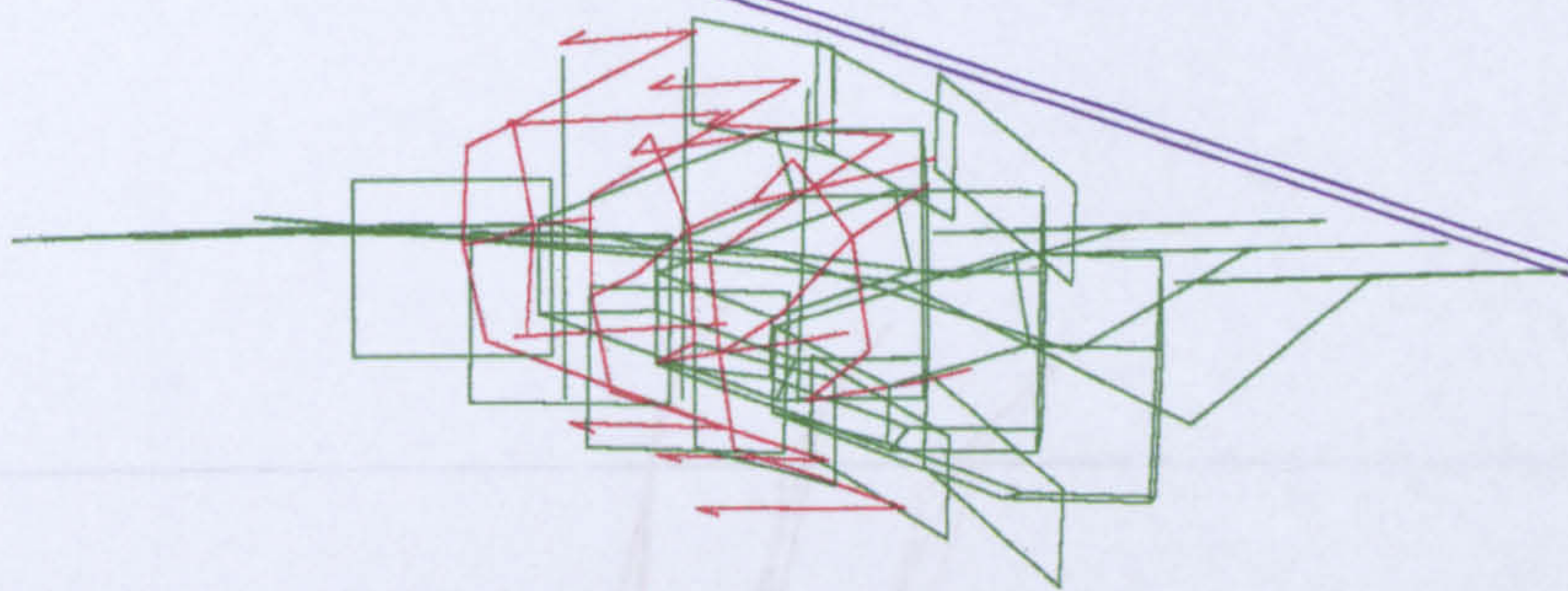


Figure 9.16a Plan view of Run 10

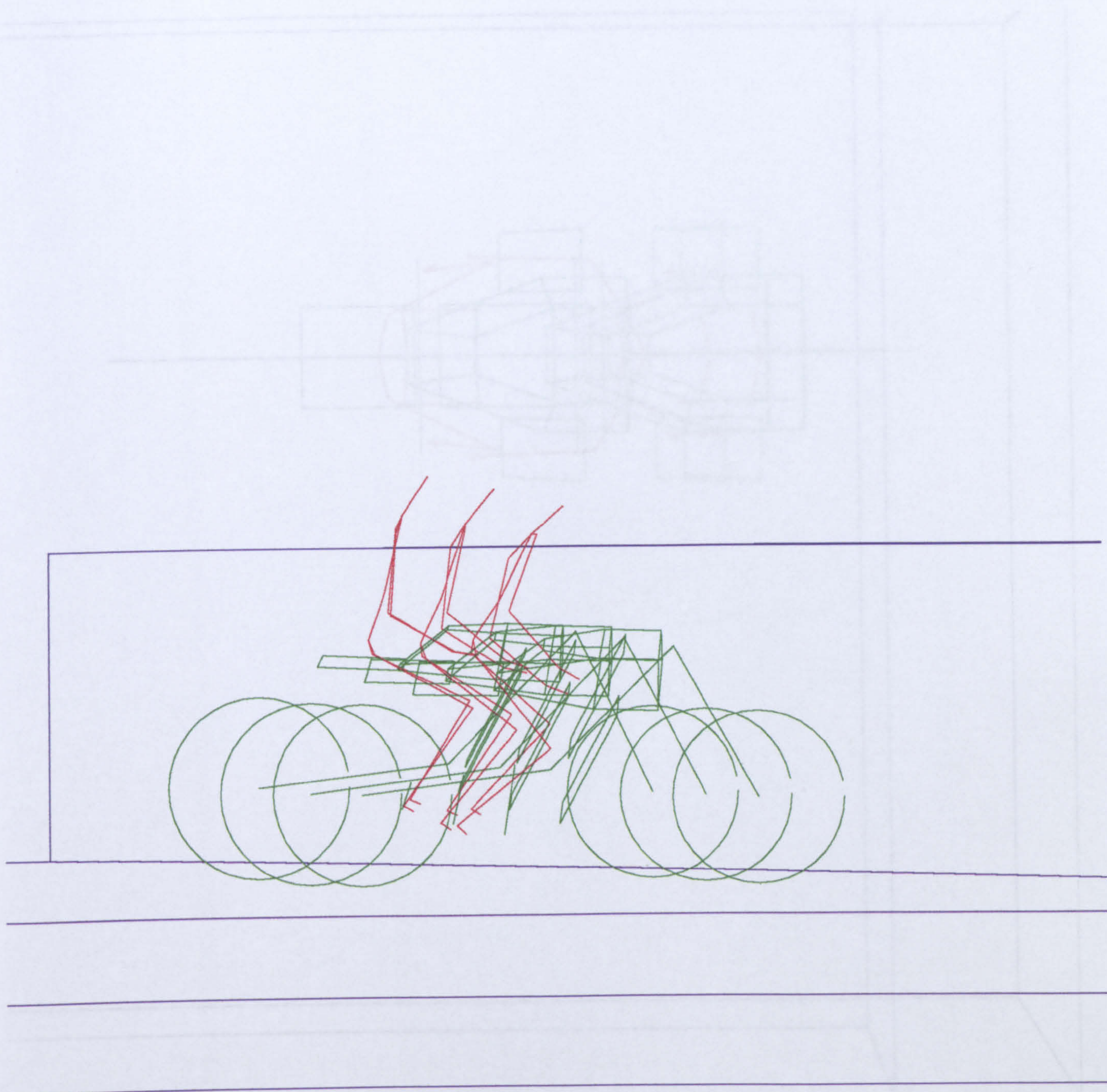


Figure 9.16b Elevation view of Run 10

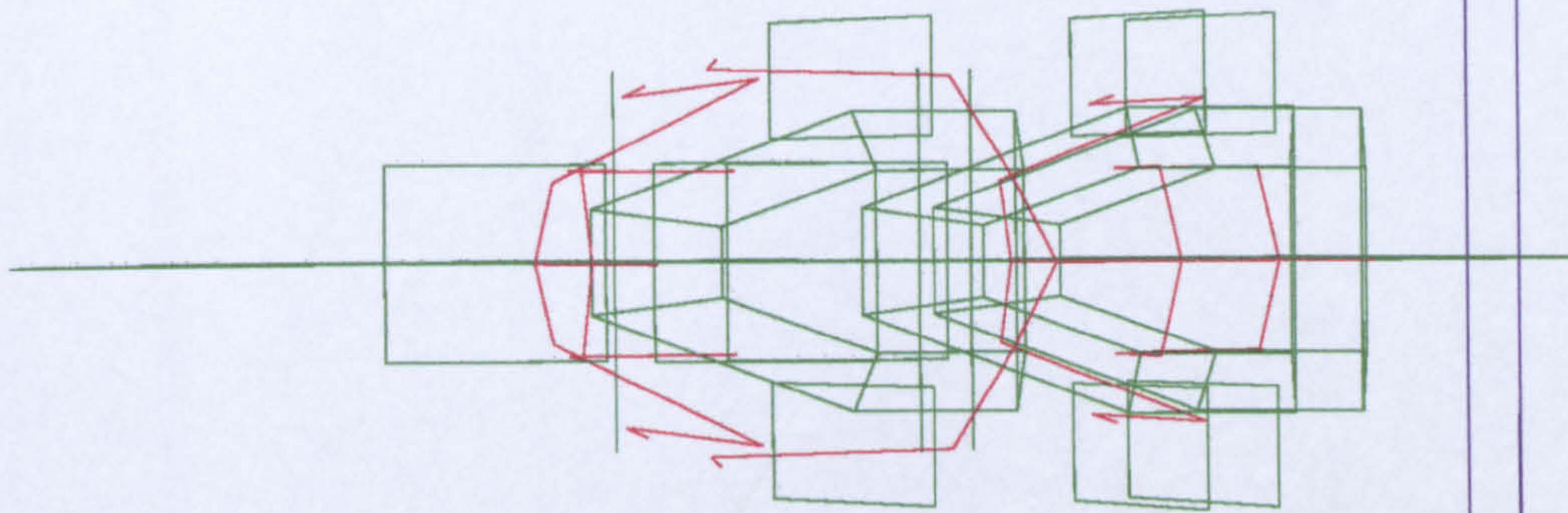


Figure 9.17a Plan view of Run 11

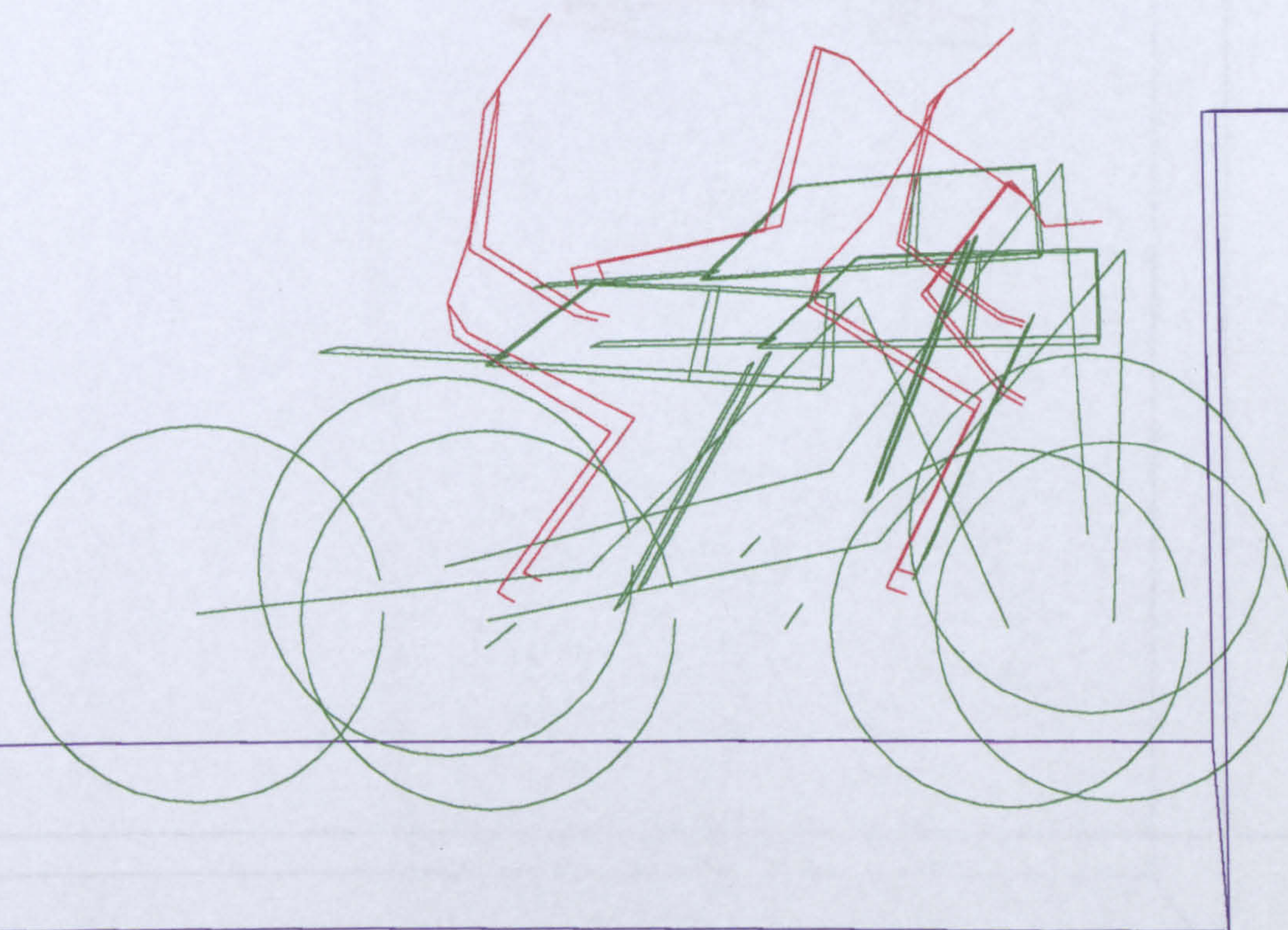


Figure 9.17b Elevation view of Run 11

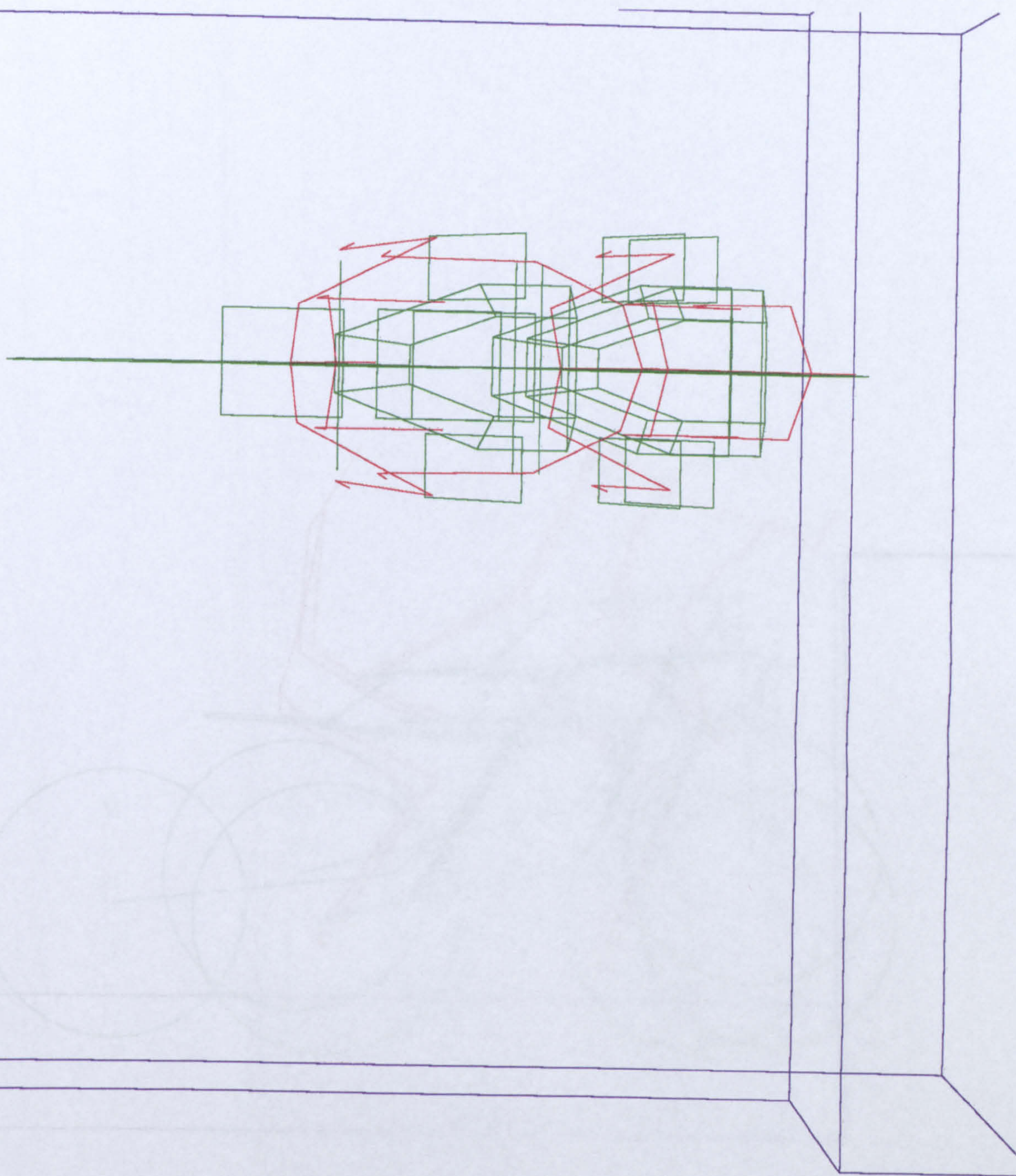


Figure 9.18a Plan view of Run 12

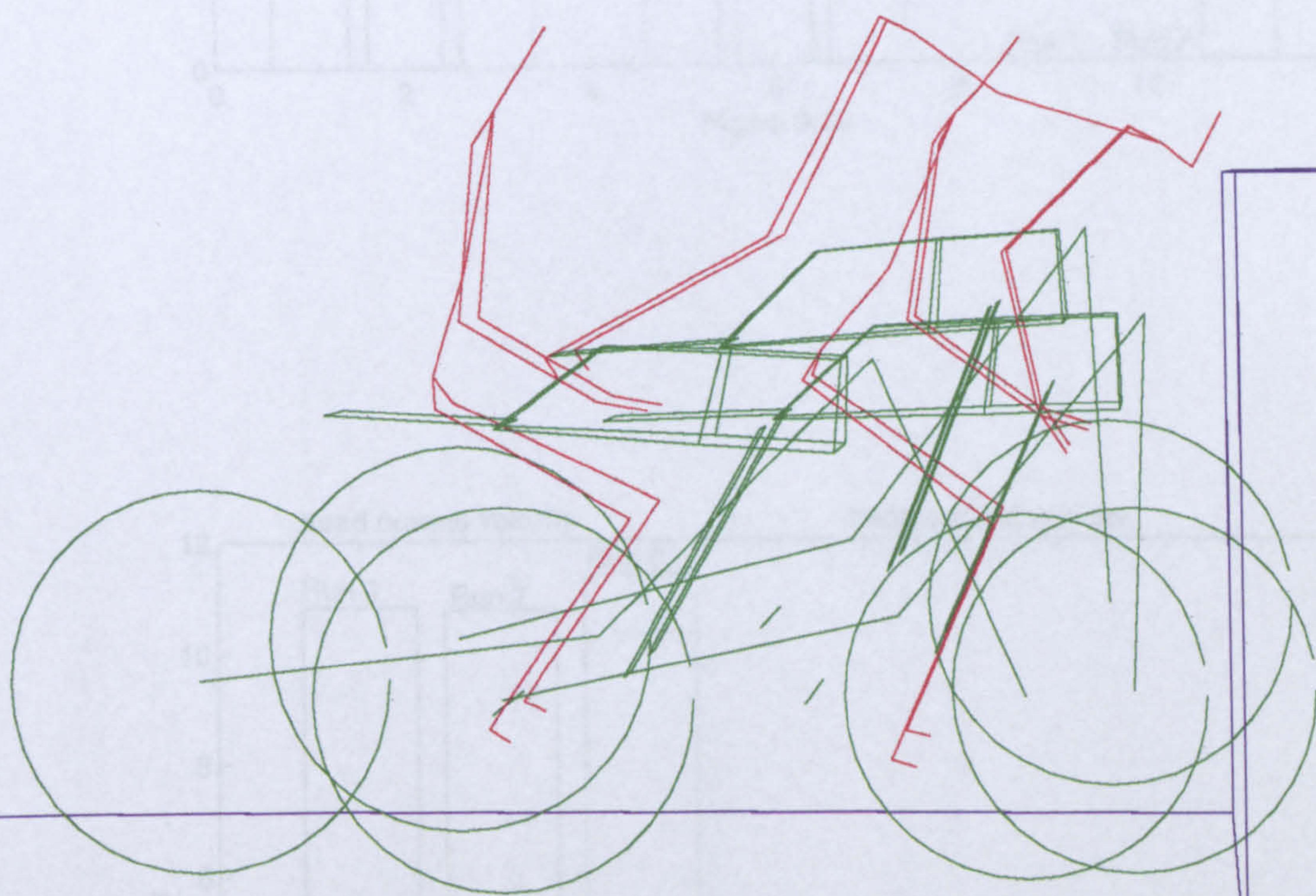
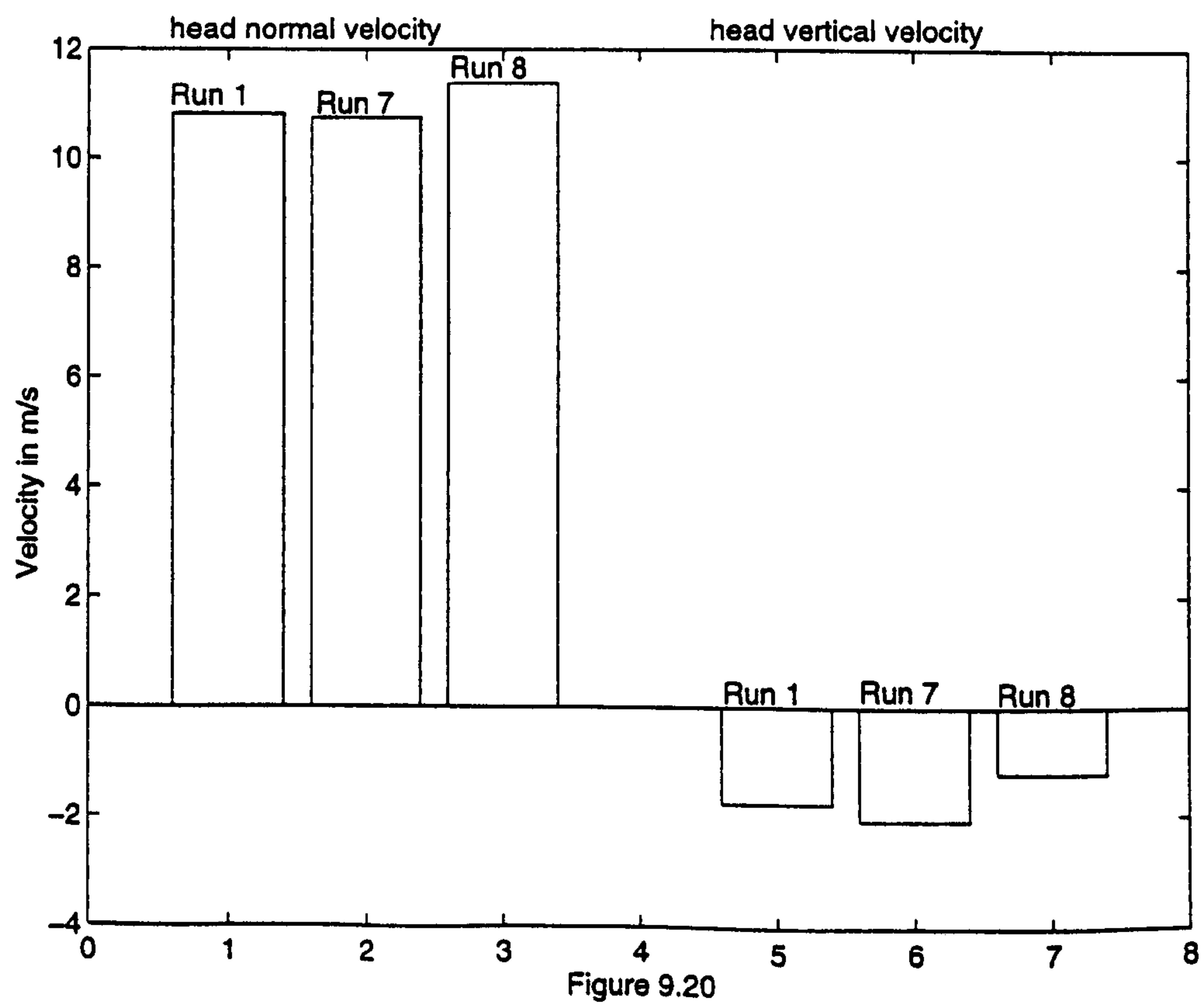
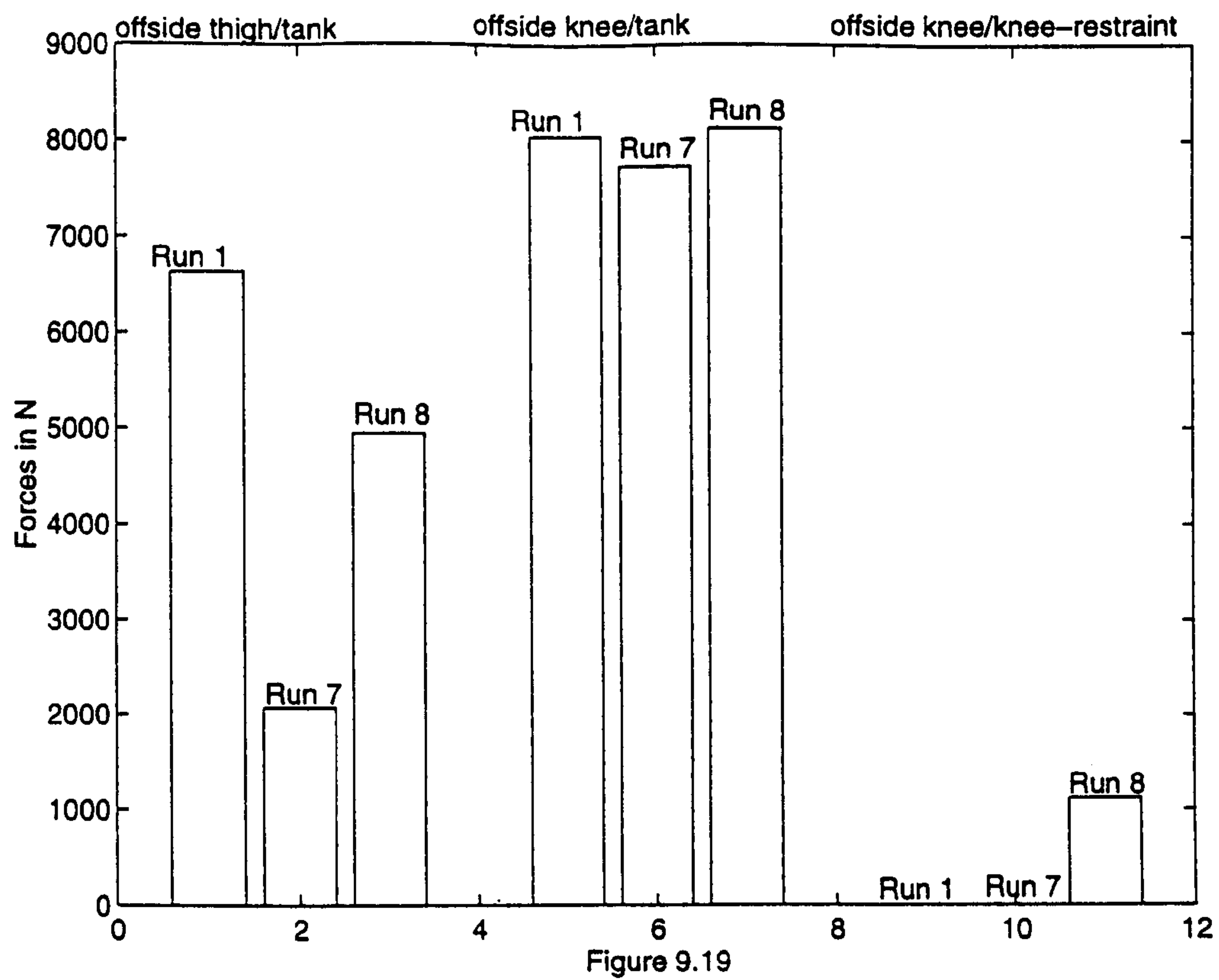
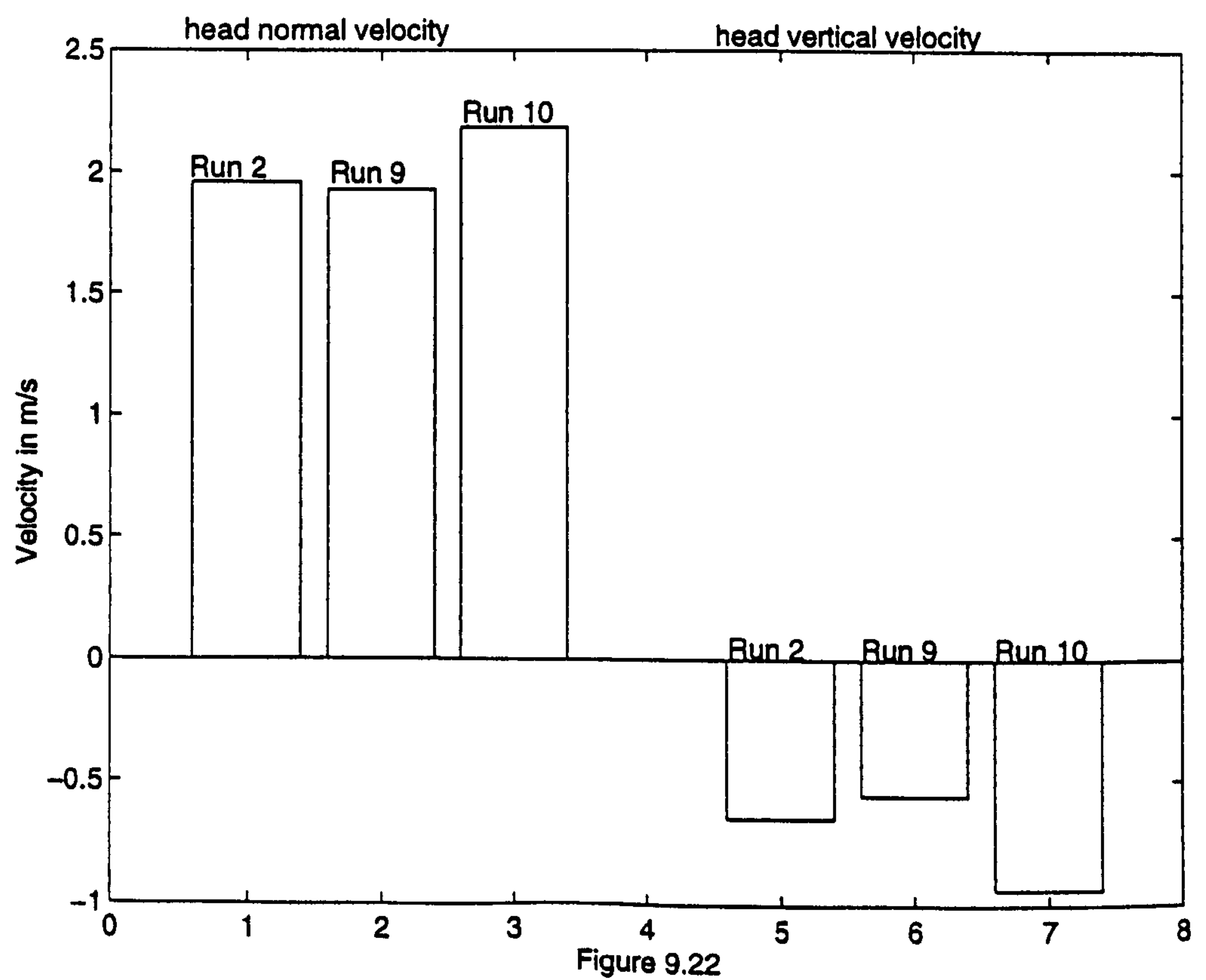
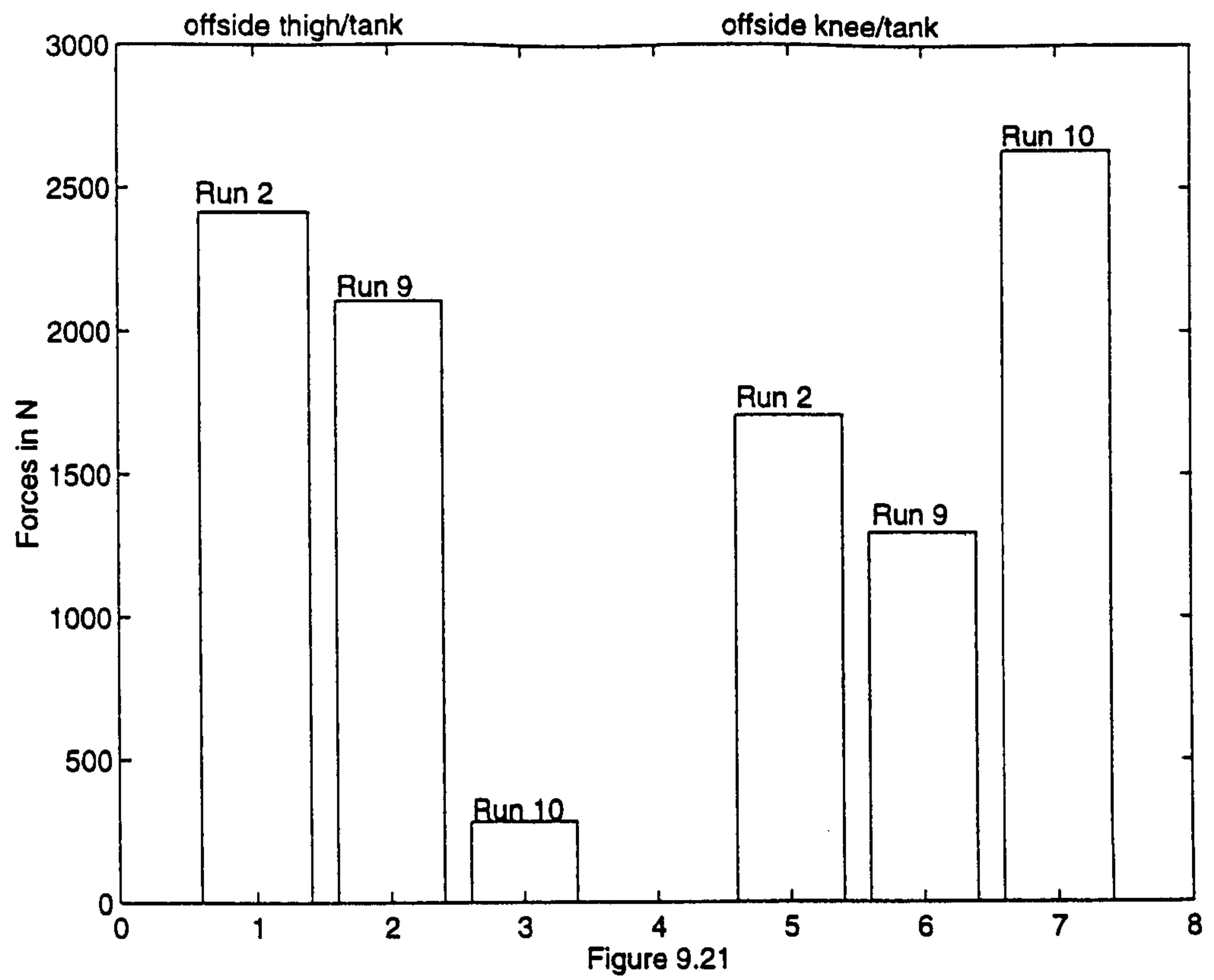
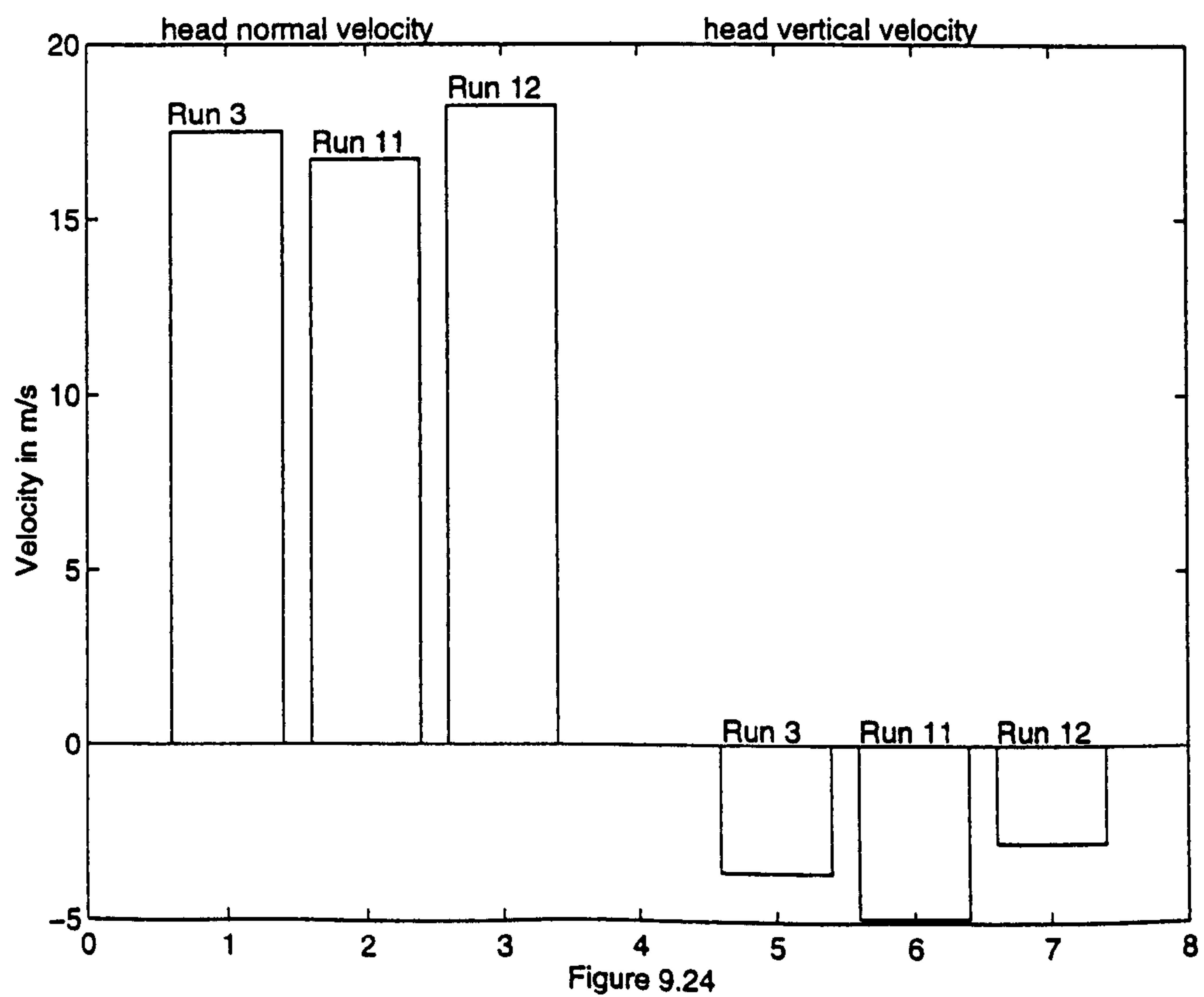
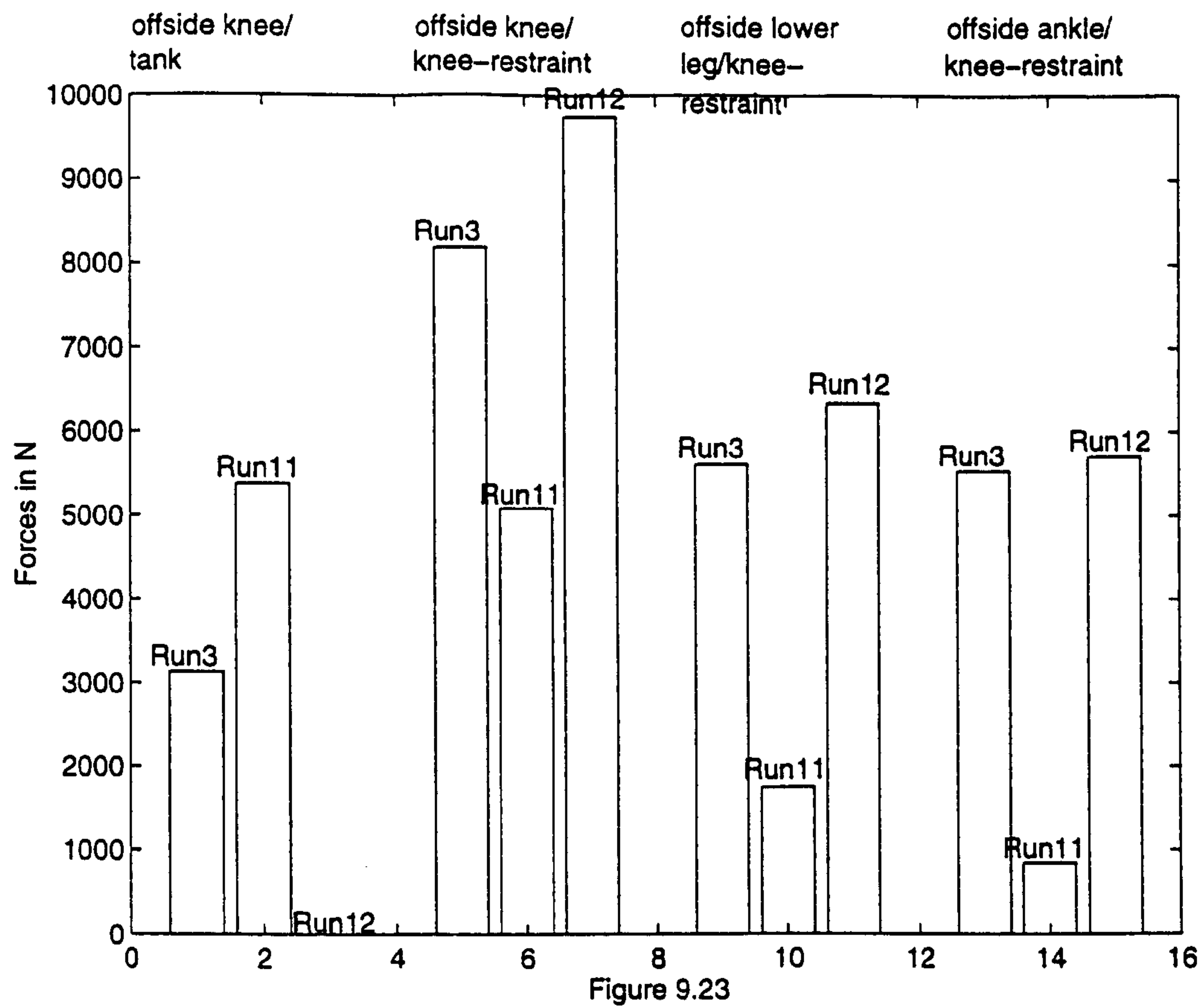


Figure 9.18b Elevation view of Run 12







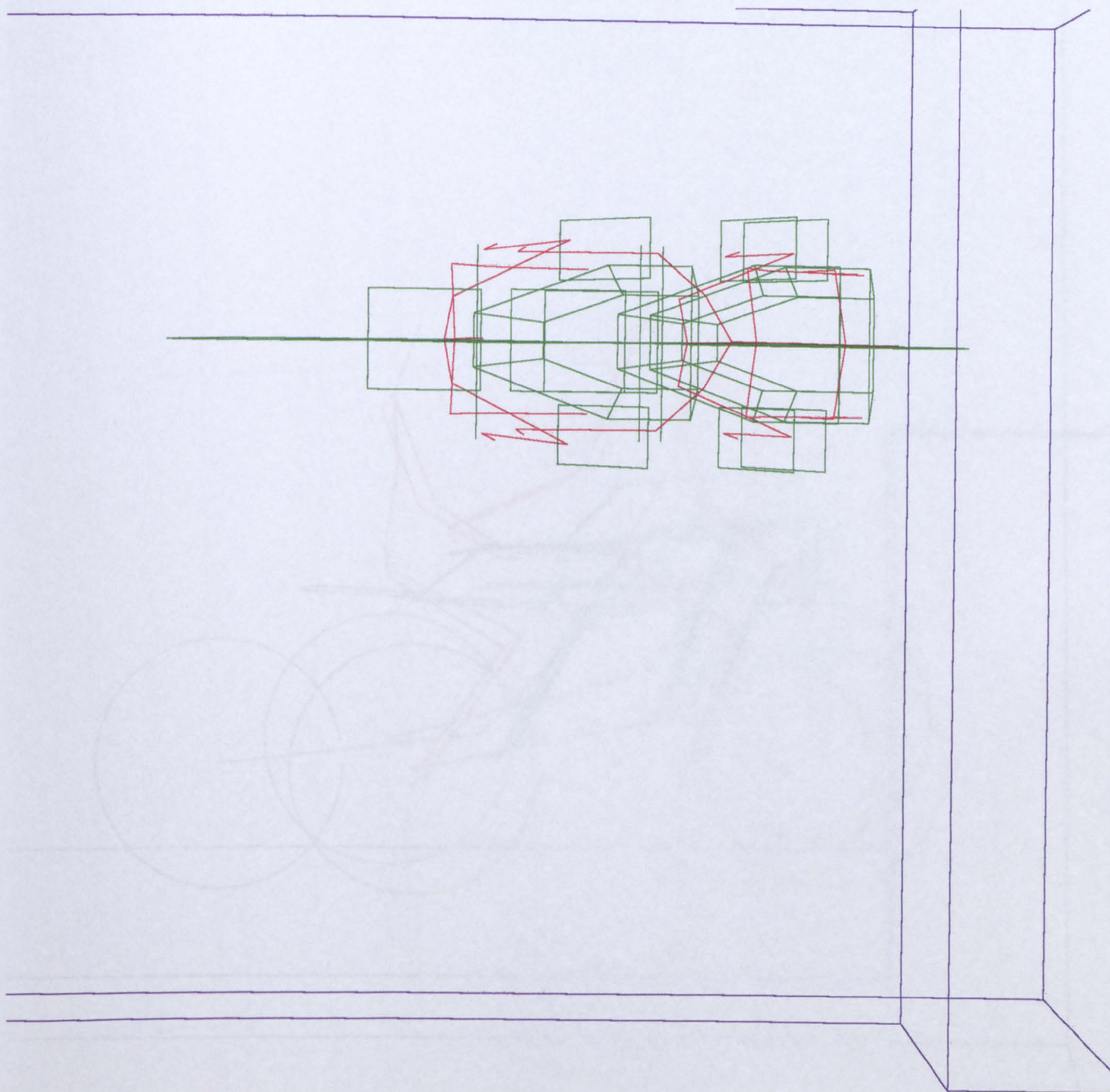


Figure 9.25a Plan view of Run 13

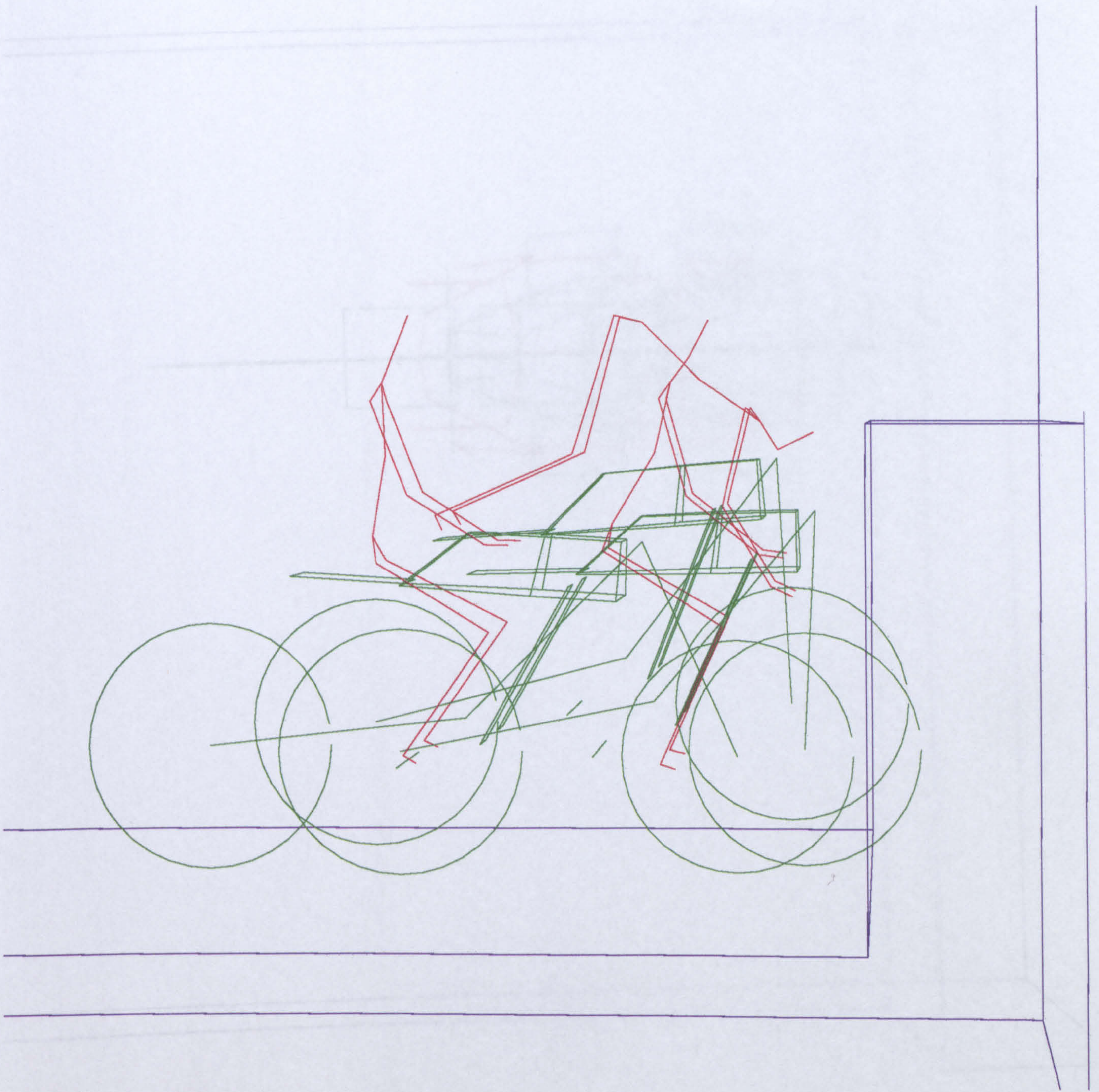


Figure 9.25b Elevation view of Run 13

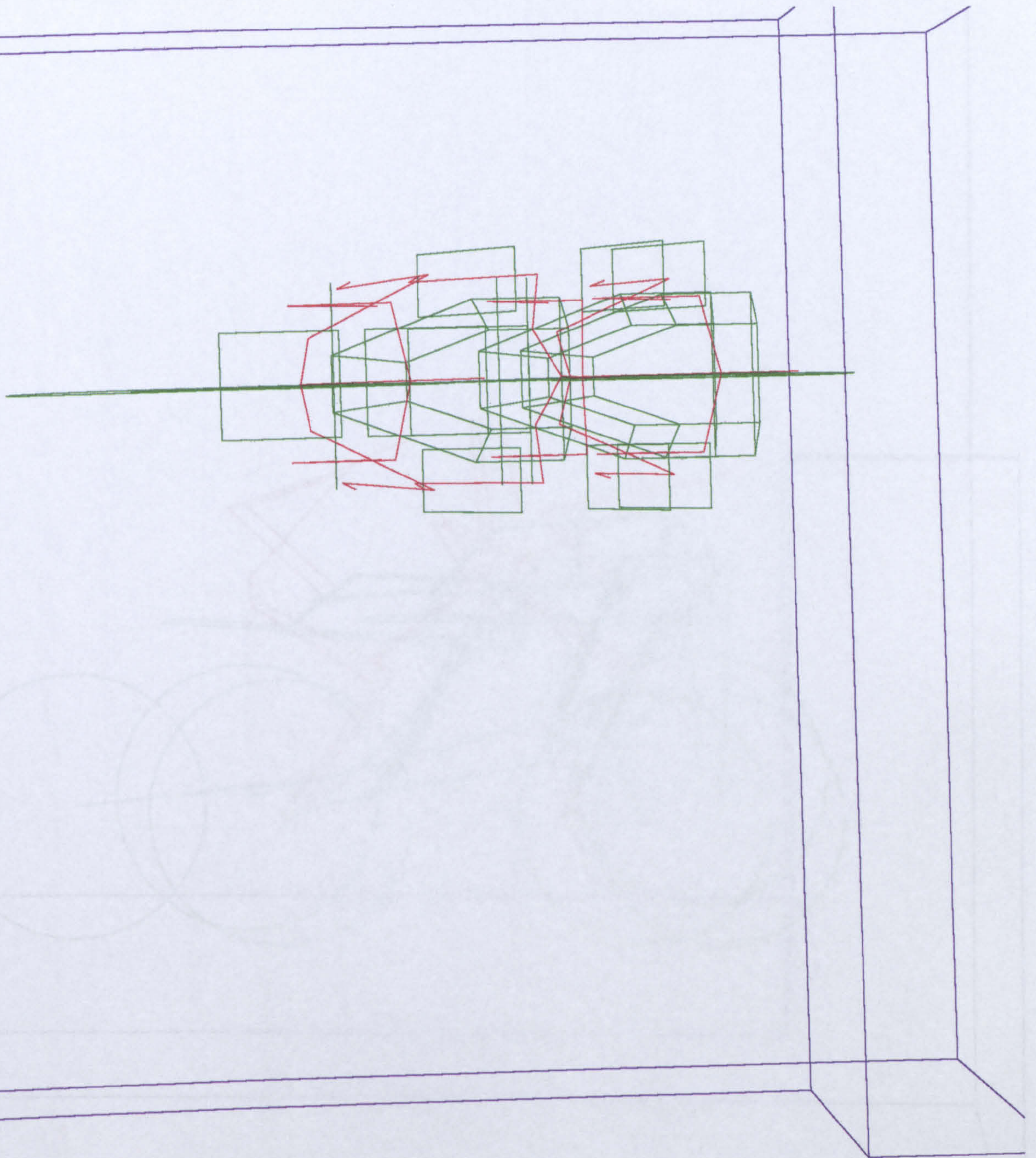


Figure 9.26a Plan view of Run 14

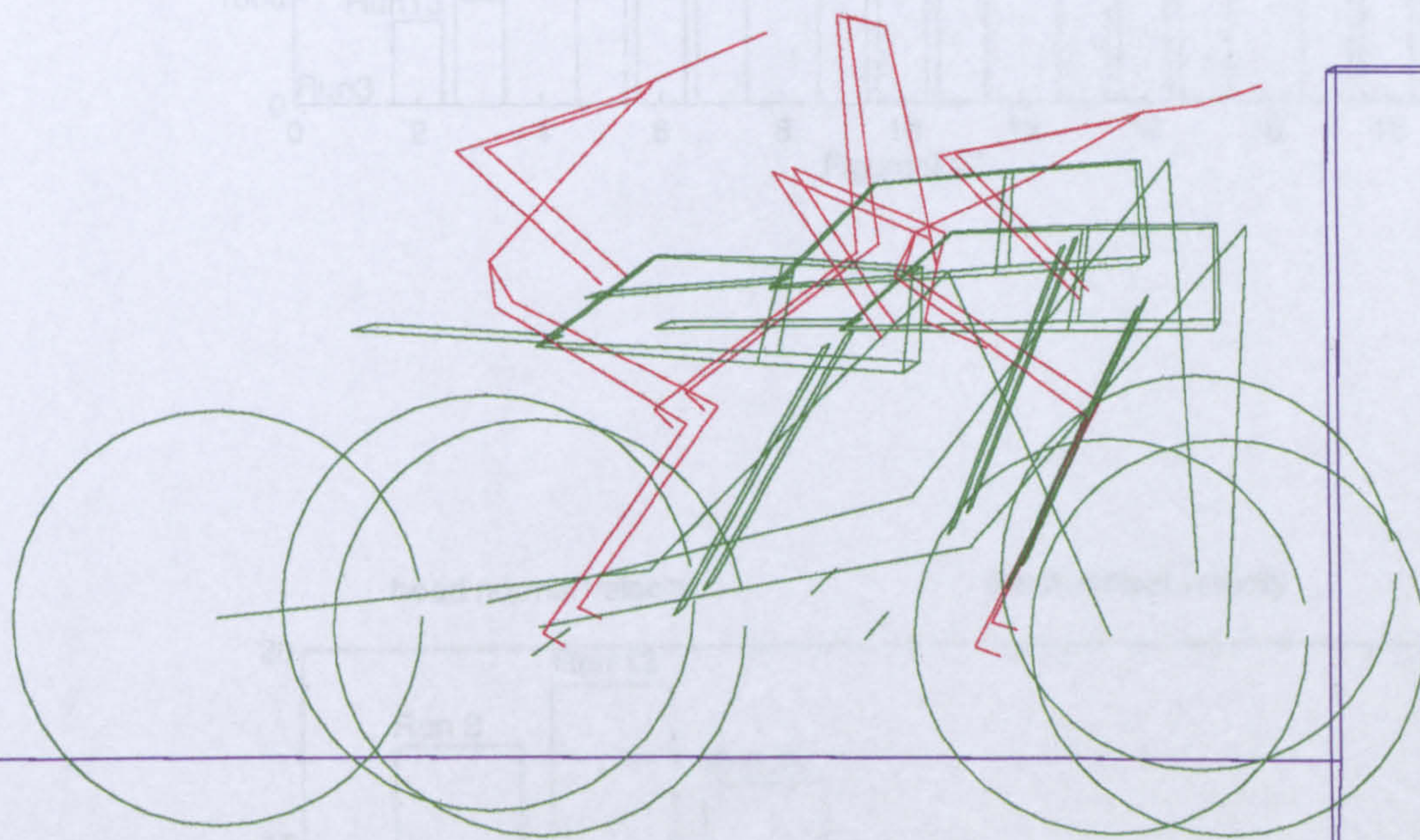
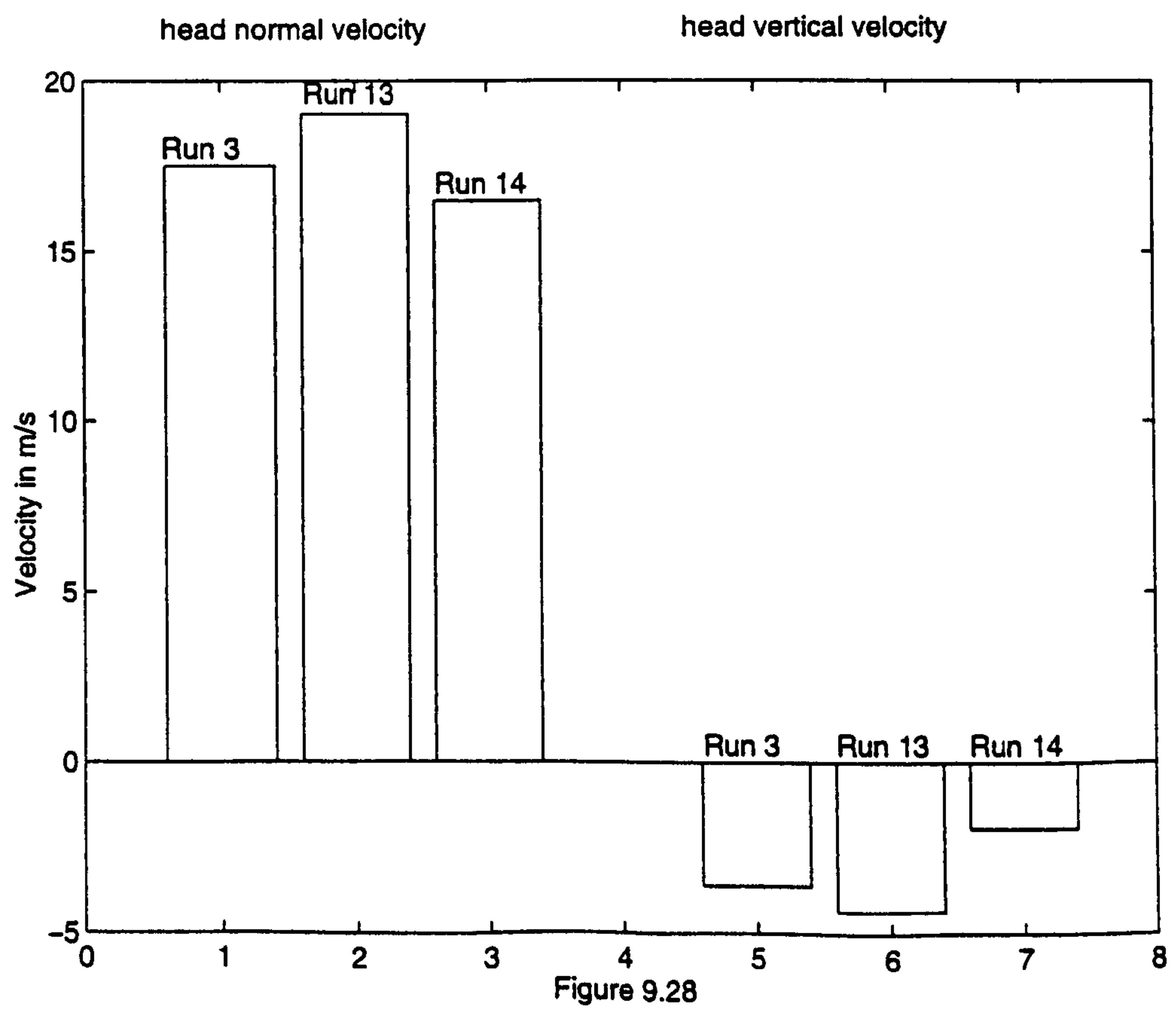
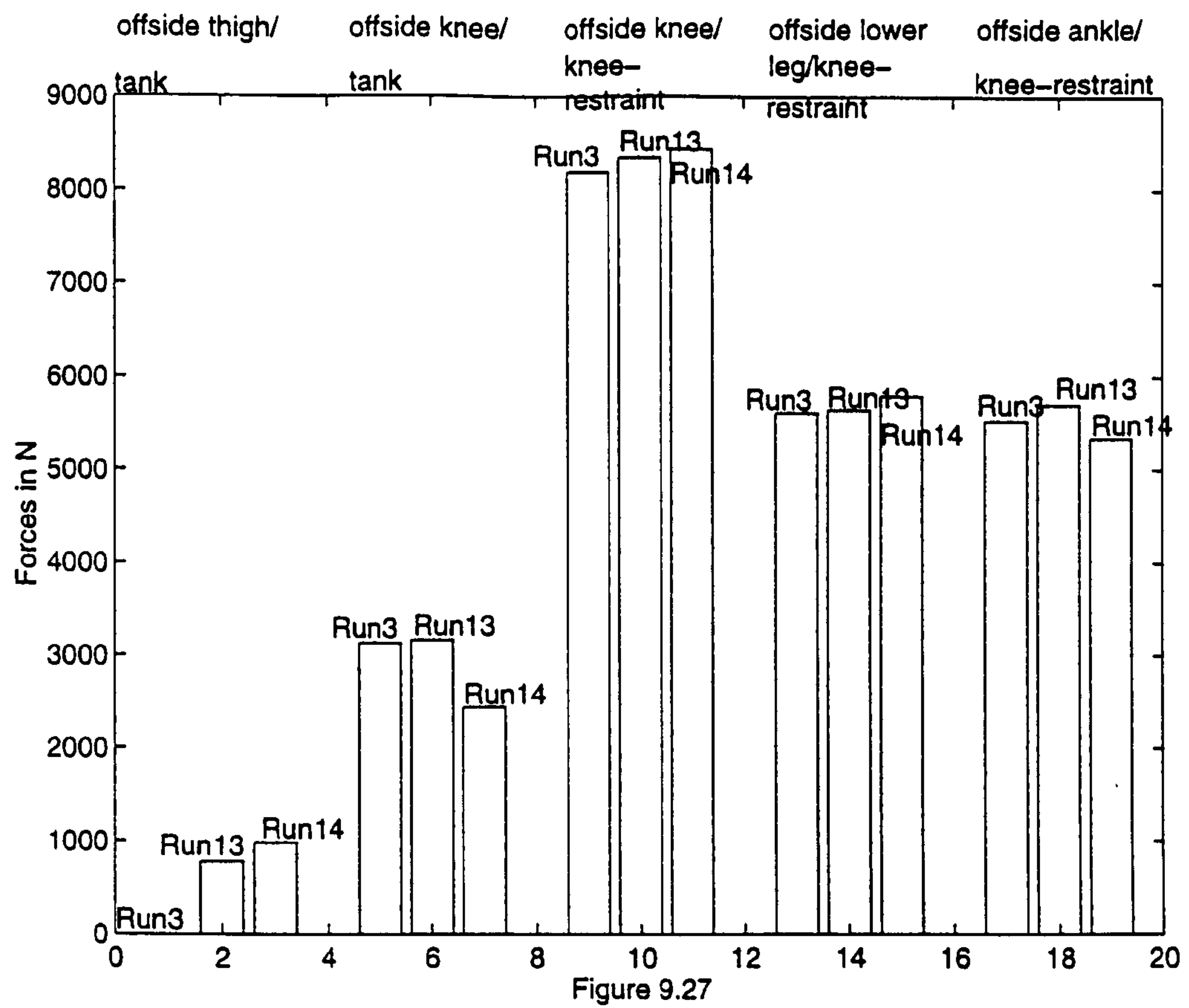


Figure 9.26b Elevation view of Run 14



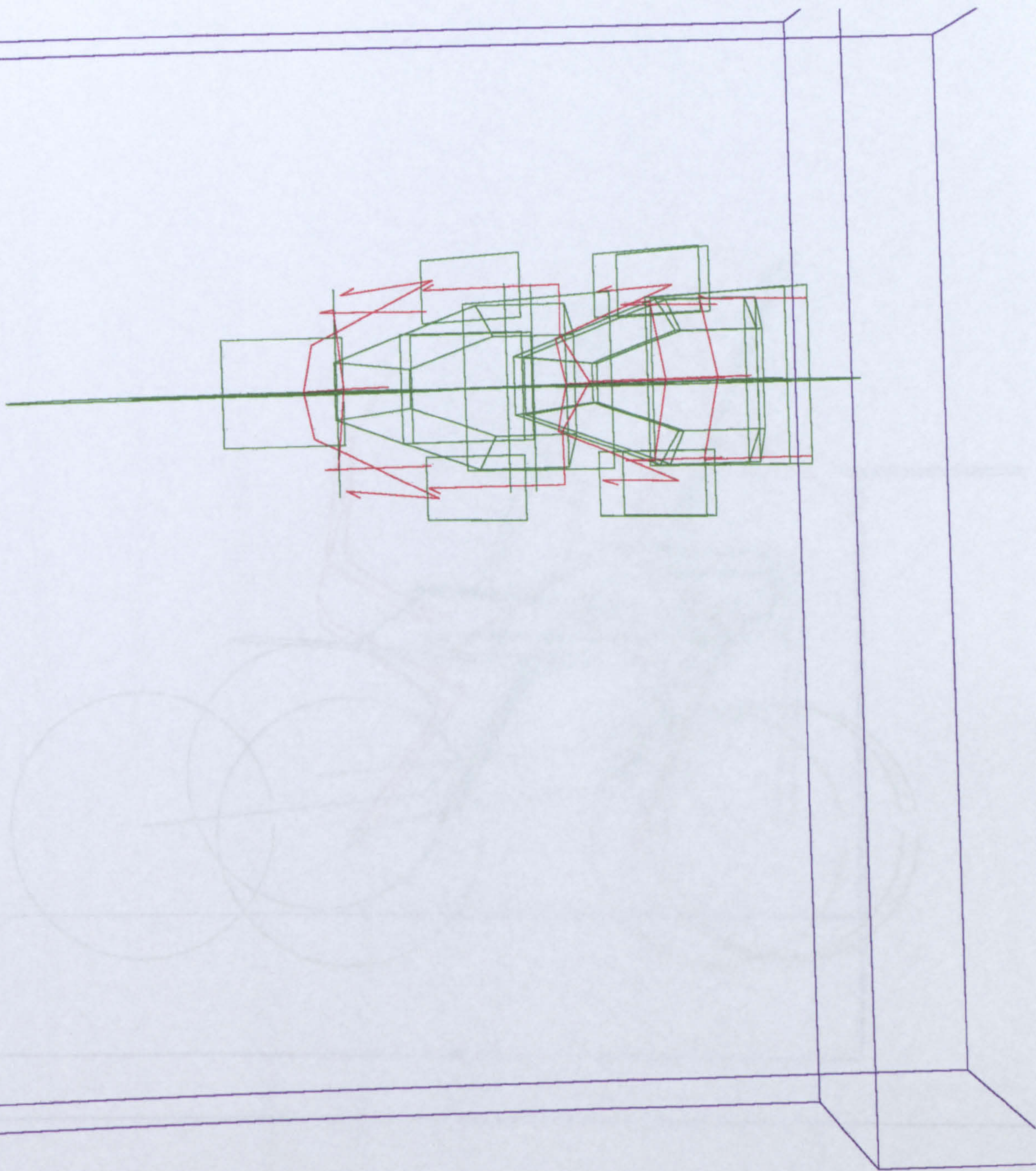


Figure 9.29a Plan view of Run 15

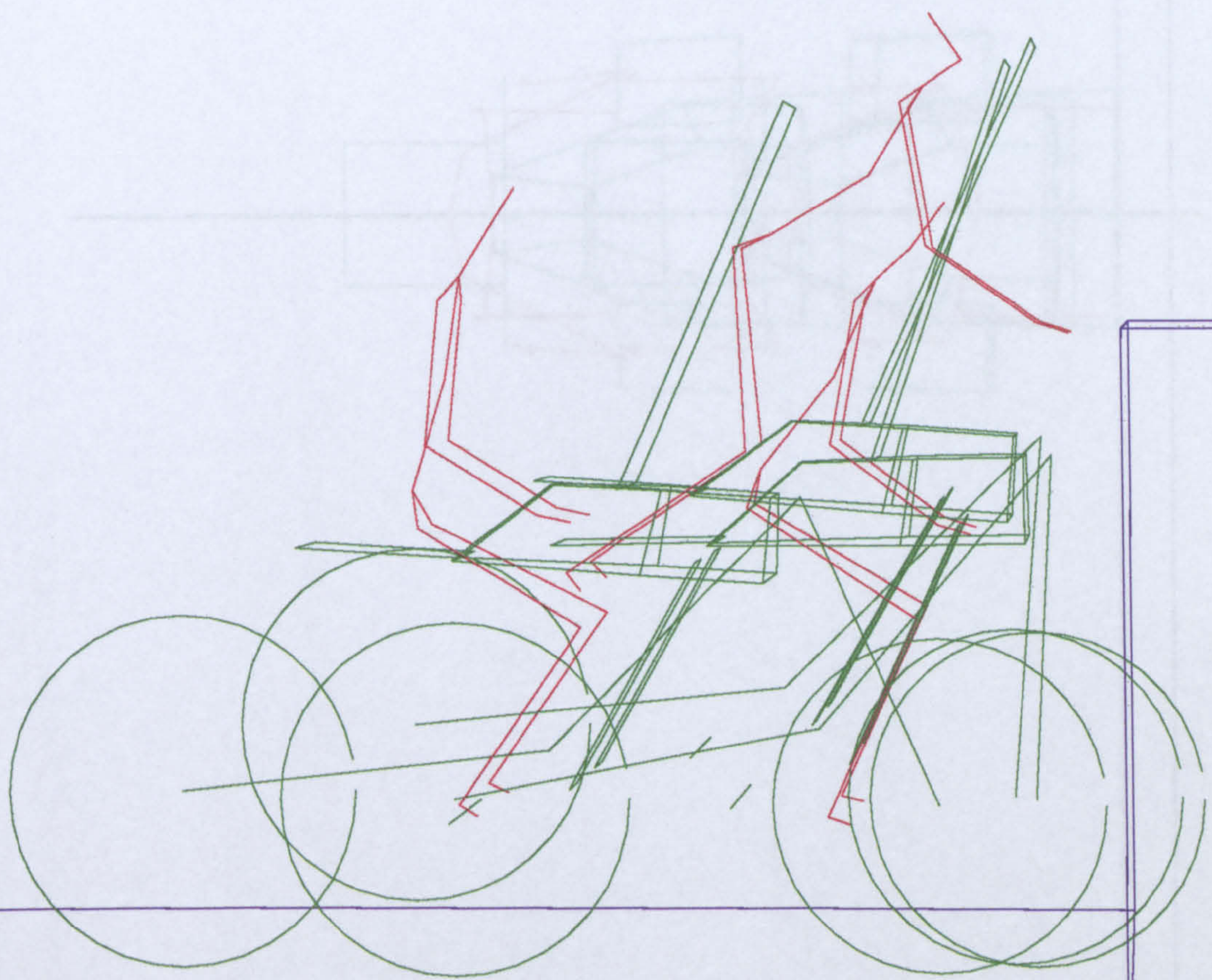


Figure 9.29b Elevation view of Run 15

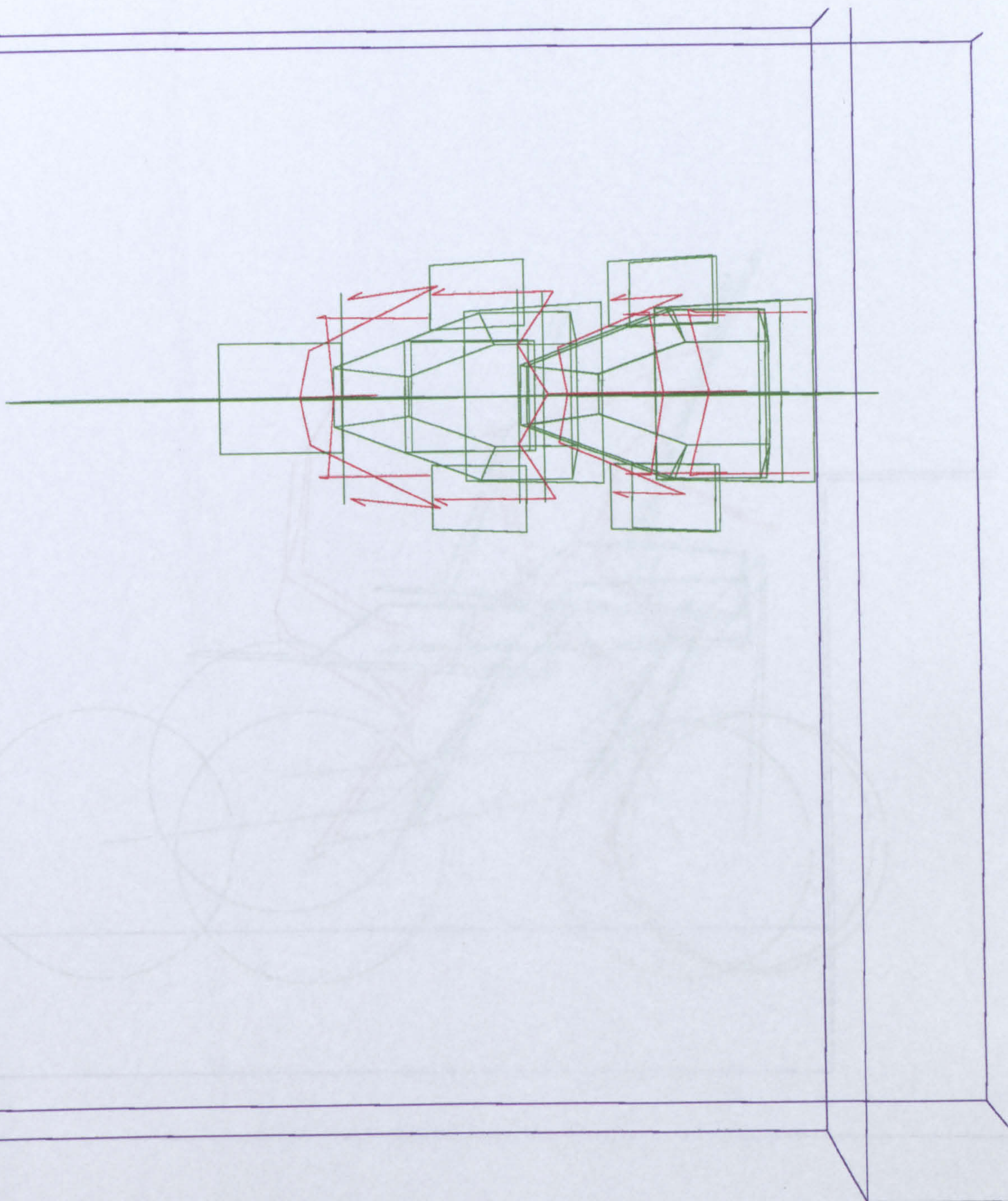


Figure 9.30a Plan view of Run 16

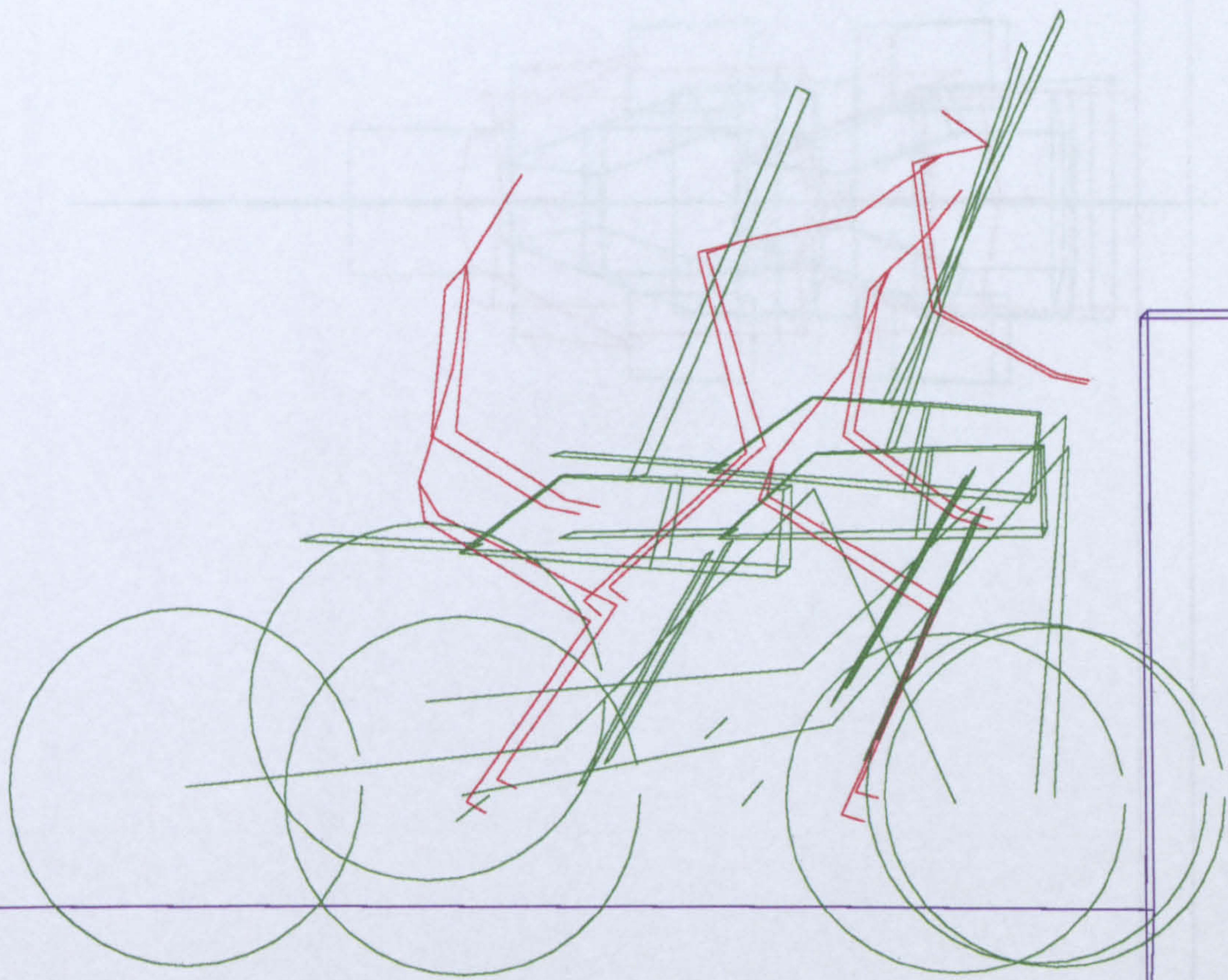


Figure 9.30b Elevation view of Run 16

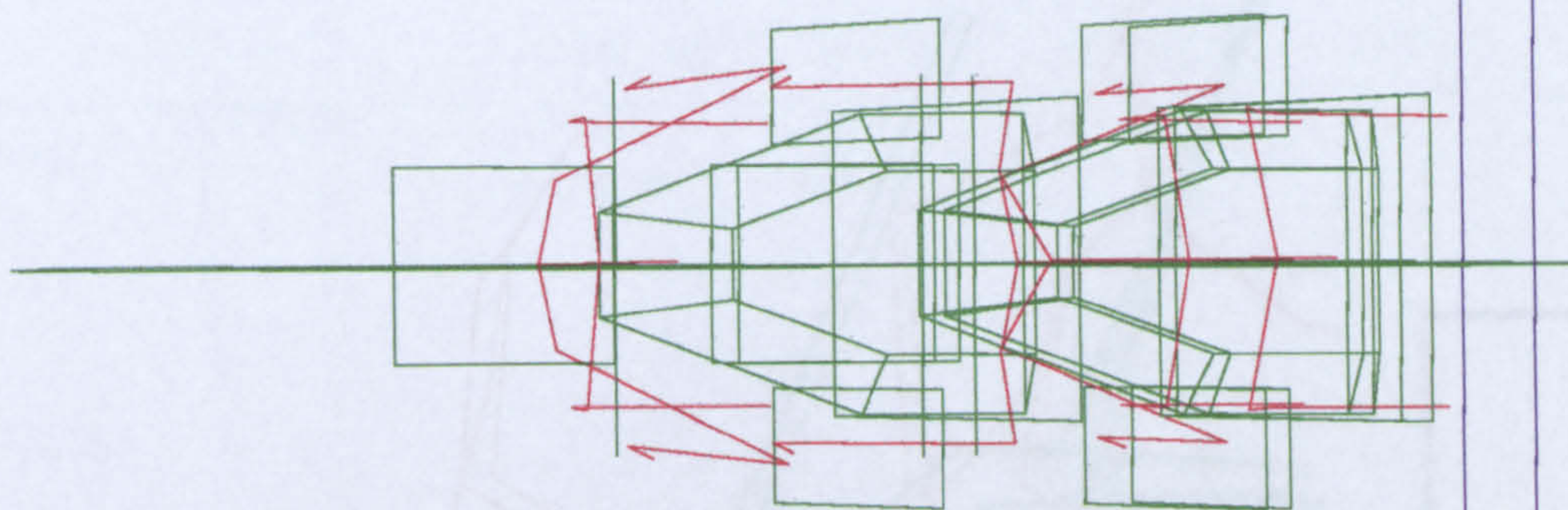


Figure 9.31a Plan view of Run 17

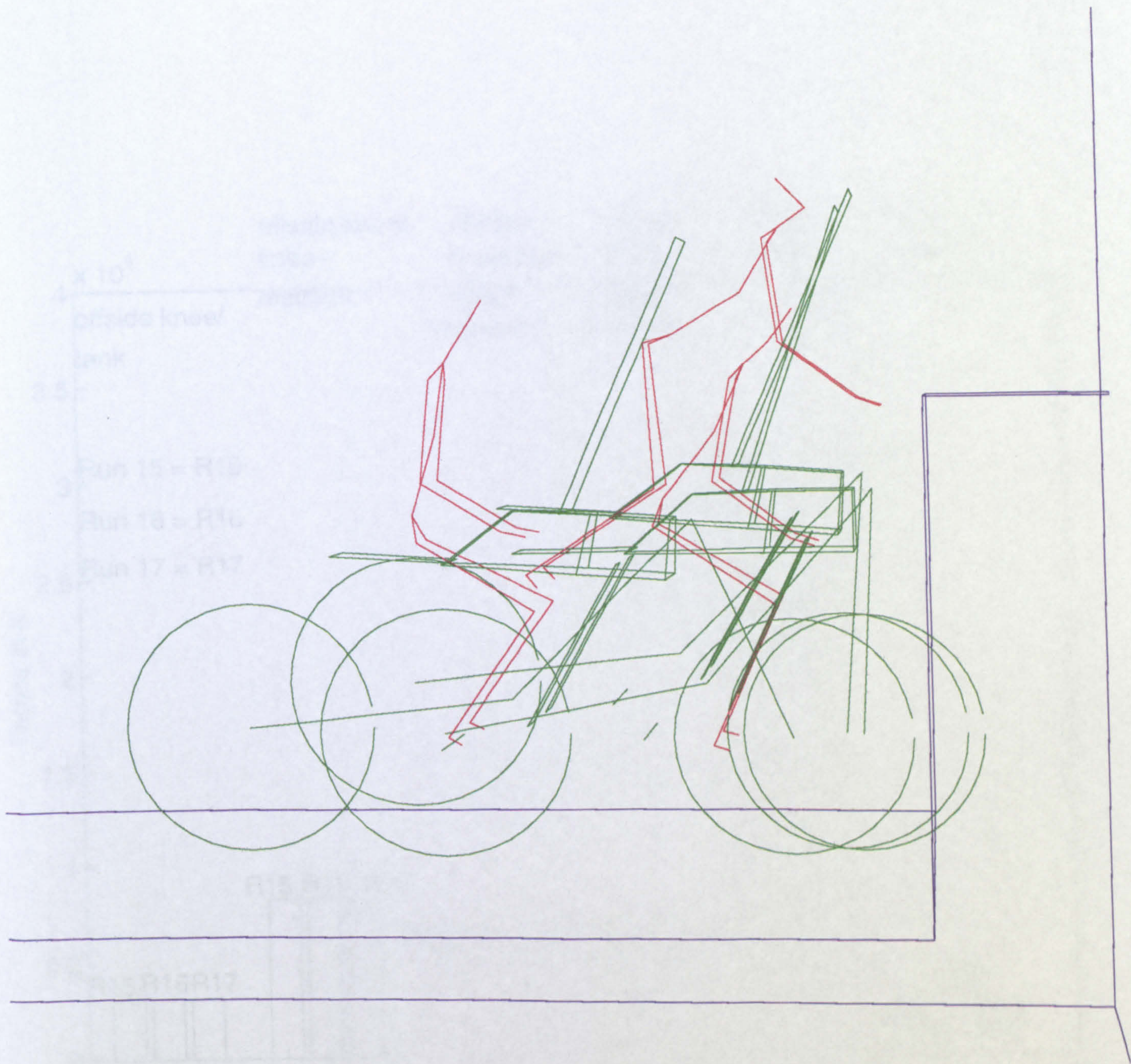


Figure 9.31b Elevation view of Run 17

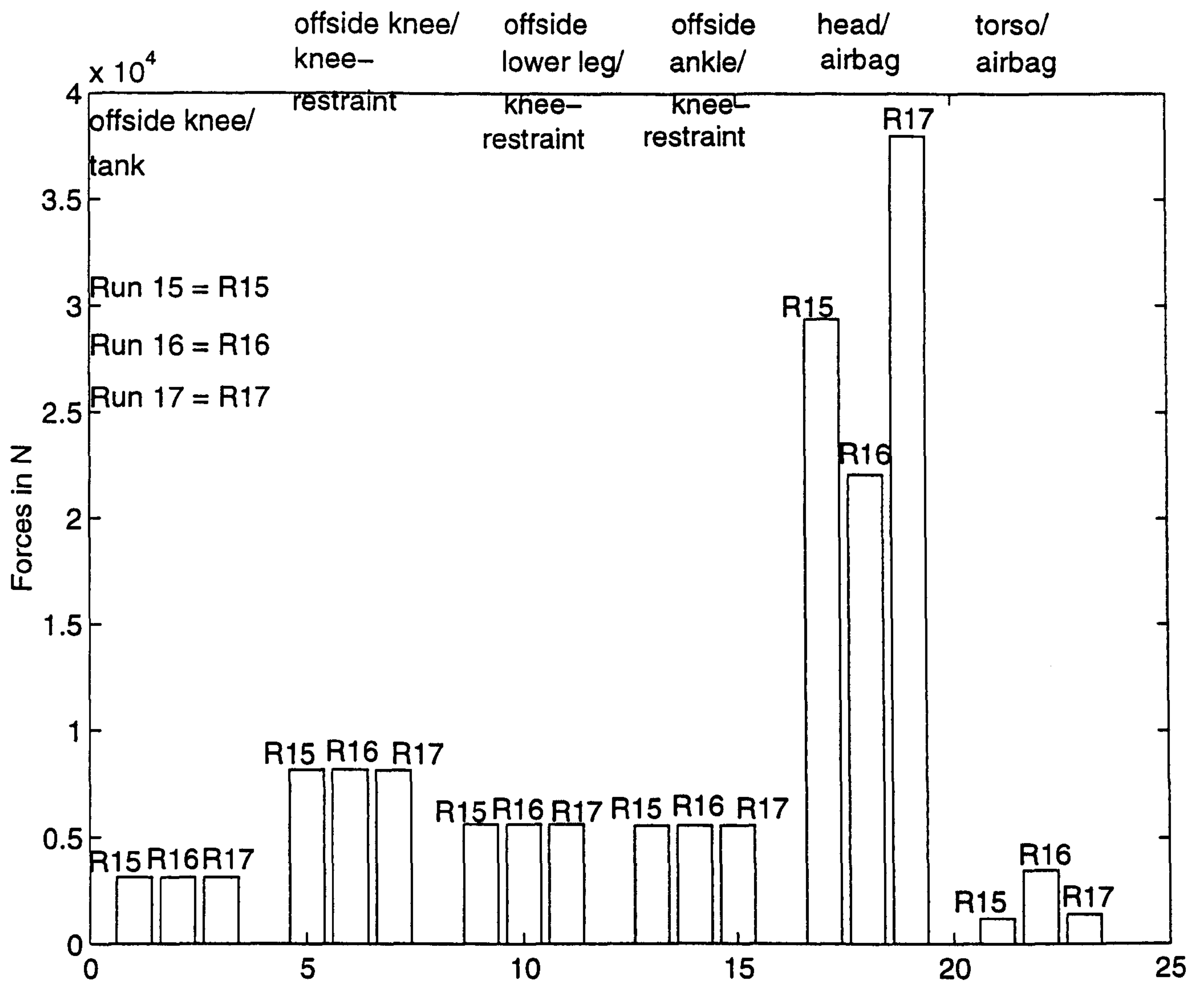


Figure 9.32

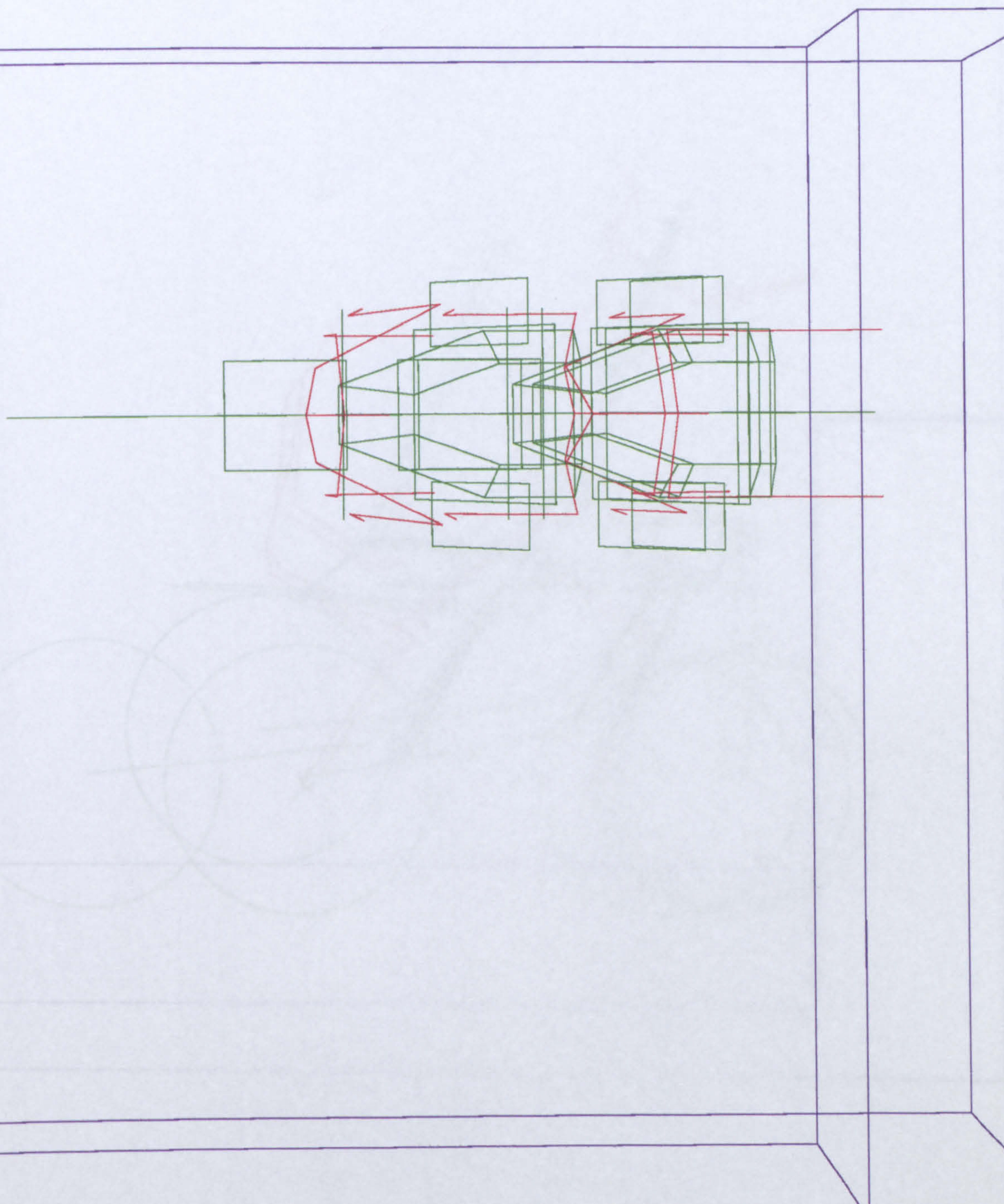


Figure 9.33a Plan view of Run 18

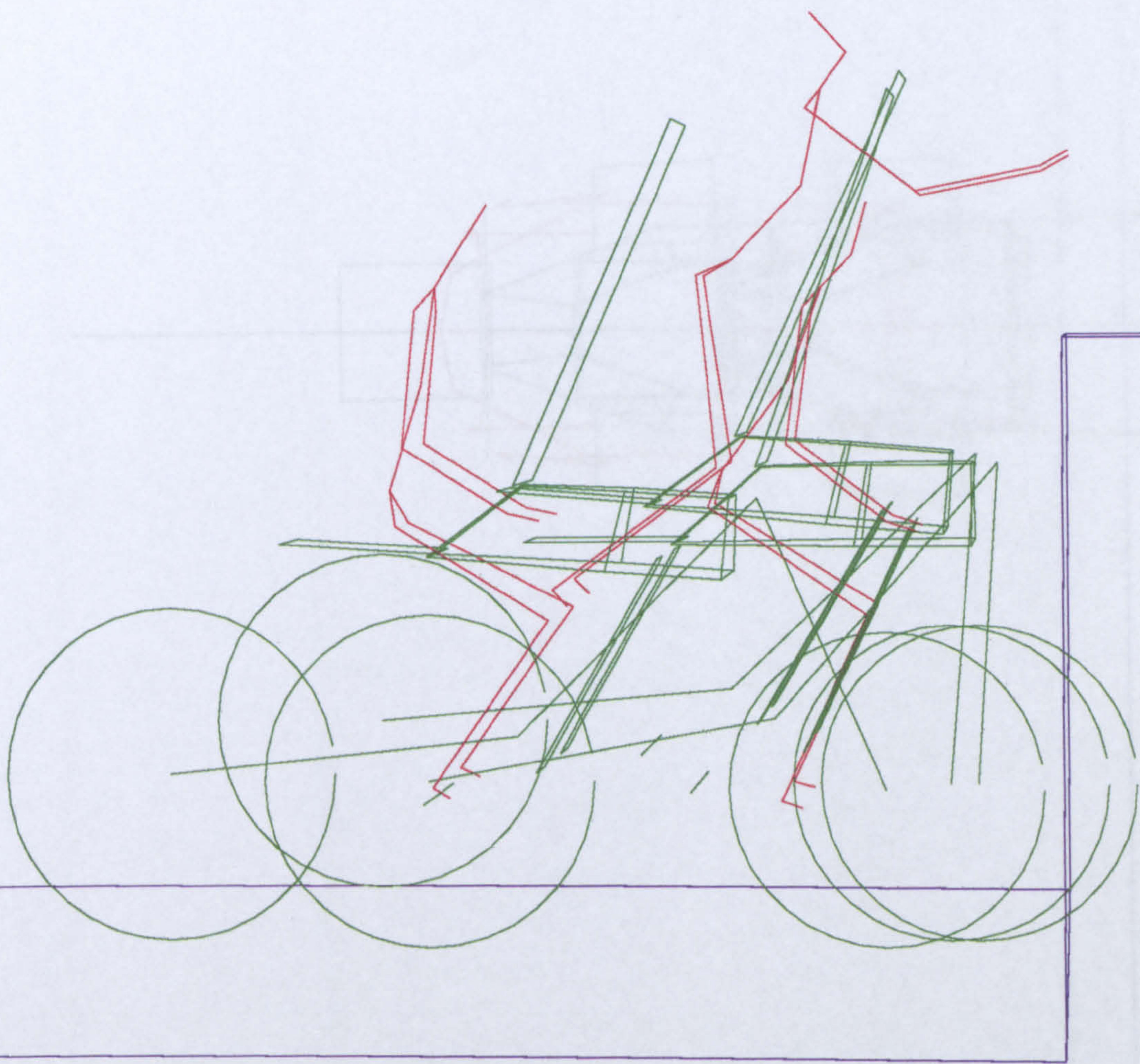


Figure 9.33b Elevation view of Run 18

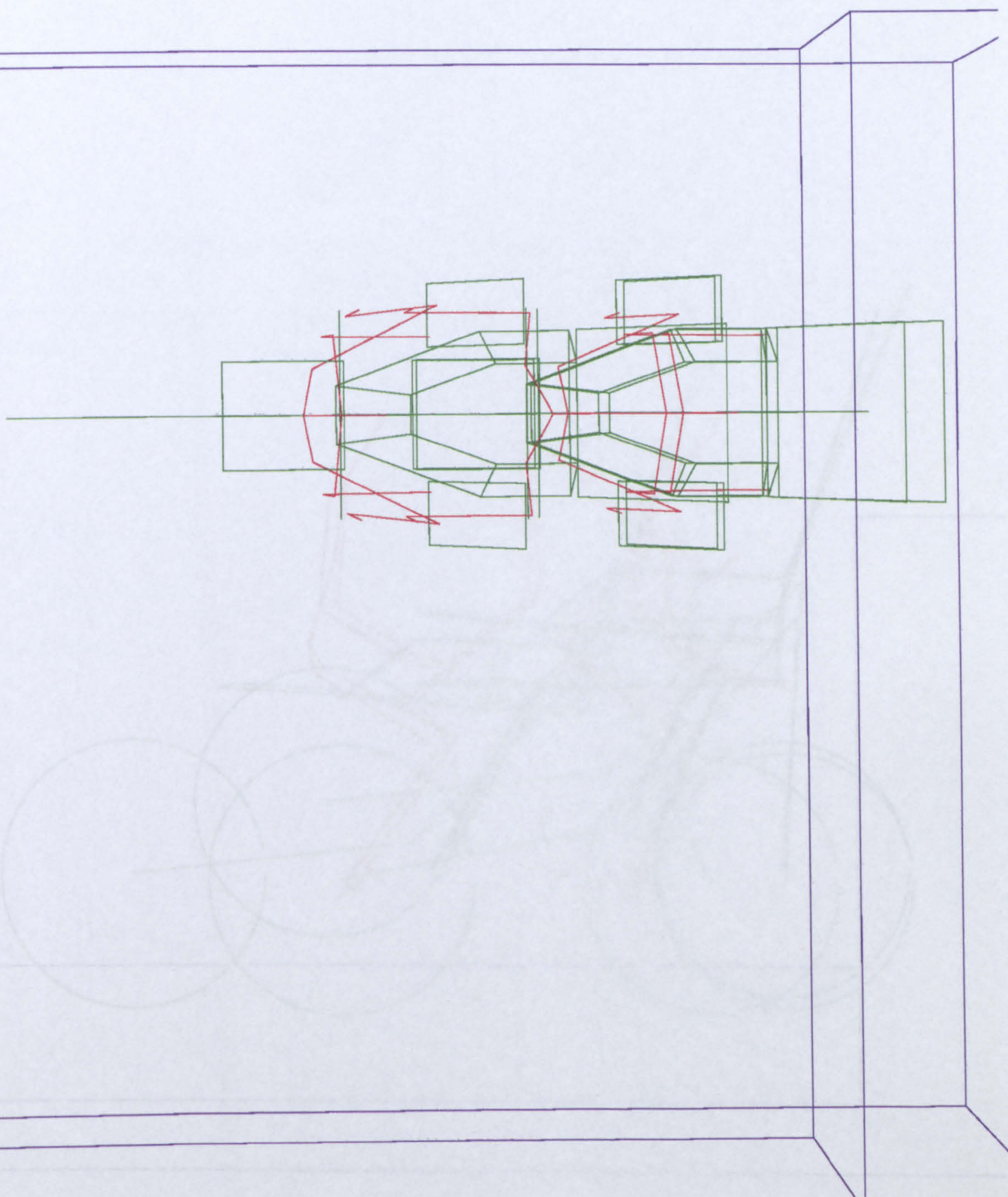


Figure 9.34a Plan view of Run 19

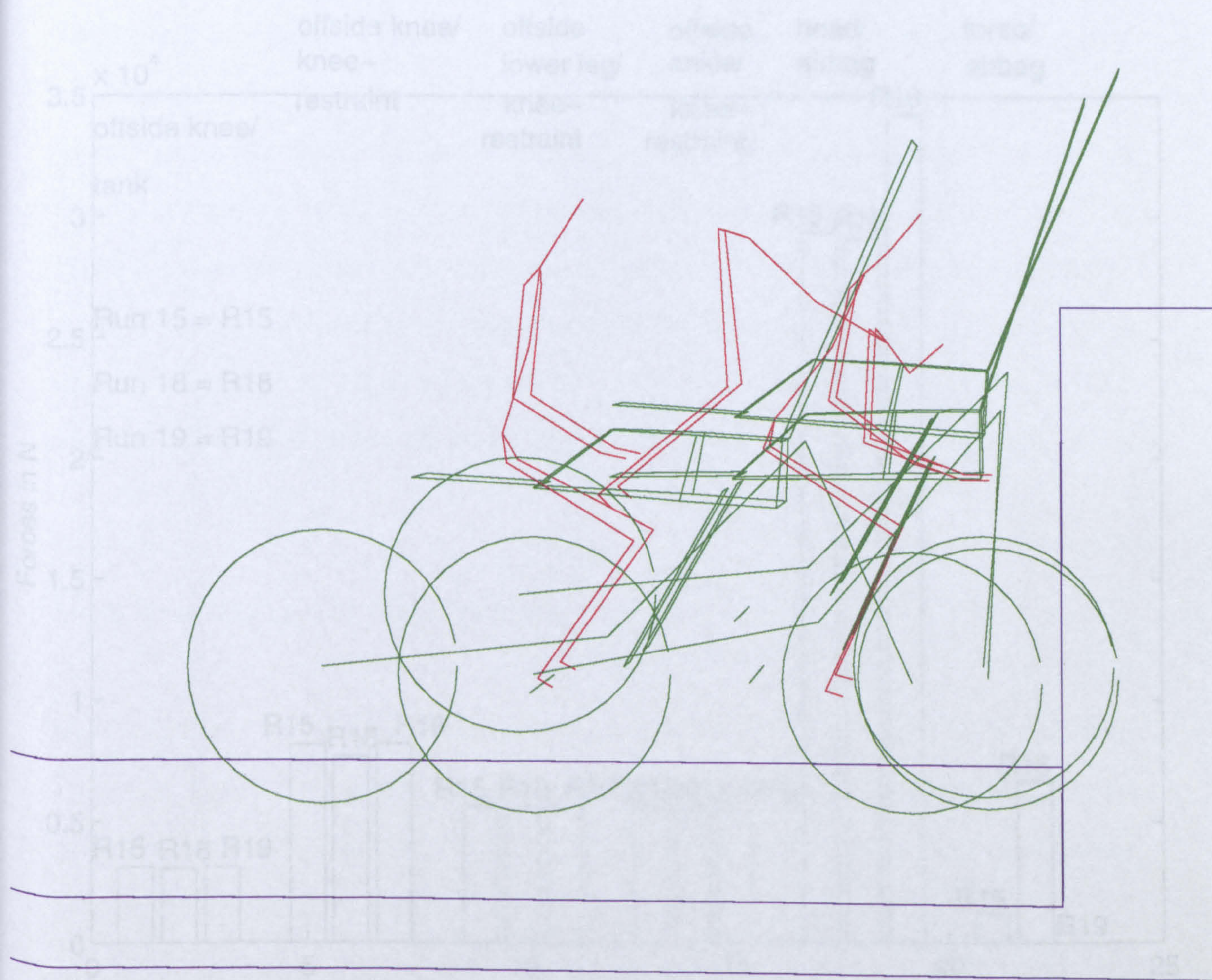


Figure 9.34b Elevation view of Run 19

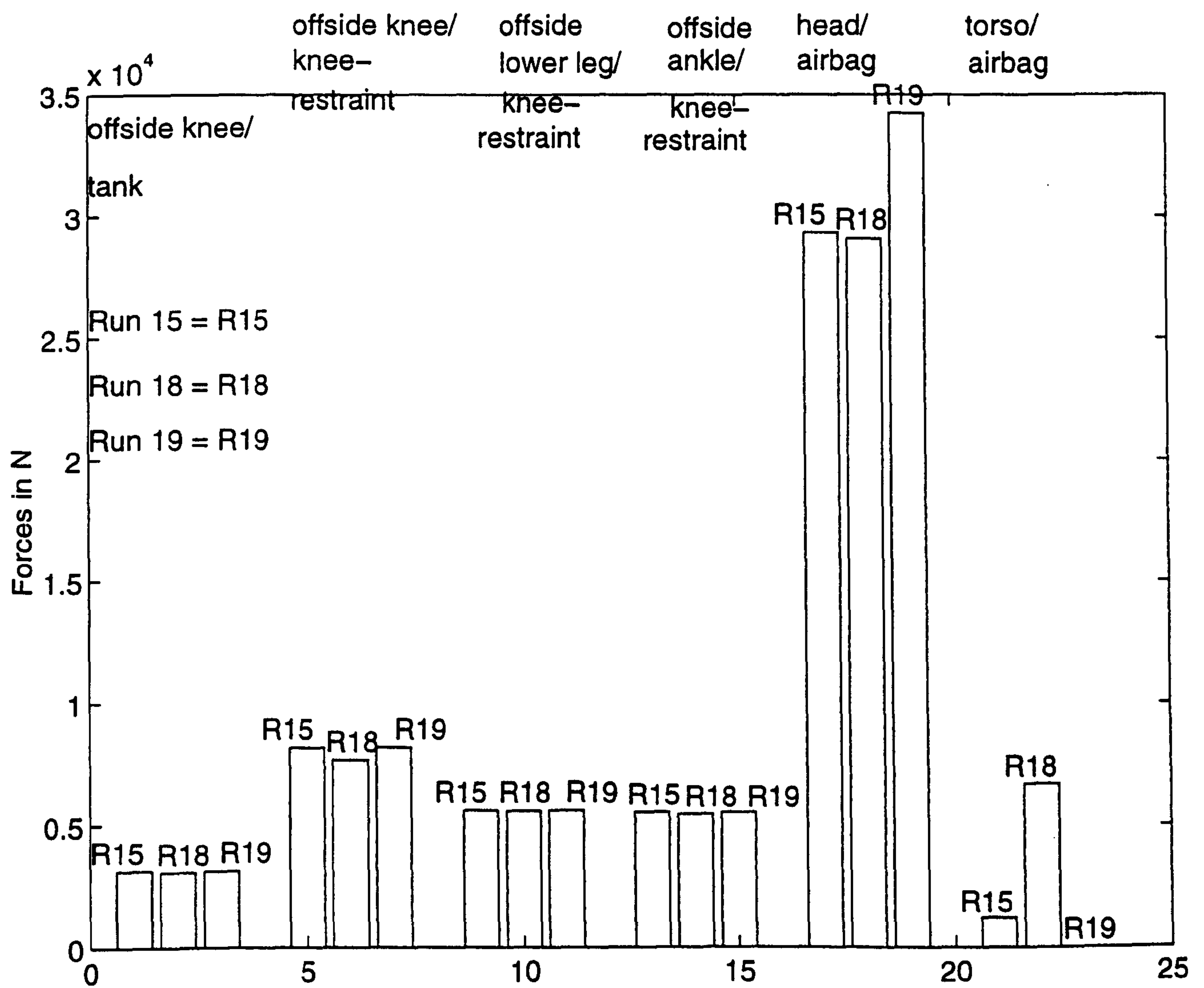


Figure 9.35

CHAPTER 10

CONVERSION OF DUMMY TO HYBRID3

10.0 Introduction

Up to this point, the work has involved a computer simulation model of an OPAT dummy rider, on a motorcycle, in differently configured impacts with a rigid barrier. However, the recent ISO draft standard specifies a HYBRID3 dummy and an automobile to be used as the target. This chapter will explain the conversion in the simulation from the design of the OPAT to that of the HYBRID3 dummy, and also analyse some comparable computer runs, with the target being a rigid barrier. The equivalents but with an automobile as a target will be described in the next chapter.

10.1 The Design Of The HYBRID3

Apart from the obvious differences of body dimensions, mass and inertia distributions between the OPAT and HYBRID3 dummies, there are two main different mechanical features between the two, they are:

- (i) where the trunk of the OPAT's body is divided into an upper and a lower torso, the HYBRID3's consists of only

one main torso,

- (ii) where the neck of the OPAT is a joint connecting the upper torso and the head, the bulk of the head of the HYBRID3 is made up of a head and a neck component, each having its own mass and inertias, with the neck also acting as a joint,

in addition, TRL suggested that

- (iii) the legs, both femora and tibiae should be frangible in order to examine the effect of leg breakage on the trajectory of the dummy rider.

Thus the following details have been incorporated into the new dummy in accordance with the specified alterations.

- (a) The upper torso is assigned with zero mass and zero inertias, with the lower torso more centrally positioned in the trunk of the body.
- (b) The neck is assigned mass and inertias but also functions as a three-dimensional joint which comprises a pin and universal joint connection.
- (c) Each of the femora and tibiae is split into two sections, as opposed to each being only one in the OPAT, and a three-dimensional joint connects the two parts. Breakage

will be simulated by the absence of joint stiffness once a certain amount of rotation has been reached.

The new designs, along with information of body dimensions, mass and inertia distributions, have been used in the mechanical construction of the HYBRID3 dummy by the use of SD/FAST, and a listing of the layout format is given in Figure 10.1 (similar in form to Figure 4.2c for the OPAT dummy in Chapter 4).

Note that the modifications and additions to the HYBRID3 dummy lead to a model of 21 bodies connected by 20 compliant joints, with a total of 47 d.o.f., instead of the OPAT design of 16 bodies connected by 15 compliant joints, with a total of 35 d.o.f.. The extra are mainly due to the insertion of frangible legs. A diagrammatic layout of the HYBRID3 dummy is given in Figure 10.2.

TRL had also provided joint stiffnesses for the HYBRID3 dummy to be inserted into the main ACSL program. However, due to process complication and a lack of time, flesh characteristics were not provided and will be assumed to be the same as for the OPAT dummy.

10.2 The Computer Runs

In addition to the new design, the following four computer runs were set up to simulate impact between the new dummy and the target of a rigid barrier, they are

Runs	Initial velocity	Barrier angle
1	17.8ms^{-1}	30°
2	13.4ms^{-1}	90°
3	8.9ms^{-1}	45°
4	6.7ms^{-1}	30°

These configurations have been applied to the simulation model and completed successfully. In the next two sections, some observations are drawn from the computer runs along with the comparisons with similar, though not identically configured, computer runs with the rider being the OPAT dummy.

10.3 Observations

In general, the behaviour of the motorcycle is similar to the previous computer runs. While the motorcycle yawed, in the case of impact with an acute barrier angle, the dummy rider was still travelling forwards, and initially yawing in an anti-clockwise direction, as opposed to that of the motorcycle, but the whole

dummy was gradually brought along on the trajectory of the motorcycle. This applies to the acute barrier angle runs with the exception of Run 1, where the dummy was still attached to the motorcycle as it spun, but the top part of the body was still yawing in the opposition direction. This is the effect of the high impact speed of the rider and the motorcycle. In the case of the head-on impact, the dummy rider was thrown high in the air, and both legs have spread out significantly.

From observations based on only these four runs, some patterns have emerged.

- (i) The legs have straightened out appreciably during impact, in the case of an acute barrier angle, this applies chiefly to the offside leg.
- (ii) The legs spread out wide during impact, in the case of an acute barrier angle, this applies particularly to the offside leg.
- (iii) The legs have been broken in the femora. In most cases the greatest rotation occurred chiefly in the yawing (twisting) motion, followed by the pitching motion.

10.4 Comparisons

Three runs from the calibration stage of the computer program

development phase have been chosen for comparisons, they are

Runs	Initial velocity	Barrier angle
L4	12.4ms ⁻¹	90°
L7	13.8ms ⁻¹	30°
L8	9.2ms ⁻¹	50°

Though these are not identical to the configured impacts as with those of the HYBRID3 dummy, comparisons can still be drawn between similar runs, and the following are a few general points which emerged. These can be demonstrated by referring to Figures 10.3 to 10.9, where a plan and elevation of each of the runs 1 to 4, and runs L4, L7 and L8, is given.

- (i) In the case of an acute barrier angle impact, the OPAT tended to yaw towards the barrier as opposed to the motorcycle which yawed away from the barrier. However, this yawing action not only affected the top half of the body but also both legs. This is different to the HYBRID3 where the top half of the body did yaw, but the offside leg had spread out significantly more around the petrol tank upon the spinning of the motorcycle. In the case of a head-on impact, the HYBRID3 dummy had definitely spread more outwards on both legs when compared to the OPAT dummy.
- (ii) In all cases, the offside leg, in an acute impact, and

both in a head-on impact, had straightened out more than the OPAT dummy did.

- (iii) Generally, the spine of the OPAT, though not broken, appeared to have bent more downwards than that of the HYBRID3.
- (iv) The motorcycle reacted similarly in the early stage of impacts, but in the case of an acute barrier angle, as the motorcycle along with the HYBRID3 dummy were spinning away from the barrier, the motorcycle stayed more upright than the motorcycle with the OPAT dummy.

These are the very general patterns observed between comparable impacts. In the next section a few comments are made to discuss the differences.

10.5 Discussion

We have observed that not only the HYBRID3's legs have spread wider, but they also straightened out more than those of the OPAT. This can be partly explained by the different joint stiffnesses, but the chief reason being the extra joints in the femora and tibiae. This leads to the flexible rotation as the offside thigh hit the petrol tank while the motorcycle yawed. Also because of the extra joints, the legs were effectively less restricted in their movements such that they can straighten out

more than those of the OPAT dummy.

Since the trunk of the HYBRID3 dummy is assigned one main mass with its position higher up in the kinematic chain than that of the OPAT dummy, there would be the need of a longer moment arm to rotate the spine. Thus the spine of the OPAT dummy is seen to have flexed more.

It is also this mass distribution on the HYBRID3's torso which leads to the more upright position of the motorcycle, which unlike with the OPAT dummy, with effectively more mass attached to the motorcycle, led to not only yawing action of the motorcycle but also a significant amount of rolling action.

* simple HYBRID3 dummy model

```

gravity      = 0.0 0.0 -9.8066?
body         = pelvis
mass         = 11.6?
inertia      = 0.1? 0.0821? 0.0637?

body         = ltorso  inb = pelvis  joint = gimbal
mass         = 17.56?
inertia      = 0.295? 0.231? 0.195?
inbtojoint   = 0.0? 0.0? 0.095?
bodytojoint  = 0.0? 0.023? -0.24?
pin          = 1 0 0
pin          = 0 1 0
pin          = 0 0 1

body         = utorso  inb = ltorso  joint = pin
mass         = 0.0?
inertia      = 0.0? 0.0? 0.0?
inbtojoint   = 0.0? -0.018? 0.137?
bodytojoint  = 0.0? 0.0? 0.0?
pin          = 1 0 0
prescribed   = 1?

body         = neck    inb = utorso  joint = pin
mass         = 1.32?
inertia      = 0.0032? 0.003? 0.0011?
inbtojoint   = 0.0? 0.031? 0.08?
bodytojoint  = 0.0? 0.0? 0.0?
pin          = 1 0 0

body         = head    inb = neck    joint = ujoint
mass         = 5.9?
inertia      = 0.0399? 0.049? 0.041?
inbtojoint   = 0.0? 0.0? 0.0?
bodytojoint  = 0.0? -0.023? -0.12?
pin          = 0 1 0
pin          = 0 0 1

body         = uarmr   inb = utorso  joint = ujoint
mass         = 2.1?
inertia      = 0.0115? 0.0112? 0.0012?
inbtojoint   = 0.19? 0.0? -0.071?
bodytojoint  = 0.0? 0.0? 0.13?
pin          = 1 0 0
pin          = 0 1 0

body         = larmr   inb = uarmr   joint = pin
mass         = 1.73?
inertia      = 0.0134? 0.0127? 0.00078?
inbtojoint   = 0.0? 0.0? -0.135?
bodytojoint  = 0.0? 0.0? 0.147?
pin          = 1 0 0

body         = handr   inb = larmr   joint = ujoint
mass         = 0.59?
inertia      = 0.00129? 0.0013? 0.00053?
inbtojoint   = 0.0? 0.0? -0.103?
bodytojoint  = 0.0? 0.0? 0.057?
pin          = 1 0 0
pin          = 0 0 1

body         = uarm1   inb = utorso  joint = ujoint
mass         = 2.1?
inertia      = 0.0115? 0.0112? 0.0012?
inbtojoint   = -0.19? 0.0? -0.071?
bodytojoint  = 0.0? 0.0? 0.13?
pin          = 1 0 0
pin          = 0 1 0

body         = larm1   inb = uarm1   joint = pin
mass         = 1.73?
inertia      = 0.0134? 0.0127? 0.00078?
inbtojoint   = 0.0? 0.0? -0.135?
bodytojoint  = 0.0? 0.0? 0.147?
pin          = 1 0 0

body         = handl   inb = larm1   joint = ujoint
mass         = 0.59?
inertia      = 0.00129? 0.0013? 0.00053?
inbtojoint   = 0.0? 0.0? -0.103?
bodytojoint  = 0.0? 0.0? 0.057?
pin          = 1 0 0
pin          = 0 0 1

body         = uplegur  inb = pelvis  joint = gimbal
mass         = 4.88?
inertia      = 0.0278? 0.0287? 0.0108?
inbtojoint   = 0.1? 0.01? -0.045?
bodytojoint  = 0.0? 0.0? 0.091?
pin          = 1 0 0
pin          = 0 1 0
pin          = 0 0 1

body         = upleglr  inb = uplegur joint = gimbal
mass         = 3.1?
inertia      = 0.146? 0.153? 0.007?
inbtojoint   = 0.0? 0.0? -0.139?
bodytojoint  = 0.0? 0.0? 0.128?
pin          = 1 0 0
pin          = 0 1 0
pin          = 0 0 1

body         = lwlegur  inb = upleglr joint = pin
mass         = 3.05?
inertia      = 0.0299? 0.0293? 0.0058?
inbtojoint   = 0.0? 0.0? -0.052?
bodytojoint  = 0.0? 0.0? 0.147?
pin          = 1 0 0

body         = lwleglr  inb = lwlegur joint = gimbal
mass         = 0.77?
inertia      = 0.00055? 0.00055? 0.00015?
inbtojoint   = 0.0? 0.0? -0.162?
bodytojoint  = 0.0? 0.0? 0.067?
pin          = 1 0 0
pin          = 0 1 0
pin          = 0 0 1

body         = footr   inb = lwleglr joint = ujoint
mass         = 1.59?
inertia      = 0.0019? 0.0062? 0.0065?
inbtojoint   = 0.0? 0.0? -0.036?
bodytojoint  = 0.0? 0.0? 0.04?
pin          = 1 0 0
pin          = 0 1 0

body         = uplegul  inb = pelvis  joint = gimbal
mass         = 4.88?
inertia      = 0.0278? 0.0287? 0.0108?
inbtojoint   = -0.1? 0.01? -0.045?
bodytojoint  = 0.0? 0.0? 0.091?
pin          = 1 0 0
pin          = 0 1 0
pin          = 0 0 1

body         = uplegll  inb = uplegul joint = gimbal
mass         = 3.1?
inertia      = 0.146? 0.153? 0.007?
inbtojoint   = 0.0? 0.0? -0.139?
bodytojoint  = 0.0? 0.0? 0.128?
pin          = 1 0 0
pin          = 0 1 0
pin          = 0 0 1

body         = lwlegul  inb = uplegll joint = pin
mass         = 3.05?
inertia      = 0.0299? 0.0293? 0.0058?
inbtojoint   = 0.0? 0.0? -0.052?
bodytojoint  = 0.0? 0.0? 0.147?
pin          = 1 0 0

body         = lwlegll  inb = lwlegul joint = gimbal
mass         = 0.77?
inertia      = 0.00055? 0.00055? 0.00015?
inbtojoint   = 0.0? 0.0? -0.162?
bodytojoint  = 0.0? 0.0? 0.067?
pin          = 1 0 0
pin          = 0 1 0
pin          = 0 0 1

body         = footl   inb = lwlegll joint = ujoint
mass         = 1.59?
inertia      = 0.0019? 0.0062? 0.0065?
inbtojoint   = 0.0? 0.0? -0.036?
bodytojoint  = 0.0? 0.0? 0.04?
pin          = 1 0 0
pin          = 0 1 0

```

Figure 10.1 A SD/FAST definition of the HYBRID3 dummy.

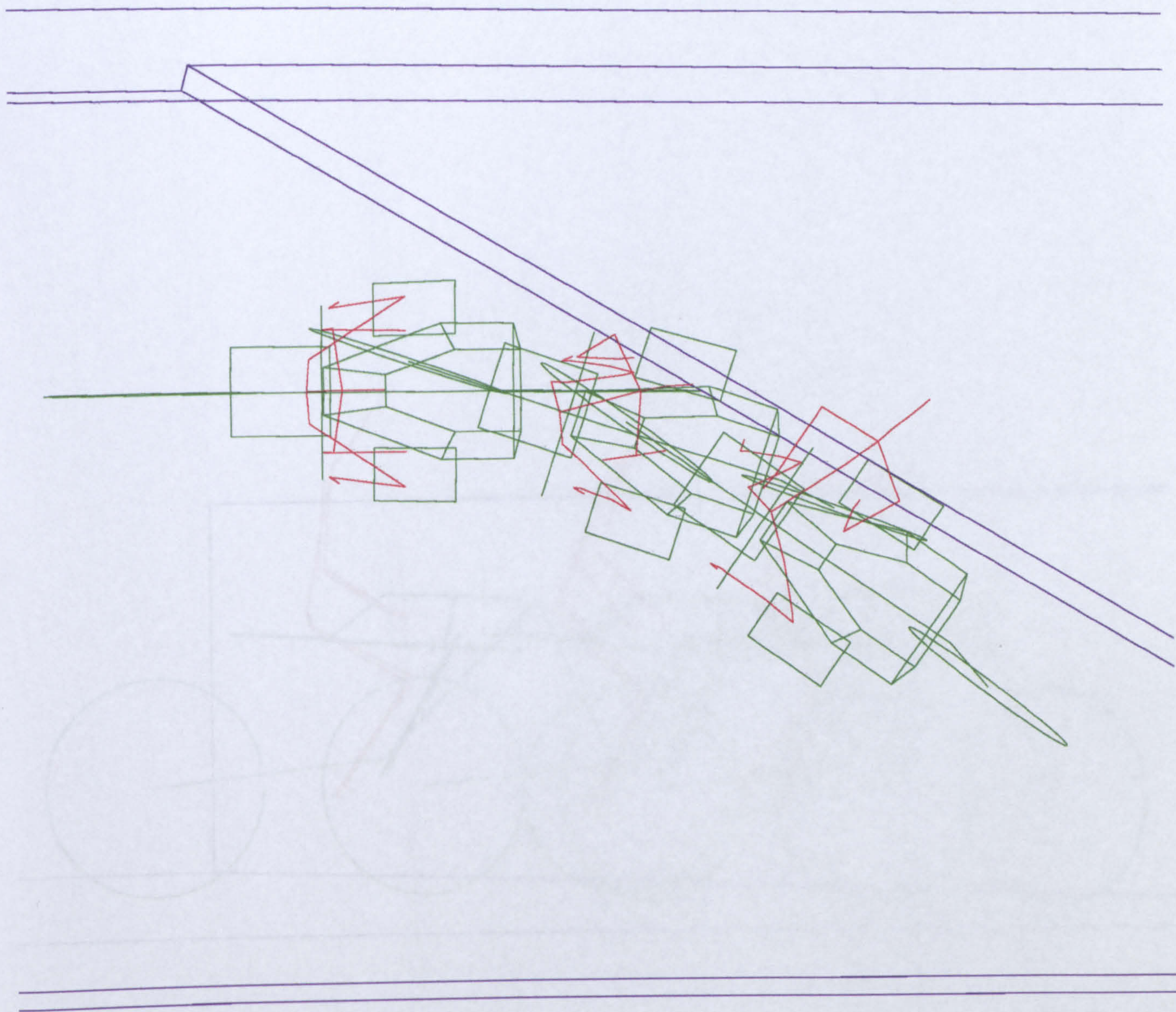


Figure 10.3a Plan view of Run 1

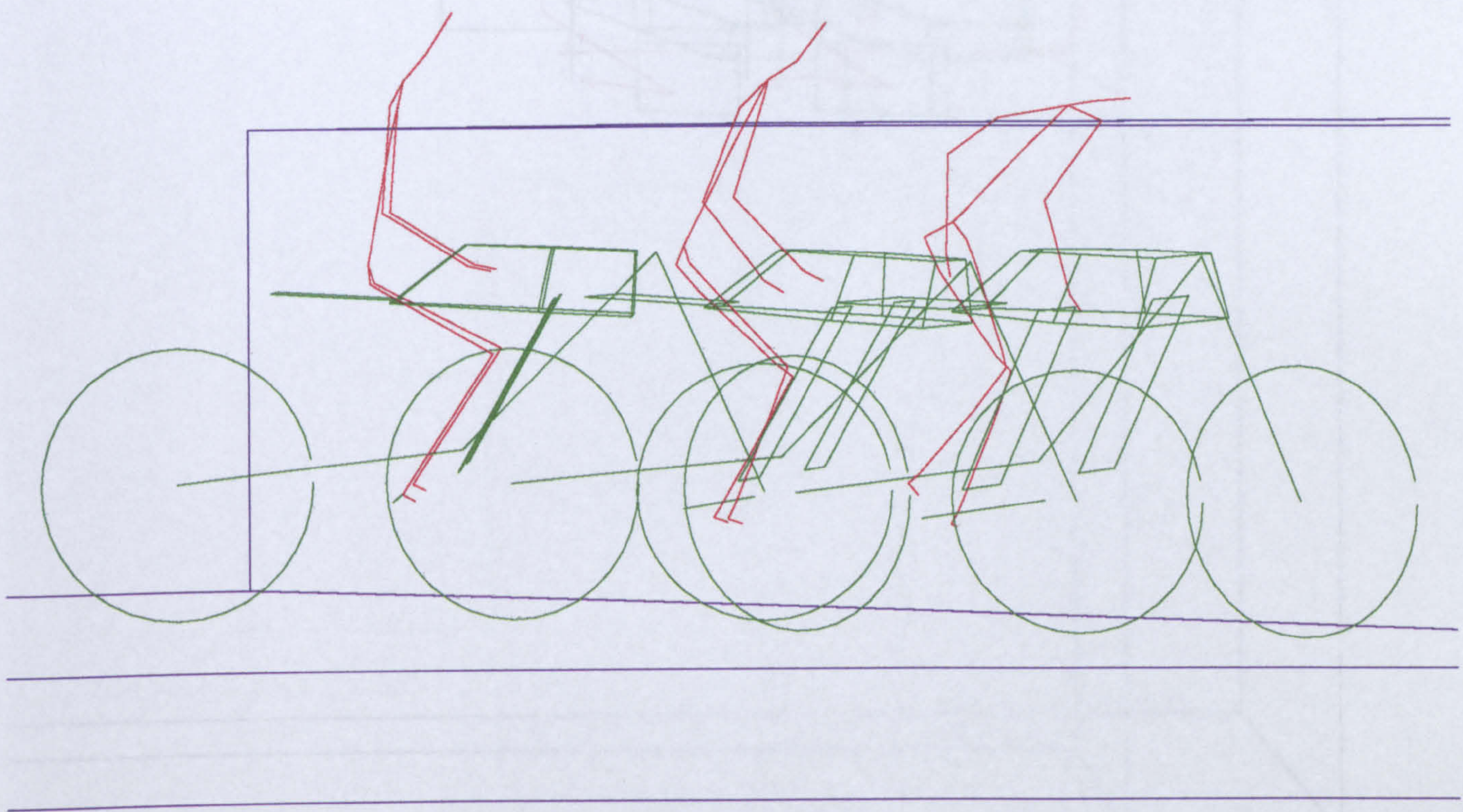


Figure 10.3b Elevation view of Run 1

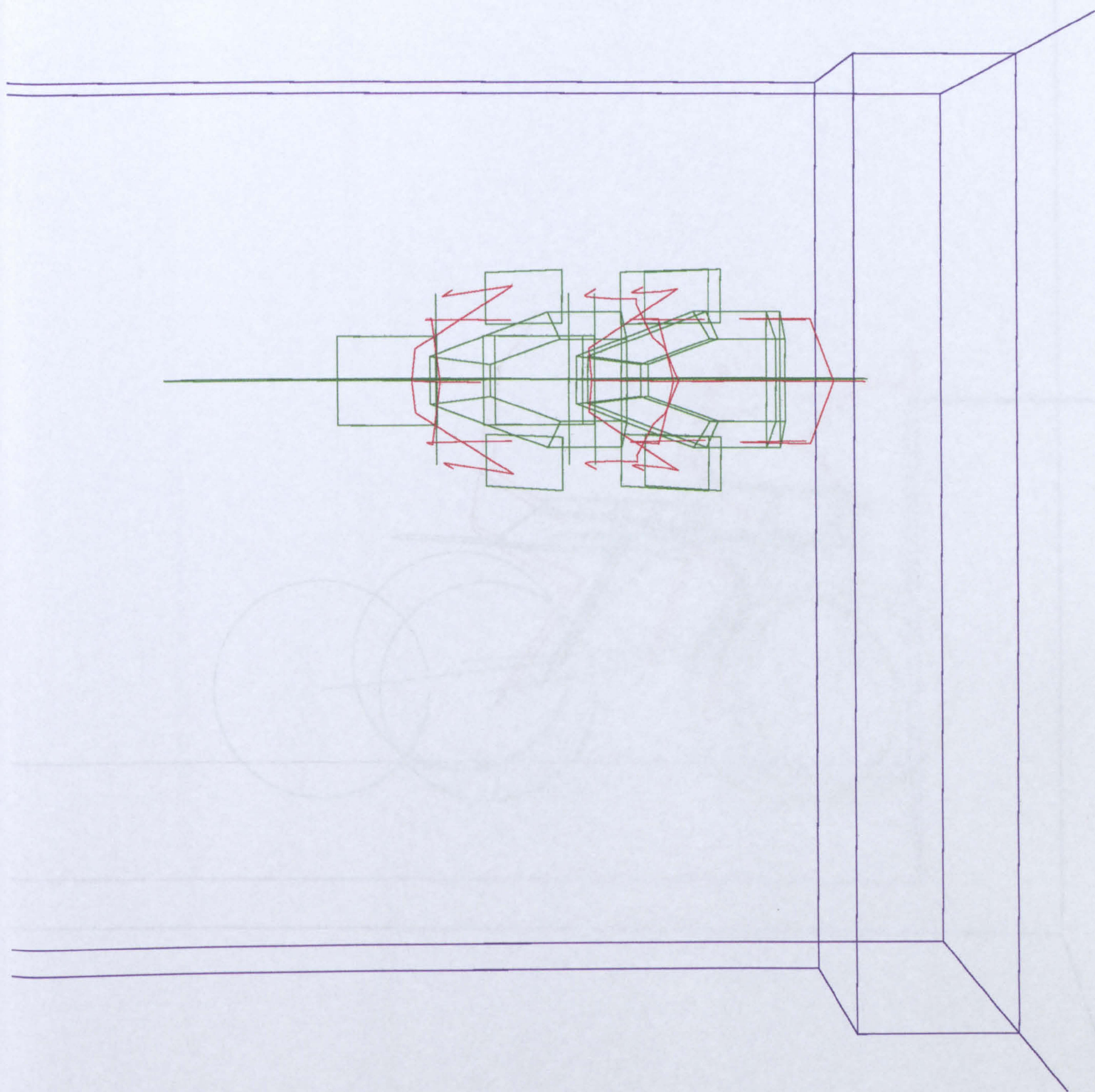


Figure 10.4a Plan view of Run 2

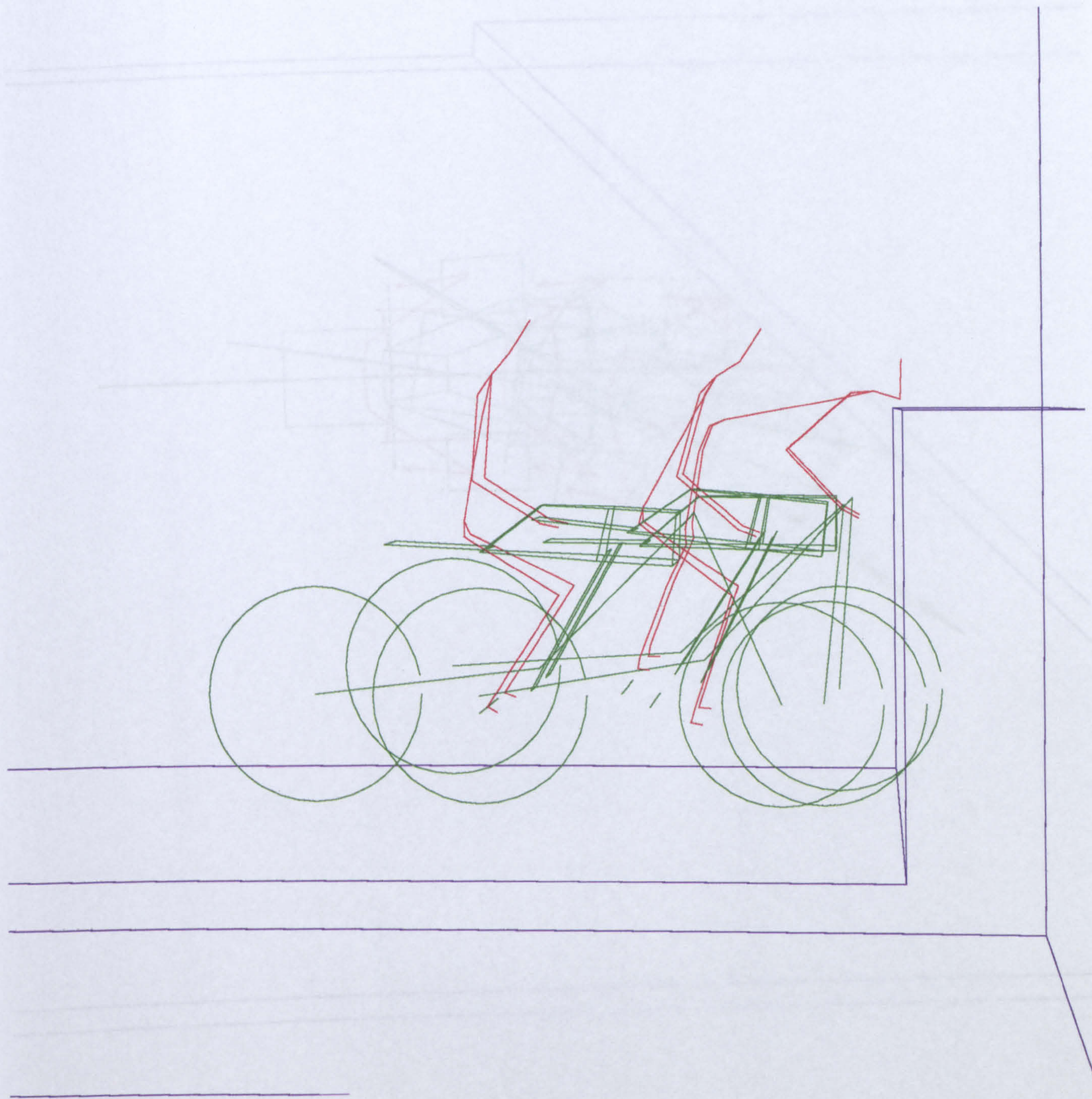


Figure 10.4b Elevation view of Run 2

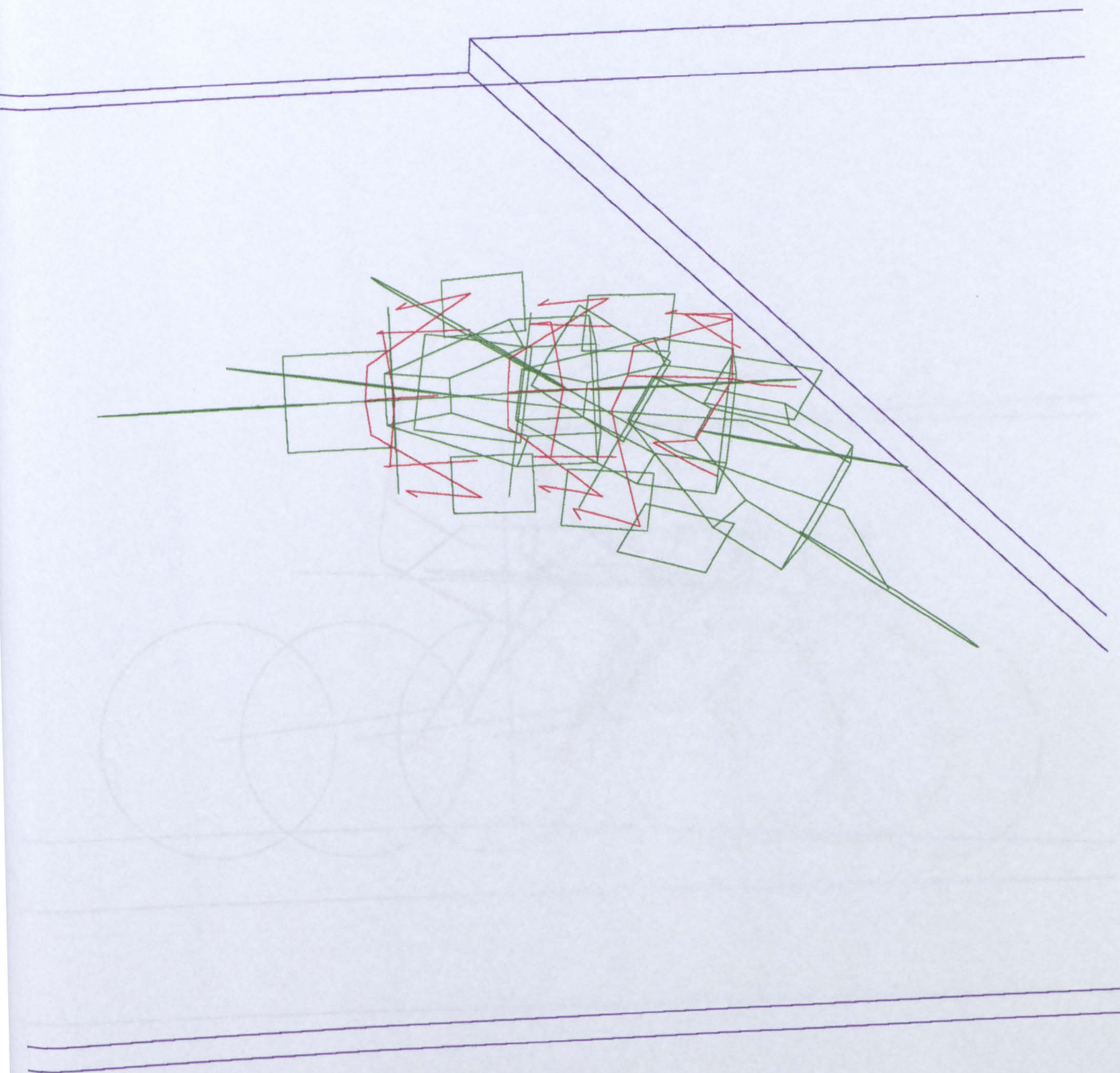


Figure 10.5a Plan view of Run 3

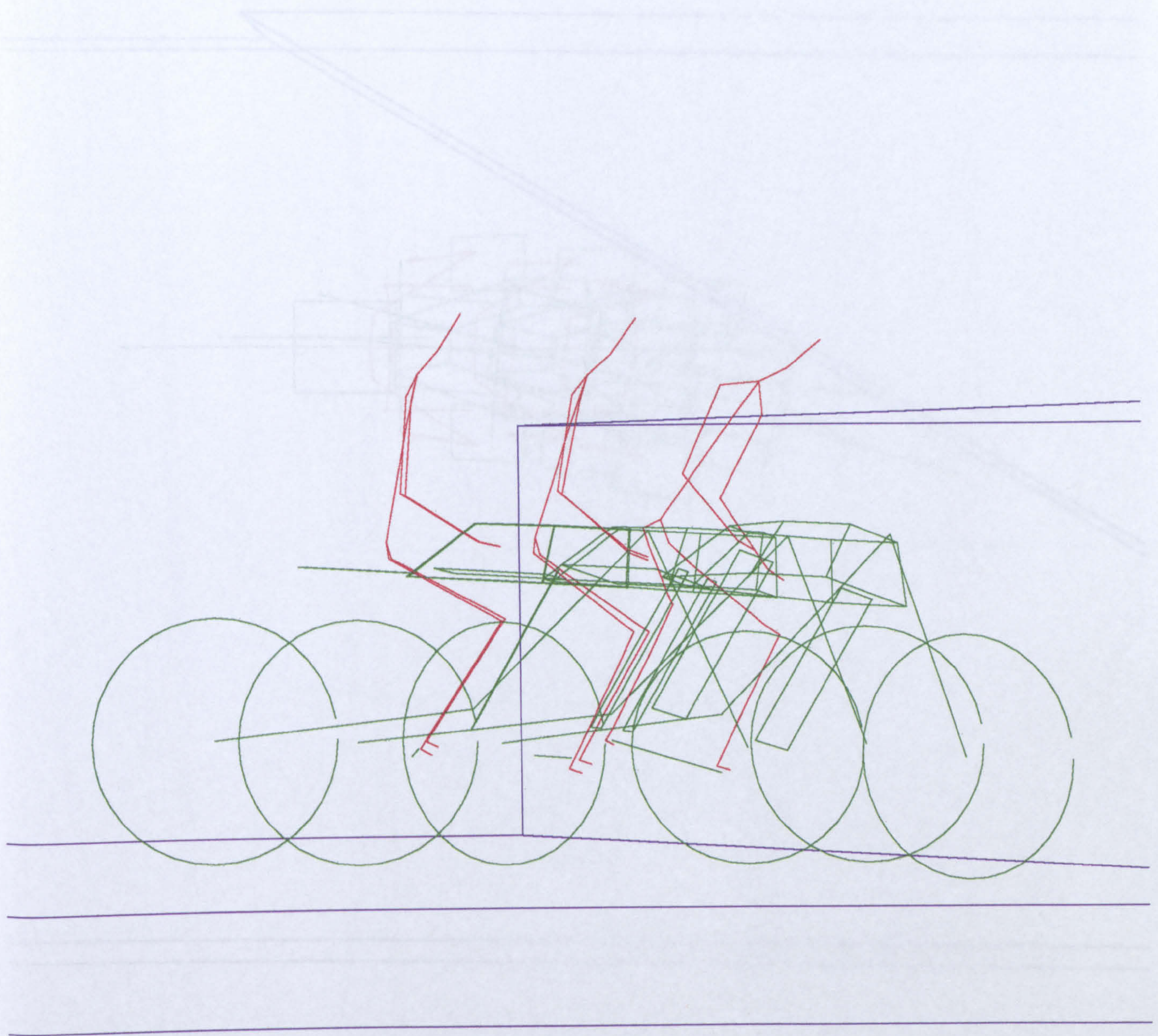


Figure 10.5b Elevation view of Run 3

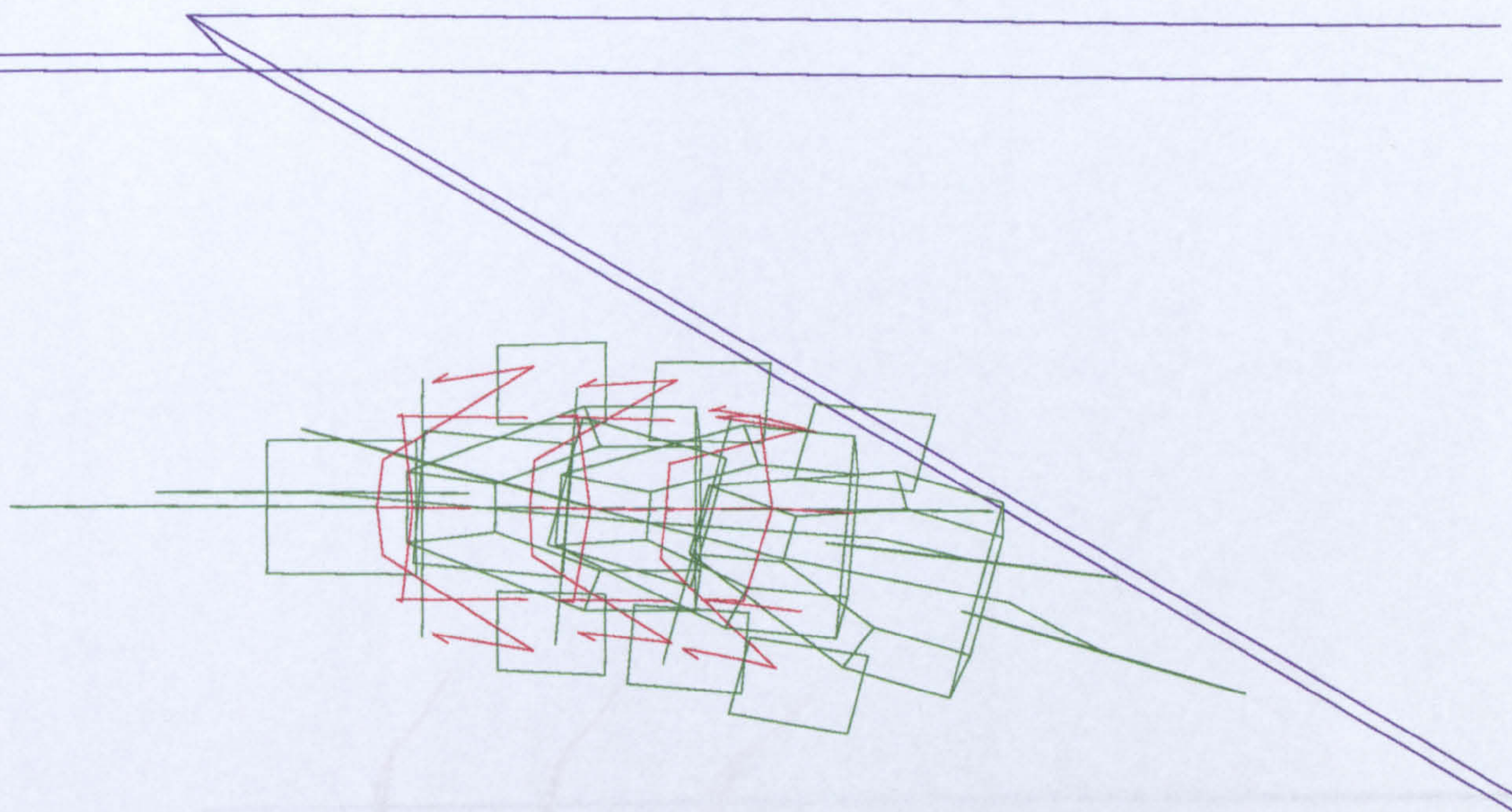


Figure 10.6a Plan view of Run 4

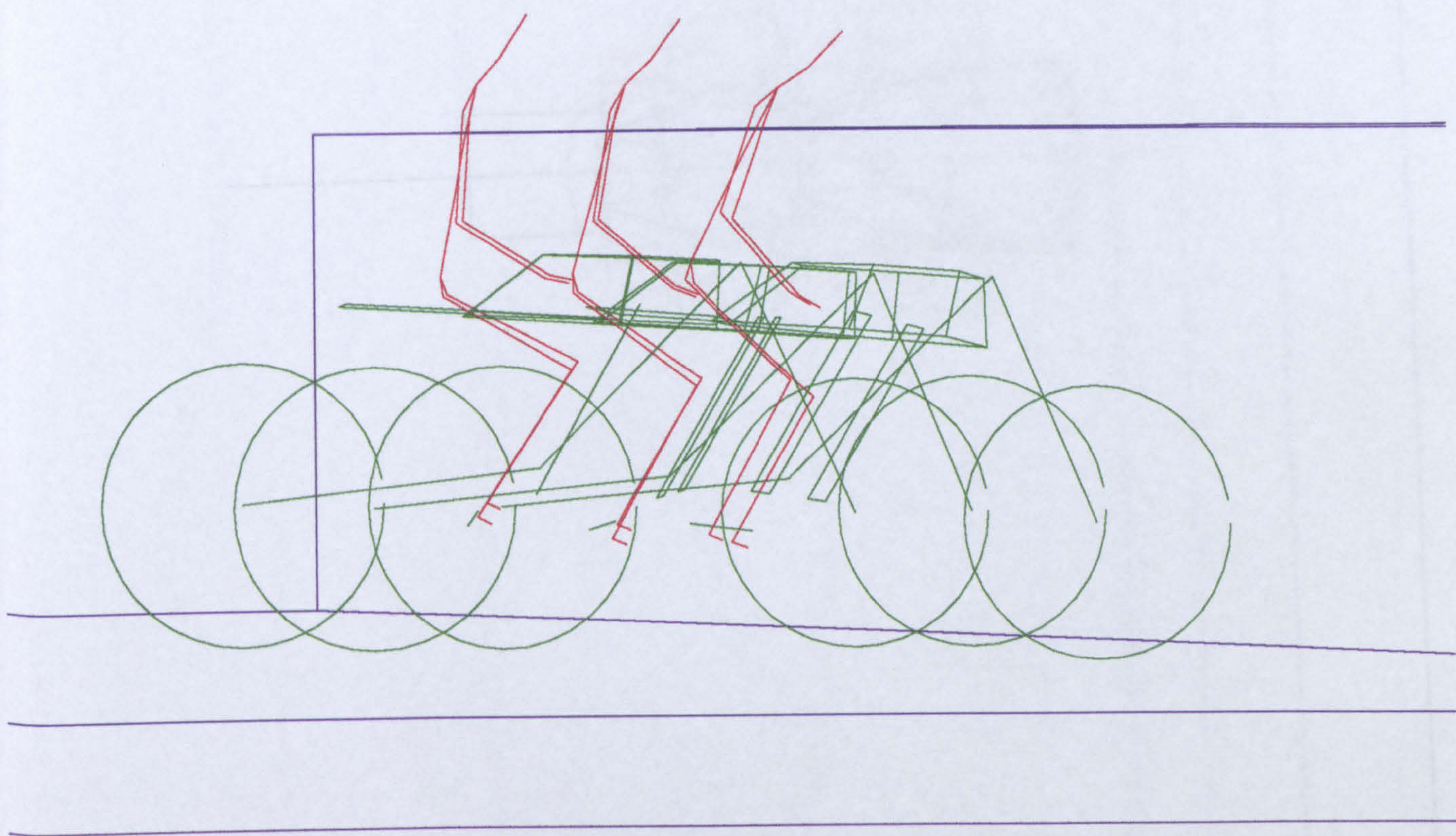


Figure 10.6b Elevation view of Run 4

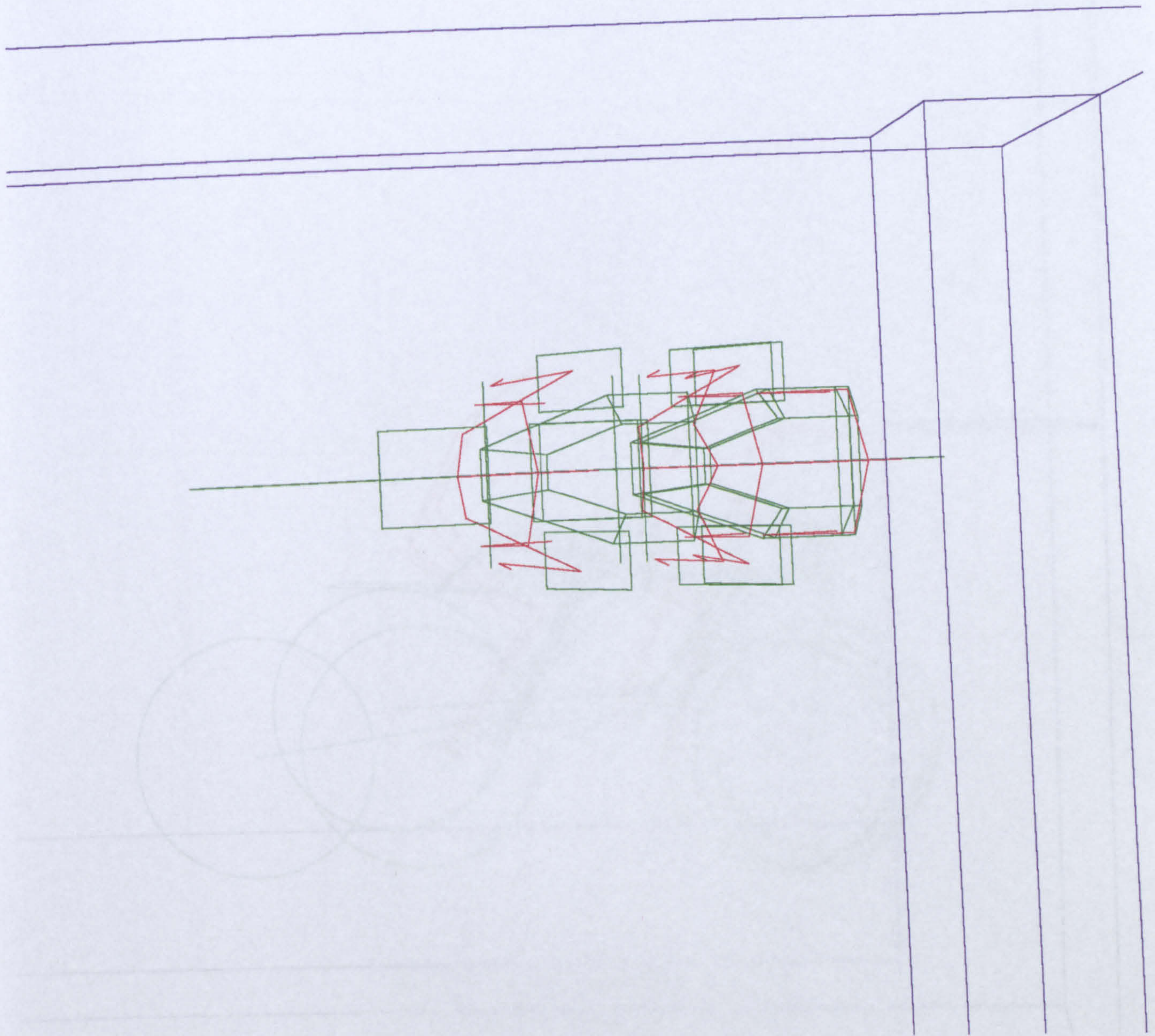


Figure 10.7a Plan view of L4

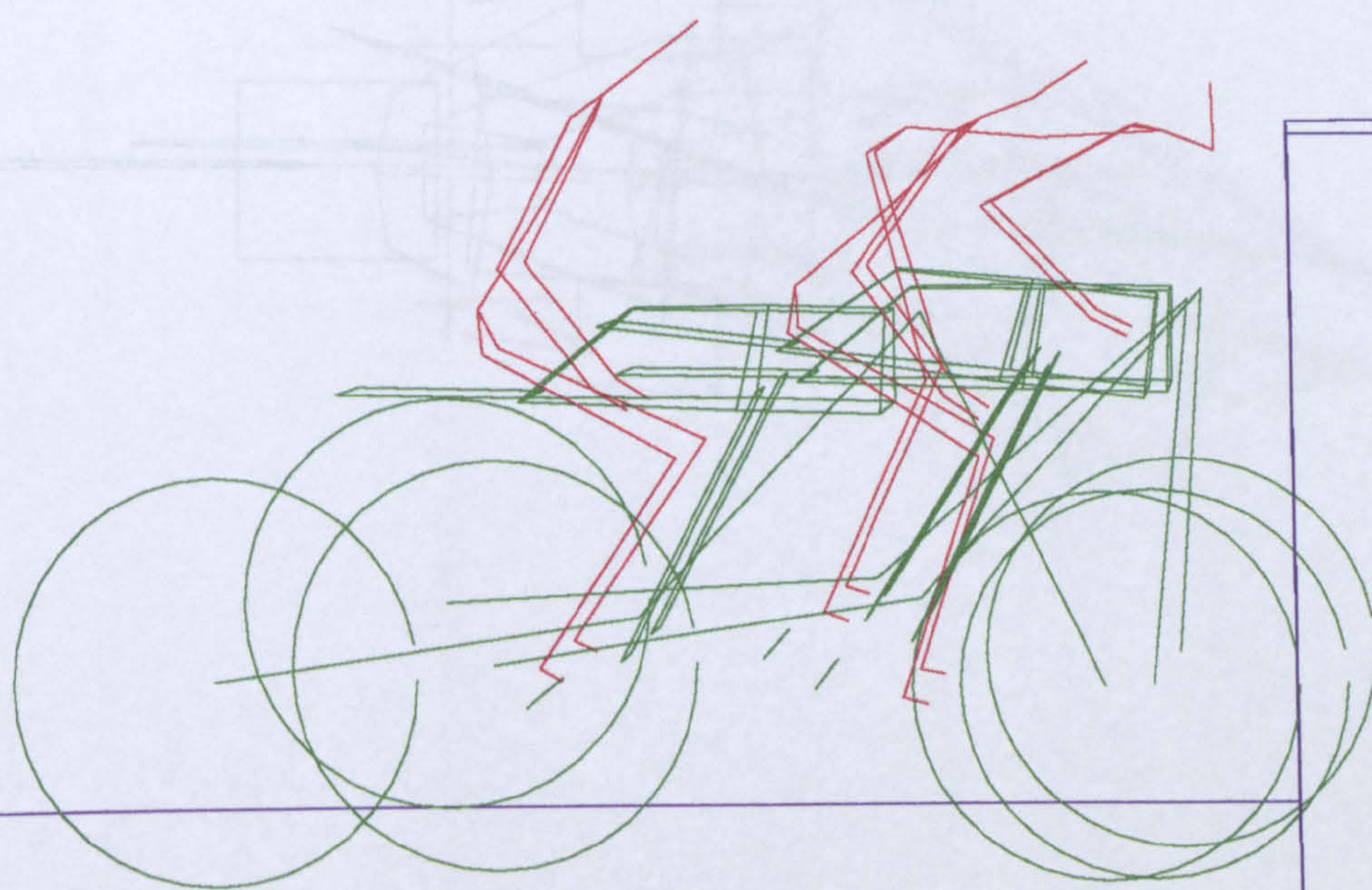


Figure 10.7b Elevation view of L4

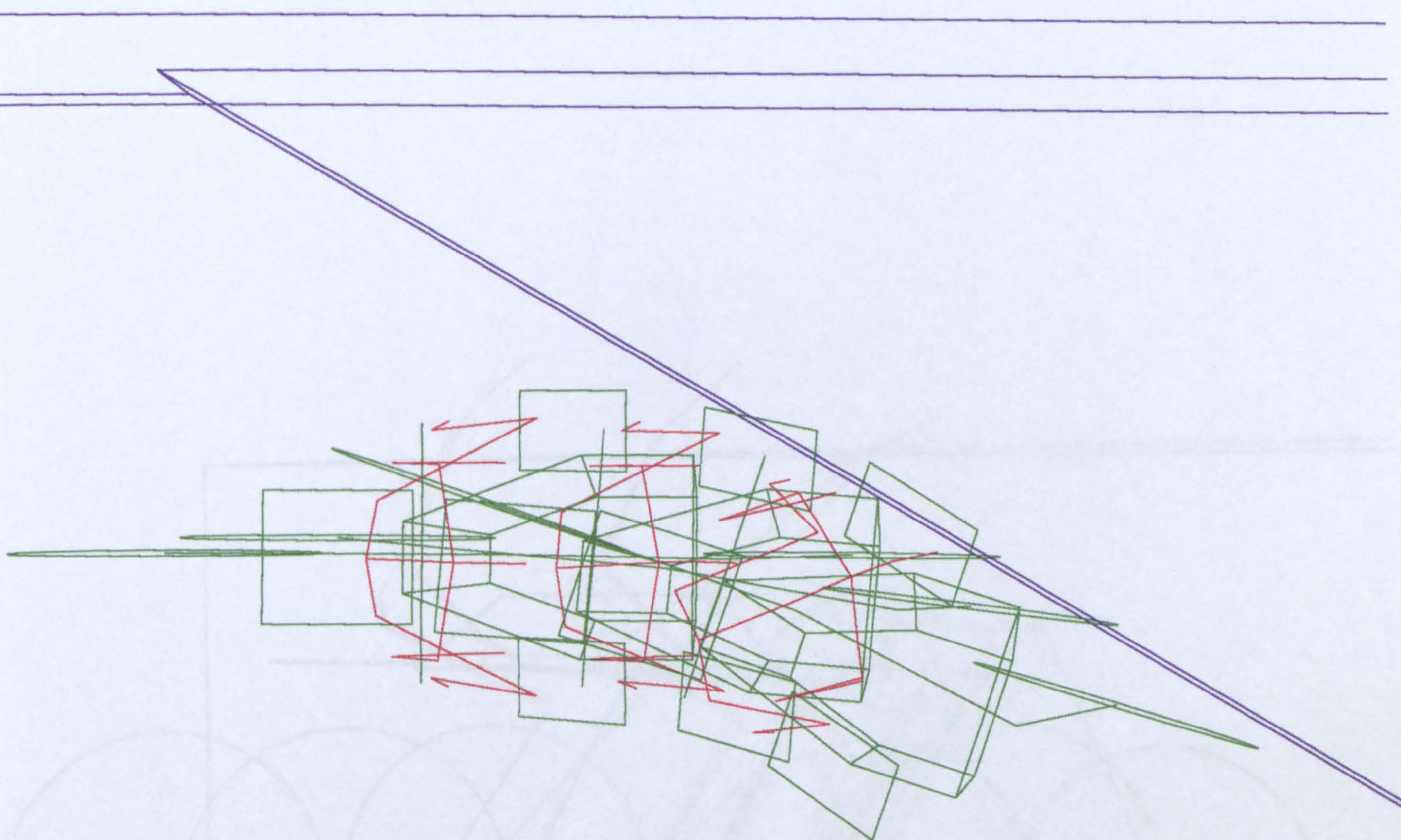


Figure 10.8a Plan view of L7

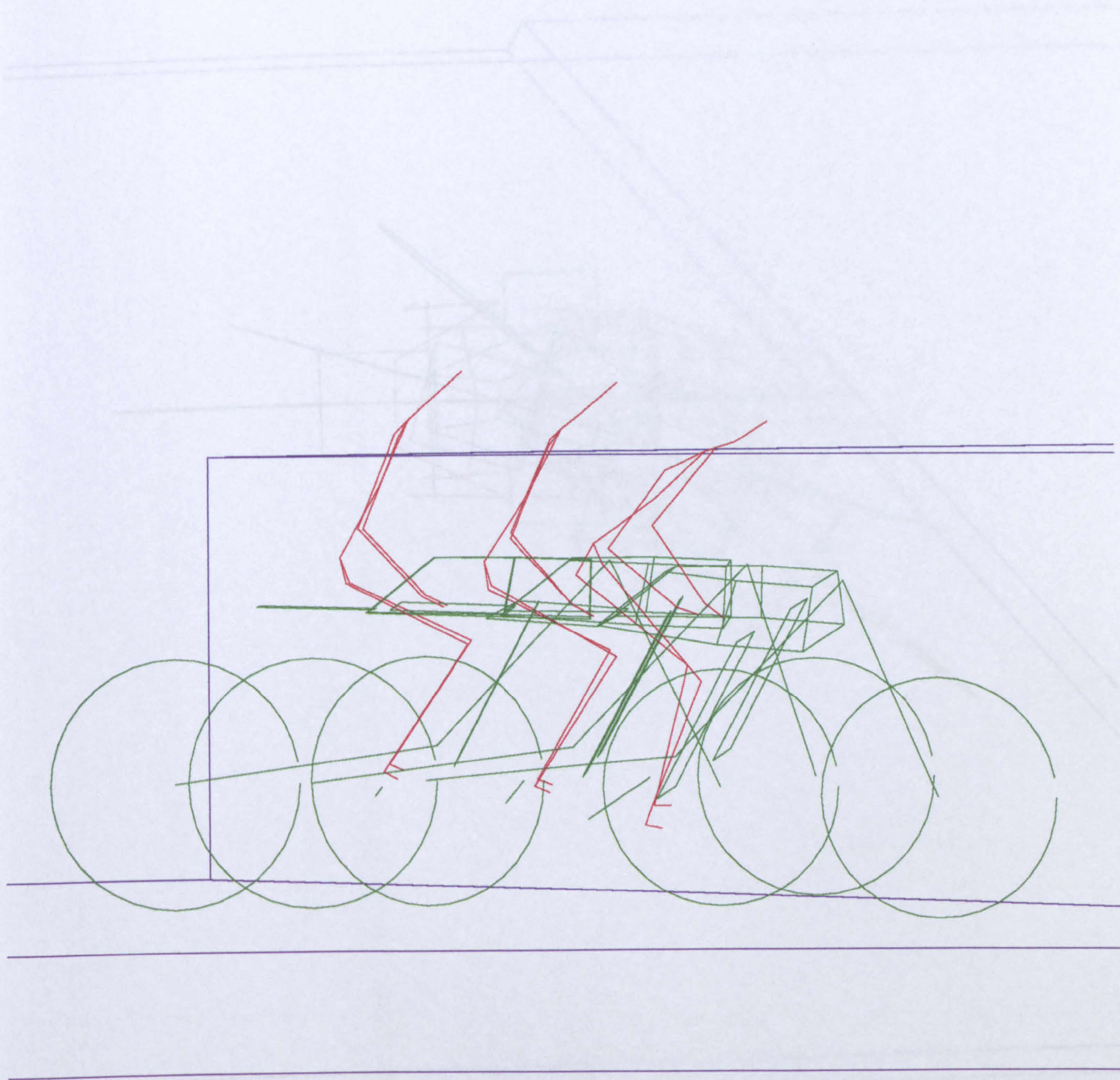


Figure 10.8b Elevation view of L7

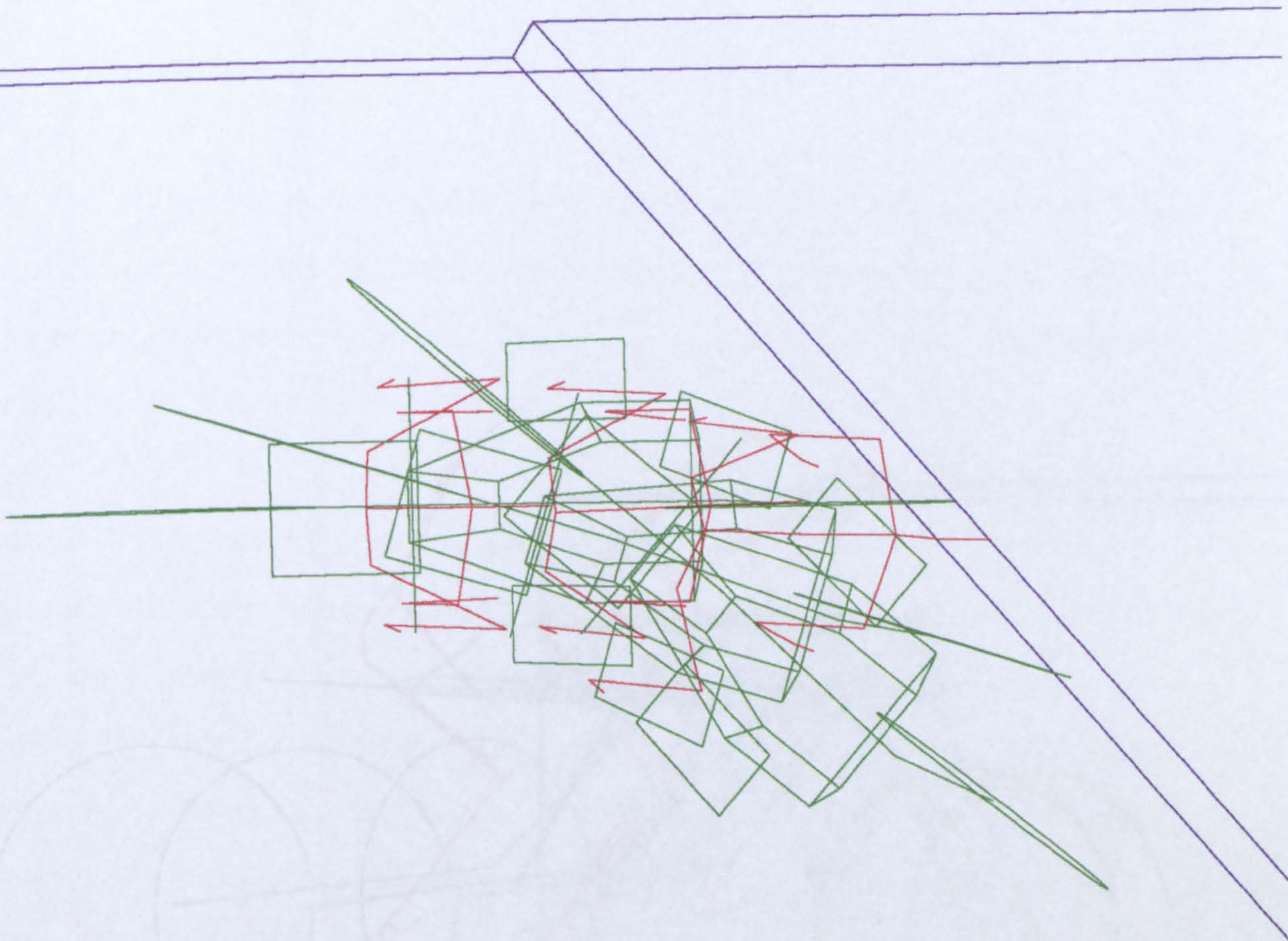


Figure 10.9a Plan view of L8

EXTENSION OF SIMULATION FOR IMPACT INTO A NEW AREA

11.1 Introduction

The first step in the simulation of impact into a new area is the selection of a suitable model. This model should be able to represent the physical processes involved in the impact, and should be able to be used to predict the results of the impact. The model should also be able to be used to predict the results of the impact for a range of different impact conditions.

It was decided that the model should be able to represent the physical processes involved in the impact, and should be able to be used to predict the results of the impact. The model should also be able to be used to predict the results of the impact for a range of different impact conditions.

11.2 The Design of the Simulation

The first step in the design of the simulation is the selection of a suitable model. This model should be able to represent the physical processes involved in the impact, and should be able to be used to predict the results of the impact.

The next step in the design of the simulation is the selection of a suitable model. This model should be able to represent the physical processes involved in the impact, and should be able to be used to predict the results of the impact.

Figure 10.9b Elevation view of L8

CHAPTER 11

EXTENSION OF SIMULATION FOR IMPACT INTO A MOTOR CAR

11.0 Introduction

After the HYBRID3 dummy rider was successfully implemented into the simulation model, the object was to replace the target, which had been a stationary rigid barrier until now, by a deformable and moving automobile.

It was decided that the car would be a single body of mass and inertias, with various panels arranged to form the outer surfaces of the car. Because of this simple structure, the car was not designed by the use of SD/FAST, but by conventional programming techniques. However, car impact simulation still needed to be created, dependent upon car dimensions and panel properties.

11.1 The Design Of An Automobile

As mentioned earlier, the car is basically a single-massed body with inertias, but simulated panels are used to form its outer structure. These panels are given names, as listed below, for the purpose of simulation programming:

- (i) car side door - PLANE B
- (ii) car side window - PLANE D
- (iii) car roof - PLANE J
- (iv) car windscreen - PLANE I
- (v) car bonnet - PLANE H
- (vi) car grille - PLANE G

An illustration of the above named panels forming a car is given in Figure 11.1.

For reason of economy, only a limited number of panels are chosen for a certain type of impact. For example, imagine a side impact towards planes B, D and J, it is justifiable to argue that a one-sided car is sufficient for impact simulation. Then, as long as the interest of the impact is centred on the side of the car, the planes I, H and G will not be necessary in this particular simulation. Likewise for a frontal impact towards the grille area, only planes G, H, I and J are required.

The principle of contact remains the same of that of a two-body impact as described in Chapter 3. However, since any particular panel making up the car consists of a large area, it is expected that the stiffness will not remain uniform throughout, therefore a different principle has been derived to separate a panel into a number of segments, with each segment possibly having a different non-linear spring stiffness. A diagram of this

principle is given in Figure 11.2.

As one can see, at present the panel is separated into six segments, but the same principle can be applied in future to obtain a variable number of segments.

Finally, the decision as to which plane of the car is considered to be in contact with the potential positions on the dummy and the motorcycle has to be made. Taking the dummy's head as an example, the head can potentially contact planes B, D and J in the case of a side impact, but not all three planes at the same time. It is obvious that the head cannot contact planes B and J at the same time, but if given the case that the head first contacted plane D and gradually reaching plane J, a switch is employed to indicate this situation. This principle is similar to the head to barrier contact as described in Chapter 4.

11.2 Data Collection

TRL had supplied dimensions of a Ford Mondeo Hatchback, along with mass and inertias. However, for panel stiffness, only that of a car side door has been supplied. This proved to be very stiff because of the inclusion of a side-impact beam. Due to the lack of other data it was decided that this value could be applied to the whole section of the car side door. In addition,

TRL had also supplied stiffnesses to simulate the car wheels and suspensions. These are in the form of a constant stiffness value throughout.

11.3 The Computer Runs

As with the conversion from an OPAT to a HYBRID3 dummy, four computer runs were chosen with the car as the target of impact, they are

Runs	Rider and Motorcycle velocity	Car velocity	Angle of impact	Car contact location
5	13.4ms ⁻¹	0.0ms ⁻¹	90°	side
6	13.4ms ⁻¹	6.7ms ⁻¹	90°	side
7	13.4ms ⁻¹	6.7ms ⁻¹	45°	side
8	13.4ms ⁻¹	6.7ms ⁻¹	45°	frontal

Note that in Run 7, the motorcycle is approaching to the side of the car with its starboard side nearer to the car, and in Run 8, the motorcycle is approaching to the grille of the car with its port side nearer to the car.

Similar to the observations and comparisons made in the previous chapter, the equivalents will be given in the next two sections.

11.4 Observations

For each of the four runs, the front wheel had only contacted one target, namely plane B in Runs 5, 6 and 7, and plane G in Run 8. In the cases of the more direct head-on impact with the side of the car, Runs 5 and 6, the head had hit plane D, but no other parts of the dummy's body had impacted with the car. In Runs 7 and 8 the head did not hit any of the panels, with parts of the right leg hitting plane B in Run 7, and parts of the left leg hitting plane G in Run 8. This is consistent with the proposed location of the target.

The above are the results obtained from the simulation, but on observation, one can clearly see from the Figures below, that the car is actually diving into the ground, especially after contact has been made with the motorcycle. This is due to the simple modelling of car suspension by using only a linear spring.

For the frangible legs on the rider, they have been broken in most cases, and similar to the runs with the barrier as a target, a trend of the yaw axis causing the greatest rotation, followed by the pitch axis, has emerged.

11.5 Comparisons

The object of this comparison exercise is to examine the difference between impacts involving a target being a rigid barrier and a target being a deformable car. Therefore comparable computer runs are those specified in the previous and the current chapter. Figures 11.3 to 11.6 show the plan and elevation of each of the runs 5 to 8. Note that the yellow lines form the various panels of the car.

One emerging pattern from the runs indicated clearly that the front wheel was still hitting into the car compared to the front wheel being trapped between the motorcycle frame and the barrier, especially in the more head-on impacts. The other distinct pattern is that the dummy's head was still diving towards the car by the end of the simulation, and hence the pelvis had pitched higher than the pitching action of the pelvis in cases of a barrier contact.

But to compare more specific computer runs, Run 1 and Run 5 are chosen first to draw primary indications. It is noticeable that the whole motorcycle had pitched significantly higher in Run 5 than in Run 1. Though the car is stationary in Run 5 but of deformable properties, the motorcycle had yawed during impact and also rolled slightly. Because of the yawing of the motorcycle in Run 5, the dummy's offside leg had spread out more than both of

the legs in Run 1.

Comparison between Run 5 and Run 6 is more direct, the difference being that in Run 5 the car is stationary but moving in Run 6. It is significant that the front wheel in Run 6 had yawed greater than in Run 5, but the interesting difference is that in Run 5, the motorcycle had rolled slightly anti-clockwise, but in Run 6, the motorcycle had rolled greatly in the opposite direction. However, during this process, the car was travelling away from the motorcycle.

Because of the great amount of rolling and yawing actions in Run 6, both legs of the dummy had actually spread wider than those in Run 5. While the legs had to counter the motion of the motorcycle in Run 6, its pelvis did not pitch as high as that in Run 5, thus the head had not dived as low as that in Run 5.

For comparison between Run 3 and Run 7, one needs to bear in mind that in Run 3 the motorcycle is approaching the target with its port side nearer to the barrier, but in Run 7 the motorcycle is approaching the target with its starboard side nearer to the car. The two motorcycles behaved quite similarly to each other, both had rolled towards the target, but one can observe the motorcycle in Run 7 had rolled slightly more than that in Run 3. However, because of this, the dummy's nearside leg had been trapped more directly between the motorcycle and the car in Run 7 than the

equivalent in Run 3. The pelvis had also pitched higher in Run 7 than that in Run 3 thus the head is striking towards the target lower in Run 7 than in Run 3.

Run 8 cannot readily be compared with any of the other runs, because even in Run 7, which is the nearest comparison possible, the target areas between the two are very different. This is because the bonnet is a lot lower down than the car roof, therefore only general observations will be given.

As the motorcycle hit the grille and then yawed away from the car, the offside leg had spread wide as the petrol tank yawed towards this leg. From there on, the dummy straightened its legs and the whole dummy had launched itself from the motorcycle, striking towards the bonnet. This happened as the motorcycle yawed away from the car but rolled slightly towards it.

11.6 Discussion

The clear difference between impacts where the target is a rigid barrier and a deformable car is that the car has a finite mass and is deformable, thus softening the impact. However, from the limited comparisons conducted it has emerged that impact with a car had caused greater rotations of the motorcycle with respect to all three axes. This can be verified by comparing Run 5 and

Run 6 where pitch, roll and yaw have all increased in Run 6, with the only difference between the two runs is that in Run 5 the car is stationary but moving in Run 6.

This is so since the car is able to absorb more energy and thus while the front wheel is being trapped between the motorcycle frame and the barrier, the front wheel can still travel further if impacted into a car. Thus the initial impact is not as sharp or sudden as would be in the case of a barrier, allowing more time to generate other movements. The motorcycle motion is also influenced by the rotations of the car hence the distinct difference between Run 5 and Run 6.

Because of the greater rotations of the motorcycle, this caused the dummy to rotate, especially in pitch motion. However, when the head was still diving towards the car, it was observed that the pelvis is pitching greater than in the cases of a barrier impact. This is because of the further distance of the car roof relative to the dummy, as compared with the relative distance between the dummy and the barrier.

These are the general observations made by the limited number of computer runs to date. In order to examine the results in more detail and hence draw more definitive conclusions, one needs to build a more refined model, and also carry out a greater number of computer runs.

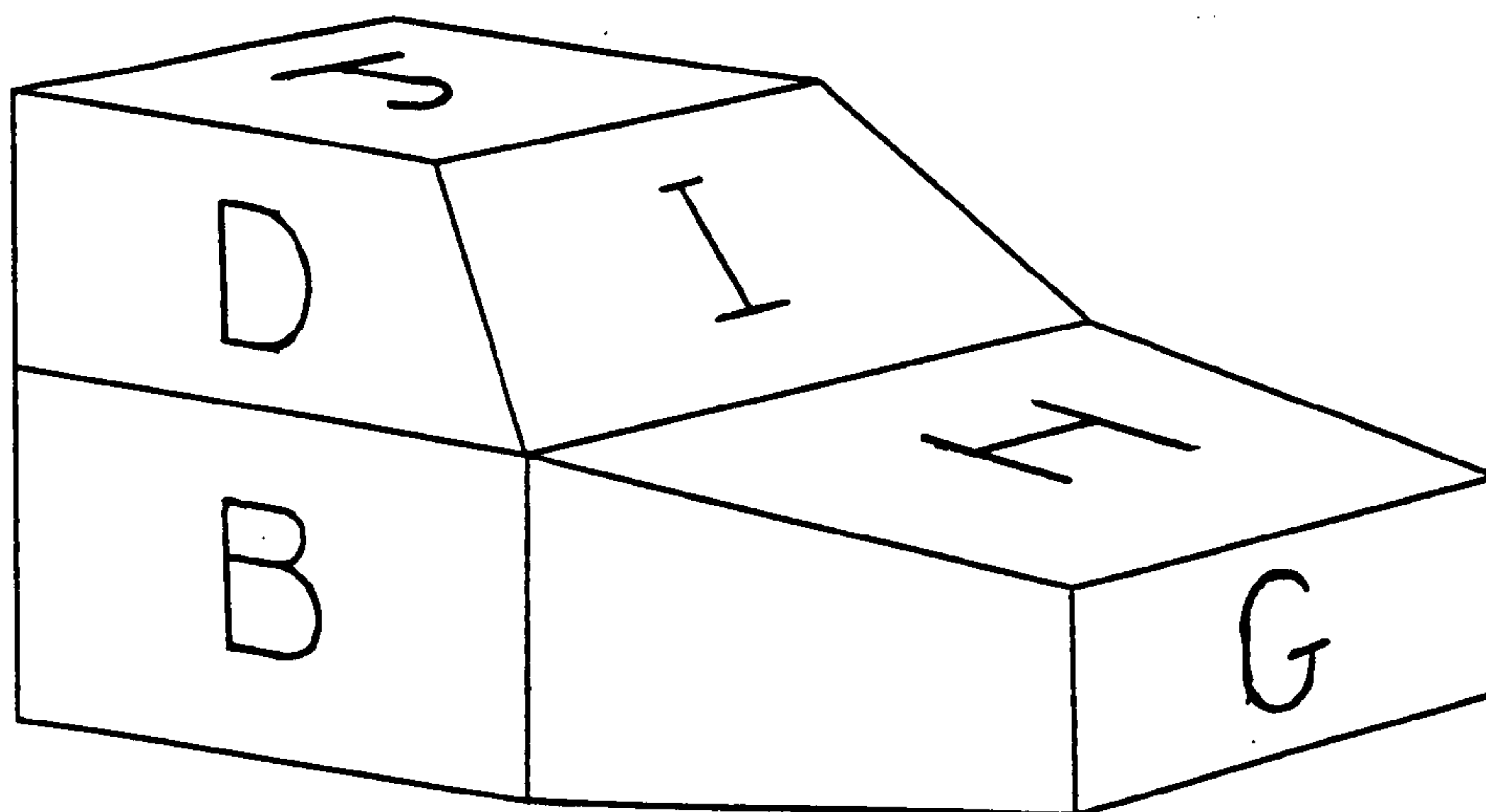


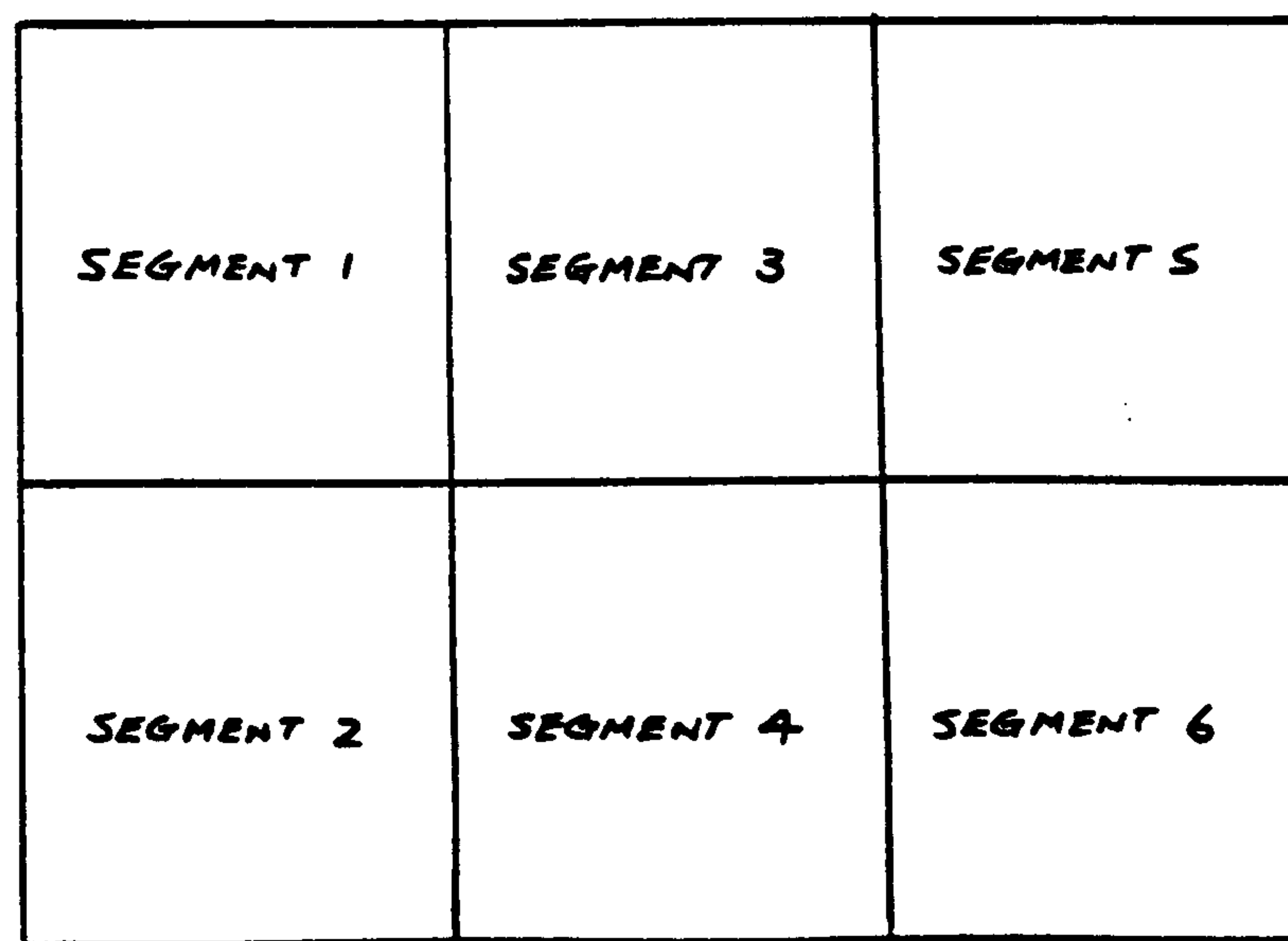
Figure 11.1 A diagram of the different panels in forming a motor car.

local y-axis

y3

y2

y1



x1

x2

x3

x4

local x-axis

Figure 11.2 Each panel is divided into segments.

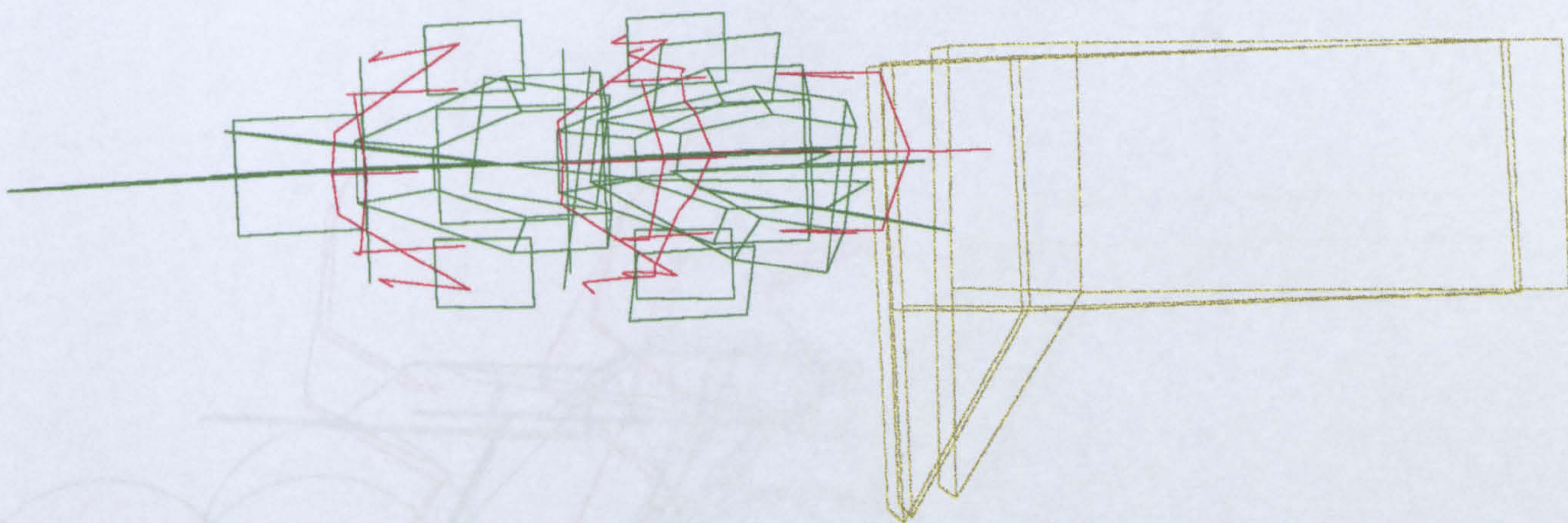


Figure 11.3a Plan view of Run 5

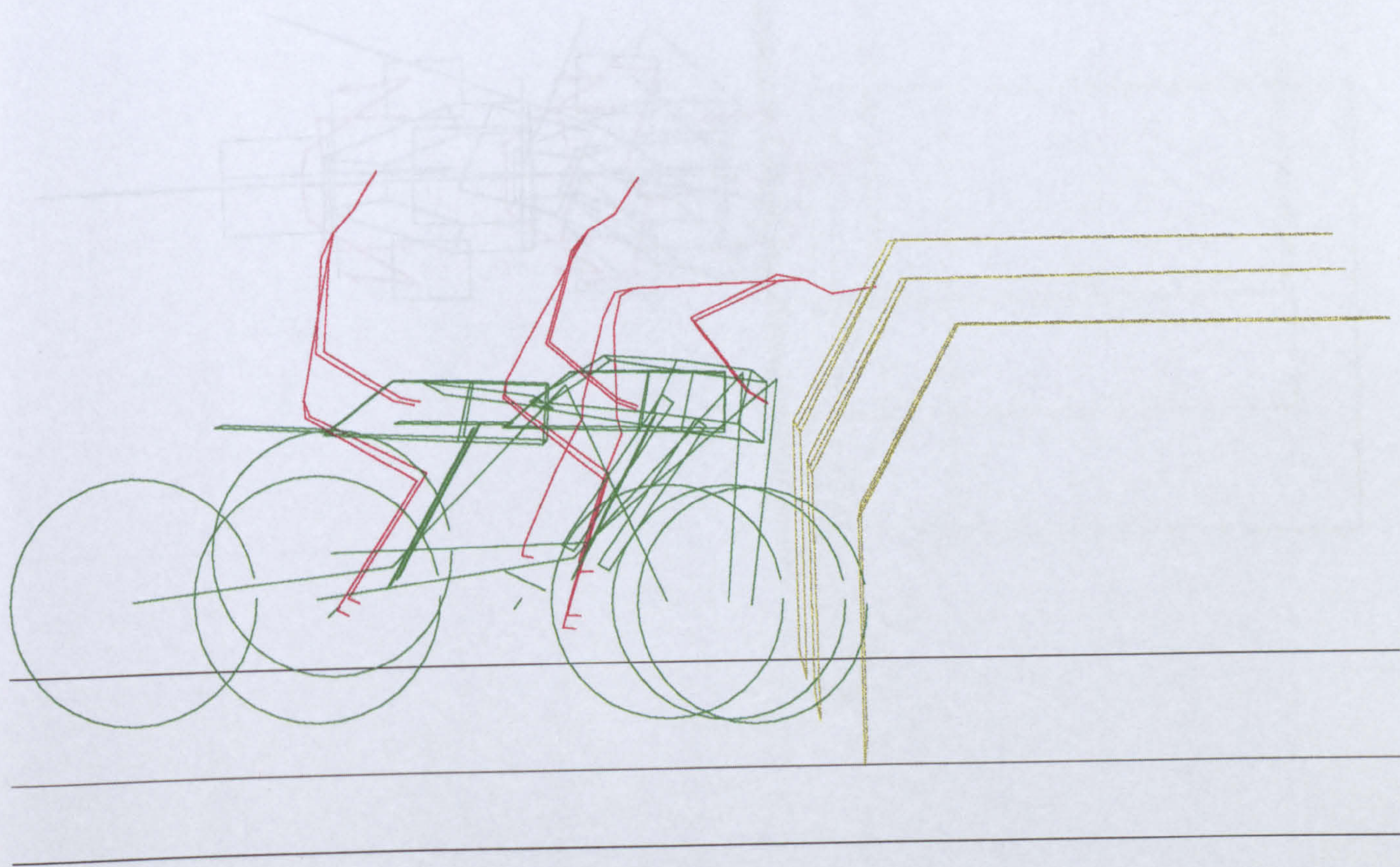


Figure 11.3b Elevation view of Run 5

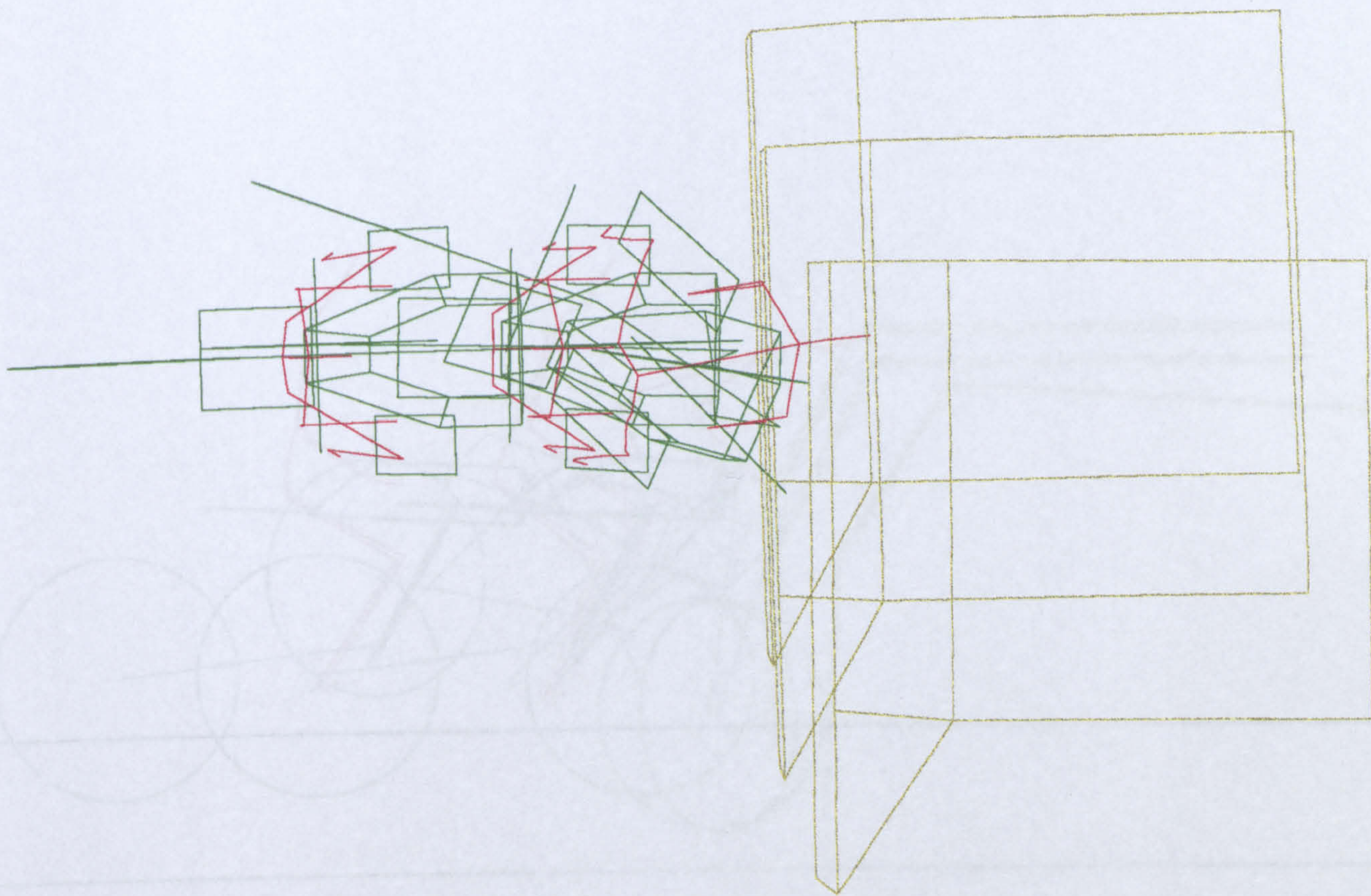


Figure 11.4a Plan view of Run 6

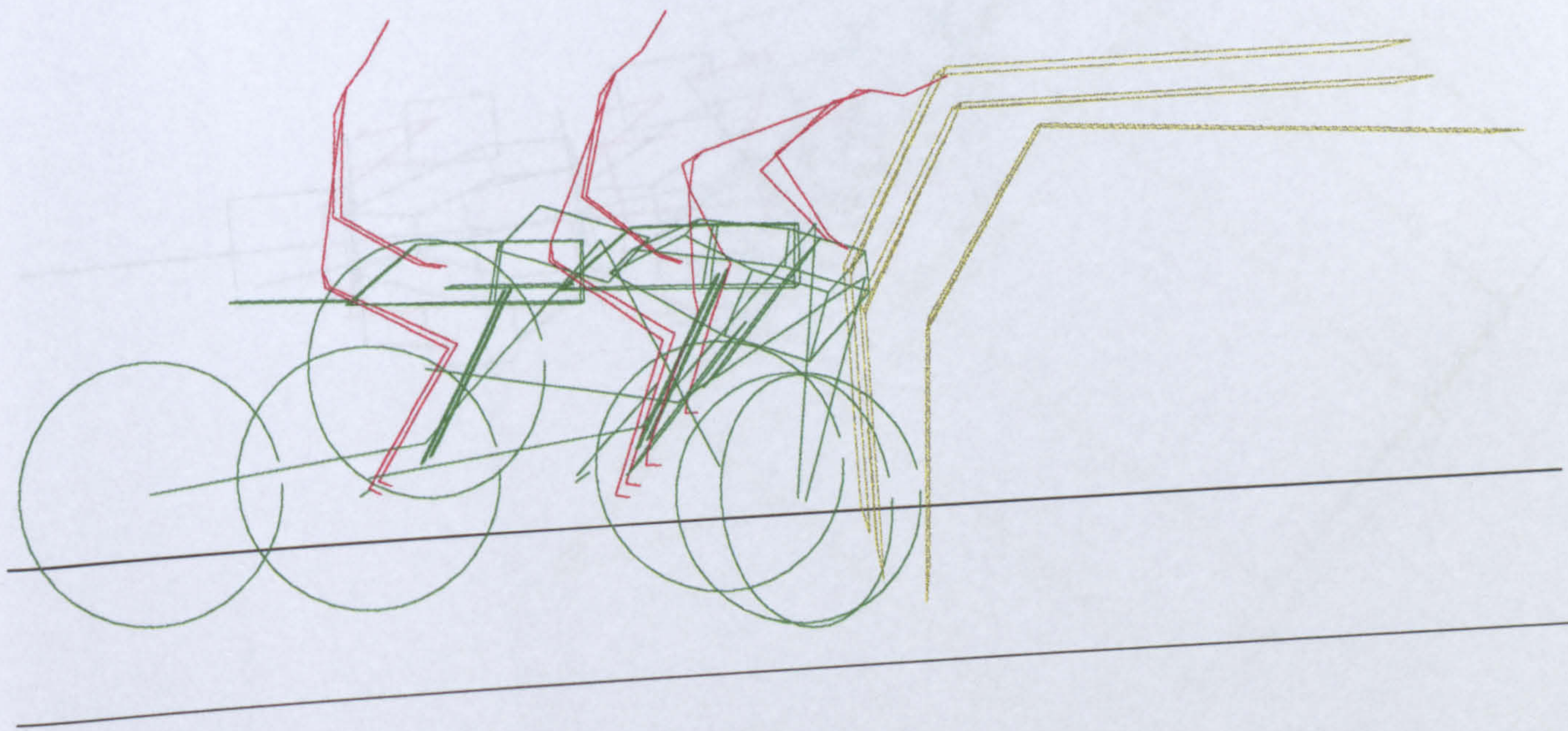


Figure 11.4b Elevation view of Run 6

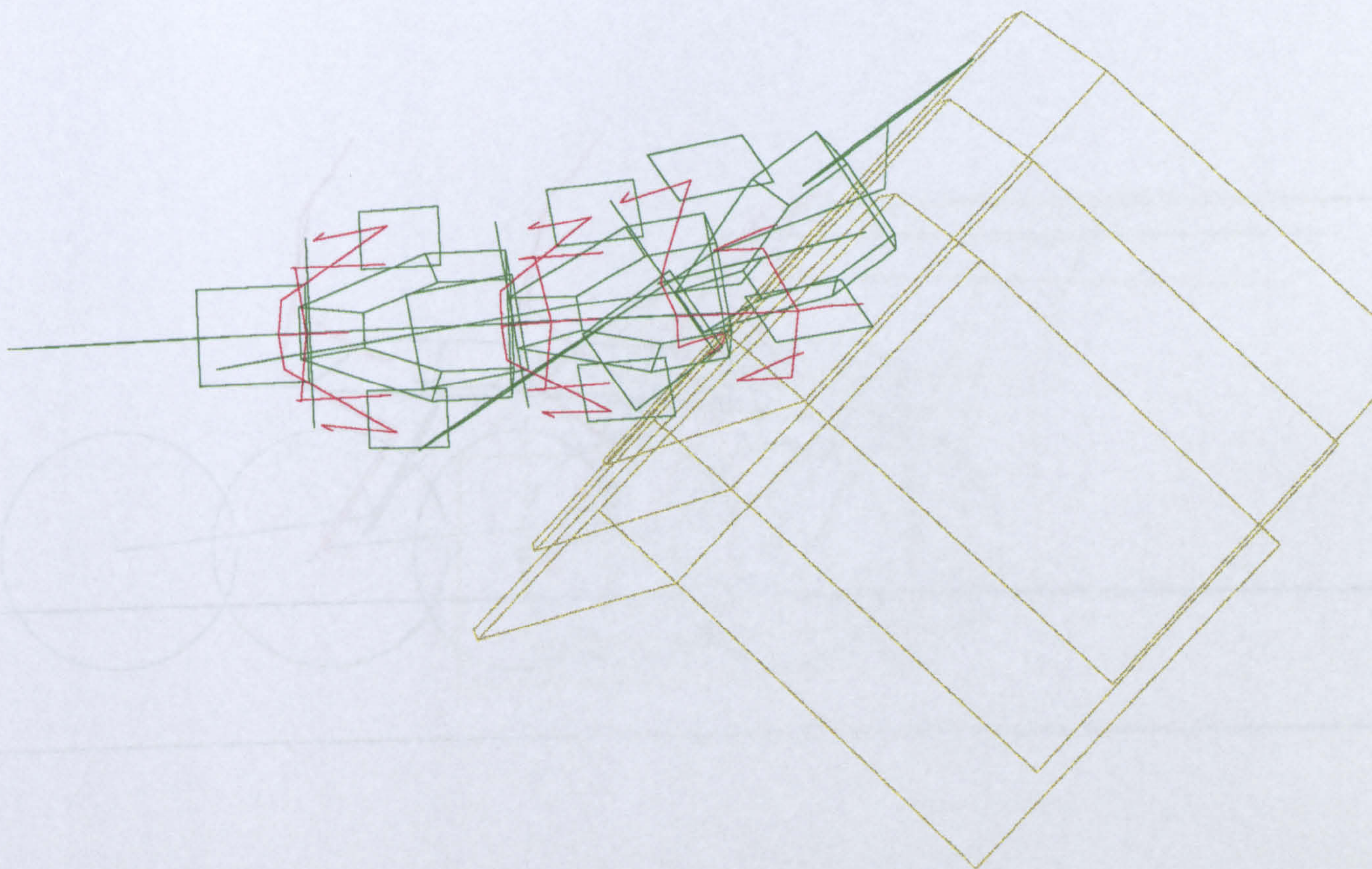


Figure 11.5a Plan view of Run 7

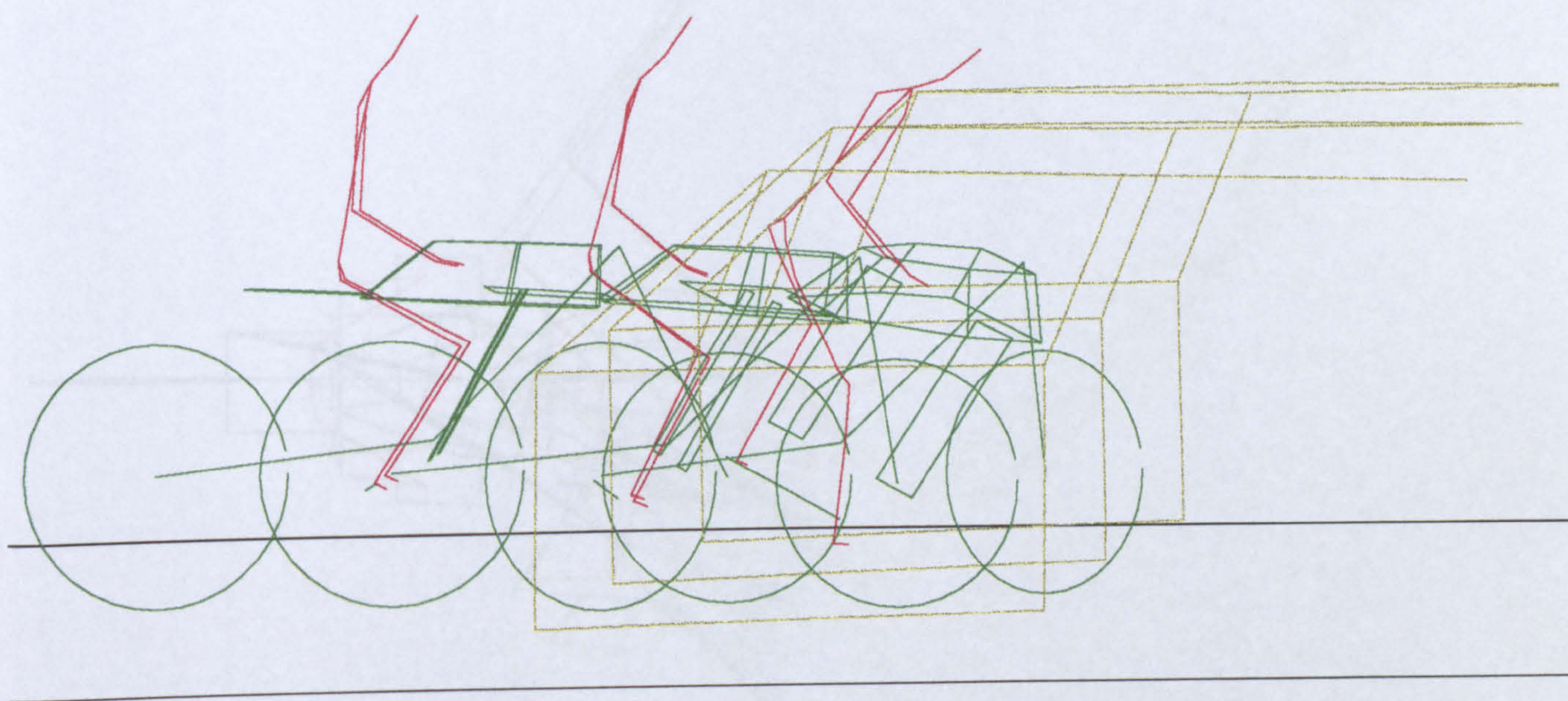


Figure 11.5b Elevation view of Run 7

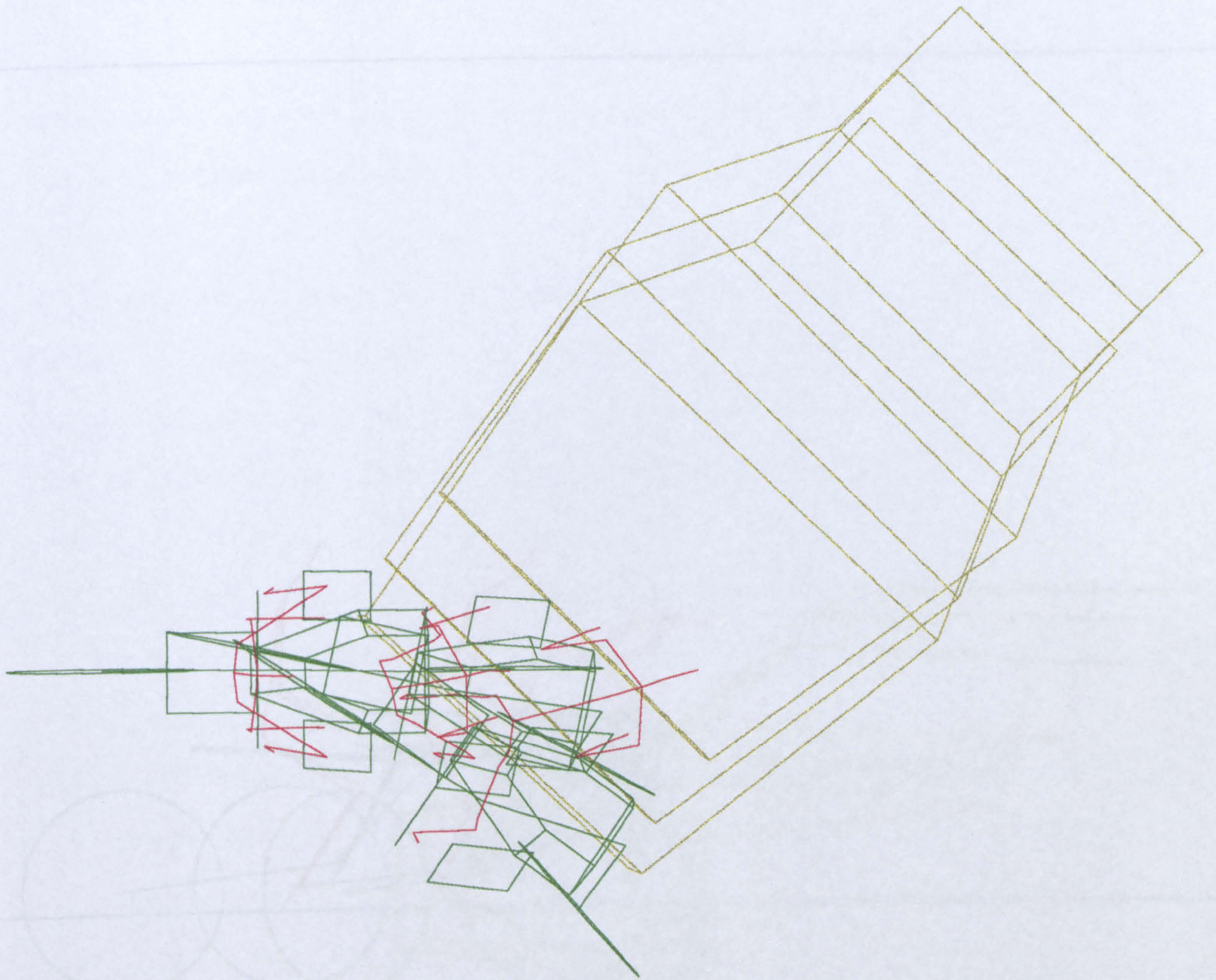


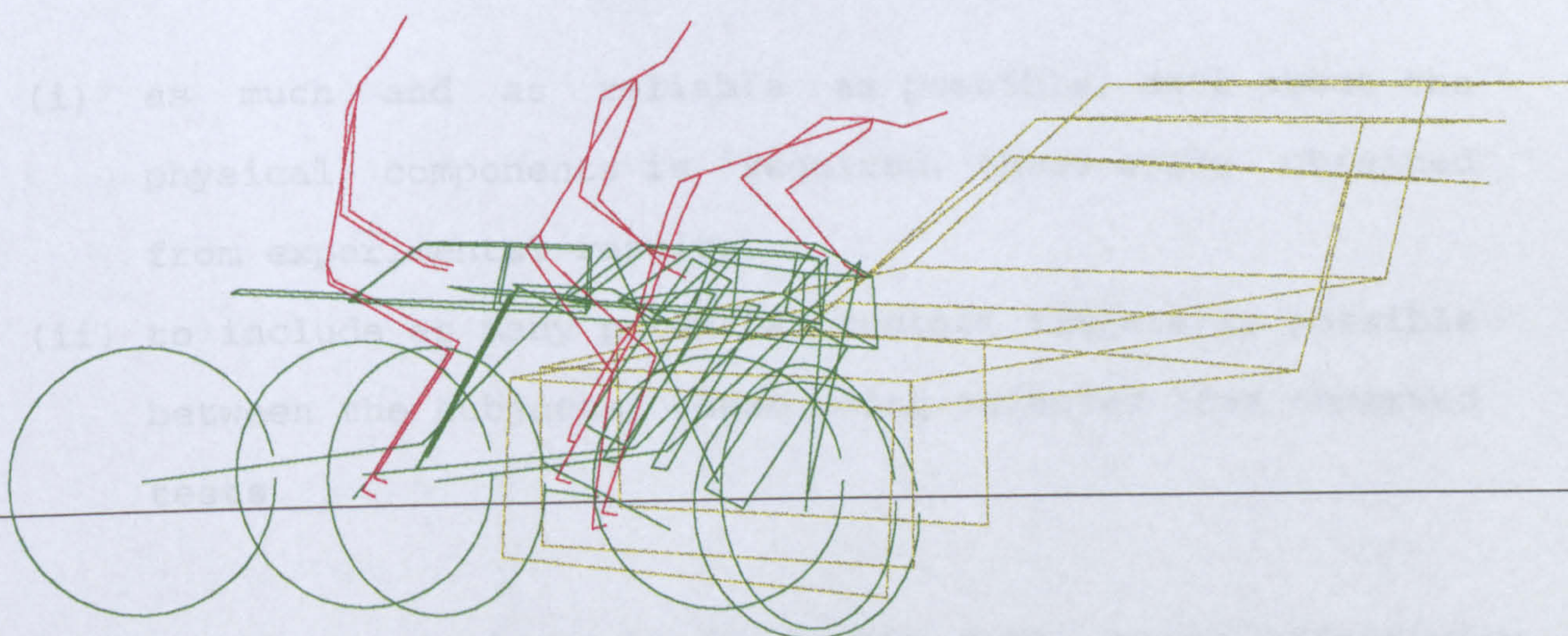
Figure 11.6a Plan view of Run 8

CONCLUSIONS AND FURTHER WORK

12.0 General Conclusions

Some general conclusions can be drawn with respect to the findings from this work.

With regard to the calibration and validation of the computer model, it was found that in order to produce results as closely-matched as possible to those of the test work, the following two factors are of prime importance:



However, one test bear is that the model is able to predict the behavior of the system under test.

It is less clear whether the model is able to predict the behavior of the system under test.

as basic guides within which the model is able to predict the behavior of the system under test.

time and cost are the two main factors which are of prime importance in the design of a machine.

more potential contacts in the work.

Figure 11.6b Elevation view of Run 8

CHAPTER 12

CONCLUSIONS AND FURTHER WORK

12.0 General Conclusions

Some general conclusions can be drawn with respect to the findings from this work.

With regard to the calibration and validation of the computer model, it was found that in order to produce simulation results as closely-matched as possible to those of the real crash tests, the following two factors are of primary concern:

- (i) as much and as reliable as possible, data about the physical components is required, these being obtained from experimental results,
- (ii) to include as many potential contact targets as possible between the subjects, these being selected from observed tests.

However, one must bear in mind that data, being effectively limitless under different circumstances, then they can only serve as basic guides within certain constraints. Also computational time and cost are but two factors governing the desire of putting more potential contacts in the model.

There are also two important findings observed from the calibration work, and they are:

- (i) that one can improve the computer model to produce as closely matching reality as possible but even then it is unlikely to re-produce exact events,
- (ii) a mathematical model is extremely sensitive when there are ill-conditioned situations, such as the discontinuity in head to barrier force generation as described in Chapter 4 which thus produces a singularity in the system. Hence a mathematical model is never as refined as the real-life events it attempts to simulate.

Investigations were made to compare the effects of differentiation and integration using simulated results as original functions. The main findings are :

- (i) where cubic splines were used in the differentiation exercise, it was found that there was an increase in accuracy in the subsequent derivatives if there was an increase in the number of knots used in prescribing the original function, but
- (ii) where the Butterworth filter was used in the integration exercise, it was found that the subsequent integrals were similar but as the cut-off frequency is lowered, there was less noise emitted from the original curve

such that the profile of the curve will be smoother, and that

- (iii) between the two methods, the integration process did produce better results such that they resemble more to those produced by the program.

From the statistical analyses the following were concluded:

- (i) angle of impact and the initial velocity of both the motorcycle and dummy rider, are the two variables that correlated the best with the various forces endured by the dummy rider,
- (ii) for the tibiae, there is an increase in force if the knee is positioned closer to the knee-restraint, and also if the leg protector is made less stiff,
- (iii) for the offside thigh, it was found that the angle of impact is significant at oblique angles, and
- (iv) in general, the profile of the leg protector, i.e. whether it was of a more or less rounded shape, has an insignificant effect.

Where various other factors were investigated, including the use of different sized dummies, to compare with three datum runs, it was found that

- (i) in general, the legs suffered more when the dummy rider

was riding a motorcycle with larger leg protector than when the protector was minimal,

- (ii) where different sized dummies are concerned, it was found that the large male suffered more force on his legs against the fairings, but less on his upper legs against the sides of the petrol tank,
- (iii) when the dummy rider was sitting at different angles to the horizontal, it was at its most up-right (80°) where in general it had suffered the most,
- (iv) for the different stiffnesses in airbags, it was found that the stiffer the airbag, the higher the force transmitted to the dummy's head, but the least to its torso, and
- (v) this was also the case when the airbag was situated furthest away from the dummy rider.

When the OPAT dummy, which had been the modelled subject in most of this work, was changed to that of the HYBRID3 specification, with frangible legs, it was found that

- (i) the HYBRID3's legs have both spread wider and straightened out more than those of the OPAT. This is because of the extra flexible joint in each of the femora and tibiae, indicating fracture of these bones,
- (ii) the HYBRID3 had flexed less in its spine than the OPAT. This is because of the higher position of the massed-

torso, relative to the pelvis, along its spine than that of the OPAT,

- (iii) it is also due to this higher position of torso, that caused the motorcycle to stay up-right longer than when the OPAT dummy was riding the motorcycle.

Similar to the extension of the dummy rider, when the target of impact was replaced by a motor car, it was found that

- (i) the car had softened the initial impact as compared with the impact between the motorcycle and the barrier. This is because the car is able to absorb more energy, but
- (ii) the car is able to cause greater rotations of the motorcycle with respect to all three axes, and
- (iii) because of the motorcycle's rotations, it also led to greater rotations of the dummy rider, especially in pitch motion.

12.1 Overall Conclusions

The simulation of a motorcycle and rider in impact is generally realistic. There had been situations when events were not anticipated, such as the occasion when the dummy dived down at the front of the motorcycle, but this can be rectified by providing further contact surfaces between the dummy rider and

the target. However, since the real-life full scale crash test is highly ill-conditioned such that a slight discrepancy in the set up can cause large changes in the subsequent impact, it follows that the simulation model of such an event, is also extremely sensitive.

The current approach to the modelling has the advantage of being simpler to use than the popular F.E. (Finite Element) approach, although it does require a different kind of experimental data such as stiffness and damping values of components as opposed to the actual material. Furthermore the SD/FAST library can provide kinematic information of a multi-body system thus saving the long and costly conventional programming. The use of ACSL as a programming language is ideal in collaboration with SD/FAST such that it describes the actual situation being modelled, and is extremely useful as an integrator of the system.

But a practical point is one which is concerned with cost. At TRL, where full scale crash tests are carried out, it is in the order of £25-30K to conduct such a test [35]. This covers the basic instrumentation, photography and also specifications to the ISO standard, along with the actual cost of the motorcycle and the motor car. However, based on the internal computational charge of running the simulation model at TRL, it was found that a sum of around £1,500 can cover a typical simulation run. Thus the cost-effectiveness of a mathematical simulation model, can

be justified.

However, one must bear in mind that a simulation model can only provide the likelihood of events happening under a certain circumstance; it does not represent the exact replica of a real-life situation.

12.2 Further Work

It is conceivable that for any mathematical model, one can improve its performance further. The following are but a few ideas that are specific to the present model.

- (i) The use of F.E. analysis to obtain stiffness and damping properties for the individual components, rather than for the whole system, could thus replace the difficult and costly task of obtaining these data by experimental means could be worthwhile.
- (ii) Further data, collected by whatever means, about the impact, would help to improve the model. This could include more detailed information about the car, such as the non-linear and non-uniform stiffnesses on the various panels and the non-linear properties of the wheel suspensions, along with more observed performance from the actual crash test.

- (iii) Improvements to the computational speed of the simulation model could be made. This can be done by investigating and developing the mathematical algorithm currently used in the computational stage.
- (iv) Any further and necessary contacts can be added into the simulation. This will be based on the observed data mentioned in (ii), but is directly linked to the computational speed mentioned in (iii).

However, besides these further improvements, one should bear in mind the following in the event of future development.

- (i) To make direct comparison between a motorcycle with leg protection and one without is a clear necessity before a definitive valuation of leg protectors can be made.
- (ii) To develop a full impact-generated inflated airbag for a motorcycle, as a simulation model is indicated.
- (iii) At present, the dummy's hands, in accordance with the full scale crash test, are not attached to the handle bars. A model of a more life-like riding position would be useful.
- (iv) The coefficients of frictions, between any contacting surfaces, or indeed within the joints, is of particular importance. More experimental investigation needs to be done in order to yield more realistic values for these.

Based on these further points, more detailed analyses of the designs and effectiveness of the motorcycle safety devices, can be evaluated.

REFERENCES

1. Dynamics of Motorcycle Impact 1971-1973, vol. I, II and III. September 1973. U.S. Department of Transportation, National Highway Traffic Saffic Administration, Washington, D.C.
2. Happian-Smith J., Motorcycle and Rider Dynamics in Frontal Collision, Simulation and Verification. Ph.D. thesis, Brunel University, 1988.
3. ACSL Reference Manual, edition 10.0, 1991. Mitchell & Gauthier Associates, U.S.A.
4. Motor cycles - Test and analysis procedures for research evaluation of rider crash protective devices fitted to motor cycles. Part 7 : Standardized procedures for performing computer simulations of motor cycle impact tests. ISO/CD 13232-7. First edition - 1994-05-24.
5. Bly P.H., A Review of Motorcycle Safety. Proc. 14th ESV Conference, Munich, 1994. Paper no. 94-S7-O-08.
6. Chinn B.P., Injuries to Motorcyclists' Legs : Testing Procedures and Protector. Ph.D. thesis, Brunel University, 1985.
7. Chinn B., Hopes P., Macaulay M., Leg Protection for Riders of Motorcycles. Proc. 10th ESV Conference, Oxford, 1985. p1055-1058.
8. Tadokoro H., Fukuda S., Miyazaki K., A Study of Motorcycle Leg Protection. Proc. 10th ESV Conference, Oxford, 1985.

p1100-1108.

9. Sakamoto S., Difficulties in Leg Protection Research. Proc. 12th ESV Conference, Goteborg, 1989. p1328-1335.
10. Chinn B., Hopes P., Finnis M., Leg Protection and Its Effect on Motorcycle Rider Trajectory. Proc. 12th ESV Conference, Goteborg, 1989. Paper no. 89-6B-O-002.
11. Sporner A., Langwieder K., Polauke J., Risk of Leg Injuries of Motorcyclists - Present Situation and Counter-measures. Proc. 12th ESV Conference, Goteborg, 1989. p1279-1287.
12. Rogers N.M., Evaluation of TRL Designed Leg Protectors for A Medium Sized Sport Motorcycle. Proc. 14th ESV Conference, Munich, 1994. Paper no. 94-S7-W-16.
13. Chinn B.P., Happian-Smith J., Macaulay M.A., The Effect of Leg Protecting Fairings on the Overall Motion of a Motorcycle in a Glancing Impact. International Journal of Impact Engineering, vol.8, no.3, 1989.
14. Chinn B., Donne G, Hopes P., Motorcycle Rider Protection in Frontal Impacts. Proc. 10th ESV Conference, Oxford, 1985. p1116-1119.
15. Finnis M.P., Air Bag and Motorcycle : Are They Compatible? SAE International Congress, Detroit, 1990. Paper no. 900744
16. Ramet M., Bouquet R., Bouallegue M., Bermond F., Cesari D., The Effect of Air Bag Inflation on the Cinematic and the Lesions of a Motorcyclist. Proc. 14th ESV Conference, Munich, 1994. Paper no. 94-S7-O-11.

17. Zellner J.W., Newman J.A., Rogers N.M., Preliminary Research into the Feasibility of Motorcycle Airbag Systems. Proc. 14th ESV Conference, Munich, 1994. Paper no. 94-S7-O-07.
18. Happian-Smith J., Chinn B.P., Simulation of Airbag Restraint Systems in Forward Impacts of Motorcycles. SAE International Congress, Detroit, 1990. Paper no. 900752.
19. Happian-Smith J., Macaulay M.A., Chinn B.P., Motorcycle Impact Simulation and Practical Verification. Proc. 11th ESV Conference, Washington, 1987. p858-865.
20. Happian-Smith J., Macaulay M.A., Chinn B.P., Computer Simulation of a Simple Motorcycle in Glancing Impacts with a Rigid Barrier. Proc. SAE International Congress, Detroit, 1990. Paper no. 900754.
21. Nieboer J.J., Wismans J., Vermissen A.C.M., van Slagmaat M.T.P., Kurawaki I., Ohara N., Motorcycle Crash Test Modelling. Proc. SAE International Congress, Texas, 1993. Paper no. 933133.
22. MADYMO User's Manual 3D, version 4.2. TNO Road-Vehicles Research Institute, Holland, 1988.
23. Yettram A.L., Happian-Smith J., Mo L-S.M., Macaulay M.A., Chinn B.P., Computer Simulation of Motorcycle Crash Tests. Proc. 14th ESV Conference, Munich, 1994. Paper no. 94-S7-O-10.
24. Chinn B.P., Yettram A.L., Mo L-S.M., Macaulay M.A., Computer Simulation of Motorcycle Impact Tests : A

- Parametric Study. Proc. IMECHE Conference, London. 1994.
25. Hollars Michael.G., Rosethal Dan.E., Sherman Michael.A.,
SD/FAST User's Manual, version B.1.1, Symbolic Dynamics
Inc., U.S.A. 1990.
 26. Phillips Mark.B., Viewwld, University of Maryland, U.S.A.,
1989.
 27. Phillips Mark, Levy Stuart, Munzner Tamara, Geomview.
Software Development Group, Geometry Center, Minneapolis,
U.S.A., 1993.
 28. The Numerical Algorithms Group Ltd. The NAG Fortran Library
Manual. Mark 13, vol.2, 1988.
 29. Lennart Ljung, Pro-Matlab User's Guide, The MathWorks, Inc.,
1988.
 30. Taylor D., Private Communication.
 31. Norušis Marija J., SPSS Base System User's Guide, SPSS Inc.,
U.S.A. 1990.
 32. Norušis Marija J., SPSS/PC+ Advanced Statistics 4.0, SPSS
Inc., U.S.A., 1990.
 33. Anthropometric Specifications, Transportation Research
Institute, The University of Michigan, U.S.A., 1983.
 34. Nieboer J.J., Wismans J., de Coe P.J.A., Airbag Modelling
Techniques. Proc. SAE International Congress, Detroit,
1990. Paper no. 902322.
 35. Chinn B., Private Communication.

BIBLIOGRAPHY

1. Morrison J.L.M., Crossland B., An Introduction to the Mechanics of Machines, second edition. 1970. William Clowes & Sons, Ltd.
2. Bacon D.H., Stephens R.C., Mechanical Technology. 1977. Butterworths.
3. Brach Raymond M., Mechanical Impact Dynamics. Rigid Body Collisions. 1991. John Wiley & Sons.
4. Macaulay M.A., Introduction to Impact Engineering. 1987. Chapman and Hall.
5. Humphrey D., Intermediate Mechanics. Dynamics. 1955. Longmans, Green and Co. Ltd.
6. Cohn P.M., Solid Geometry, third impression. 1965. Latimer, Trend & Co. Ltd.
7. Feineman George, Garrett Samuel, Kraus Allan, Applied Differential Equations. 1965. Macmillan and Co., Ltd.
8. Burden Richard.L., Faires Douglas.J., Numerical Analysis, third edition. 1985. Prindle, Weber & Schmidt.
9. Macon Nathaniel, Numerical Analysis. 1963. John Wiley and son, Inc.
10. Mathews John.H., Numerical Methods for Mathematics, Science, and Engineering, second edition. 1992. Prentice-Hall International Editions.
11. Phillips G.M., Taylor P.J., Theory and Applications of Numerical Analysis. 1973. Academic Press : London and New

York.

12. Watson G.A., Approximation Theory and Numerical Methods. 1980. John Wiley & Sons Ltd.
13. Scheid Francis, Numerical Analysis. 1968. Schaum's Outline Series. McGraw-Hill Book Company.
14. Beauchamp K.G., Signal Processing using Analog and Digital Techniques. 1973. George Allen & Unwin Ltd.
15. Willemssen Eleanor.W., Understanding Statistical Reasoning. 1974. W.H. Freeman and Company.
16. Hope K., Elementary Statistics. 1967. Pergamon Press Ltd.
17. Backhouse J.K., Statistics. An Introduction to Tests of Significance, third impression. 1968. Spottiswoode, Ballantyne & Co. Ltd.
18. Blank Leland, Statistical Procedures for Engineering, Management, and Science. 1980. McGraw-Hill, Inc.
19. Berenson Mark.L., Levine David.M., Goldstein Matthew, Intermediate Statistical Methods and Applications, Prentice-Hall.

APPENDIX A.1

USE OF PROGRAM

A.1.0 Introduction

In this appendix a brief user's guide to the ACSL program will be given. This will include commands to execute and run the program, the dumping of results and the graphical plotting facilities. This will involve a number of related files and their significance will also be explained.

However, this will only give the general running commands of the existing program. Thus, if for any reason the user feels a parameter from the program needs to be updated, for example the damping value of the front wheel, one needs to know the way to change this parameter and also if it has significant effect on the set up, or the stability of the running of the program. Therefore, a section with reference to the modification of parameters will also be given.

A.1.1 Compilation

Imagine that two SD/FAST data files which describe the motorcycle and the dummy, and an ACSL program with access to the SD/FAST

libraries of routines have all been written, the next step the user needs to take is to compile these files so that the ACSL program can run. First, the SD/FAST data files need to be compiled, then the ACSL program can link to the libraries in its compilation.

Suppose we have two SD/FAST data files called 'opat.dat' for the dummy rider, and 'cycle.dat' for the motorcycle. To compile these into their relevant FORTRAN files we type

```
sdfast -ge opat.dat
```

where 'ge' means 'generate everything'. This will lead to the creation of the following four files: opat_dyn.f, opat_sar.f, opat_info and sdlib.f

The 'dyn' file is the 'Dynamic file', which contains all the system equations and system-specific generated code. The 'sar' file is the 'Simplified Analysis file', which contains system-specific analyses for common operations. The 'info' file is an 'Information file', which contains a roadmap and information about the specific system. The 'sdlib' file is a 'Library file', which contains numerical library routines used by the subroutines in the Dynamic and Simplified Analysis files. A similar procedure is carried out on cycle.dat.

All the routines within the above files will have a meaningful mnemonic name with preceding letters 'SD'. This would be highly inconvenient in our case where two SD/FAST models are used, such that there will be two Information files, and the two models sharing the same routine names. However, there is an option to give a specific name to a model or to distinguish the routines when more than one SD/FAST model is being used, this is done by typing

```
                sdfast -ge -pdmy opat.dat  
and             sdfast -ge -pcyc cycle.dat
```

This will generate a Library file of the name 'dmylib.f', and routine names preceding with the letters 'DMY' in the case of the dummy rider. Similarly, a 'cyclib.f' Library file and routine names preceding with letters 'CYC' in the case of the motorcycle.

After these files have been generated, the task is to compile them into object codes. This is done by typing

```
f77 opat_dyn.f opat_sar.f dmylib.f
```

This will lead to the generation of the following object files: opat_dyn.o, opat_sar.o and dmylib.o. Equivalent files will also be generated for the motorcycle by typing the above with the appropriate files.

When these object-coded files have been generated, they are ready to be linked to the ACSL main program for compilation. Suppose our ACSL program is called 'barrier.csl', in order to compile this file type

```
acsl barrier cycle_dyn.o cycle_sar.o cyclib.o
      opat_dyn.o opat_sar.o dmylib.o
```

This will generate three files. One file is the subsequent generated FORTRAN file of the same name with the extension '.f' i.e. 'barrier.f', the second is the object-coded file with the extension '.o', i.e. 'barrier.o', and finally the executable file with the name simply 'barrier'.

These are the tasks in the compilation stage of the running of the program. Note that these are the general commands since the installation of software is dependent on the local network. In addition, there are options available with the FORTRAN compiler, for example a '-x' for double-precision formatted variables, and these will be machine-dependent.

A.1.2 Running Of The Program

When the ACSL program is ready to run, the user simply keys in the executable name of the program, in our case, it would be

'barrier'. By typing this word, it will bring us into the ACSL environment and it has a leading prompt as follows:

```
ACSL>
```

ACSL-specific commands can now be typed following the prompt.

There is a whole range of ACSL-specific routine commands, for more details consult the ACSL user's guide [3]. Here we will outline some of the widely used commands. Below is a list of these and a description of their functions. Letters in upper case are the actual typed runtime commands. Note that the list of commands is used prior to the start of the simulation.

(a) PREPARE

This is to prepare the variables whose names follow this command. This is a very important command since variables whose names are not in this 'prepare' list will not be available for dumping as output or for interactive analysis after the simulation. Alternately, the user can type

```
PREPAR /ALL
```

This will prepare every variable in the program. However, if the program is immensely large such that the number of variables used is enormous, this command will not be advisable since this will

use too much of the available memory and computational time.

(b) SET

This is a powerful command. Its function is to provide the user the option of changing certain parameters already set in the program, say a coefficient of friction called MEW to a different value. This is done by typing, for example,

```
SET MEW = 0.5
```

The syntax of this command is very simple but the significance of this command will be highlighted later.

(c) OUTPUT

This is an optional command. Its purpose is to output values of the variables whose names follow at every communication stage during the simulation. This is a useful tool in that the user then has knowledge of how the simulation is still in progress, or an indication of how far the simulation has performed. This of course involves a large amount of input and output between the processor and the display unit, so a decision needs to be made as to the benefit of applying this command. For example, if a short program has been tested to work correctly, and its processing time is short, therefore it may be beneficial just to run the simulation without the interactive output.

(d) START

This command simply allows the simulation to commence. After the simulation has completed, the user would like to extract results from the computation for analysis purposes. However, while the program is still in the ACSL environment the user can communicate with the simulation interactively. There are various analysing facilities provided by ACSL, but here we will outline some typical plotting commands.

The command to display graphs in interactive mode or for hardcopy is simply 'PLOT'. Let us consider the following command.

```
PLOT Y
```

This will display the graph of Y against time T. T is automatically taken as the x-axis if the user did not specify the variable to be plotted as the x-axis variable against Y. However, if the user would like to plot, say X against Y, then typing

```
PLOT /XAXIS = X, Y
```

will display the above curve.

Suppose we have inspected the graph of X against Y, and would like to zoom into a certain area of the curve, say between (x_1, x_2) and (y_1, y_2) . This is done by typing

PLOT /XAXIS = X , /XLO = x_1 , /XHI = x_2 ,
Y , /LO = y_1 , /HI = y_2

Note that if the user does not feel that one of the axes needs to be specified, this can be achieved by the omission of the appropriate scaling commands.

It has been mentioned that the plotting commands for display unit and for hardcopy are the same, but choosing the device will signify the status of the output. There is a default list in the ACSL manual. For example to display plots in an X-window one types

SET DEVPLT = 6

but the device drivers are usually dependent on local network therefore it is advisable to check with the installation of the ACSL software.

However, once the user has chosen for a particular plotting device to produce graphical hardcopy, the following command needs to be keyed in before the actual plotting command

SET PLT = N

where N is an integer greater than 10. This will produce the

appropriate formatted file, according to the device driver chosen, thus if N=12, then plot12.

After having made relevant hardcopies of the required plots, the user may wish to examine certain variables closely. This is done by piping out data into a logging file. The command is simply, say

```
PRINT T , X , Y
```

This will produce the values of T, X and Y at every communication level of the simulation. However if the user wishes only to pipe out data at say, every tenth communication level, it can be done by typing

```
PRINT T , X , Y , /NCIPRN = 10
```

But where do all these data go? They are automatically dumped into a file of the same name with the extension '.log', in our case, it would be 'barrier.log'. Indeed, whilst the user is in interactive mode inside the ACSL environment, all the commands typed and the output displayed on the terminal screen, if any, are stored automatically in this .log file.

While the simulation is being executed, another file of the same name but with the extension '.rrr', here 'barrier.rrr', is being

created. This is called a 'raw run record' file. This file has not been extensively used by the author and the understanding of the purpose of this file is for simulation reassurance, such that the same simulation can be repeated exactly.

A.1.3 The ACSL Command File

There may arise a situation when the user is interested in repeating the same simulation but with a few changes to certain parameters. Furthermore it is conceivable that the user is only interested in certain resulting variables from the simulation. It would be a cumbersome task, and an increase in the risk of mis-typing, if the user were to key in these commands interactively every time a new simulation was to commence. ACSL provides a facility called a 'command' file with the extension '.cmd', in our case, it would be 'barrier.cmd'.

Inside a command file the user may type in the parameters of interest, and edit the assignments to these values if changes are needed. Output and print commands can also be keyed in to to this command file. However, it is obvious that these commands need to be activated separately. ACSL provides the means to do this by introducing a command called 'PROCEDURE'. Common commands can be bounded by such a procedure with a name assigned to it, for example

```

PROCED SETDATA
SET .....
.....
.....
END

PROCED OUTDATA
PRINT .....
.....
.....
END

```

Note that each procedure is bracketted by 'PROCED' and its appropriate 'END' statements.

When the user enters the ACSL environment, ACSL will activate the input facility of a command file, if it existed, but this does not mean it automatically reads in all the commands inside a command file. This is done by the user keying in the appropriate procedure name, for example SETDATA as above. The commands within this procedure will be read by ACSL and the setting of the enclosed parameters will be updated accordingly. Similarly, after the simulation has completed, by typing OUTDATA the appropriate variable values will be outputted and dumped automatically in the '.log' file.

A.1.4 Modifying The Parameters

As was mentioned earlier the setting of parameters and the reading of the simulated variable values needs to be considered. What is the significance of the setting of parameters and how do they differ from variables? In this section, these variations will be explained.

In an ACSL program there are two basic groups of mnemonic variables. One group belongs to the class of parameters in that their values have already been set inside the program. The other group is the genuine class of variables whose values are computed at every stage of the simulation.

In the case of the group of parameters, they are defined by the ACSL statement `CONSTANT`, which is not an executable statement. For example, the mnemonic for the stiffness of the front wheel, may be defined as

```
CONSTANT  KFWHL = 10000.0
```

This signifies the constant value of KFWHL as being 10000.0 throughout the simulation. However, variable mnemonics whose declaration type are `CONSTANT` are the only variables that can be updated in future editions of the program, either by `SET` statements either when the user is in interactive mode with ACSL

or by use of command file as mentioned earlier.

In the case of the group of the genuine variables, their values are generated by the actual computation. In most cases, these variables need not be assigned an initial value, but they do need to be declared in terms of their status. In ACSL programming, all mnemonic names are taken to be real, single-valued numbers. Therefore variables whose status are different need to be declared at the start of the program. For example, arrays and an integer are as follows

```
ARRAY  HEAD(3)
ARRAY  INERTIA(3,3)
DOUBLEPRECISION  PLANE(4)
INTEGER  SWITCH
```

Note that if double-precision formatted computation is required, arrays need to be declared as DOUBLEPRECISION as above.

Since all mnemonic names are taken to be real single-valued numbers unless otherwise declared, it follows that these real single-valued variables do not need to be defined in the declaration of variables.

Therefore, by using SET commands the command file, if used, provides the convenience of testing different values of

parameters, but more importantly, it does not require repeated compilation every time the user edits a `CONSTANT` value, or more, within the program. This is because each program change requires new compilation, as with most programming languages, but setting parameters in an ACSL environment means the actual ACSL program remains physically unchanged. It follows that the `CONSTANT`-declared parameters can be viewed as user-supplied data for experimental testing.

It may be thought that ACSL is quite an odd language in that variables need to be assigned specific values inside the program, whereas programs written say, in FORTRAN, will have variables either assigned mathematically, or in a form of user-supplied data such that they need not hold specific values unless the user otherwise wishes. This requirement of assigning initial values in `CONSTANT`-typed parameters in an ACSL program is because ACSL is a continuous simulation modelling language. It has a special feature in that it can itself sort out program statements so that the programmer needs not arrange these statements in any specific order. This is quite unlike most of the other programming languages where statements are executed in the order in which they are coded. In addition, a `CONSTANT` can appear anywhere in an ACSL program so that these parameters need to hold actual, constant values.

A.1.5 Changes To The Current Program

Up until now, the explanation to the running of the program has been very general; it is applicable to most ACSL programs. In this section, a brief guideline will be given if the user wishes to make changes in the current simulation program. Two examples will be given.

The usefulness of the SET command has been highlighted. However, these kind of parameters contain single values which are sometimes inadequate in describing realistic objects, such as the stiffness of the front wheel, which is highly non-linear. However, ACSL does provide another form of data parameter. This is in a form of a table. Note that a table called one-dimensional in the ACSL language interrelates two variables, and so on. This is our first example of changes in the current model.

An ACSL table is basically a data list accessed by one, two or three independent variables, and like other variables, the table is given a mnemonic name. In the current program, the one-dimensional table data lists have been extensively used, and most of these are tables representing force or stiffness against deflection. For example, there is a force-deflection curve for the crushing of the front wheel, the program can extract numerical values on the curve, which is the force against the displacement, and obtain two columns of numbers. These are then

put into an ACSL tabular form so that a force value can be accessed based upon the compression of the front wheel. It is obvious that this list contains a finite pairing of data, but ACSL can extrapolate beyond the two limits so that the programmer needs only to supply an adequate number of data points and make an arrangement at either limit for extrapolation purposes.

However, this form of data cannot be declared as `CONSTANT` thus the `SET` command does not apply to table-formatted data. Therefore if the user wishes to put in another table, say to represent another type of wheel, the table needs to be keyed in , or if it is already inside the program, it needs to be referred to by a different mnemonic name.

The second example involves changes made to the defined planes in the current model. Referring back to Chapter 5 a plane is defined by four points in space. To achieve an alignment of the planes with the global coordinate axes system each plane is given its local axes system so that a direction cosine matrix can be derived. In the current model, a consistent local axes system is used for each plane such that the x and z axes lie on, or in the same orientation of the plane, and the y-axis, appointed to be the direction of the line of action of the force if contact occurred, is the axis pointing outwards from the plane. This is shown in Figure 5.2.

Note that this local axes system still follows the standardised right-hand rule.

At the moment, each plane in the program has been given its own local axes system, but it is conceivable that the user may like to put the plane in a different location. If the changed location is translational such that the movement is only a certain distance relative to one of the axes, but its distance is fixed relative to this axis, the user needs only to supply the four new corner locations defining the plane, since the plane's orientation still remains unaltered.

However, if the orientation of the plane has to be altered, the user must remember to supply the new local axes system in addition to the four points defining the plane. Fortunately, these values have all been declared as `CONSTANT` in the current program so that the user can either key in the new points and local axes interactively or edit the command file by the use of the `SET` command.

APPENDIX A.2

MATHEMATICAL DERIVATIONS

A.2.0 Introduction

In this Appendix the mathematical derivations to the various formulae used in Chapter 7 will be given.

A.2.1 Cubic Spline Interpolation

Cubic splines are polynomials of degree three on each sub-interval, $S_i(x)$, such that the first two derivatives of $S_i(x)$ are continuous. However, the construction of cubic splines does not assume that the derivatives of the interpolant S agree with those of the original function f , even at the nodes.

Let us define a function f on $[a,b]$ and a set of nodes, $a=x_0 < x_1 < \dots < x_n = b$. The interpolant, S , is called a cubic spline if it satisfies the following conditions (see Figure A.2.1):

- (i) S is a cubic polynomial, denoted S_i for $x \in [x_i, x_{i+1}]$ for $i=0, 1, \dots, n-1$
- (ii) $S(x_i) = f(x_i)$ for $i=0, 1, \dots, n$

The spline passes through each data point.

$$(iii) \quad S_{i+1}(x_{i+1}) = S_i(x_{i+1}) \text{ for } i=0,1,\dots,n-2$$

The spline forms a continuous function.

$$(iv) \quad S'_{i+1}(x_{i+1}) = S'_i(x_{i+1}) \text{ for } i=0,1,\dots,n-2$$

The spline forms a smooth function.

$$(v) \quad S''_{i+1}(x_{i+1}) = S''_i(x_{i+1}) \text{ for } i=0,1,\dots,n-2$$

The second derivative is continuous.

Let us define a cubic polynomial

$$S_i(x) = a_i + b_i(x-x_i) + c_i(x-x_i)^2 + d_i(x-x_i)^3$$

$$\text{for } i = 0, 1, \dots, n-1$$

$$\text{Clearly, } S_i(x_i) = a_i = f(x_i)$$

Applying condition (iii)

$$\begin{aligned} a_{i+1} &= S_{i+1}(x_{i+1}) = S_i(x_{i+1}) \\ &= a_i + b_i(x_{i+1}-x_i) + c_i(x_{i+1}-x_i)^2 + d_i(x_{i+1}-x_i)^3 \end{aligned}$$

$$\text{for } i = 0, 1, \dots, n-2$$

If we introduce $h_i = x_{i+1} - x_i$ for $i = 0, 1, \dots, n-1$ and define $a_n = f(x_n)$, it follows that

$$a_{i+1} = a_i + b_i h_i + c_i h_i^2 + d_i h_i^3$$

$$\text{for } i = 0, 1, \dots, n-1$$

Similarly, applying condition (iv) and define $b_n = S'(x_n)$ we have

$$\begin{aligned}
b_{i+1} &= S'_{i+1}(x_{i+1}) = S_i(x_{i+1}) \\
&= b_i + 2c_i(x_{i+1} - x_i) + 3d_i(x_{i+1} - x_i)^2
\end{aligned}$$

i.e. $b_{i+1} = b_i + 2c_i h_i + 3d_i h_i^2$

for $i = 0, 1, \dots, n-1$

Finally, applying condition (v) and define $c_n = \frac{S''(x_n)}{2}$ we have

$$\begin{aligned}
c_{i+1} &= \frac{S''_{i+1}(x_{i+1})}{2} = \frac{S''_i(x_{i+1})}{2} \\
&= c_i + 3d_i h_i
\end{aligned}$$

for $i = 0, 1, \dots, n-1$

A.2.2 The Butterworth Filter

The second-order low-pass Butterworth filter transfer function is defined as:

$$H(s) = \frac{1}{1 + 2(s/w_c) + (s/w_c)^2}$$

where $w_c = \tan(\pi f_c T)$

f_c being the cut-off frequency.

By using z-transfer

$$s = \frac{z-1}{z+1}$$

we have
$$H(z) = \frac{1}{1 + \frac{2 \cdot \frac{z-1}{z+1}}{w_c} + \frac{1}{w_c^2} \frac{z-1}{z+1}^2}$$

and the difference equation for the second-order Butterworth filter is

$$y_i = Cx_i + 2Cx_{i-1} + Cx_{i-2} - Dy_{i-1} - Ey_{i-2}$$

where

$$C = \frac{1}{1 + [\pi 2 \cot(\pi f_c T)] + [\cot(\pi f_c T)]^2} ,$$

$$D = 2[1 - (\cot(\pi f_c T))^2] ,$$

and

$$E = 1 - [\pi 2 \cot(\pi f_c T)] + [\cot(\pi f_c T)]^2 .$$

The filter gain is $1/C$.

However, a phenomenon called phase shift can happen when this filter is applied. This is due to the order of the filter which determines the fall-off rate. The higher the order, the more attenuation of frequencies above the cut-off frequency, see Figure A.2.2. However, the phase shift is remedied by applying the filter again backwards through the data points.

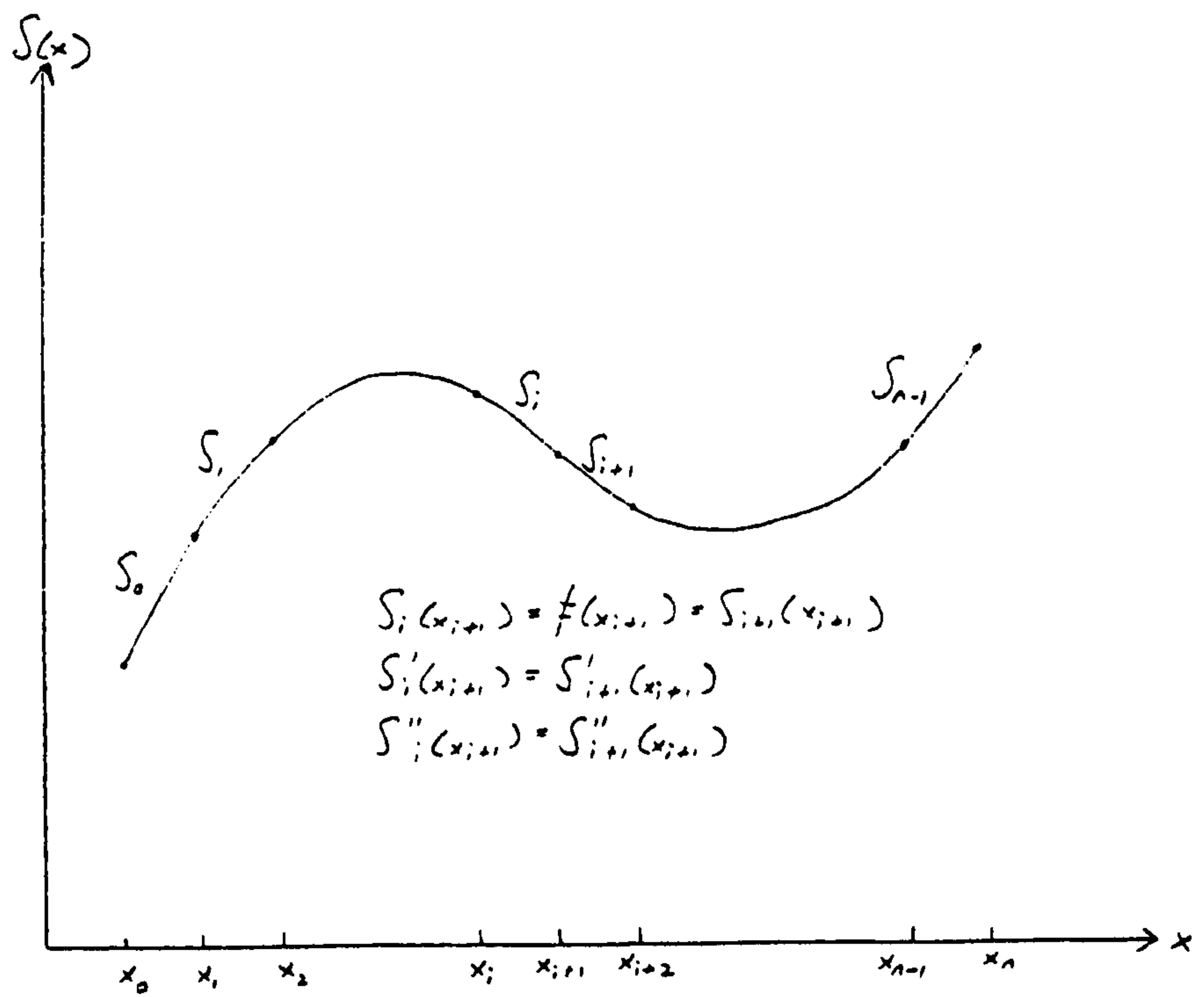


Figure A.2.1 Cubic spline S interpolant.

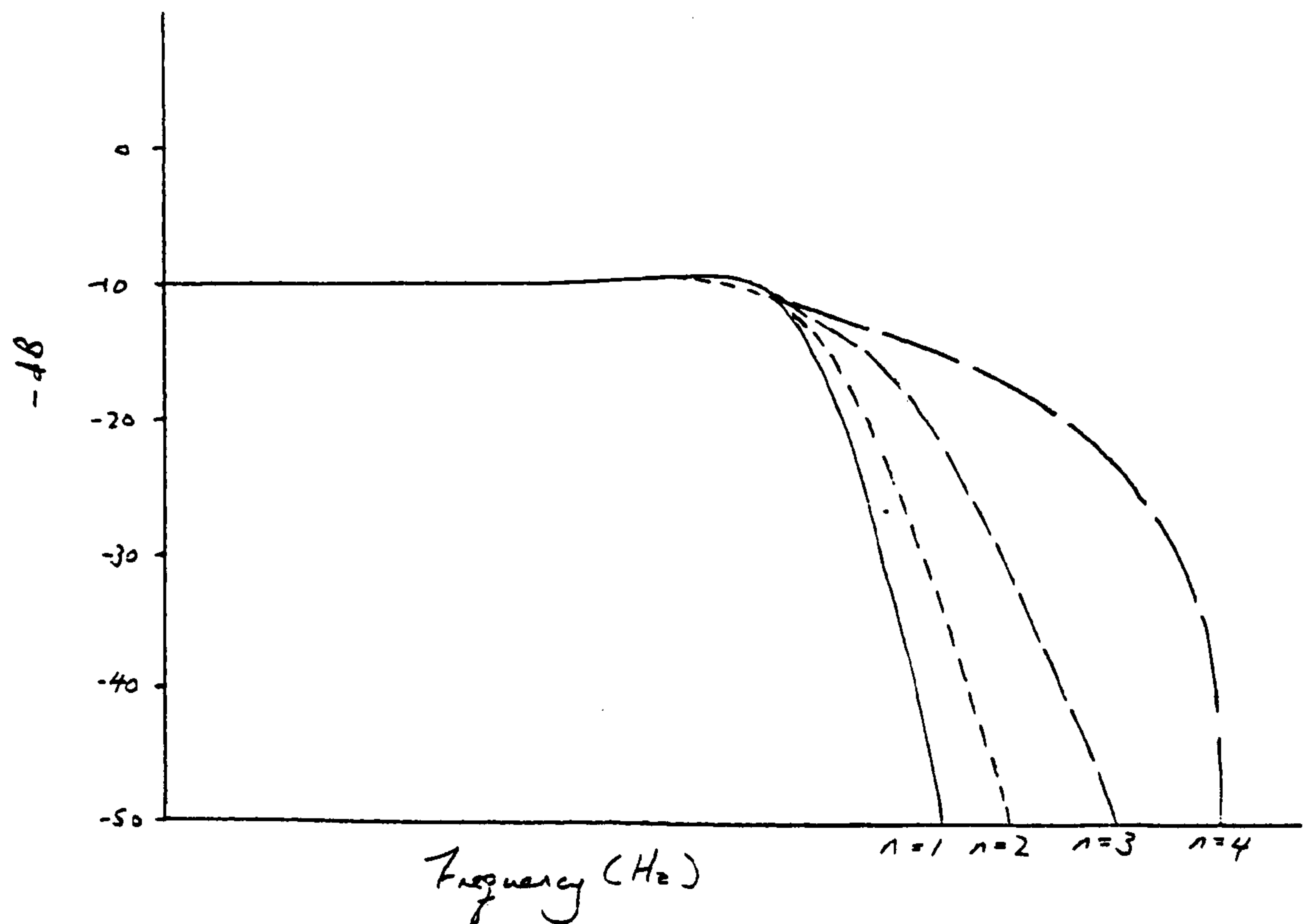


Figure A.2.2 The different order of attenuations.